Phenotypically and transcriptionally characterising hidden reservoirs of *Plasmodium falciparum* in paediatric severe malaria patients

Lauren Galloway
BSc (Hons), MSci

Submitted in fulfilment of the requirement for the Degree of Doctor of Philosophy

Institute of Infection and Immunity
College of Medical, Veterinary and Life Sciences
University of Glasgow

March 2024

Abstract

Malaria is a tropical infectious disease of global health importance which is caused by protozoan parasites of the genus *Plasmodium*. Most fatal malaria cases occur in children under five years old in sub-Saharan Africa where the dominant parasite species is *Plasmodium falciparum*. Recent studies have demonstrated that the haematopoietic spaces of the bone marrow (BM) represent an important hidden parasite reservoir of asexual and sexual stages, largely independent of classical vascular sequestration. Moreover, the spleen may represent a secondary haematopoietic organ with similar functions in extravascular parasite sequestration. The existence of hidden reservoirs has important implications for malaria eradication efforts as parasite reservoirs in these tissues may contribute to recrudescent infections, ongoing transmission, and the emergence of antimalarial resistance.

The aim of this thesis was to systematically investigate parasite sequestration in the BM and spleen in paediatric severe *P. falciparum* malaria cases, and the transcriptional pathways driving the switch from asexual to sexual stage development that may occur within these tissues. Specifically, this thesis aimed to determine whether the spleen harboured a significant parasite biomass compared to other tissues, to investigate the existence of an endosplenic life cycle, to determine the contribution of the spleen towards gametocyte formation and development in relation to the BM, and to deconvolute the transcriptional signatures of sexual commitment in two parasite strains with different sensitivities to environmental induction.

To evaluate the splenic reservoir, parasite distribution, density, and biomass were compared between the spleen, BM, lung, and peripheral circulation. Within the spleen, an enrichment of rings/early trophozoites was observed across all splenic compartments. While there were significantly higher parasite densities in the spleen compared to other tissues and peripheral circulation, there was no significant difference in the total parasite biomass between tissues. Furthermore, the parasite density in the spleen could be explained by the retention of peripherally circulating rings at a rate of 9.52%. Together, this suggests that in paediatric severe *P. falciparum* malaria, there is not a substantial hidden biomass

of parasites in the spleen that is supported by an endosplenic life cycle. This contrasts with previous observations in chronic asymptomatic malaria in adults.

The spleen and BM were investigated for their contribution towards gametocyte formation and development. In the spleen, very few gametocytes and sexually committed schizonts were identified. In contrast, 13% of parasites identified in the BM were gametocytes, with 9% identified as sexually committed schizonts. This demonstrates the role of the BM in gametocyte formation and development.

To investigate the transcriptional signatures of asexual and sexually committed schizont populations which may exist in the BM, an *in vitro* single cell RNA sequencing (scRNAseq) experiment was performed. Sexual commitment was induced by growing parasites in medium depleted of the serum phospholipid lysophosphatidylcholine (LysoPC). Two parasite strains were used, Pf2004 and Dd2, with different sensitivities to LysoPC. In LysoPC depleted conditions, two transcriptionally distinct schizont populations were identified: i) an asexual population, which exhibited upregulation of cytoadherence associated genes and genes associated with purine metabolism, and ii) a sexually committed population, which exhibited upregulation of genes associated with sexual commitment and gene regulation. These two populations shared a metabolic signature in response to nutrient depletion. A final schizont population in steady state conditions exhibited higher expression of nutrient channel components and invasion related genes. In both asexual populations, a non-coding RNA (ncRNA), PF3D7_1370800, was identified. The expression patterns of PF3D7_1370800 in relation to sexual commitment markers, and the association of this ncRNA with asexual populations, suggests that this ncRNA may function in repressing sexual commitment; however, this remains unknown.

Overall, this thesis has revealed that the magnitude of the splenic parasite reservoir varies with disease severity. It has provided histological evidence of sexual commitment in the BM, suggesting that an endogenous asexual replication cycle in the BM contributes to gametocyte enrichment and development. In parallel, it has provided insight into the transcriptional signatures of sexually committed and asexual schizonts which are hypothesised to exist within the BM.

Table of Contents

Abstract 2

List of Tables 8

List of Figures 9

Acknowledgements 13

Author's Declaration 15

Abbreviations 16

Chapter 1 | Introduction 19

1.1 Introduction to Malaria 20
1.1.1 Global Burden and Epidemiology 20
1.1.2 *Plasmodium* Life Cycle 20
1.1.3 The Pathogenesis of Severe Malaria 22
1.1.4 Malaria Elimination 26

1.2 Hidden Parasite Reservoirs 27
1.2.1 Classical Vascular Sequestration 27
1.2.2 Cryptic Parasite Reservoirs 30
1.2.3 The Bone Marrow (BM) Reservoir 30
1.2.4 The Splenic Reservoir 31
1.2.5 Evidence for an Endosplenic Life Cycle 33

1.3 Structure of the BM and the Spleen 33
1.3.1 Structure and Function of the BM 34
1.3.2 Structure and Function of the Spleen 36
1.3.3 Anaemia and Extramedullary Haematopoiesis 38
1.3.4 Differences Between Human and Mouse Haematopoietic Niches 40

1.4 Gene Regulation and Sexual Commitment 40
1.4.1 The *Plasmodium* Genome 41
1.4.2 Gene Regulation 41
1.4.3 Gene Regulation in Sexual Commitment 45
1.4.4 The Kennedy Pathway and Environmental Induction 46

1.5 Summary and Aims 49

Chapter 2 | Materials and Methods 50

2.1 Malawi Cohort 51
2.1.1 Patient Samples and Ethical Approval 51
2.1.2 Selection of Samples 52

2.2 Basic Histology and Mouse Work 53
2.2.1 *P. berghei* Infections 53
2.2.2 Standard Tissue Processing and Embedding 53
2.2.3 BM Tissue Processing and Reverse Processing 53
2.2.4 BM Decalcification 54
2.2.5 Haematoxylin and Eosin (H&E) Staining 55
2.2.6 Giemsa Staining 55
2.2.7 Periodic Acid Schiff (PAS) Staining 56
2.2.8 Histopathology Scoring 56

2.3 IHC and RNAscope 57
2.3.1 IHC 57
2.3.2 Antigen Retrieval Method and Materials 59
2.3.3 IHC Controls 60
2.3.4 Parasite Quantification and Calculations 61
2.3.5 RNAscope: *Mm-PolR2A* RNAscope 65

2.3.6 Statistics 67

2.4 *Plasmodium* Culture 68
2.4.1 Parasite Strains 68
2.4.2 Thawing and Freezing Parasite Stocks 68
2.4.3 *In vitro* Culture Maintenance 69
2.4.4 Parasite Synchronisation 69
2.4.5 Parasite Induction (Sexual Conversion Assay) 70
2.4.6 Sexually Committed and Gametocyte FFPE Blocks 71

2.5 Single Cell RNA Sequencing (scRNAseq) 72
2.5.1 Experimental Outline 72
2.5.2 Parasite Induction 72
2.5.3 Cell Harvesting 72
2.5.4 Sample Preparation 73
2.5.5 10X Run and Library Preparation 73

2.6 scRNAseq Data Analysis 74
2.6.1 Demuxlet and Quality Control 74
2.6.2 Sample Integration, Unsupervised Clustering and Mapping to the Malaria Cell Atlas 75
2.6.3 Differential Gene Expression (DGE) Analysis 75
2.6.4 Pseudotime Trajectory Inference 75
2.6.5 Data Visualisation Methods and Tools 76

Chapter 3 | Using basic histological stains to evaluate the histopathology and parasite distribution in the BM and spleen 77

3.1 Introduction 78
3.1.1 BM and Splenic Reservoirs 78
3.1.2 Histopathology of the BM 79
3.1.3 Histopathology of the Spleen 80
3.1.4 Reticulocytes and Endosplenic Life Cycles 81
3.1.5 Malawi Cohort 82
3.1.6 Chapter Aims and Hypotheses 83

3.2 Case Selection and Cohort Characterisation 85

3.3 Technical Considerations: BM Decalcification 92
3.3.1 Basic Staining: H&E and Giemsa 93
3.3.2 HSP70 IHC 94
3.3.3 *Mm-PolR2A* RNAscope 95

3.4 Histopathology of the BM and Spleen 97
3.4.1 Histopathology of the BM: Whole Cohort 97
3.4.2 Histopathology of the BM: Per Clinical Group 99
3.4.3 Multivariant Analysis of BM Histopathological and Patient Clinical Parameters 100
3.4.4 Histopathology of the Spleen: Whole Cohort 103
3.4.5 Multivariant Analysis of Splenic Histopathological and Patient Clinical Parameters 107

3.5 Evaluating Parasite Accumulation in the Spleen 109
3.5.1 Defining Spleen Compartments 109
3.5.2 Defining Giemsa Counting Methodology 111
3.5.3 Splenic Distribution and Accumulation of Parasites by Giemsa 114
3.5.4 Evidence of an Endosplenic Life Cycle? 117

3.6 Chapter Discussion 120
3.6.1 BM Decalcification 120
3.6.2 Histopathology of the BM and Spleen 121
3.6.3 Parasite Accumulation in the Spleen 126
3.6.4 Evidence of an Endosplenic Life Cycle 129
3.6.5 Chapter Summary 131

Chapter 4 | Using IHC to determine splenic tropism and the presence of an endosplenic life cycle 132

4.1 Introduction 133
4.1.1 Sequestration Across Multiple Organs 133
4.1.2 Reticulocytes in the Spleen 134
4.1.3 Gametocytes in the Spleen 135
4.1.4 Sexual Commitment in the Tissue 136
4.1.5 Chapter Aims and Hypotheses 138

4.2 Parasite Accumulation in the Spleen, BM, and Lung 140
4.2.1 Validating Giemsa Counts 140
4.2.2 Parasite Distribution in the Spleen, BM, and Lung 142
4.2.3 Comparison of Parasite Accumulation Between Organs 150
4.2.4 Splenic Parasite Retention vs Endosplenic Life Cycle 151
4.2.5 Comparison of Parasite Biomass Between Organs 152

4.3 Confirmation of Non-Phagocytosed Parasites 154
4.3.1 Splenic Macrophage Distribution 154
4.3.2 Free vs Phagocytosed Splenic Parasites 156
4.3.3 Investigating Splenic Parasitic "Nests" 157

4.4 Reticulocyte Co-Localisation and Invasion 159
4.4.1 Reticulocyte Density in the Spleen and Lung Vessels 159
4.4.2 Parasites Infection of Reticulocytes in the Spleen and BM 163

4.5 Gametocyte Distribution in the Spleen and BM 165
4.5.1 Gametocytes in the Spleen 165
4.5.2 Gametocytes in the BM 166

4.6 Sexually Committed Schizonts in the Spleen and BM 168

4.7 Chapter Discussion 171
4.7.1 Conservative Counting Methodology 171
4.7.2 Ineffective Splenic Parasite Clearance 174
4.7.3 No Evidence of an Endosplenic Life Cycle 176
4.7.4 Gametocyte Formation and Development 179
4.7.5 The Role of the Spleen as a Parasite Reservoir 181
4.7.6 Chapter Summary 183

Chapter 5 | Deconvolving the transcriptional signature of sexual commitment in schizonts 185

5.1 Introduction 186
5.1.1 Transcriptomics in *Plasmodium* 187
5.1.2 The 10X Chromium Single Cell Pipeline 191
5.1.3 *Plasmodium* Strains, Conversion Rates, and Transmission Settings 193
5.1.4 Aims and Hypotheses 194

5.2 Experimental Outline 195

5.3 Sexual Conversion Assay 197

5.4 Quality Control, Clustering and Annotation 201
5.4.1 Separating Pooled Strains 201
5.4.2 Quality Control 203
5.4.3 Sample Integration & Unsupervised Clustering 207
5.4.4 Correlating Clusters with Published Datasets 209

5.5 Global Differences Between mFA vs Serum 211
5.5.1 DGE: mFA vs Serum 211
5.5.2 DGE: mFA vs Serum in Early and Late Schizonts 216

5.6 Defining Asexual and Sexual Populations 223
5.6.1 Mapping Known Sexual Commitment Markers 223
5.6.2 Mapping 'Sexual' and 'Asexual' Markers 228
5.6.3 DGE: *ap2-g* High vs *ap2-g* Low Clusters in Pf2004 231
5.6.4 Investigating DGE Hits in Dd2 238

5.7 Chapter Discussion 242
5.7.1 DGE: mFA vs Serum 242
5.7.2 DGE: *ap2-g* High vs *ap2-g* Low Clusters 246
5.7.3 Commitment in Dd2 250
5.7.4 Limitations of scRNAseq 252
5.7.5 Chapter Summary 253

Chapter 6 | General Discussion 257

6.1 General Discussion 258

6.2 Model of Splenic Accumulation in Malaria 258

6.3 Deconvoluting Transcriptional Signatures of Sexual Commitment 261

6.4 Future Directions 266

6.5 Summary 269

Appendices 270

Appendix 1 271

Appendix 2 272

References 273

List of Tables

Table 2-1. Histopathology scoring. 57
Table 2-2. IHC conditions. 59
Table 2-3. IHC controls. 61
Table 2-4. RNAscope conditions. 67
Table 2-5. ACD qualitative scoring criteria. 67
Table 2-6. Quality control thresholds. 74
Table 3-1. Patient information for malaria cases and non-malarial controls. 88
Table 3-2. Baseline characteristics of malaria cases and non-malarial controls. 91
Table 3-3. Summary of BM histopathology scoring. 100
Table 3-4. Summary of spleen histopathology scoring. 105
Table 5-1. Cell ranger outputs and cell counts. 206
Table 5-2. Top 25 DGE genes between mFA vs Serum. 215
Table 5-3. Top 25 DGE genes between mFA vs Serum in early schizonts. 221
Table 5-4. Top 25 DGE genes between mFA vs Serum in late schizonts. 222
Table A1-1. Histopathologic bone marrow (BM) scoring criteria. 271
Table A1-2. Histopathologic spleen scoring criteria. 271
Table A2-1. Top 25 differentiallly expressed (DGE) genes between *ap2-g* high and *ap2-g* low clusters (Pf2004). 272

List of Figures

Figure 1-1. The life cycle of *P. falciparum*. 22
Figure 1-2. Severe malaria organ involvement with age. 25
Figure 1-3. Classical vascular sequestration. 28
Figure 1-4. *P. falciparum* host cell remodelling. 30
Figure 1-5. Cellularity of the bone marrow (BM) alters with age. 35
Figure 1-6. The bone marrow (BM) is organised into distinct niches. 36
Figure 1-7. The structure of the spleen. 38
Figure 1-8. The biosynthesis of phosphatidylcholine (PC) in *Plasmodium*. 48
Figure 3-1. Granulocytic left shift. 80
Figure 3-2. Flow chart of case selection. 87
Figure 3-3. Baseline characteristics of malaria cases and non-malarial controls. 91
Figure 3-4. Bone marrow (BM) decalcification experimental outline. 93
Figure 3-5. Decalcification does not induce changes in H&E and Giemsa-stained bone marrow (BM) sections. 94
Figure 3-6. Decalcification does not induce changes in IHC staining. 95
Figure 3-7. Decalcification does not Induce changes in RNAscope staining. 96
Figure 3-8. Infected RBCs (iRBC), eosinophils, macrophages, and pigment in the bone marrow (BM) of paediatric severe malaria patients. 99
Figure 3-9. Multivariant analysis reveals no distinct subgroups in the bone marrow (BM). 101
Figure 3-10. Multivariant analysis reveals several significant correlations in the bone marrow (BM). 102
Figure 3-11. Pigment, infected red blood cells (iRBCs), and disorganisation of the splenic microarchitecture in the spleen of severe malaria patients and non-malarial controls. 106
Figure 3-12. Multivariant analysis reveals no distinct subgroups in the spleen. 107
Figure 3-13. Multivariant analysis reveals several significant correlations in the spleen. 108
Figure 3-14. Representative images of splenic compartments. 110
Figure 3-15. The perifollicular zone of the spleen. 111
Figure 3-16. Periodic acid Schiff (PAS) stain on a spleen section highlighting sinusoids. 111
Figure 3-17. Morphological appearance of non-phagocytosed parasites and pigmeted phagocytes in Giemsa-stained spleen sections. 112
Figure 3-18. Splenic ring identifications using polarised light. 113
Figure 3-19. Infected spleens primarily exhibited rings/early trophozoites, with the largest concentration of asexual parasites observed in the splenic cords. 115

Figure 3-20. Heterogenous parasite distribution in the spleen. _____ 116
Figure 3-21. Identification of parasitic "nests". _____ 116
Figure 3-22. Density of asexual parasites in each splenic compartment. _____ 117
Figure 3-23. Ring and trophozoite densities are highest across all splenic compartments. _____ 118
Figure 3-24. Proportions of asexual stages are not consistent with an endosplenic life cycle. _____ 119
Figure 3-25. No correlation was observed between post-mortem interval (PMI) and pigmentation. _____ 124
Figure 3-26. Inconsistent Giemsa staining in Malawi bone marrow (BM). _____ 128
Figure 4-1. Parasite distribution in the spleen was comparable between immunohistochemistry (IHC) and Giemsa counts. _____ 141
Figure 4-2. Counts performed by immunohistochemistry (IHC) and Giemsa were comparable. _____ 141
Figure 4-3. Distribution of parasites in the spleen, bone marrow (BM), and lung. ___ 143
Figure 4-4. Splenic distribution of *P. falciparum* by immunohistochemistry (IHC). __ 144
Figure 4-5. Parasite density is significantly higher in small vessels and cords compared to non-circulatory spaces. _____ 145
Figure 4-6. Heterogeneous distribution of parasites in the spleen. _____ 146
Figure 4-7. Bone marrow (BM) distribution of *P. falciparum* by immunohistochemistry (IHC). _____ 147
Figure 4-8. Parasite densities were significantly higher in the BM parenchyma compared to the small vessels (SV). _____ 148
Figure 4-9. Lung distribution of *P. falciparum* by immunohistochemistry (IHC). ____ 149
Figure 4-10. Parasite densities were significantly higher in the small vessels (SV) of the lung compared to the lung parenchyma. _____ 150
Figure 4-11. Spleen parasite densities are significantly higher than bone marrow (BM), lung, and peripheral blood parasite densities. _____ 151
Figure 4-12. The spleen did not have a significantly higher parasite biomass compared to other organs. _____ 153
Figure 4-13. Parasite localisation with splenic macrophages. _____ 155
Figure 4-14. There is no significant difference in macrophage numbers between malaria cases and non-malaria controls. _____ 155
Figure 4-15. Free parasites in the spleen are positively correlated with macrophages and phagocytosed parasites. _____ 156
Figure 4-16. Parasites in the spleen were predominantly non-phagocytosed. _____ 157
Figure 4-17. Splenic "nests" likely represent phagocytic events. _____ 159

Figure 4-18. Reticulocyte (CD71) immunohistochemistry (IHC) in the lung and spleen. 161
Figure 4-19. Reticulocytaemia was not significantly different between spleen and peripheral blood. 163
Figure 4-20. Parasites predominantly infect mature red blood cells (RBCs) over reticulocytes in the spleen. 164
Figure 4-21. The spleen does not contribute to gametocyte development. 166
Figure 4-22. The bone marrow (BM) parenchyma has the largest proportion of gametocytes. 167
Figure 4-23. Identification of sexually committed schizonts in the bone marrow (BM). 169
Figure 4-24. Correlation between MSRP1 parasitaemia and Pfs16 parasitaemia in the bone marrow (BM) parenchyma. 170
Figure 4-25. Proportion of unclassifiable counts by immunohistochemistry (IHC). 173
Figure 4-26. Model of parasite accumulation in the spleen in malaria. 183
Figure 5-1. Droplet based single cell RNA sequencing (scRNAseq) workflow. 192
Figure 5-2. Representative images of Pf2004 and Dd2 in vitro cultures at 26/28 hours post invasion (hpi). 197
Figure 5-3. single cell RNA sequencing (scRNAseq) experimental outline. 197
Figure 5-4. Gating strategy for sexual conversion assay flow cytometry in Pf2004. 198
Figure 5-5. Parasite multiplication rate (PMR) and conversion rate for Pf2004 and Dd2. 199
Figure 5-6. Blood smear of Pf2004 and Dd2 in vitro cultures confirms the presence of gametocytes following the sexual conversion assay. 200
Figure 5-7. Separating pooled parasite strains computationally. 201
Figure 5-8. Heatmap of the top 10 differentially expressed marker genes between Pf2004 and Dd2. 203
Figure 5-9. single cell RNA sequencing (scRNAseq) quality control (QC) thresholds for each sample. 205
Figure 5-10. Minimal fatty acid (mFA) and Serum samples from each replicate were integrated into single Seurat objects depending on strain identity using Harmony. 208
Figure 5-11. Pf2004 and Dd2 uniform manifold approximation and projections (UMAPs). 208
Figure 5-12. Assignment of asexual developmental stages to cells and their proportions after quality control. 209
Figure 5-13. Uniform manifold approximation and projection (UMAP) of Pf2004 and Dd2 cells coloured by the expression level of cell stage marker genes. 211

Figure 5-14. Global transcriptional changes between minimal fatty acid (mFA) and Serum for Pf2004 and Dd2. _____ 213
Figure 5-15. Venn diagram comparisons of differentially expressed genes in minimal fatty acid (mFA) vs Serum for Pf2004 and Dd2. _____ 216
Figure 5-16. Transcriptional changes between schizonts in minimal fatty acid (mFA) and Serum in Pf2004. _____ 218
Figure 5-17. Transcriptional changes between schizonts in minimal fatty acid (mFA) and Serum in Dd2. _____ 219
Figure 5-18. Venn diagram comparisons of differentially expressed genes between minimal fatty acid (mFA) vs Serum for Early and Late Schizonts (Pf2004 and Dd2). __ 220
Figure 5-19. Regions of similarity between 3 non-coding RNAs (ncRNA) of chromosome, 8, 11. and 13. _____ 223
Figure 5-20. Representative figures demonstrating the ordering of cells along pseudotime. _____ 224
Figure 5-21. Temporal order of sexual commitment markers in mFA and Serum. __ 227
Figure 5-22. Expression of sexual commitment markers. _____ 228
Figure 5-23. *clag3.1* and *rhoph3* were not markers of the cluster separation identified in Pf2004. _____ 229
Figure 5-24. Uniform manifold approximation and projection (UMAP) of Pf2004 and Dd2 cells coloured by expression *ap2-g*, *garp*, and *pf332*. _____ 231
Figure 5-25. Differential gene expression (DGE) between *ap2-g* high and *ap2-g* low clusters. _____ 233
Figure 5-26. Uniform manifold approximation and projection (UMAPs) coloured by the expression of genes representing three identified schizont populations in Pf2004. __ 236
Figure 5-27. Average expression of differentially expressed genes identified in *ap2-g* high vs *ap2-g* low clusters over pseudotime in Pf2004. _____ 237
Figure 5-28. *surf8.2* is co-expressed with msrp1 in Pf2004 late schizonts. _____ 238
Figure 5-29. Uniform manifold approximation and projection (UMAPs) of Dd2 cells coloured by the expression of genes which represented three schizont populations identified in Pf2004. _____ 240
Figure 5-30. Average expression of markers over pseudotime in Dd2._____ 241
Figure 5-31. The RhopH complex and plasmodial surface anion channel (PSAC). ____ 245
Figure 5-32. Summary of the transcriptional signatures of hypothesised schizont populations in the bone marrow (BM). _____ 255

Acknowledgements

First and foremost, I would like to thank my primary supervisor, Professor Matthias Marti. Thank you for your support, guidance, and supervision throughout my PhD. Your unwavering enthusiasm throughout and belief in my abilities has served as a constant source of motivation. You have been the perfect PhD supervisor, and I am grateful for your mentorship over the past four years.

To my supervision team, Professor Thomas Otto, Dr. Chris Moxon, and Professor Alex Rowe, thank you for sharing your expertise and for your guidance throughout my PhD. To my lab, both in Glasgow and in Switzerland, thank you for being supportive. In particular, I would like to thank Fiona Achcar, Barbara Stokes, Lauriane Sollelis and Priscilla Ngotho for your help with my scRNAseq experiment and the data analysis. It was a nightmare, but I couldn't have done it without you all. I would like to thank Gillian Parker for being incredibly supportive, a great listener and for having my back throughout my PhD. Importantly, I would like to thank Matt Gibbins. You have been an integral part of the development of my PhD project and of me as a scientist. Your positive attitude and encouragement throughout have been invaluable. The Gibbins lab will go far with you as a leader!

I would like to thank several people for their technical support and assistance. In no particular order, I thank: Fiona McMonagle, Ross Laidlaw, Olympia Hardy, Joao Da Silva Filho, Frazer Bell, Julie Galbraith and Glasgow Polyomics. I would also like to thank Charalampos Attipa as the pathologist on this project, not only for his contribution to the histopathological evaluation of tissues, but for being a great teacher on the pathology of the bone marrow and spleen. To those involved in the Blantyre Malaria Project, Malawi, thank you for kindly providing tissues for this project, as well as your expertise.

Most importantly, I would like to thank my family and friends. I am so incredibly fortunate to have such supportive and loving people in my life. To the boys, Rob, Gavin, Ryan, and Hector, thank you for all the amazing memories we share together in Glasgow. To Lena, Alicia, and Ine, thank you for sending me flowers, for bringing me hot chocolate, and buying me lunch when I was too busy to make time. To the "lunchables", Andrew, Emily, Annie, Kieran, and Patricia, thank you for bringing joy and laughter to an ordinary day at work. To Lewis, thank you for

ice cream therapy, who knew ice cream would be the answer to so many problems. To Mimi, thank you for all that you do, you are a great friend, and I am so grateful that the field of malaria has brought us together. To Andrew, thank you for always making me smile, for being my biggest hype man, and for making me feel calm whenever I felt overwhelmed. Finally, to my family, Mum, Dad, Katie, Kerren, and Anna, you are my happy place. Kerren, thank you for being you, I would be lost without you. Mum and Dad, you've always believed in us and motivated us to strive for bigger and better things. You have taught us the meaning of hard work and how to never give up. We are endlessly grateful for everything you have done for us. Thank you.

Author's Declaration

I declare that the work presented in this thesis is my own work, except where reference is made to the contribution of others. It does not consist of work submitted for any other degree at the University of Glasgow or any other institution.

Signature: …….

Printed Name: Lauren Jane Galloway

Abbreviations

All gene names are abbreviated according to their annotation in PlasmoDB release 66.

ACT	Artemisinin combination therapy
Adm	Admission
ApiAP2	Apicomplexan apetala-2
ARDS	Acute respiratory distress syndrome
asRNA	Antisense RNA
BCIP/NBT	5-bromo-4-chloro-3-indolyl phosphate/nitroblue tetrazolium
BLAST	Basic local alignment search tool
BSA	Bovine serum albumin
BV	Blood volume
CA	Central artery
CCT	CTP:phosphocholine cytidylytransferase
cDNA	Complement DNA
CDP-Cho	cytidine-diphosphocholine
CEPT	choline/ethanolamine phosphotransferase
ChIP	Chromatin immunoprecipitation
CI	Confidence interval
CK	Choline kinase
CM	Cerebral malaria
COC	Cause of coma
Contrib	Contribution
CSA	Chondroitin sulphate A
DAB	3, 3-diaminobenzidine
DAG	diacylglycerol
Decal	Decalcified
DGE	Differential gene expression
DGE	Differential gene expression
DNA	Deoxyribonucleic acid
DPX	Dibutylphthalate polystyrene xylene
EDTA	Ethylene-diamine-tetraacetic acid
EK	ethanolamine kinase
EPCR	Endothelial cell protein C receptor
FC	Fold change
FFPE	Formalin-fixed, paraffin embedded
GC	Germinal centre
GEM	Gel bead in emulsion
H&E	Haemotoxylin and eosin
HPF	High powered fields
Hpi	Hours post invasion
ICAM-1	Intracellular adhesion molecule 1
IHC	Immunohistochemistry
IQR	Interquartile range

iRBC	Infected red blood cell
LF	Lymphoid follicle
lncRNA	Long non-coding RNA
LV	Large vessels
LysoPC	Lysophosphatidylcholine
M:E	Myeloid to erythroid
ManZ	Mantle zone
MarZ	Marginal zone
mFA	Minimal fatty acid
NA	Not assigned
NBF	Neutral buffered formalin
ncRNA	Non-coding RNA
NCS	Non-circulatory spaces
NGS	Next generation sequencing
NMC	Non-malarial control
NS	Not significant
P-Cho	phosphocholine
P-Eth	phophoethanolamine
P%	Parasitaemia
PALS	Periarteriolar lymphoid sheath
PAS	Periodic acid Schiff
PBS	Phosphate buffered saline
PC	phosphatidylcholine
PCA	Principal component analysis
PCV	Packed cell volume
PE	phosphatidylethanolamine
PECAM	Platelet endothelial cell adhesion molecule
PfEMP1	*Plasmodium falciparum* Erythrocyte Membrane Protein 1
PfHRPII	*Plasmodium falciparum* histidine rich protein II
PFZ	Perifollicular zone
pLDH	*Plasmodium* lactate dehydrogenase
PM	Post-mortem
PMI	Post-mortem interval
PMR	Parasite multiplication rate
PMT	phophoethanolamine methyltransferase
PSAC	Plasmodial surface anion channel
PV	Parasitophorous vacuole
QC	Quality control
Qn	Quinine dihydrochloride
RBC	Red blood cell
RNA	Ribonucleic acid
RP	Red pulp
RPMI	Roswell Park Memorial Institute
SAH	S-adenosyl-l-homocysteine
SAHH	S-adenosyl-l-homocysteine hydrolase
SAM	s-adenosylmethionine

scRNAseq	Single cell RNA sequencing
SL	Sinus lumen
SMA	Severe malarial anaemia
SNP	Single nucleotide polymorphisms
SV	Small vessels
TBST	Tris buffered saline 0.05% tween
UMAP	Uniform manifold approximation and projection
UMI	Unique molecular identifier
uRBC	Uninfected red blood cell
WHO	World health organisation
WP	White pulp

Chapter 1 | Introduction

1.1 Introduction to Malaria

Malaria is an ancient disease, with the earliest documented reference believed to originate from a Chinese document dating back to around 2700 BC (Cox, 2010). However, the spread of disease to the Americas was relatively recent coinciding with the slave trade (Rodrigues et al., 2018). Shortly after the development of the germ theory of disease by Louis Pasteur and Robert Koch in the 1870s, Alphonse Laveran demonstrated that the causative agent of malaria was the protozoan parasite, *Plasmodium*. In 1897, Ronald Ross and Battista Grassi determined that malaria was a vector borne disease with the identification of parasites stages in the midgut of *Anopheles* mosquitoes (Cox, 2010).

1.1.1 Global Burden and Epidemiology

Malaria remains a major global health threat, with an estimated 249 million cases and 608,000 deaths in 2022. Over 90% of all malaria cases and deaths occur in sub-Saharan Africa with children under 5 years old, pregnant women, travellers, and patients with HIV/AIDS at the highest risk of severe malaria. In this region, children under 5 years old accounted for 80% of all malaria deaths (WHO, 2023b).

Five species of *Plasmodium* are known to infect humans. The species associated with the most fatalities is *Plasmodium falciparum* which is the predominant *Plasmodium* species in sub-Saharan Africa. *P. vivax*, initially regarded as only causing benign disease, is the most geographically widespread species. Over the past decade, there has been a rise in reports of severe *P. vivax* malaria (Phyo et al., 2022). *P. ovale* (*P. ovale curtisi* and *P. ovale wallikeri*) and *P. malariae* rarely cause severe disease. *P. knowlesi* is a zoonotic species which primarily infects long tailed and pig tailed macaques. However, increasing reports of human infections have been described throughout Southeast Asia (Singh et al., 2004, Cox-Singh and Singh, 2008, Singh and Daneshvar, 2013). This thesis will focus on *P. falciparum*.

1.1.2 *Plasmodium* Life Cycle

Plasmodium spp. have a complex yet conserved life cycle which encompasses both a vertebrate host and mosquito vector (**Figure 1-1**). A *Plasmodium* infection is established when an infected mosquito injects sporozoites into the skin of a vertebrate host during a blood meal (**Figure 1-1A**). A proportion of these highly

motile sporozoites enter blood capillaries and travel to the liver where they traverse several hepatocytes before actively invading a hepatocyte forming a parasitophorous vacuole (PV) within which they asexually replicate (Mota et al., 2001, Amino et al., 2006, Tavares et al., 2013, Loubens et al., 2021). This asexual replication results in the production of up to 100,000 merozoites which are released into the liver sinusoids by budding from the host hepatocytes in membrane bound vesicles termed merosomes (**Figure 1-1B**) (Sturm et al., 2006, Vaughan et al., 2012). Within the blood, free merozoites invade red blood cells (RBCs) to establish an intraerythrocytic cycle of asexual replication. Parasites undergo three morphologically distinct developmental stages within RBCs: ring, trophozoite and schizont. The duration of the intraerythrocytic asexual replication cycle varies between species and strains ranging from 24 to 72 hours. *P. falciparum* exhibits an asexual replication cycle of ca. 48 hours. After this asexual replication cycle, up to 32 daughter merozoites (varies depending on species) are produced which are released following schizont rupture for further RBC invasion (**Figure 1-1C**). It is during this stage of the life cycle where patients become symptomatic. During this intraerythrocytic developmental cycle, a subset of parasites will undergo sexual commitment to produce the transmissible gametocytes. Gametocytes (male and female) progress through gametocytogenesis from stages I-V over 8-10 days. It is only the mature stage V gametocytes, circulating at low densities in the blood, that are transmissible to the mosquito vector (**Figure 1-1C**). Gametocytes are transmitted to the mosquito vector during a blood meal where they enter the mosquito midgut and egress from the RBC to form either eight microgametes (male) or one macrogamete (female) (Sologub et al., 2011). Microgametes and macrogametes fuse to produce a zygote which undergoes meiosis to produce an ookinete. These ookinetes traverse the midgut wall to form an oocyst. Asexual replication occurs within the oocyst producing thousands of sporozoites which, upon rupture, migrate through the haemolymph to the salivary glands (**Figure 1-1D**). From here, the cycle is initiated again through the transfer of these sporozoites to a vertebrate host following bloodmeal.

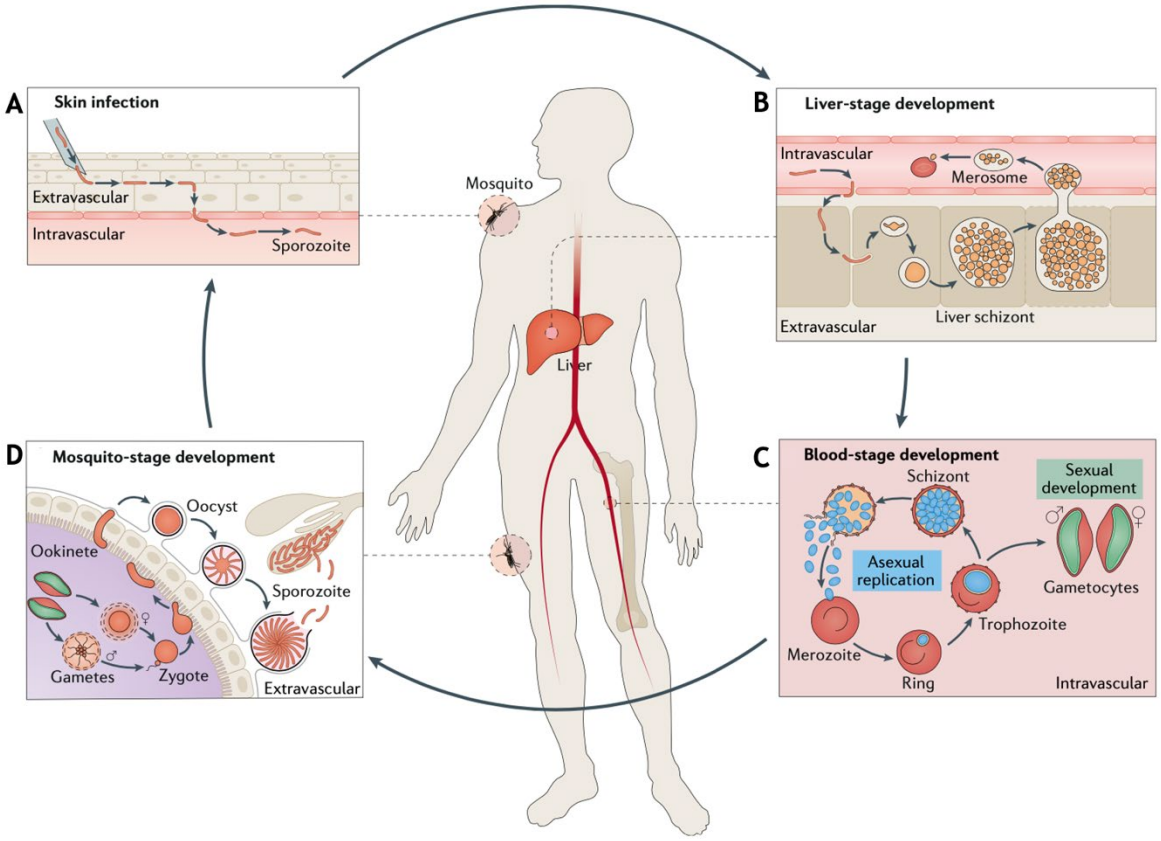

Figure 1-1. The life cycle of *P. falciparum*. (**A**) The life cycle is initiated when an infected female *Anopheles* mosquito injects sporozoites into the skin during a bloodmeal. (**B**) Sporozoites migrate to the liver where they invade hepatocytes. Here, parasites asexually replicate forming liver schizonts which bud from the infected hepatocyte releasing merosomes, and therefore merozoites, into the peripheral circulation for invasion of RBCs. (**C**) Within RBCs, parasites establish an asexual replication cycle undergoing three main stages: ring, trophozoite and schizont. After ca. 48 hours, schizonts rupture releasing merozoites for further invasion. A subset of asexual parasites will undergo sexual commitment resulting in the production of female or male gametocytes in the subsequent cycle. (**D**) During a bloodmeal, the mosquito vector will ingest gametocytes which will develop into macrogametes (female) or microgametes (male) in the midgut. These will fertilise to form a zygote which undergoes meiosis forming an ookinete. This ookinete penetrates through the midgut wall into the haemolymph. Within the haemolymph, ookinetes develop into oocysts where asexual sporogony produces sporozoites; these sporozoites migrate to the salivary glands upon rupture. The cycle continues when an infected mosquito takes another blood meal injecting sporozoites into the skin. Figure from Venugopal *et al.*, 2020 (Venugopal et al., 2020).

1.1.3 The Pathogenesis of Severe Malaria

The clinical presentation of malaria is critically influenced by level of exposure and acquired protective immunity. *P. falciparum* malaria disease severity ranges from asymptomatic to uncomplicated to severe malaria, with the severity of disease being multifactorial. Asymptomatic malaria is prevalent in adults in malaria endemic countries through years of exposure and acquired immunity. These low density, asymptomatic infections likely contribute to ongoing transmission (Gupta et al., 1999, Langhorne et al., 2008, Weiss et al., 2010,

Laishram et al., 2012, Gonzales et al., 2020). Symptoms of uncomplicated malaria typically present 10-15 days after an infectious bite. These symptoms are non-specific, classically presenting as cyclical fever, chills, and headache, however, vomiting, diarrhoea, fatigue, and anaemia are common. Without treatment, uncomplicated malaria can rapidly progress to severe malaria. Severe malaria can present in one or more clinical manifestations which include a neurological syndrome with unrousable coma (cerebral malaria (CM)), severe malarial anaemia (SMA) and respiratory distress in relation to metabolic acidosis (WHO, 2024). Severe malaria in non-immune patients (e.g., young children in malaria endemic countries) is associated with the production of pro-inflammatory cytokines and chemokines, leading to systemic inflammation (Farrington et al., 2017). With re-exposure, pro-inflammatory mediators are downregulated coinciding with less severe disease (Portugal et al., 2014).

In children, CM and SMA are the most frequent complications attributed to *Plasmodium* infection. CM is associated with the highest mortality rates, with case fatality rates, even with treatment, between 15% to 30% (Haldar et al., 2007). Clinical CM is defined as unrousable coma (Blantyre Coma Scale score $\leq$ 2 or Glasgow Coma Scale score $\leq$ 10), with no improvement following correction of hypoglycaemia, peripheral parasitaemia, and no other obvious cause of coma (Taylor et al., 2004). The Blantyre Coma Scale was adapted from the Glasgow Coma Scale (adults) to assess malarial coma in preverbal children. A characteristic feature of CM is the accumulation of sequestered parasites in the vasculature of the brain (classical vascular sequestration is reviewed in **Section 1.2.1**). It was previously assumed that parasite sequestration, and the associated cerebral histopathological changes, was the cause of death in CM cases. Between 1996 and 2010, a large severe malaria post-mortem study was conducted in Blantyre, Malawi. In this Malawi cohort, a strong positive correlation was identified between the level of sequestered parasites, and the histopathological changes in the brain (Taylor et al., 2004). However, Taylor *et al.* revealed that not all patients with clinical CM exhibited histopathological changes with a subset of patients exhibiting a "sequestration only" pattern (Taylor et al., 2004, Milner et al., 2014). In a pioneering study of 168 paediatric fatal and non-fatal CM cases in Malawi, magnetic resonance imaging was used to reveal that fatal cases of CM exhibited increased brain volume, whereas non-fatal cases either exhibited no brain

swelling, or brain swelling that resolved. These results suggested that the cause of death in CM cases, was not due to histopathological changes caused by parasite sequestration, but by increased intracranial pressure (Seydel et al., 2015).

Malaria associated anaemia is common in chronic and acute malaria across age groups. In areas of high transmission, SMA (haemoglobin < 50 g/L; packed cell volume (PCV) < 15%) is the main clinical manifestation in children below two years old (White, 2018). The pathogenesis of SMA is complex involving multiple contributing factors. Direct parasite factors include the inherent rupture of host RBCs to release merozoites for further invasion and the binding of infected RBCs (iRBCs) and uninfected RBCs (uRBCs) to vascular endothelial cells which removes RBCs from circulation. Similarly, malaria induces reduced RBC deformability in both iRBCs and uRBCs, predisposing them to splenic clearance. Immune factors that contribute to the development of SMA include immune mediated haemolysis and infection induced eryptosis. Additionally, there is decreased RBC production attributed to iron depletion and dyserythropoiesis in the bone marrow (BM) (White, 2018, Moxon et al., 2020, Scovino et al., 2022).

The pathogenesis of malaria varies depending on age and host immunity (**Figure 1-2**). In high transmission settings, protective immunity increases with age explaining the higher frequency of asymptomatic infections observed in adults (Lindblade et al., 2013). Severe malaria in adults occurs in non-immune patients and presents differently to severe malaria in children (Moxon et al., 2020). The frequent complication of SMA in children below two years old may relate to the function of the spleen in parasite clearance. Buffet *et al*. proposed that the high prevalence of SMA in young children was related to highly active splenic clearance of ring-iRBCs and uRBCs. As such, this clearance prevents trophozoite/schizont-iRBC sequestration in the tissues, thereby preventing severe complications such as CM. However, this enhanced iRBC and uRBC clearance results in severe anaemia (Buffet et al., 2011). Children aged two to sixteen years old are more susceptible to CM. An explanation for this shift in frequency of SMA and CM with age, is that the clearance activity of the spleen alters with age and host immunity. Less active parasite clearance in the spleen of children older than two years old is protective against anaemia but increases the risk of CM (**Figure 1-2**) (Buffet et al., 2011, Moxon et al., 2020). Other organ associated complications of malaria such as renal

failure, pulmonary oedema, and acute respiratory distress syndrome (ARDS) is less common in severe malaria in children (**Figure 1-2**) (Moxon et al., 2020).

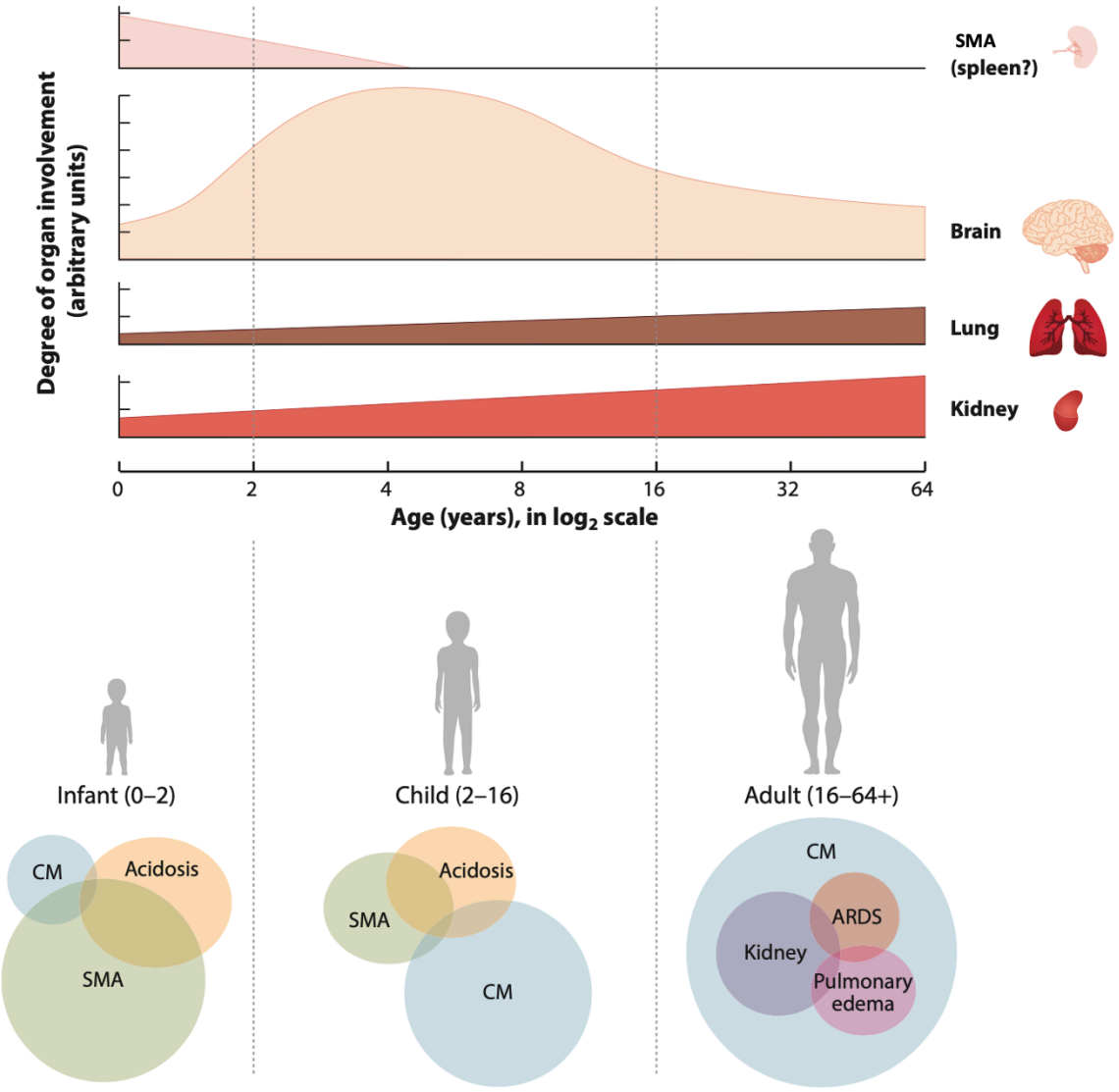

Figure 1-2. Severe malaria organ involvement with age. In children less than two years old in high transmission settings, severe malarial anaemia (SMA) is a common complication which is attributed, at least in part, to high splenic clearance of RBCs. With age, reduced splenic clearance may protect against SMA, however, this increases susceptibility to cerebral malaria (CM). In adults, severe malaria involves multiple organ syndromes. The dogma on severe malaria in adults is evolving with evidence of brain involvement, similar to that of CM, in adults with non-cerebral severe malaria (Mohanty et al., 2022). Venn diagrams represent the approximate relative frequency and degree of interactions between different clinical syndromes. Abbreviations: CM, cerebral malaria; SMA, severe malarial anaemia; ARDS, acute respiratory distress syndrome. Figure adapted from Moxon *et al.*, 2020.

1.1.4 Malaria Elimination

The Global Technical Strategy for malaria 2016-2030 presents a comprehensive framework aimed to accelerate the progress towards malaria elimination. Here, the overall target is to reduce the global burden of malaria by 90% by 2030, interrupt transmission, and prevent the re-establishment of malaria in all malaria free countries (WHO, 2021). Between 2015 and 2019, global malaria deaths declined from 864,000 to 576,000 in 2019. However, in 2020, with the impact of the SARS-CoV-2 pandemic on fragile health care systems, the number of deaths increased by 10% to 631,000. While malaria cases continue to rise, the global number of deaths has decreased in 2022 (WHO, 2023b). However, despite these recent improvements in case management, there are multiple biological challenges that threaten the achievement of the Global Technical Strategy targets. One such challenge is the emergence and spread of antimalarial resistance.

The current first line treatment for uncomplicated malaria is artemisinin combination therapy (ACT) which combines the fast-acting artemisinin derivative with a longer acting partner drug. For treatment of severe malaria, the recommended treatment is intravenous or intramuscular artesunate for at least 24 hours until patients can tolerate oral ACT (WHO, 2023a). Artemisinin offers superior activity against all parasite stages compared to the previous gold standard treatment, quinine, which is only effective on sequestered parasites (ter Kuile et al., 1993, Dondorp et al., 2010, Saidi et al., 2023). Consequently, the World Health Organisation (WHO) recommended the use of artemisinin and derivatives over quinine. This transition to ACTs was adopted by global health boards, including the Blantyre Malaria Project at the Queen Elizabeth Central Hospital, Blantyre, Malawi, in 2014 (Saidi et al., 2021). Despite the relatively recent implementation of artemisinin as the frontline therapy in sub-Saharan Africa, resistance has emerged.

In 2008, the first reports of partial artemisinin resistance were described in *P. falciparum* in the Greater Mekong subregion of Cambodia (Noedl et al., 2008, Dondorp et al., 2009). Here, partial resistance refers to delayed clearance of parasites following treatment from ACT. More recently, partial resistance has emerged independently in Rwanda, Uganda and the Horn of Africa (Rosenthal et

al., 2024). There is therefore an urgent need to identify novel drug and/or vaccine targets. In line with the Global Technical Strategy goal to interrupt transmission, novel transmission blocking targets need to be identified. It is therefore imperative to understand gametocyte formation and development, and the tissue reservoirs which may contribute to cryptic infections and ongoing transmission.

1.2 Hidden Parasite Reservoirs

One of the challenges faced with malaria elimination is the establishment of cryptic or hidden infections. In *P. falciparum,* parasites modify the host cell architecture to allow sequestration of late stages (trophozoites and schizonts) in the capillary beds of deep tissues such as the brain. As a result, diagnosis by blood smear and light microscopy underestimates total parasite biomass as only peripherally circulating rings can be quantified (Dondorp et al., 2005, Hendriksen et al., 2012, Watson et al., 2022). There is growing evidence to suggest that the haematopoietic niches of the host, such as the BM and spleen, serve as significant parasite reservoirs, largely independent of classical vascular sequestration.

1.2.1 Classical Vascular Sequestration

To avoid immune clearance, *P. falciparum* substantially remodels the architecture of the host RBC. During the intraerythrocytic cycle, parasites export proteins which alter the RBC architecture, topology, and membrane deformability (Nash et al., 1989, Glenister et al., 2002, Maier et al., 2009). Under normal circumstances, this lack of deformability would result in clearance from the spleen; however, *P. falciparum* avoids immune clearance through the export of the variant surface antigen *P. falciparum* erythrocyte membrane protein 1 (PfEMP1) which facilitates cytoadherence to the vasculature of deep tissues (Leech et al., 1984). These proteins can bind to a range of receptors on the vasculature such as CD36, intracellular adhesion molecule 1 (ICAM-1), platelet endothelial cell adhesion molecule (CD31/PECAM), endothelial cell protein C receptor (EPCR), and chondroitin sulphate A (CSA) (**Figure 1-3**) (Barnwell et al., 1989, Hsieh et al., 2016, Berendt et al., 1989, Smith et al., 2000, Treutiger et al., 1997, Turner et al., 2013, Rogerson et al., 1995, Robert et al., 1995). PfEMP1 is encoded by approximately 60 *var* genes and exhibits monoallelic expression (Su et al., 1995, Baruch et al., 1995, Smith et al., 1995). As before described in the context of CM,

vascular sequestration results in significant adhesion-mediated pathogenesis, largely attributed to vascular occlusion and inflammation, which is exacerbated by rosetting (the binding of uRBCs to iRBCs) (Lee et al., 2022).

Specific PfEMP1 variants are associated with specific disease manifestations. For example, in pregnancy associated malaria, iRBCs exhibit a tissue specific binding phenotype whereby parasites bind to CSA on placental syncytiotrophoblasts. Here, a specific PfEMP1 variant, VAR2CSA, was identified to mediate this binding interaction. As a consequence of parasite accumulation in the placenta, there are substantial immunological changes in the placenta which can lead to complications such as anaemia, hypertension, low birth weights and stillbirths (Salanti et al., 2003, Gamain et al., 2021). Therefore, specific binding interactions can facilitate organ specific sequestration and pathology.

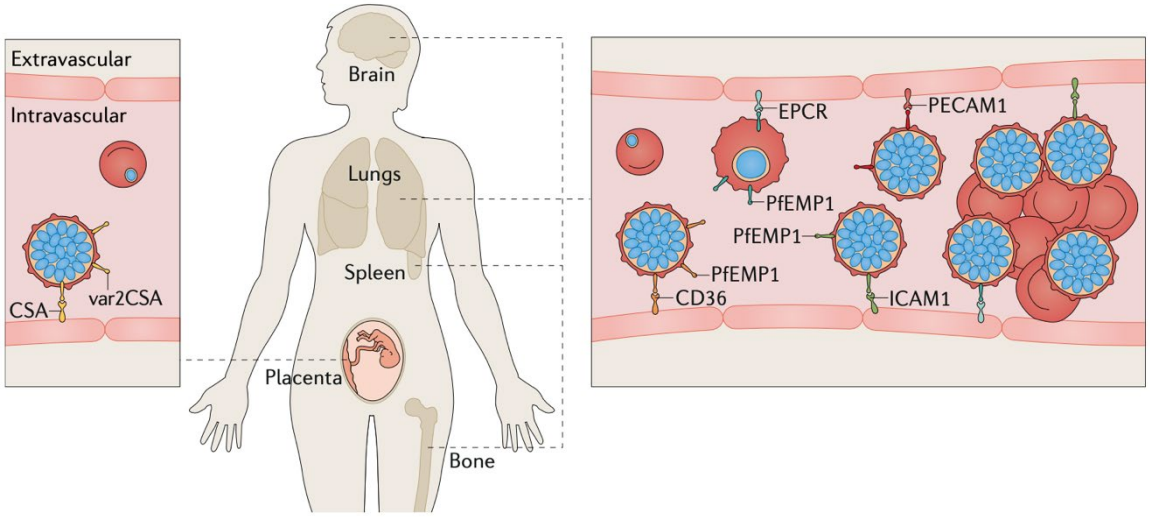

Figure 1-3. Classical vascular sequestration. *P. falciparum* trophozoites and schizonts sequester in the capillaries and post capillary venules of deep tissues such as the brain, lung, spleen, and bone marrow (BM). This sequestration is mediated through binding interactions between the parasite exported protein, *P. falciparum* erythrocyte membrane protein 1 (PfEMP1) and endothelial cell receptors such as CD36, ICAM1, PECAM1 and EPCR. Specific variants of PfEMP1 are associated with tissue specific sequestration; for example, the PfEMP1 variant VAR2CSA binds to chondroitin sulphate A (CSA) in the placenta resulting in pregnancy associated malaria. Rosetting can occur in capillaries where uninfected RBCs (uRBCs) bind to infected RBCs (iRBC). Vascular sequestration and rosetting can cause capillary occlusion and inflammation. Abbreviations: ICAM-1, intracellular adhesion molecule-1; PECAM; platelet endothelial cell adhesion molecule; EPCR, endothelial cell protein C receptor. Figure from Venugopal *et al.*, 2020 (Venugopal et al., 2020).

In order to display PfEMP1 above host cell receptors, *Plasmodium* modifies the RBC membrane cytoskeleton through protein export to form electron-dense protrusions called knobs. Shortly after invasion, ring stage *P. falciparum* release the ring erythrocyte surface antigen (RESA) which binds to spectrin, the main component of the host RBC cytoskeleton, functioning to stabilise the cytoskeleton (Culvenor et al., 1991, Foley et al., 1991, Pei et al., 2007). After 16 hours post invasion (hpi), knobs appear on the surface of the RBC with significant remodelling of the host cell cytoskeleton (Langreth et al., 1978, Gruenberg et al., 1983). The *Plasmodium* mature erythrocyte surface antigen (MESA) then replaces RESA binding to band 4.1, a host protein which contributes to the stabilisation of the spectrin-actin network. This binding interaction at the spectrin-actin network allows free spectrin to anchor knobs to the host cell cytoskeleton (Waller et al., 2003). Underneath the host cell membrane of knobs, the essential knob associated histidine rich protein (KAHRP) self-assembles as individual protein modules into a conical shaped complex which supports the spiral scaffold of the knob protrusion (Taylor et al., 1987, Crabb et al., 1997, Rug et al., 2006, Looker et al., 2019). With the formation of the knob, between 16 and 20 hpi, PfEMP1 accumulates on the surface with the cytoplasmic tail (acidic terminal segment) anchored to the knob and the amino terminal domain exposed at the surface of the iRBC to engage in binding interactions (**Figure 1-4**) (Kriek et al., 2003, Maier et al., 2009, Warncke et al., 2016).

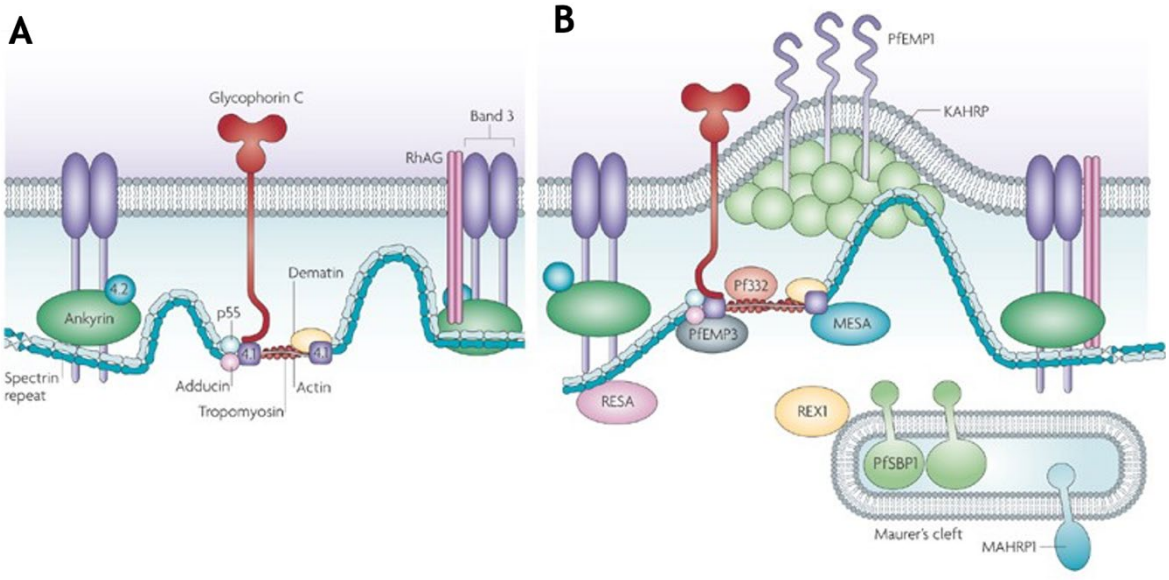

Figure 1-4. *P. falciparum* host cell remodelling. (**A**) Uninfected red blood cell (uRBC). The host cytoskeleton comprises spectrin heterodimers, capable of folding and unfolding in response to deformation stress, which are linked to form tetramers. Spectrin tails connect to short actin filaments. These junctions are stabilised by band 4.1R and other molecules. Multiple vertical interactions connect the cytoskeleton to the membrane such as interactions between glycophorin C, band 4.1R and p55 which forms a ternary complex. Another vertical interaction between the cytoskeleton and the RBC membrane involves band 3 and ankyrin. (**B**) Infected RBC (iRBC). During the intraerythrocytic developmental stages, *P. falciparum* exports numerous proteins to disrupt the host cell cytoskeleton forming knob protrusions which allow the variant surface antigen PfEMP1 to be displayed above host cell receptors. In ring stages, RESA binds to spectrin to stabilise the membrane. KAHRP self-assembles beneath the host cell membrane to form ring structures. From 16 hours post invasion (hpi), MESA binds to band 4.1 which allows spectrin to fold and interact with KAHRP. Mature RBCs are transcriptionally and translationally inactive and therefore the parasite requires its own trafficking machinery for protein export. Maurer's clefts are intermediate parasite compartments for sorting and trafficking exported proteins. Several proteins are associated with protein trafficking and the Maurer's clefts such as REX1, PfSBP1 and MAHRP1. Pf332 interacts with both the cytoplasmic side of the Maurer's clefts and, in late stages of the parasite, with the host cell cytoskeleton. Abbreviations: RBC, red blood cell; RESA, ring-infected erythrocyte surface antigen; KAHRP, knob associated histidine rich protein; hpi, hours post invasion; MESA, mature erythrocyte surface antigen; REX1, ring exported protein 1; PfSBP1, *P. falciparum* skeleton binding protein 1; MAHRP, membrane associated histidine rich protein 1. Figure from Maier *et al.*, 2009 (Maier et al., 2009, Nilsson et al., 2012, Warncke et al., 2016).

1.2.2 Cryptic Parasite Reservoirs

In 1887, the physician WS Thayer described a case of relapsing malaria which was 21 months following an initial attack. In 1900, Sir Patrick Manson used *P. vivax* infected *Anopheles* mosquitoes to infect his son, Patrick Thornburn Manson, and laboratory technician, George Warren, who were both successfully treated with quinine. However, after a 9-month latency period, his son experienced a relapse without any additional exposure to *P. vivax* (Manson, 1900, Manson, 1901, White, 2011). Decades later, the dormant non-replicating liver stage of *P. vivax* was discovered, the hypnozoite (Krotoski, 1985). Hypnozoites represent cryptic stages in a tissue reservoir (the liver) which are difficult to detect and therefore have important implications for malaria eradication (Markus, 2017). While liver stage hypnozoites were considered as the only hidden reservoir of *Plasmodium,* recently the haematopoietic niches of the BM and spleen have been demonstrated to be important and poorly explored reservoirs of malaria parasites.

1.2.3 The Bone Marrow (BM) Reservoir

The presence of only mature stage V gametocytes in circulation implied that immature stages developed within the tissues, analogous to the sequestration of late asexual stages. Gametocytes were initially observed in post-mortem BM and

spleen tissue samples by Marchiafava and Bignami in 1894 (Marchiafava, 1894). Several case studies utilising post-mortem tissues, BM biopsies and BM aspirates have consistently demonstrated the presence of immature gametocytes and asexual stages in both the BM and spleen for *P. falciparum* and *P. vivax* malaria (Thomson and Robertson, 1935, Smalley et al., 1981, Wickramasinghe et al., 1987, Farfour et al., 2012, Baro et al., 2017). In 2014, two independent studies provided the first quantitative evidence for the enrichment of gametocytes in the BM using post-mortem tissues and BM aspirates in paediatric *P. falciparum* malaria (Joice et al., 2014, Aguilar et al., 2014). Gametocyte enrichment in the BM and spleen was also demonstrated in *P. falciparum* infection in humanised mice (Duffier et al., 2016). Similarly, quantitative evidence of gametocyte enrichment in the BM was found in *P. vivax* infections of splenectomised non-human primates (Obaldia et al., 2018). While the extravascular spaces of the BM exhibit a marked enrichment of gametocytes, sequestration of asexual parasites in these extravascular compartments have been observed independent of classical vascular sequestration (De Niz et al., 2018). In a study of gametocyte dynamics over time in *P. berghei* infected mice, intravital microscopy revealed the homing of early gametocyte stages to the BM and spleen. Parasite accumulation in these organs coincided with increased vascular leakage due to inflammation. The location of gametocyte formation remains unknown, raising questions about whether the distinct microenvironments of the haematopoietic niches might also contribute to gametocyte formation.

1.2.4 The Splenic Reservoir

The total parasite biomass is underestimated by measuring peripheral parasitaemia alone as only circulating stages can be quantified. To better estimate the total parasite biomass, including sequestered stages, biomarkers such as *Plasmodium falciparum* histidine rich protein II (PfHRPII) and *Plasmodium* lactate dehydrogenase (pLDH) can be measured in the plasma. While PfHRPII is the most widely used biomarker in rapid diagnostic tests (WHO, 2023b), its use for assessing biomass is limited due to the persistence of the glycoprotein in peripheral circulation following parasite clearance (Mayxay et al., 2001, Houzé et al., 2009). In contrast, pLDH does not persist in the blood and can be used to evaluate total

biomass for five human infective species (Iqbal et al., 2004, Brown et al., 2004, McCutchan et al., 2008).

In a study of non-immune adults in Malaysia with severe or non-severe *P. vivax* infection, the relationship between disease severity, total parasite biomass, and endothelial activation was investigated (Barber et al., 2015). Using plasma pLDH to measure parasite biomass, it was found that the total parasite biomass was correlated with markers of inflammation (IL-6, IL-10) and disease severity. However, biomass was not correlated with endothelial activation. In contrast, peripheral parasitaemia was correlated with endothelial activation. This latter correlation could be explained by endothelial activation by circulating iRBCs through the peripheral microvasculature. The lack of correlation between endothelial activation and total parasite biomass suggests the existence of a hidden reservoir of parasites in tissue compartments with non-typical endothelium (Barber et al., 2015). The cords of the splenic red pulp (RP) are lined with sinuses containing a discontinuous endothelium with a poorly developed basal membrane. The endothelial cells of the sinuses, known as “stave cells”, are elongated and arranged longitudinally creating inter-endothelial slits which facilitate the filtration function of the spleen (Gifre-Renom et al., 2022). Barber *et al*. therefore hypothesised that the lack of correlation between endothelial activation and parasite biomass was due to an accumulation of parasites in the splenic cords (Barber et al., 2015).

The first detailed immunohistopathological characterisation of an untreated human intrasplenic infection was performed in a case study of a *P. vivax* infected patient who was splenectomised due to splenic rupture. This case study revealed large numbers of non-phagocytosed parasites in the cords of the spleen, as well as several histopathological changes such as white pulp (WP) expansion (Machado Siqueira et al., 2012). More recently, a study of the spleen from 22 adult chronic asymptomatic malaria patients undergoing splenectomy in Indonesia revealed that 93.1% and 98.7% of the total parasite biomass was in the spleen for *P. falciparum* and *P. vivax* malaria respectively (Kho et al., 2021b). Note that this calculation of biomass was based on spleen, peripheral blood, and estimates of BM biomass; no other tissues were analysed. It is currently unknown whether the spleen in

paediatric severe *P. falciparum* malaria harbours a significant parasite biomass of intact parasites.

1.2.5 Evidence for an Endosplenic Life Cycle

Evidence for a cryptic life cycle in the haematopoietic niches was first demonstrated in *P. berghei* infected mice. Here, parasites utilised the erythroid precursor rich environments of the BM and spleen to establish a cryptic asexual lifecycle. Importantly, in *P. berghei* infected mice, artemisinin-induced haemolysis drove erythropoiesis providing ample host cells for reinvasion which subsequently resulted in recrudescent infection. Furthermore, parasites which invaded erythroid precursors in the BM and spleen were less sensitive to antimalarials indicating a niche by which resistance could emerge (Lee et al., 2018). In chronic asymptomatic *P. vivax* infection in adults, Kho *et al*., identified parasites of all developmental stages in proportions consistent with the duration of each stage in the intraerythrocytic life cycle (Kho et al., 2021a). Together with the observation that parasite magnitudes in the spleen could not be explained by peripheral parasitaemia alone, this suggests the existence of an endosplenic life cycle. Furthermore, a pool of retained reticulocytes were observed in the spleen of *P. vivax* and *P. falciparum* patients which could facilitate reinvasion events. These findings suggest the existence of an endosplenic cycle in chronic asymptomatic malaria.

It is important to note that there are physiological differences between the spleen in adult mice and humans (reviewed in **Section 1.3.4**). The primary difference between these two species is the erythropoietic activity of the spleen, where there is limited evidence of erythropoiesis in the spleen of humans, in particular as a consequence of malaria (Gupta et al., 2022). The role of the spleen in parasite growth is currently unknown in paediatric severe malaria cases.

1.3 Structure of the BM and the Spleen

To investigate the spleen and BM parasite reservoirs, it is important to gain an understanding of the structure and function of each of these organs. Many studies on the haematopoietic niches have been performed on mouse models of malaria.

However, as previously alluded to, there are fundamental differences between these organs in human and mice.

1.3.1 Structure and Function of the BM

In humans, the BM is the primary site of haematopoiesis, the production of blood cells, and can be found within the cavities of bones accounting for approximately 4% of the total body weight. Structurally, the BM consists of haematopoietic cords which localise to sinusoidal vascular networks, and adipocytes which together are supported by a web of reticular fibres and bony trabeculae (Mescher, 2018, Travlos, 2006, Lucas, 2021). Based on gross anatomy, the BM can be broadly divided into two: the red marrow, which is haematopoietically active, and the yellow (fatty) marrow, which consists of adipocytes and is haematopoietically inactive (Griffith, 2017).

In utero and in early childhood, the BM occupies the medullary cavity of long and spongy bones and is almost entirely haematopoietically active. However, BM composition and skeletal site distribution changes with age (Griffith, 2017). As individuals age, the appendicular (limb) marrow converts to fatty marrow in a centripetal and symmetrical manner, a process known as BM conversion. In adults, haematopoietically active marrow is localised to the axial (central) skeleton and the proximal ends of the femur and humerus (Di Iorgi et al., 2008, Griffith, 2017). Accordingly, the BM cellularity, which refers to the percentage of haematopoietically active cells compared to fatty marrow or adipocytes, can be estimated in histopathological examinations, and is directly related to age (**Figure 1-5**). For example, the BM cellularity in children under 3 months is usually 80% or more. For children between 18 months and 11 years old, the BM cellularity is typically between 50% and 70% (Sturgeon, 1951, Proytcheva, 2013).

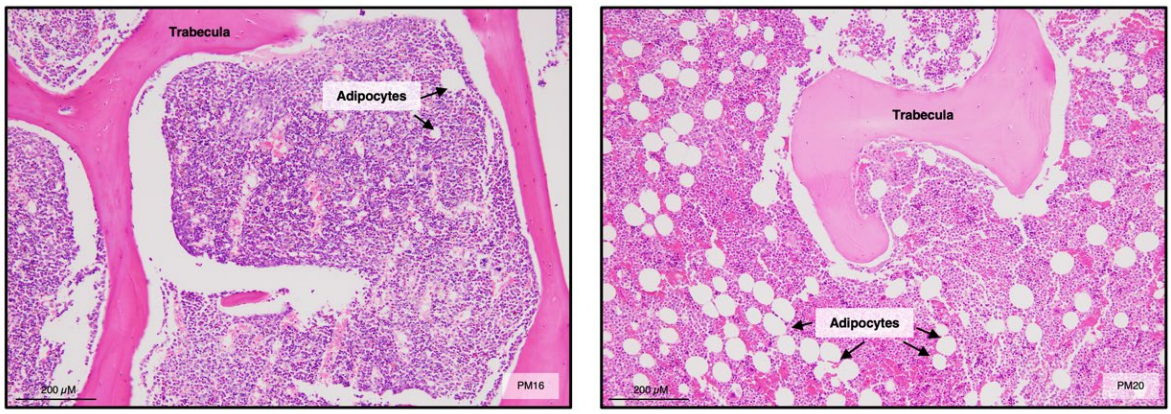

Figure 1-5. Cellularity of the bone marrow (BM) alters with age. Haematoxylin and eosin (H&E)-stained BM sections. The cellularity of the BM (the proportion of haematopoietically active cells to adipocytes) decreases with age; this is evident in H&E-stained sections from PM16 (4 years old) compared to PM20 (8 years old) where PM20 has a greater proportion of adipocytes. Abbreviations: PM, postmortem.

Our understanding of how haematopoietic stem cells differentiate into distinct myeloid and lymphoid cell lineages has advanced in recent years; however, our understanding of the spatial organisation of BM microenvironments to support haematopoiesis is less comprehensive (Lucas, 2021). Haematopoiesis, differentiation and/or cell maturation, occurs in the BM in distinct microenvironments or niches (Lucas, 2017). For example, erythropoiesis occurs in specialised niches known as erythroblastic islands (**Figure 1-6A**). Erythroblastic islands were first identified in the BM by the French haematologist, Marcel Bessis, using transmission electron micrographs. They described erythroblastic islands as developing erythroblasts surrounding a central macrophage, often termed a 'nursing macrophage'. These nursing macrophages provide iron for erythroblasts and promote enucleation (Bessis, 1958, Chasis and Mohandas, 2008). Megakaryocytes, the largest haematopoietic cell, localise adjacent to marrow sinusoids where they deposit platelets directly into circulation via proplatelet extensions (**Figure 1-6B**) (Stone et al., 2022). In contrast, granulopoiesis, or granulocytes, do not have distinct foci within the BM (Travlos, 2006). Haematopoietic cells in the BM demonstrate plasticity, adapting their cell proportions in response to external stimuli such as increased demand due to inflammation (e.g., infection) or anaemia. This dynamic responsiveness allows for alterations in the cellular composition of the BM microenvironment which can be evaluated in histopathological examinations.

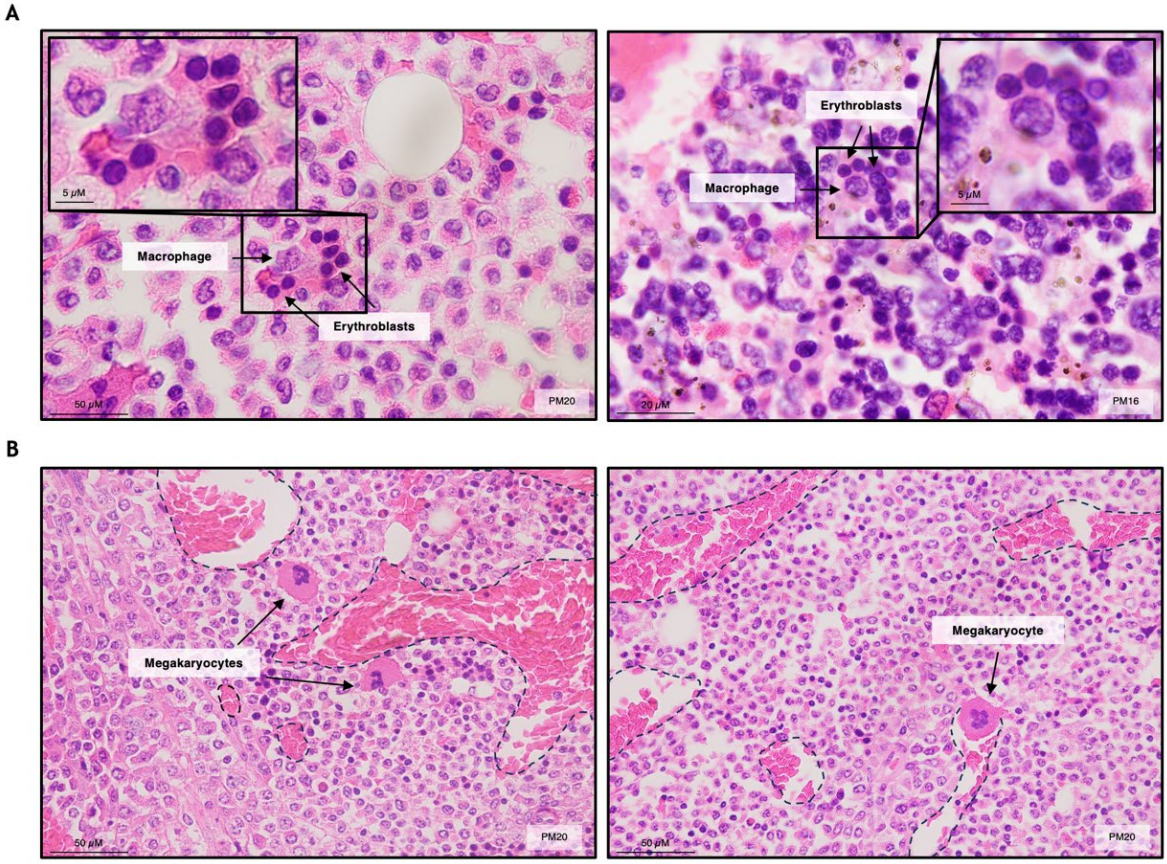

Figure 1-6. The bone marrow (BM) is organised into distinct niches. Haematoxylin and eosin (H&E)-stained BM sections. (A) Erythropoiesis occurs in specialised niches called erythroblastic islands. Erythroblastic islands consist of a central macrophage surrounded by erythroblasts undergoing maturation and enucleation. (B) Megakaryocytes localise to sinusoids where they deposit platelets into circulation. Dashed black lines mark the sinusoidal lining.

1.3.2 Structure and Function of the Spleen

The spleen can be regarded as a secondary haematopoietic organ, exhibiting haematopoietic activity during foetal development. The function of the spleen is to filter blood by removing aged or damaged RBCs, recycle iron, and to initiate adaptive immune responses against blood-borne pathogens and antigens. Positioned intraperitoneally, the spleen resides in the upper left abdomen, situated behind the stomach (Kapila et al., 2023). Based on structure and function, the spleen can be divided into two major compartments: the red pulp (RP) and the white pulp (WP) (Mebius and Kraal, 2005).

The spleen is encased within a capsule consisting of connective tissue containing myofibroblasts which allows the spleen to contract and expand. In humans, the RP occupies most of the splenic tissue and consists of the macrophage lined splenic cords and sinusoids (**Figure 1-7A**). The RP features a slow and "open" circulation, where RBCs navigate through narrow inter-endothelial slits (1-2 μm) within venous sinuses before re-entering circulation (Schmidt et al., 1993). This passage through inter-endothelial slits acts as a site of RBC quality control where young, healthy, and deformable RBCs can pass through, and aged, damaged, or iRBCs are trapped in the reticular meshwork of the cords (Groom et al., 1991, Buffet et al., 2006, Safeukui et al., 2008). Trapped RBCs are subsequently phagocytosed by cordal macrophages or undergo a process called 'pitting'. Pitting allows for the RBC to be recycled where RBC particulates, such as Howell-Jolly bodies (nuclear remnants), Heinz bodies (denatured haemoglobin) or *Plasmodium,* are removed and phagocytosed (Schnitzer et al., 1972, Ghosh and Stumhofer, 2021).

The WP is composed of lymphatic tissue where adaptive immune responses to blood-borne pathogens or antigens are initiated. In the centre of the WP is the germinal centre which is occupied by B lymphocytes and serves as the site of antigen presentation and antibody production (Stebegg et al., 2018). Beyond the germinal centre are the mantle and marginal zones (**Figure 1-7B**). In humans, an additional compartment, the perifollicular zone, exists beyond the marginal zone separating the WP from the RP (**Figure 1-7A**). Approximately 90% of splenic blood flow entering the marginal zone will enter the fast circulation of the perifollicular zone. The remaining 10% enters the slow circulation of the RP (Safeukui et al., 2008). Surrounding central arterioles is the periarteriolar lymphoid sheath (PALS), which is predominantly occupied by T lymphocytes; in humans, PALS are sparsely distributed and tend to occur around larger arteries (**Figure 1-7A**) (Steiniger et al., 2001, Steiniger, 2015, Lewis et al., 2019).

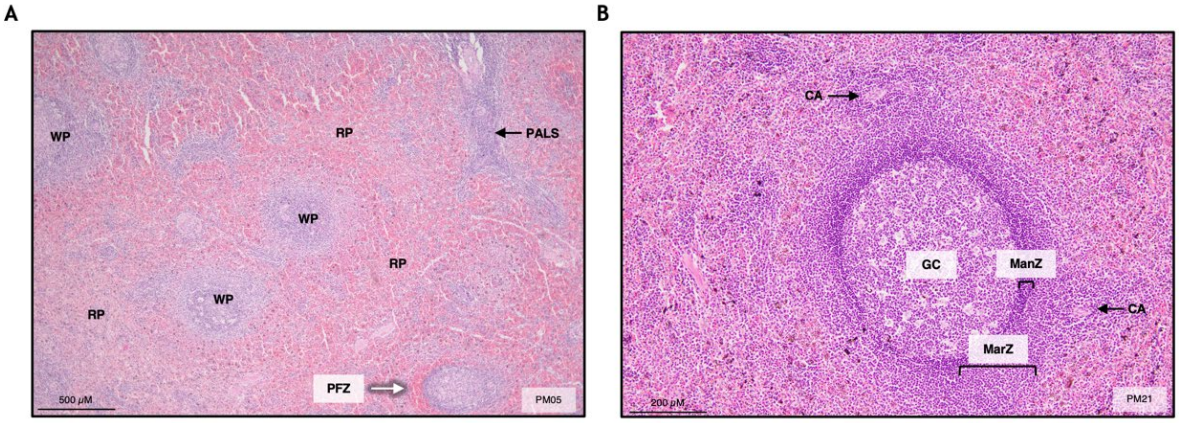

Figure 1-7. The structure of the spleen. Haematoxylin and eosin (H&E)-stained spleen sections. (A) The structure of the spleen can be broadly separated into two distinct compartments: the red pulp (RP) and the white pulp (WP). Surrounding large vessels is the periarteriolar lymphoid sheath (PALS). Beyond the WP is an area of fast circulation known as the perifollicular zone (PFZ). (B) Structure of the WP. The germinal centre (GC) is surrounded by the mantle zone (ManZ) followed by the marginal zone (MarZ). CA, central artery. Abbreviations: RP, red pulp; WP, white pulp; PFZ perifollicular zone; PALS, periarteriolar lymphoid sheath; CA, central artery; GC, germinal centre; ManZ, mantle zone; MarZ, marginal zone.

1.3.3 Anaemia and Extramedullary Haematopoiesis

Haematopoiesis is the process by which all blood cells are produced. During embryonic and foetal development, primitive haematopoiesis begins in the yolk sac, followed by the aorta-gonad mesonephros region and then in the liver and the spleen. After birth, the BM is the primary site for definitive haematopoiesis throughout life in humans (Galloway and Zon, 2003, Mikkola and Orkin, 2006, Orkin and Zon, 2008, Gupta et al., 2022). Haematologic disorders such as chronic haemolytic anaemia, thalassaemia, sickle cell anaemia, and myelofibrosis, as well as some cancers such as leukaemia and lymphoma, can lead to BM dysfunction and ineffective haematopoiesis. In rare instances, this BM dysfunction forces haematopoiesis to occur in extramedullary sites. Extramedullary haematopoiesis is a compensatory response to peripheral blood cells cytopenias (anaemia, neutropenia, thrombocytopenia) or increased cell demand which occurs most commonly in sites that were involved in primitive haematopoiesis such as the spleen and liver (Orphanidou-Vlachou et al., 2014, Gupta et al., 2022, Reichard et al., 2023).

In sub-Saharan Africa, there is a high prevalence of anaemia in children less than five years old (Tesema et al., 2021). In Malawi, several factors were independently

associated with the prevalence of severe anaemia in children, including HIV, bacteriaemia, hookworm infection, vitamin A and B12 deficiency, and malaria (Calis et al., 2008). Anaemia in sub-Saharan Africa is often associated with haemoglobinopathies, such as sickle cell disease and thalassaemia (Weatherall, 2008, Taylor et al., 2012, Adigwe et al., 2023). These conditions are prevalent in areas with a high incidence of malaria due to a level of protection provided by the haemoglobinopathy; both thalassaemia and sickle cell disease have been associated with extramedullary haematopoiesis (Gupta et al., 2022).

As previously described (**Section 1.1.2**), malarial anaemia is multifactorial. The nature of *Plasmodium* infection results in the destruction of iRBCs through schizont rupture. However, a larger contributor to malarial anaemia is the destruction of uRBCs compounded by BM dysfunction and subsequent dyserythropoiesis (White, 2018). Given the severity of malarial anaemia, and examples of extramedullary haematopoiesis in patients with haemoglobinopathies sharing the same geographical distribution, it has been hypothesised that extramedullary haematopoiesis may occur as a consequence of malaria (Ghosh and Stumhofer, 2021).

In mice, erythropoiesis in the BM was reduced in early infection with no compensatory increase in erythropoietin, a glycoprotein hormone which stimulates RBC production. This decrease in erythropoietic activity in the BM was associated with splenomegaly which was in turn associated with an increase in erythroid progenitors in the spleen during peak parasitaemia (Weiss et al., 1989, Villeval et al., 1990, Yap and Stevenson, 1992, Lamikanra et al., 2007, Ghosh and Stumhofer, 2021). Interestingly, when comparing fatal *P. berghei* infection with non-fatal *P. yoelii* infection, *P. yoelii* infected mice exhibited more marked splenomegaly and a greater degree of erythroid progenitors in the spleen (Asami et al., 1992). Similar findings were generated when comparing *P. chabaudi* infection in resistant compared to susceptible mice (Yap and Stevenson, 1992). This suggests that the degree of extramedullary haematopoiesis during malaria in mice could relate to the severity of disease. However, to date there have been no studies demonstrating extramedullary haematopoiesis in the spleen in human *Plasmodium* infection.

1.3.4 Differences Between Human and Mouse Haematopoietic Niches

As before described, many studies have been performed in mouse models to investigate extramedullary haematopoiesis, or stress erythropoiesis. However, there are a few key differences between the human and murine spleen. One such difference is the splenic microarchitecture. For example, in humans the separation between the RP and the WP is the perifollicular zone; however, this is absent in mice where the marginal zone separates the two primary compartments of the spleen (Steiniger, 2015, Lewis et al., 2019). The major difference between mice and human spleen lies in their respective roles in erythropoiesis.

As before described, the primary site of erythropoiesis in humans is the BM. The production of RBCs in the BM in humans is dynamic and can respond to increasing RBC demands allowing for a 20-fold increase in RBC production. In mice, both the BM and spleen are haematopoietically active. However, in adult mice, the BM has limited capacity to increase RBC production (Liu et al., 2013). The spleen in adult mice is the primary site of erythropoiesis which is able to respond to increased RBC production demands during anaemia (Weiss et al., 1989, Villeval et al., 1990, Yap and Stevenson, 1992, Lamikanra et al., 2007, Paulson et al., 2011, Bennett et al., 2018, Paulson et al., 2020, Ghosh and Stumhofer, 2021, Chen et al., 2021). Furthermore, it has also been demonstrated in *P. berghei* infected and naïve mice, that treatment with low doses of artemisinin had a stimulatory effect on haematopoiesis in the spleen (Lee et al., 2018). The spleen in mice is therefore a haematopoietically active organ, whereas in humans, the spleen is haematopoietically inactive. Consequently, it is important to avoid overgeneralising findings from studies on extramedullary haematopoiesis/stress erythropoiesis in mice in the context of human malaria.

1.4 Gene Regulation and Sexual Commitment

The haematopoietic niches of the host serve as crucial parasite reservoirs for onward transmission. As such, gaining a deeper understanding of how parasites sequestered in these organs are distinct, particularly in terms of sexual commitment, is important. One approach to investigating this is the use of transcriptomics.

1.4.1 The *Plasmodium* Genome

In the three decades since the nuclear genome of *P. falciparum* was sequenced, our comprehension of its intricacies and gene regulation mechanisms has advanced significantly. Like other higher eukaryotes, *Plasmodium* possesses both nuclear and mitochondrial genomes. However, in 1991, Wilson *et al*. identified a third organellar genome leading to the discovery of the apicoplast - a non-photosynthetic but chloroplast-derived organelle with a circular genome present in organisms of the phylum Apicomplexa (Wilson et al., 1991). In 1996, an international consortium was established to sequence and annotate the genome of *P. falciparum* (Hoffman et al., 1997). Building on this initiative, the nuclear genome of *P. falciparum* (clone 3D7) was successfully sequenced in 2002 marking the establishment of the first *Plasmodium* reference genome (Gardner et al., 2002). Since 2002, ongoing efforts have enhanced the genome assembly, addressing closure of gaps, conducting full chromosome sequencing (from telomere to telomere), rectifying mis-assemblies and sequencing errors, and incorporating the apicoplast and mitochondrial genomes into the reference (Berry et al., 2004, Otto et al., 2010a, Hunt et al., 2015, Böhme et al., 2019). The nuclear genome of *P. falciparum* spans 22.8 Mbp with a total of 5438 genes (v. 3.2, 2019) distributed across 13 chromosomes (Gardner et al., 2002, Böhme et al., 2019). Unusually, the *Plasmodium* nuclear genome is highly AT-biased, one of the most AT-rich nuclear genomes, with an average of 87% AT bases found within exons in *P. falciparum* (Dechering et al., 1998).

1.4.2 Gene Regulation

Plasmodium spp. transition through many morphologically and functionally distinct stages during their complex life cycle suggesting the requirement for strict control of gene regulation (**Section 1.1.2**). This regulation can occur at the epigenetic, transcriptional, post-transcriptional and/or post-translational level (Vembar et al., 2016). Shortly after the nuclear genome was sequenced, the transcriptomes of *P. falciparum* intraerythrocytic stages were published independently by Bozdech *et al*. and Le Roch *et al*. Both studies utilised microarrays to reveal a cyclic pattern of expression whereby peak expression levels in transcripts during the intraerythrocytic cycle correlated with the function

of the encoded protein. This type of expression pattern has been described as a "just-in-time" model of transcription where expression occurs immediately prior to when the protein is required (Bozdech et al., 2003, Le Roch et al., 2003, Llinás et al., 2006). These intraerythrocytic gene expression programmes were found to be highly conserved among different strains when comparing the geographically distant strains HB3 (originating from Latin America), 3D7 (West Africa) and Dd2 (Southeast Asia) (Llinás et al., 2006).

Transcription factors are proteins involved in the initiation and regulation of transcription. They operate by recognising deoxyribonucleic acid (DNA) motifs containing regulatory elements, which influences the initiation of the pre-initiation complex for transcription. The sequencing of the *Plasmodium* genome revealed a lack of known specific transcription factors which regulate subsets of genes in other eukaryotes. The lack of specific transcription factors in *P. falciparum* lead to the hypothesis that gene regulation in *Plasmodium* was mainly via post-transcriptional regulation (Painter et al., 2011). However, through sensitive sequencing profiling methods, Balaji *et al*. identified a novel family of DNA binding proteins known as the Apicomplexan apetala-2 (ApiAP2) protein family found in *Plasmodium, Cryptosporidium, Theileria,* and later *Toxoplasma* (Balaji et al., 2005, Altschul et al., 2010). These proteins contain at least one of the AP2 (Apetala-2 integrase) DNA binding domains of approximately 60 amino acids analogous to those found in the plant AP2/ethylene response factor (Ap2/ERF) transcription factor family (Riechmann and Meyerowitz, 1998). The *P. falciparum* ApiAp2 family, often described as the principal family of transcription factors in *Plasmodium,* has 27 orthologs, some of which have been shown to act in a stage specific manner. For example, AP2-L (PF3D7_0730300) in liver stages is involved in development within hepatocytes, AP2-I (PF3D7_1007700) acts in merozoites for invasion, AP2-EXP (PF3D7_1466400) acts in rings for expression of multigene families, and AP2-G (PF3D7_1222600) is the master regulator of sexual commitment in trophozoites/schizonts (Yuda et al., 2010, Iwanaga et al., 2012, Santos et al., 2017, Martins et al., 2017, Kafsack et al., 2014, Sinha et al., 2014, Poran et al., 2017). Despite the discovery of this principal transcription factor family, *Plasmodium* has relatively few specific transcription factors. Indeed, when compared to other eukaryotes, the ratio of proteins to predicted specific transcription factors was found to be 800 in *Plasmodium* in contrast to 29 in

Saccharomyces cerevisiae (Templeton et al., 2004). Therefore, other gene regulation mechanisms must be at play to compensate for the relative scarcity of transcription factors in *Plasmodium*.

In addition to specific transcription factors, an important level of gene regulation in *Plasmodium* is through chromatin structure modifications and epigenetic mechanisms. Epigenetics have been implicated in antigenic variation, solute transport, and sexual commitment (Cortés and Deitsch, 2017). At the core of this regulation is the nucleosome, the fundamental unit of chromatin in eukaryotes. The nucleosome is composed of a histone octamer (two copies of H2A, H2B, H3 and H4) with approximately 147 base pairs of DNA arranged in a superhelix surrounding it (Luger et al., 1997). This packaging into nucleosomes, and the positioning of nucleosomes along the genome, regulates gene expression by altering the access of transcription factors to promoter regions (Hollin and Le Roch, 2020). Overall, the chromatin landscape of *P. falciparum* was found to be predominantly euchromatic (open DNA structure) with distinct "heterochromatic islands" (closed DNA structure) (Salcedo-Amaya et al., 2009). Through investigation of nucleosome positioning during asexual and sexual stages, it was found that euchromatin was mostly observed in trophozoites and gametocytes coinciding with high transcriptional activity in these stages (Bunnik et al., 2014, Ponts et al., 2011, Bozdech et al., 2003, Le Roch et al., 2003). The histones of each nucleosome are subject to post translational modifications (in particular, acetylation and methylation) through their N terminal tails exposed outside of nucleosomes. These modifications affect the chromatin structure and, consequently, transcriptional activity. Using mass spectrometry approaches and monoclonal antibodies against these conserved modifications, many post-translational modifications have been identified in *Plasmodium* (Miao et al., 2006, Salcedo-Amaya et al., 2009, Trelle et al., 2009, Saraf et al., 2016, Coetzee et al., 2017, Shrestha et al., 2022). Specifically, in asexual stages and gametocytes, 232 and 90 distinct post-translational modifications were identified respectively (Saraf et al., 2016, Shrestha et al., 2022). From such studies, certain epigenetic marks emerged as distinctive markers of heterochromatic or euchromatic states, analogous to such marks in other eukaryotic systems. For example, heterochromatin, and therefore inactive promoters, is associated with H3K9me3 (i.e., trimethylation at lysine position 9 of the histone 3 protein) and H3K36me3

epigenetic marks. These modifications are mutually exclusive with H3K9ac (i.e., acetylation at lysine position 9 of the histone 3 protein) and H3K4me3 modifications which are associated with euchromatin and therefore active promoters (Cui et al., 2007, Cui et al., 2008, Trelle et al., 2009, Salcedo-Amaya et al., 2009, Lopez-Rubio et al., 2009, Fraschka et al., 2018, Bártfai et al., 2010, Gupta et al., 2013, Ruiz et al., 2018). Post-translational modifications can be modified by histone modifiers deemed as "writers", such as histone acetyltransferases or histone lysine methyltransferases, or "erasers", such as histone lysine deacetylases and histone lysine demethylases (Cui et al., 2007, Cui et al., 2008, Chaal et al., 2010). Such histone marks can be recognised by specific recognition proteins, such as heterochromatin protein 1 (HP1; PF3D7_1220900) which binds to the repressive mark H3K9me3 resulting in heterochromatin formation. This binding interaction has been demonstrated to silence multigene families (e.g., *var* genes in antigenic variation/cytoadherence) as well as *ap2-g* (sexual commitment) by maintaining a repressive centre in the nuclear periphery (Lomberk et al., 2006, Pérez-Toledo et al., 2009, Flueck et al., 2009, Bunnik et al., 2018, Brancucci et al., 2014).

For decades, it has been evident that *Plasmodium,* and other Apicomplexans, encode numerous noncoding ribonucleic acid (RNA) (ncRNAs), including long noncoding RNAs (lncRNAs), however their functions have been relatively unknown (Raabe et al., 2010, Broadbent et al., 2011, Patil et al., 2012, Siegel et al., 2014, Broadbent et al., 2015, Chappell et al., 2020, Li et al., 2021b, Batugedara et al., 2023). Due to recent advances in "omic" technologies, identification of ncRNAs has improved and their specific functions are starting to be elucidated. ncRNAs exhibit functional diversity depending on their type. They can modify gene expression by recruiting transcription factors or transcriptional machinery, modulate the chromatin landscape through interactions with epigenetic factors, and block protein function through their own binding interactions, among other functions (Simantov et al., 2022). Indeed, it has recently been demonstrated that some ncRNAs correlate with changes in gene expression suggesting their involvement with epigenetic and transcription factors (Batugedara et al., 2023). Many ncRNAs were found to be transcribed from bidirectional promoters resulting in noncoding antisense RNA (asRNA) "transcriptionally linked" to coding mRNA which are coregulated (Chappell et al., 2020). Such asRNA have been implicated

in the monoallelic expression of *var* genes, as "activators" of their corresponding *var* gene. Chromatin immunoprecipitation (ChIP) with RNA revealed the integration of *var* gene asRNA into chromatin, with linked *var* mRNA and corresponding asRNA exhibiting distinct perinuclear co-localisation as identified by RNA fluorescence *in situ* hybridisation (Epp et al., 2009, Amit-Avraham et al., 2015). Indeed, the induction of asRNA from a particular silent *var* gene intron leads to a switching event resulting in the expression of this silent *var* gene (Amit-Avraham et al., 2015, Jing et al., 2018). While nearly 2000 ncRNAs have been identified, many of which novel to *P. falciparum,* few have been functionally characterised. Consequently, the extent to which ncRNAs regulate gene expression remains largely unknown (Batugedara et al., 2023).

While **Section 1.4.2** provides an overview of gene regulation mechanisms in *Plasmodium,* this has been extensively reviewed elsewhere (Painter et al., 2011, Vembar et al., 2016, Toenhake and Bártfai, 2019, Hollin and Le Roch, 2020, Hollin et al., 2023, Simantov et al., 2022).

1.4.3 Gene Regulation in Sexual Commitment

Sexual commitment and gametocytogenesis are great examples of the dynamic interplay between gene regulation mechanisms. As described previously in **Section 1.4.2**, the transcription factor AP2-G was identified as the master regulator of sexual commitment (Kafsack et al., 2014, Sinha et al., 2014). In asexual parasites, the *ap2-g* locus is silenced through the interaction between HP1 with the epigenetic modification H3K9me3, resulting in a heterochromatic state. In collaboration with HP1, the histone modifying HDA2 (PF3D7_1008000) acts by removing histone acetylation marks (e.g., H3K9ac), thus promoting repression of the *ap2-g* locus (Brancucci et al., 2014, Coleman et al., 2014). During sexual commitment, the perinuclear protein GDV1 (PF3D7_0935400) dissociates HP1 from the *ap2-g* locus resulting in its euchromatic state and triggering the expression of *ap2-g* (Eksi et al., 2012, Filarsky et al., 2018). GDV1, and therefore sexual commitment, is negatively regulated by the ncRNA *gdv1 antisense* (GDV1as, PF3D7_0935390) which is (indirectly) responsive to environmental triggers of sexual commitment such as lysophosphatidylcholine (LysoPC) depletion (Filarsky et al., 2018, Brancucci et al., 2017). Several proteins have been found to have AP2-G binding sites; among these is MSRP1 (PF3D7_1335000), a merozoite surface

protein 7 (MSP7)-related protein which has been consistently upregulated in sexually committed cells (Poran et al., 2017, Brancucci et al., 2018, Perrin et al., 2015, Kadekoppala et al., 2010).

1.4.4 The Kennedy Pathway and Environmental Induction

Phospholipids are essential components of cell membranes. In *Plasmodium* phosphatidylcholine (PC) and phosphatidylethanolamine (PE) are the primary membrane phospholipids which represent 40-50% and 35-40% of the total phospholipids in *Plasmodium* respectively (Vial et al., 2003). Phospholipid levels vary throughout the life cycle with a 6-fold rise in phospholipid levels observed in trophozoites and schizonts (Tran et al., 2016). *Plasmodium* can synthesise PC and PE *de novo* from exogenous choline sources, ethanolamine or serine (**Figure 1-8**) (Déchamps et al., 2010b). PC is largely derived from exogenous LysoPC which is hydrolysed into choline and fatty acids via the parasite derived exported lipase 2 (XL2) before entering the Kennedy pathway (Liu et al., 2024). Choline is phosphorylated via choline kinase (CK) to produce phosphocholine (P-Cho). P-Cho is then metabolised to cytidine-diphosphocholine (CDP-Cho) via CTP:phosphocholine cytidylytransferase (CCT). The final step of the Kennedy pathway adds a choline headgroup to diacylglycerol (DAG) which is catalysed by choline/ethanolamine phosphotransferase (CEPT) resulting in the production of PC (Déchamps et al., 2010b, Déchamps et al., 2010a, Wein et al., 2012). In circumstances where exogenous LysoPC is less abundant, an alternative substrate arm of the Kennedy pathway is upregulated. This alternative Kennedy pathway arm utilises ethanolamine or serine from the environment via ethanolamine kinase (EK) to ultimately synthesise PC. This requires the s-adenosylmethionine (SAM)-dependent transmethylation of phosphoethanolamine (P-Eth) which is catalysed by phosphoethanolamine methyltransferase (PMT) (Pessi et al., 2004, Pessi et al., 2005, Flammersfeld et al., 2018). The methylation from SAM results in the production of S-adenosyl-l-homocysteine (SAH) which is recycled by SAH hydrolase (SAHH) (Tanaka et al., 2004). The metabolic pathways and enzymes involved in phospholipid synthesis have been demonstrated to be essential for the parasite and hence are excellent drug targets (**Figure 1-8**) (Ancelin et al., 2003, Déchamps et al., 2010b, Wein et al., 2012).

Sexual commitment, and consequently sexual conversion rates, have been shown to be responsive to environmental factors. Several factors have been demonstrated to alter conversion rates, including antimalarial treatment, host cell age, extravascular vesicles, and endoplasmic reticulum stress (Buckling et al., 1999, Peatey et al., 2013, Mantel et al., 2013, Regev-Rudzki et al., 2013, Chaubey et al., 2014). A strong inducer of sexual commitment is the depletion of the serum lipid LysoPC, a major substrate for PC biosynthesis (Brancucci et al., 2017). This negative correlation between plasma LysoPC and *ap2-g* has been demonstrated *in vivo* in two human cohort studies of *P. falciparum* malaria (Usui et al., 2019, Abdi et al., 2023). Using blood samples collected from uncomplicated malaria cases in Ghana, Usui *et al.* observed an association between high levels of plasma LysoPC and low gametocyte-to-asexual ring ratios (Usui et al., 2019). Subsequently, Abdi *et al.* demonstrated a significant negative correlation between LysoPC levels and *ap2-g* transcription levels in a large cohort (n=235) of severe, uncomplicated and asymptomatic malaria cases in Kenya. This relationship was associated with high inflammatory responses during low transmission seasons (Abdi et al., 2023). Furthermore, a local LysoPC depletion was observed in the BM in mice which was hypothesised to be the result of serum albumin binding to LysoPC in the plasma preventing the passage of the complex to the extravascular space (Brancucci et al., 2017, Kim et al., 2007). This local depletion in LysoPC suggests that sexual commitment, at least in part, could be tissue specific.

LysoPC is an inflammatory mediator acting as a chemoattractant for monocytes and T lymphocytes. The phospholipid induces the production of pro-inflammatory cytokines such as IFNγ and IL-18, and promotes the polarisation of macrophages into the pro-inflammatory M1 phenotype (Quinn et al., 1988, McMurray et al., 1993, Huang et al., 1999, Qin et al., 2014). In turn, the inflammatory response can trigger the turnover of LysoPC to PC, resulting in reduced LysoPC concentrations in serum (Law et al., 2019). Indeed, this was also observed by Abdi *et al.* where markers of the inflammatory response were associated with reduced plasma concentrations of LysoPC, which in turn was associated with *ap2-g* expression. This relationship between sexual commitment, inflammation and low LysoPC levels was most significant during low transmission seasons (Abdi et al., 2023). Therefore, parasites can adjust their investment in reproduction in

response to changes in the host environment, which is subject to transmission intensity.

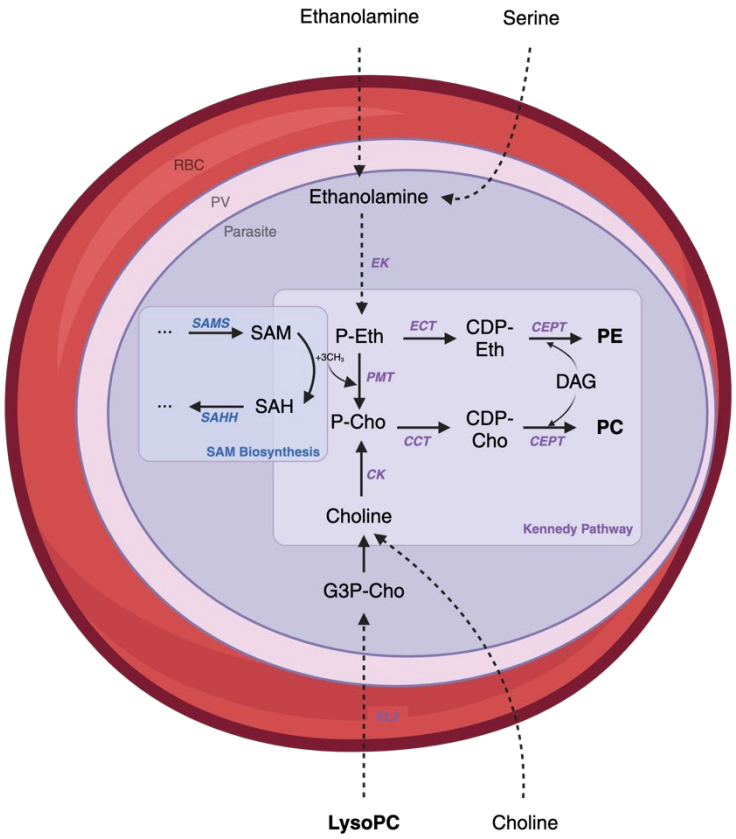

Figure 1-8. The biosynthesis of phosphatidylcholine (PC) in *Plasmodium*. *Plasmodium* synthesises PC *de novo* predominantly through the Kennedy pathway. Here, the parasite uptakes exogenous lysophosphatidylcholine (LysoPC) (which is hydrolysed to glycerophosphocholine (G3P-Cho)) via exported lipase 2 (XL2)) or exogenous choline. Choline is phosphorylated via choline kinase (CK) to phosphocholine (P-Cho). This is then metabolised to CDP-choline through the action of CCT:phosphocholine cytidyltransferase (CCT). The choline headgroup is then added to diacylglycerol (DAG) via choline/ethanolamine phosphotransferase (CEPT) to produce PC. When exogenous LysoPC/choline is not available, an alternative substrate arm of the Kennedy pathway is triggered whereby PC can be synthesised from ethanolamine or serine. Here, ethanolamine kinase (EK) phosphorylates ethanolamine to phosphoethanolamine (P-Eth). P-Eth is trimethylated from the methyl donor s-adenosylmethionine (SAM) which is catalysed by phosphoethanolamine methyltransferase (PMT) to form P-Cho. This reaction results in the release of S-adenosyl-l-homocysteine (SAH) which is recycled by SAH hydrolase (SAHH) in the SAMS biosynthesis pathway. P-Cho is then metabolised as before to produce PC. Abbreviations: EK, ethanolamine kinase; P-Eth, phosphoethanolamine; SAMS, S-adenosyl-l-methionine synthase; SAH, S-adenosyl-l-homocysteine; SAHH, SAH hydrolase; PMT, phosphoethanolamine methyltransferase; P-Cho, phosphocholine; CK, choline kinase; G3P-Cho, glycerophosphocholine; XL2, exported lipase 2; LysoPC, lysophosphatidylcholine; CCT, CCT:phosphocholine cytidyltranferase; CDP-Cho, cytidine-diphosphocholine; CEPT, choline/ethanolamine phosphotransferase; PC, phosphatidylcholine; ECT, ethanolaminephosphate cytidylyltransferase; CDP-Eth, cytidine-diphosphoethanolamine; PE, phosphatidylethanolamine; DAG, diacylglycerol. PV, parasitophorous vacuole; RBC, red blood cell. Figure created with BioRender.com.

1.5 Summary and Aims

In summary, the spleen and BM represent two important reservoirs of *Plasmodium* which contribute to ongoing transmission and may contribute to the development of resistance and recrudescent infection. Studies in chronic asymptomatic malaria in adults revealed that the spleen harbours a large hidden biomass of intact parasites of all stages of the life cycle, including gametocytes, with evidence to suggest the existence of an endosplenic life cycle. However, the contribution of the spleen towards the total parasite biomass in paediatric *P. falciparum* severe malaria cases, responsible for most malaria associated mortality, remains unknown. Furthermore, the role of the spleen in gametocyte formation and development has not been systematically investigated. The BM reservoir has been demonstrated to exhibit an enrichment of gametocytes in the extravascular spaces. However, it remains unclear whether the unique environment of the BM (characterised by active erythropoiesis and a local LysoPC depletion) directly facilitates sexual commitment within the BM. Consequently, parasites sequestered in the BM may exhibit transcriptional differences from those sequestered elsewhere in the body, specifically in relation to sexual commitment. The specific nature of these distinctions between parasite populations in the body requires further investigation.

This thesis is structured around two overarching aims: firstly, to characterise the splenic reservoir of *P. falciparum* in paediatric severe malaria cases, and secondly, to investigate the transcriptional differences between sequestered schizont populations.

This thesis specifically aims to:

- Determine if there is a significantly higher biomass of intact *P. falciparum* in the spleen compared to other tissues in paediatric severe malaria patients.
- To investigate the existence of an endosplenic life cycle in the spleen of paediatric severe malaria patients.
- To determine the contribution of the spleen towards gametocyte formation and development in relation to the BM.
- To deconvolute the transcriptional signature of sexual commitment in *P. falciparum* schizonts.

Chapter 2 | Materials and Methods

2.1 Malawi Cohort

2.1.1 Patient Samples and Ethical Approval

Tissues obtained for this study were collected as part of a severe paediatric malaria post-mortem study in Blantyre, Malawi between 1996 and 2010. Patients were admitted to the Malaria Research Ward in the Queen Elizabeth Central Hospital in Blantyre, Malawi. Clinical observations were made every 2 hours with parasitaemia assessed every 6 hours using finger prick blood samples. All patients were treated with intravenous quinine dihydrochloride with infusions continuing until four consecutive blood smears were interpreted as negative for malaria parasitaemia. A clinical diagnosis was made during life except for cases where the time to death was too short to make a clinical diagnosis (indeterminant cases). Full details of the clinical management of patients has been previously described (Taylor et al., 2004).

Over 2000 children were enrolled in the study, with 404 cases resulting in mortality giving a mortality rate of 20% for the study. In the event of death, families were met with a Malawian clinician who discussed the possibility of a post-mortem. Consent to perform a post-mortem was sought for 335 cases. In total, 103 post-mortems were performed with post-mortem intervals (PMI) between 2 and 14 hours after death. The cause of death was determined at post-mortem forming the basis for the classification into clinical groups. Collected tissues were stored in 10% neutral buffered formalin (NBF) and processed and embedded in paraffin to generate formalin-fixed, paraffin embedded (FFPE) tissue blocks using standard protocols at the time of collection.

Most patients enrolled in the study had clinically defined cerebral malaria (CM) which was defined as coma (Blantyre Coma Scale score ≤ 2 or Glasgow Coma Scale score ≤ 10) with no improvement following correction of hypoglycaemia, *P. falciparum* peripheral parasitaemia, and no other obvious cause of coma such as meningitis (Taylor et al., 2004). For cases meeting this clinical definition during life, three patterns of cerebral histopathology were observed at post-mortem generating the following histologically defined CM definitions: CM1 cases exhibited sequestration of infected red blood cells (iRBC) with no further cerebral histopathological changes; CM2 cases had sequestration of iRBCs with cerebral

histopathological changes such as ring haemorrhages, cerebral microthrombi and extra-erythrocytic pigment; and CM3 cases presented with clinical CM however there was limited evidence of cerebral sequestration, and an alternative cause of death was identified. Non-CM parasitaemic cases included in the study consisted of severe malarial anaemia (SMA) and incidental parasitaemia cases where malaria was not the primary cause of death. Non-malarial controls (*P. falciparum* negative) included patients presenting with coma attributed to non-malarial causes such as bacterial meningitis (Milner et al., 2014).

The post-mortem cohort study was approved by the institutional review boards at the University of Malawi College of Medicine, Michigan State University, and the Harvard School of Public Health (Taylor et al., 2004, Milner et al., 2013b, Milner et al., 2014).

2.1.2 Selection of Samples

For this thesis, spleen, bone marrow (BM), and lung (right lung) tissues were used. From the initial 103 post-mortem cases, the following exclusion criteria were applied: HIV positivity, a high PMI of greater than 12 hours and a lack of a determined diagnosis prior to death. HIV cases were removed due to the known impacts of the infection on organ structure, cellular composition, function, and on parasite accumulation (Delacrétaz et al., 1987, Khalil et al., 1996, Flateau et al., 2011, Williams et al., 2016, Joice et al., 2016, Heller et al., 2023). Cases with a high PMI were removed due to poor structural preservation and immunohistochemistry (IHC) staining in cases with a PMI exceeding 12 hours (Joice et al., 2014). Indetermined diagnoses are cases where a clinical diagnosis was not made prior to death. Due to the lack of a clinical diagnosis during life, these cases were excluded. Case selection was further refined based on the availability of matched BM FFPE blocks in the Glasgow repository. Finally, cases that were previously utilised by Joice *et al*. and De Niz *et al*. (**Figure 3-4**) were prioritised (Joice et al., 2014, De Niz et al., 2018). Selection of post-mortem cases is described in detail in **Section 3.2.**

2.2 Basic Histology and Mouse Work

2.2.1 *P. berghei* Infections

TO mice were infected with *P. berghei* to achieve a parasitaemia of ~4%. Mice were culled on day 4-7 post infection; spleen and leg bones (femurs and tibias) were harvested. In addition, tissues were collected from naïve TO mice as a negative control. Harvested tissues were submerged in 10% NBF for a maximum of 24 hours before being transferred to 70% ethanol. Spleen tissue was processed using a standard tissue processing protocol (**Section 2.2.2**). The processing of bones followed a bone specific tissue processing protocol (**Section 2.2.3**). Due to the mineralisation of bones, decalcification was required which was executed either before or after tissue processing (**Section 2.2.4**).

2.2.2 Standard Tissue Processing and Embedding

Tissue processing was performed using the Expredia Excelsior AS tissue processor. For the standard tissue processing procedure, tissues initially underwent four consecutive 30 minute incubations in a series of alcohol (70%, 90%, 95% and 100%) at 37ºC. Following these incubations, tissues were incubated in 100% alcohol twice for 45 minutes for each incubation. Tissues were then incubated in xylene for an initial 15 minutes followed by two incubations for 30 minutes each. After xylene incubations, tissues were submerged in wax for 30 minutes, then two subsequent 1 hour incubations at 65ºC. Tissues were usually processed overnight and therefore held in 70% alcohol until start time.

After tissue processing, tissues were positioned as desired and embedded in paraffin wax. Wax was allowed to solidify on a cold plate for between 30 minutes to 1 hour.

2.2.3 BM Tissue Processing and Reverse Processing

Tissue processing was performed using the Expredia Excelsior AS tissue processor. For tissue processing BM, tissues initially underwent three consecutive 1 hour incubations in 70%, 90% and 95% alcohol at 37ºC. Tissues were subsequently incubated in 100% alcohol for 30 minutes, 1 hour, and 1.5 hours at the same temperature. Following this, tissues underwent three 1 hour xylene incubations. Tissues were then submerged in wax three times at 65ºC for 1 hour, 2 hours, and

3 hours. This process was run overnight with tissues held in 70% alcohol to delay start time.

After tissue processing, bones were positioned to allow transverse sections to be made. This was done by pouring a small volume of paraffin wax into a cassette, positioning the bone with tweezers, and then fully embedding the bone in paraffin wax in that position. Blocks were then allowed to solidify on a cold plate for between 30 minutes to 1 hour.

To reverse process FFPE bone blocks, blocks were melted for 10-15 minutes, or until all wax had melted, and individual bones were blotted with blue roll to remove excess wax. Bones were then slowly reverse processed by submerging in xylene in a sealed container incubated at room temperature for 1 hour on a rocker. Following xylene incubation, bones were submerged in a series of alcohol baths (100%, 90%, 70%) undergoing two consecutive 30 minute incubations at room temperature on a rocker for each concentration. Finally, bones were rinsed twice in nuclease free water.

2.2.4 BM Decalcification

To preserve mRNA integrity, a gentle decalcification protocol was utilised using 10% ethylene-diamine-tetraacetic acid (EDTA) in RNA*later* (Belluoccio et al., 2013). RNA*later*/EDTA solution was prepared by adding 3 g of EDTA to 30 mL of RNA*later* Stabilisation Solution (Invitrogen™, cat# AM7021). The pH was adjusted to pH 8.8 to dissolve EDTA. Once EDTA was dissolved, the pH was adjusted to pH 5.2 for decalcification. Tissues were incubated on a shaker for 24 hours at 4°C. The decalcification solution was replaced every 24 hours until two consecutive calcium tests were negative (Belluoccio et al., 2013).

To test the progress of decalcification, two methods were used. Firstly, a physical test was performed where tissue was removed from the RNA*later*/EDTA solution, and the rigidity was tested by gently bending the tissue by hand. Second, calcium levels were tested using 5% ammonium hydroxide and 5% ammonium oxalate. Equal volumes of the used decalcification solution, 5% ammonium hydroxide and 5% ammonium oxalate were combined in a falcon tube and mixed by inversion. The solution was allowed to stand at room temperature overnight to check for

precipitation of calcium oxalate. Decalcification was complete when two consecutive calcium tests were negative (IHC-World, 2022).

Decalcification times varied between tissues. To accurately determine decalcification endpoint, it was important to decalcify tissues separately.

2.2.5 Haematoxylin and Eosin (H&E) Staining

FFPE tissues were sectioned at 3-5 microns and mounted on SuperFrost Plus™ Adhesion Slides (Fisher Scientific, 1014870). Sections were dried overnight at room temperature. These sections were then baked in a histology oven at 60ºC for 35 minutes and then deparaffinised by immersion in xylene for 3 minutes twice. Tissues were hydrated through a series of alcohol baths (100%, 90%, 70%) and rinsed in deionised water (twice for 3 minutes each). Slides were stained with the nuclear stain Harris haematoxylin for 2.5 minutes before rinsing in running tap water. They were then dipped in 1% acid/alcohol twice, rinsed in running tap water, and incubated in Scott's Tap Water Substitute for 30 seconds, before rinsing again in running tap water. Sections were dipped in 70% alcohol 10 times and then incubated in 1% alcoholic eosin for 2.5 minutes. Sections were then dehydrated by incubating in 90% alcohol (2x30 seconds), 100% alcohol (2x3 minutes) and xylene (2x3 minutes). Finally, coverslips were mounted using dibutylphthalate polystyrene xylene (DPX) mountant and allowed to dry in the fume hood.

2.2.6 Giemsa Staining

FFPE tissues were sectioned at 2-3 microns and mounted on SuperFrost Plus™ Adhesion Slides (Fisher Scientific, 1014870) and dried overnight at room temperature. Sections were baked at 60ºC for 1 hour before deparaffinisation in xylene for 2x3 minutes. Tissue was then hydrated by dipping slides in a series of alcohol baths (100%, 90%, 70%) and final submersion in deionised water. Slides were laid on a rack and flooded with 100% filtered Giemsa stain and incubated for 1 minute. After 1 minute, flooded Giemsa stain was diluted 5 times by addition of tap water using a Pasteur pipette. Slides with diluted Giemsa were incubated for a further 10 minutes. After this incubation, the stain was differentiated in 1% acetic acid (by dipping 2-3 times) and then immediately rehydrated through briefly dipping in 100% alcohol twice and submersion in xylene. Coverslips were mounted using DPX mountant and allowed to dry in the fume hood.

For parasite quantification using Giemsa-stained sections, tissues were analysed on an Olympus BX43 microscope with an Olympus DP22 camera. For each splenic tissue, 10 high powered fields (HPF) were examined in each splenic compartment (red pulp (RP) cords, RP sinus lumen, perifollicular zone, and non-circulatory spaces) at 1000x magnification. Red blood cells (RBCs) and iRBCs were counted in each region; iRBCs were classified by their developmental stages (rings/early trophozoites, trophozoites, schizonts, gametocytes, or unclassifiable). Quantification required assessment of various Z-planes with fine focus. Parasitaemia in each splenic compartment, and overall, was calculated as a percentage of iRBCs over total RBCs in the given area:

$$\text{Parasitaemia (\%)} = \frac{\text{(total iRBC counts for 10 HPF/total RBC counts for 10 HPF)}}{} \times 100$$

2.2.7 Periodic Acid Schiff (PAS) Staining

FFPE tissues were sectioned at 2-3 microns and mounted on SuperFrost Plus™ Adhesion Slides (Fisher Scientific, 1014870) which were dried overnight at room temperature. Sections were baked at 60ºC for 35 minutes before deparaffinising in xylene and hydrating in an alcohol series (100%, 90%, 70%) to deionised water (2x 3 minutes each). Sections were then oxidised by submerging in 0.5% periodic acid solution for 5 minutes. To wash, sections were briefly washed in deionised water and then submerged in Schiff reagent for 15 minutes. Haematoxylin was used to counterstain sections for 1 minute with excess stain washed in running tap water for 5 minutes. Sections were then dehydrated in an alcohol series (90%, 100%) to xylene (2x3 minutes for each alcohol and xylene incubation) and coverslip mounted using DPX mountant.

2.2.8 Histopathology Scoring

Histopathology scoring of H&E stained tissues (**Section 2.2.5**) was performed by a comparative pathologist based on the International Council for Standardisation in Haematology guidelines. The pathologist was blinded to patient details and clinical information. The scoring criteria was modified to include additional parameters of interest such as the presence of iRBCs, pigmentation,

extramedullary haematopoiesis, and immature RBC counts. Scoring criteria can be found **Appendix 1.** Each parameter was qualitatively scored between 0 and 4 where 0 denoted a feature that was not present and 4 denotated a marked appearance of that feature (**Table 2-1**). Binary parameters such as the presence of iRBCs (i.e., yes/no) were marked by 1/Y for the presence of that parameter or 2/N for the absence of that parameter. Relative lesion burden in the spleen was scored between 0 and 5 where 0 denoted no lesions and 5 denoted extensive lesions that occupied most of the spleen section (**Table 2-1**).

Table 2-1. Histopathology scoring.

Score	Description
Relative Lesion Burden	
0	No lesions
1	Focal lesions
2	Multiple focal lesions
3	One or more focal severe lesions
4	Multiple focal lesions that are extensive and coalesce
5	Extensive lesions that occupy the majority of the spleen section
All Other Parameters	
0	Not present
1	Minimal
2	Mild
3	Moderate
4	Marked

2.3 IHC and RNAscope

2.3.1 IHC

IHC was performed using the Impress® Polymer detection system (Vector Laboratories). FFPE blocks were sectioned at 3 microns, mounted on SuperFrost Plus™ Adhesion Slides (Fisher Scientific, 1014870), and allowed to dry overnight. Slides were baked in a histology oven at 60°C for at least 35 minutes. Sections were then deparaffinised and hydrated through xylene and a graded alcohol series (100%, 90%, 70%) to deionised water with each step repeated twice for a duration of 3 minutes each. Endogenous enzyme activity was quenched using BLOXALL® (Vector Laboratories, SP-6000-100) for 10 minutes at room temperature before

washing slides in Tris buffered saline 0.05% tween (TBST) for 3 minutes. Antigen retrieval was performed according to optimised conditions for the given antibody (**Table 2-2, Section 2.3.2**). Slides were allowed to cool in the antigen retrieval solution in a container surrounded by running tap water. Sections were then washed in deionised water followed by TBST each for 3 minutes. Non-specific binding was blocked with 2.5% normal horse blocking serum (Vector Laboratories, S-2012-50) together with 2.5% species specific serum. The choice of species-specific serum was dependent on the host of the tissue; for example, human serum (ThermoFisher Scientific, 31876) was used for all sections derived from human tissues. Blocking was performed at room temperature for 1 hour. After blocking, primary antibodies or the isotype control was added to tissue sections at the optimised concentration (**Table 2-2**) and incubated overnight in a humidified chamber at 4^{o}C.

On day 2, slides were brought to room temperature and then washed for 3 minutes in TBST. An Immpress polymer detection kit specific to the species for which the primary antibody was raised, and specific for the desired substrate to be used, was added to sections, and incubated for 30 minutes at room temperature (**Table 2-2**). Slides were then washed for 3 minutes in TBST before incubating with the desired substrate for the optimised time. For improved staining with Vector Red (Vector Laboratories, SK-5105), Vector Blue (Vector Laboratories, SK-5300) and BCIP/NBT (Vector Laboratories, SK-5400) substrates, substrate incubation was performed protected from light. Slides were washed twice for 3-5 minutes in TBST. For double staining protocols, washing was immediately followed by antigen retrieval performed according to optimised conditions for the given antibody (**Table 2-2**). The same procedures were followed as before where slides were washed in deionised water, TBST and then blocked for 1 hour at room temperature before incubating the primary antibody at 4^{o}C overnight.

As described before, slides were brought to room temperature, washed for 3 minutes in TBST before incubating with the specific polymer detection kit for that antibody for 30 minutes. Slides were then washed for 3 minutes in TBST. The desired substrate for that specific antibody was added to section and incubated for the optimised time (**Table 2-2**). Slides were then washed for 3 minutes in TBST followed by a 3 minute wash in deionised water. Counterstaining was performed

by dipping slides in Harris haematoxylin twice and washing in running tap water. Slides were then alcohol dehydrated as previously described to xylene or Histo-Clear® (GeneFlow, A2-0101) depending on the substrate used. Coverslips were mounted using DPX or VectaMount® Mounting Medium (Vector Laboratories, H-5000).

The following double IHC combinations were performed: CD31/HSP70 (spleen, BM, lung), CD68/HSP70 (spleen), CD31/CD71 (lung), CD71/HSP70 (spleen, BM), MSRP1/Pfs16 (spleen, BM). Most IHC experiments described in this thesis involved double staining, as described above, except for HSP70 IHC experiments in *P. berghei* decalcification experiments (**Section 3.3.2**). For single staining, after the substrate was applied, slides were washed in TBST followed by deionised water for 3 minutes each, counter stained, alcohol dehydrated and mounted as described at the end of the double staining protocol.

Table 2-2. IHC conditions.

Antibody	Antigen Retrieval	Antigen Retrieval Conditions	Antibody Concentration (µg/mL)	Ab Host Species	Immpress Polymer Detection Kit	Substrate	Substrate Incubation Time	Clearing Agent	Mountain
CD31*	pH 6 Citrate	Microwave	2	Rabbit	HRP Horse Anti-Rabbit IgG (MP-7801-15) or AP Horse Anti-Rabbit IgG (MP-5401)	DAB (SK-4105) or BCIP/NBT (SK-5400)	30s or 2-3 minutes	Xylene or Histo-Clear	DPX or VectaMount
CD68	pH Citrate	Microwave	3.33	Mouse	AP Horse Anti-Mouse IgG (MP-5402)	Vector Blue (SK-5300)	2-3 minutes	Histo-Clear	VectaMount
CD71	pH 8.5 Tris EDTA	Pressure Cooker	2.5	Rabbit	HRP Horse Anti-Rabbit IgG (MP-7801-15)	DAB (SK-4105)	30s	Xylene	DPX
HSP70	pH 9 Tris EDTA	Pressure Cooker	2.5	Rabbit	AP Horse Anti-Rabbit IgG (MP-5401)	Vector Red (SK-5105)	2-3 minutes	Xylene	DPX
Pfs16	pH 6 Citrate	Pressure Cooker	1.04	Rabbit	AP Horse Anti-Rabbit IgG (MP-5401)	Vector Red (SK-5105)	2-3 minutes	Xylene	DPX
MSRP1	pH 9 Tris EDTA	Pressure Cooker	4.17	Rabbit	HRP Horse Anti-Rabbit IgG (MP-7801-15)	Vector Blue (SK-5300)	2-3 minutes	Histo-Clear	VectaMount

*HRP Horse Anti-Rabbit IgG Immpress polymer detection kit and DAB substrate was used for CD31/HSP70 stains. For CD31/CD71 staining in the lung, the AP Horse Anti-Rabbit IgG Immpress polymer detection kit and BCIP/NBT substrate was used.
Abbreviations: EDTA, ethylene-diamine-tetracetic acid; HRP, horseradish peroxidase; AP, alkaline phosphatase; DAB, 3,3-diaminobenzidine; BCIP/NBT, 5-bromo-4-chloro-3-indolyl phosphate/nitroblue tetrazolium; DPX, dibutylphthalate polystyrene xylene.

2.3.2 Antigen Retrieval Method and Materials

Two methodologies were used for IHC antigen retrieval: microwave and pressure cooker/benchtop autoclave. For antigen retrieval performed by microwave (1000W), slides were immersed in the given antigen retrieval solution and microwaved on full power until the antigen retrieval solution began to boil. At this point, the power of the microwave was reduced to 20% for 10 minutes. After this 10 minute incubation, the container with the antigen retrieval solution and slides

was cooled down by placing within a dish containing running tap water. The IHC protocol was followed from this point as described in **Section 2.3.1**.

For antigen retrieval performed by pressure cooker/benchtop autoclave, slides were immersed in the given antigen retrieval solution and placed in a benchtop autoclave (Prestige Medical Classic 2100). The pressure cooker was allowed to reach pressure at which point the pressure cooker was turned off and slides were incubated within for 10 minutes. After this 10 minute incubation, slides were removed from the benchtop autoclave and cooled down as before described. The IHC protocol was followed from this point as described in **Section 2.3.1**.

Three antigen retrieval solutions were used: pH 6 citrate, pH 8.5 Tris EDTA and pH 9 Tris EDTA. pH 6 citrate buffer (1X) was made using pH 6 citrate antigen retrieval buffer (10X) (TCS Biosciences Ltd, HDS05-100). Tris-EDTA based antigen retrieval buffers were made with 10 mM Tris base and 1 mM EDTA solution. The pH of the buffer was adjusted to either pH 9 or pH 8.5 once Tris and EDTA had dissolved. For pH 9 Tris EDTA antigen retrieval buffer, Tween 20 was also added at 0.05%.

2.3.3 IHC Controls

To assess antibody specificity for each parasite stage, FFPE blocks of blood clots containing asexual, sexual, and sexually committed parasites from *in vitro* cultured *P. falciparum* were generated. Parasites were grown between 2-5% parasitaemia at 5% haematocrit (500 μL packed cell volume (PCV)). To generate blood clots, parasite cultures were centrifuged at 1600 rpm for 5 minutes in a 50 mL falcon tube and the supernatant was removed. To 500 μL PCV, 150 μL of foetal bovine plasma and 150 μL of thrombin was added in a dropwise manner and mixed by gently swirling. The falcon tube was then placed at an angle (approximately 45^{o}) to allow the solution to form a "puddle" in the bottom cone of the falcon tube. The pellet was allowed to rest at room temperature for 30-60 minutes until the pellet had agglutinated. Using a 2 mL glass pipette, the blood clot was transferred to clean lens paper. The blood clot was folded within the lens paper to form a small square which was placed into a histology cassette (Joice et al., 2014). Cassettes were transferred to 10% NBF for 18-24 hours. After fixation, blood clots were processed as standard (**Section 2.2.2**). Specific details for the

generation of sexually committed and gametocyte blood clot FFPE blocks are found in **Section 2.4.6**. In addition to parasite blood clot controls, tissue controls were used as detailed in **Table 2-3.** For every tissue section, an isotype control (non-immune antibody of the same class or subclass of the primary antibody used) was included to identify any non-specific interactions.

Table 2-3. IHC controls.

	Positive Control	Negative Control
CD31	Tonsil	Mouse Spleen/Parasite Blood Clot
CD68	Tonsil/Uninfected Spleen (USA origin)	Parasite Blood Clot
CD71	Uninfected BM (USA origin)	Parasite Blood Clot
HSP70	Parasite Blood Clot	Tonsil/Naive Mouse Spleen
Pfs16	Gametocyte Blood Clot	Tonsil/Naive Mouse Spleen
MSRP1	Sexually Committed Schizont Blood Clot	Tonsil/Naive Mouse Spleen

2.3.4 Parasite Quantification and Calculations

Sections were analysed on an Olympus BX43 microscope with an Olympus DP22 camera. An initial evaluation of staining quality was made at 400x magnification. For IHC based parasite quantification in tissue samples from the Malawi cohort, 10 HPF were examined per tissue compartment at 1000x magnification. For MSRP1/Pfs16 counts in the BM, 25 HPF per compartment was quantified. RBC counts for splenic compartments were derived from the corresponding Giemsa-stained section. For BM and lung tissues without a corresponding Giemsa-stained tissue section, RBC counts were made based on their appearance on IHC stained sections. Quantification required assessment of various Z-planes with fine focus.

2.3.4.1 Tissue Parasitaemia

Parasitaemia in each splenic compartment, and overall, was calculated as a percentage of iRBCs over total RBCs in the given area:

Parasitaemia (%) =

$$\frac{\text{(total iRBC counts for total HPF/total RBC counts for total HPF)}}{} \times 100$$

Total organ parasitaemia was calculated based on the total iRBCs and total RBCs counts in all HPF counted for that organ. For BM and lungs, the total organ parasitaemia excluded large vessels from this calculation.

This same calculation was used to determine the reticulocytaemia of the spleen and large vessels of the lung. Here, CD71+ (reticulocyte) counts replaced iRBCs in the equation above.

2.3.4.2 Organ Biomass

The biomass in peripheral blood, spleen, BM, and lung was determined. Organ biomass calculation was based on Obaldia *et al*. 2018 and Kho *et al*. 2021 (Obaldia et al., 2018, Kho et al., 2021a).

To determine the parasite biomass in peripheral blood, the number of iRBCs per μL of blood and the total body blood volume (BV) was required. The total body BV was determined based on the relationship between total BV and body weight (Howie, 2011, Koperska, 2023). For parasite biomass in peripheral blood, the last parasitaemia reading prior to death was used.

Parasite biomass in peripheral blood =

$$\frac{(\text{iRBCs per } \mu\text{L peripheral blood} \times \text{total body BV}) \times 10^6}{}$$

To determine spleen parasite biomass, the following parameters were required: iRBC count per HPF, splenic weight, number of HPF analysed per tissue, the spleen volume per HPF, and the spleen density where the density of human paediatric spleen is 1.06 g/cm^3 (ICRP, 2020). Spleen weight was measured at post-mortem; the mean spleen weight for the cohort was 94 g.

To calculate the spleen volume per HPF, the area of a HPF (area = πr^2) needs to be determined. The radius of a HPF at 1000x magnification on the Olympus BX43 was measured at 0.11 mm. Section depth of tissues was 0.003 mm.

i) Spleen volume per HPF (cm^3) =

$$\frac{\text{(area of HPF } (mm^2) \text{ x section depth (mm))}}{1000}$$

ii) Total spleen parasite biomass =

$$\frac{\text{(iRBC count in HPFs x spleen weight (g))}}{\text{(spleen volume per HPF } (cm^3) \text{ (i) x number of HPF x spleen density } (g/cm^3))}$$

Here, the total number of HPF was taken for the whole tissue. Each splenic compartment (cords, sinus lumen, perifollicular zone, and non-circulatory spaces) had 10 HPF evaluated. Since the perifollicular zone was not evaluated in IHC stained spleen sections, counts from this compartment were removed to calculate the mean count in HPF between the two methods (Giemsa and IHC). The number of HPF evaluated in the spleen was therefore 30.

The parasite biomass in the BM was calculated like the spleen biomass (ii). Here, the BM weight was calculated based on the assumption that the BM constitutes 4% of the total body weight. The mean weight of the cohort was 9.75 kg; therefore, based on the before mentioned assumption, the BM weight used here was 390 g. The density of the BM was calculated using the volume (cm^3) and mass (g) of active marrow. These values alter with age; therefore the density was determined for each case and the mean density of 1.03 g/cm^3 was determined for the cohort (ICRP, 2020).

iii) BM density (g/cm^3) =

$$\frac{\text{mass (g)}}{\text{volume } (cm^3)}$$

iv) Total BM parasite biomass =

$$\frac{\text{(iRBC count in HPFs x BM weight (g))}}{\text{(BM volume per HPF } (cm^3) \text{ (i) x number of HPF x BM density } (g/cm^3) \text{ (iii))}}$$

For BM calculations, two compartments (parenchyma and small vessels) were counted and therefore the number of HPF was 20.

The parasite biomass in the lung was calculated in the same way as the spleen and BM biomass (ii and iv). The density of lung tissue varies with age; therefore the density was determined for each case and the mean density of 0.45 g/cm^3 was determined for the cohort (ICRP, 2020). The right lung mean weight for the cohort was 72.8 g.

iv) Total lung parasite biomass =

$$\frac{\text{(iRBC count in HPFs x lung weight (g)) /}}{\text{(lung volume per HPF (cm}^3\text{) (i) x number of HPF x lung density (g/cm}^3\text{) (iii))}}$$

For lung calculations, two compartments (parenchyma and small vessels) were counted and therefore the total number of HPF was 20.

2.3.4.3 Splenic Retention Rate

To calculate the parasite retention rate, the following values were required: the spleen weight, body weight, the total body BV, the total splenic BV, splenic parasitaemia and peripheral blood parasitaemia. Splenic BV was determined based on *ex vivo* flushing experiments revealing a splenic BV of 15 mL/100 g of tissue (Kho et al., 2021a).

To determine the parasite retention rate, the splenic input parasitaemia must be established based on the ratio of total BV to splenic BV (v).

v) Ratio of total blood volume to splenic blood volume =

$$\frac{\text{total body BV (mL)/ total splenic BV (mL)}}{}$$

Using this ratio, the splenic input parasitaemia can be determined. For this calculation, the mean splenic parasitaemia of the cohort was used which was 1.82% excluding patients who had received a blood transfusion during hospitalisation. With the mean splenic parasitaemia and the ratio of total blood

to splenic blood volume (v), the input splenic parasitaemia can be determined. This is the input splenic parasitaemia we would expect to generate the total splenic parasitaemia observed (**Section 2.4.2**).

vi) Splenic input parasitaemia (%) =

$$\frac{\text{mean splenic parasitaemia (\%)}}{\text{ratio of total BV to splenic BV (v)}}$$

With the splenic input parasitaemia determined, the proportion of peripheral parasitaemia retained in the spleen (i.e., the retention rate) can be determined. Here, peripheral parasitaemia was determined using the parasitaemia determined in the large vessels of the lung independent of classical vascular sequestration (**Section 2.3.4.1**).

iii) Retention rate (%) =

$$\frac{\text{(splenic input parasitaemia (\%) (vi)}}{\text{peripheral parasitaemia (\%))}} \times 100$$

2.3.5 RNAscope: *Mm-PolR2A* RNAscope

All reagents used for RNAscope were sourced from Advanced Cell Diagnostics (ACD). For RNAscope, sections were cut no more than 24 hours prior to the experiment. Sections were baked in a histology oven at 60°C for 1 hour. Slides were then submerged in xylene twice for 5 minutes each before submerging in 100% ethanol twice for 1 minute each. Using an empty staining bin, slides were allowed to dry at room temperature before proceeding with the next step. Endogenous enzyme activity was blocked using RNAscope® hydrogen peroxide (ACD, 32235) for 10 minutes at room temperature and then washed in nuclease free water 3-5 times. In a steamer, slides were briefly dipped in a staining bin containing nuclease free water for approximately 10 seconds to acclimate them before conducting antigen retrieval (1X Target Retrieval, ACD, 322000) at 94 °C to 100°C for the duration specific to the tissue type (**Table 2-4**). After antigen retrieval, slides were briefly washed in nuclease free water 3-5 times, allowed to dry, and then submerged in 100% ethanol 3-5 times before airdrying again.

Samples were permeabilised with RNAscope® Protease Plus (ACD, 322331) at 40°C in a HybEZ™ oven for the required duration of time depending on the tissue (**Table 2-4**). Protease plus was discarded into a waste container and slides were washed briefly in nuclease free water twice. Slides were incubated with RNAscope probes for 2 hours at 40°C in the HybEZ oven. For RNAscope in mouse bones (**Section 3.3.3**), the *Mm-PolR2A* (ACD, 312471) positive control probe and the dihydrodipicolinate reductase, *dapb* (ACD, 310043), negative control probe was used.

Following hybridisation with probes, excess liquid was discarded into a waste container and slides were washed twice in RNAscope® 1x Wash Buffer (ACD, 310091) for 2 minutes each at room temperature. After washing, a series of amplification steps were performed. Amplification was performed at 40°C in the HybEZ oven for Amp1 (30 minutes), Amp2 (15 minutes), Amp3 (30 minutes) and Amp4 (15 minutes). The remaining two amplification steps were performed at room temperature (Amp5 (45 minutes) and Amp6 (15 minutes)) (ACD, 322360). Between each amplification step, slides were washed twice in RNAscope 1x Wash Buffer for 2 minutes each. After amplification, signal was detected using RNAscope Fast Red (1 volume of Red-B to 60 volumes of Red-A reagent) (ACD, 322360) which was incubated on sections for 10 minutes at room temperature protected from light. After 10 minutes, stain was discarded, and slides were washed in nuclease free water 3-5 times. Slides were counterstained in 50% haematoxylin for 2 minutes at room temperature and then washed in running tap water. They were then immersed in Scott's Tap Water Substitute for 10 seconds and washed again in running tap water. Slides were then dried at 60°C in a histology oven before dipping slides in xylene and coverslip mounting with EcoMount (Biocare, EM897L). Stained sections were qualitatively scored using the ACD scoring system (**Table 2-5**).

Table 2-4. RNAscope conditions.

Tissue	Target Retrieval Time (minutes)	Protease Plus Time (minutes)
Mouse Spleen	18	35
Mouse BM	18	35
Human BM	24	16
Tonsil/HeLa Cell Pellet Control	15	15

Table 2-5. ACD qualitative scoring criteria.

ACD Score	Scoring Criteria
0	No staining or < 1 punctate dot/10 cells
1	1-3 dots/cell
2	4-9 dots/cell and none or very few dot clusters
3	10-15 dots/cell and/or <10% of dots are in clusters
4	>15 dots/cell and/or >10% of dots are in clusters

2.3.6 Statistics

Analysis for Giemsa, IHC and RNAscope was performed using GraphPad Prism (v. 10.0.3) (GraphPad, California). Counting and imaging was performed on an Olympus BX43 microscope with an Olympus DP22 digital camera. Minor adjustments were applied to the brightness of some images, ensuring that no original features were altered in the process. The Mann-Whitney test was applied for between group comparisons. The Wilcoxon matched pairs signed rank test was used to compare paired datasets. For multiple comparisons, the Friedman test was used for matched pairs comparisons and the Kruskal-Wallis test was used for non-matched comparisons. To assess pairwise differences, post-hoc Dunn's test was performed.

2.4 *Plasmodium* Culture

2.4.1 Parasite Strains

Two *P. falciparum* strains were used in this thesis: Pf2004/164tdt (Pf2004) and Dd2 WT (Dd2). Throughout this thesis, Pf2004/164tdt is referred to as Pf2004 and Dd2 WT as Dd2. This strain was previously transfected with the reporter plasmid 164tdTomato under the control of the gametocyte specific promoter, PF3D7_1016900 (Brancucci et al., 2015). These two culture-adapted strains originated from geographically distant locations which differ in transmission intensity. Pf2004 originated from West Africa, where transmission is high, and Dd2 from Southeast Asia, where transmission is low (Elliot, 2007, Hommel et al., 2010, Wellems et al., 1990). These different transmission settings may promote strains which differ in their investments in reproduction, or sexual commitment, and therefore, could provide insights into different sexual commitment transcriptional signatures (Abdi et al., 2023).

2.4.2 Thawing and Freezing Parasite Stocks

To thaw frozen parasite stocks from liquid nitrogen, cryovials were retrieved and brought to room temperature. The total volume was measured, usually approximately 1 mL, and transferred to a 50 mL falcon tube. To this, 0.1 volumes of 12% sodium chloride (NaCl) was added in a dropwise manner whilst gently shaking the falcon tube. Falcon tubes were left to stand at room temperature for 2 minutes. After this incubation, 10 volumes of 1.6% NaCl was added in a dropwise manner whilst gently shaking. The resulting solution was centrifuged at 1600 rpm for 4 minutes before discarding the supernatant. Parasites were washed in 10x volume of incomplete Roswell Park Memorial Institute (RPMI) medium 1640 with additives L-glutamine and 25 mM HEPES (Gibco, 22400089) supplemented with 5 mM hypoxanthine and 1 mg/mL gentamycin. Parasites were centrifuged at 1600 rpm for 4 minutes before discarding the supernatant. Finally, the remaining pellet was resuspended in complete RPMI (incomplete RPMI as described above with 10% human serum (Interstate Blood Bank, Inc)) at 5% haematocrit using washed O-positive blood. Parasites were maintained in culture as described in **Section 2.4.3**.

Aliquots of parasite cultures were frozen shortly after thawing once the parasite culture had reached at least 3% ring parasitaemia. To freeze parasites, parasite

cultures were transferred to an appropriately sized falcon tube and centrifuged at 1600 rpm for 3 minutes to remove media. To the cell pellet, 1.2 volumes of human serum was added in a dropwise manner whilst gently shaking the falcon tube. Drop by drop, 2 volumes of freezing solution (sorbitol-glycerolyte freezing solution) were added while gently shaking the falcon tube. From the resulting solution, 1 mL was then transferred to a labelled sterile cryovial and stored in liquid nitrogen.

2.4.3 *In vitro* Culture Maintenance

Asexual parasites were routinely cultured according to protocols described in Lambros and Vanderberg, 1979 & Trager and Jensen, 1976 (Trager and Jensen, 1976, Lambros and Vanderberg, 1979). Parasites were grown in complete medium composed of RPMI 1640 with L-Glutamine, 25 mM HEPES, 5 mM hypoxanthine and 1 mg/mL gentamycin, supplemented with 10% O-positive human serum (Interstate Blood Bank, Inc). Parasites were typically grown at 5% haematocrit, unless stated otherwise, and maintained at 0.5-5% parasitaemia in petri dishes. For Pf2004 cultures, addition of 4 nM WR99210 (Jacobus Pharmaceutical) was required to select for stable maintenance of episomes. Petri dishes were placed in a modulator incubator chamber which was gassed using a mixture containing 1% O_2, 5% CO_2 and 94% N_2 and incubated at 37^{o}C. Parasitaemia was determined by blood smear and light microscopy. RBCs used in routine culture were obtained from O-positive blood which were washed twice in incomplete RPMI before use. Washed RBCs were then stored at 4^{o}C and replaced weekly. To maintain parasite cultures, media was changed daily and parasitaemia was counted every 48 hours following reinvasion. Parasite cultures were diluted depending on parasitaemia and parasite multiplication rate (PMR).

2.4.4 Parasite Synchronisation

To synchronise parasites, sorbitol synchronisation was performed as outlined by (Lambros and Vanderberg, 1979). This allows ring stage parasites to be selected for while trophozoites and schizonts are permeabilised and thus removed. The first sorbitol synchronisation was performed on cultures containing predominantly ring stage parasites at approximately 10-12 hours post invasion (hpi). Parasite cultures were transferred to an appropriately sized falcon tube and centrifuged at 1600 rpm for 3 minutes before aspirating media. The remaining cell pellet was resuspended in 10 volumes of pre-warmed 5% sorbitol and incubated at 37^{o}C for

10 minutes. After incubation, parasites were centrifuged again at 1600 rpm for 3 minutes to remove sorbitol. The cell pellet was washed in incomplete RPMI to remove any remaining sorbitol. To confirm successful enrichment of ring stages, blood smears can be made to check parasitaemia and staging. Parasites were then resuspended in complete media at 5% haematocrit, placed in a modular incubator chamber, gassed, and returned to 37°C. Sorbitol synchronisation was repeated 16 hours after the first sorbitol synchronisation.

To create a tighter window of synchronicity, the double sorbitol synchronisation described above can be repeated approximately 32 hours after the second sorbitol when parasites have reinvaded.

2.4.5 Parasite Induction (Sexual Conversion Assay)

The sexual conversion assay for controlled *in vitro* stage conversion was adapted from Brancucci *et al*. 2018 (Brancucci et al., 2018). This assay utilised the depletion of the serum phospholipid lysophosphatidylcholine (LysoPC) in minimal fatty acid (mFA) media to induce sexual commitment and conversion (Brancucci et al., 2017). mFA was generated by supplementing incomplete RPMI with 0.39% fatty acid-free bovine serum albumin (BSA), 30 μM oleic acid, and 30 μM palmitic acid. Prior to parasite induction, cultures were synchronised with four sorbitol treatments as described in **Section 2.4.4**. At 26/28 hpi, parasites were grown in mFA media at 2.5% haematocrit and 0.5% parasitaemia for 20-22 hours before returning to complete (serum) media (day 0). Starting parasitaemia was measured by flow cytometry using SybrGreen staining (1/5000). Cultures were maintained as described in **Section 2.4.3** until the end of the experiment.

Two days after the sexual conversion assay was initiated, reinvasion parasitaemia was measured by flow cytometry using SybrGreen staining. This allowed the calculation of the PMR. The PMR was calculated by dividing parasitaemia measured on day 2 by the starting parasitaemia measured on day 0:

PMR =

$$= \text{parasitaemia}_{d0} / \text{reinvasion parasitaemia}_{d2}$$

To block further reinvasion, heparin was added to cultures at 0.23 mg/mL for 2 consecutive days. On day 6 at stage III gametocytes, gametocytaemia was measured by flow cytometry using SybrGreen and Tubulin Tracker™ Deep Red (Invitrogen, T34077) to stain gametocytes. Conversion rate was calculated by diving gametocytaemia with the reinvasion parasitaemia measured on day 2 multiplied by 100:

Conversion Rate (%) =

$$\frac{(\text{gametocytaemia}_{d6}/\text{parasitaemia}_{d2}) \times 100}{}$$

Flow cytometry was performed on the MACSQuant VYB flow cytometer (Miltenyi Biotec), and data analysed using FlowJo software (v. 10.7.2).

2.4.6 Sexually Committed and Gametocyte FFPE Blocks

To assess antibody specificity of anti-MSRP1 and anti-Pfs16 antibodies, sexually committed schizonts and gametocyte FFPE blocks were generated from *in vitro* cultured *P. falciparum*. Here, the sexual conversion assay described in **Section 2.4.5** was modified. Synchronised Pf2004 parasites were grown at 2-5% parasitaemia and 5% haematocrit in 2 mL PCV. At 26/28 hpi, the 2 mL PCV was divided into four, to establish two mFA plates and two complete (serum) media plates. To measure PMR and conversion rate, an additional 96 well plate was prepared to run in parallel. At 44-46 hpi, parasites were harvested from one mFA plate and one serum plate. Parasite cultures were transferred to a 50 mL falcon tube and centrifuged at 1600 rpm for 5 minutes. Media was removed and to each 500 μL PCV, 150 μL of foetal bovine plasma and 150 μL of thrombin was added in a dropwise manner and mixed by gently swirling. The falcon tube was positioned as described in **Section 2.3.3** and the resulting blood clot was packaged in lens paper and placed into a histology cassette (Joice et al., 2014). Cassettes were transferred to 10% NBF for 18-24 hours.

After reinvasion, at 18 hpi, the remaining mFA and serum cultures were transferred to a 50 mL falcon and blood clots were generated as previously described. Gametocyte and asexual ring blood clots were packaged in lens paper and placed into a histology cassette which was transferred to 10% NBF. After fixation, blood clots were processed as standard (**Section 2.2.2**).

2.5 Single Cell RNA Sequencing (scRNAseq)

2.5.1 Experimental Outline

For scRNAseq, the sexual conversion assay described in **Section 2.4.5** was modified. At 26/28 hpi, the sexual conversion assay was initiated by growing Pf2004 and Dd2 in either mFA or complete (serum) media. Two time points were taken during schizont growth and stored in the preservation medium Hypothermasol® FRS (STEMCELL technologies, 07935) at 4ºC. Parasite strains and time points were pooled together according to growth medium to form two samples per replicate.

2.5.2 Parasite Induction

Pf2004 and Dd2 were synchronised in parallel to induce at the same time. Prior to the sexual conversion assay, synchronised *P. falciparum* was grown at 4-6% parasitaemia in 2.5% haematocrit. At 26/28 hpi, parasite cultures were transferred to 15 mL falcon tubes and centrifuged at 1600 rpm for 3 minutes. Parasites were washed twice by resuspending in mFA and centrifuging at 1600 rpm for 3 minutes. Parasites were then resuspended in mFA or serum at 2.5% haematocrit and transferred to a 24 well plate (2 mL per well with 50 μL PCV). A sexual conversion assay was prepared in a 96 well plate as outlined in **Section 2.4.5** to run in parallel allowing measurement of PMR and conversion rate.

2.5.3 Cell Harvesting

At 16 hours post induction, blood smears were made to confirm the presence of early schizonts. After confirmation of early schizonts, parasite cultures from the 24 well plate were transferred to LoBind Eppendorfs (Eppendorf, 0030108078) and centrifuged at 2000 rpm for 5 minutes. Supernatants were removed and pellets were resuspended in 1.5x Hypothermasol® FRS (STEMCELL technologies, 07935) and stored at 4ºC. At this time point, media was changed on the 96 well induction plate and in the 24 well plate with the remaining time points.

At 6 hours after the first time point was taken, blood smears were made to confirm the presence of late schizonts. Once late schizonts were confirmed, parasites were prepared for cold storage as before described.

2.5.4 Sample Preparation

Before proceeding with sample preparation, blood smears were made to check for the presence of live parasites. Samples were processed in batches on ice to limit cell loss. Serum samples were processed first by centrifuging at 2000 rpm for 5 minutes to remove Hypothermasol. Parasites were then washed in 5 volumes of cold 1xphosphate buffered saline (PBS):0.2% BSA and centrifuged at 2000 rpm for 5 minutes. To lyse RBCs, the supernatant was aspirated, and pellets were gently resuspended in 5 volumes of 0.1% saponin. Parasites were incubated in 0.1% saponin for 2-5 minutes on ice. After saponin lysis, parasites were gently washed twice with cold 1xPBS:0.2% BSA at 2000 rpm for 5 minutes. At this point, parasites were very fragile and prone to lysis; therefore, wide pore pipette tips were used from this point onwards. Parasites were counted by flow cytometry (MACSQuant VYB flow cytometer (Miltenyi Biotec)) and by Neubauer haemocytometer. Whilst counting was being performed, the next batch of mFA samples were prepared as previously described.

To calculate cell concentration from haemocytometer counts, the following calculation was performed:

Cell concentration (cell/mL) =

$$\frac{(\text{number of cells counted} \,/\, (\text{number of squares counted} \times \text{dilution factor})) \times 2.5\times10^{5}}{}$$

After cells were counted by both methods, the mean of the two methods was taken and samples were diluted to 2.5×10^{5} cells/mL in cold 1xPBS:0.2% BSA. The two time points and two parasite strains were pooled together per condition (i.e., per growth medium) generating two samples: mFA and serum. Each sample was counted as beforementioned immediately before loading onto the 10X Chromium machine by Glasgow Polyomics.

2.5.5 10X Run and Library Preparation

After cell preparation, approximately 1×10^{6} cells/mL were loaded onto the 10X Chromium Chip which was loaded onto the 10X Chromium machine to recover 10,000 cells per inlet. Amplification, library preparation and Illumina sequencing was performed by Glasgow Polyomics following the standard 10X protocol. An

initial sequencing depth of 30,000 reads per cell was generated before increasing sequencing depth to 50,000 reads per cell.

2.6 scRNAseq Data Analysis

Raw Illumina reads were mapped against the *P. falciparum* reference genome 3D7 (PlasmoDB (v. 53)) with extended 3' untranslated regions, or a combination of PfDd2 and Pf2004 (Aurrecoechea et al., 2009, Otto et al., 2018). Mapping was performed by Thomas Otto using 10X Genomics Cell Ranger using default settings (v. 7.0.0) (Zheng et al., 2017). Data analysis was performed in R (v. 4.1.0) using Seurat (v. 4.4.0) (Hao et al., 2021).

2.6.1 Demuxlet and Quality Control

The computational tool Demuxlet (v. 0.1.0) was used to assign strain identity (Pf2004 or Dd2) to cells which were pooled together based on genetic variation between the two strains. In addition, Demuxlet was used to isolate singlets thereby removing doublets, cells which were too ambiguous to call, and cells that were not annotated (Kang et al., 2018).

Low quality cells and empty droplets were removed according to individual thresholds for each sample (**Table 2-6**). Cells that had greater than 1% mitochondrial counts and less than 100 total unique molecular identifiers (UMIs), i.e., transcripts, were removed.

Table 2-6. Quality control thresholds.

Sample	nFeature_RNA	nCount_RNA
mFA_1	3100	17,000
Serum_1	3510	26,000
mFA_2	3900	30000
Serum_2	3500	24,000
mFA_3A	3300	18,000
mFA_3B	3300	18,000
Serum_3A	3400	23,000

2.6.2 Sample Integration, Unsupervised Clustering and Mapping to the Malaria Cell Atlas

Pf2004 and Dd2 were analysed separately using the same analysis pipeline. Single cell transcriptomes were normalised using Scran normalisation (v.1.20.1) (Lun et al., 2016). The seven samples generated for each strain were integrated into single Seurat objects (i.e., an object for Pf2004 and an object for Dd2) using Harmony (Korsunsky et al., 2019). Uniform manifold approximation and projection (UMAP) nonlinear dimensionality reduction was performed with the first 30 principal components of the armony corrected principal component analysis (PCA) and clusters were identified using a resolution of 0.2 and 0.25 for Pf2004 and Dd2. An additional quality control step was performed removing clusters with low UMI counts, clusters expressing *pfs16* (PF3D7_0406200), or clusters/cells expressing *kahrp* (PF3D7_0202000**)** (in the cells marked as Dd2 only) as a large deletion in chromosome 2 has been previously described in Dd2 (Ribacke et al., 2007, Jiang et al., 2008). Clusters were annotated according to their correlation with cell stage marker genes and *P. falciparum* scRNAseq Malaria Cell Atlas reference which was mapped onto each dataset using scmap (v. 1.14.0) (Reid et al., 2018, Howick et al., 2019, Kiselev et al., 2018).

2.6.3 Differential Gene Expression (DGE) Analysis

Differential gene expression (DGE) analysis between clusters was performed using the FindMarkers function in the Seurat package in R. The test used was MAST which is designed for single cell datasets. A threshold of 0.5 $\log_2$fold change (FC) (unless stated otherwise) was set and hits were deemed significant with an adjusted p value < 0.05.

2.6.4 Pseudotime Trajectory Inference

To perform pseudotime, Pf2004 and Dd2 Seurat objects were split according to media condition generating four Seurat objects: ‘mFA_Pf2004’, ‘mFA_Dd2’, ‘serum_Pf2004’ and ‘serum_Dd2’. Ring clusters were removed and the resolution of the UMAP for each Seurat was reduced. Cluster resolution for Pf2004_mFA, Pf2004_serum, Dd2_mFA. Dd2_serum was reduced to 0.05, 0.08, 0.08 and 0.05 respectively. Trajectories were determined using slingshot (v. 2.0.0) with start and end clusters defined according to life cycle progression (Street et al., 2018).

2.6.5 Data Visualisation Methods and Tools

Plots in **Chapter 5** were performed in R from the Seurat library (v. 4.0.0) including UMAPs, heatmaps, feature plots, violin plots and co-expression plots. Volcano plots were generated in R using the Enhanced Volcano library (v. 1.13.2) and bar plots and pseudotime expression line plots were generated using the ggplot2 library (v. 3.4.4).

Chapter 3 | Using basic histological stains to evaluate the histopathology and parasite distribution in the BM and spleen

3.1 Introduction

In this chapter, I began my investigations into hidden parasite reservoirs in the bone marrow (BM) and spleen in paediatric *P. falciparum* severe malaria cases using basic histological techniques. To phenotypically characterise these reservoirs, I initially investigated the histopathological changes in the BM and spleen in severe malaria cases and non-malarial controls. I then investigated parasite stage distribution across the different compartments of the spleen.

3.1.1 BM and Splenic Reservoirs

The BM and spleen represent two important parasite reservoirs which are largely independent of classical vascular sequestration. Through a histopathological survey of post-mortem tissues collected from paediatric severe *P. falciparum* malaria cases in Malawi, Joice *et al.* provided histological and molecular evidence for an enrichment of immature gametocytes in the extravascular spaces (i.e., the parenchyma) of the BM (Joice et al., 2014). In the same cohort, the presence of mature asexual stages was confirmed by immunohistochemistry (De Niz et al., 2018). In a separate cohort of anaemic children in Mozambique, Aguilar *et al.*, similarly provided molecular evidence for the enrichment of immature gametocytes in the BM (Aguilar et al., 2014). This enrichment of gametocytes in the BM is not constricted to *P. falciparum* cases in sub-Saharan Africa. The enrichment of *P. vivax* gametocytes was observed in BM aspirates collected from a *P. vivax* infected patient from Brazil and in *P. vivax* infected non-human primates (Baro et al., 2017, Obaldia et al., 2018). The BM is therefore an important parasite reservoir for ongoing transmission.

The spleen has historically been considered an organ of parasite destruction during malaria infection. However, in a study of 22 chronic asymptomatic malaria patients (12 to 46 years old) undergoing splenectomy due to splenic rupture in Timika, Indonesia, an accumulation of non-phagocytosed parasites of all stages of the life cycle were identified using Giemsa-stained tissue sections. In *P. vivax* malaria, the parasite biomass was found to be 81 times higher in the spleen compared to peripheral blood. In *P. falciparum* malaria, the parasite biomass was 12 times higher in the spleen, therefore the accumulation of parasites in the spleen is more marked in *P. vivax* malaria than *P. falciparum* malaria. This

suggests that the spleen may represent an important reservoir for asexual replication outside of circulation. While this study was able to compare parasite densities and biomass between the spleen and peripheral circulation, it was not able to investigate parasite accumulation in other organs (Kho et al., 2021a, Kho et al., 2021b).

3.1.2 Histopathology of the BM

Despite the importance of the BM and spleen in malaria infection, few in-depth studies into their histopathology during infection have been performed to date. A common feature of BM observed during infection is a shift in the myeloid-to-erythroid ratio (proportion of myeloid to erythroid cells) in favour of myelopoiesis. This is coupled with dyserythropoiesis and an increase in the presence of granulocytic precursors in the BM (granulocytic left shift) (Bain et al., 2019, Ghosh and Stumhofer, 2021). Here, a left shift in a blood cell lineage, for example, the granulocytic lineage, refers to the increase in immature cell types (**Figure 3-1**). Consequently, this results in an increase in BM cellularity (Bain et al., 2019). The most comprehensive study on the histopathology of the BM was performed in 1986 using BM aspirates from 9 patients with cerebral malaria (CM) in Eastern Thailand (Wickramasinghe et al., 1987). Here, an increase in macrophages, eosinophils and plasma cells was observed. In addition, the presence of infected red blood cells (iRBCs) and pigmented macrophages was noted (Wickramasinghe et al., 1987). In a separate study of fatal paediatric severe malaria cases in Malawi, pigmented macrophages and free pigments were consistently observed across cases (Milner et al., 2014).

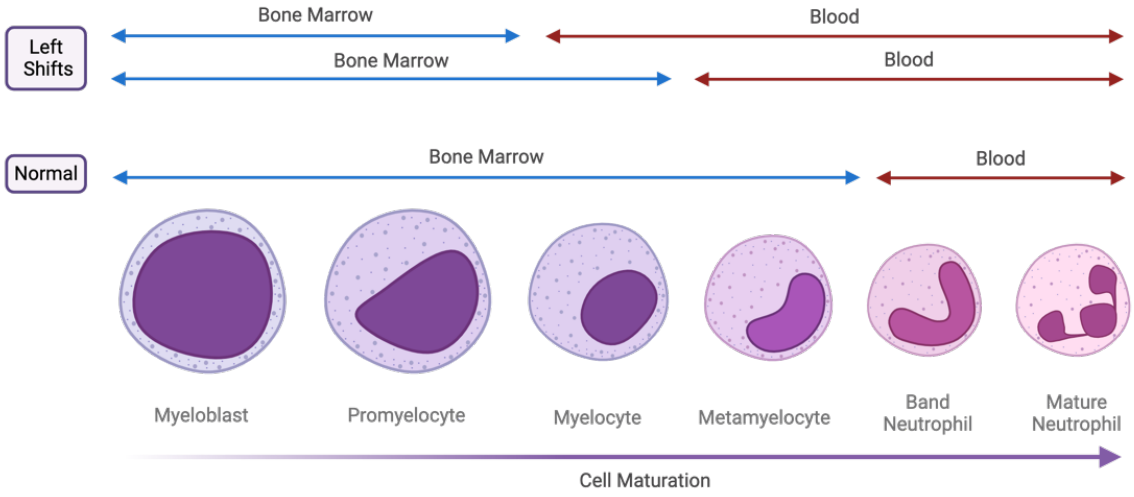

Figure 3-1. Granulocytic left shift. Granulopoiesis, or granulocyte cell maturation, involves the development of granulocytes such as neutrophils, eosinophils and basophils. A left shift in a blood cell lineage describes an increased presence of immature cell types in the blood or a higher proportion of immature cell types relative to mature cell types in the bone marrow (BM). Figure created with BioRender.com.

3.1.3 Histopathology of the Spleen

Compared to the BM, more studies have been performed on the histopathology of the spleen in the context of malaria. A hallmark of malaria infection is splenomegaly (enlargement of the spleen) which is often associated with expansion of the red pulp (RP) and white pulp (WP) (Urban et al., 2005a, Buffet et al., 2011, Milner et al., 2014). The most common histopathological changes observed as a result of blood-borne infections, including *Plasmodium,* is the disruption or disorganisation of the splenic architecture (Pongponratn et al., 1987, Pongponratn et al., 1989, Urban et al., 2005b, da Silva et al., 2012, Bauomy et al., 2014, Milner et al., 2014, Gómez-Pérez et al., 2014, Alves et al., 2015, Hermida et al., 2018). This includes disruption of germinal centre architecture, blurring of limits between the RP and WP, and dissolution of the marginal zone. In malaria cases, abundant pigment and pigment latent macrophages were observed throughout splenic tissue (Pongponratn et al., 1987, Pongponratn et al., 1989, Urban et al., 2005a, Milner et al., 2014, Alves et al., 2015). The amount of pigment and pigment latent macrophages was demonstrated to increase with disease progression in *P. falciparum* infected non-human primates (Alves et al., 2015). Loss of B lymphocytes and congestion of red blood cells (RBCs) including

RBC infiltration of lymphoid tissue was also frequently observed in malaria cases (Pongponratn et al., 1987, Urban et al., 2005a, Gomez-Perez et al., 2014, Alves et al., 2015). Further, haemorrhage, necrosis, inflammation and lesions were recently observed among histopathological changes in the spleen of *P. berghei* infected mice (Hentzschel et al., 2022). These histopathological alterations in the spleen during malaria infection are likely to impact splenic function, affecting both the clearance of iRBCs and the immune response.

3.1.4 Reticulocytes and Endosplenic Life Cycles

As before described in **Section 1.1.5** of this thesis, there is evidence to suggest the presence of an ongoing endosplenic life cycle. This was first demonstrated in *P. berghei* infected mice where the reticulocyte rich environments of both the BM and spleen facilitated an intraerythrocytic asexual replication cycle. Here, Lee *et al*. emphasised the importance of cryptic life cycles in the development of antimalarial drug resistance and recrudescent infection (Lee et al., 2018). In chronic asymptomatic malaria cases in adults, infected spleens exhibited a substantial pool of retained reticulocytes (Kho et al., 2021a). In contrast to mice, the spleen in humans is rarely haematopoietically active; however, the spleen does play a role in reticulocyte maturation (Gupta et al., 2022, Griffiths et al., 2012, Li et al., 2021a). It is unknown whether retained reticulocytes in the spleen of chronic asymptomatic malaria patients is the result of extramedullary haematopoiesis, or retention of reticulocytes during their maturation phase in the spleen. However, it was hypothesised that these retained reticulocytes may support an endosplenic life cycle, similar to what was previously observed in *P. berghei* infected mice. This is particularly relevant for *P. vivax* which is restricted to reticulocytes. Note that while *P. falciparum* can invade both normocytes (mature RBCs) and reticulocytes, it has a predilection for reticulocytes (Leong et al., 2022).

In the same study of chronic asymptomatic malaria cases in adults, parasites were found to co-localise with reticulocytes. Of particular importance, schizonts were observed in the splenic cords, which under normal circumstances, would be cleared in the spleen due to their lack of deformability. Furthermore, schizonts in the cords were observed in proportions consistent with their duration in the

intraerythrocytic life cycle. The cords represent an area of the spleen which is characterised by slow circulation. Therefore, Kho *et al*. proposed that the co-localisation of reticulocytes and schizonts in the slow circulation of the cords provides a niche for successful reticulocyte invasion and parasite replication.

3.1.5 Malawi Cohort

Between February 1996 and June 2010, a large prospective post-mortem study was conducted on fatal paediatric malaria cases and non-malarial controls in Blantyre, Malawi. In this study, over 2000 children were enrolled, with 404 cases resulting in mortality. Consent to perform a post-mortem was sought for 335 cases. In total, 103 post-mortems were performed on patients between the ages of 6 months and 13 years old. Clinical diagnoses were determined prior to post-mortem and reclassified based on post-mortem findings (Taylor et al., 2004, Milner et al., 2014).

Most patients in the study had clinical CM; here, clinical CM is defined as coma (Blantyre Coma score ≤ 2 and Glasgow Coma Scale score ≤ 10) with no improvement following correction of hypoglycaemia, *P. falciparum* peripheral parasitaemia, and no other obvious cause of coma such as meningitis (Taylor et al., 2004). Among clinically defined CM cases, three patterns of cerebral histopathology were observed: CM1 cases exhibited sequestration of iRBCs with no further cerebral histopathological changes; CM2 cases had sequestration of iRBCs with cerebral histopathological changes such as ring haemorrhages, cerebral microthrombi and extra-erythrocytic pigment; and CM3 cases presented with clinical CM however there was limited evidence of cerebral sequestration, and an alternative cause of death was identified.

Non-CM parasitaemic cases were also enrolled in the study which included severe malarial anaemia (SMA) cases without coma and incidental parasitaemia cases where malaria was not the primary cause of death. Non-malarial controls included comatose patients with non-malarial causes of coma. Based on these final clinical diagnoses, the cohort comprised CM1 (n=13), CM2 (n=42), CM3 (n=20), SMA (n=4), incidental parasitaemia (n=3), non-malarial coma (n=17), non-malarial death (n=1) and indeterminant cases (where a clinical diagnosis was not made prior to death; n=4) (Taylor et al., 2004, Milner et al., 2013b, Milner et al., 2014).

3.1.6 Chapter Aims and Hypotheses

Recent evidence has demonstrated that the BM and spleen are important hidden reservoirs of malaria parasites for both asexual and sexual stages (Joice et al., 2014, Aguilar et al., 2014, De Niz et al., 2018, Kho et al., 2021a, Kho et al., 2021b). The existence of such hidden reservoirs has important implications for malaria eradication efforts as parasite reservoirs in the haematopoietic niches may contribute to recrudescent infections, ongoing transmission, and the emergence of drug resistance. Despite the importance of these two organs in malaria infection, few in-depth studies into their histopathology in paediatric severe *P. falciparum* malaria have been performed. Specifically, no in-depth histopathological studies in the BM in paediatric cases have been performed with previous work only investigating the BM in adults (age range 15 to 78 years old) (Wickramasinghe et al., 1987).

The spleen has been demonstrated to harbour a large biomass of intact parasites of all developmental stages in proportions consistent with their duration in the intraerythrocytic life cycle (Kho et al., 2021b, Kho et al., 2021a). This suggests that the spleen may serve as a tissue site for asexual replication. However, it remains unknown whether large magnitudes of intact parasites accumulate in the spleen in paediatric severe *P. falciparum* malaria patients. Additionally, it remains unclear whether the spleen in these cases could function as a tissue site of asexual replication, as evidenced by high densities of non-phagocytosed parasites of all developmental stages in proportions indicative of an endosplenic life cycle.

In this chapter, I aimed to apply basic histological stains, such as Haematoxylin and Eosin (H&E) and Giemsa, to explore the histopathology of these two important organs in paediatric severe *P. falciparum* malaria cases and non-malarial controls (**Section 3.1.5**). Using Giemsa, I began to explore the density and stage distribution of non-phagocytosed parasites in the different compartments of the spleen.

Specifically, I aimed to:

- Perform a detailed histopathological scoring of spleen and BM samples from paediatric severe *P. falciparum* malaria and non-malarial controls.
- To perform multivariant analysis between histopathological and clinical parameters to identify key associations.
- To explore parasite density and distribution in the spleen using a Giemsa-based counting methodology.
- To determine if there is any evidence of an endosplenic life cycle based on the proportion of intraerythrocytic developmental stages.

3.2 Case Selection and Cohort Characterisation

To investigate the histopathology and parasite reservoirs in the spleen and BM in paediatric severe *P. falciparum* malaria, tissues from a severe malaria post-mortem study between 1996 and 2010 in Blantyre, Malawi, were utilised (described in **Section 3.1.5**) (Taylor et al., 2004). From the initial 103 post-mortem cases, patients were only included if they were HIV-negative (n=77), had a post-mortem interval (PMI) less than 12 hours (n=62) and a determined clinical diagnosis (n=61). Removal of HIV-positive patients was based on known effects on the histopathology, organ function, and parasite accumulation in the BM and spleen during HIV infection (Delacrétaz et al., 1987, Khalil et al., 1996, Flateau et al., 2011, Williams et al., 2016, Joice et al., 2016, Heller et al., 2023). Exclusion of cases with a PMI of greater than 12 hours was based on previous findings of poor structural preservation of tissues and poor immunohistochemistry (IHC) staining in cases with a PMI greater than 12 hours (Joice et al., 2014). Indeterminant cases were patients who died before a clinical diagnosis could be made and were therefore also excluded. The remaining cases were categorised into six clinical groups based on diagnosis. In the severe malaria post-mortem study, 72% of patients were diagnosed with CM (details on the specific CM classifications can be found in **Section 2.1.1**) (Taylor et al., 2004, Milner et al., 2014). It was hypothesised that anaemia could drive histopathological changes in the BM and spleen and may influence the parasite reservoir within these organs. Since there were few SMA cases in this study, CM cases were grouped according to their anaemic status:

- CM1/CM2 without SMA [CM1/CM2 (-SMA)] (n=9),
- CM2 with SMA [CM2 (+SMA)] (n=7),
- CM3 (n=11),
- SMA (n=2),
- incidental parasitaemia (n=3) and
- non-malarial controls (n=6).

Several cases were reclassified for this study following discussions with clinicians. Originally, PM40 was diagnosed with a non-malarial encephalopathy of infectious origin and therefore categorised as a non-malarial control. However, this case had a parasitaemia on admission of 597 parasites/μL with blood infection cleared

before death (time to death 64 hours). This case was subsequently reclassified as an incidental parasitaemia case, defined as a patient with parasitaemia. PM05, PM48 and PM61 were originally classified as CM2 cases without SMA; however, based on their packed cell volume (PCV), either on admission or in the last reading prior to death, their anaemic status was considered severe. They were therefore reclassified as CM2 cases with SMA (**Table 3-1**).

From this, only cases with matched BM and spleen formalin-fixed, paraffin embedded (FFPE) tissue blocks in the Glasgow repository were selected (n=46). The CM1/CM2 (-SMA) clinical group was further refined by prioritising cases that had been previously utilised by Joice *et al.*, and De Niz *et al.* (Joice et al., 2014, De Niz et al., 2018). After applying the above exclusion criteria and selection methods, a cohort of 38 patients was established to take forward for histological analyses (**Figure 3-2, 3-3A, Table 3-1**). Within the cohort, there were 32 malaria cases and 6 non-malarial controls. All non-malarial controls had non-malarial encephalopathy with an infectious aetiology, apart from 2 cases.

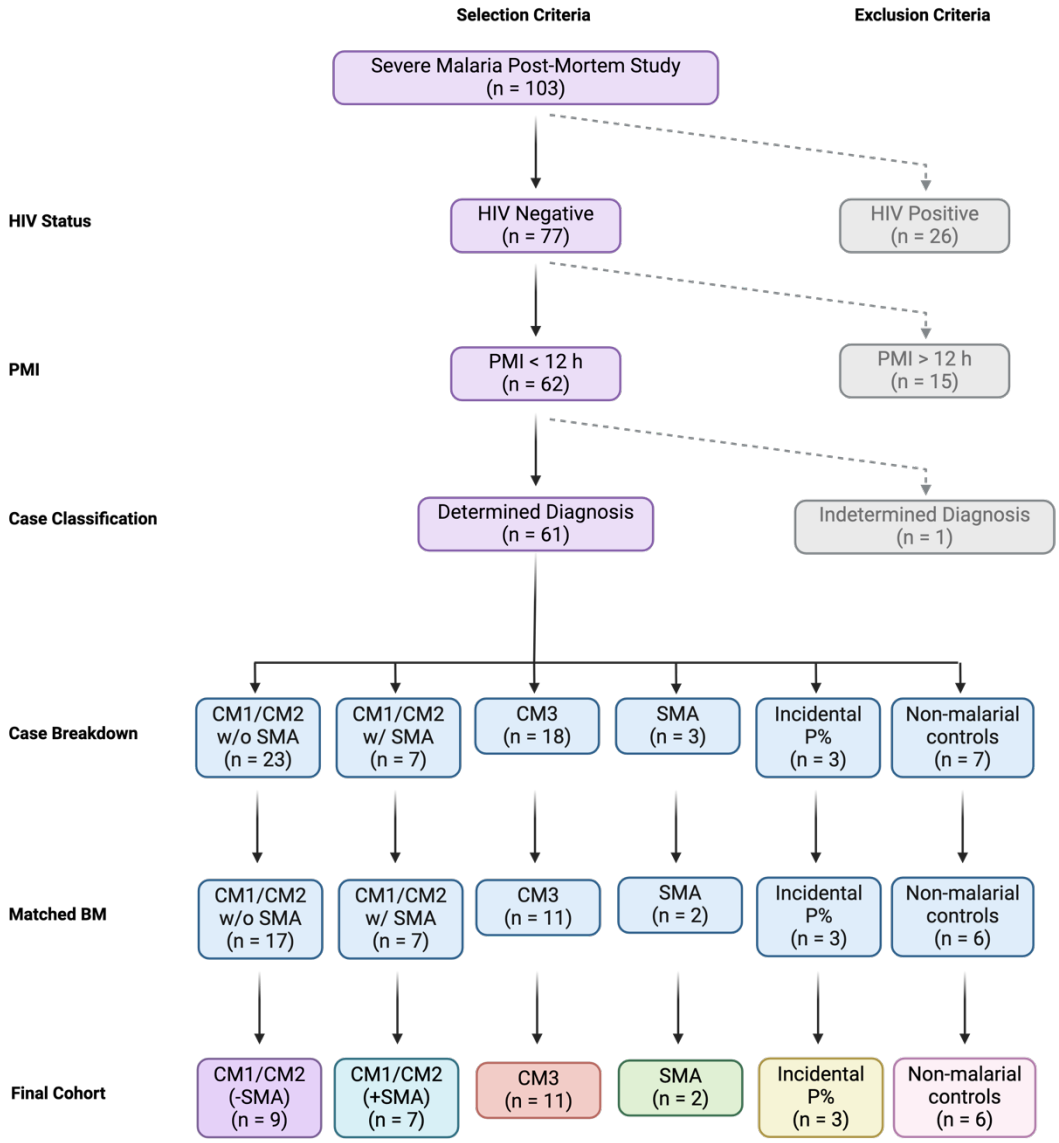

Figure 3-2. Flow chart of case selection. From the 103 patients enrolled in the severe malaria post-mortem study, cases were selected based on HIV status, post-mortem interval (PMI) and case determination. Cases were grouped into 6 categories based on diagnosis and anaemic status. Cases without matched bone marrow (BM) and spleen formalin-fixed, paraffin embedded (FFPE) tissue blocks in the Glasgow repository were excluded. Finally, CM1/CM2 cases without severe malarial anaemia (SMA) were further refined by prioritising cases used in Joice *et al.* and De Niz *et al.* (Taylor et al., 2004, Joice et al., 2014, De Niz et al., 2018). Abbreviations: PMI, postmortem interval; BM, bone marrow; CM, cerebral malaria; SMA, severe malarial anaemia. Figure created with BioRender.com.

Table 3-1. Patient information for malaria cases and non-malarial controls.

PM case	Age (months)	Height (cm)	Weight (kg)	Clinical Diagnosis	Adm PCV (%)	Last PCV (%)	Normal Hct Ranges (%)	Anaemia Status on Adm	Last Anaemia Status	Duration of Fever (h)	Parasitaemia on Admission (parasites/µL)	Last Parasitaemia Before Death (parasites/µL)	Time to death (h)	Spleen Weight (gm)	Normal Spleen Weight Ranges (gm)	Splenomegaly Status	Pre-admission Treatment	Blood Transfusion	PMI (h)	Study Group
CM1/CM2 w/o SMA																				
16	51	93	15	Clinical CM	27	18	23.60-38.80	Normal	Anaemic	24	125950	70990	5	100	16-98	Splenomegaly	Qn	No	3	CM1/2 (-SMA)
21	25	93	11.8	Clin CM	29		21.5-39.10	Normal		18	9464	280	12	127	16-86	Splenomegaly	N/A	No	7.75	CM1/2 (-SMA)
26	30	90	10.3	Clin CM	23	18	21.5-39.10	Normal	Anaemic	48	442705	45358	30	80	16-98	Normal	Qn	Yes	6.5	CM1/2 (-SMA)
28	61	92	9.5	Clin CM	18	18	21.90-50.40	Anaemic	Anaemic	120	424000	424000	0	105	19-105	Normal	SP	No	2.25	CM1/2 (-SMA)
66	14	71	7.4	Clinical CM	35	28	26.30-40.70	Normal	Normal	28	1458425	840	40	68	19-59	Splenomegaly	N/A	No	3.75	CM1/2 (-SMA)
78	15	79	9.5	Clinical CM	28	28	26.30-40.70	Normal	Normal	12	637000	637000	2	125	22-55	Splenomegaly	N/A	No	3.75	CM1/2 (-SMA)
82	31	93	12	Clinical CM + pneumonia	17	27	21.5-39.10	Anaemic	Normal	72	197820	0	56	116	16-86	Splenomegaly	SP	Yes	6.25	CM1/2 (-SMA)
83	26	84	10.8	Clinical CM	20	20	21.5-39.10	Anaemic	Anaemic	72	22000	6000	22	83	16-86	Normal	CQ	No	4.75	CM1/2 (-SMA)
102	42	86	10.7	Clinical CM	20	17	23.60-38.80	Anaemic	Anaemic	120	364	0			20-90		SP	No	4	CM1/2 (-SMA)
CM1/CM2 w/ SMA																				
5	14	73	9.1	Clin CM	21	13	26.30-40.70	Anaemic	Severe	72	81700	43700	18	76	19-59	Splenomegaly	N/A	No	2.25	CM2 (+SMA)
6	17	72	8.1	Clin CM + SMA	15	15	26.30-40.70	Severe	Severe	72	69,230	69230	1	47	23-71	Normal	N/A	No	4	CM2 (+SMA)
15	8	64	6.8	Clin CM + SMA	12	21	26.40-40.80	Severe	Anaemic	22	11300	0	12	50	17-43	Splenomegaly	N/A	Yes	5.25	CM2 (+SMA)
36	22	75	7.5	Clinical CM + SMA	13		22.70-44.10	Severe		72	11399	6348	11	44	18-88	Normal	N/A	Yes	10.75	CM2 (+SMA)
48	48	93	10	Clinical CM	15	15	23.60-38.80	Severe	Severe	72	425	425	22	88	16-98	Normal	CQ/Qn	No	2	CM2 (+SMA)
61	26	82	10	Clinical CM	15	15	21.5-39.10	Severe	Severe	120	42027	42027	4	78	16-86	Normal	Qn	No	4.75	CM2 (+SMA)
85	33	79	9.3	Clinical CM + SMA	16	15	21.50-39.10	Anaemic	Severe	72	103	0	10	111	16-86	Splenomegaly	Qn	Yes	8.45	CM2 (+SMA)
CM3																				
22	18	82	12.2	Clin CM - hepatic necrosis	16	15	26.30-40.70	Anaemic	Severe	120	250	250	135	125	18-72	Splenomegaly	SP	No	2.5	CM3
33	25	73	10.5	Clinical CM - path viral pneumonia Reye's	25	22	21.50-39.10	Normal	Normal	24	4716	5845	15	80	16-86	Normal	N/A	No	2.5	CM3
45	28	75	8.7	Clinical CM, S. pn pneumonia	40	38	21.50-39.10	Polycythaemia	Normal	9	100519	100519	28	107	16-86	Splenomegaly	N/A	No	9	CM3
47	22	83	8.8	Clinical CM - viral pneumonia Reye's	30	24	22.70-44.10	Normal	Normal	12	338303	133	44	73	18-88	Normal	Qn	No	4.25	CM3
67	48	104	16	Clinical CM, S. pn pneumonia	30	30	23.60-38.80	Normal	Normal	48	266	266	5	169	16-98	Splenomegaly	N/A	No	10.25	CM3
71	60	104	13.9	Clinical CM; subdural/intracerebral hematomas	39	39	23.60-38.80	Polycythaemia	Polycythaemia	12	314	314	2	157	19-105	Splenomegaly	N/A	No	5	CM3
73	14	72	8.5	Clinical CM; ? Severe pneumonia	31	22	26.30-40.70	Normal	Anaemic	18	35000	0	84	57	19-59	Normal	SP	No	7.25	CM3
80	63	110	15	Clinical CM, meningoencephalitis	28	27	21.90-50.40	Normal	Normal	7	23700	63200	8	144	19-105	Splenomegaly	N/A	No	9.25	CM3
81	21	88	11	Clinical CM, pneumonia, meningoencephalitis	42	41	22.70-44.10	Normal	Normal		1460	0	16	32	15-73	Normal	N/A	No	7	CM3
87	34	89	10	Clinical CM, severe pneumonia with spread to meninges	36	25	21.50-39.10	Normal	Normal		1040520	0	60	96	16-86	Splenomegaly	N/A	No	3.75	CM3
103	31	88	12	Clinical CM, fatal pneumonia	34	35	21.50-39.10	Normal	Normal	9	226800	0			16-86		Qn	No	5.75	CM3
SMA																				
30	7	71	7.3	SMA	8	8	26.40-40.80	Severe	Severe	48	302400	302400	2	43	13-49	Normal	N/A	Yes	2.25	SMA
57	49	84	10	Severe malarial anemia Reye's	7	7	23.60-38.80	Severe	Severe	168	164	164	4	90	16-98	Normal	SP	No	10.75	SMA
Incidental Parasitaemia																				
70	108	122	26	Acute renal failure + incidental parasitemia	18	16	21.90-50.40	Anaemic	Anaemic		87	0	37	110	27-179	Normal	N/A	No	9	IP
77	7	68	6.6	Small bowel obstrx, incidental parasitemia	25	25	26.40-40.80	Anaemic	Anaemic		66844	66844	7	50	13-49	Splenomegaly	SP/Qn	No	4.5	IP
40	26	97	10.7	COC (probable sepsis)	40	38	21.50-39.10	Polycythaemia	Normal	24	597	0	64	45	16-86	Normal	Qn	No	5.25	IP
Non-Malarial Controls																				
12	6	59	6.5	COC (anemia, sepsis)	11	11	24-50-40-80	Severe	Severe	72	0	0	4	88	11--43	Splenomegaly	SP	No	11.5	NMC
18	7	68	6.4	COC (H. flu meningitis)	27	27	26.40-40.80	Normal	Normal	48	0	0	14	16	13-49	Normal	SP	No	8.5	NMC
20	96	122	20.5	COC (TB meningitis)	49	58	21.90-50.40	Normal	Polycythaemia	72	0	0	20	48	18-164	Normal	N/A	No	6.5	NMC
56	63	98	12	Coma, unknown etiology	25	27	21.90-50.40	Normal	Normal		0	0	60	53	19-105	Normal	Qn	No	4.75	NMC
72	96	112	16	COC-Salmonella sepsis	26	26	21.90-50.40	Normal	Normal		0	0	26	91	18-164	Normal	SP	No	3.5	NMC
88	63	87	9	Non-malarial coma (subdural haematoma due to head trauma)	25	25	21.90-50.40	Normal	Normal		0	0	4	83	19-105	Normal	N/A	No	12	NMC

Table is colour coded according to clinical group. Where a case was reclassified, the colour of the post-mortem (PM) number is coloured to match that of the original classification. Clinical diagnosis was taken from the original diagnosis of cases (Taylor et al., 2004). Normal packed cell volume (PCV) reference ranges were taken from

age related changes in haematological parameters in healthy Malawians (Mandala et al., 2017). Normal spleen weight reference ranges were based on age, taken from Molina *et al.,* 2019 (Molina et al., 2019).
Abbreviations: PM, post-mortem; CM, cerebral malaria; SMA, severe malaria anaemia; S. pm, *Streptococcus pneumoniae;* obstrx, obstruction; COC, cause of coma; Adm, admission; PCV, packed cell volume, PMI, post-mortem interval; Qn, quinine dihydrochloride.

Baseline characteristics were generated for the cohort, and for individual clinical groups (summarised in **Table 3-2**). The median age of the cohort was 27 months with a range of 6 months to 9 years old. All patients were treated with intravenous quinine dihydrochloride. Quinine infusions continued until four consecutive blood smears were deemed negative for parasitaemia (Taylor et al., 2004). Haematocrit, or packed cell volume (PCV), was measured six-hourly throughout hospitalisation. The median PCV of patients was 25% (interquartile range (IQR): 16% to 31%) which in general was reduced during hospitalisation to a median PCV of 22% (IQR: 15% to 28%). Based on PCV, 17 (45%) patients were anaemic on admission (including SMA) and 18 (47%) patients were anaemic according to the last measurements taken prior to death. Anaemic status was classified according to PCV reference ranges per age group for healthy Malawians where cases with a PCV less than 15% were considered severe (Mandala et al., 2017). At post-mortem, all organs were weighed including the spleen. The median spleen weight of the cohort was 83 g (IQR: 50 g to 110 g) where 16 (42%) patients were considered to have splenomegaly based on paediatric spleen weight reference ranges (Molina et al., 2019). Blood transfusions were administered to 6 (16%) patients during hospitalisation (**Table 3-2**).

Across clinical groups, the highest median admission parasitaemia was in CM1/CM2 (-SMA) cases. In general, all clinical groups observed a reduction in parasitaemia throughout hospitalisation (**Figure 3-3B**). As expected, admission and last PCV measurements were lowest for clinical groups with SMA. CM2 (+SMA) and SMA cases had a median admission PCV of 15% (IQR: 14% to 16%) and 8% (IQR: 7% to 8%) respectively (**Figure 3-3C)**. The same clinical groups had the shortest median time to death of 11 h (IQR: 7 to 15 h) and 3 (IQR: 3 to 4 h) for CM2 (+SMA) and SMA respectively (**Figure 3-3D**). Splenomegaly was most frequently observed in CM1/CM2 (-SMA) cases with 5 (56%) patients considered to have splenomegaly, followed by 6 (55%) CM3 patients and 3 (43%) CM2 (+SMA) patients. Due to small sample sizes within some clinical groups, most analyses in this thesis focused on comparing malaria cases to non-malarial controls to achieve statistical significance. Where relevant, comparisons were made between clinical groups.

Table 3-2. Baseline characteristics of malaria cases and non-malarial controls.

		Clinical Groups					
Parameters	All Patients (n = 38)	CM1/CM2 (-SMA) (n=9)	CM2 (+SMA) (n=7)	CM3 (n=11)	SMA (n=2)	IP (n=3)	NMC (n=6)
Age in months (median [IQR])	27 (17-48)	30 (25-42)	22 (16-30)	28 (21-41)	28 (18-39)	26 (17-67)	63 (7-88)
Adm parasitaemia (median [IQR])	29350 (554-212310)	197820 (22000-442705)	11399 (5863-55629)	23700 (887-163660)	151282 75723-226841)	587 (342-33721)	N/A
Last parasitaemia before death (median [IQR])	370 (0-44529)	6000 (280-700990)	6348 (213-42864)	250 (0-3080)	1282 (75723-226841)	0 (0-33422)	N/A
Adm PCV (median [IQR])	25 (16-31)	23 (20-28)	15 (14-16)	31 (29-38)	8 (7-8)	25 (22-33)	26 (25-27)
Last PCV (median [IQR])	22 (15-28)	19 (18-27)	15 (15-15)	27 (23-37)	8 (7-8)	25 (21-32)	27 (26-27)
Anaemic Status on Adm (n/N [%])	17 (45)	4/9 (44)	7/7 (100)	1/11 (9)	2/2 (100)	2/3 (67)	1/6 (17)
Last Anaemic Status (n/N [%])	18 (47)	5/9 (56)	6/7 (86)	2/11 (16)	2/2 (100)	2/3 (67)	1/6 (17)
Duration of fever (median [IQR])	48 (20-72)	48 (24-72)	72 (72-72)	12 (9-24)	108 (78-138)	24 (24-24)	72 (60-72)
Time to death (median [IQR])	14 (5-37)	17 (4-33)	11 (7-15)	22 (10-56)	3 (3-4)	37 (22-51)	17 (14-25)
Treatment pre-admission (n/N [%])	20 (53)	6/9 (67)	3/7 (43)	4/11 (36)	1/2 (50)	2/3 (67)	4/6 (67)
Spleen weight in grams (median [IQR])	83 (50-110)	103 (82-118)	76 (49-83)	102 (75-139)	67 (55-78)	50 (48-80)	68 (48-87)
Splenomegaly (n/N [%])	16 (42)	5/9 (56)	3/7 (43)	6/11 (55)	0/2 (0)	1/3 (33)	1/6 (17)
Transfusion during hospitalisation (n/N [%])	6/38 (16)	2/9 (22)	3/7 (43)	0/11 (0)	1/2 (50)	0/3 (0)	0/6 (0)

Abbreviations: IQR, interquartile range; Adm, admission; PCV, packed cell volume; CM, cerebral malaria; SMA, severe malarial anaemia; IP, incidental parasitaemia; NMC, non-malarial controls.

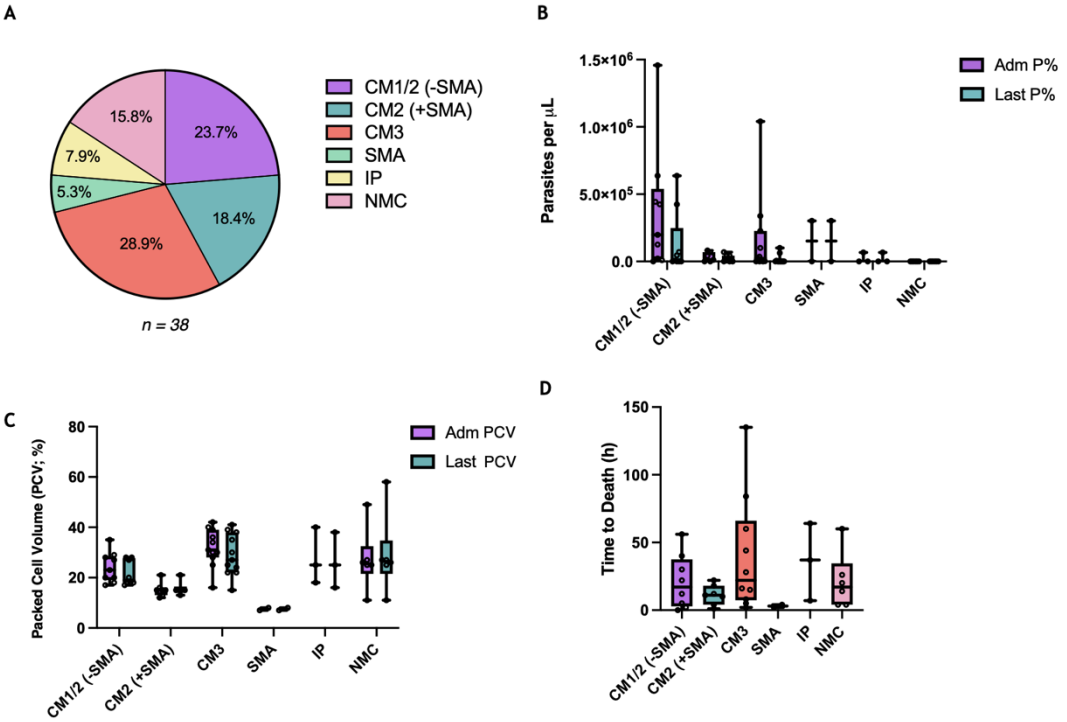

Figure 3-3. Baseline characteristics of malaria cases and non-malarial controls. (**A**) Pie chart showing the proportion of each clinical group in the cohort. (**B**) Parasitaemia (P%) as parasites per µL of blood on admission (Adm %) and last reading before death (Last P%) per clinical group. (**C**) Packed cell volume (PCV), per clinical group on admission (Adm PCV) and last reading before death

(Last PCV). (**D**) Time to death from admission in hours. Symbols represent individual patients. Abbreviations: CM, cerebral malaria; SMA, severe malarial anaemia; IP, incidental parasitaemia; NMC, non-malarial controls, Adm, admission; P%, parasitaemia.

3.3 Technical Considerations: BM Decalcification

Before performing histological studies, tissue blocks were assessed for quality. Many BM samples were not sufficiently decalcified prior to tissue processing and embedding limiting their use. Without decalcification, mineralised tissue such as bone is difficult to section without tissue damage. Therefore, I investigated whether decalcifying bone post processing and embedding would have a detrimental effect on tissue structure and epitopes. Routinely used methods of decalcification and fixation can cause significant mRNA degradation (Masuda et al., 1999, Shao et al., 2006, Salmon et al., 2012, Belluoccio et al., 2013, Miquelestorena-Standley et al., 2020, Al-Maawi et al., 2022). Since these tissues will ultimately be used for spatial transcriptomic approaches, it was imperative to use a method of decalcification that will optimally preserve mRNA. Therefore, a novel decalcification approach proposed by Belluoccio *et al.*, which utilises 10% ethylene-diamine-tetraacetic acid (EDTA) in RNA*later* to decalcify bone whilst preserving mRNA integrity, was tested (Belluoccio et al., 2013). Before applying this technique to human samples, this approach was tested on bones harvested from mice.

Femurs were harvested from *P. berghei* infected (n=3) or naïve mice (n = 1). From each mouse, one bone was immediately decalcified, forward processed, and embedded to generate a FFPE BM block (decal prior). The second bone was processed and embedded immediately without decalcification. This latter FFPE block was then melted, reverse processed and decalcified for the required length of time (**Section 2.2.4**). Decalcification times for mouse bones were typically between 5 to 7 days. Now decalcified, the bone was forward processed as before and embedded in wax to generate a decalcified FFPE BM block (decal post). Sections were cut for H&E staining, Giemsa staining, IHC and RNAscope. Staining intensity and/or signal was compared between the two conditions (**Figure 3-4**)

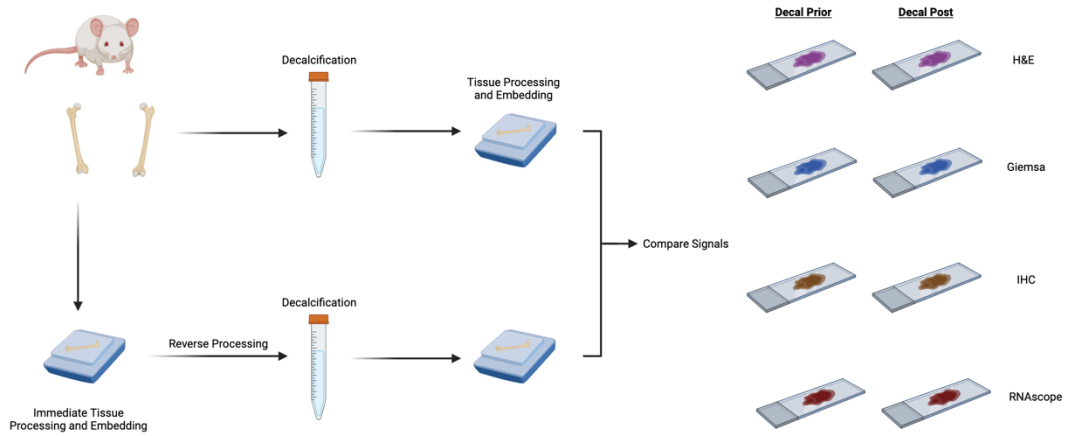

Figure 3-4. Bone marrow (BM) decalcification experimental outline. Bones were harvested from *P. berghei* infected or naïve TO mice. Bones were either processed and embedded immediately or underwent decalcification. Decalcified bones were processed and embedded after decalcification (decal prior) to generate a formalin fixed, paraffin embedded (FFPE) tissue block. FFPE blocks from bones that were immediately processed without decalcification were melted, reverse processed and decalcified. They were then re-processed and re-embedded to generate FFPE blocks (decal post). Sections were subjected to histological stains: haematoxylin & eosin (H&E), Giemsa, immunohistochemistry (IHC) and RNAscope in parallel. Staining intensity and/or signal was compared between the two conditions. Abbreviations: H&E, haematoxylin and eosin; IHC, immunohistochemistry.

3.3.1 Basic Staining: H&E and Giemsa

To determine whether time at which tissues were decalcified in relation to processing and embedding resulted in basic staining variation and tissue morphology alterations, two basic histological stains were performed: H&E and Giemsa. No differences were observed in staining patterns or tissue morphology for both H&E and Giemsa-stained sections. By Giemsa, *P. berghei*-iRBCs in both 'decal prior' and 'decal post' BM were identified (**Figure 3-5**).

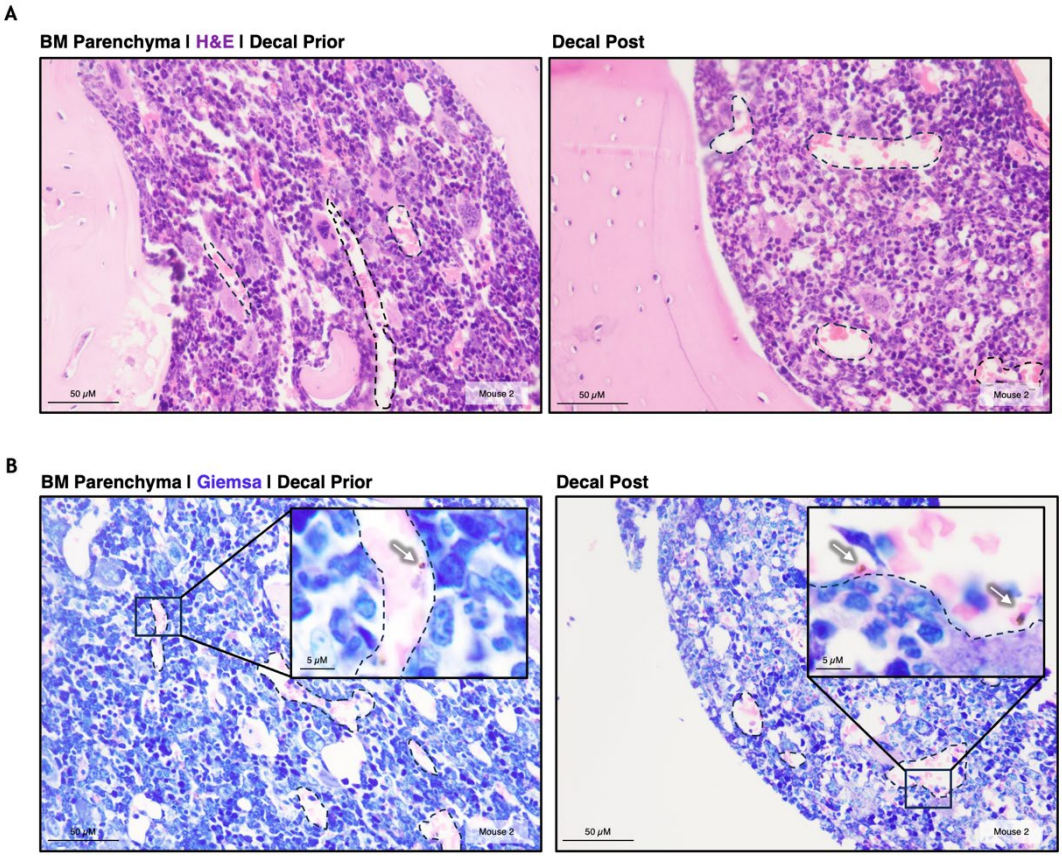

Figure 3-5. Decalcification does not induce changes in H&E and Giemsa-stained bone marrow (BM) sections. Bones from *P. berghei* infected mice were harvested and either decalcified prior to (decal prior) or post (decal post) tissue processing and embedding. (**A**) H&E-stained BM sections. (**B**) Giemsa-stained BM sections. Zoomed in panels highlight *P. berghei* infected RBCs (iRBC, indicated by white arrows) in the sinus lumen. Dashed black line represents the sinusoidal lining. Abbreviations: BM, bone marrow; H&E, haematoxylin and eosin; decal, decalcified.

3.3.2 HSP70 IHC

To determine whether decalcifying post tissue processing and embedding had a detrimental effect on tissue epitopes, IHC was performed using antibodies against the conserved constitutive parasite protein, heat shock protein 70, HSP70 (LSBio; LS-C109068) (Shonhai et al., 2007). IHC was successful in all BM tissues with no differences observed in staining intensity between 'decal prior' and 'decal post' BM (**Figure 3-6A**).

It was assumed that parasite load would be similar between parallel bones from within the same mouse. Therefore, HSP70+ parasites were quantified in each tissue and compared to determine if there was a significant difference indicative of false negatives. There was no significant difference between counts in 'decal

prior' bones compared to 'decal post' bones (p=0.82) (**Figure 3-6B**). Therefore, decalcification after tissue processing and embedding does not have a detrimental effect on tissue epitopes for IHC.

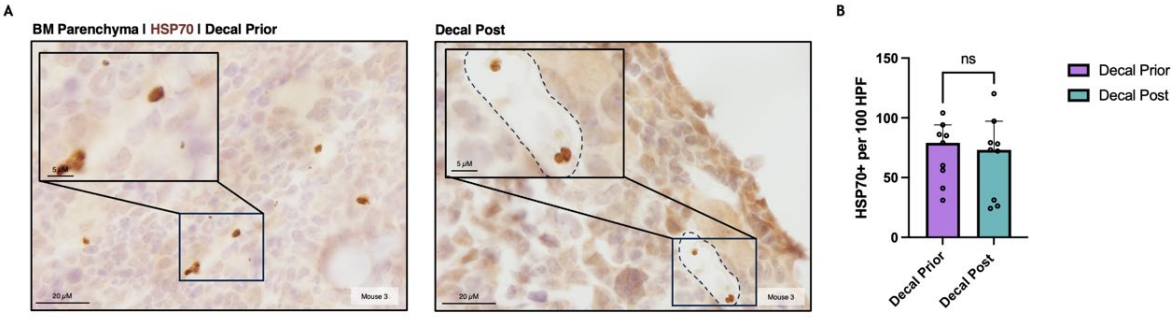

Figure 3-6. Decalcification does not induce changes in IHC staining. (**A**) Detection of *P. berghei* infected RBCs (iRBCs) in mouse bone marrow (BM). Representative images of BM from *P. berghei* infected mice which were either decalcified prior to (decal prior) or post (decal post) tissue processing and embedding. Parasites were labelled using antibodies against HSP70 (brown; chromogen DAB). Black dashed lines represent sinusoid lining. (**B**) Quantification of parasite loads in BM tissue. Number of HSP70+ parasites per 100 high powered fields (HPF) for each organ. Parasite loads are shown as median with 95% confidence interval. There was no statistical difference (ns) between parasite loads in BM decalcified before or after processing and embedding (p=0.82). Statistical test used was Wilcoxon matched pairs signed-rank test. Symbols represent individual replicates (3 biological replicates with 3 technical replicates). Abbreviations: BM, bone marrow; decal; decalcified; HPF, high powered field.

3.3.3 *Mm-PolR2A* RNAscope

RNA *in situ* hybridisation was used to determine whether decalcifying BM post tissue processing and embedding had a detrimental effect on RNA integrity (Wang et al., 2012). Here, the standard positive control probe which targets murine RNA polymerase II subunit A mRNA, *Mm-Polr2A*, was used (ACD, NM_009089.2). Naïve murine spleen was used as a positive control tissue. Spleen was fixed for the same amount of time as BM, however, did not undergo any decalcification. This enabled an assessment of the potential impact of decalcification on RNA integrity. There was expression of *polr2a* throughout splenic tissue, however, expression was highest in the WP likely due to the higher nuclear cell density in this compartment (**Figure 3-7A, B**).

Variation in the distribution of *polr2a* expression by RNAscope was observed across all BM tissues (**Figure 3-7C**). This may suggest some level of mRNA degradation

occurred in some areas. Overall, signal intensity was similar between decal prior and decal post BM tissue. To quantify expression levels, qualitative scoring was performed based on ACD scoring guidelines (detailed in **Section 2.3.5, Table 2.5**). This was performed by hand however image analysis software tools such as Visiopharm® have been considered. Staining intensity, indicative of gene expression levels, was assessed in five randomly selected regions of interest within each tissue and scored between 0 and 4. Scores between tissues which were decalcified prior to or post processing and embedding were not different (**Figure 3-7B**).

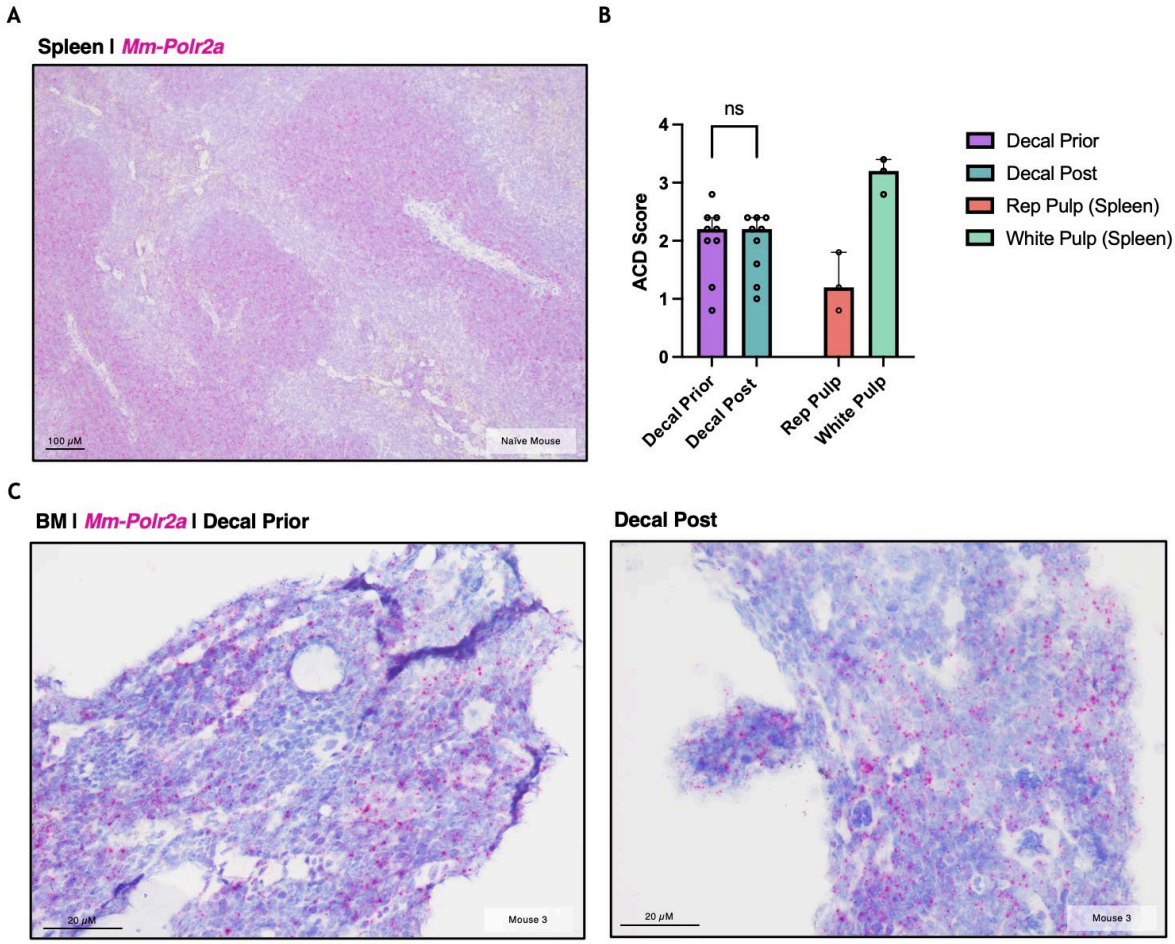

Figure 3-7. Decalcification does not Induce changes in RNAscope staining. RNAscope targeting *Mm-Polr2a* was performed on matched *P. berghei* infected bone marrow (BM) that was either decalcified prior ('decal prior') or post ('decal post') forward processing and embedding. (**A**) Representative image of *Mm-Polr2a* expression in naïve murine spleen. (**B**) Scoring was performed based on the number of punctate dots observed in each cell over five regions of interest per tissue. Each punctate dot represents a single copy of mRNA. Data is displayed as median with 95% confidence interval. There was no significant difference (ns) between scores in BM decalcified prior (decal prior) compared to BM decalcified after (decal post) processing and embedding ($p = 0.93$). Statistical test used was Wilcoxon matched pairs signed-rank test. Symbols represent individual replicates (3 biological replicates with 3 technical replicates for BM; 3 technical

replicates for spleen control). (**C**) Representative images of *Mm-Polr2a* expression in decalcified Abbreviations: BM. BM, bone marrow; decal, decalcified.

Overall, decalcification after tissue processing and embedding does not have a detrimental effect on tissue structure, staining patterns, or tissue epitopes. The process of decalcification itself will likely result in a level of degradation of mRNA, however, the protocol used here is designed to minimise this degradation.

3.4 Histopathology of the BM and Spleen

No in-depth studies into the histopathology of the BM and spleen in paediatric severe malaria have been performed. Therefore, I aimed to perform a detailed semi-quantitative histopathological scoring of the BM and spleen in the Malawi cohort of paediatric severe malaria and non-malarial controls. Based on previously identified histopathological features of the spleen and BM, as described in **Section 3.1.2** and **Section 3.1.3**, a detailed histopathological scoring criteria was generated.

3.4.1 Histopathology of the BM: Whole Cohort

BM sections were stained with H&E and scored by a comparative pathologist (board certified of the American College of Veterinary Pathologists) blinded to patient and clinical information. Where available, Giemsa-stained sections were used to assist with scoring. Parameters for scoring included cellularity, pigmentation, number and distribution of megakaryocytes, myeloid-to-erythroid (M:E) ratio, presence of suspected iRBCs, and elevation of eosinophils and macrophages. Left shifts, characterised by a higher proportion of immature cell types relative to mature cell types (**Figure 3-1**), were also evaluated in the megakaryocytic, granulocytic, and erythroid lineages. Note that complete evaluation of these cell lineages requires cytology aspirates which were not available for this cohort. Parameters were scored between 0-4 where 0 denotes that the feature is not present and 4 denotes a marked appearance (**Section 2.2.8**). In total, histopathological scoring was performed on 19 BM sections. The findings from this histopathological scoring are summarised in **Table 3-3**.

Malaria cases (consisting of all parasitaemic cases) were first compared to non-malarial controls. The presence of iRBCs was noted in 78% of malaria cases and largely absent in non-malarial controls as expected (**Figure 3-8A**). Note that a lower number of tissues were analysed for the presence of iRBCs as it was not always possible to define the sinusoids. Mild pigmentation throughout the BM was observed in malaria cases, while no pigmentation was evident in non-malarial controls (**Figure 3-8**). The absence of pigment in non-malarial controls implies that the observed pigment is likely haemozoin; however, it is not possible to determine if this pigment is haemozoin, haemosiderin, or formalin pigment using H&E-stained sections alone. To distinguish between pigments, Prussian blue stains should be performed (Rebelatto, 2018).

Megakaryocytes had a diffuse distribution across all cases. Dysplastic changes in megakaryocytes, such as hyperlobated megakaryocytes or micro-megakaryocytes, were observed in 47% of malarial cases and 25% of non-malarial controls (Mair et al., 2013). Complete granulocytic and erythroid lineages were observed in both malaria cases and non-malarial controls. In malaria cases, a left shift in the erythroid lineage was observed in 7% of cases with 47% exhibiting a left shift in the granulocytic lineage. In contrast, there were no cases of left shifts in the erythroid lineage for non-malarial control, with only 1 case exhibiting a left shift in the granulocytic lineage. An elevation in eosinophils was observed in 53% of malaria cases but not observed in non-malarial controls. Similarly, there was a mild increase in macrophages in malaria cases while non-malarial cases showed only a minimal increase (**Figure 3-8B, Table 3-3**).

The M:E ratio compares the proportion of myeloid (granulocytes and monocytes) to erythroid cells (Elmore, 2006). The M:E ratio can be informative with high M:E ratio indicative of increased demand/granulopoiesis (e.g., due to infection and inflammation) or decreased erythroid lineage, whereas a low M:E ratio can be indicative of decreased leukopoiesis or erythroblast proliferation (e.g., secondary to anaemia). In malaria and non-malarial cases, the M:E ratio was within the reference range for the median age of the cohort, although note that there were few cases where this M:E ratio exceeded the limits of the reference range for this age (2 years and 3 months, reference M:E ratio: 3-4:1) (Proytcheva, 2013).

There was no gross evidence of haemorrhage, inflammation, necrosis or fibrosis across malaria patients and non-malarial controls as evaluated by a comparative pathologist specialising in these organs using H&E stained tissue sections.

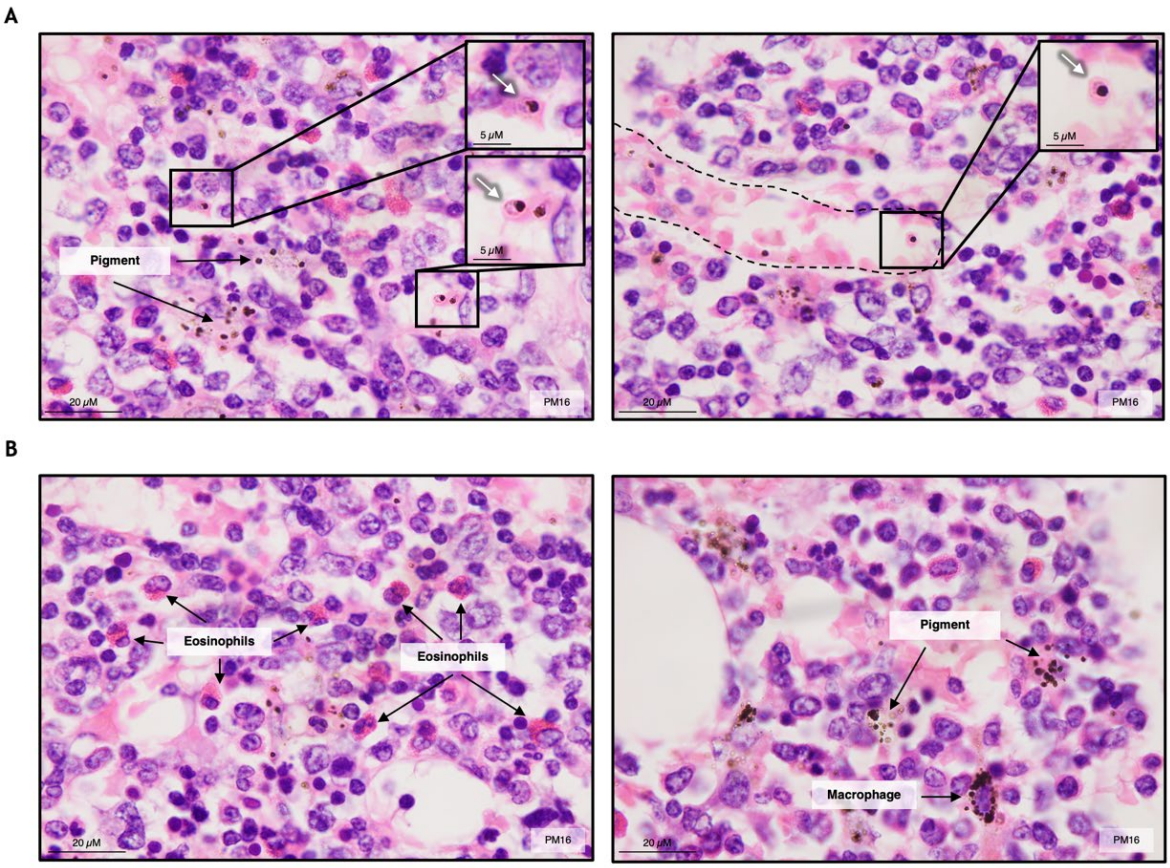

Figure 3-8. Infected RBCs (iRBC), eosinophils, macrophages, and pigment in the bone marrow (BM) of paediatric severe malaria patients. Pigment was observed throughout malaria cases. (**A**) iRBCs were identified in the BM parenchyma and in BM sinusoids. White arrows are used to indicate iRBCs. (**B**) Malaria cases displayed an elevation of eosinophils and a mild increase in macrophages. A macrophage containing phagocytosed pigment is indicated. Black dashed lines outline sinusoids.

3.4.2 Histopathology of the BM: Per Clinical Group

Despite the low sample numbers for some clinical groups, an impression of overall differences between each clinical group can be obtained. While the brain was not the focus of this study, it is unclear whether different CM classifications exhibit distinct BM responses to *Plasmodium* infection. In CM1/CM2 cases, there was mild to moderate pigmentation observed in the BM whereas in CM3, SMA and incidental parasitaemia cases, there was minimal to no pigment observed. iRBCs were observed in all CM1/CM2 cases, however, they were less frequently observed in

other malaria clinical groups. Left shifts in the megakaryocytic and granulocytic lineages were only observed in CM1/CM2 cases. Only one SMA case exhibited a left shift in the erythroid lineage. In general, the M:E ratio was higher in CM1/2 cases, compared to non-CM and CM3 cases (**Table 3-3**).

Table 3-3. Summary of BM histopathology scoring.

Histological Parameter	Malaria	Non-malarial controls	CM1/CM2 (-SMA)	CM2 (+SMA)	CM3	SMA	IP
Number analysed	15	4	5	4	3	2	1
Pigmentation	Mild	Not Present	Mild	Moderate	Minimal	Minimal	Not Present
Presence of iRBCs (n/N [%])	7/9 (78)	1/4 (25)	5/5 (100)	1/1 (100)	1/2 (50)	0/1 (0)	N/A
Megakaryocytic Lineage							
Average number under 40x (Median [range])	4 (2-7)	3 (2-3)	3 (2-3.5)	5 (4-7)	5 (4-5)	4 (4-5)	2
Left shift (n/N [%])	4/15 (27)	0/4 (0)	2/5 (40)	3/4 (75)	0/3 (0)	0/2 (0)	0/1 (0)
Possible dysplastic changes (n/N [%])	7/15 (47)	1/4 (25)	4/5 (80)	3/4 (75)	0/3 (0)	0/2 (0)	0/1 (0)
Granulocytic Lineage							
Left shift (n/N [%])	7/15 (47)	1/4 (25)	4/5 (80)	3/4 (75)	0/3 (0)	0/2 (0)	0/1 (0)
Elevation in eosinophils (n/N [%])	8/15 (53)	0/4 (0)	3/5 (60)	3/4 (75)	1/3 (33)	1/2 (50)	0/1 (0)
Erythroid Lineage							
Left Shift (n/N [%])	1/15 (7)	0/4 (0)	0/5 (0)	0/4 (0)	0/3 (0)	1/2 (50)	0/1 (0)
Elevated macrophages	Mild	Minimal	Mild	Moderate	Not Present	Mild	Not Present
Estimation of M:E ratio (Median [range])	4 (0.8-5.5)	3 (1-6)	5 (4.5-5.5)	4 (3.5-5)	3 (2-4)	2 (0.8-4)	3

Abbreviations: iRBC, infected red blood cell; M:E ratio, myeloid:erythroid ratio; CM, cerebral malaria; SMA, severe malarial anaemia; IP, incidental parasitaemia.

3.4.3 Multivariant Analysis of BM Histopathological and Patient Clinical Parameters

To investigate whether histopathological parameters alone were enough to separate clinical groups, a principal component analysis (PCA)-biplot was generated. This would allow the determination of distinct groups based on histopathological and clinical parameters, and the parameters responsible for these group separations. Here, binary transformation was applied to dichotomous parameters, such as the presence of iRBCs, assigning a value of 1 for 'yes/present' and 0 for 'no/not present'.

The PCA-biplot was initially coloured according to malaria cases and non-malarial controls (**Figure 3-9A**). From this initial PCA-biplot, malaria cases and non-malarial controls did not cluster separately. To determine whether each clinical

group clustered separated, the PCA-biplot was coloured according to clinical diagnosis. Individual clinical groups did not form distinct clusters (**Figure 3-9B**).

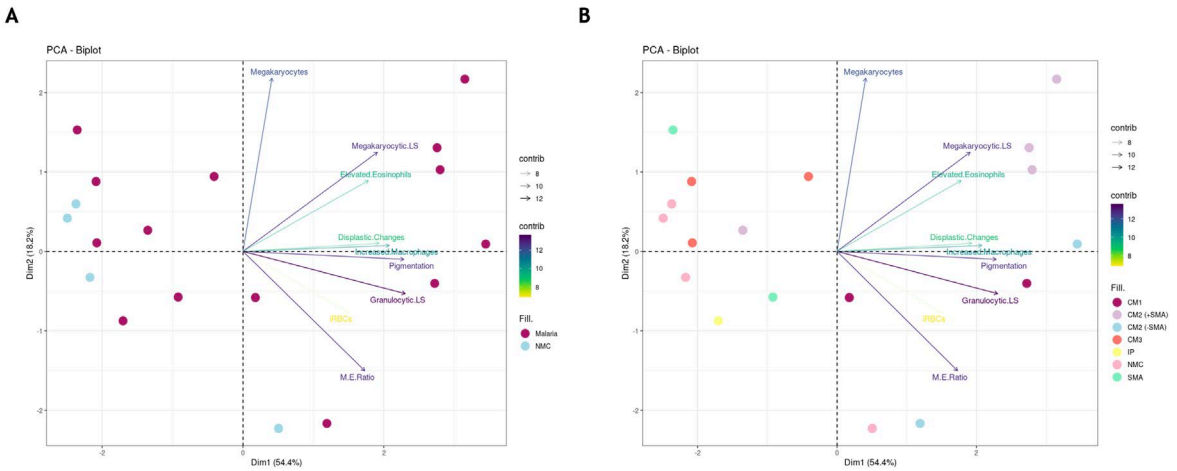

Figure 3-9. Multivariant analysis reveals no distinct subgroups in the bone marrow (BM). (**A**) PCA-biplot categorising malaria (purple) patients and non-malarial controls (blue). (**B**) PCA-biplot categorising patients according to clinical diagnosis. Abbreviations: LS, left shift; M.E.Ratio; myeloid:erythroid ratio; contrib, contribution; CM, cerebral malaria; SMA, severe malarial anaemia; IP, incidental parasitaemia; NMC, non-malarial controls.

PCA-biplots give an indication of correlations between parameters. To expand on this, a correlation matrix plot was generated to investigate the significant correlations between histopathologic parameters and clinical parameters. Clinical parameters included age, admission parasitaemia, last parasitaemia before death, admission PCV, last PCV before death, time to death, and duration of fever.

From this correlation matrix, several significant correlations were identified. Several parameters relating to parasites in the BM (presence of iRBCs and pigmentation) positively correlated with dysplastic changes in megakaryocytes, granulocytic left shifts, increased macrophages, and a higher M:E ratio. In turn, admission parasitaemia was positively correlated with both pigmentation and the presence of iRBCs. Elevated eosinophils were also positively correlated with increased macrophages, megakaryocytic left shift, pigmentation, and presence of iRBCs. Therefore, the presence of parasites in the BM impacts several histopathological features (**Figure 3-10**).

There were several significant negative correlations between clinical and histopathological parameters in the BM. Elevated macrophages were negatively correlated with both time to death and last PCV. Since the time to death was positively correlated with last PCV, this suggests that an increased number of macrophages is associated with a low PCV (i.e., anaemia), which in turn is associated with a short time to death (**Figure 3-10**).

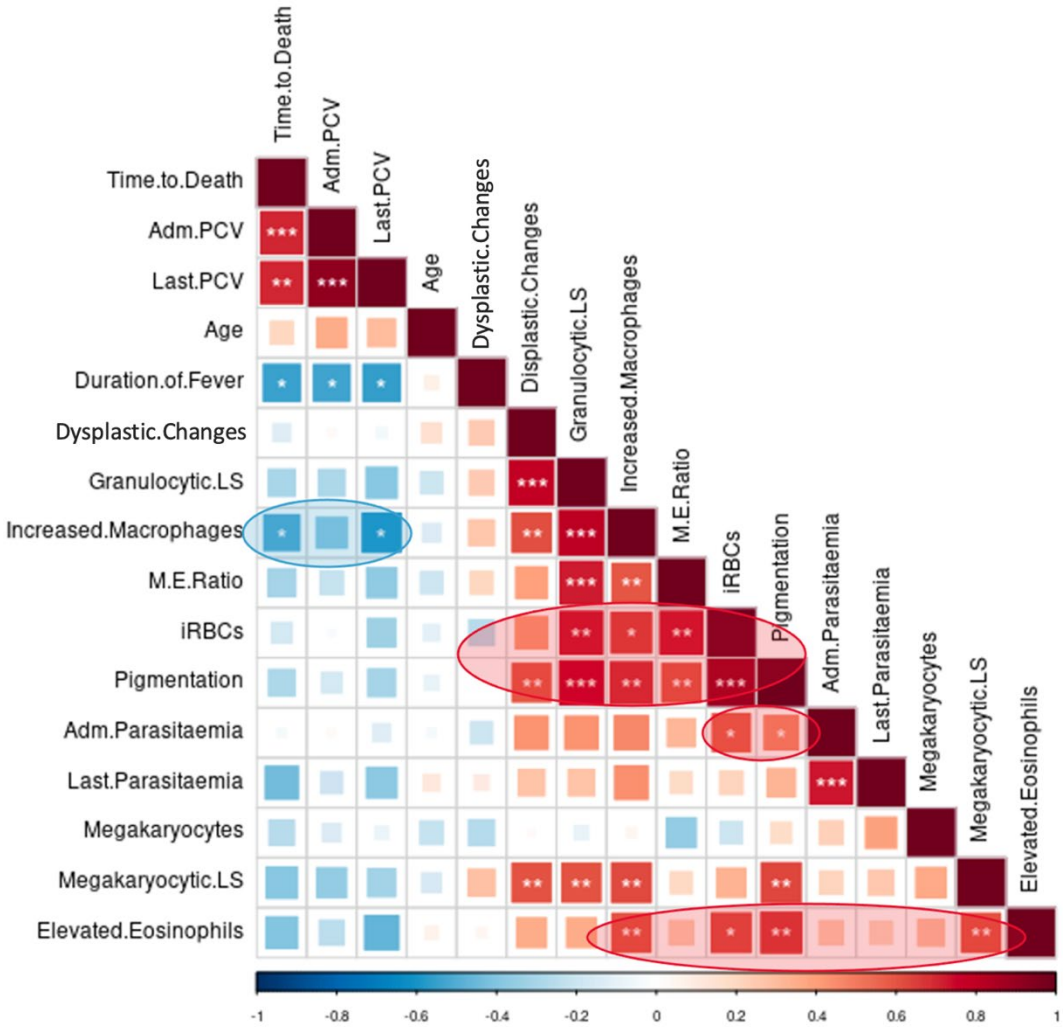

Figure 3-10. Multivariant analysis reveals several significant correlations in the bone marrow (BM). Pearson correlation matrix calculated for all malaria cases and non-malarial controls. Correlations were made between clinical parameters and BM histopathological parameters. Significant correlations are depicted by asterisks. Red boxes highlight positive correlations and blue boxes represent negative correlations. The box size and colour intensity convey the degree of correlation between the two parameters. Coloured bubbles indicate relevant correlations. Abbreviations: Adm, admission; PCV, packed cell volume, LS, left shift, M.E.Ratio, myeloid:erythroid ratio; iRBC, identification of infected RBC; Dysplastic.Changes, dysplastic changes in the megakaryocytic lineage.

3.4.4 Histopathology of the Spleen: Whole Cohort

Spleen sections were stained with H&E and scored by a pathologist blinded to clinical information as before described. Parameters for scoring included degree of macrophages and pigment latent macrophages in the RP and WP, WP hyperplasia, haemorrhage or congestion, and parameters indicating disorganisation of splenic microarchitecture such as dissolution of the marginal zones and disruption of germinal centre architecture. The presence of suspected iRBCs was also noted. Relative lesion burden, an aggregate of multiple parameters, was scored from 0 to 5 where 0 represents no lesions and 5 represents extensive lesions that occupy most of the spleen section. All other parameters were scored between 0-4 where 0 denotes a feature that is not present and 4 denotes a marked appearance (**Section 2.2.8**). In total, histopathological scoring was performed on 17 spleen sections. The findings from this histopathological scoring are summarised in **Table 3-4**.

Overall, there were no major differences in spleen histopathology between malaria cases and non-malarial controls. Throughout the cohort, there was no evidence of inflammation, necrosis, or fibrosis. A moderate amount of pigment latent cells was present in the RP for both malaria cases and non-malarial controls. It was noted that a large amount of pigment was present throughout the spleen, considerably more than observed in BM sections (**Figure 3-11A**). There was a minimal amount of pigment observed in the WP which was largely localised to the germinal centre (**Figure 3-11B**). Like the BM, it is not possible to determine if this pigment is haemozoin, haemosiderin, or formalin pigment using H&E-stained sections alone. The main difference between the two groups was the presence of iRBCs which were confidently identified in malaria cases but absent in non-malarial controls (**Figure 3-11C**).

In terms of splenic microarchitecture, there was minimal blurring of the RP to WP boundaries and minimal dissolution of the marginal/mantle zones for both malaria cases and non-malarial controls. For non-malarial controls, there was mild germinal centre architecture disruption compared to minimal disruption in malaria cases. Both groups had minimal WP hyperplasia and a mild increase in macrophages (**Figure 3-11D**).

In mice, the BM is unable to respond to an increase in RBC production demands, however, the spleen has been demonstrated to be able to induce stress erythropoiesis to increase RBC production (Liu et al., 2013, Weiss et al., 1989, Villeval et al., 1990, Yap and Stevenson, 1992, Lamikanra et al., 2007, Paulson et al., 2011, Bennett et al., 2018, Paulson et al., 2020, Ghosh and Stumhofer, 2021, Chen et al., 2021). It has been long been hypothesised that the human spleen might trigger a comparable response in malaria, demonstrating extramedullary haematopoiesis, a phenomenon observed rarely in patients with haemoglobinopathies (Gupta et al., 2022). Stress erythropoiesis in the spleen has been demonstrated to occur in response to inflammation in mice models where the BM alters haematopoiesis in favour of myeloid cells (Bennett et al., 2019, Paulson et al., 2020). Indeed, in CM1/CM2 cases, a higher M:E ratio was observed likely in response to inflammation and infection (**Table 3-3**). The presence of extramedullary haematopoiesis was therefore investigated in the spleen of this cohort. In addition, the percentage of RBC precursors (following 500 RBC count) in the spleen was evaluated which may indicate retention of reticulocytes as observed in chronic asymptomatic malaria cases (Kho et al., 2021a). Based on the sections evaluated from this cohort, there was no evidence of extramedullary haematopoiesis in the spleen. In addition, no cases exhibited a notably high percentage of RBC precursors present in the spleen.

To conclude, the spleen in both malaria cases and non-malarial controls display minimal to mild splenic disruption. Since disruption was observed in non-malaria cases as well, it is likely that factors other than *Plasmodium* contribute to this splenic disruption.

Table 3-4. Summary of spleen histopathology scoring.

Histological Parameter	Malaria	Non-malarial controls	CM1/CM2 (-SMA)	CM2 (+SMA)	CM3	IP
Number analysed	14	3	6	6	1	1
Presence of iRBCs (n/N [%])	7/11 (64)	1/3 (33)	3/4 (75)	3/3 (100)	N/A	N/A
Pigment Latent Cells						
Red Pulp (RP)	Moderate	Moderate	Mild	Mild	Moderate	Minimal
White Pulp (WP)	Minimal	Minimal	Minimal	Minimal	Minimal	Minimal
White Pulp Hyperplasia	Minimal	Minimal	Minimal	Minimal	Mild	Minimal
Elevated Macrophages	Mild	Mild	Mild	Mild	Minimal	Minimal
Disorganised Microarchiecture						
Blurred limits between RP and WP	Minimal	Minimal	Minimal	Minimal	Minimal	Mild
Disruption of germinal centre architecture	Minimal	Mild	Minimal	Minimal	Minimal	Minimal
Dissolution of mantle zone	Not Present	Not Present	Minimal	Minimal	Not Present	Moderate
Dissolution of marginal zone	Minimal	Minimal	Minimal	Minimal	Minimal	Minimal
Extramedullary Haematopoiesis	Not Present	Not Present	Not Present	Not Present	Not Present	Not Present
Haemorrhage/Congention	Mild	Mild	Mild	Moderate	Minimal	Moderate
Immature RBC% (following 500 RBC count)	0.25%	0.2%	0.33%	0.33%	Inconclusive	0.75%
Evidence of Inflammation	Not Present	Not Present	Not Present	Not Present	Not Present	Not Present
Necrosis	Not Present	Not Present	Not Present	Not Present	Not Present	Not Present
Fibrosis	Not Present	Not Present	Not Present	Not Present	Not Present	Not Present
Relative Lesion Burden	Multiple Focal Lesions	Multiple Focal Lesions	Multiple Focal Lesions	Multiple Focal Lesions	Multiple Focal Lesions	Multiple Focal Lesions

Abbreviations: iRBC, infected red blood cell; RBC, red blood cell; CM, cerebral malaria; SMA, severe malarial anaemia; IP, incidental parasitaemia.

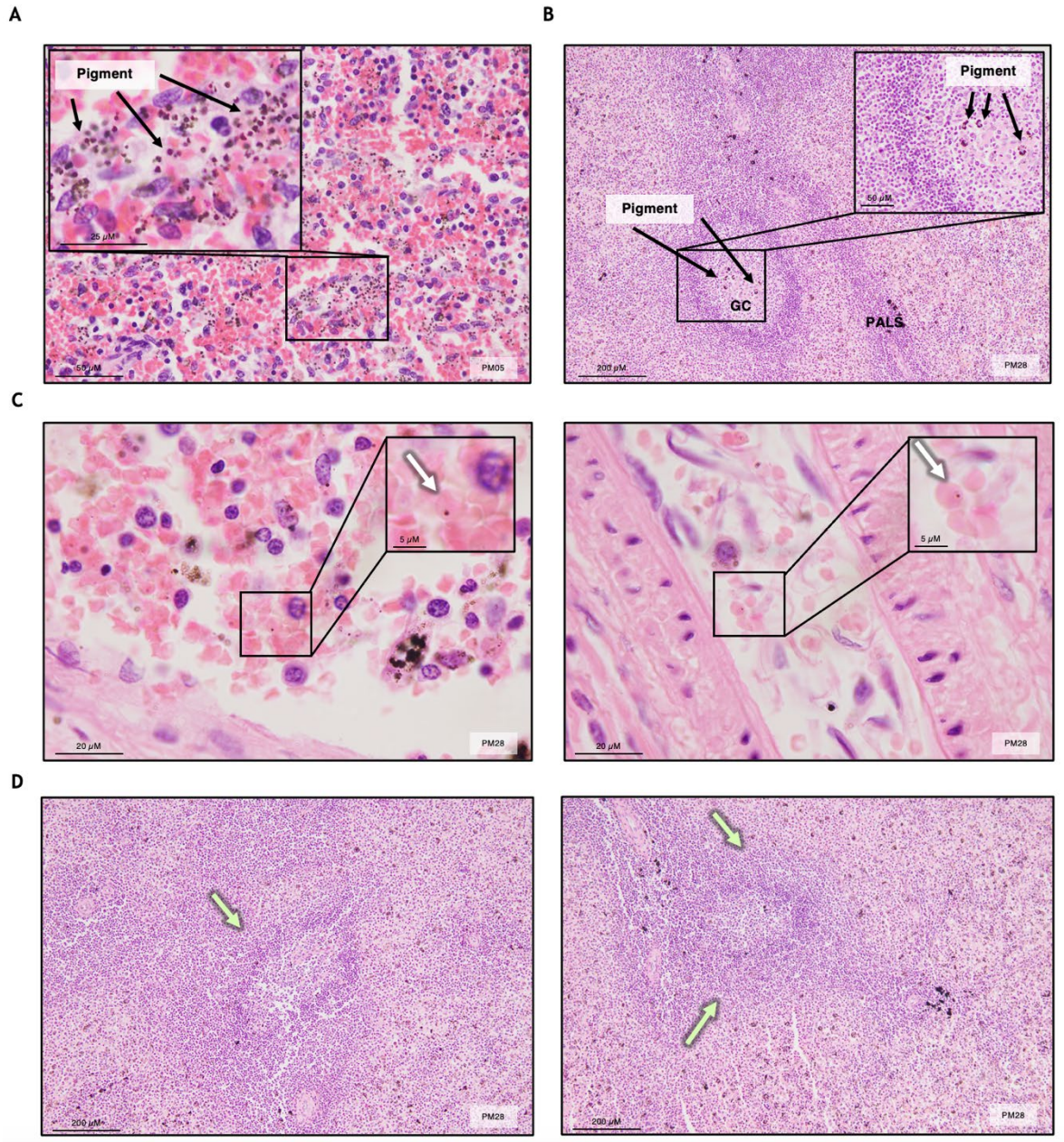

Figure 3-11. Pigment, infected red blood cells (iRBCs), and disorganisation of the splenic microarchitecture in the spleen of severe malaria patients and non-malarial controls. (**A**) There was a moderate appearance of pigment throughout the red pulp (RP). (**B**) Where pigment was present in the white pulp (WP), it was predominantly found in the germinal centre (GC). The GCs of the spleen are specialised microenvironments containing B cells which initiate an adaptive immune response upon antigen recognition. (**C**) iRBCs were observed in malaria cases as indicated by white arrows. (**D**) Blurred limits between the RP and WP indicated by green arrows. The structure of the WP is more diffused with less distinctive boundaries between splenic compartments, as shown in **Figure 1-7**. Abbreviations: GC, germinal centre; PALS, periarteriolar lymphoid sheath.

3.4.5 Multivariant Analysis of Splenic Histopathological and Patient Clinical Parameters

Malaria and non-malarial controls appear to exhibit similar splenic histopathology. This was supported by PCA-biplot which demonstrates no distinct clusters based on histopathological parameters alone, even when coloured by clinical group (**Figure 3-12**).

To investigate correlations between histopathologic parameters and clinical parameters, a correlation matrix plot was generated. The same clinical parameters used in BM correlations were used here with the addition of spleen weight. As expected, parameters related to disruption of splenic architecture were positively correlated such as disruption of the marginal zone and blurred limits between the RP and WP. Relative lesion burden was positively associated with haemorrhage and congestion, consistent with splenic disruption or damage. Relative lesion burden was also positively correlated with pigment in the WP. Parasitaemia (both on admission and before death) was positively correlated with the presence of immature RBCs in the spleen and negatively correlated with time to death. This latter correlation aligns with the understanding that higher parasitaemia is associated with disease severity and therefore a shorter time to death (Bilal et al., 2016, Antwi-Baffour et al., 2023). Pigment in the RP was associated with a higher degree of splenic macrophages, further suggesting that pigment, at least in malaria cases, is likely haemozoin (**Figure 3-13**).

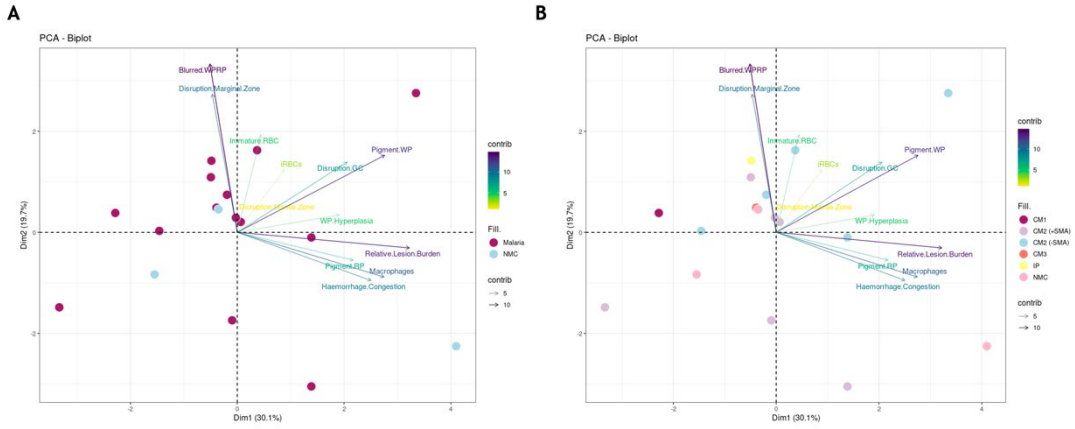

Figure 3-12. Multivariant analysis reveals no distinct subgroups in the spleen. (**A**) PCA-biplot categorising malaria (purple) patients and non-malarial controls (blue). (**B**) PCA-biplot categorising patients according to clinical diagnosis. Abbreviations: WP, white pulp; RP, red pulp; iRBC,

infected red blood cells; GC, germinal centre; CM, cerebral malaria; SMA, severe malarial anaemia; IP, incidental parasitaemia; NMC, non-malarial control; contrib, contribution.

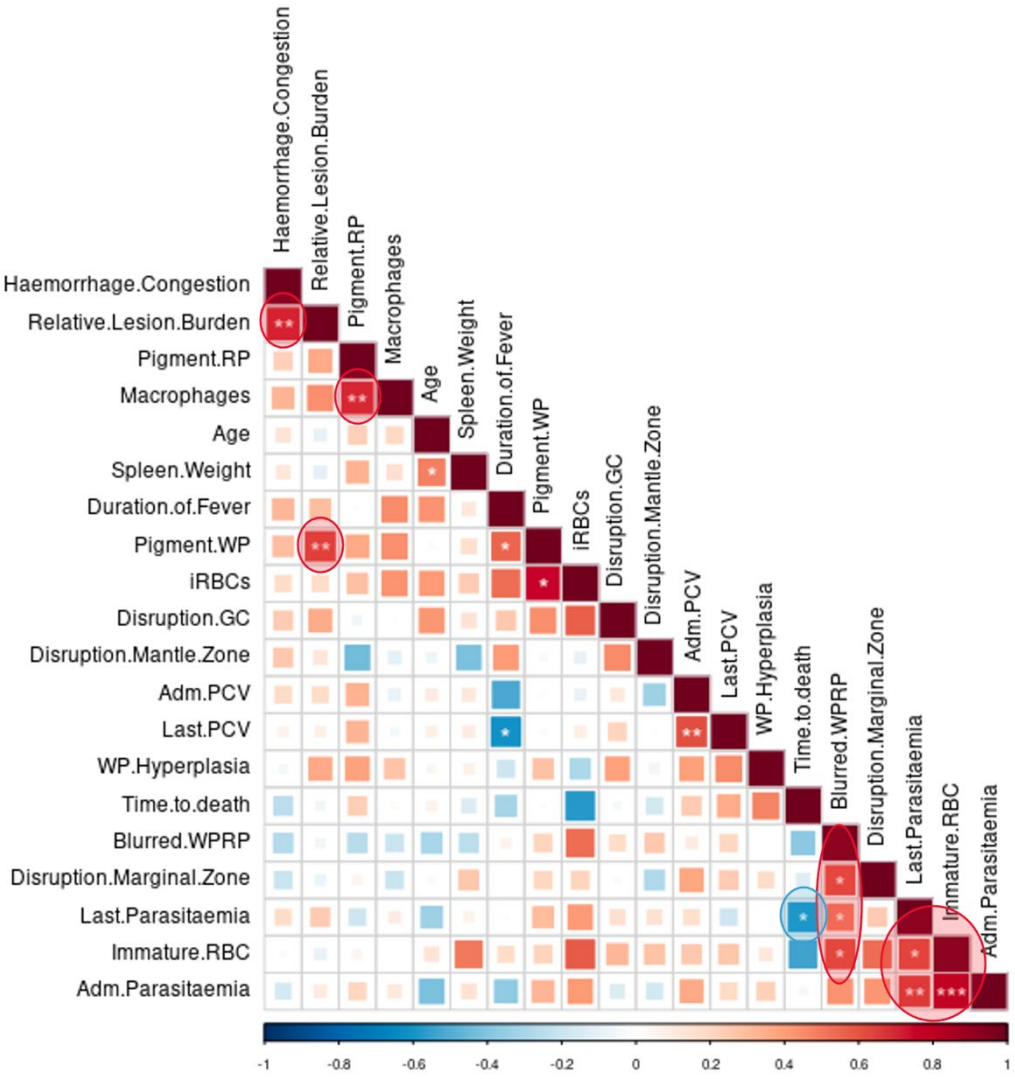

Figure 3-13. Multivariant analysis reveals several significant correlations in the spleen. Pearson correlation matrix calculated for all malaria and non-malarial control patients. Correlations were made between clinical parameters and spleen histopathological scoring parameters. Significant correlations are depicted by asterisks. Red boxes highlight positive correlations and blue boxes represent negative correlations. The box size and colour intensity convey the degree of correlation between the two parameters. Coloured bubbles indicate relevant correlations. Abbreviations: Pigment.RP, pigment in the red pulp; Pigment.WP, pigment in the white pulp; iRBCs, presence of infected red blood cells; Disruption.GC, disruption of the germinal centre; Adm.PCV, admission packed cell volume; WP.hyperplasia; white pulp hyperplasia; blurred.WPRP, blurred limits between the red pulp and white pulp; Immature.RBC, percentage of immature red blood cells; Adm.parasitaemia, admission parasitaemia.

PCA-biplot did not identify distinct groups based solely on histopathological parameters; however, many histopathological parameters were positively

correlated with clinical parameters. Like the BM, severity of infection (i.e., high parasitaemia) corresponded with significant histopathological alterations in the spleen, leading to splenic disruption. Overall, these findings suggest that, based on histopathology alone, the spleen in malaria cases and non-malarial controls are very similar. This implies that the mild splenic disruption observed here may be influenced by other factors or past infections.

3.5 Evaluating Parasite Accumulation in the Spleen

The spleen was recently revealed to harbour a large hidden reservoir of non-phagocytosed *P. falciparum* and *P. vivax* in adults with chronic asymptomatic malaria. Using Giemsa-stained spleen sections, all developmental stages were identified, including gametocytes in *P. falciparum* cases. Parasite densities were highest in the splenic cords where all blood stages were identified in proportions consistent with their duration in the intraerythrocytic life cycle. The magnitude of parasite densities in the spleen was more marked for *P. vivax* cases than *P. falciparum* suggesting a level of heterogeneity in terms of the splenic reservoir (Kho et al., 2021b, Kho et al., 2021a). It is unknown whether the spleen in paediatric severe malaria cases, which account for the majority of malaria related deaths, harbour similarly high densities of non-phagocytosed parasites. Such high splenic parasite densities may be the result of an endosplenic life cycle which would be evidenced through the presence of schizonts in proportions consistent with their duration in the intraerythrocytic life cycle. For *P. falciparum*, rings and trophozoites constitute ~75% of the lifecycle (0-36 hours post invasion (hpi)) while schizonts constitute ~25% (36-48 hpi).

3.5.1 Defining Spleen Compartments

To determine whether there was a marked accumulation of non-phagocytosed parasites present in the spleen, an initial parasite screen on Giemsa-stained tissue sections was performed. For this initial screen, the spleen was compartmentalised into the splenic cords, sinus lumens, perifollicular zones, and non-circulatory spaces (**Figure 3-14**). These splenic compartments have previously been used to explore the distribution of parasites in the spleen where the majority of parasites were found in the splenic cords, followed by sinus lumens and then perifollicular zones (Kho et al., 2021a, Kho et al., 2021b).

The perifollicular zone is not a well-defined compartment of the spleen; it is a region of fast circulation between the WP and the RP with a reticular cell framework (Groom et al., 1991, Safeukui et al., 2008, Buffet et al., 2011, Sasou, 2021). For the purposes of these counts, the boundary of the perifollicular zone was defined as the point where the first sinus lumen of the RP was visible, and the reticular framework was no longer obvious (**Figure 3-15**). To gain familiarity with the structure of the sinus lumen in the RP, periodic acid Schiff (PAS) stain was used to stain polysaccharides making sinus lumens more obvious (**Figure 3-16**).

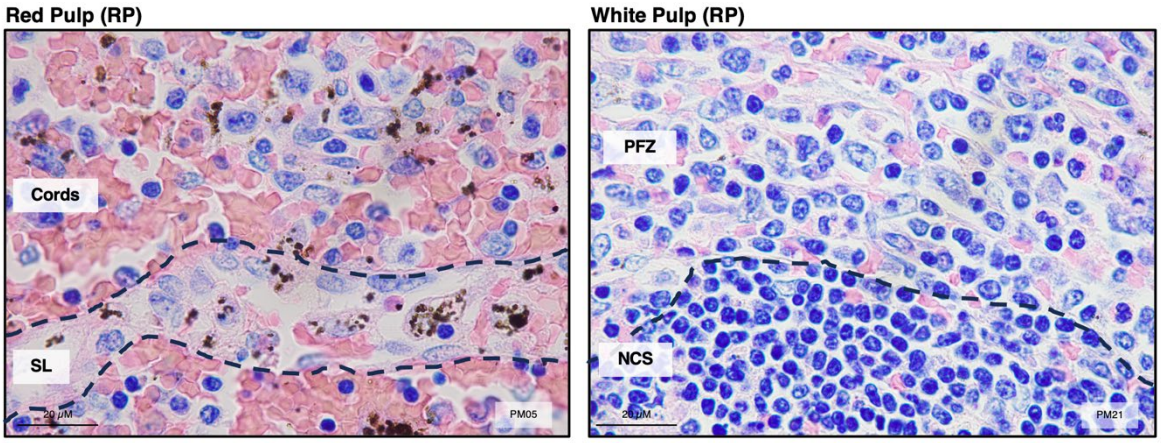

Figure 3-14. Representative images of splenic compartments. Sections from *P. falciparum* infected spleens stained with Giemsa. Two major compartments of the spleen exist: the red pulp (RP) and the white pulp (WP). These can be further divided into the following compartments: splenic cords, sinus lumens (SL), perifollicular zones (PFZ) and non-circulatory spaces (NCS). Dashed lines indicate the separation between these compartments. Abbreviations: SL, sinus lumen, PFZ, perifollicular zone; NCS, non-circulatory spaces.

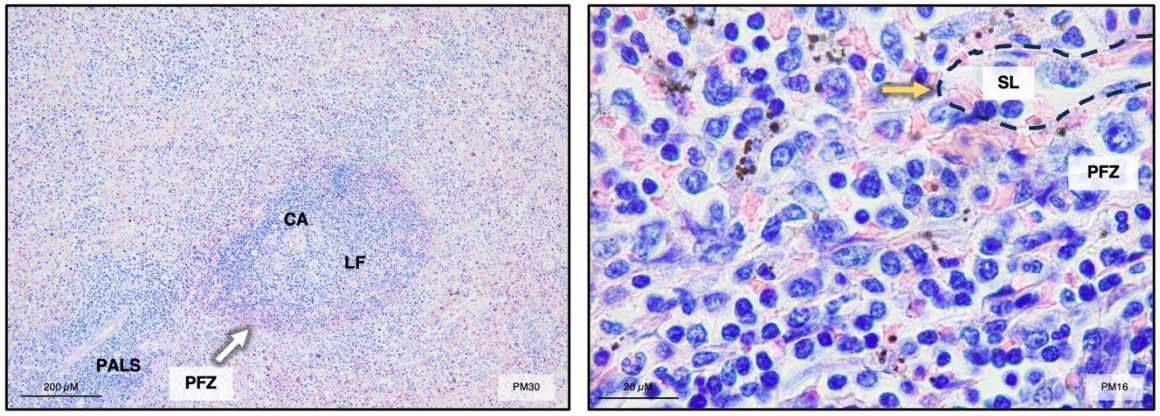

Figure 3-15. The perifollicular zone of the spleen. Sections from *P. falciparum* infected spleens were stained with Giemsa. (A) The perifollicular zone (PFZ) can be observed as an RBC rich area surrounding the WP. The white arrow indicates the perifollicular zone. (B) Representative image of the first sinus lumen observed at the periphery of the PFZ indicated by a yellow arrow. Dashed lines indicate outline the first sinus lumen. Abbreviations: CA, central artery; LF, lymphoid follicle; PALS, periarteriolar lymphoid sheath; PFZ, perifollicular zone; SL, sinus lumen.

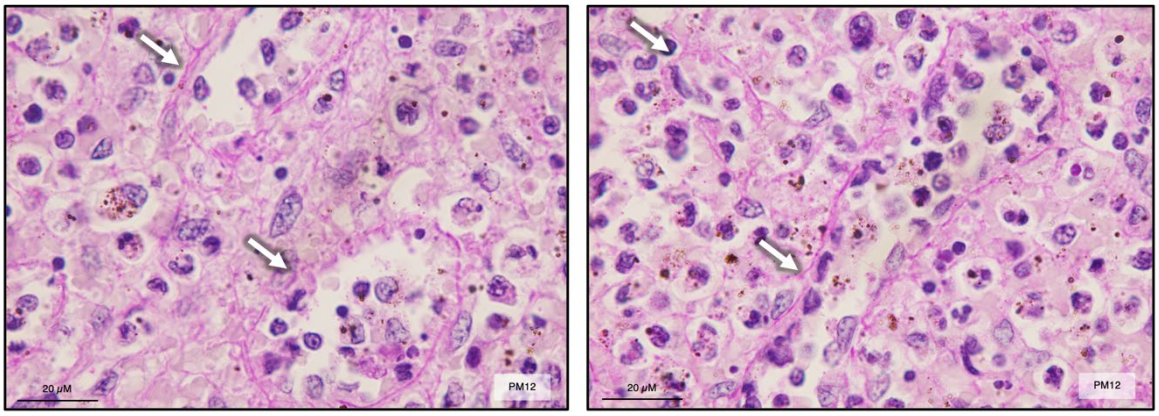

Figure 3-16. Periodic acid Schiff (PAS) stain on a spleen section highlighting sinusoids. Spleen sections were subjected to a PAS stain to stain polysaccharides allowing identification of sinus lumens. White arrows indicate sinuses.

3.5.2 Defining Giemsa Counting Methodology

Staging was based on morphological appearance (parasite nuclei, cytoplasm, and haemozoin distribution) which has previously been described (Safeukui et al., 2008, Kho et al., 2021a, Kho et al., 2021b). Rings were identifiable by a RBC containing a light brown nucleus less than 1 μM in diameter, often with either a faint blue hue (cytoplasm) or pale circular zone originating at the nucleus. Trophozoites appear similar with a marked blue cytoplasmic hue and larger nucleus. Schizonts contained a large brown pigment more than 1 μM, or multiple brown dots, occupying half the diameter of the erythrocyte with a thick blue cytoplasm. Late gametocytes contain a large central pigment surrounded by oblong blue cytoplasmic staining matching the modified shape of the gametocyte-infected erythrocyte. Non-phagocytosed parasites were clearly distinguishable from pigmented phagocytes, likely pigmented due to parasite destruction or engulfment of free pigment in the spleen (**Figure 3-17**).

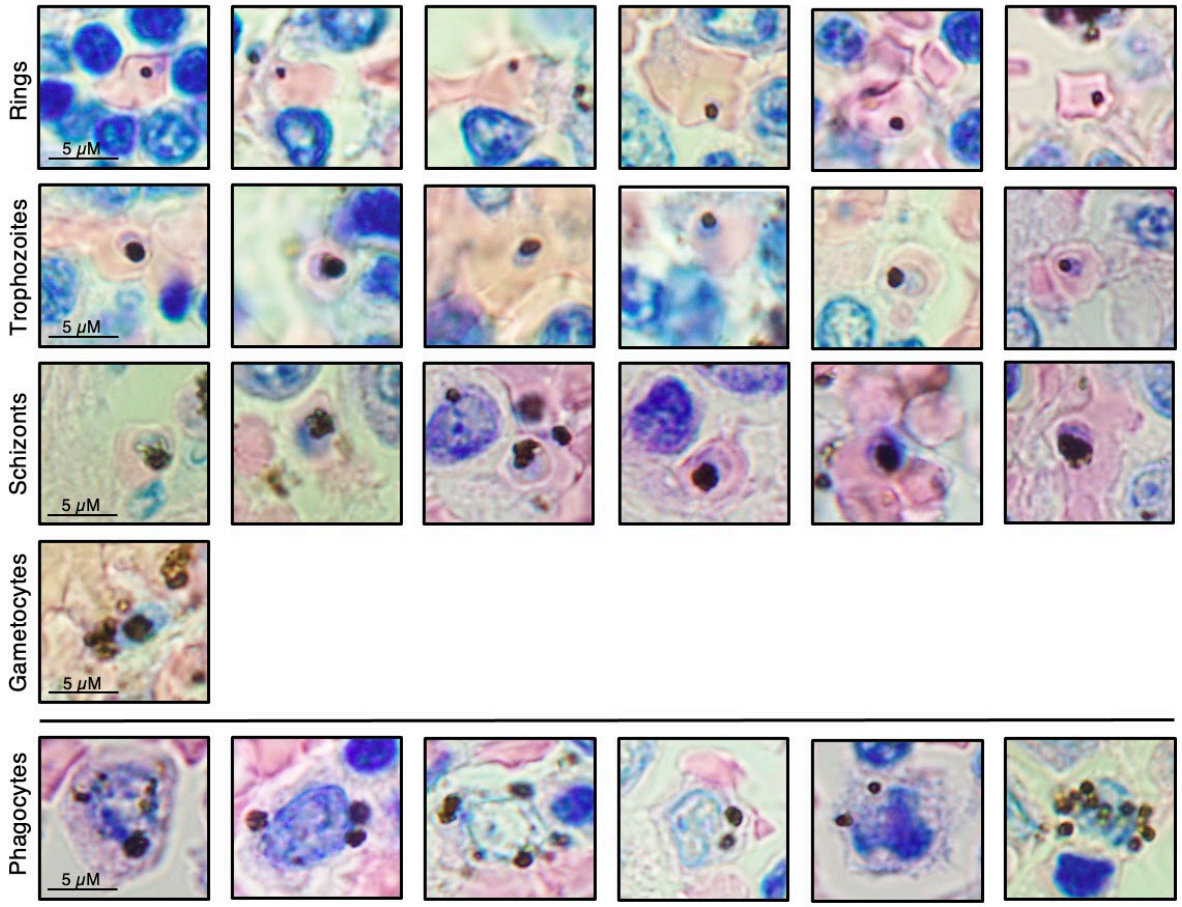

Figure 3-17. Morphological appearance of non-phagocytosed parasites and pigmeted phagocytes in Giemsa-stained spleen sections.

To aid parasite stage identification, the use of polarised light was investigated. Polarising light filters can be used for the detection of haemozoin due to the unique optical properties of this parasite crystal which render it birefringent. Since rings have been suggested to lack haemozoin, the use of polarising light may assist in distinguishing rings from early trophozoites which are morphologically similar in Giemsa-stained tissues (Rebelo et al., 2012, Shapiro et al., 2013, Delahunt et al., 2014). Using polarised light microscopy, early rings were distinguishable from late rings/early trophozoites which, by Giemsa, were morphologically the same (**Figure 3-18**). While this technique was simple to implement, the addition of a polarising filter onto the objective made identifications by brightfield microscopy of Giemsa-stained sections more challenging. In addition, as previously described, a substantial amount of pigment was observed throughout the splenic tissue. While polarising light microscopy

could aid in distinguishing haemosiderin from haemozoin, formalin pigment is also birefringent and therefore makes the use of this technique in these tissues challenging (Rogerson and Ordi, 2014). For the purposes of this study, rings and early trophozoites were grouped together for counts by brightfield microscopy alone. Trophozoites, schizonts, late gametocytes and unclassifiable stages were counted separately.

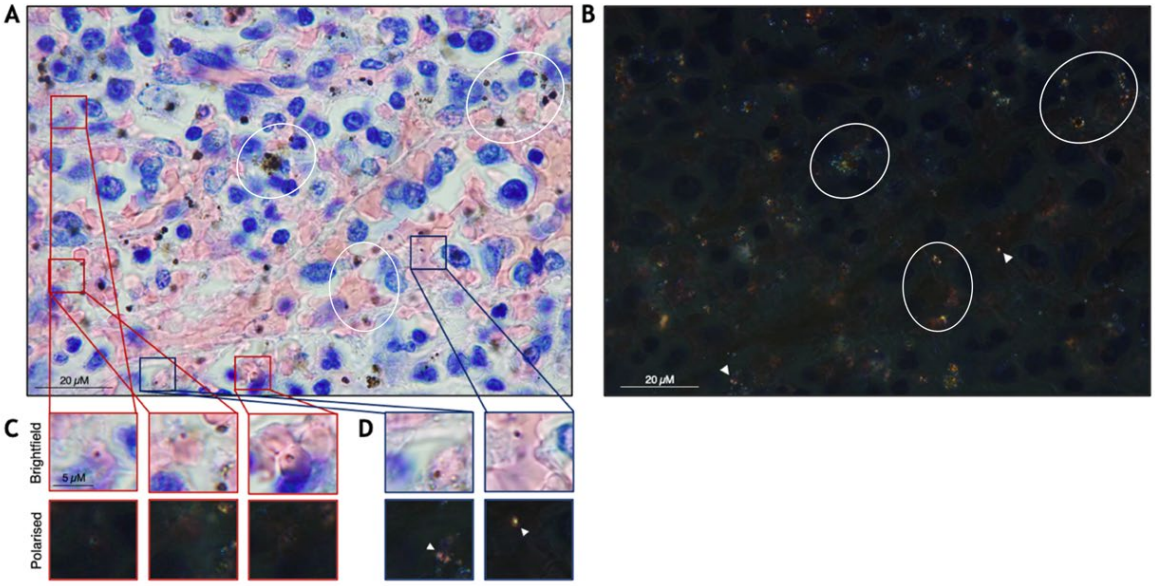

Figure 3-18. Splenic ring identifications using polarised light. (**A**) Giemsa-stained spleen section. (**B**) Matching field of view of Giemsa-stained spleen section with a polarising light filter. White arrowheads indicate birefringent pigment corresponding to parasite identifications highlighted in (**D**). White rings represent birefringent particles (likely formalin) which do not resemble parasites in the corresponding brightfield image. (**C**) Images of rings from infected spleen using brightfield and polarised light microscopy. Brown nuclear dots show no evidence of birefringence confirming early ring identification. (**D**) Images of infected red blood cells (iRBCs) from infected spleen using brightfield and polarised light microscopy. White arrowheads indicate birefringent pigment within iRBCs. These parasites are morphologically the same as rings identified in (**C**) but differ in pigment, indicating later parasite stages.

Parasite counts were performed in each splenic compartment defined in **Section 3.5.1**. For each compartment, 10 high powered fields (HPF) were counted. Only clearly defined perifollicular zones were counted with the first sinus lumen of the RP marking the boundary between the perifollicular zone and the RP (**Figure 3-15B**). For each HPF, total RBCs were counted allowing parasitaemia to be determined in each splenic compartment.

3.5.3 Splenic Distribution and Accumulation of Parasites by Giemsa

In total, 24 stained tissues were counted where parasites were identified in all 24 spleens, including non-malarial controls. Few parasites were identified in non-malarial controls and consisted of only rings/early trophozoites which could be confused with free pigment. However, without further validation by IHC (performed in **Chapter 4**), these will be considered as genuine parasite identifications.

In all infected spleens, most non-phagocytosed parasites identified were asexual, comprising a mean of 64.8% (95% confidence interval (CI): 54.2% to 75.3%), with gametocytes accounting for only 0.1% of parasites identified (95% CI: -0.1% to 0.4%). Of these asexual stages, 48.1% were identified as rings/early trophozoites (95% CI: 37.9% to 58.28), with 10.5% (95% CI: 5.3% to 15.6%) identified as trophozoites and 6.2% as schizonts (95% CI: 2% to 10.4%) (**Figure 3-19A**). An unclassifiable category was included for counts where a confident identification of the nature (parasite or pigment) and stage could not be determined. If this category is removed, a mean of 99.5% of all stages identified were asexual (95% CI: 98.9% to 100%). Of these asexual stages, 77.3% (95% CI: 66.8% to 88.1%) were rings/early trophozoites, 13.9% (95% CI: 7.7% to 20.1%) were trophozoites, and 8.3% (95% CI: 3.0% to 13.6%) were schizonts (**Figure 3-19B**).

Most of the non-phagocytosed parasites within the spleen were found in the splenic cords with a mean of 51% (95% CI: 43.7% to 59.6%) of asexual stages localised to this splenic compartment. The sinus lumens occupied the next largest fraction of asexual parasites with a mean of 31% (95% CI: 22.3% to 40.9%) of asexual stages localised here. The WP occupied the smallest fractions of total asexual parasite distribution (**Figure 3-19C**). Gametocytes were only found in the splenic cords.

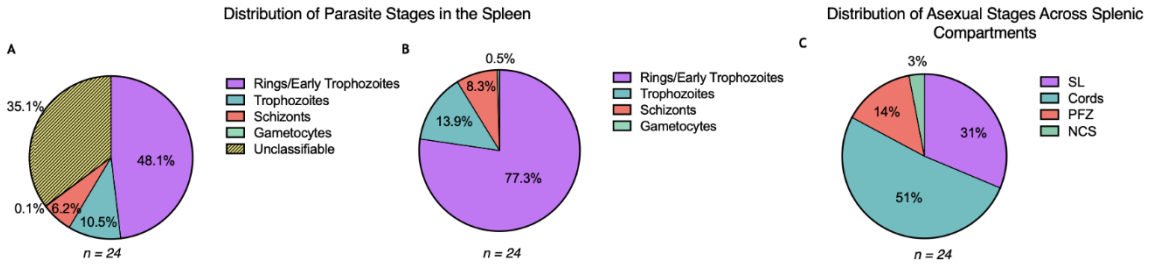

Figure 3-19. Infected spleens primarily exhibited rings/early trophozoites, with the largest concentration of asexual parasites observed in the splenic cords. (**A**) Pie chart showing the mean proportion of each parasite stage found in the spleen. (**B**) Pie chart showing the mean proportion of each parasite stage found in the spleen when the unclassifiable category was removed. (**C**) Pie chart showing the mean distribution of asexual parasite stages (rings, trophozoites and schizonts) in each splenic compartment. SL, sinus lumen; PFZ, perifollicular zone; NCS, non-circulatory spaces.

While investigating the distribution of parasite stages, it was observed that the distribution of parasites in the cords was not always uniform. In some cases, a higher density of parasites was observed on the periphery of the WP beyond the perifollicular zone (**Figure 3-20A**). This accumulation of parasites consisted of predominantly mature stages (late trophozoites and schizonts) (**Figure 3-20B**). In these areas, aggregates of parasites and pigment that appeared to be enclosed within a membrane, were identified. These structures, previously undescribed, are referred to as parasitic “nests” in this thesis (**Figure 3-21**). It was hypothesised that these “nests” could represent parasites within a large macrophage, far larger than the pigmented phagocytes that were previously defined (**Figure 3-17**). The presence of a macrophage nucleus was not always clear in parasitic “nests”. Therefore, specific labelling for macrophages will need to be performed to confirm whether these aggregates of parasites are examples of phagocytosis (**Figure 3-21**).

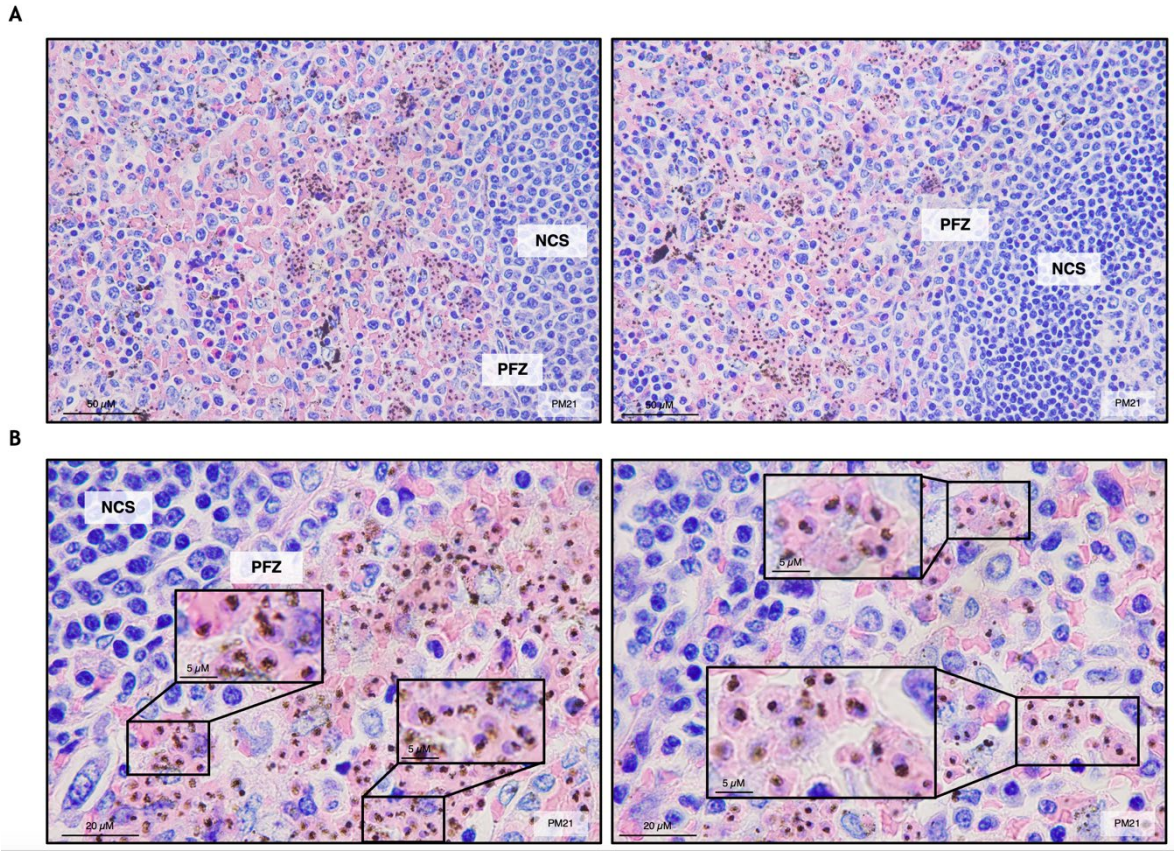

Figure 3-20. Heterogenous parasite distribution in the spleen. (**A**) An accumulation of parasites was observed beyond the perifollicular zone (PFZ) in the red pulp (RP) cords. (**B**) The parasite stage distribution in these areas were predominantly mature stages (late trophozoites/schizonts) identifiable by lobulated pigment and a large blue cytoplasm within red blood cells (RBCs). Abbreviations: NCS, non-circulatory space; PFZ, perifollicular zone; PM, postmortem.

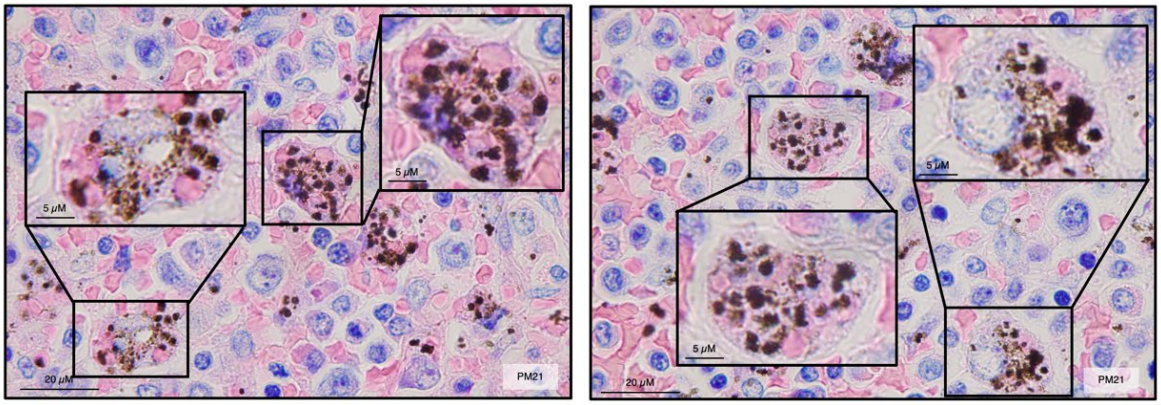

Figure 3-21. Identification of parasitic "nests". On the periphery of the white pulp (WP), aggregates of parasites and pigment were identified. These aggregates appeared to be enclosed within a membrane and were larger in size compared to typical splenic macrophages, or pigmented phagocytes (**Figure 3-17**).

The parasitaemia of the spleen and within each splenic compartment was calculated based on RBC counts. The mean splenic parasitaemia was found to be 2.1% (95% CI: 1.0 to 3.2). In each compartment, the highest splenic parasitaemia was found in splenic cords (1.2% [95% CI: 0.4 to 2.1]). No significant differences were identified between the parasitaemia in splenic compartments except for between the splenic cords and sinus lumens compared to non-circulatory spaces of the WP where far fewer parasites were observed (**Figure 3-22**).

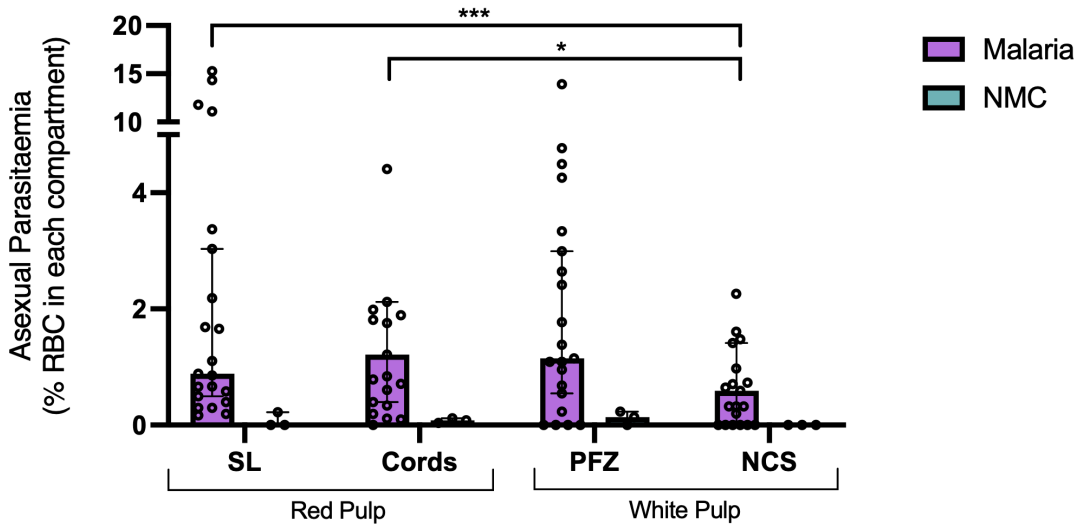

Figure 3-22. Density of asexual parasites in each splenic compartment. The density, or parasitaemia, of *P. falciparum* in each splenic compartment was determined (n=24). No significant differences in parasite densities were observed between splenic compartments with the exception of sinus lumens (SL) and cords compared to non-circulatory spaces (NCS) (p=0.0008 and p=0.02, respectively). Parasitaemia is shown as median with 95% confidence interval. Symbols represent individual patients. Statistical test used for each compartmental comparison was the Friedman test, followed by post-hoc Dunn's test to assess pairwise differences. Abbreviations: RBC, red blood cell; SL, sinus lumens; PFZ, perifollicular zone; NCS, non-circulatory spaces; NMC, non-malarial control.

3.5.4 Evidence of an Endosplenic Life Cycle?

Recent evidence has suggested the presence of a cryptic endosplenic life cycle in *P. berghei* and *P. vivax* (Lee et al., 2018, Kho et al., 2021a). For an endosplenic cycle to be present, three conditions are anticipated to be met: firstly, all asexual stages are expected to be present within the spleen, secondly, the proportions of each parasite stage are expected to be consistent with their duration in the lifecycle, and thirdly, the magnitude of parasite densities in the spleen cannot be explained by peripheral parasitaemia alone. Assuming parasite growth in the

spleen is similar to *in vitro* conditions, *P. falciparum* rings and trophozoites constitute approximately 75% of the lifecycle (0-36 hpi), while schizonts account for the remaining 25% (36-48 hpi).

The stage distribution of parasites within each splenic compartment was first investigated. For this, rings and trophozoites were combined into a single category. Throughout splenic compartments, there was a significantly higher density of rings and trophozoites compared to schizonts and gametocytes across all splenic compartments (**Figure 3-23**). Ring and trophozoite parasitaemia was highest in the splenic sinus lumens with a median parasitaemia of 1.2% (95% CI: 0.5% to 2.34%) which was significantly higher than median parasitaemia observed for schizonts and gametocytes ($p<0.0001$). This pattern was consistent throughout splenic compartments where rings and trophozoites had significantly higher densities than gametocytes ($p<0.0001$) and schizonts (in cords $p<0.0001$, in perifollicular zones $p=0.007$, and in non-circulatory spaces $p=0.03$) (**Figure 3-23**).

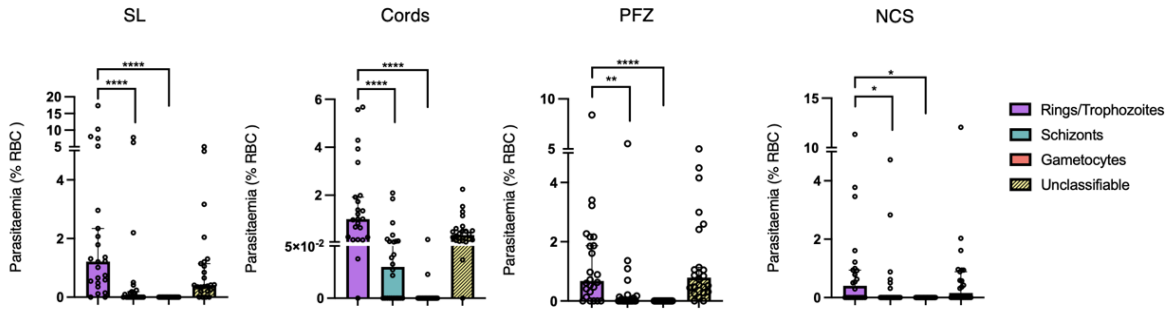

Figure 3-23. Ring and trophozoite densities are highest across all splenic compartments. The density, or parasitaemia, of each stage of *P. falciparum* in each compartment was determined (n=24). Rings and trophozoites had consistently significantly higher densities compared to schizonts and gametocytes across all four splenic compartments analysed. Parasitaemia is shown as median with 95% confidence interval. Symbols represent individual patients. Statistical tests used for each compartmental comparison was the Friedman test, followed by post-hoc Dunn's test to assess pairwise differences. Abbreviations: RBC, red blood cell; SL, sinus lumen; PFZ, perifollicular zone; NCS, non-circulatory spaces.

Across the Malawi cohort, all stages of the intraerythrocytic cycle were observed in the spleen. However, while all asexual stages were observed, the mean proportions of rings/trophozoites in the whole cohort was 91.3% (95% CI: 85.9% to 96.8%) compared to 8.3% (95% CI: 3.0% to 13.6%) for schizonts. This proportion of

schizonts deviates from the anticipated proportion for an endosplenic life cycle (~25%), even when considering the 95% CI. When investigating the proportions of rings/trophozoites to schizonts across clinical groups, a few cases had higher proportions of schizonts, notably CM1 cases. CM1 cases appeared to have the highest proportion of schizonts present in the spleen with 61.9% (95% CI: 45.51% to 78.2%) of stages identified as rings/trophozoites and 38.1% (95% CI: 21.8% to 54.5%) of stages identified as schizonts (**Figure 3-24**). These proportions are more suggestive of an endosplenic cycle. It is important to note that in both CM1 cases, an accumulation of schizonts was observed on the periphery of the WP/perifollicular zones. It is possible that this accumulation is due to parasites entering the cords via the marginal zone and getting trapped due to a lack of deformability. Alternatively, this parasite accumulation could be explained by an ongoing endosplenic cycle localised to these sites.

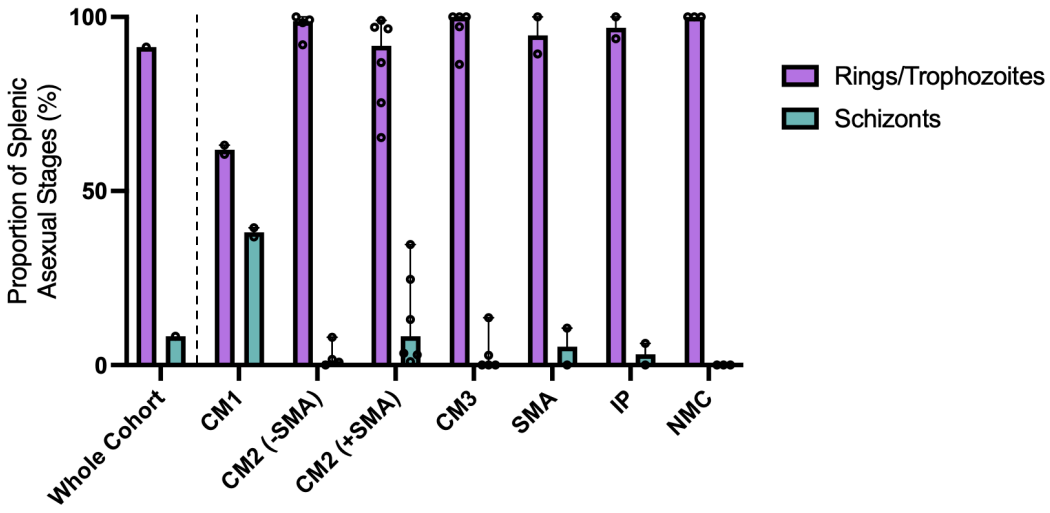

Figure 3-24. Proportions of asexual stages are not consistent with an endosplenic life cycle. The proportion of rings/trophozoites and schizonts were determined according to the total asexual counts in the spleen. This was determined for the whole cohort where proportions calculated were not consistent with an endosplenic cycle. Proportions for each clinical group were plotted where only CM1 cases had proportions that would be consistent with an endosplenic life cycle. Abbreviations: SMA, severe malarial anaemia; IP, incidental parasitaemia; NMC, non-malarial control.

3.6 Chapter Discussion

3.6.1 BM Decalcification

Due to the precious nature of these historic samples, the expertise of the Veterinary Diagnostics Services (University of Glasgow) was employed for sectioning BM samples, given their extensive experience working with bone tissues. As part of this service, they evaluated the quality of BM blocks for sectioning and would not proceed with sectioning tissues that were insufficiently decalcified. From this evaluation, several tissues were not suitable for sectioning limiting their use. As a result, I investigated whether reverse processing and decalcifying tissues would have a detrimental effect on staining.

Using *P. berghei* infected tissues, it was demonstrated that the time at which decalcification was performed did not have a detrimental effect (**Section 3.3**). However, it was noted that staining using RNAscope was not consistent throughout tissues (regardless of when decalcified). It is possible that the inconsistent staining in the BM was due to mRNA degradation as a consequence of decalcification, despite using a protocol designed to preserve mRNA and an ultrasensitive RNA *in situ* hybridisation assay (RNAscope) (Belluoccio et al., 2013, Wang et al., 2012).

The use of RNAscope on BM from the Malawi cohort was tested. It has previously been demonstrated in BM tissues from this cohort that there was a negative correlation between RNA integrity number and PMI (Joice et al., 2014). RNAscope was therefore tested on three BM samples from cases with varying PMIs. Successful RNAscope has previously been performed on trephine BM core biopsies to investigate B lymphocyte clonality (Guo et al., 2018) and therefore their optimised protocol for BM was used on the Malawi BM tissues. In all BM tissues, it was not possible to generate consistent labelling throughout the tissue regardless of PMI. While further optimisation of RNAscope for these tissues would be recommended, it is possible that RNA quality may not be good enough to perform mRNA targeting approaches. Indeed, in work by Guo *et al.*, only 22% of cases exhibited satisfactory RNA preservation for the implementation of RNAscope (Guo et al., 2018).

Other factors that may affect RNA integrity in tissues is formalin fixation. The modification of nucleic acid by formaldehyde can block base pairing in

hybridisation techniques such as RNAscope (Evers et al., 2011). Moreover, the duration of decalcification time may affect RNA integrity, especially in larger tissues necessitating extended decalcification periods. A similar experimental approach as described in **Figure 3-4** was established with longer decalcification times to determine the effect of duration of decalcification on staining by RNAscope. Histological experiments have yet to be completed to determine if longer decalcification times has a significant impact on RNA integrity.

Taking this into consideration, a quality control step to identify tissues with good RNA preservation would be necessary to select suitable cases for mRNA-based approaches. It is likely that only a subset of tissues would be suitable. Following the transcriptional characterisation of *P. falciparum* hypothesised to exist in the BM (**Chapter 5**), it was aimed to validate the identified transcriptional markers in the tissues using RNAscope. However, due to time constraints, this was not achieved.

3.6.2 Histopathology of the BM and Spleen

To investigate the histopathology and parasite accumulation in the spleen and BM in paediatric severe malaria patients, a number of exclusion criteria were applied to the Malawi cohort (**Section 3.2**). One of these criteria was the exclusion of patients with HIV as HIV infection is known to impact the histopathology, organ function, and parasite accumulation in the BM and spleen (Delacrétaz et al., 1987, Khalil et al., 1996, Flateau et al., 2011, Williams et al., 2016, Joice et al., 2016, Heller et al., 2023). In 2022, the total number of children aged 0 to 9 years old living with HIV was estimated at 930,000. Of these cases, nearly 85% localised to sub-Saharan Africa (UNAIDS, 2023b). In Malawi, it was estimated that 57,000 children under 15 years old were living with HIV in 2022 (UNAIDS, 2023a). Indeed, in the Malawi cohort nearly 20% of patients were HIV positive. Therefore, HIV positive patients represent a highly relevant population in Malawi. Consequently, the exclusion of these patients is a limitation.

To date, only one detailed study on the histopathology of the BM in patients with malaria has been performed. This study was performed in Eastern Thailand (1986) where 9 patients with CM were enrolled aged 15 to 78 years old (Wickramasinghe

et al., 1987). BM aspirates were taken from the sternum or iliac crest, smeared onto glass slides, and then fixed and stained with Giemsa for evaluation. Using these BM aspirates, Wickramasinghe *et al*. observed an increase in the proportions of eosinophils, macrophages and plasma cells. Phagocytosed parasites within macrophages, or pigmented macrophages, were frequently observed in the parenchyma of the BM. iRBCs were observed in both the extravascular spaces and binding to sinusoidal endothelial cells in the BM (Wickramasinghe et al., 1987).

Here, a detailed histopathological analysis of the BM in paediatric severe malaria was performed by a board-certified comparative pathologist from the American College of Veterinary Pathology, specialising in haematopoietic organs. Similar to the findings of Wickramasinghe *et al*. there was a mild elevation of macrophages in the BM in malaria cases compared to a minimal elevation in non-malarial controls (**Table 3-3**) (Wickramasinghe et al., 1987). The increase in macrophages observed in both malaria cases and non-malarial controls, although minimal in controls, is likely a response to infection. The cause of coma in non-malarial controls included meningitis caused by *Haemophilus influenzae* and *Mycobacterium tuberculosis,* and sepsis. The role of macrophages in each of these infectious agents, including *Plasmodium*, has been well documented; therefore, the increase in macrophages observed in the BM across groups may be expected (Chua et al., 2013, Zhang and Wang, 2014, Ackland et al., 2019, Ahmad et al., 2022).

Elevated eosinophils were observed in 53% of malaria patients, particularly for CM1/CM2 cases, whereas such an increase was not observed in non-malarial controls. Eosinophilia is frequently observed in children and pregnant women in sub-Saharan Africa due to the high prevalence of helminth infections and malaria (Huang and Appleton, 2016, Orish et al., 2021, Emmanuel et al., 2023). In this cohort, no helminth infections were diagnosed. The observed increase in eosinophils in the BM is likely attributed to *P. falciparum* infection alone, as this parasite is known to induce eosinophilia in children even in the absence of concurrent helminth infection (Orish et al., 2021). This finding of elevated eosinophils aligns with early observations in BM aspirates from patients with CM (Wickramasinghe et al., 1987).

The most notable histopathological parameters that varied between malaria patients and non-malaria controls were largely attributed to CM1 and CM2 cases. The presence of iRBCs was noted in all CM1/CM2 cases with mild to moderate pigment compared to minimal or no pigment present in SMA, incidental parasitaemia, and non-malarial controls (**Table 3-3**). Both iRBCs and pigment were positively correlated with a high M:E ratio, granulocytic left shift, and increased macrophages, all features associated with the response to infection. Further, these features were positively correlated with admission parasitaemia indicating that the BM is responsive to peripheral parasite load (**Figure 3-8**).

In both BM and spleen sections, pigment was noted throughout the tissue (**Figure 3-8, 3-11**). As discussed in **Section 3.4.1** and **Section 3.4.4**, it is not possible to determine whether this pigment is haemozoin, haemosiderin or formalin pigment using H&E-stained sections alone. To help decipher what this pigment is, prussian blue stains could be used which would allow differentiation between haemozoin and haemosiderin, an iron storage complex (Rebelatto, 2018). The higher amount of pigment observed in the spleen compared to the BM might be related to splenic clearance of parasites and therefore an abundance of haemozoin (Groom et al., 1991, Buffet et al., 2006, Safeukui et al., 2008). Alternatively, the higher levels of pigment might be due to general erythrocyte destruction releasing haemosiderin as a consequence of this process (Rebelatto, 2018). The pigment observed may also be formalin pigment, which is harder to distinguish from haemozoin since they are both brown/black with a granular appearance (Rogerson and Ordi, 2014). Formalin pigment deposition has been demonstrated to be positively correlated with PMI (Chatzopoulos et al., 2020). It was therefore investigated whether pigmentation in the BM or splenic RP was positively correlated with PMI. Pigmentation was not significantly correlated (p value > 0.05) with PMI in this cohort for both tissues (**Figure 3-25**). This lack of correlation further supports the hypothesis that this pigment is largely attributed to haemozoin.

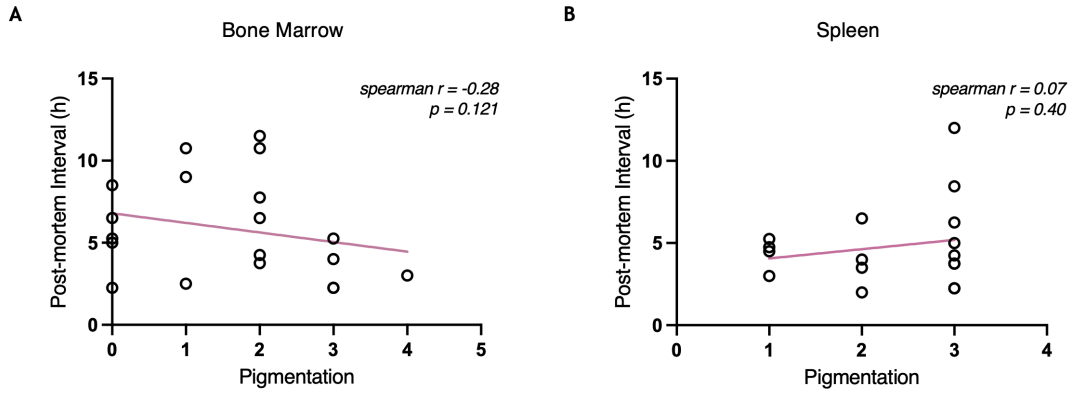

Figure 3-25. No correlation was observed between post-mortem interval (PMI) and pigmentation. Spearman correlations were performed for pigmentation (semi-quantitative scoring between 0 and 4) and PMI in the bone marrow (BM) (**A**) and spleen (**B**). For the spleen, pigmentation scores were taken from splenic red pulp (RP).

Where pigment was visible in the splenic WP, this pigment localised to germinal centres. Germinal centres are the site of somatic hypermutation of genes encoding the B cell receptor generating a panel of B lymphocytes which, based on antigen affinity, proliferate, and differentiate into antibody producing plasma cells or memory B cells. To engage in the germinal centre response, B cells must recognise antigens on their B cell receptor through antigen presentation (Mesin et al., 2016, Stebegg et al., 2018). The localisation of pigment to the germinal centres is consistent with antigen presentation from phagocytes which have phagocytosed either iRBCs or free haemozoin (**Figure 3-11B**).

Overall, the histopathology in the spleen did not differ greatly between malaria cases and non-malarial controls. Both groups exhibited minimal disorganisation/disruption of the splenic microarchitecture, mild elevation in eosinophils, minimal WP hyperplasia and mild haemorrhage/congestion. Further, there was no evidence of inflammation, necrosis, or fibrosis. These mild alterations in histopathology are consistent with previous findings investigating splenic histopathology in 15 adults with fatal severe *falciparum* malaria in Vietnam. This cohort consisted of 8 patients with CM and 7 patients that had at least one additional malaria-related complication such as hyperparasitaemia, anaemia, or acute respiratory failure. Here, authors stressed that even mild disorganisation of splenic architecture could disrupt splenic function affecting the generation of an effective and long-lasting immune response (Urban et al., 2005a).

Parameters relating to splenic architecture disruption were positively correlated such as disruption of the marginal zones and the blurring of limits between the RP and WP (**Figure3-13**). The relative lesion burden was positive correlated with haemorrhage, congestion and pigment in the WP, and other parameters indicative of splenic damage.

The lack of apparent differences in the spleen between malaria cases and non-malarial controls may be due to general disruption of the spleen due to other infection, previous episodes of malaria or an inflammatory driven response. For example, one non-malarial control had *Salmonella* septicaemia (PM72, **Table 3-1**). *Salmonella* has been demonstrated to disrupt splenic microarchitecture and cause expansion of macrophages and RBCs (Rosche et al., 2015, St John and Abraham, 2009, Jackson et al., 2010, Marcial-Juárez et al., 2023). It is unknown what the long-term effect of malaria on the histopathology of the spleen is. Effective antimalarial therapy typically resolves splenomegaly, a consequence of histopathological changes such as RP and WP expansion (McGregor et al., 2015). This indirectly suggests that splenic histopathology would return to normal after treatment, however, this remains unknown. The most marked changes in splenic histopathology among non-malarial controls were observed in PM56, a case diagnosed with coma of unknown aetiology. This patient had the highest relative lesion burden in the cohort with multiple lesions that were extensive and coalesce. It was evident that in this cohort, there is splenic disruption/damage observed throughout cases regardless of malaria status. The addition of spleens from healthy controls would provide a non-infectious control which will likely not exhibit infection/inflammatory driven histopathological changes allowing for a more suitable case comparison.

Several studies have demonstrated stress erythropoiesis in the spleen of *Plasmodium* infected mice, the degree of which is related to disease severity (Weiss et al., 1989, Villeval et al., 1990, Yap and Stevenson, 1992, Lamikanra et al., 2007, Ghosh and Stumhofer, 2021). No studies to date have investigated extramedullary haematopoiesis in *P. falciparum* severe malaria in humans. In our cohort, there was no evidence of extramedullary haematopoiesis across all clinical groups. It is important to note that this cohort was predominantly comprised of CM cases rather than SMA cases. No cases with SMA alone were histopathologically

scored here; however, there was no evidence of extramedullary haematopoiesis in CM cases with SMA. While no evidence of extramedullary haematopoiesis was found, the role of the spleen in stress erythropoiesis may differ in patients with SMA or chronic anaemia.

3.6.3 Parasite Accumulation in the Spleen

The spleen has recently been demonstrated to harbour a substantial non-phagocytosed parasite biomass in cases of chronic asymptomatic malaria in adults (Kho et al., 2021b, Kho et al., 2021a). Parasites of all intraerythrocytic developmental stages, with proportions aligning with the duration of each stage in the intraerythrocytic life cycle, were observed. Using a similar approach, the same splenic compartments were analysed to determine whether a comparable accumulation of non-phagocytosed parasites was present in the spleen of paediatric *P. falciparum* severe malaria cases. The use of Giemsa enabled identification of each parasite stage in each splenic compartment. For the existence of an endosplenic life cycle, all stages of the intraerythrocytic cycle should be present in the spleen and in proportions matching their duration in the life cycle (e.g., *P. falciparum* schizonts are expected to comprise ~25% of total asexual parasites based on observations from *in vitro* cultures).

Staging was based on morphological appearance of Giemsa-stained parasites in the tissue as described previously (**Figure 3-17**) (Safeukui et al., 2008, Kho et al., 2021a, Kho et al., 2021b). Note that the appearance of Giemsa-stained parasites in the tissues differs to that of peripheral blood smears. Parasite counts by Giemsa in the spleen was initially challenging due to the high levels of pigment throughout the RP (**Section 3.4.4**). Areas with a high level of pigment can obscure parasite identification. This is particularly challenging for identifying rings/early trophozoites where a blue cytoplasm is not visible within the RBC. This may have been the case for non-malarial controls where rings and early trophozoites were identified, albeit in far lower densities than observed in malaria cases (**Figure 3-22**). To validate these counts, IHC using a marker of all parasite stages, such as the constitutive parasite protein HSP70, is required (Shonhai et al., 2007).

Although Giemsa-based counts of early gametocytes in the spleen have been previously reported, the morphological appearance of this stage was not distinct enough to identify here and therefore this stage was not included. Further, very few mature gametocytes were identified throughout the spleen. As a fraction of the total parasite counts, including unclassifiable counts, only 0.1% of parasites were identified as gametocytes (95% CI: -0.1% to 0.4%) (**Figure 3-19A**). This contrasts with previous studies in chronic asymptomatic *falciparum* malaria in adults where 8.3% of total parasites (including unclassifiable stages) were identified as gametocytes (Kho et al., 2021a). To validate this finding, IHC targeting the gametocyte marker Pfs16 should be performed (Joice et al., 2014).

For all counts, an unclassifiable category was included. This category was used where a confident identification of the nature (parasite or pigment) and/or stage could not be made. This category comprised 35.1% of all counts and therefore parasite counts made here are conservative. The large fraction of unclassifiable parasites or stages may be due to the high levels of pigment throughout splenic compartments. If this category is removed, parasite distribution in all splenic compartments was 77.3% (95% CI: 66.8% to 88.1%) identified as rings/early trophozoites, 13.9% (95% CI: 7.7% to 20.1%) as trophozoites and 8.3% (95% CI: 3-13.6%) as schizonts (**Figure 3-19B**). Importantly, the spleen revealed the presence of all stages of the intraerythrocytic cycle, contrary to the classical view of the spleen comprising only rings/early trophozoites through circulation and normal splenic filtration.

The distribution of these parasites was not even throughout the spleen. The highest parasitaemia was observed in splenic cords followed by perifollicular zones. Parasitaemia between compartments was significantly different between splenic cords and non-circulatory spaces ($p=0.02$) and sinus lumens and non-circulatory space ($p=0.0008$). In some cases, a large accumulation of parasites outside the perifollicular zone was observed consisting predominantly of schizonts (**Figure 3-20**). It is possible that this accumulation of parasites represents parasites which have entered the slow circulatory system from the marginal zone and, due to the magnitude of parasites present, caused obstruction of the splenic cords. This obstruction may lead to an accumulation of parasites, in particular schizonts which lack deformability, in this area (Schmidt et al., 1993, Safeukui et

al., 2008, Cranston et al., 1984, Deplaine et al., 2011). Notably, in the same areas of intense parasite accumulation, aggregates of parasites that appeared to be enclosed within a membrane were identified which I have termed parasitic "nests". I hypothesised that these "nests" represent expanded macrophages that are morphologically distinct from pigmented phagocyted as represented in **Figure 3-17.** However, the presence of nuclear staining, as expected for macrophages, was not always clear or visible (**Figure 3-21**). Therefore, labelling with the macrophage marker anti-CD68 is necessary to determine if these are parasites within macrophages (Betjes et al., 1991, Chistiakov et al., 2017).

The original aim was to investigate both the spleen and BM by Giemsa; however, issues were encountered with the quality of Giemsa staining in BM sections for the Malawi cohort (**Figure 3-26**). To improve this, the Veterinary Diagnostics Services (University of Glasgow) was employed to stain selected tissues. However, it was not possible to achieve consistent good quality Giemsa staining across all BM sections despite being able to achieve this in Malawi spleen sections and in mouse BM sections (**Section 3.3.1** and **Section 3.5**). Further investigation into why staining failed in Malawi BM sections is required. For example, staining too many slides in a single batch could result in under or over-staining. It may be that the protocol used for staining these specific tissues could be modified to improve the quality of staining by increasing/decreasing the dilution of Giemsa used. It is important to determine whether the staining issues observed here are derived from the protocol or from the tissues themselves.

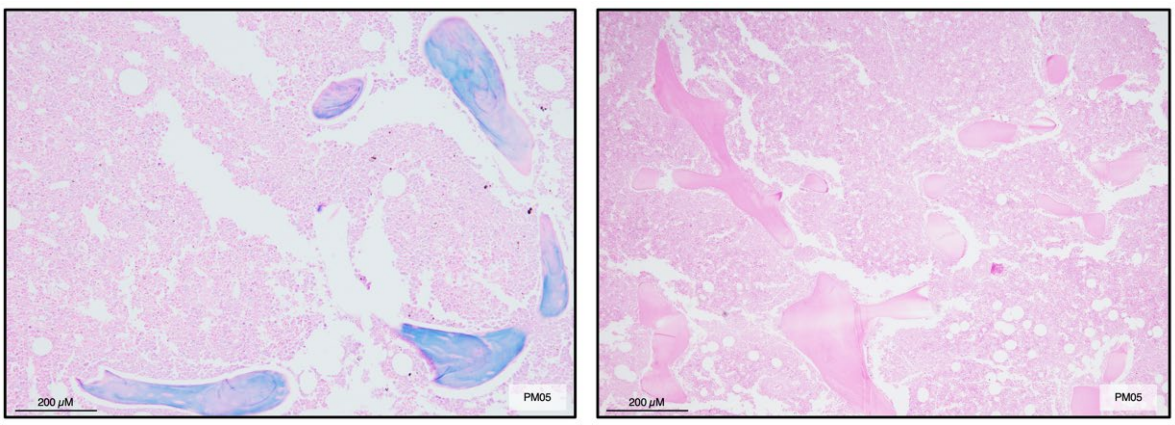

Figure 3-26. Inconsistent Giemsa staining in Malawi bone marrow (BM).

Overall, using Giemsa-stained sections alone, a large density of non-phagocytosed parasites in the spleen in paediatric severe *P. falciparum* malaria was revealed. This methodology is advantageous due to its simplicity, time efficiency, and the ability to define splenic compartments and stage parasites (**Section 3.5.1** and **Section 3.5.2)**. However, the substantial presence of pigment, as observed in this cohort, introduces challenges in parasite identification and staging. Further, this methodology may be considered subjective, necessitating counts from a second reader. IHC should be performed to validate counts derived from Giemsa-stained tissues.

3.6.4 Evidence of an Endosplenic Life Cycle

The existence of cryptic asexual replication in haematopoietic niches has been hypothesised, however, it has received limited investigation. This is largely due to ethical and technical considerations where investigation of such cryptic life cycles is challenging, especially in severe malaria. Therefore, previous investigations have been performed in mouse models or using splenectomised patient samples. Evidence of a cryptic life cycle in the spleen and BM has been demonstrated in *P. berghei* where invasion of early reticulocytes promotes gametocytogenesis (Lee et al., 2018). More recently, Kho *et al*. revealed the presence of schizonts in the spleen in proportions matching the duration of schizonts in the intraerythrocytic cycle for each species (*P. vivax* and *P. falciparum*) in chronic asymptomatic malaria in adults. Assuming that parasite growth rate in the spleen closely matches that observed *in vitro*, it is expected that *P. falciparum* rings and trophozoites would constitute approximately 75% of the lifecycle (0-36 hpi), while schizonts would constitute ~25% (36-48 hpi).

As mentioned before, all stages of the intraerythrocytic cycle were observed. Where schizonts were found, they were predominantly localised to the splenic cords in lower densities than observed for rings and trophozoites combined (**Figure 3-23**). If the proportion of rings and trophozoites is compared to schizonts, 91.2% (95% CI: 85.9% to 96.8%) of parasites identified were rings and trophozoites and 8.3% (95% CI: 3.0% to 13.6%) were schizonts. This fraction of schizonts, including the 95% CI, does not match their duration in the life cycle and therefore does not

suggest that there is an ongoing endosplenic cycle. Further, a large contribution of schizonts in the cords may be due to cord obstruction of schizonts on the periphery of the WP/perifollicular zone in some cases (**Figure 3-20**).

If you consider each stage independently, over 77% of asexual stages identified were rings/early trophozoites suggesting an enrichment of rings in the spleen in this cohort. There are several possible explanations for this enrichment of rings. One explanation is that rings from peripheral circulation are entering the spleen and are being retained in the spleen. Alternatively, quinine, which was the gold standard treatment for malaria in Malawi at the time, is only effective against mature stages. It is therefore possible that the enrichment of rings observed here is due to the activity of quinine which all patients were treated with on admission (ter Kuile et al., 1993, Dondorp et al., 2010, Saidi et al., 2023). To address this, tissue sections from a comparator organ, such as the lung, could be stained with Giemsa to assess parasite stage distribution in a similar manner to the spleen. In this cohort, lung involvement and respiratory complications were modest (Milner et al., 2013a). The lung is an organ of moderate sequestration which, like the spleen, is highly vascularised and therefore a good organ for comparing intravascular vs extravascular parasite accumulation (Milner et al., 2015). An alternative way to view the data is in relation to the parasite multiplication rate (PMR). In rapidly growing parasite populations with high PMRs, you may observe a higher ring to mature stage ratio. In populations with a high PMR, for every schizont from the last generation, there will be considerably more young stages from the new generation. Whereas, in parasite populations with a low PMR, there would be a lower ratio of next generation young stages to last generation mature stages (Khoury et al., 2014). Therefore, in this cohort where schizonts are not observed in proportions consistent with their duration in the life cycle, as observed in chronic asymptomatic cases, there may be a rapidly growing parasite population. The use of a comparator tissue could help to address the question of whether parasites in the spleen are growing with a higher PMR than in other tissues.

When considering the whole cohort, there is insufficient evidence to suggest that there is an ongoing endosplenic cycle based on parasite stage proportions alone. To investigate this further, it is necessary to determine if the magnitude of

parasite densities in the spleen could be explained by peripheral circulation alone. If parasite densities are so high that they cannot be explained by peripheral parasitaemia, this would suggest that an active endosplenic life cycle was ongoing. Since this is a treated cohort, it is also important to compare splenic accumulation to other tissues. This would reveal whether this parasite accumulation is unique to the spleen, revealing a splenic tropism.

3.6.5 Chapter Summary

The overall aim of this chapter was to use basic histological stains, H&E and Giemsa, to investigate the histopathology of the BM and spleen, and to begin to investigate the parasite reservoir in the spleen of paediatric severe *P falciparum* malaria cases and non-malarial controls. Overall, in both the spleen and BM, histopathological alterations were mild. In the BM, malaria cases displayed a greater presence of macrophages, eosinophils, iRBCs, pigment, and a higher M:E ratio. These histopathological changes were largely attributed to CM1/CM2 cases. In the spleen, no major differences in histopathology were observed between malaria and non-malarial controls. Minimal to mild disruption of the splenic microarchitecture was observed across all cases which was positively correlated with last parasitaemia before death. There was no evidence of extramedullary haematopoiesis, high reticulocyte percentages, and only mild congestion.

Evaluation of splenic accumulation of parasites by Giemsa revealed a large magnitude of non-phagocytosed parasites in the spleen. The distribution of parasites was predominantly in the splenic cords with rings and trophozoites comprising the greater life cycle fraction. Overall, there was insufficient evidence to suggest that there is an ongoing endosplenic life cycle based on intraerythrocytic stage proportions alone. Further investigation into the magnitude of splenic accumulation compared to peripheral circulation and other organs is required (**Chapter 4**).

Chapter 4 | Using IHC to determine splenic tropism and the presence of an endosplenic life cycle

4.1 Introduction

In the previous chapter, the accumulation of non-phagocytosed parasites started to be investigated using the basic histological stain, Giemsa. This allowed the distribution of parasites to be determined revealing that the highest parasite densities were found in the splenic cords. In this same compartment, there was evidence of all stages of the intraerythrocytic cycle, including few gametocytes. To validates these findings, immunohistochemistry (IHC) was performed to label specific host and parasite markers in the tissue.

4.1.1 Sequestration Across Multiple Organs

Kho *et al.,* investigated splenic parasite accumulation in asymptomatic patients undergoing splenectomy mostly due to splenic injury caused by trauma. Only spleen tissue and peripheral blood could be analysed in this cohort from Timika, Indonesia, where transmission is unstable (Kho et al., 2021a, Kho et al., 2021b). While estimates were made for the biomass in the BM, it was not possible to compare parasite biomass between organs using the same methodology as the spleen which would confirm the presence of a splenic tropism. In *P. falciparum,* a major virulent factor is the *Plasmodium falciparum* erythrocyte membrane protein 1 (PfEMP1) which allows the parasite to sequester in deep tissues through binding interactions between PfEMP1 and endothelial cell receptors (**Section 1.2.1**). Consequently, parasites sequester in all tissues, including the spleen.

In the same cohort presented here from Blantyre, Malawi, sequestration in the capillary beds in multiple organs was assessed. In all patients, sequestration intensity was highest in the brain, followed by the gastrointestinal tract (Milner et al., 2015). In the brain, parasite sequestration was associated with cerebral malaria (CM), the cause of death for most patients in this cohort (**Table 3-1**). The impact of gastrointestinal sequestration remains poorly defined (Sey et al., 2020). However, murine models of malaria (*Plasmodium yoelii*) have revealed that *Plasmodium* infection is associated with intestinal inflammation, dysbiosis of the intestinal microbiome, increased intestinal permeability, and increased colonisation of *Escherichia coli* and non-typhoidal *Salmonella* (Chau et al., 2013,

Mooney et al., 2015). Higher sequestered parasite densities were associated with cases of more rapid disease (CM1) across all organs analysed, in particular the spleen. Cases of CM associated with slightly more prolonged disease and histopathological changes in the brain (CM2), were associated with intense parasite sequestration in the skin. The lung, heart, stomach and spleen (exception in CM1 cases) represented organs with medium sequestration (Milner et al., 2015). This was supported by a separate study in Malawi utilising *Plasmodium* lactate dehydrogenase (pLDH) in the plasma to assess parasite organ distribution. This study revealed that the highest pLDH levels, and therefore parasite loads, were in the cerebral cortex, intestine, and skin for paediatric CM cases (Seydel et al., 2006). Due to this multiorgan sequestration, evaluating other organs and their respective compartments enable the determination of specific organ tropisms.

4.1.2 Reticulocytes in the Spleen

Previous studies investigating cryptic life cycles in the haematopoietic niches of the host have noted that the spleen is rich in erythroid precursors, or reticulocytes, providing young red blood cells (RBCs) to support an endosplenic life cycle (Lee et al., 2018, Kho et al., 2021a). In *P. berghei* infected mice, the invasion of erythroid precursors by *Plasmodium* in these niches renders parasites less susceptible to artemisinin, potentially facilitating the emergence of resistance (Lee et al., 2018). In chronic asymptomatic malaria cases (*P. vivax* and *P. falciparum*), an enrichment of reticulocytes was observed in the spleen compared to peripheral blood (Kho et al., 2021a). Indeed, it is known that the spleen contributes to the final maturation of reticulocytes (Li et al., 2021a). Reticulocytes in the spleen under normal circumstances are equally deformable as mature RBCs (Ovchynnikova et al., 2018). However, reticulocytes in the spleen of adults with chronic asymptomatic malaria, were observed to have reduced deformability which allowed for mechanical retention (Kho et al., 2021a). Furthermore, reticulocyte densities were highest in the splenic cords co-localising with parasites. (Kho et al., 2021a). Reticulocytes are known to have reduced deformability compared to mature RBCs, however, under normal circumstances they are not retained in the spleen (Moura et al., 2019). It is possible that during *Plasmodium* infection, reticulocytes become less deformable through an unknown mechanism resulting in their retention in the spleen providing a niche for parasite

invasion. It is known that parasite invasion induced increased host cell deformability (Groomes et al., 2022). However, in this study, it was not determined whether parasites were invading splenic reticulocytes (Kho et al., 2021a).

It is unknown whether paediatric severe *P. falciparum* malaria results in splenic retention of reticulocytes. In the previous chapter, the presence of extramedullary haematopoiesis, and therefore production of reticulocytes, in the spleen was investigated in malaria cases and non-malarial controls. No evidence was found for extramedullary haematopoiesis in the spleen based on histopathology (**Section 3.4.4**). Moreover, histopathological evaluation of the percentage of immature RBCs in the spleen indicated low proportions of reticulocytes. To validate these findings, IHC labelling of the reticulocyte marker, CD71, should be performed. It is important to note that for both *P. berghei* and *P. vivax*, where cryptic life cycles in the haematopoietic niches were associated with reticulocyte pools, parasites are restricted to reticulocytes for invasion (Lee et al., 2018, Kho et al., 2021a). Therefore, a pool of reticulocytes in the spleen may not be necessary to support an endosplenic life cycle for *P. falciparum*.

4.1.3 Gametocytes in the Spleen

The first identification of gametocytes in the spleen was in 1894 by Marchiafava and Bignami (Marchiafava, 1894). More recently, gametocytes were identified by Kho *et al.,* using Giemsa-stained spleen sections from chronic asymptomatic malaria patients. For *P. vivax* cases (n=6), gametocytes were only observed in one patient localised to the perifollicular zones of the spleen. For *P. falciparum* cases, gametocytes were observed in 6 cases (n=9) accounting for 8.3% of parasites identified in the spleen (Kho et al., 2021a). It is not clear whether the gametocyte stages identified in the spleen were immature stages or stage V gametocytes which are normally found in circulation. From this data, there may be a role of the spleen in either gametocyte formation or development for *P. falciparum,* but not for *P. vivax,* although note the small sample sizes. The contribution of the spleen towards gametocyte formation and development in paediatric severe *P. falciparum* malaria cases remains unknown.

In the previous chapter, the presence of gametocytes using Giemsa-stained spleen section from paediatric severe *P. falciparum* malaria cases and non-malarial controls was evaluated. Here, few gametocytes were observed accounting for 0.1% of parasite stages identified in the spleen (**Figure 3-18**). Only mature gametocytes could be evaluated based on their distinct morphology in Giemsa-stained tissue sections (**Figure 3-16**); these gametocytes were exclusively localised to the splenic cords (**Figure 3-22**). Due to the difficulties in identifying gametocytes in the spleen by Giemsa, it is necessary to perform IHC using a gametocyte specific antibody to confirm the lack of gametocytes in the spleen in these cases.

4.1.4 Sexual Commitment in the Tissue

The bone marrow (BM) has been identified as the site of gametocyte development; however, it remains unknown where gametocyte formation occurs. Two models have been proposed to explain how an enrichment of immature gametocytes is established in the BM in humans: either through selective homing of sexually committed merozoites or early gametocytes to the BM, where sexual commitment occurs outside of the BM, or via an endogenous asexual replication cycle within the BM that promotes sexual commitment (Nilsson et al., 2015). To investigate this, De Niz *et al*. utilised intravital microscopy to monitor gametocyte behaviour during *P. berghei* infection. This revealed that, early in infection, early gametocytes preferentially homed to the haematopoietic niches of the mouse (BM and spleen). The parasite accumulation in the BM increased during disease progression coinciding with vascular leakage in the BM and spleen, likely the result of inflammation. From this study, the following model was proposed: early in infection, early gametocyte stages preferentially home to the haematopoietic niches entering the extravascular compartment. As the disease progresses, high levels of inflammation result in vascular leakage in the sinusoids of the haematopoietic niches which results in extravasation of sexually committed and asexual merozoites into the extravascular spaces. Here, an endogenous asexual replication cycle can be established. Gametocytes mature in the extravascular compartment of the BM before a deformability switch which allows their release into circulation for onward transmission (De Niz et al., 2018).

Sexual commitment is environmentally sensitive. One environmental factor which has been demonstrated to regulate sexual commitment is the serum phospholipid lysophosphatidylcholine (LysoPC) (Brancucci et al., 2017). Specifically, depletion of LysoPC triggers sexual commitment and gametocyte formation in *Plasmodium* species with LysoPC responsive genes. Primate *Plasmodium* species, such as *P. falciparum, P. vivax* and *P. knowlesi*, possess LysoPC responsive genes such as *gdv1* (PF3D7_0935400) and therefore, at least in theory, are inducible by LysoPC depletion. However, rodent *Plasmodium* species lack these LysoPC responsive genes and consequently have different mechanisms for sexual commitment compared to primate species. Most notably, *P. berghei* exhibits same cycle commitment where commitment occurs in ring stages with gametocyte development occurring within the same cycle (Mons, 1986, Voss and Brancucci, 2024). In contrast, *P. falciparum* exhibits next cycle commitment, where commitment occurs in the cycle preceding gametocyte development (Bancells et al., 2019, Voss and Brancucci, 2024). While regulation of sexual commitments varies between primate and rodent *Plasmodium* species (as reviewed by Voss and Brancucci (Voss and Brancucci, 2024)), mouse models can still provide insights into physiological variation in LysoPC levels during *Plasmodium* infection. In *P. berghei* infected mice, LysoPC concentrations were demonstrated to be reduced systemically compared to uninfected controls. This reduction in LysoPC levels may be explained through the uptake and turnover of LysoPC by high parasite densities. Furthermore, BM aspirates from infected mice were found to exhibit a depletion in LysoPC compared to serum (Brancucci et al., 2017). This suggests that the local depletions in LysoPC concentration in the BM may trigger sexual commitment in a tissue specific manner. Additionally, inflammatory environments during acute or severe infection may also promote sexual commitment, possibly outside of the BM.

In a study of 828 children in Kilifi, Kenya, with asymptomatic, uncomplicated, and severe malaria, inflammatory responses were associated with reduced plasma LysoPC concentrations, which in turn was associated with markers of sexual reproduction (i.e., *ap2-g* expression) (Abdi et al., 2023). This validated previous findings in mouse models that inflammation results in physiological variation in LysoPC concentration which is linked to sexual reproduction. Therefore,

physiological variation in LysoPC concentrations, either systemically or in specific tissue compartments, may regulate sexual commitment and gametocytogenesis.

4.1.5 Chapter Aims and Hypotheses

In the previous chapter, high densities of non-phagocytosed parasites of all blood developmental stages were identified in the spleen of paediatric severe malaria cases. These parasites were found predominantly in the splenic cords. The proportion of schizonts observed in these cases does not suggest the existence of an endosplenic life cycle. To explore this further, it is necessary to determine whether parasite densities in the spleen could be explained by the retention of peripherally circulating parasites alone. To determine if there is a hidden biomass of intact parasites in the spleen, and therefore a splenic tropism, it is necessary to compare parasite biomass between different organs and the blood.

Erythroid precursors and reticulocytes have been implicated in supporting cryptic life cycles in the haematopoietic niches in *P. berghei, P. vivax,* and *P. falciparum* (Lee et al., 2018, Kho et al., 2021a). In **Chapter 3**, histopathological evaluation of the spleen in paediatric severe *P. falciparum* malaria cases revealed that there was no extramedullary haematopoiesis in the spleen, and the percentage of immature RBCs was low. To confirm that the spleen does not exhibit an enrichment of reticulocytes, it is necessary to perform IHC targeting reticulocytes and compare splenic reticulocytaemia with peripheral reticulocytaemia.

In chronic asymptomatic *P. falciparum* malaria, 8.3% of parasites identified in the spleen were gametocytes suggesting a possible role of the spleen in gametocyte formation and/or development. However, the contribution of the spleen towards gametocyte formation and development in paediatric *P. falciparum* severe malaria remains unknown. It has previously been demonstrated that the BM is enriched in gametocytes; however, it is unknown how this enrichment is facilitated in humans.

The overall aim of this chapter was to validate and expand on findings from **Chapter 3** and to explore the role of the spleen and the BM in gametocyte formation and development in paediatric severe *P. falciparum* malaria using IHC.

Specifically, in this chapter I aimed to:

- Investigate the presence of an endosplenic life cycle in paediatric severe *P. falciparum* malaria cases.
- To determine if there is a significant parasite biomass in the spleen, and therefore, a splenic tropism.
- To investigate the role of the spleen in gametocyte formation and development.
- To determine if there is evidence of sexual commitment in the BM.

4.2 Parasite Accumulation in the Spleen, BM, and Lung

To validate the previous observation that there was a large accumulation of non-phagocytosed parasites, predominantly in the splenic cords, IHC was performed using antibodies against the conserved constitutive parasite protein, heat shock protein 70, HSP70 (LSBio; LS-C109068), and the endothelial marker, CD31 (Novus Biologicals; NB100-2284). To determine if there is a splenic tropism in this cohort, a comparative analysis between the spleen, BM, and lung was performed. Here, the lung was used as a comparator tissue; the lung is a highly vascularised organ (like the spleen) with a mixture of vessel sizes and moderate sequestration (Milner et al., 2015).

4.2.1 Validating Giemsa Counts

By IHC, it was difficult to distinguish the perifollicular zone. Therefore, the perifollicular zone was not included in IHC counts for the spleen. Among the 24 spleens analysed, a mean of 66.3% (95% CI: 57.4% to 75.3%) of parasites were found in the splenic cords. The sinus lumens contained the next highest proportion of splenic parasites, with a mean of 29.9% (95% CI: 20% to 39.8%), followed by the non-circulatory spaces, which had a mean of 3.8% (95% CI: 0.9% to 0.6%) (**Figure 4-1A**). These proportions were comparable to those observed in Giemsa-stained spleen sections (**Figure 4-1B**). The discrepancy in mean proportion of parasites localised to the splenic cords between the two methods is likely due to the exclusion of the perifollicular zone in IHC counts.

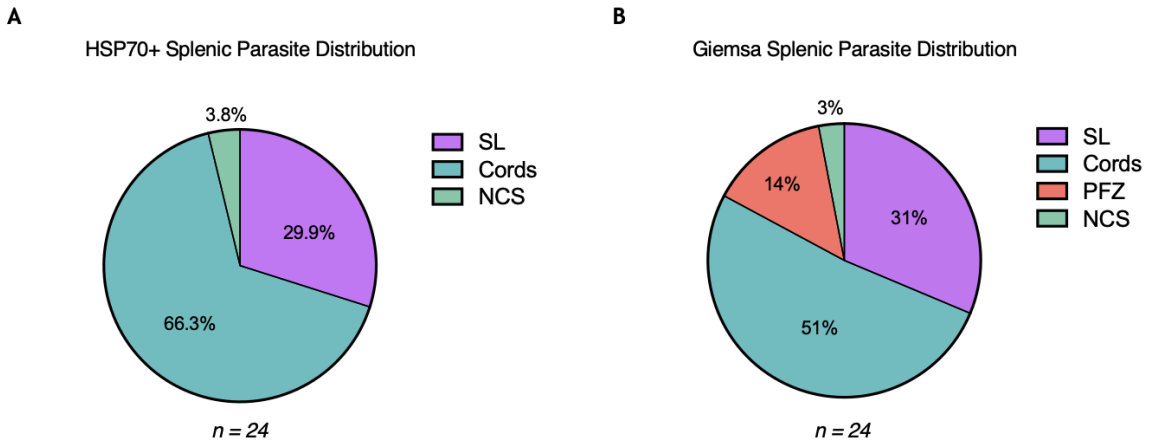

Figure 4-1. Parasite distribution in the spleen was comparable between immunohistochemistry (IHC) and Giemsa counts. Pie charts showing the mean proportion of parasites within each splenic compartment quantified by IHC and Giemsa. Each pie chart represents proportions across all clinical groups. Abbreviations: SL, sinus lumen; NCS, non-circulatory spaces; PFZ, perifollicular zone.

To measure the agreement between Giemsa and IHC counts, a Bland-Altman plot was generated determine the mean difference between the two counting methodologies (Bland and Altman, 1986, Myles and Cui, 2007). Most counts cluster around the mean difference, however, there were two outliers which fall out with the limits of agreement. Overall, the two counting methodologies are in agreement (**Figure 4-2**).

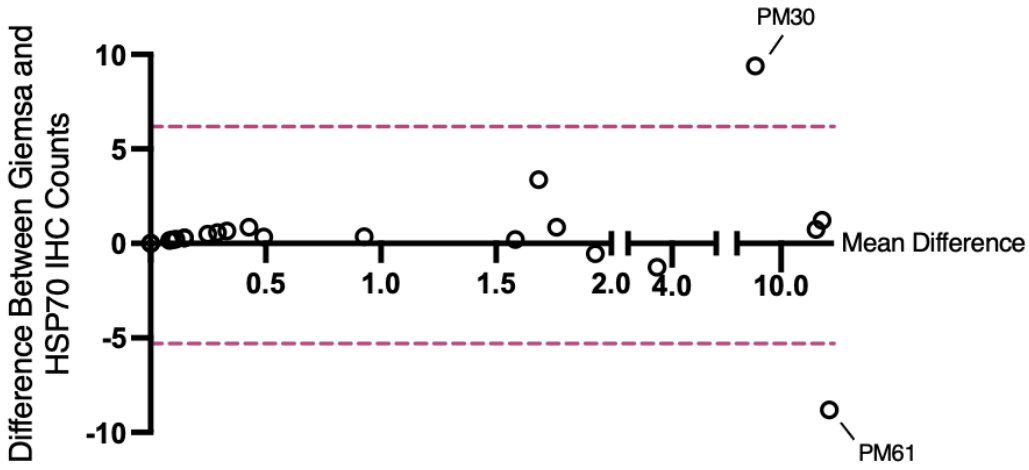

Figure 4-2. Counts performed by immunohistochemistry (IHC) and Giemsa were comparable. Bland-Altman plot showing the level of agreement between Giemsa and IHC counts. The distribution of differences between the two counting methodologies is shown giving an insight into their concordance. Purple dashed lines mark 95% confidence intervals (CI), or the limits of

agreement. Abbreviations: IHC, immunohistochemistry; PM, post-mortem (i.e., the number of the post-mortem performed used for patient identification).

4.2.2 Parasite Distribution in the Spleen, BM, and Lung

The distribution of *P. falciparum* in spleen, BM, and lung compartments was determined by HSP70/CD31 dual IHC staining. Since comparable results were achieved between Giemsa and IHC counts, the mean counts between these two methodologies were used in all subsequent analyses. As a result, a total of 25 spleens were analysed. In the interest of having consistent nomenclature between organs, sinus lumens, capillaries and post-capillary venules are classified as small vessels (denotated as SV in figures). Large vessels (denotated as LV in figures) can be distinguished from small vessels based on morphology and staining intensity of CD31. Counts within large vessels can be used to determine peripheral parasitaemia using the same modality as in the tissues. Using large vessels allows counting of parasites in vessels which are independent of classical sequestration (i.e., parasites in circulation).

Taking both Giemsa and IHC counts into consideration, a mean proportion of 62.6% (95% CI: 54.7% to 70.38%) of parasites were localised to the splenic cords. A similar mean proportion of 69.6% (95% CI: 51.6% to 87.56%) of parasites identified in the BM were found to localise to the extravascular space of the parenchyma. This contrasts with the lung where most parasites were found in small vessels. Here, a mean proportion of 68.7% (95% CI: 44.7% to 92.8%) of parasites were localised to the small vessels. Therefore, the distribution of parasites in the spleen and BM differs from that of the lung, where the vascular spaces are the predominant compartments of parasite accumulation (**Figure 4-3**).

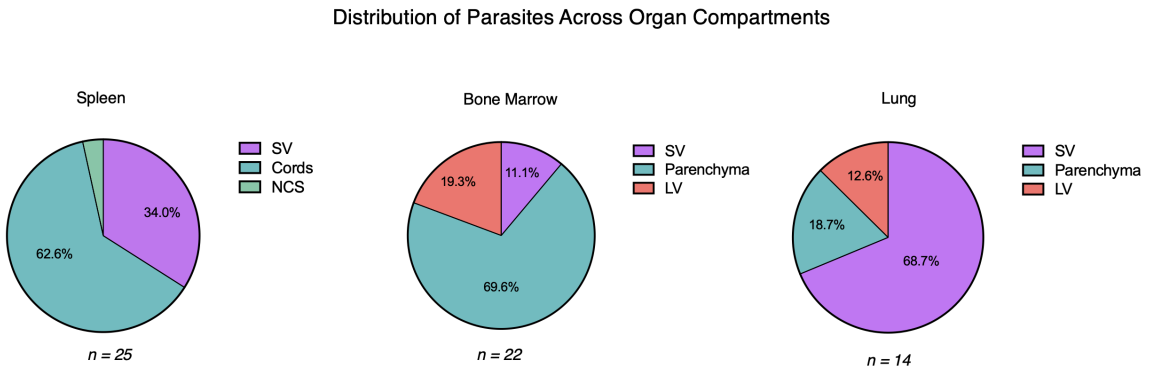

Figure 4-3. Distribution of parasites in the spleen, bone marrow (BM), and lung. Pie charts showing the mean proportion of parasites within each organ compartment by IHC (CD31/HSP70). Spleen distributions are based on both Giemsa and IHC counts. Each pie chart represents proportions across all clinical groups. Abbreviations: SV, small vessels; NCS, non-circulatory spaces; LV, large vessels.

Through IHC, splenic *P. falciparum* infection was found in 14/25 (56%) patients. Interestingly, one patient (PM56), which was classified as a non-malarial control, had HSP70+ parasites despite undetectable peripheral parasitaemia by PCR as measured on admission. Among non-malarial controls, this case also had the most marked histopathological changes in the spleen. Across the patients analysed for histopathological changes in the spleen, this patient had the highest relative lesion burden overall (**Section 3.6.2**). The presence of splenic parasites in cases where no parasites were detected by peripheral parasitaemia has previously been observed in chronic asymptomatic malaria cases in adults (*P. falciparum* and *P. vivax*) (Kho et al., 2021b, Kho et al., 2021a). In this cohort, all patients were treated with intravenous quinine dihydrochloride upon admission. However, where treatment is based on the identification of peripherally circulating *P. falciparum*, these cases would likely be missed which could lead to relapses.

To determine the parasitaemia, or parasite density, for each splenic compartment (cords, sinus lumen and non-circulatory spaces), the mean parasite count between Giemsa and IHC, and the RBC count from Giemsa-stained tissues, was used (**Section 2.3.4.1**). The parasite density was significantly higher in the small vessels ($p = 0.002$) and the splenic cords ($p = 0.012$) compared to the non-circulatory spaces of the spleen (**Figure 4-4, 4-5**).

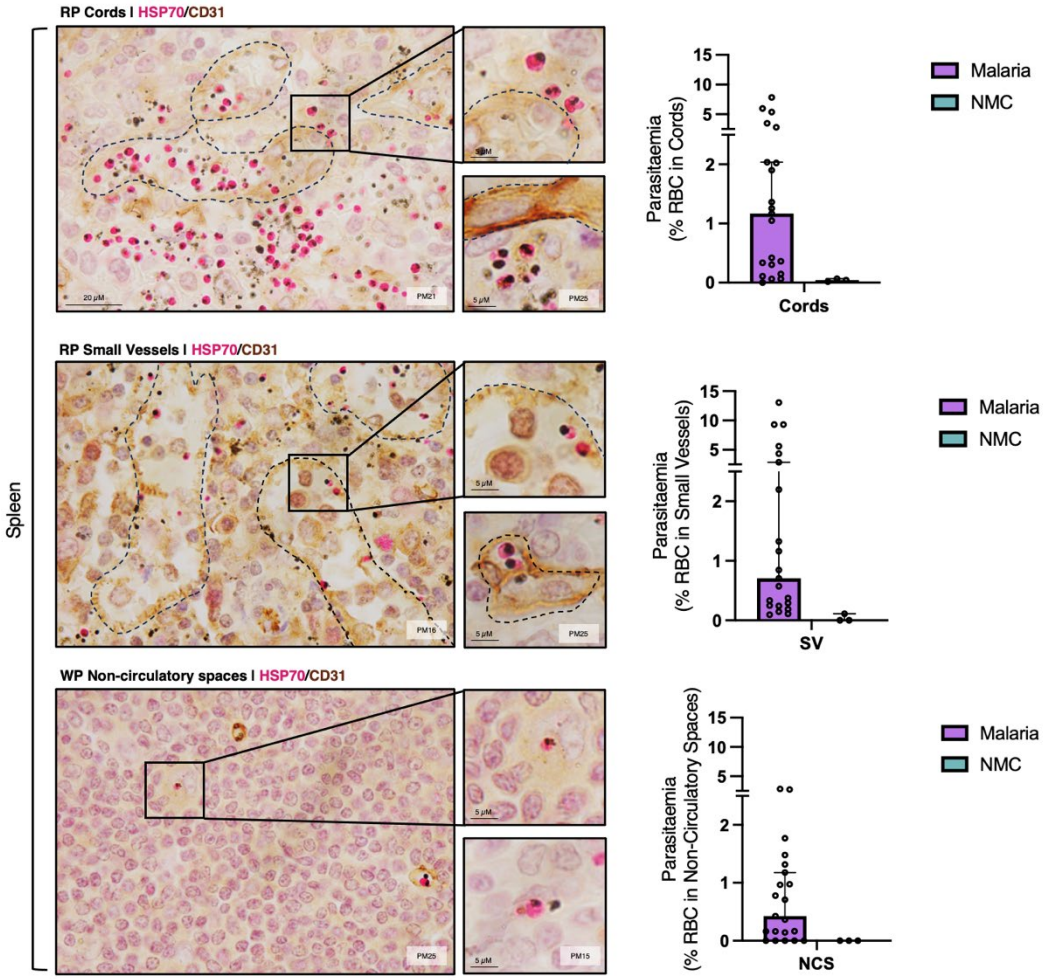

Figure 4-4. Splenic distribution of *P. falciparum* by immunohistochemistry (IHC). Representative images of splenic compartments and parasites with corresponding parasite densities (parasitaemia). Parasites were labelled using antibodies against HSP70 (pink; chromogen Vector Red). Intravascular compartments were determined using antibodies against CD31 (brown; chromogen DAB). Black dashed lines represent sinusoid lining. Parasitaemia is shown as median with 95% confidence interval. Symbols represent individual patients. Abbreviations: RP, red pulp; RBC, red blood cell, NMC, non-malarial control; SV, small vessels; NCS, non-circulatory spaces.

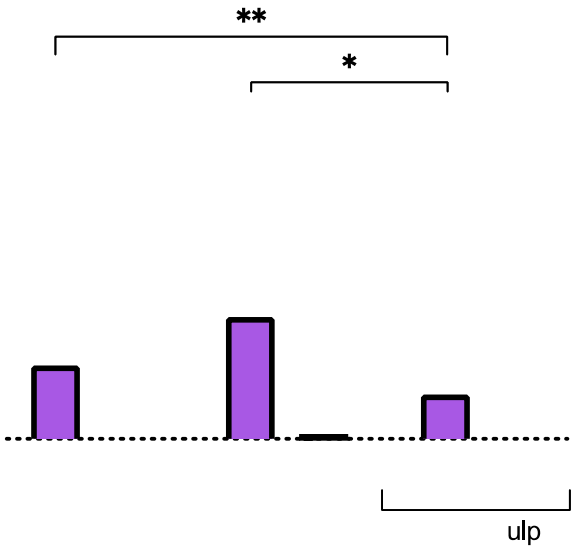

Figure 4-5. Parasite density is significantly higher in small vessels and cords compared to non-circulatory spaces. The density, or parasitaemia, of *P. falciparum* in each splenic compartment was determined (*n=24*). Parasitaemia is shown as median with 95% confidence interval. Symbols represent individual patients. Statistical tests performed was the Friedman test, followed by post-hoc Dunn's test to assess pairwise differences. Abbreviations: RBC, red blood cell; SV, small vessels; NCS, non-circulatory spaces; NMC, non-malarial control.

By Giemsa, in some cases, a notable enrichment of parasites was observed surrounding the WP (**Figure 3-20**). Using HSP70, this heterogenous distribution was confirmed (**Figure 4-6**). The heterogeneous distribution of parasites within the RP cords could be attributed to obstruction of the cords in these regions where substantial parasite accumulation impacts the local microcirculation.

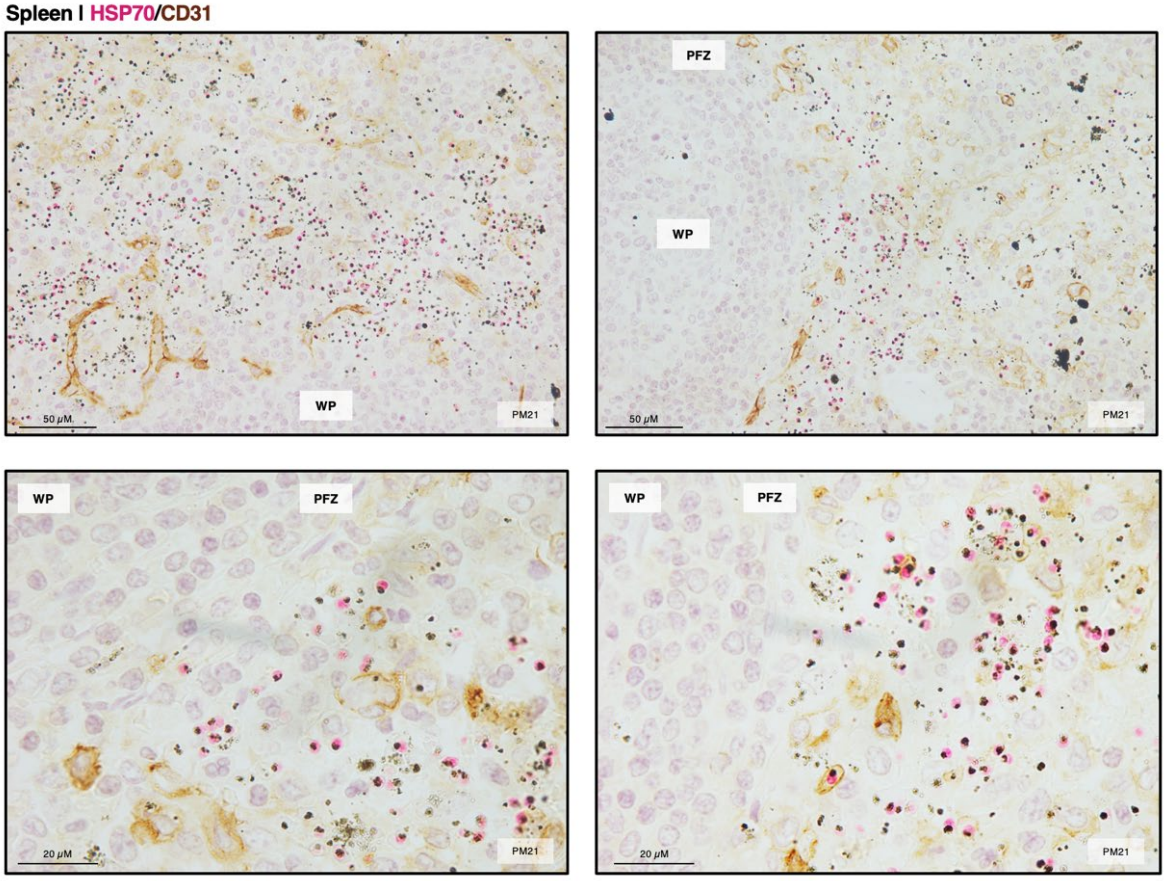

Figure 4-6. Heterogeneous distribution of parasites in the spleen. Representative images of parasite accumulation surrounding the white pulp (WP) beyond the perifollicular zone (PFZ). Parasites were labelled using antibodies against HSP70 (pink; chromogen Vector Red). Endothelial cells were labelled using antibodies against CD31 (brown; chromogen DAB). Abbreviations: WP, white pulp, PFZ, perifollicular zone.

For the BM, three distinct compartments – parenchyma, sinuses (which were classified as small vessels), and large vessels – were identified based on CD31 labelling. Among the 22 patients analysed, BM parasitaemia was identified in 14 cases (63.6%). For each compartment, RBCs were quantified based on their appearance by IHC allowing calculation of parasitaemia for each compartment. Parasite densities were significantly higher in the BM parenchyma ($p = 0.028$) compared to the small vessels of the BM. It is important to note that BM vessel parasitaemia may not be representative of peripheral parasitaemia due to the difficulty in counting RBCs and parasites in the vessels of the BM (**Figure 4-7, 4-8**).

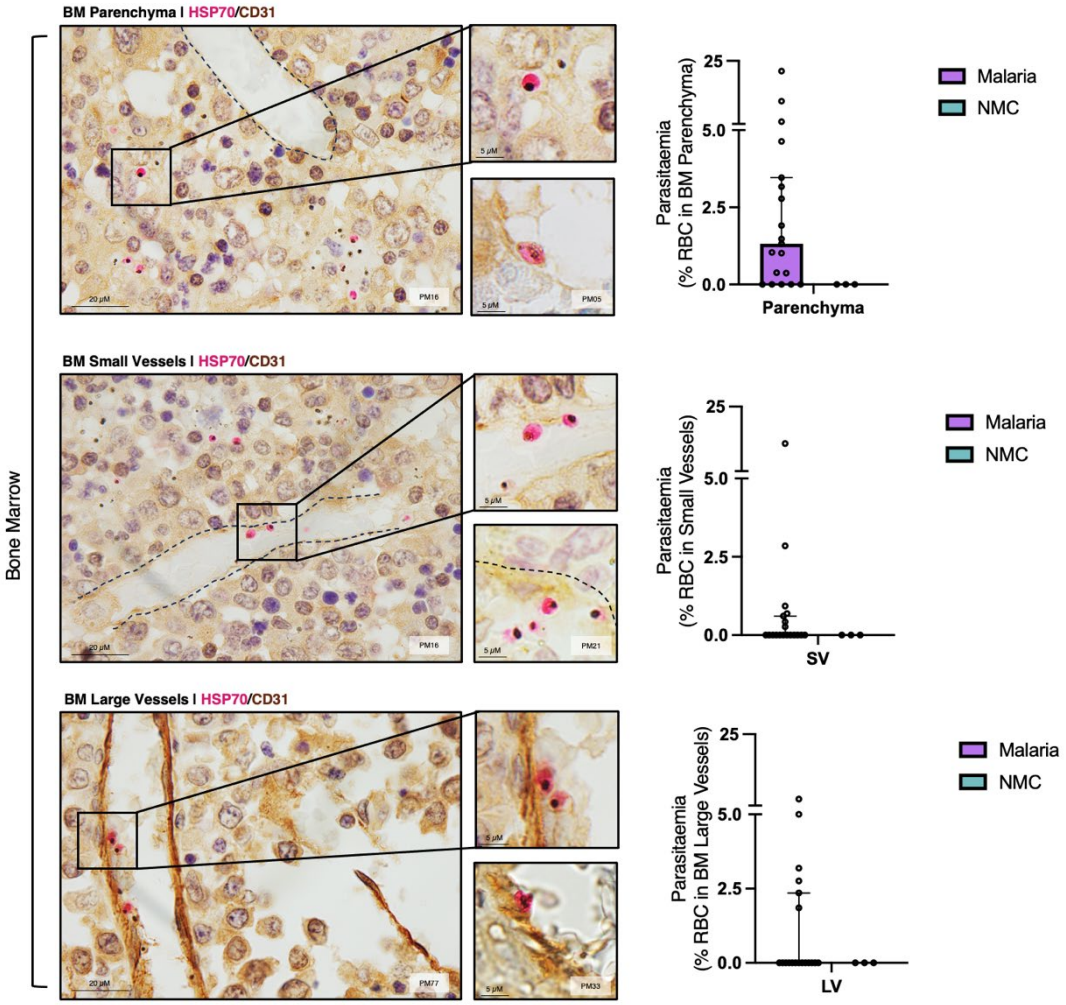

Figure 4-7. Bone marrow (BM) distribution of *P. falciparum* by immunohistochemistry (IHC). Representative images of BM compartments and parasites with corresponding parasite densities (parasitaemia). Parasites were labelled using antibodies against HSP70 (pink; chromogen Vector Red). Intravascular compartments were determined using antibodies against CD31 (brown; chromogen DAB). Black dashed lines represent sinusoid lining. Parasitaemia is shown as median with 95% confidence interval. Symbols represent individual patients. Abbreviations: BM, bone marrow; RBC, red blood cells; SV, small vessels; LV, large vessels; NMC, non-malarial control.

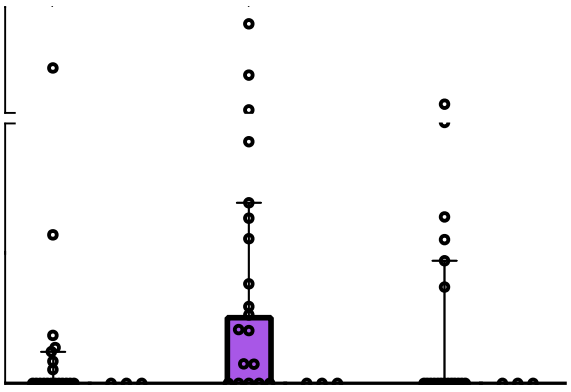

Figure 4-8. Parasite densities were significantly higher in the BM parenchyma compared to the small vessels (SV). The density, or parasitaemia, of *P. falciparum* in each BM compartment was determined (*n*=22). Parasitaemia is shown as median with 95% confidence interval. Symbols represent individual patients. Statistical tests used for each compartmental comparison was the Friedman test, followed by post-hoc Dunn's test to assess pairwise differences. Abbreviations: RBC, red blood cells; SV, small vessel; LV, large vessel; NMC, non-malarial control.

The lung was included as a comparator organ since it is a highly vascularised organ with moderate sequestration (Milner et al., 2015). For the lung, three compartments were identified based on CD31 labelling – the parenchyma, capillaries and post capillary venules (which are grouped as small vessels), and large vessels. Across all clinical groups, parasites were identified in 9 of 11 (81.8%) patients. Parasite densities were significantly higher in the small vessels ($p = 0.043$) of the lung compared to the lung parenchyma. The parasite densities in the small vessels of the lung likely represents classical sequestration (**Figure 4-9, 4-10**).

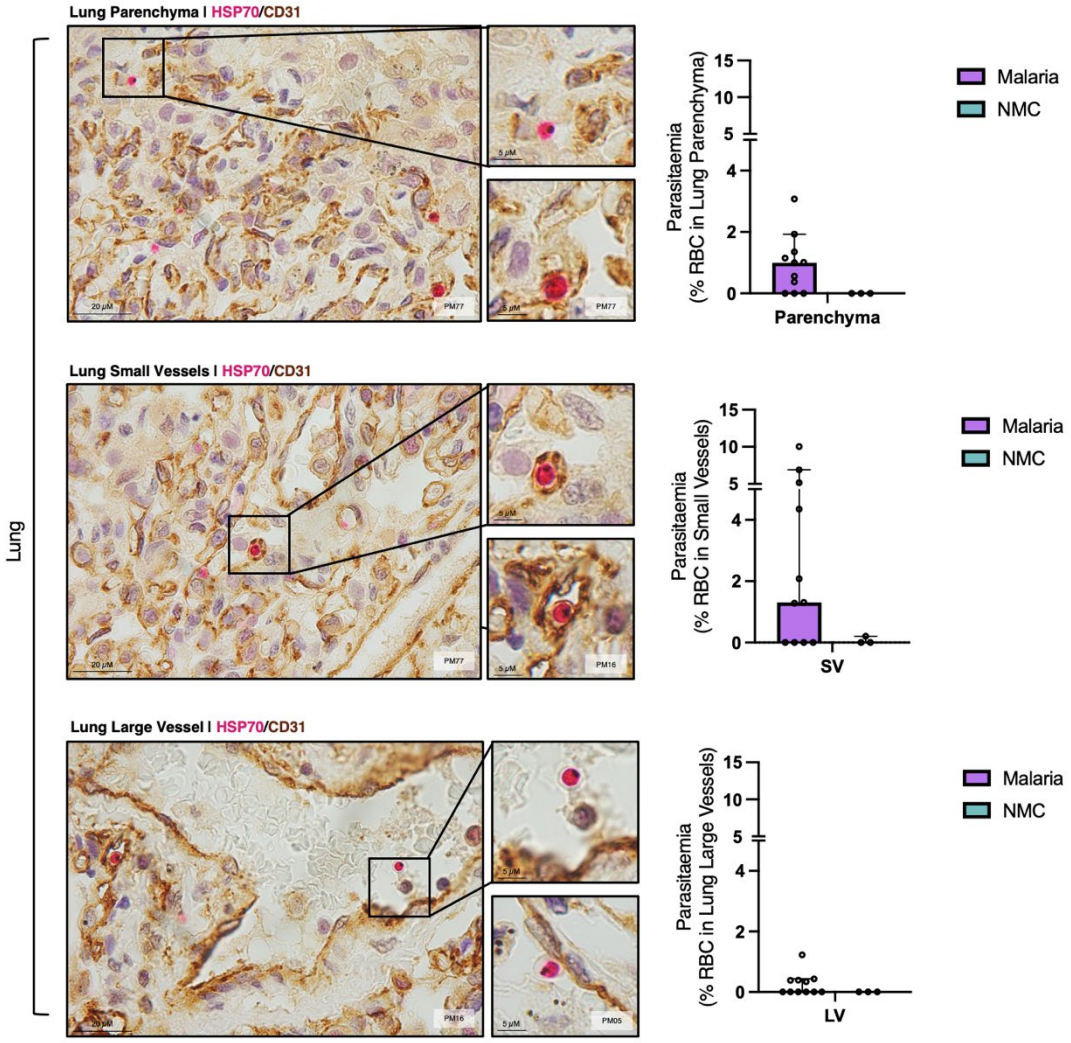

Figure 4-9. Lung distribution of *P. falciparum* by immunohistochemistry (IHC). Representative images of lung compartments and parasites with corresponding parasite densities (parasitaemia). Parasites were labelled using antibodies against HSP70 (pink; chromogen Vector Red). Intravascular compartments were determined using antibodies against CD31 (brown; chromogen DAB). Parasitaemia is shown as median with 95% confidence interval. Symbols represent individual patients. Abbreviations: RBC, red blood cells; SV, small vessels; LV, large vessels; NMC, non-malarial control.

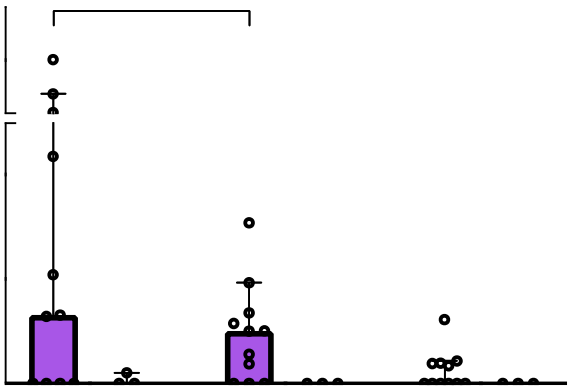

Figure 4-10. Parasite densities were significantly higher in the small vessels (SV) of the lung compared to the lung parenchyma. The density, or parasitaemia, of *P. falciparum* in each lung compartment was determined (*n=11*). Parasitaemia is shown as median with 95% confidence interval. Symbols represent individual patients. Statistical tests used for each compartmental comparison was the Friedman test, followed by post-hoc Dunn's test to assess pairwise differences. Symbols represent individual patients. Abbreviations: RBC, red blood cells; SV, small vessel; LV, large vessel; NMC, non-malarial control.

Overall, the parasite distribution between organs differs where parasite densities were predominantly in the intravascular spaces of the lung in contrast to the BM and spleen. This intravascular parasite density is likely attributed to classical vascular sequestration.

4.2.3 Comparison of Parasite Accumulation Between Organs

To determine whether a marked splenic tropism occurs in paediatric severe malaria, the total organ parasitaemia was calculated in the spleen, BM, and lung. In addition, peripheral parasitaemia at the time of death was determined using the large vessels of the lung allowing the calculation of peripheral parasitaemia by the same modality as tissues. The spleen, BM, and lung parasitaemia excluded parasite counts from large vessels.

The mean total parasitaemia in each organ was 1.86% (95% CI: 0.73% to 2.99%), 0.02% (95% CI: 0.00% to 0.04%) and 0.02% (95% CI: 0.00% to 0.03%) for the spleen, BM, and lung respectively. The mean peripheral parasitaemia based on parasitaemia in large lung vessels was 0.23% (95% CI: 0.00% to 0.46%). The mean spleen parasitaemia in severe malaria cases (1.86%) was comparable to the mean spleen parasitaemia in the Kho *et al*. chronic asymptomatic *P. falciparum* malaria cohort (1.53%) (Kho et al., 2021a). However, the mean peripheral parasitaemia between the two cohorts differed from 0.23% in the Malawi cohort to 0.007% in chronic asymptomatic *P. falciparum* malaria cases. Therefore, the difference between splenic and peripheral parasitaemia is more drastic in chronic asymptomatic adults compared to this cohort of paediatric severe malaria. Parasite densities were significantly higher in the spleen compared to the BM ($p < 0.0001$), lung ($p = 0.0006$), and peripheral parasitaemia ($p = 0.0008$; lung large vessels) (**Figure 4-11**). Parasites therefore accumulate in higher densities in the spleen compared to the organs analysed here.

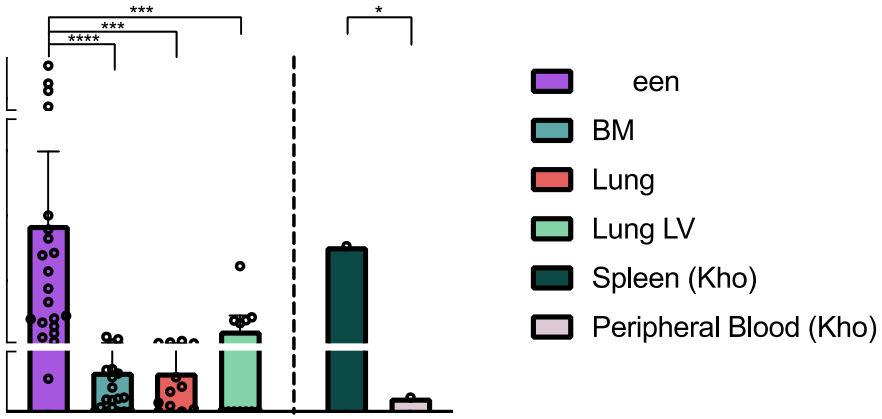

Figure 4-11. Spleen parasite densities are significantly higher than bone marrow (BM), lung, and peripheral blood parasite densities. The mean density, or parasitaemia, of *P. falciparum* in each organ and in the large lung vessel (LV) as a proxy for peripheral circulation. Total organ parasitaemia for BM and lung did not include large vessel parasitaemia. Parasitaemia is shown as mean with 95% confidence interval (CI). Splenic parasitaemia was significantly higher than parasitaemia observed in the BM ($p<0.0001$), lung ($p=0.0006$), and in the large vessels of the lung ($p=0.0008$). Statistical tests used for each compartmental comparison was the Kruskal-Wallis test, followed by post-hoc Dunn's test to assess pairwise differences. Symbols represent individual patients. Data from Kho *et al.*, 2021 was included as a comparator cohort of chronic asymptomatic malaria (*P. falciparum*) (Kho et al., 2021a). Abbreviations: RBC, red blood cell; BM, bone marrow; LV, large vessel.

4.2.4 Splenic Parasite Retention vs Endosplenic Life Cycle

Based on parasite densities alone, there was a significantly higher parasite density observed in the spleen compared to the BM, lung, and peripheral circulation. The parasite densities in the spleen were observed to be 8 times higher than in peripheral circulation. Like Kho *et al*, the aim was to investigate whether the extent of *P. falciparum* accumulation in the spleen could be attributed to splenic retention or whether this difference could be explained by the existence of an endosplenic life cycle. To determine if the magnitude of parasite densities in the spleen were the result of either parasite retention or a possible endosplenic life cycle, the following considerations needed to be made. Of the patients analysed

here, 5 patients received blood transfusions during hospitalisation (**Table 3-2**). Since the estimations for splenic retention require total blood volume and splenic blood volume, these patients were removed from the subsequent calculations. After removing these patients, the mean splenic parasitaemia of malaria cases was 1.97% and peripheral parasitaemia was 0.33%. For each patient, total blood volume was calculated based on the relationship between total blood volume and body weight. The total blood volume of a child is ~75-80 mL/kg depending on their age; for this cohort, all children were above 3 months old and therefore the age factor was 75 mL/kg (Howie, 2011, Koperska, 2023). Based on this, the mean total blood volume of the cohort was determined to be 830 mL.

Through *ex vivo* flushing experiments, the splenic blood volume was found to be 15 mL/100g of splenic tissue (Kho et al., 2021a). The mean splenic blood volume of malaria cases without blood transfusions was 13.39 mL. To determine the retention rate, the splenic input parasitaemia was calculated based on the ratio of total blood volume to splenic blood volume giving an input parasitaemia of 0.032%. Based on a mean peripheral parasitaemia of 0.33%, 9.52% of circulating parasites were retained in the spleen. This retention rate is consistent with ring retention rates determined by *ex vivo* spleen perfusion experiments to be ca. 10% (Safeukui et al., 2008). This observation is supported by the enrichment of rings/early trophozoite stages observed in Giemsa-stained tissues (**Section 3.5.3**, **Figure 3-18, 3-22**). Therefore, the splenic parasitaemia in acute paediatric *P. falciparum* could be explained by retention of peripherally produced *P. falciparum* infected RBCs (iRBCs) alone. Calculations for retention rate is detailed in **Section 2.3.4.3**.

4.2.5 Comparison of Parasite Biomass Between Organs

While the spleen exhibits higher parasite densities compared to other organs and the peripheral blood, it is important to know the total parasite load, or biomass, within each organ. This may provide a better indication of the true parasite organ distribution, and therefore, determine if there is a splenic tropism in these cases. The total parasite biomass was calculated for each organ based on organ weight and density. For peripheral biomass calculations, the iRBCs/μL of blood and total body blood volume was used (calculations detailed in **Section 2.3.4.2**).

The parasite biomass in the spleen ($p < 0.0001$), BM ($p=0.004$), and lung ($p=0.012$), were significantly higher than the circulating parasite biomass. However, there was no significant difference in parasite biomass between organs. This suggests that there is not a splenic tropism in terms of parasite biomass in paediatric severe malaria cases (**Figure 4-12**). The higher parasite biomass in tissues compared to peripheral blood is likely due to quicker clearance of parasites in circulation compared to in the tissues following antimalarial treatment. It is likely that the biomass in other organs, such as the brain which is known to have the high levels of parasite sequestration, is higher than the biomasses determined here (Milner et al., 2015).

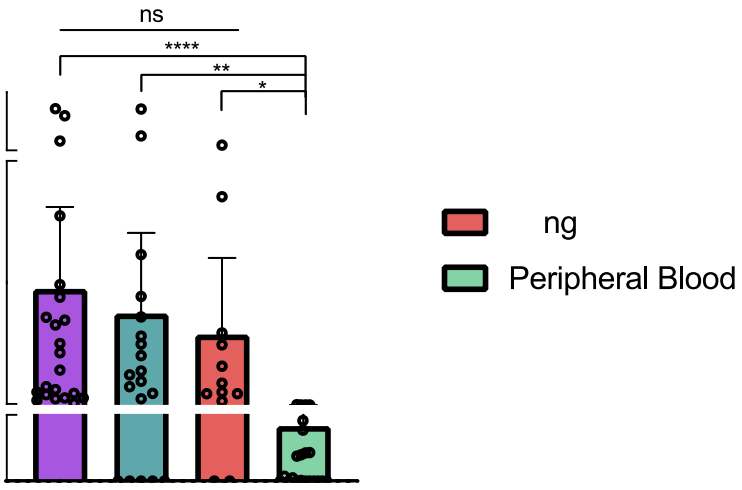

Figure 4-12. The spleen did not have a significantly higher parasite biomass compared to other organs. The parasite biomass was determined for each organ and peripheral blood. Calculation of bone marrow (BM) and lung biomass did not include large vessels. Parasitaemia is shown as mean with 95% confidence interval (CI). Parasite biomass was significantly higher in the spleen ($p<0.0001$), BM ($p=0.004$), and lung ($p=0.012$) compared to peripheral parasite biomass. However, there was no significant difference (ns) in parasite biomass between organs. The statistical test used for each compartmental comparison was the Kruskal-Wallis test, followed by post-hoc Dunn's test to assess pairwise differences. Symbols represent individual patients. Abbreviations: BM, bone marrow.

Overall, there were significantly higher parasite densities in the spleen compared to the BM, lung, and peripheral circulation. While the magnitude of parasite densities was high compared to other organs, the density could be explained be retention of peripherally circulation parasites alone and therefore not suggestive of an endosplenic life cycle. Furthermore, when comparing the parasite biomass between organs and peripheral blood, there was no significant difference observed between organ biomasses suggesting that there is not a splenic tropism in paediatric severe malaria cases. Note that these findings are based on the tissue sections analysed from this cohort.

4.3 Confirmation of Non-Phagocytosed Parasites

4.3.1 Splenic Macrophage Distribution

To confirm observations made in Giemsa-stained tissue that most parasites were non-phagocytosed, spleen sections were stained with the macrophage marker anti-CD68 and HSP70 (**Figure 4-13**) (Betjes et al., 1991, Chistiakov et al., 2017). Phagocytosed parasites were identified as pink HSP70+ parasites within a blue CD68+ macrophage. Overall, there were significantly more macrophages observed in the RP compared to the WP for both severe malaria patients ($p = 0.02$) and non-malarial controls ($p = 0.05$). There was no significant difference observed in macrophage numbers between malaria cases and non-malarial controls (**Figure 4-14**).

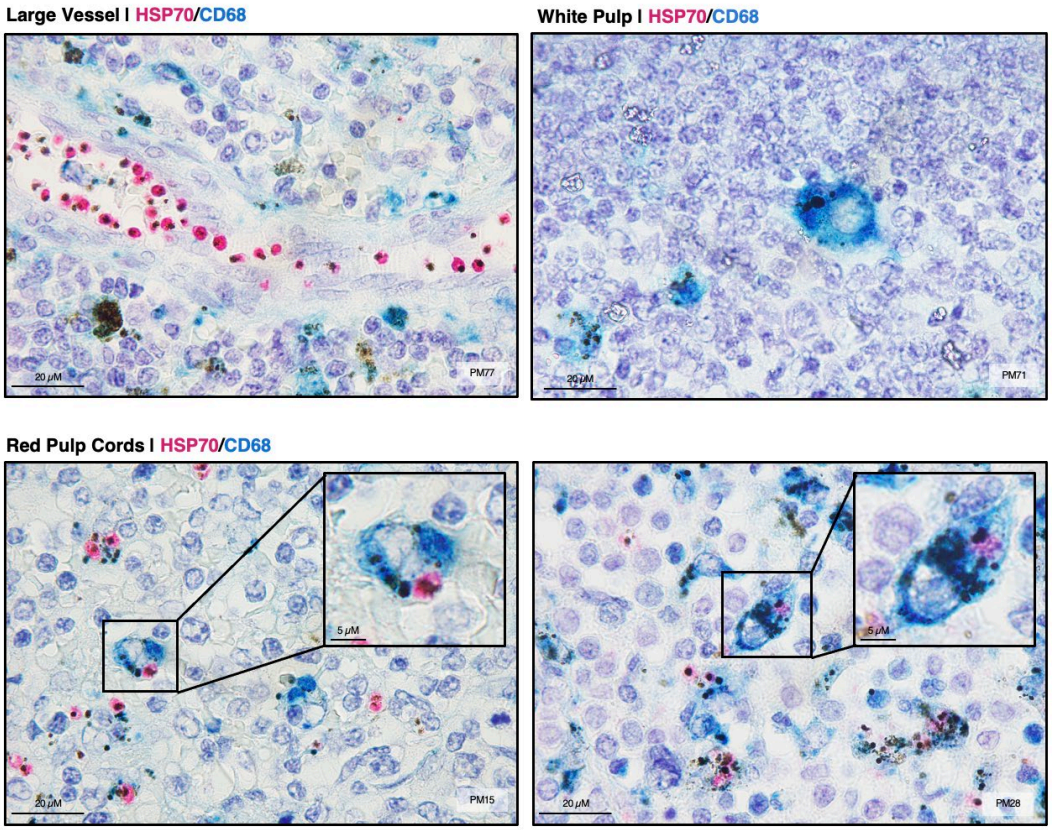

Figure 4-13. Parasite localisation with splenic macrophages. Representative images of the localisation of macrophages and parasites in spleen sections. Macrophages were labelled with the macrophage marker anti-CD68 (blue; chromogen Vector Blue) and parasites were labelled with anti-HSP70 (pink; chromogen Vector Red). Zoomed in image panels highlight phagocytosed parasites with dual HSP70/CD68 staining.

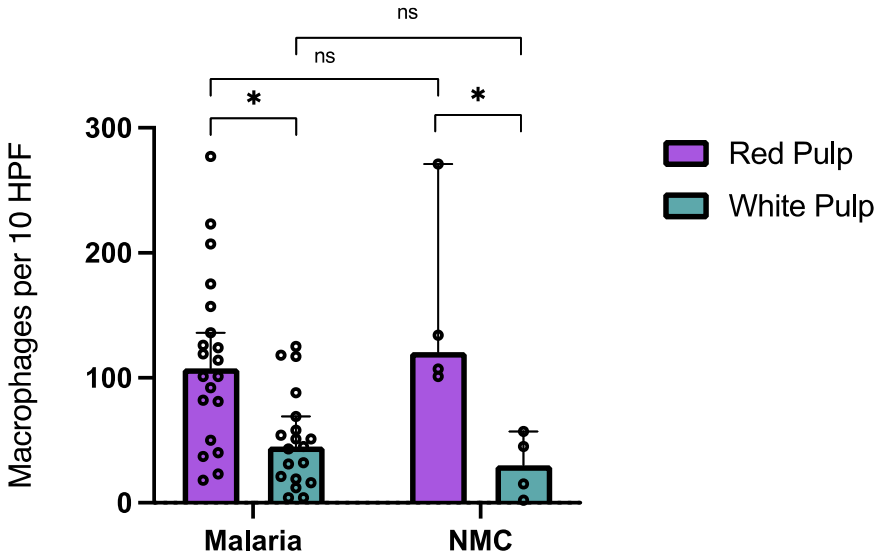

Figure 4-14. There is no significant difference in macrophage numbers between malaria cases and non-malaria controls. Median macrophage counts per 10 high powered fields (HPF) in the splenic red and white pulp across severe malaria cases and non-malarial controls (NMC). Data is presented as median values with 95% confidence interval (CI). There were significantly more macrophages in the red pulp (compared to the white pulp in both severe malaria cases (p=0.02) and non-malarial controls (p=0.05). The statistical test used for each comparison was the Kruskal-

Wallis test, followed by post-hoc Dunn's test to assess pairwise differences. Symbols represent individual patients. Abbreviations: HPF, high powered fields; NMC, non-malarial controls.

4.3.2 Free vs Phagocytosed Splenic Parasites

The visualisation of phagocytosed parasites across all spleens provided direct *in vivo* evidence of the host-protective role of the spleen. Next, the relationship between splenic parasite densities, macrophages and phagocytosed parasites was investigated. Spearman correlations were performed for 'free parasites' (HSP70+/CD68-) vs either macrophages (CD68+/HSP70-) or phagocytosed parasites (CD68+/HSP70+). Free parasites were weakly (r = 0.34) but significantly (p = 0.0478) positively correlated with splenic macrophages. Similarly, free parasites were moderately (r = 0.56, p = 0.0017) correlated with phagocytosed parasites within the spleen (**Figure 4-15**). Splenic macrophages however were not significantly correlated with peripheral parasitaemia (r = -0.11, p = 0.3806) as measured by HSP70+ cell counts in the large vessels of the lung. Therefore, elevated splenic parasites loads were associated with increased macrophage numbers, possibly leading to a heightened capacity for phagocytosis of iRBC.

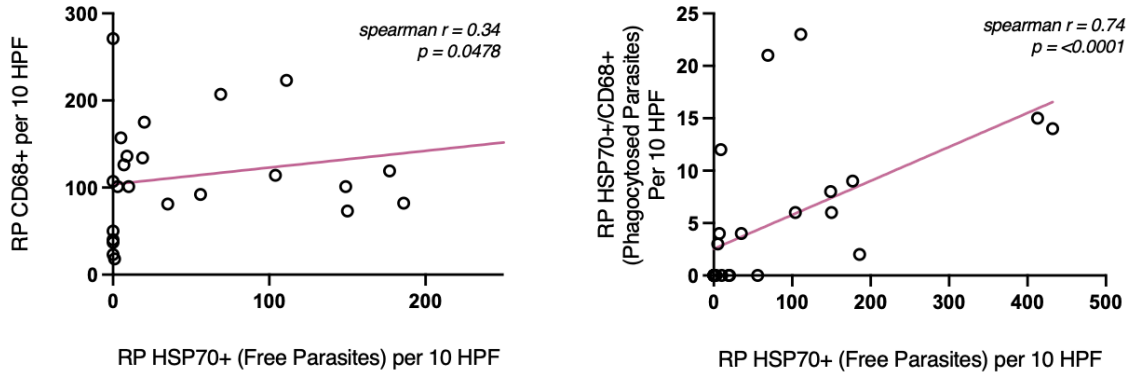

Figure 4-15. Free parasites in the spleen are positively correlated with macrophages and phagocytosed parasites. Spearman correlations were performed between 'free parasites' (HSP70+/CD68-) and either macrophages (CD68+/HSP70-) or phagocytosed parasites (CD68+/HSP70+) in the red pulp (RP) where macrophages predominate. Free parasites positively correlated with RP macrophages (r=0.35, p = 0.0478) and phagocytosed parasites (r = 0.56, p = 0.0017). Abbreviations: RP, red pulp; HPF, high powered field.

The number of free parasites (HSP70+/CD68-) were compared with the number of phagocytosed parasites (HSP70+/CD68+). There were significantly more free parasites than phagocytosed parasites in the spleen (p=0.0002). This suggests that while the number of macrophages, and phagocytosed parasites increase with the accumulation of parasites in the spleen, the vast majority of parasites are non-phagocytosed (**Figure 4-16A**). The impact of excluding phagocytosed parasitaemia from previous calculations was assessed. The mean splenic parasitaemia without removing phagocytosis counts was 1.86% (95% CI: 0.73% to 2.99%) whereas the mean splenic parasitaemia once these phagocytosis counts were removed was 1.84% (95% CI: 0.72% to 2.46%). Therefore, excluding phagocytosed parasitaemia does not drastically alter the splenic parasitaemia.

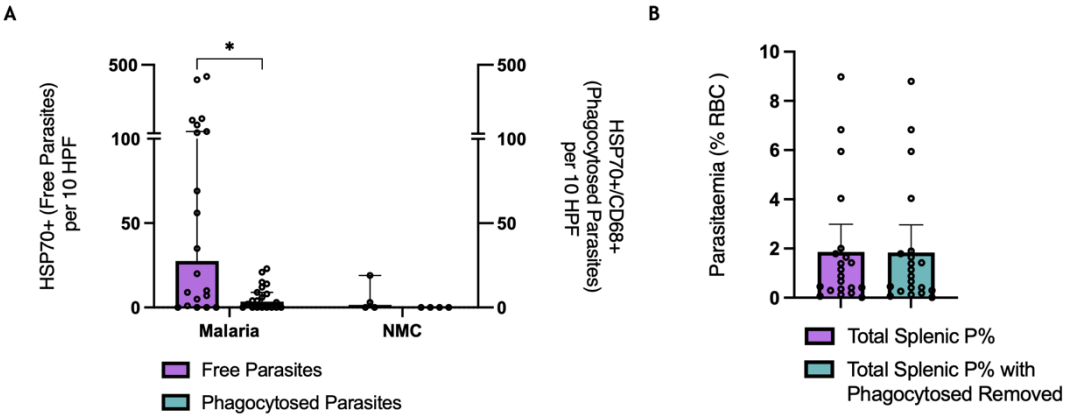

Figure 4-16. Parasites in the spleen were predominantly non-phagocytosed. (**A**) Number of free parasites and phagocytosed parasites in severe malaria cases and non-malarial controls. There were significantly more free parasites compared to phagocytosed parasites in the spleen (p=0.0002). Data is displayed as median values with 95% confidence intervals (CI). The statistical test performed was the Wilcoxan test. (**B**) Splenic parasitaemia with or without phagocytosed parasites. Symbols represent individual patient values. Abbreviations: HPF, high powered field; RBC, red blood cell; NMC, non-malarial control; P%, parasitaemia.

4.3.3 Investigating Splenic Parasitic "Nests"

By Giemsa, parasitic "nests" were identified in some cases on the periphery of the splenic WP beyond the PFZ. By IHC, parasitic "nests" were also observed (**Figure 4-17A**). These "nests" appeared as a cluster of parasites with a membrane surrounding the cluster. Often these "nests" consisted of a combination of

parasites, and parasite-like cells, which were categorised as unclassifiable. Here, unclassifiable parasites typically appear as a pigmented RBCs with an inner membrane (like that of the parasitophorous vacuole (PV)). I hypothesised that these clusters of parasites and unclassifiable parasites may be within large macrophages with parasite-like cells representing dead parasites. Based on this hypothesis, the co-staining patterns of CD68 and HSP70 in the context of parasitic "nests" was evaluated.

Many "nests" exhibited dual staining; these were only observed in CM1/CM2 cases (**Figure 4-17B**). The number of double stained "nests" were notably high for PM28 and PM78 which were both CM2 (-SMA) cases. However, many "nests" did not exhibit obvious CD68 staining (**Figure 4-17C**). It is not clear whether such "nests" without CD68 labelling are the result of inconsistent CD68 labelling or due to macrophage cell death.

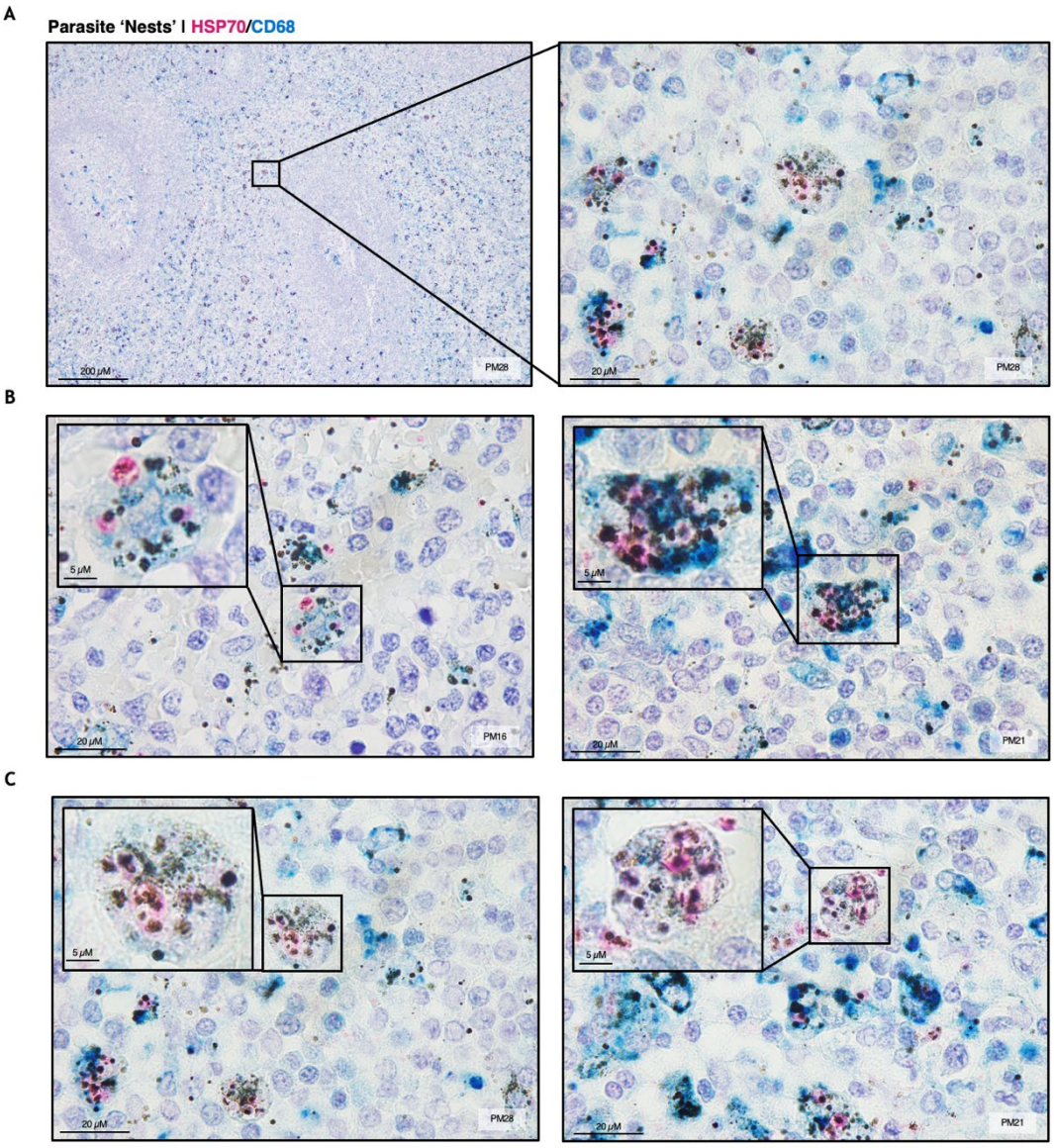

Figure 4-17. Splenic "nests" likely represent phagocytic events. (**A**) Parasitic "nests" were observed on the periphery of the white pulp (WP), beyond the perifollicular zone. They appear as a large cluster of parasites and pigmented red blood cells (RBCs). (**B**) Nest with clear CD68+ macrophage staining (blue, chromogen Vector Blue) and HSP70+ parasite staining (pink, chromogen Vector Red). (**C**) Nests lacking obvious CD68+ macrophage staining but with a visible membrane and HSP70+ parasite staining.

4.4 Reticulocyte Co-Localisation and Invasion

4.4.1 Reticulocyte Density in the Spleen and Lung Vessels

The spleen has a role in the final maturation of reticulocytes (Lee et al., 2018). Reticulocytes are equally deformable to RBCs, and therefore, under normal circumstances, can pass though the cords of the spleen with ease (Ovchynnikova

et al., 2018). However, Kho *et al*. demonstrated that in chronic asymptomatic malaria cases (*P. vivax* and *P. falciparum*), reticulocytes exhibited reduced deformability and consequently were retained in the spleen providing a pool of reticulocytes for invasion (Kho et al., 2021a). In **Chapter 3**, the presence of extramedullary haematopoiesis and immature RBCs was investigated in a histopathological evaluation of the spleen. This revealed that there was no extramedullary haematopoiesis in the spleen in this cohort, and therefore reticulocytes were not being produced in this tissue. Reticulocytes also accounted for a low percentage of the total splenic RBCs. To confirm that there is not an enrichment of reticulocytes in the spleen, IHC using antibodies against transferrin receptor of reticulocytes, CD71, was performed (Malleret et al., 2013). To compare reticulocytaemia in the spleen to peripheral circulation, reticulocytes in the large vessels of the lung were quantified (**Figure 4-18**). Note that extramedullary haematopoiesis can occur in the lung in rare occasions, although never reported in malaria cases, and therefore reticulocytaemia was compared only to peripheral circulation as measured using the large vessels of the lung (Singh et al., 2017, Yang et al., 2017, Fujimoto et al., 2022).

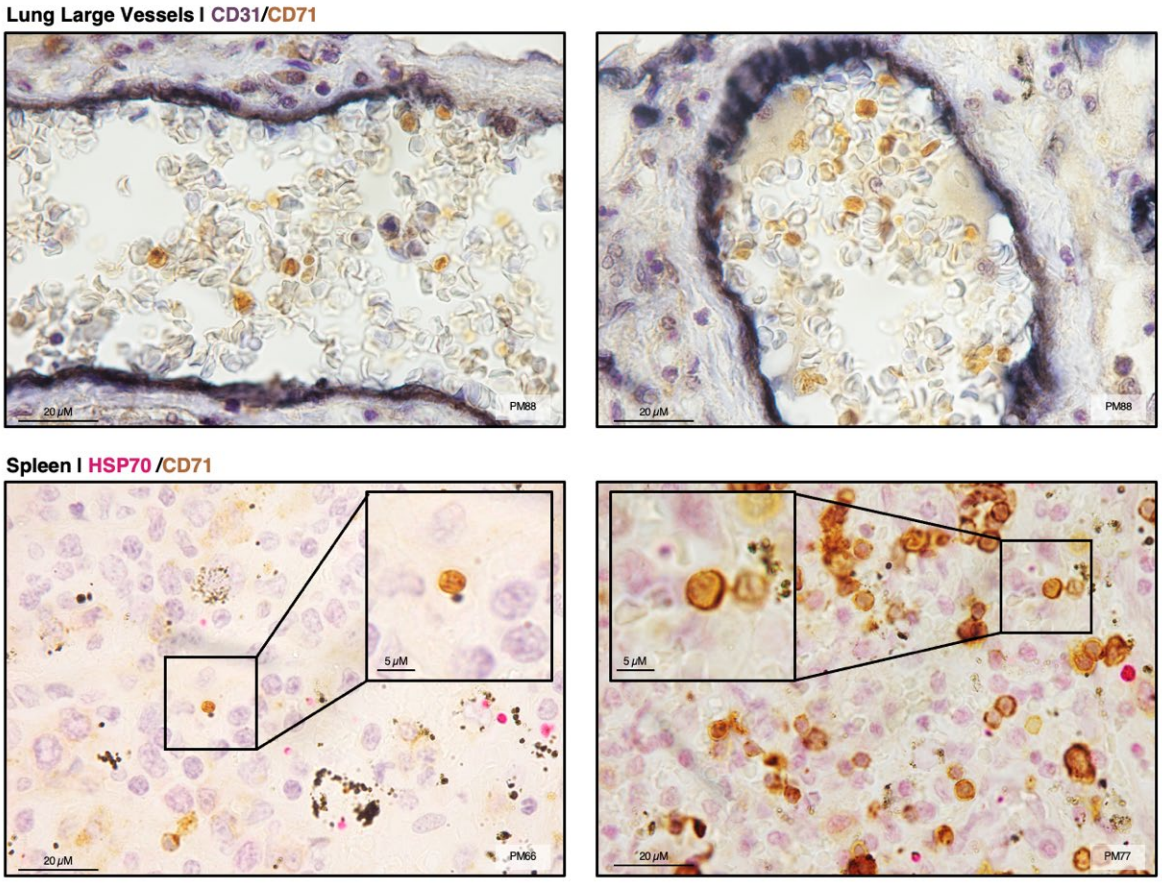

Figure 4-18. Reticulocyte (CD71) immunohistochemistry (IHC) in the lung and spleen. (**A**) IHC in the large vessels of the lung staining reticulocytes (CD71; brown, chromogen DAB) and endothelial cells (CD31; indigo, chromogen BCIP/NBT). (**B**) Reticulocyte IHC in the spleen. This was performed as a double stain with the parasite marker HSP70 (pink, chromogen Vector Red).

Throughout the spleen, many cells stained positive for CD71. To distinguish reticulocytes from other CD71 positive cells, only cells with CD71 staining lacking a nucleus were classified as reticulocytes. Reticulocytaemia was calculated in the same way as tissue parasitaemia. For spleen reticulocytaemia counts, RBC counts were obtained from the corresponding Giemsa-stained spleen section. For the large vessels of the lung, RBC counts were obtained from IHC stained tissues (**Section 2.3.4.1, Figure 4-18**). Comparisons were made between matched spleen and lung samples. Overall, there was a mean splenic reticulocytaemia of 1.08% (95% CI: -0.94% to 3.10%) compared to a mean peripheral reticulocytaemia of 0.38% (95% CI: -0.23% to 0.98%) (**Figure 4-19A**). This difference in reticulocytaemia was deemed not significant based on the Wilcoxon matched-pairs sign ranked test (p=0.313) (**Figure 4-19A**).

I hypothesised that high reticulocytaemia in the spleen may be driven by anaemia, and therefore highest in cases with SMA due to increased reticulocyte production to counteract anaemia (Leowattana et al., 2008, Dumarchey et al., 2022). I therefore compared matched reticulocytaemia spleen and lung between each clinical group. While it is difficult to draw conclusions from such small sample sizes, reticulocytaemia was notably higher in the SMA case and incidental parasitaemia case evaluated here (**Figure 4-19B**). In these two cases (PM30 and PM77 respectively), both children had anaemia. In comparing splenic reticulocytaemia within each group, these two patients exhibited abnormally high splenic reticulocytaemias. For instance, in cases with incidental parasitaemia, PM77 demonstrated a splenic reticulocytaemia of 10.07%, whereas PM70, another incidental parasitaemia case, exhibited a splenic reticulocytaemia of 0.03%. Similarly, for SMA cases, PM30 had a splenic reticulocytaemia of 1.16%, while PM57 had a splenic reticulocytaemia of 0%. PM70 and PM57 did not have matched lung samples and so a comparison between the spleen and peripheral circulation could not be performed. Therefore, although splenic reticulocytaemia was higher than peripheral reticulocytaemia in the cases of SMA (PM30) and incidental parasitaemia cases (PM77) evaluated here, these two cases may represent outliers in this cohort.

The reticulocyte densities were compared between this cohort and the Kho *et al*. cohort of adult chronic asymptomatic malaria (*P. falciparum* and *P. vivax*) (Kho et al., 2021a). In the Kho *et al*. cohort, the median splenic reticulocytaemia was 2.4% (n=10; *P. vivax* (n=4) and *P. falciparum* (n=6)) compared to the median splenic reticulocytaemia in this cohort of 0.2% (95% CI: 0% to 1.16%). This difference is likely due to chronic anaemia in chronic asymptomatic malaria cases driving RBC production. In the Kho *et al*. cohort, deformability of reticulocytes in the spleen were also observed to be reduced (Kho et al., 2021a). While it is unknown in paediatric severe malaria if reticulocytes are more deformable than in chronic asymptomatic cases, this may be the case due to lower reticulocyte densities observed in this cohort (**Figure 4-19**). Alternatively, the short time to death of patients in this cohort may not allow sufficient time to establish a reticulocyte response comparable to that of patients with chronic malaria and anaemia (Mayer and Donnelly, 2013).

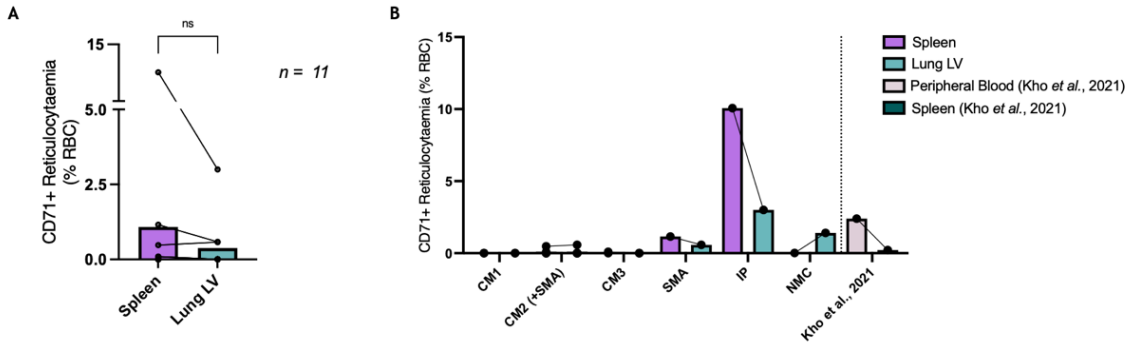

Figure 4-19. Reticulocytaemia was not significantly different between spleen and peripheral blood. (**A**) Reticulocytaemia was compared between the spleen and the large vessels of the lung as a measure of peripheral reticulocytaemia (*n=11*). There was no significant difference (p=0.312) between reticulocytaemia in the spleen and the peripheral circulation. Statistical test performed was a Wilcoxon matched pairs signed rank test. (**B**) Reticulocytaemia was compared between the spleen and peripheral circulation in each clinical group. Data from Kho *et al.*, 2021 was included as a comparator cohort of chronic asymptomatic adult infections (*P. falciparum* (n=6) and *P. vivax* (n=4)) (Kho et al., 2021a). Symbols represent individual patients. Abbreviations: RBC, red blood cell; CM, cerebral malaria; SMA, severe malaria anaemia; IP, incidental parasitaemia; NMC, non-malarial control; LV, large vessels.

4.4.2 Parasites Infection of Reticulocytes in the Spleen and BM

To assess the extent to which *P. falciparum* invades reticulocytes in the spleen and BM, the number of parasites within reticulocytes was quantified based on HSP70+/CD71+ double staining (**Figure 4-20A**). In both the spleen and BM, parasites were predominantly in normocytes (mature RBC, HSP70+/CD71-) compared to reticulocytes (HSP70+/CD71+). In the spleen, the mean normocyte infecting parasitaemia was of 1.83% (95% CI: 0.71% to 2.96%) which was significantly higher than the mean reticulocyte infecting parasitaemia of 0.02% (95% CI: 0.00% to 0.03%) ($p < 0.0001$) (**Figure 4-20B**). Since the splenic reticulocytaemia was low (**Section 4.4.1**), the low reticulocyte infecting parasitaemia observed here could be expected. If the splenic reticulocytaemia was high, it is possible that the reticulocyte infecting parasitaemia would be higher due to the preference of *Plasmodium* for reticulocytes (Leong et al., 2022).

In the BM, there was no significant difference between parasites within reticulocytes and normocytes (**Figure 4-20B**). However, due to the lower parasite densities observed in the BM, it is likely that 10 high powered fields (HPF) per BM compartment were not sufficient to draw conclusions. Additional HPFs would be

required to confirm these observations. The BM is the primary site of erythropoiesis in humans after birth providing a large pool of erythroid precursors for invasion (Galloway and Zon, 2003, Mikkola and Orkin, 2006, Orkin and Zon, 2008, Gupta et al., 2022). Furthermore, the BM has previously been demonstrated to be enriched in gametocytes (Joice et al., 2014, Aguilar et al., 2014, Baro et al., 2017, Obaldia et al., 2018). In BM aspirates collected from an adult patient with *P. falciparum* malaria in India, gametocytes were identified within erythroid precursors (Neveu et al., 2020). Joice *et al*. observed that 50-90% of gametocytes in the BM were in contact with erythroblastic islands (described in **Section 1.3.1, Figure 1-6**) in paediatric cases of severe *P. falciparum* malaria. Most early gametocytes (stage I) were localised to within CD71+ cells in the BM, while more mature gametocytes (stage II/III) were found within CD71- cells suggesting that gametocyte development coincides with host cell maturation (Joice et al., 2014). It is possible that the higher reticulocyte densities in the BM, alongside higher reticulocyte infecting parasite densities, not only support a possible asexual replication cycle, but may also contribute to creating a BM niche conducive of gametocyte formation and development.

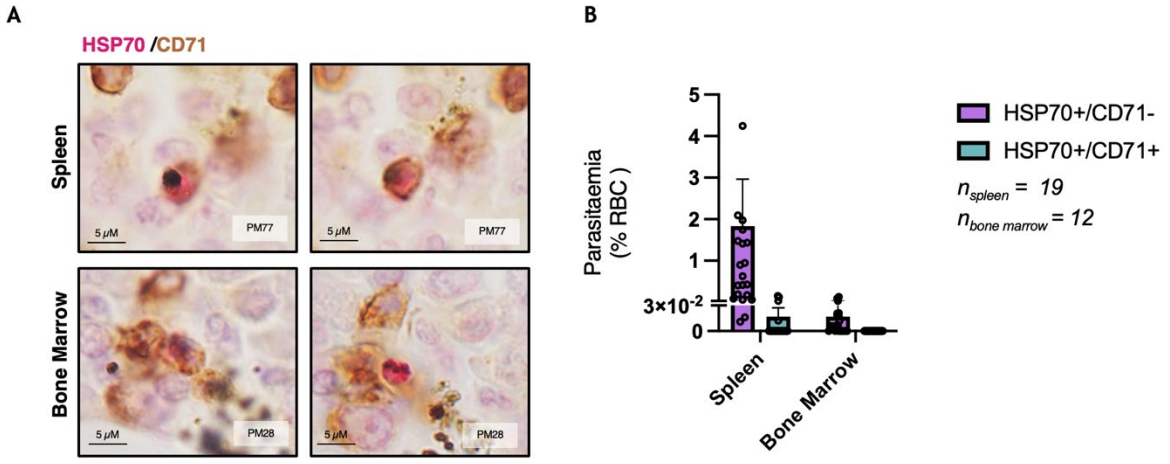

Figure 4-20. Parasites predominantly infect mature red blood cells (RBCs) over reticulocytes in the spleen. Dual immunohistochemistry (IHC) was performed on spleen and bone marrow (BM) sections using the parasite marker, anti-HSP70 (pink, chromogen Vector Red), and reticulocyte marker, anti-CD71 (brown, chromogen DAB) (**A**) Representative images of parasite infected reticulocytes in the spleen and BM. The left and right panels represent the same image but in a different plane of focus. (**B**) Spleen and BM parasitaemia for parasite infected mature RBCs or normocyte (HSP70+/CD71-) and parasite infected reticulocytes (HSP70+/CD71+). There was significantly higher mature RBC parasitaemia compared to reticulocyte parasitaemia ($p<0.0001$). Statistical tests used for each comparison was the Kruskal-Wallis test, followed by post-hoc Dunn's test to assess pairwise differences. Symbols represent individual patients. Abbreviations: RBC, red blood cell.

4.5 Gametocyte Distribution in the Spleen and BM

4.5.1 Gametocytes in the Spleen

In chronic asymptomatic *P. falciparum* malaria cases in adults, 8.3% of parasites in the spleen were identified as gametocytes by Giemsa suggesting that the spleen may contribute to gametocyte development in *P. falciparum* cases. Since quinine is not effective against gametocytes stages, assessment of gametocytes will more closely reflect parasite densities during infection (Peatey et al., 2012). Using Giemsa-stained tissue sections, the gametocyte fraction of all parasites identified in the spleen of paediatric severe malaria cases was 0.1% (**Figure 3-18**). By Giemsa, identification of gametocytes, other than mature gametocytes, is challenging. Therefore, evaluation of gametocyte densities in the spleen was performed using the gametocyte marker, anti-Pfs16 (**Figure 4-21A**) (Joice et al., 2014). Pfs16 labelling was part of a dual IHC partnered with antibodies against the sexual commitment marker, MSRP1 (provided by Gavin Wright, University of York), to assess gametocyte formation (analysed in **Section 4.6**). Since few gametocytes are expected to be identified in the spleen based on Giemsa data (**Section 3.5.3)**, the number of HPFs analysed was increased to 25 HPFs per tissue compartment.

In the spleen, gametocytes were identified in 4 cases, among them PM56, which was originally classified as a non-malarial control. Gametocytes were found exclusively in the RP of the spleen (**Figure 4-21B**). When considering the entire cohort, only 1% of parasites within the spleen were gametocytes, a considerably lower proportion than that observed in chronic infections in adults (8.3%) (**Figure 4-21C**) (Kho et al., 2021a). This fraction was higher than observed by Giemsa highlighting difficulties in evaluating gametocyte densities based on this stain alone. Therefore, the spleen does not contribute towards gametocyte maturation in paediatric severe malaria cases.

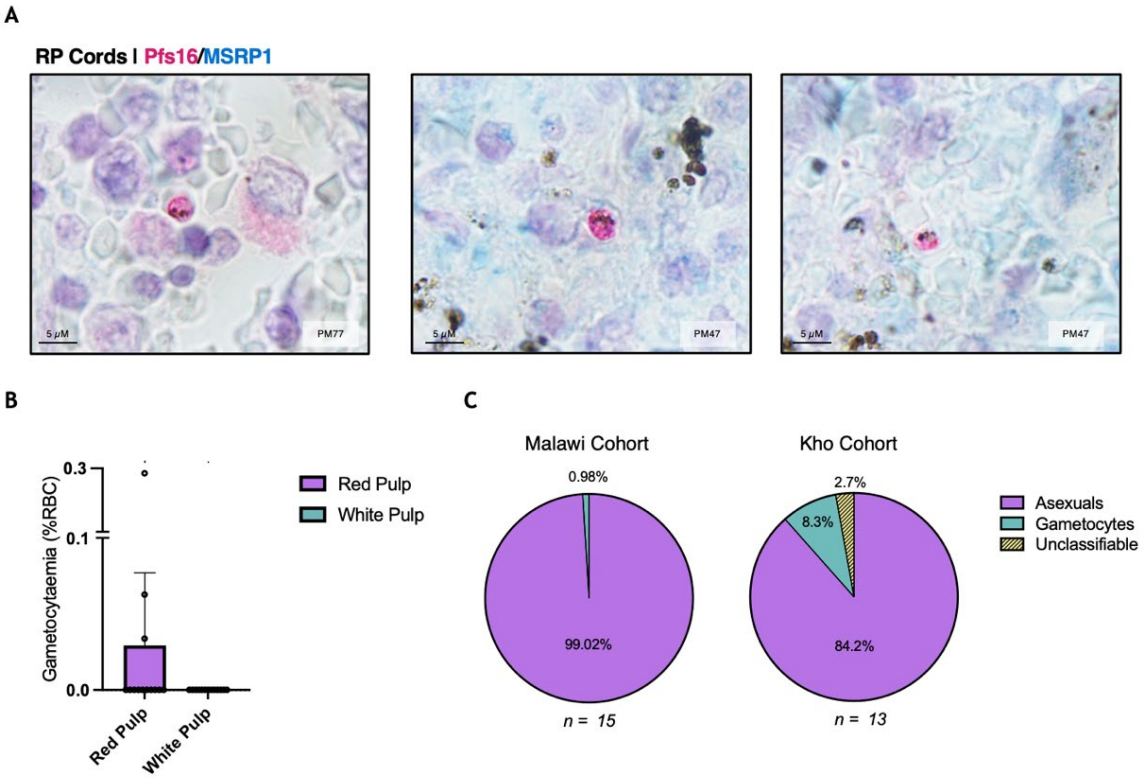

Figure 4-21. The spleen does not contribute to gametocyte development. Spleen sections were stained with Pfs16, a marker of gametocytes, and MSRP1, a marker of sexual commitment. No MSRP1+ parasites were identified in the spleen. (**A**) Representative images of gametocytes in the spleen labelled with antibodies against Pfs16 (pink, chromogen Vector Red). (**B**) Gametocytaemia in the red pulp (RP) and white pulp (WP) of the spleen. Data is presented as mean with 95% confidence interval. (**C**) Pie charts showing the proportion of asexual, sexual, and unclassifiable stages in the spleen for the Malawi cohort (paediatric severe *P. falciparum* malaria cases) and the Kho cohort (adult chronic asymptomatic *P. falciparum* malaria cases) (Kho et al., 2021a). Symbols represent individual patients. Abbreviations: RBC, red blood cell; RP, red pulp.

4.5.2 Gametocytes in the BM

Through a previous histopathological survey of CM1/CM2 cases in the Malawi cohort, the BM was identified as a major reservoir for asexual and sexual stages (Joice et al., 2014, De Niz et al., 2018). To effectively compare the spleen reservoir, and to confirm previous findings in a larger cohort, IHC was performed on BM sections using anti-Pfs16 (**Figure 4-22A**). As was the case for the spleen, Pfs16 labelling was part of a dual IHC partnered with antibodies against the sexual commitment marker, MSRP1. Similarly, the number of HPF analysed was increased to 25 HPF per tissue compartment.

Gametocyte quantification was performed in both the parenchyma and small vessels (sinus lumens) of the BM. As previously described (**Section 4.2.2**), the BM parenchyma had significantly higher parasite densities compared to parasite densities in the small vessels of the BM (p = 0.01) (**Figure 4-22B**). Therefore, the extravascular spaces contribute more towards the total parasite densities and biomass in the BM. There was no significant difference between gametocyte densities in the parenchyma compared to the small vessels (**Figure 4-22B**).

Overall, in the BM (combining the parenchyma and small vessels), 13% of parasites identified were gametocytes based on the number of HPFs counted. When examining specific compartments, gametocytes constituted 18% of parasites in the BM parenchyma. A lower fraction of gametocytes was found in the small vessels of the BM, constituting 7.9% of parasites in the small vessels. Compared to the spleen in this cohort, there is a far greater proportion of gametocytes in the BM compared to the spleen highlighting the role of the BM in gametocyte development (**4-22C, 4-21C**).

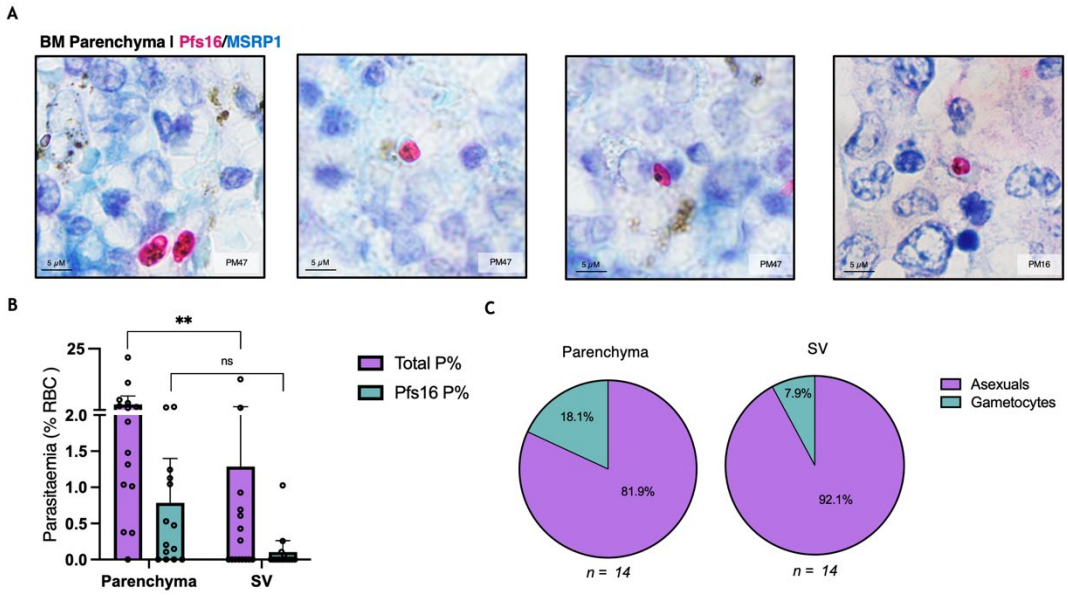

Figure 4-22. The bone marrow (BM) parenchyma has the largest proportion of gametocytes. BM sections were stained with Pfs16, a marker of gametocytes, and MSRP1, a marker of sexual commitment. Identification of MSRP1+ parasites are discussed in **Section 4.6**. Therefore, no images of MSRP1+ parasites are presented in this figure. (**A**) Representative images of gametocytes in the BM labelled with antibodies against Pfs16 (pink, chromogen Vector Red). (**B**) Parasitaemia and gametocytaemia in the parenchyma and small vessels (SV) of the BM. Data is presented as mean with 95% confidence interval. (**C**) Pie charts showing the proportion of asexual and sexual stages in the BM parenchyma and BM small vessels for the cohort. The statistical tests used for each compartmental comparison was the Kruskal-Wallis test, followed by post-hoc Dunn's test to

assess pairwise differences. Symbols represent individual patients. Abbreviations: BM, bone marrow; RBC, red blood cell; SV, small vessels; P%, parasitaemia.

4.6 Sexually Committed Schizonts in the Spleen and BM

During the intraerythrocytic developmental cycle, a subset of parasites will undergo sexual commitment which results in the production of gametocytes. As confirmed in **Section 4.5.2,** there is an enrichment of gametocytes in the extravascular spaces of the BM (Joice et al., 2014, Aguilar et al., 2014). Enrichment of gametocytes in this compartment could be explained by two previously proposed models: preferential homing of sexually committed merozoites or early gametocytes to the BM, or sexual commitment directly in the BM where an endogenous asexual replication cycle takes place (Nilsson et al., 2015, De Niz et al., 2018). To investigate gametocyte formation in the tissues, IHC was performed using an antibody against the sexual commitment marker, MSRP1 (**Figure 4-23A**) (Kadekoppala et al., 2010, Perrin et al., 2015, Poran et al., 2017, Brancucci et al., 2018). Since sexually committed cells are a rare population, the number of HPF analysed for each compartment was increased to 25 HPF.

To determine the role of the spleen in gametocyte formation in paediatric severe malaria cases, MSRP1 was quantified in the RP, WP, and large vessels of the spleen (n=15). In total, only 2 MSRP1+ parasites were identified in the RP of the spleen which were found in one case, PM21 (CM1); no gametocytes were observed in this case. The lack of MSRP1+ parasites in the spleen is consistent with the low number of observed gametocytes. This finding supports the hypothesis that the spleen does not contribute to gametocyte formation and development.

In the BM, MSRP1+ cells were identified in 5 out of 14 (36%) of the quantified BM samples. These cases corresponded to CM1/2/3 cases, i.e., those that met the clinical definition of CM (**Section 2.1.1**). Sexually committed parasites (MSRP1+) were found predominantly in the BM parenchyma at a mean parasitaemia of 0.45% (95% CI: -0.16% to 1.07%) (**Figure 4-23B**). When compared to other populations identified in the BM, gametocytes accounted for 13% of the total parasites, while

sexually committed parasites accounted for 9% of the total parasites in the BM (**Figure 4-23C**).

The correlation between the density of MSRP1+ parasites and gametocytes were investigated in the BM. Although there was a moderate correlation between the density of MSRP1+ parasites and gametocytes in the BM parenchyma, this correlation was not significant (Spearman correlation r = 0.37, p value = 0.077) (**Figure 4-24**).

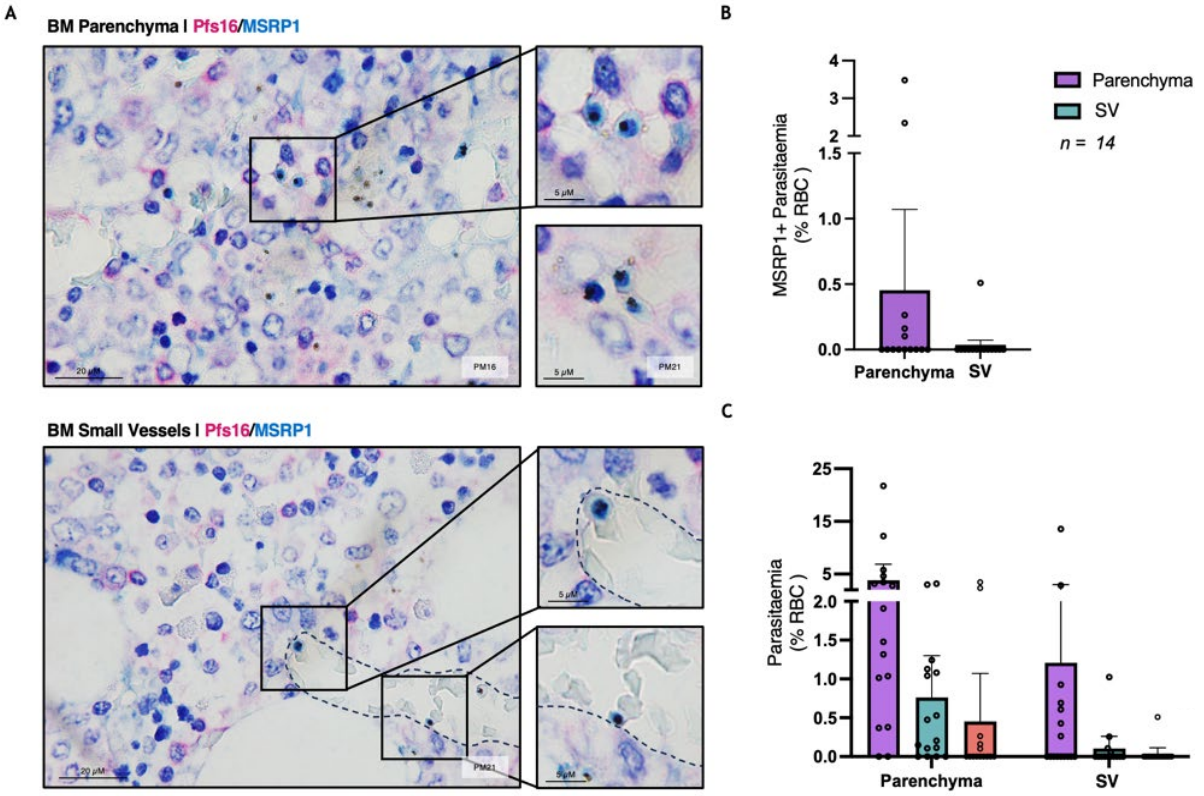

Figure 4-23. Identification of sexually committed schizonts in the bone marrow (BM). (**A**) Representative images of MSRP1+ schizonts in the BM parenchyma and small vessels (SV). Morphology of sexually committed schizonts was confirmed using formalin fixed, paraffin embedded (FFPE) blood clots of *P. falciparum* schizonts grown in minimal fatty acid (mFA, i.e., sexual commitment inducing conditions) (**Section 2.3.3**). (**B**) MSRP1 parasitaemia in the parenchyma and SV of the BM across the whole cohort. Data is presented as mean parasitaemia with 95% confidence interval (CI). (C) Parasitaemia in the BM represented as mean values with 95% CI. Symbols represent individual patients. Abbreviations: BM, bone marrow, RBC, red blood cells, SV, small vessels.

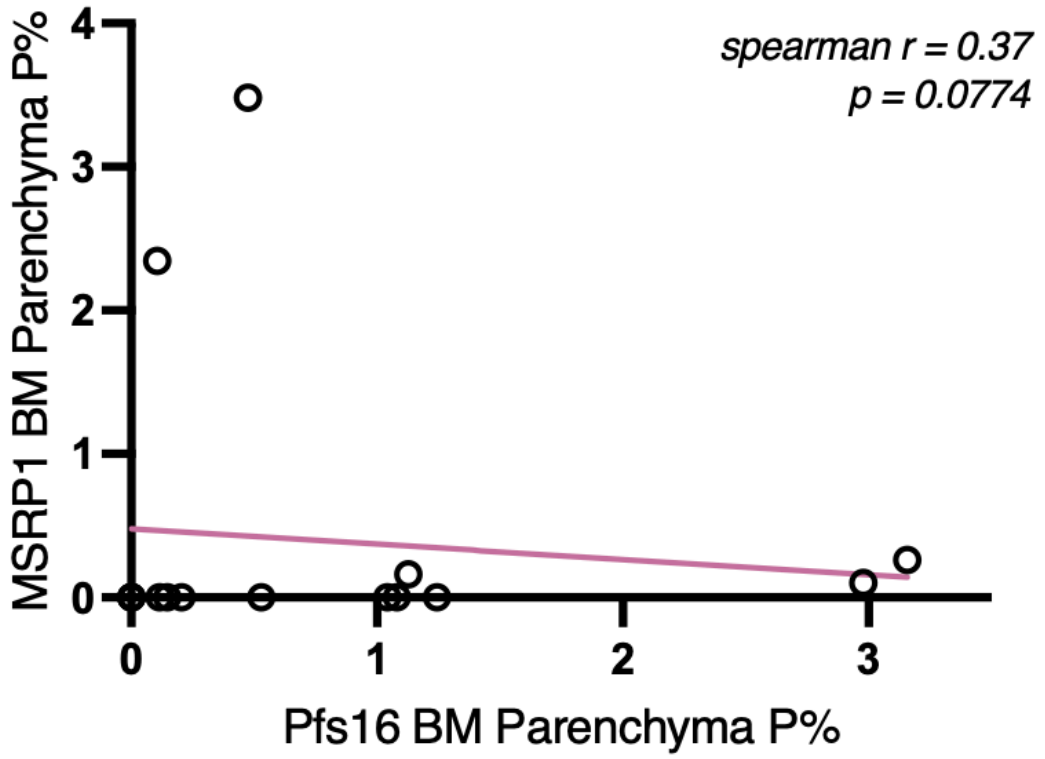

Figure 4-24. Correlation between MSRP1 parasitaemia and Pfs16 parasitaemia in the bone marrow (BM) parenchyma. Spearman correlations were performed on MSRP1+ parasitaemia vs Pfs16+ parasitaemia in the BM parenchyma. MSRP1 parasitaemia did not significantly correlate with Pfs16 parasitaemia (r = 0.37, p = 0.774). Abbreviations: BM, bone marrow. P%, parasitaemia.

The presence of sexually committed cells in the BM suggests that sexual commitment can occur directly in the BM. This confirms the model of gametocyte enrichment in the BM where the microenvironment of the BM supports endogenous sexual commitment. The spleen was the only other tissue analysed here; however, it is possible that other tissues may contribute to the enrichment of gametocytes in the BM. In this scenario, sexually committed merozoites, or early gametocytes, could home to the BM for gametocyte maturation. It would therefore be necessary to perform a larger organ screen to determine if sexual commitment can occur in other tissues. In *P. berghei* infected mice, parasite density was associated with depletion in LysoPC (Brancucci et al., 2017). It is possible that in organs with high parasite sequestration, such as the brain or the gastrointestinal tract, that there is higher turnover of LysoPC resulting in a local LysoPC depletion and sexual commitment within that tissue. It would therefore be interesting to investigate the presence of MSRP1 positive parasites in multiple organs of differing levels of sequestration. Since this is a rare parasite population, it will likely be necessary

to increase the number of HPF analysed to ensure sexually committed parasites are captured, both in the BM and in other tissues.

4.7 Chapter Discussion

In a recent study by Kho *et al.*, the spleen was revealed to harbour a large hidden biomass of intact *P. vivax* and *P. falciparum* in chronic asymptomatic malaria in adults, with evidence to suggest the existence of an endosplenic life cycle. It is unknown whether a similar hidden biomass exists in the spleen of paediatric severe *P. falciparum* malaria cases. In the previous chapter, a large density of non-phagocytosed parasites was identified using the basic histological stain, Giemsa. To confirm the presence of these non-phagocytosed parasites, and to compare the parasite density and biomass between other organs and peripheral blood, immunohistochemistry was utilised. This approach also allowed the investigation of gametocyte formation and development in the BM and the spleen.

4.7.1 Conservative Counting Methodology

To avoid overestimating parasite accumulation in the spleen, BM, and lung, an 'unclassifiable' category was introduced to most counts. This category was applied for HSP70/CD31, HSP70/CD71 and Pfs16/MSRP1 IHC experiments (**Figure 4-25**). In HSP70 IHC, unclassifiable cells encompassed two forms: cells with weak Vector Red staining lacking a definitive nucleus or cells lacking Vector Red staining completely but exhibiting morphological features resembling iRBCs, as evidenced by the shape of pigment with a faint halo surrounding indicative of the PV. The latter, which can be deemed as parasite-like cells, may represent "coffin-RBCs" – RBCs containing dead parasites following treatment with artesunate or quinine (Ndour et al., 2014). These possible "coffin-RBCs" were not counted; however, it may be interesting to quantify them to determine if they were associated with treatment time, or other parasite or clinical parameters. To determine whether these unclassifiable parasites are indeed dead parasites, it would be necessary to generate formalin-fixed, paraffin embedded (FFPE) *P. falciparum* parasite clots on quinine treated and untreated cultures.

The inclusion of an unclassifiable category in these instances serves to avoid misclassifying cells as parasites, although it may lead to a potential underestimation of parasite accumulation in each organ. As an additional strategy to address IHC staining and count variation, and considering the agreement between Giemsa and IHC counts, the mean count for each splenic compartment was calculated between Giemsa and IHC counts and used for all subsequent analysis (**Figure 4-2**).

The proportion of unclassifiable reticulocyte-like cells was highest in the BM (57.2%) compared to the spleen (35.4%) and lung (33.5%). Given that the BM serves as the primary site of erythropoiesis in humans, the abundance of CD71+ cells, a marker of cells in the erythroid lineage (Malleret et al., 2013, Fröbel et al., 2021), made it more challenging to distinctly identify CD71+ reticulocytes within this tissue. The final step in erythropoiesis, before reticulocytes are released into circulation, is enucleation by a nursing macrophage in erythroblastic islands (**Figure 1-6A**) (Klei et al., 2017). Consequently, it should be possible to distinguish reticulocytes from earlier cells of the erythroid lineage, or erythroblasts. Nuclear staining was not always clear with the IHC protocol used here (**Section 2.3.1**). The contrast of nuclear staining by haematoxylin could be easily enhanced using Scott's Tap Water Substitute. This would eliminate the need to use an additional erythroid cell lineage marker expressed in erythroblasts but not in reticulocytes. Additionally, distinguishing between erythroblasts and reticulocytes could be interesting in the context of gametocytes. Neveu *et al*. recently demonstrated that gametocytes can develop within late erythroblasts *in vitro*. Furthermore, gametocytes were found within nucleated cells of the erythroid lineage in BM smears collected from an Indian adult with *P. falciparum* malaria (Neveu et al., 2020). While co-staining of CD71 and Pfs16 was not performed due to time constraints, improving the distinction between reticulocytes and erythroblasts could substantiate findings from Neveu *et al*.

For MSRP1, unclassifiable counts were particularly high. This is primarily due to suboptimal optimisation of the MSRP1 antibody causing issues with background staining in these tissues. While I was able to confidently quantify MSRP1+ cells, quantification would be made easier by fully optimising this antibody using

induced schizont blood clots. However, due to the lack of the Pfs16+ gametocytes present in splenic tissue, it is unlikely that MSRP1+ cells are present in the spleen.

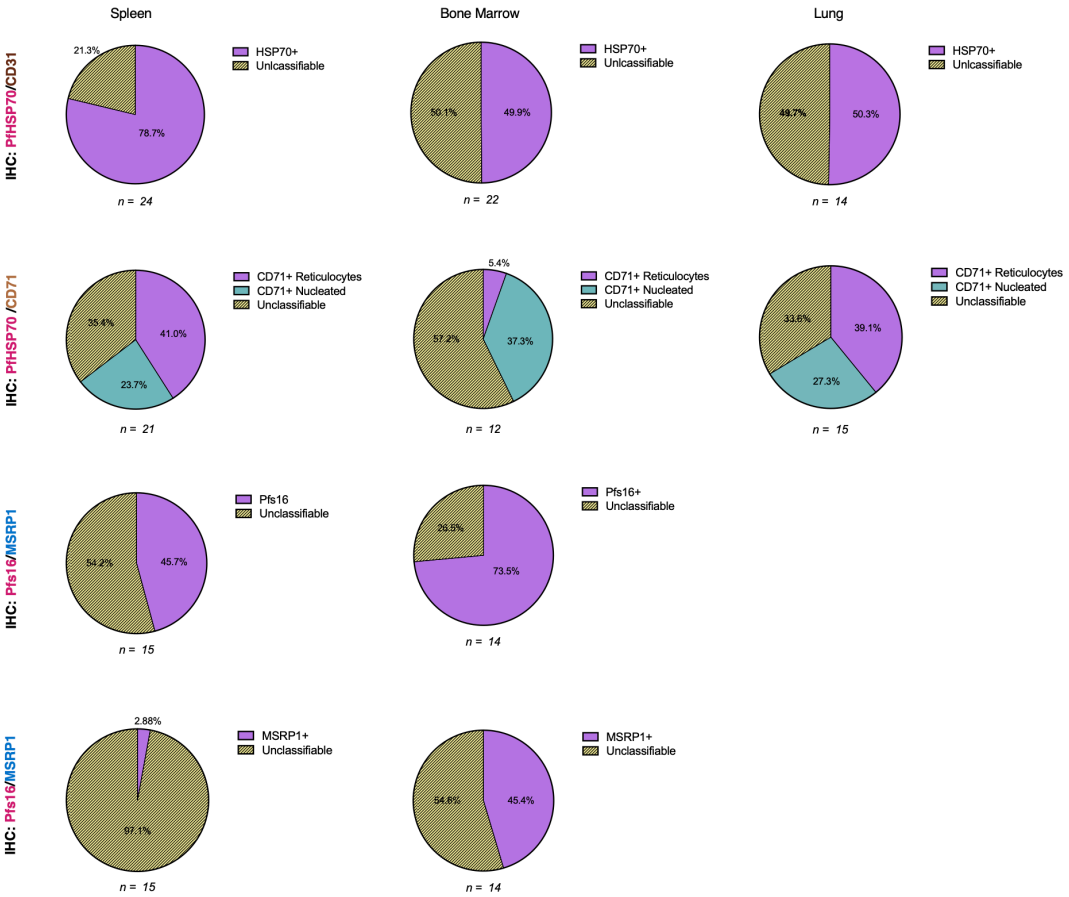

Figure 4-25. Proportion of unclassifiable counts by immunohistochemistry (IHC).

Stained sections were analysed directly on the Olympus BX43 microscope with an Olympus DP22 camera. By analysing tissues in person, rather than from a scanned image, multiple planes of focus could be quickly and easily analysed. This was essential for Giemsa quantifications as morphology can be obscured, particularly by the high level of pigment observed in tissues. Similarly, for quantifying parasite infected reticulocytes, moving through multiple planes of focus was necessary to identify the reticulocyte and parasite within (**Figure 4-20A**). To validate all Giemsa and IHC based quantifications, a second microscopist would be required to evaluate 30% of patients. Alternatively, image analysis software such as

Visiopharm®, which utilises deep learning algorithms based on artificial intelligence and neural networks, could be employed for quantifications. As such, image analysis pipelines could be designed to initially identify tissue compartments and then quantify stained cells within each compartment.

4.7.2 Ineffective Splenic Parasite Clearance

The unique architecture of the spleen facilitates the filtration of aged, damaged, or iRBCs, whereby RBCs must traverse narrow inter-endothelial slits within sinuses (Groom et al., 1991, Buffet et al., 2006, Safeukui et al., 2008). This passage from macrophage lined RP cords, through inter-endothelial slits, and eventually into the venous system, requires mechanical sensing of RBC deformability, a quality trophozoite- and schizont- iRBCs lack (Groom et al., 1991, Deplaine et al., 2011, Cranston et al., 1984). In the context of malaria, cordal macrophages play several crucial roles in this filtering process: (i) During pitting, the parasitised portion of the RBC is unable to pass, and thereby gets trapped and subsequently released into the reticular meshwork of the cords where cordal macrophages engulf the remains. (ii) In some instances, macrophages themselves engage in pitting of iRBCs, where the parasitised portion is engulfed, and the remaining RBC is pinched and released into circulation. (iii) Macrophages in the cords can directly phagocytose iRBCs. (iv) Additionally, macrophages can engulf debris, such as haemozoin, released from parasites (Schnitzer et al., 1972, Ghosh and Stumhofer, 2021). Some of these protective roles were evidenced here as visualised by phagocytosed parasites and pigmented macrophages (**Figure 4-13**). These pigmented macrophages have likely phagocytosed haemozoin released from rupturing schizonts, a clear example of which can be found in the WP panel of **Figure 4-13** where the field of view lacks pigment outside of the macrophage (Arese and Schwarzer, 1997). This absence of pigment outside the macrophage eliminates the possibility of confusion with other forms of pigment such as formalin pigment (Arese and Schwarzer, 1997).

As before mentioned, a high number of possible “coffin-RBCs” were identified in splenic tissue. The RBC “coffin” can be recycled through pitting in the spleen (Schnitzer et al., 1972, Buffet et al., 2006). Pitting rates are highest in antimalarial treated children aged between 1.5-4 years, aligning with the average

age of this cohort, which falls within this range at 2 years and 3 months (Ndour et al., 2015). However, pitting rates and parasite clearance rates are less pronounced in quinine treated patients than in artesunate treated patients (Chotivanich et al., 2000, Newton et al., 2001, Jauréguiberry et al., 2014, Saidi et al., 2021, Saidi et al., 2023). This lower contribution of pitting observed in quinine treated patients may explain the accumulation of "coffin-RBCs" in the spleens of the Malawi cohort. It would be interesting to compare splenic tissue from artesunate treated patients to determine if a similar fraction of potential "coffin-RBCs" are present in the spleen. Alternatively, as evidence from histopathological scoring data, the high density of "coffin-RBC" may simply be due to reduced splenic function.

In previous post-mortem studies in Southeast Asian adults with severe *P. falciparum* malaria, a downregulation of cordal macrophages was observed compared to patients with bacterial sepsis and control patients (Urban et al., 2005b). In the Malawi cohort, there was not a significant reduction in macrophage numbers observed between malaria patients and non-malarial controls in both splenic compartments analysed (**Figure 4-14**). In fact, with parasitaemia, the number of macrophages and phagocytosed parasites increased (**Figure 4-15**). Therefore, the presence of low levels of phagocytosed parasites is unlikely to be solely attributed to low macrophage levels in malaria cases.

While direct *in vivo* evidence of parasite phagocytosis in the spleen was provided, most parasites within the spleen were non-phagocytosed (**Figure 4-16**). This ineffective phagocytic activity might be due to the considerable antigenic challenge in the spleen where parasite densities were high (Ho et al., 1990). Indeed, it was noted that parasite distribution in the splenic RP was heterogenous. In particular, higher parasite densities were often observed on the periphery of the WP beyond the fast circulation of the perifollicular zone (**Figure 4-6**). Interestingly, the presence of parasitic "nests" was also observed on the periphery of the WP beyond the perifollicular zone (**Figure 4-17**). I hypothesised that these parasitic "nests" containing clusters of HSP70+ parasites and parasite-like cells were large macrophages in a phagocytic state. The hypothesis that these cell clusters reside within macrophages aligns with the identification of parasite-like cells as "coffin-RBCs" i.e., RBCs harbouring a dead parasite. In many cases, co-

localisation of HSP70+ and CD68+ staining was observed confirming this hypothesis. However, there were many cases where CD68+ staining, or nuclear staining by Giemsa, was not clear (**Figure 3-21, 4-17C**). In these instances, the lack of CD68 staining may be due to macrophage cell death. Alternatively, these clusters of cells may represent rosettes, which form when mature iRBCs bind to uRBCs, a phenomenon first identified in *P. falciparum* in the 1980s (Handunnetti et al., 1989). Rosettes have been demonstrated to hamper phagocytic activity of monocytes (Lee et al., 2020). Therefore, it is possible that rosettes form in the tissue, particularly in the spleen where there is an abundance of iRBCs and uRBCs. These large rosettes could affect the phagocytic activity of resident macrophages, as previously demonstrated *in vitro,* resulting in their cell death (Lee et al., 2020). Currently, there is no evidence of rosette formation in infected tissues (Lee et al., 2022).

Ineffective phagocytic activity and parasite clearance could be attributed to high levels of haemozoin, where pigment was frequently observed in the splenic tissue of this cohort (Tyberghein et al., 2014). Phagocytosis of haemozoin, or late parasite stages harbouring haemozoin, has been associated with prolonged oxidative burst and subsequently inhibition of phagocytosis. Here, iron released from haemozoin has been attributed to these toxic effects on monocytes and macrophages (Schwarzer et al., 1992). In addition, the toxic effects of haemozoin alters processing of antigens and reduces macrophage bactericidal activities resulting in susceptibility to secondary bacterial infections (Fiori et al., 1993, Scorza et al., 1999, Lokken et al., 2018, Chua et al., 2021). The high levels of intact parasites may, in part, be attributed to inefficient splenic clearance by cordal macrophages, influenced by high loads of haemozoin.

4.7.3 No Evidence of an Endosplenic Life Cycle

The existence of cryptic asexual replication in haematopoietic niches has been hypothesised, however, it has received limited investigation. This is largely due to ethical and technical considerations where investigation of such cryptic life cycles is challenging, especially in severe malaria. Therefore, investigations have been performed in mouse models or using splenectomised patient samples. Evidence of a cryptic life cycle in the spleen and BM has been demonstrated in *P.*

berghei where invasion of early reticulocytes promotes gametocytogenesis. Note that in adult mice, the spleen is haematopoietically active (Lee et al., 2018). In a human case study of spontaneous splenic rupture, a large reservoir of intact *P. vivax* was identified (Machado Siqueira et al., 2012). More recently, Kho *et al.* unveiled the existence of a substantial biomass of intact *P. vivax* and *P. falciparum* which co-localised with a retained pool of reticulocytes in the spleens of adults with chronic asymptomatic malaria (Kho et al., 2021b, Kho et al., 2021a). The magnitude of the splenic accumulation in both *P. vivax* and *P. falciparum* cases could not be explained by the retention of parasites from circulation alone, even at parasite retention rates greater than 90%. Therefore, due to the co-localisation of reticulocytes and parasites in the same splenic compartments (predominantly the splenic cords), the magnitude of splenic infection unexplained by peripheral parasitaemia alone, and the presence of schizonts in proportions consistent with their duration in the intraerythrocytic life cycle, Kho *et al.*, hypothesised the existence of a cryptic endosplenic life cycle (Kho et al., 2021a).

To investigate the splenic parasite reservoir, Giemsa (**Section 3.5**) and IHC (CD31/HSP70) was utilised to quantify parasite distribution, densities and biomass in the spleen. To determine if there was a splenic tropism, parasite density and biomass was compared to the BM, lung, and peripheral blood. Here the lung serves as a comparator tissue due to the high vascularity of the tissue demonstrating a range of vessel sizes and moderate parasite sequestration (Milner et al., 2015). Further, in this cohort, lung involvement, pathology, and respiratory complications, such as acute respiratory distress syndrome (ARDS), were modest (Milner et al., 2013a).

The distribution of parasites within the spleen was heterogenous, with an enrichment of parasites observed in the periphery of the WP beyond the perifollicular zone (**Figure 4-6**). The spleen has two forms of circulation: closed (fast) circulation and open (slow) circulation (Schmidt et al., 1993). Splenic blood flow enters the marginal zone where 90% will enter the fast circulation of the perifollicular zone. The remaining 10% directly enters the RP cords in the slow circulation through venous sinuses. It is possible that the large accumulation of parasites observed in many cases outside the WP, beyond the marginal zone and perifollicular zone, represents parasites that have just entered the slow

circulatory system and, due to sheer abundance, have caused obstruction of the splenic cords resulting in an accumulative effect (**Figure 4-6**). Here, macrophages are unable to clear the high density of parasites, forming what have been classified in this thesis as parasitic "nests" (**Figure 4-17**). Based on Giemsa data presented in **Chapter 3**, this accumulation of parasites on the periphery of the WP is predominantly mature stages (late trophozoites/schizonts) (**Figure 3-23**). Mature stages are less deformable than rings, and therefore cannot pass through the inter-endothelial slits of the splenic cords (Schmidt et al., 1993, Safeukui et al., 2008, Cranston et al., 1984, Deplaine et al., 2011). These stages are therefore more likely to cause obstruction of the splenic cords. Furthermore, since these stages contain haemozoin, the high levels of haemozoin in these areas may affect the phagocytic activity of macrophages localised here (Schwarzer et al., 1992, Tyberghein et al., 2014).

Parasite densities were compared between the spleen, BM, lung, and peripheral circulation. For peripheral circulation, parasitaemia was determined by counting HSP70+ parasites and RBCs in the large vessels of the lung. This should be representative of peripheral circulation as sequestration would not be expected in the large vessels. This also allows parasite densities to be determined using the same modality as applied to the tissues. In paediatric *P. falciparum* severe malaria cases, the mean splenic parasitaemia was 1.86%, which was comparable to the mean splenic parasitaemia in chronic asymptomatic *P. falciparum* malaria in adults (1.53%) (Kho et al., 2021a). Parasite densities in the spleen were significantly higher than densities in the BM, lung, and peripheral circulation. While the parasite densities in the spleen was significantly higher than other organs and peripheral circulation, the magnitude of parasite densities in the spleen could be explained by a retention rate of 9.52% (**Section 4.2.4**). This retention rate is close to the retention rates observed in *P. falciparum* rings (ca. 10%) in the slow, open microcirculation during *ex vivo* splenic perfusion experiments (Safeukui et al., 2008). Based on Giemsa, the spleen exhibits an enrichment in rings/early trophozoites. Therefore, the higher splenic densities observed in the spleen could be explained by the natural retention of rings at a rate of 9.52%.

The parasite biomass in each organ and peripheral circulation was determined. The parasite biomass in all organs analysed was significantly higher than circulating parasite biomass, as was also observed when comparing the spleen to peripheral circulation in chronic asymptomatic cases in adults. However, there was no significant difference in parasite biomass when comparing biomasses between organs. Comparing parasite biomass between tissues is important in treated cohorts, as it is recognised that parasite clearance in the tissues is delayed compared to parasite clearance in the blood. Therefore, a splenic tropism was not observed in paediatric severe *P. falciparum* malaria cases.

In chronic asymptomatic malaria cases, the spleen exhibited a higher density of reticulocytes in the spleen compared to peripheral circulation. These reticulocytes had reduced deformability and were consequently retained in the spleen by mechanical retention (Kho et al., 2021a). Reticulocyte densities were investigated in the Malawi cohort revealing no significant difference in reticulocytaemia between the spleen and peripheral circulation (**Figure 4-18, 4-19**). Due to the small sample size, it was not possible to draw any conclusions on the reticulocyte responses in anaemic patients. However, it is possible that retention of reticulocytes is associated with chronic anaemia. *P. falciparum* is not restricted to reticulocytes for reinvasion events. However, from histopathological evaluation of the spleen in **Chapter 3**, there was not marked congestion of blood observed which would also provide ample host cells for reinvasion.

Taken together, the absence of schizonts in proportions consistent with an endosplenic life cycle, the explanation of parasite densities in the spleen by peripheral circulation alone, the lack of significant differences in parasite biomass among different organs, and the absence of alterations in the immature or mature RBC pool for reinvasion, suggest that there is no ongoing endosplenic life cycle in paediatric severe *P. falciparum* malaria in Malawi based on the sections investigated in this study.

4.7.4 Gametocyte Formation and Development

In adults with chronic asymptomatic *P. falciparum* malaria, gametocytes accounted for 8.3% of parasites identified in the spleen by Giemsa (Kho et al., 2021a). This suggests that the spleen may be involved in gametocyte

development. By Giemsa, it was challenging to identify gametocytes, particularly immature gametocytes. For example, it is not possible to distinguish early gametocyte rings from asexual rings. The gametocyte marker, Pfs16, was therefore used to quantify gametocytes in the spleen by IHC.

By IHC, gametocytes accounted for 1% of parasites identified in the spleen. This was considerably lower than the 8.3% gametocyte fraction observed in chronic asymptomatic *P. falciparum* malaria cases. A possible explanation for this is the difference in splenic reticulocytaemia between the two cohorts where chronic asymptomatic cases exhibited reticulocyte densities twice as high as those observed in paediatric severe malaria (**Section 4.4.1**). The higher density of reticulocytes in the spleen in chronic cases may provide a niche, similar to that of the reticulocyte rich BM, which supports gametocyte formation and development. This difference in reticulocyte densities in the spleen in chronic compared to acute malaria cases may be attributed to the time required to mount a reticulocyte response to anaemia. It takes 3-5 days for the BM to respond to anaemia with a peak in reticulocytaemia after 7-10 days (Mayer and Donnelly, 2013). The median time to death of the cohort analysed here was 14 hours (**Table 3-2, Section 3.2**). Therefore, it is unlikely that an appropriate reticulocyte response would have been mounted, and for reticulocytes to be retained in the spleen, as observed in adult cases likely experiencing chronic, low-grade anaemia. In contrast to the spleen, Pfs16 labelling in the BM revealed that 13% of identified parasites were gametocytes. Gametocytes were predominantly found in the extravascular spaces of the BM (parenchyma) supporting previous findings of an enrichment of immature gametocytes in the extravascular spaces of the BM (Joice et al., 2014, Aguilar et al., 2014).

To investigate gametocyte formation, IHC was performed using antibodies against the sexual commitment marker, MSRP1. In the spleen, only one case had identifiable MSRP1+ parasites which were found in the splenic cords. This suggests that the spleen does not contribute to gametocyte formation. In contrast, sexually committed schizonts were identified in the BM, predominantly found in the BM parenchyma (**Figure 4-23**). Sexual commitment is responsive to environmental triggers. The serum phospholipid LysoPC was identified as a repressor of sexual commitment; therefore, depletion in LysoPC concentrations can induce sexual

commitment (Brancucci et al., 2017). In *P. berghei* infected mice, LysoPC concentrations were shown to be lower in the BM compared to plasma concentrations (Brancucci et al., 2017). The BM microenvironment may therefore be conducive to sexual commitment and gametocyte formation. The co-localisation of sexually committed schizonts and gametocytes in the same BM compartment suggests that sexual commitment can occur directly in the BM. However, no significant correlation between MSRP1+ parasites and gametocytes were found (**Figure 4-24**). This lack of correlation may be due to a few reasons: Firstly, MSRP1+ parasites were only identified in 36% of cases. Importantly, for these BM counts, 25 HPFs were evaluated for each compartment (50 HPF total per tissue). Since sexually committed schizonts represent a rare parasite population, a higher number of HPF may need to be analysed to gain a more comprehensive understanding of their distribution. Secondly, gametocyte accumulation in the BM may be supported by another source such as the homing of sexually committed cells, or early gametocytes, to the BM. As such, sexual commitment might occur elsewhere in the body. It would therefore be necessary to perform a larger organ screen to identify tissues which may be implicated in sexual commitment. For example, the brain exhibits high parasite densities in CM cases which could result in greater uptake of LysoPC by parasites. This uptake could cause a localised depletion in LysoPC concentrations which triggers sexual commitment (Milner et al., 2015, Brancucci et al., 2017).

Overall, based on the tissue sections analaysed here, the spleen does not contribute to gametocyte formation or development. In contrast, both gametocytes and sexually committed schizonts were identified in the same compartments of the BM. This suggests that gametocyte accumulation in the BM is supported by, at least in part, by an endogenous asexual replication cycle where a subset undergo sexual commitment likely due to the local depletion in LysoPC in the BM.

4.7.5 The Role of the Spleen as a Parasite Reservoir

Based on findings from chronic asymptomatic malaria cases in adults and the data generated here in a paediatric severe malaria cohort, the following model was proposed to explain parasite accumulation in the spleen (**Figure 4-26**). In this

model, parasite accumulation in the spleen varies along a spectrum of disease severity, driven by host and parasite factors. Chronic infections in adults may lead to parasite adaptation, where a less inflammatory response could promote the survival of slower growing parasite populations which may survive better in the spleen. Furthermore, chronic infection of *Plasmodium* may induce a tolerogenic niche for parasite survival in the spleen as proposed by Kho *et al*. (Kho et al., 2021a). Splenic parasite accumulation in chronic infection may therefore be the result of immune control and parasite adaptation.

Chronic *Plasmodium* infection leads to persistent, low-grade anaemia (Chen et al., 2016, White, 2018). This likely contributes to the higher levels of reticulocytes observed in the spleen observed in chronic malaria cases but not severe malaria cases. In severe malaria, as observed in this cohort, disease onset and progression are rapid and therefore there may be insufficient time to develop a reticulocyte response. The reshaping of the splenic environment in chronic cases to generate a reticulocyte rich niche might explain higher observed parasite densities in the spleen for both asexual and sexual stages while at the same time the peripheral parasitaemia is far lower.

Another factor that may influence parasite accumulation in the spleen (and other organs) is repeated antimalarial treatment in children. In malaria endemic countries, children will regularly develop malaria symptoms, frequently due to acute malaria infection, and as a result be treated with antimalarials. These treatments will clear parasites from tissues preventing the chronic accumulation and adaptation of parasites. Indeed, in many malaria-endemic countries, children are given seasonal malaria chemoprevention which has been proven to reduce clinical episodes (Meremikwu et al., 2012, Matangila et al., 2015, WHO, 2023b). While children in the Malawi cohort presented here were not part of a seasonal malaria chemoprevention programme, 20/38 (52.6%) patients had reported pre-admission treatment.

This model is supported by unpublished data from Kho *et al*. in which uncomplicated *P. vivax* malaria patients exhibited an 8-fold increase in parasite biomass compared to peripheral circulation, which is 10 times lower than the 81-fold difference observed in asymptomatic patients (Kho et al., unpublished) (Kho

et al., 2021a). This contrasts with severe malaria described here where there was no significant difference between parasite biomass across organs. Therefore, the accumulation of parasites in the spleen varies with disease severity and is likely driven by multiple host and parasite adaptations (**Figure 4-26**).

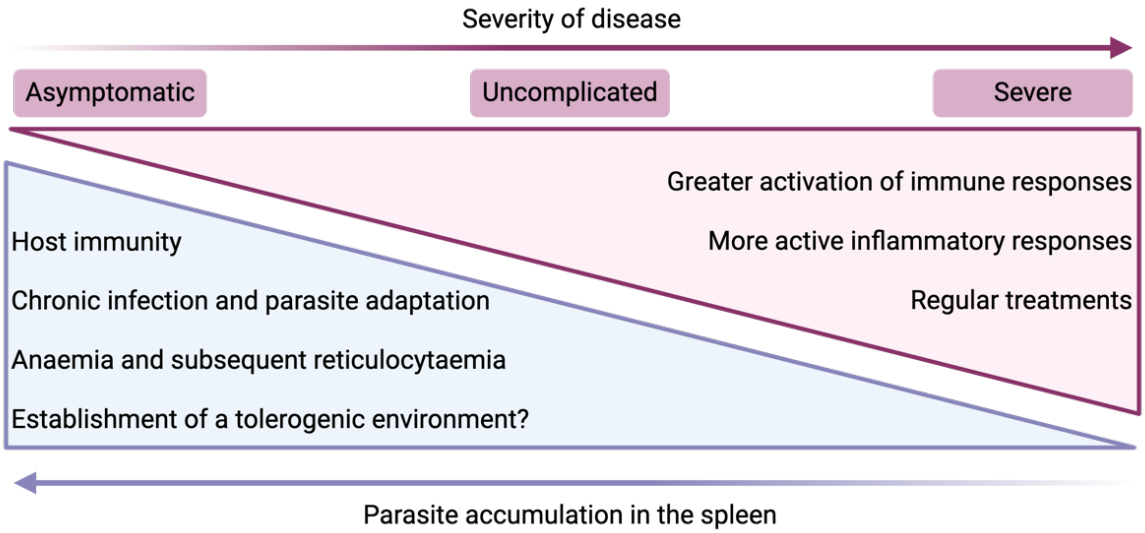

Figure 4-26. Model of parasite accumulation in the spleen in malaria. The splenic reservoir varies depending on disease severity. As such, many host and parasite factors drive the accumulation of parasites in the spleen.

4.7.6 Chapter Summary

The overall aim of this chapter was to validate and expand on findings from **Chapter 3** on the parasite distribution in the spleen and to explore the role of the spleen and the BM in gametocyte formation and development in paediatric severe *P. falciparum* malaria using IHC. Specifically, I aimed to investigate the presence of an endosplenic life cycle and to determine if there was a splenic tropism through a comparative analysis of tissues.

IHC validated parasite counts in Giemsa-stained tissues and allowed the comparison of parasite densities between organs and peripheral circulation. The spleen exhibited significantly higher parasite densities compared to the BM, lung, and peripheral circulation. However, the magnitude of parasite density could be explained by retention of ring stages in the spleen. Furthermore, while parasite

biomass was significantly higher in tissues compared to peripheral circulation, there was no significant difference in parasite biomass between tissues. Therefore, there was no splenic tropism in paediatric severe *P. falciparum* malaria as observed in chronic asymptomatic malaria cases in adults. Similarly, an enrichment of reticulocytes was not observed in the spleen in this cohort, as was observed in chronic asymptomatic malaria cases, which could support an endosplenic life cycle. Taking into consideration that *P. falciparum* is not restricted to reticulocytes, and thereby a reticulocyte response may not be required to support an endosplenic life cycle, there was only mild congestion of RBCs observed in the spleen. Together with the absence of schizonts in proportions consistent with their duration in the asexual life cycle, there is no evidence to suggest the presence of an active endosplenic life cycle in paediatric severe *P. falciparum* malaria based on the tissue sections analysed.

The role of the spleen in gametocyte formation and development was investigated; the spleen did not contribute to gametocyte formation or development in this cohort. In contrast, the BM parasite density comprised a substantial fraction of gametocytes. Furthermore, the presence of sexually committed schizonts were identified in the BM, predominantly in the extravascular spaces, suggesting that commitment can occur directly in the BM.

Based on these findings, I proposed a model of the splenic parasite reservoir whereby the accumulation of parasites varies with disease severity and is largely driven by host and parasite adaptations.

Chapter 5 | Deconvolving the transcriptional signature of sexual commitment in schizonts

5.1 Introduction

In **Chapter 3** and **4**, the splenic and BM reservoirs of *P. falciparum* in paediatric severe malaria cases from Malawi were phenotypically characterised using basic histological strains and immunohistochemistry (IHC). The BM has previously been demonstrated to be important in gametocyte maturation and consequently onward transmission (Joice et al., 2014, Aguilar et al., 2014, Baro et al., 2017, Obaldia et al., 2018). Therefore, it is important to both phenotypically and transcriptionally characterise parasites in the BM.

The BM has a unique environment which is depleted in lysophosphatidylcholine (LysoPC), a substrate for phosphatidylcholine (PC) synthesis (**Figure 1-8**). The depletion of LysoPC has been demonstrated to induce sexual commitment in *P. falciparum,* with the BM exhibiting a local LysoPC depletion in *P. berghei* infected mice (Brancucci et al., 2017). Indeed, in **Chapter 4**, both gametocytes and sexually committed schizonts were identified in the BM in paediatric severe *P. falciparum* malaria cases. Sexually committed schizonts and gametocytes collectively represented 22% of parasites in the BM (**Section 4.5, 4.6**); therefore, a population of asexual parasites also exist in the BM. The transcriptional distinctions between parasites in the BM and in other tissues is unknown.

During infection, the conversion rate of *Plasmodium* exhibits adaptive plasticity and is responsive to environmental factors such as the depletion of LysoPC. Conversion rate varies between strains from differing transmission settings (Pollitt et al., 2011). Further, based on unpublished data from the Marti Lab, LysoPC sensitivity also varies between strains originating from geographically distinct locations. The transcriptional programme underlying different parasite responses to this environmental trigger remains unclear and requires further investigation.

To deconvolute the transcriptional signature of sexual commitment in *P. falciparum* schizonts and to characterise schizont populations in the BM, single cell RNA sequencing (scRNAseq) was utilised. scRNAseq was performed on two culture-adapted parasite strains with different LysoPC sensitivities originating from West Africa (Pf2004) and Southeast Asia (Dd2) (Elliot, 2007, Hommel et al., 2010, Wellems et al., 1990). Here, Dd2 can respond to minor fluctuation in LysoPC in contrast to Pf2004, as observed in unpublished data from the Marti Lab.

5.1.1 Transcriptomics in *Plasmodium*

Transcriptomics, the study of the absolute ribonucleic acid (RNA) content of a cell, is the most widely used 'omics' approach allowing investigation of gene expression and regulation (Zhang, 2019). Advances in deoxyribonucleic acid (DNA) sequencing led to the development of microarray technology by Patrick Brown *et al* which permits the simultaneous detection of thousands of genes based on molecular hybridisation to DNA probes (Sanger and Coulson, 1975, Sanger et al., 1977, Brady et al., 1990, Schena et al., 1995, Zhang, 2019). This facilitated the profiling of gene expression patterns throughout the *Plasmodium* life cycle revealing a streamlined continuous transcriptional cascade which is largely conserved between *Plasmodium* strains and species in steady state conditions (Bozdech et al., 2003, Le Roch et al., 2003, Young et al., 2005, Llinás et al., 2006). It was microarrays that revealed the "just-in-time" model of transcription in *Plasmodium* and have provided bioinformatic resources for transcriptomic exploration in gametocyte and asexual development *in vitro* and *in vivo* (Bozdech et al., 2003, Le Roch et al., 2003, Llinás et al., 2006, Pelle et al., 2015).

In a recent study, Llorà-Batlle *et al*. produced a transgenic parasite line (background E5 (3D7 subclone)) whereby *ap2-g* (PF3D7_1222600) could be conditionally activated using rapamycin to generate conversion rates of >90%. With this parasite line, the transcriptional signature of sexually committed schizonts downstream of AP2-G (40 to 48 hours post invasion (hpi)) and early sexual stages (5 to 10 hpi and 10 to 20 hpi) was investigated using a custom Agilent microarray. Across all cell types, gene families such as *surfin* (*surf1.2* (PF3D7_0116300), *surf4.1* (PF3D7_0402200), *surf4.2* (PF3D7_0424400), *surf8.2* (PF3D7_0830800) and *surf13.1* (PF3D7_1301800)), and early transcribed membrane proteins, *etramp* (*etramp4* (PF3D7_0423700) and *etramp9* (PF3D7_0936300)) were significantly upregulated in sexually committed parasites. Using Chromatin immunoprecipitation sequencing (ChIP-seq), 71% of highly upregulated genes were found to be bound to AP2-G suggesting that they are direct targets. In contrast, gene families involved in antigenic variation and asexual development were downregulated in sexually committed parasites, such as *mesa* (PF3D7_0500800), *kahrp* (PF3D7_1016300), *pfemp3* (PF3D7_0201900),

pf332 (PF3D7_1149000), and *hrpiii* (PF3D7_1372200). These genes were not bound by AP2-G with only 5% of downregulated genes shown to be bound to AP2-G by ChIP-seq. In sexually committed schizonts specifically, only 6 genes were significantly downregulated, three of which encoded proteins of the RhopH complex or plasmodial surface anion channel (PSAC). These genes included *clag3.1* (PF3D7_0302500), *clag2* (PF3D7_0220800) and *rhoph3* (PF3D7_0905400) (Llorà-Batlle et al., 2020). Microarrays have therefore allowed the exploration of the *Plasmodium* transcriptome, shedding light on the transcriptional signature of sexual commitment. However, microarrays are limited by their dependence on a pre-defined set of oligonucleotide probes, making them hypothesis driven rather than exploratory tools.

The development of bulk RNA sequencing technologies has improved the resolution of transcriptomic datasets generated from microarrays. This approach overcomes the need for prior knowledge and technical limits of detection. Bulk RNA sequencing approaches validated microarray data, in addition to identifying transcription start sites, alternative splice sites, antisense transcripts in gene regulation, the co-transcription and stabilisation of genes, and the characterisation of untranslated flanking regions (Sorber et al., 2008, Otto et al., 2010b, López-Barragán et al., 2011, Otto et al., 2014, Zhu et al., 2016, Adjalley et al., 2016, Painter et al., 2018). Bulk RNA sequencing also revealed a large non-coding RNA (ncRNA) transcriptome in *P. falciparum,* likely involved in tight gene regulation, antigenic variation, virulence, and pathogenicity (Raabe et al., 2010). These approaches, however, represent an average gene expression across a population level masking potential biological heterogeneity. For example, only a subset of parasites (1-30%) will undergo sexual commitment. Therefore, transcriptional signatures for sexually committed schizonts could be masked using microarray or bulk RNA sequencing approaches (Pelle et al., 2015).

The first scRNAseq study was applied to a 4-cell stage mouse blastomere (cells derived from the cleavage of a zygote) in 2009 by Tang *et al.* (Tang et al., 2009). This approach was first applied to *Plasmodium* by Poran *et al,* where 18,000 transcriptomes were analysed using Dropseq to investigate sexual commitment in a *conditional ap2-g* knockdown line and wild-type NF54. This study confirmed the previously hypothesised positive feedback loop of *ap2-g* demonstrating two peaks

in *ap2-g* expression (Kafsack et al., 2014, Poran et al., 2017). Additionally, 19 genes were identified to be associated with sexual commitment upon *ap2-g* activation including *msrp1* and members of the small family of polymorphic surface antigens, *surfin*. Genes involved in gene regulation such as the ApiAP2 transcription factors, *ap2-g5* (PF3D7_1139300) and PF3D7_1222400, genes involved in chromatin remodelling such as *iswi* (ISWI chromatin remodelling complex ATPase, PF3D7_0624600) and *snf2l* (PF3D7_1104200), and histone modifying enzymes such as histone deacetylase 1 (*hda1*, PF3D7_1472200) and lysine specific histone demethylase (*lsd2*, PF3D7_0801900) were shown to be sequentially upregulated following *ap2-g* activation (Poran et al., 2017).

Following this study, the entire process of sexual commitment in response to nutrient depletion was investigated using a pseudo-single cell experimental approach and the Pf2004/164tdt reporter line (Brancucci et al., 2018). Using LysoPC depleted medium, reporter parasites were induced to undergo sexual commitment allowing the investigation of pathways upstream of *ap2-g* activation. Using this experimental design, two transcriptional signatures were defined amongst the 881 transcriptomes obtained from LysoPC depleted conditions: one reflecting a shared metabolic response between parasites grown in nutrient limiting conditions, and a distinct sexual commitment signature present in a subset of parasites. Using clustering analysis, a cluster enriched in *ap2-g* was identified and used to perform differential gene expression (DGE) analysis to define a sexually committed transcriptional signature. Transcription factors (e.g., *ap2-lt*, PF3D7_0802100), epigenetic regulators (e.g., *set9,* PF3D7_0508100), and kinases (e.g., PF3D7_1145200) were amongst genes upregulated in sexually committed cells. When comparing the sexually committed transcriptional signature with Poran *et al.*, *msrp1* was among the shared hits of upregulated genes in sexually committed cells highlighting a potential functional role in the sexual commitment trajectory (Poran et al., 2017). Previous bulk RNA sequencing data comparing parasites grown in LysoPC depleted medium and serum supplemented medium revealed an upregulation of enzymes involved in an alternative substrate arm of the Kennedy pathway in LysoPC depleted conditions (described in **Section 1.1.2**) (Brancucci et al., 2017). However, when investigating the transcriptional signature of sexually committed cells in this same medium, two key enzymes in this alternative Kennedy pathway, ethanolamine kinase (*ek*, PF3D7_1124600) and

phosphoethanolamine methyltransferase (*pmt,* PF3D7_1343000), were not differentially expressed. This suggests that in nutrient depleted conditions, there is a shared transcriptional signature relating to metabolic adaptation, with a subset of cells displaying a distinct sexual commitment transcriptional signature (Brancucci et al., 2018).

Since 2018, several scRNAseq projects have contributed to the Malaria Cell Atlas Project, a large transcriptomic database encompassing the full life cycle of several *Plasmodium spp*. at single cell resolution (Nötzel and Kafsack, 2021). Using a combination of Smart-Seq2 and the 10X Chromium platform, single cell transcriptomes have been generated for *P. berghei, P. falciparum,* and *P. knowlesi* including for mosquito stages in *P. falciparum* and *P. berghei* (Reid et al., 2018, Howick et al., 2019, Real et al., 2021, Witmer et al., 2021). Unpublished transcriptomes from circulating asexual and sexual stages collected from symptomatic *P. malariae* and *P. ovale* patients have recently been added. The most recently published additions to the Malaria Cell Atlas project investigated sexual development in *P. berghei* and *P. falciparum* (Russell et al., 2023, Dogga et al., 2024). In the latter scRNAseq study in *P. falciparum,* Dogga *et al*. focussed on transcriptional transitions from *ap2-g* positive cells in the subsequent cycle after commitment, through to differentiation into male and female gametocytes. At the earliest point of commitment identifiable in their study, they found an upregulation of members of the *etramp* family, *surfin* family, *hda1, lsd2* and *sir2a* (PF3D7_1328800) in *ap2-g* positive clusters. This cluster had a downregulation in genes associated with surface exported proteins such as *gbp130* (PF3D7_1016300), *kahrp* and *pf332* (Dogga et al., 2024). This database of published and unpublished transcriptomes provides a reference framework for scRNAseq experiments and allows the exploration of gene expression across multiple life cycle stages and *Plasmodium spp*.

Most transcriptomic analysis investigating sexual commitment has focused on stages or events downstream of *ap2-g* activation. These studies often utilised conditional expression of *ap2-g* rather than environmental induction which likely triggers a transcriptional cascade more akin to what is observed *in vivo*. A more in-depth study on the transcriptional signature of sexually committed schizonts,

which allows the exploration of events upstream of *ap2-g*, is required to unravel the complete sexual commitment transcriptional cascade.

5.1.2 The 10X Chromium Single Cell Pipeline

Since the first scRNAseq study of a single blastomere in 2009, there has been a huge expansion on single cell technologies, the scope of have been extensively reviewed (Briggs et al., 2021, See et al., 2018, Wang et al., 2019, Ziegenhain et al., 2017, Hedlund and Deng, 2018, Valihrach et al., 2018). Chromium by 10X Genomics is the most widely used single cell platform, a droplet-based microfluidic method which generates high throughputs at relatively low costs per cell (Ziegenhain et al., 2017, Haque et al., 2017, See et al., 2018). The principal steps in this methodology are detailed below and summarised in **Figure 5-1**; note that the methodological pipeline detailed here is applicable to other single cell platforms.

The first step in a scRNAseq experiment is sample preparation where the aim is to generate a cell suspension of which at least 90% of cells are viable. Cell suspensions with substantial ongoing apoptosis results in the release of ambient RNA which can be incorporated into droplets resulting in poor capture rates and contamination of live transcriptomes (Yang et al., 2020, Briggs et al., 2021). For *Plasmodium,* an additional step of host cell lysis may be required prior to loading (Reid et al., 2018, Howick et al., 2019). Single cells can be captured using a Gel bead in Emulsion (GEM) approach where cells at the desired concentration are loaded onto the Chromium chip (an 8-channel microfluidic chip), alongside gel beads and oil in separate wells. Gel beads contain oligonucleotides which consist of a 10X 14 bp oligonucleotide barcode for cellular identity, 10 bp unique molecular identifiers (UMIs) to tag transcripts, and 30 bp oligo-dTs to capture polyadenylated tails of mRNA (Zheng et al., 2017). Individual cells can then be partitioned with barcoded gel beads into single nanolitre aqueous reaction droplets, or GEMs. Within each GEM, cell lysis occurs, and poly-T primed mRNA molecules are reverse transcribed into complement DNA (cDNA) tagged with UMIs at the 3' end of the molecule. After reverse transcription, the emulsion can be broken and tagged cDNA molecules pooled together for polymerase chain reaction amplification, library construction and Illumina next generation sequencing. Reads can then be mapped to a reference genome (here, *P. falciparum* clone 3D7)

and a transcript count matrix generated for downstream data analysis and visualisation (Haque et al., 2017, See et al., 2018, Zheng et al., 2017, Briggs et al., 2021).

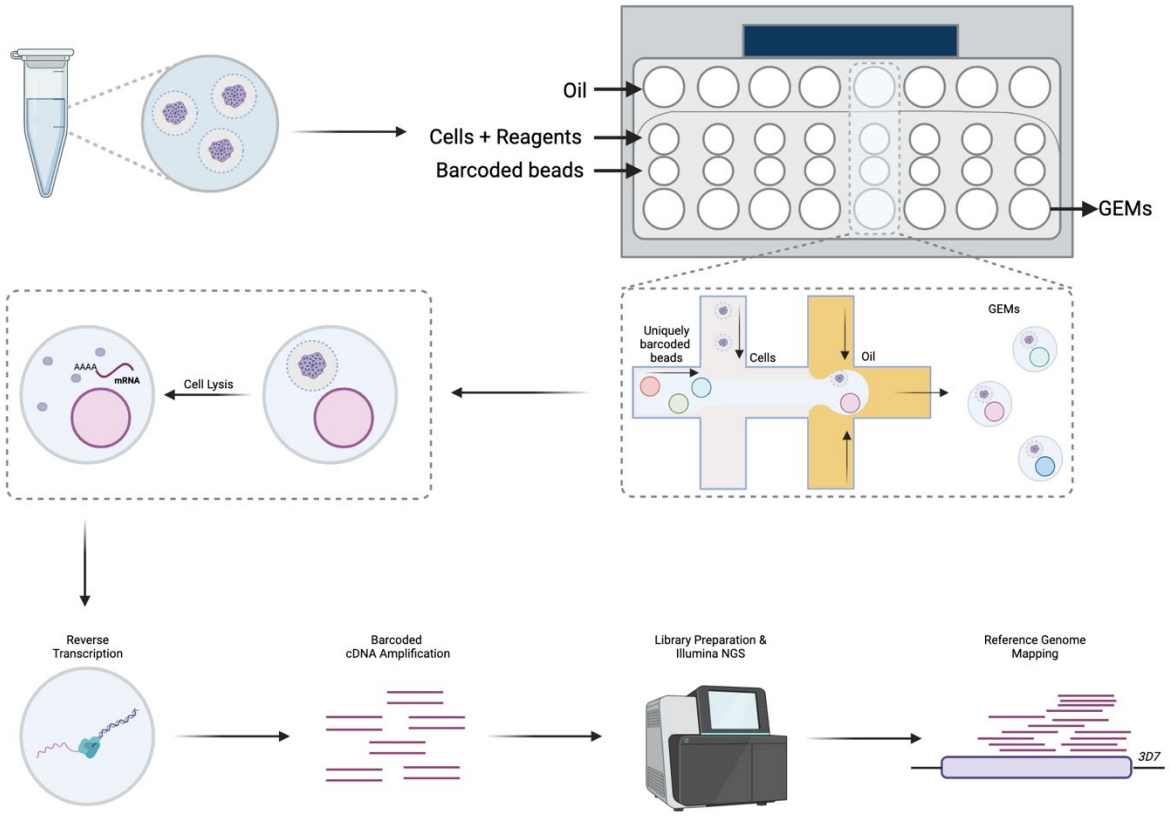

Figure 5-1. Droplet based single cell RNA sequencing (scRNAseq) workflow. A cell suspension with free *Plasmodium* (red blood cells (RBCs) lysed prior to loading) at a known concentration is loaded onto a microfluidic chip with necessary reaction reagents. In separate wells, partitioning oil and barcoded beads are loaded. Individual cells are encapsulated into single droplets containing a barcoded bead resulting in Gel bead in Emulsion or GEMs. Within each droplet, the cell is lysed and polyadenylated messenger RNA (mRNA) are reversed transcribed and tagged with a unique molecular identifier (UMI). After reverse transcription, the emulsion can be broken pooling total cDNA together for complement DNA (cDNA) amplification and library preparation. Libraries are then sequenced using Illumina next generation sequencing (NGS). Reads can then be mapped to a reference genome, in this case, *P. falciparum* clone 3D7. Abbreviations: GEMs, gel beads in emulsion; mRNA, messenger RNA; cDNA, complement DNA; NGS, next generation sequencing. Figure created with BioRender.com based on Briggs *et al.*, 2021 and Zheng *et al.*, 2017 (Zheng et al., 2017, Briggs et al., 2021).

5.1.3 *Plasmodium* Strains, Conversion Rates, and Transmission Settings

To successfully transmit to the definitive host of the mosquito vector, *Plasmodium* must undergo sexual commitment to produce gametocytes. In terms of fitness, the transmission of gametocytes to the mosquito vector corresponds to reproductive success (Schneider and Reece, 2021). This transfer of gametocytes to the mosquito represents a bottleneck in the parasite life cycle which is an attractive target for transmission blocking strategies (Nilsson et al., 2015). Parasites need to balance the within-host survival, which favours asexual replication, with between-host transmission, which favours sexual reproduction. The proportion of gametocytes produced within a given intraerythrocytic cycle is deemed the conversion rate. This conversion rate exhibits adaptive plasticity and is responsive to environmental factors such as antimalarial treatment, host cell age, extravascular vesicles, endoplasmic reticulum stress, and LysoPC depletion (Buckling et al., 1999, Peatey et al., 2013, Mantel et al., 2013, Regev-Rudzki et al., 2013, Chaubey et al., 2014, Brancucci et al., 2017, Schneider et al., 2018). Ultimately, the plasticity of conversion rate allows for the maintenance of parasite fitness in different contexts. For example, it has been demonstrated that in paediatric cases of asymptomatic, uncomplicated, and severe malaria, inflammatory responses results in a decline in plasma LysoPC concentrations which was associated with a larger investment in sexual conversion over asexual reproduction (Abdi et al., 2023).

Different geographical settings present different challenges which may alter the conversion rate of parasites. In high transmission areas, such as in sub-Saharan Africa, parasites experience greater within-host competition due to mixed genotype infections, antimalarial drug treatment and host immune responses, with more opportunities to transmit to the mosquito vector. In these circumstances, parasites invest more in asexual reproduction. The inverse is true for low transmission settings, such as in Southeast Asia, where there are fewer mixed infections and less opportunities for transmission (Greischar et al., 2016, Schneider and Reece, 2021). Indeed, it is known that the conversion rate varies between genotypes and parasite strains (Pollitt et al., 2011). For instance, the culture adapted parasite strains Pf2004 and Dd2 represent two strains of low and high background sexual conversion, respectively, and different sensitivities to

LysoPC. These two strains were originally derived from geographically distinct locations; Pf2004 originated from a high transmission setting (West Africa) while Dd2 from a low transmission setting (Southeast Asia) (Elliot, 2007, Hommel et al., 2010, Wellems et al., 1990). The transcriptional differences between geographically distinct strains in relation to sexual commitment has not been largely explored.

5.1.4 Aims and Hypotheses

During infection, the conversion rate (i.e., the proportion of gametocytes produced in a given intraerythrocytic cycle) is responsive to environmental factors such as the depletion of the serum phospholipid LysoPC (Brancucci et al., 2017). Different parasite strains exhibit different sensitivities to this environmental trigger, however, the transcriptional programme underlying different parasite responses to this environmental trigger remains unclear.

In the previous chapter, sexually committed schizonts in the BM of severe paediatric *P. falciparum* malaria cases were identified. Sexually committed parasites and gametocytes collectively represented 35% of parasites in the BM. Therefore, an additional population of asexual parasites exist in the BM. Due to the unique environment of the BM (e.g. local LysoPC depletion), this BM asexual population may be transcriptionally distinct from asexual parasites sequestered in other tissues.

The overall aim of this chapter was to use scRNAseq to deconvolute the transcriptional signatures of sexually committed and asexual schizonts across two parasite strains with different LysoPC sensitivities.

Specifically, I aimed to:

- Validate previous findings from bulk RNA sequencing.
- Investigate the sexual commitment transcriptional pathway from the initial response to LysoPC depletion and progression towards the development of sexually committed schizonts.
- Determine the transcriptional differences between asexual and sexually committed schizonts under LysoPC limiting conditions.

5.2 Experimental Outline

To investigate the transcriptional signatures of sexually committed and asexual schizonts across two parasite strains with different LysoPC sensitivities, a sexual conversion assay was adapted (Brancucci et al., 2018). This assay utilises a minimal fatty acid (mFA) medium, devoid of LysoPC, which serves as a strong inducer of sexual commitment. Two geographically distant culture-adapted *P. falciparum* strains with differing sensitivities to LysoPC were used: Pf2004/164tdt, which is less sensitive to LysoPC fluctuations as represented by a lower conversion rates in serum, and Dd2 WT, which is more sensitive to LysoPC fluctuations as represented by a higher conversion rates in serum. Pf2004 had been previously transfected with a reporter plasmid 164tdTom whereby the expression of the fluorescent protein tdTomato is under the control of a gametocyte specific promoter (PF3D7_1016900) (Buchholz et al., 2011, Aingaran et al., 2012, Brancucci et al., 2015).

At 26/28 hpi, the sexual commitment assay was initiated by growing washed parasites in either serum supplemented media or mFA (**Figure 5-2**). Two time points were collected in schizonts approximately 16 and 22 hours after induction (**Figure 5-3A**). Time points were taken in the evening and therefore parasites were stored in Hypothermasol® FRS at 4ºC until they were ready to be processed and handed over during the day to Glasgow Polyomics. After storage for <10 hours, parasites were washed in 0.2% bovine serum albumin (BSA)/phosphate buffered saline (PBS) and red blood cells (RBCs) were lysed using saponin (0.1%). Cell counts for each sample was performed by haemocytometer and flow cytometry. Parasites grown in the same media were pooled together in equal ratios to produce two samples, 'mFA' and 'serum', at a final concentration of $1x10^6$ cells/mL (**Figure 5-3B**). A final cell count was performed by flow cytometry before immediately loading onto the 10X chromium machine. The 10X cDNA libraries were sequenced on an Illumina NextSeq 550 to a sequencing depth of approximately 50,000 reads per cell. In parallel, a sexual conversion assay was established in a 96 well plate to determine the parasite multiplication rate (PMR) and the conversion rate. Full details on the methodology can be found in **Section 2.5**.

Note that throughout this chapter, Pf2004/164tdt is referred to as Pf2004, and Dd2 WT is referred to as Dd2.

Pf2004

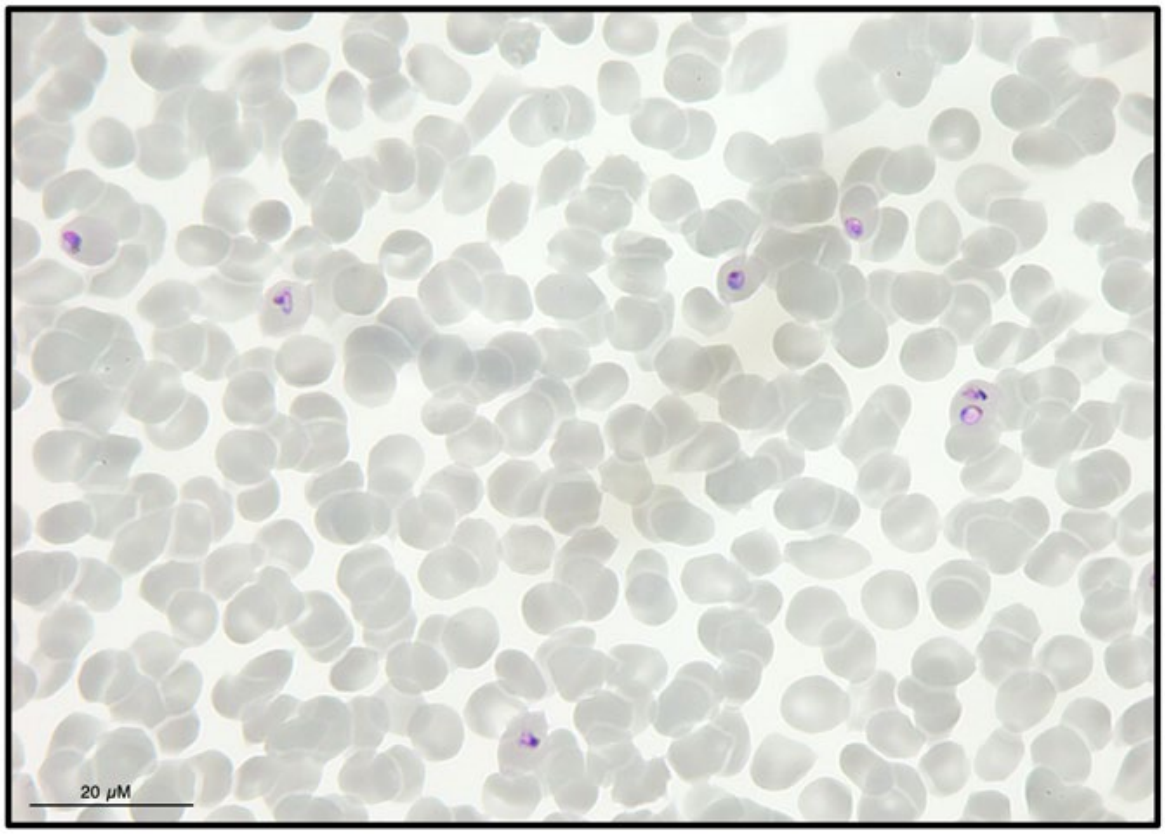

Dd2

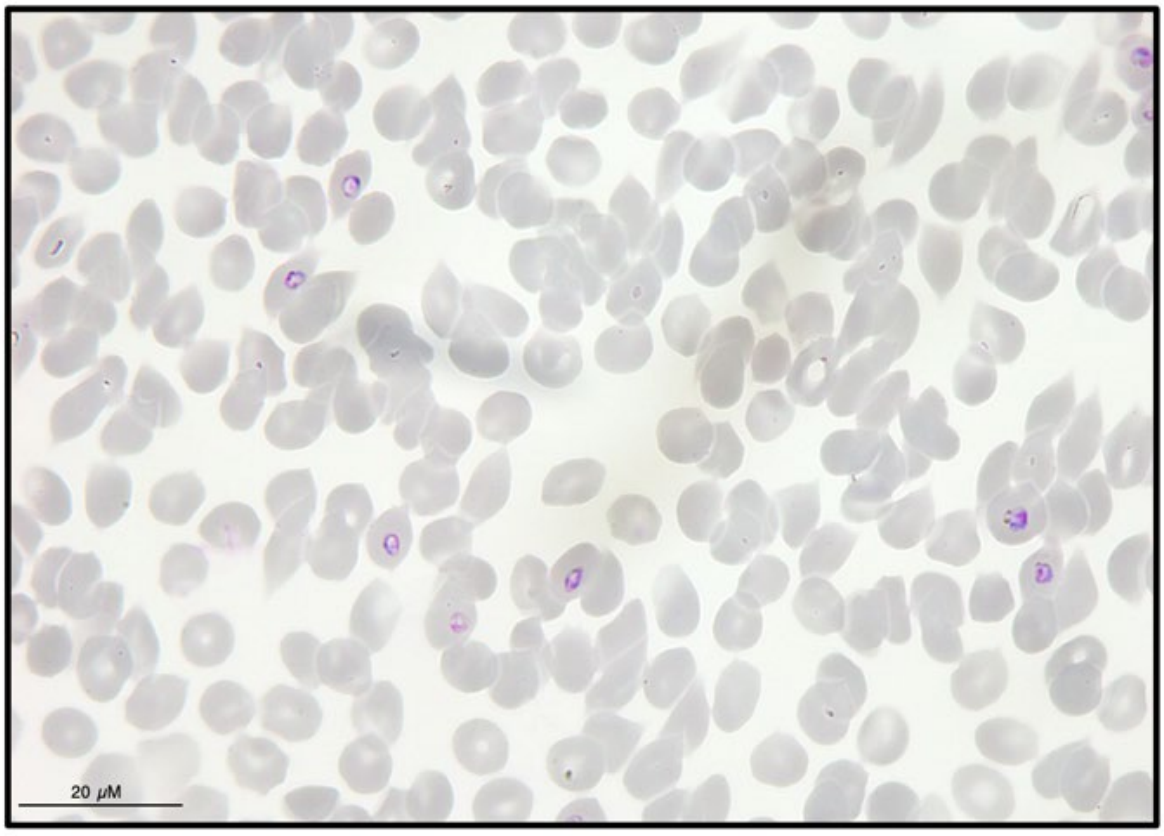

Figure 5-2. Representative images of Pf2004 and Dd2 *in vitro* cultures at 26/28 hours post invasion (hpi).

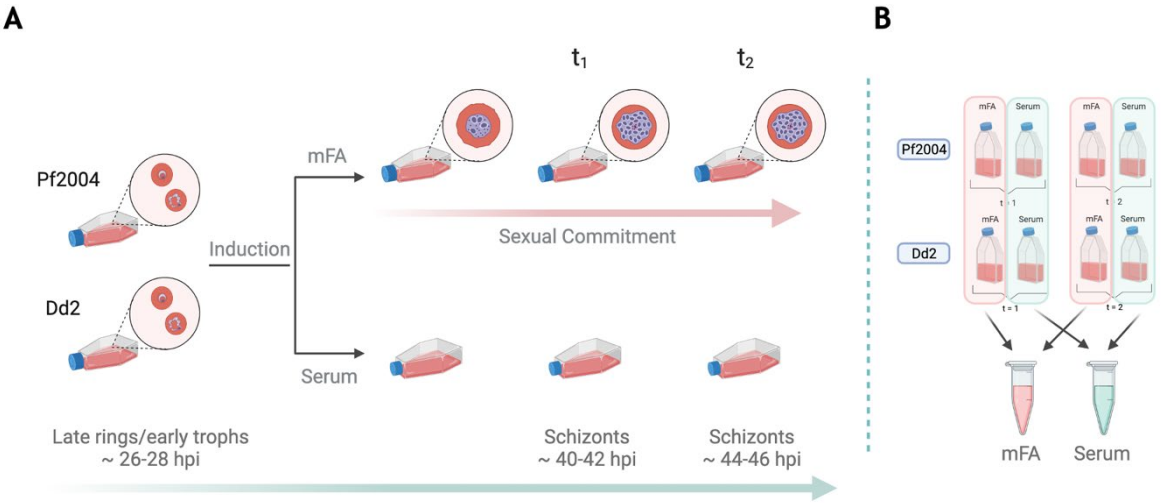

Figure 5-3. single cell RNA sequencing (scRNAseq) experimental outline. (**A**) Pf2004 and Dd2 (Pf2004/164tdt (gametocyte reporter line) and Dd2 WT) were grown *in vitro* at 4-6% parasitaemia at 2.5% haematocrit. At 26/28 hours post invasion (hpi), the sexual commitment assay was initiated by growing parasites in either minimal fatty acid medium (mFA) or serum supplemented medium (serum). Two time points were collected during schizonts and stored in Hypothermasol® FRS at 4ºC. (**B**) Parasites grown in the same media for each strain and time point were pooled together in equal ratios to generate two pooled samples, 'mFA' and 'serum', for loading onto the 10X chromium machine. Abbreviations: hpi, hours post invasion; mFA, minimal fatty acid (LysoPC depleted growth medium); t_1, time point 1; t_2, time point 2. Figure created with BioRender.com.

5.3 Sexual Conversion Assay

To determine whether the sexual conversion assay was successful, PMR and conversion rates were measured by flow cytometry. For PMR, parasites were stained with SYBRGreen+ to stain nucleic acids and measured on the MACSQuant VY flow cytometer using the GFP/FITC channel on day 0 of induction (i.e., the day the sexual conversion assay was initiated) and after parasite reinvasion on day 2. Similarly, to determine conversion rates, parasites were stained with both SYBRGreen+ and Tubulin Tracker™ Deep Red (which stains microtubule networks in gametocytes), and measured using the GFP/FITC and mKate channels (Li et al., 2022). Cells were gated to determine parasitaemia (**Figure 5-4A**) and gametocytaemia (**Figure 5-4B**). Note that the Pf2004/164tdt cell line expresses tdTomato under the control of a gametocyte specific promoter (PF3D7_1016900)

and therefore gametocytaemia read outs could be performed using the PE channel instead of the mKate channel (Buchholz et al., 2011, Aingaran et al., 2012, Brancucci et al., 2015). To be consistent between strains, gametocytaemia measurements were made using Tubulin Tracker™ Deep Red staining and the mKate channel for both strains. Flow cytometry data was analysed using FlowJo software (v. 10.7.2).

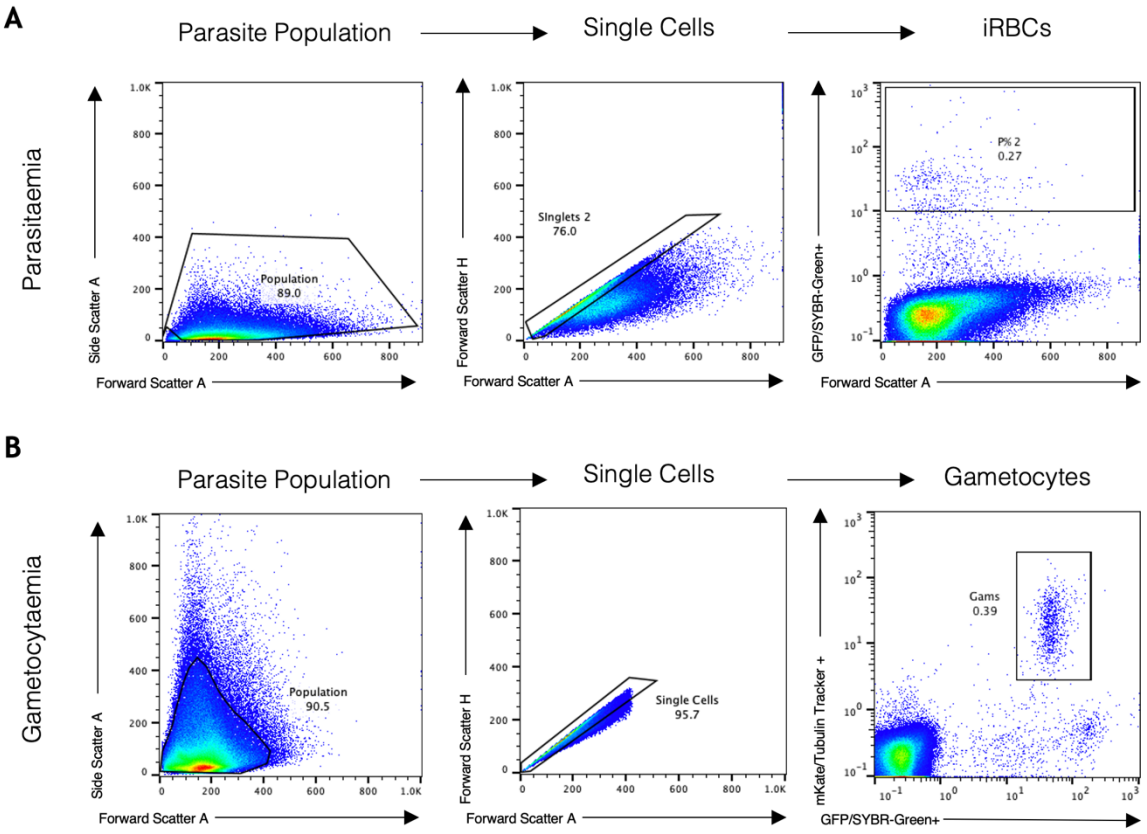

Figure 5-4. Gating strategy for sexual conversion assay flow cytometry in Pf2004. (**A**) Gating strategy for determining parasitaemia. Parasitaemia was measured by firstly selecting parasites and then isolating single cells. Parasites were measured based on GFP/SYBRGreen positivity in the GFP/FITC channel. (**B**) Gating strategy for measuring gametocytaemia. Gametocytaemia was measured by selecting parasites and then isolating single cells. Double positive parasites for SYBRGreen and Tubulin Tracker were gated allowing gametocytes to be quantified. Abbreviations: iRBCs, infected red blood cells.

PMR was lower in mFA conditions compared to serum for both strains as anticipated (Brancucci et al., 2015). The mean PMR in mFA was 2.8 (95% confidence interval (CI): 2.5 to 3.1) and 4.4 (4.2 to 4.5) for Pf2004 and Dd2 respectively. In contrast, the mean PMR in serum was 6.8 (95% CI: 6.5 to 7.0) for

Pf2004 and 7.6 (95% CI: 5.7 to 9.5) for Dd2. Conversion rates were higher in mFA compared to serum, with a mean conversion rate in mFA of 23% (95% CI: 13.2% to 33.5%) for Pf2004 and 32% (95% CI: 16.0% to 48.3%) for Dd2. This difference in conversion rate between the two strains in mFA was not significant (p = 0.118). Dd2 exhibited a higher background conversion rate of 2.7% (95% CI: 0.8% to 4.7%) reflecting the hypersensitivity of this strain to LysoPC (**Figure 5-5**). The presence of gametocytes was confirmed by microscopy (**Figure 5-6**). Calculations for PMR and conversion rate are detailed in **Section 2.4.5**.

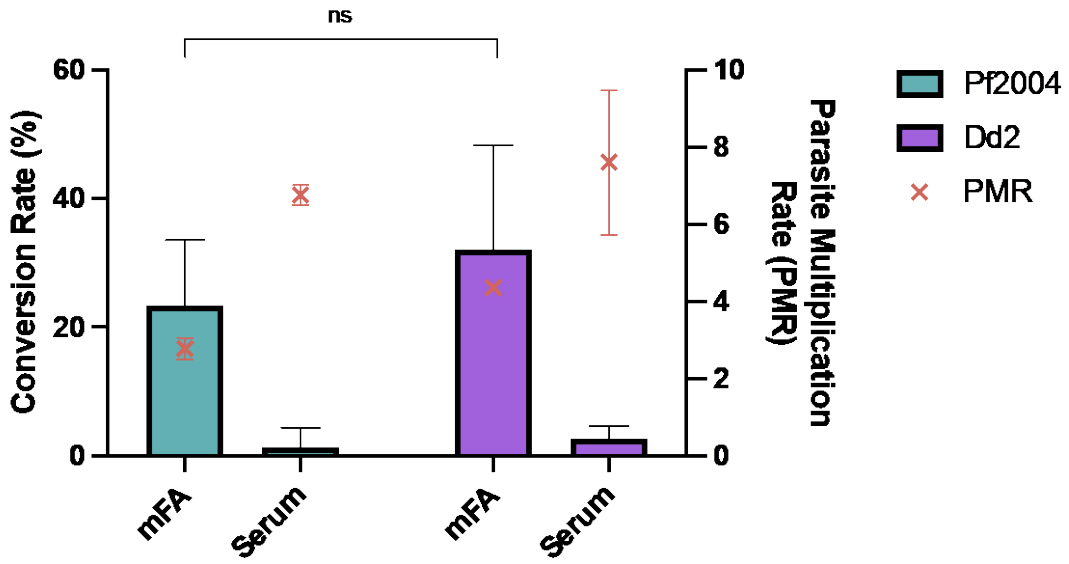

Figure 5-5. Parasite multiplication rate (PMR) and conversion rate for Pf2004 and Dd2. Bar graph showing mean (95% confidence interval (CI)) sexual conversion rates in each growth condition (mFA and Serum) for each strain (Pf2004 and Dd2). Conversion rates were measured as a percentage of gametocytes over the total reinvaded population (left axis). PMR is shown on the right axis. There was no significant difference between strain conversion rates (p=0.118). Statistical test used was unpaired t test. N=3 biological replicates with 3 technical replicates/experiment. Calculations for PMR and conversion rates can be found in **Section 2.4.5**.

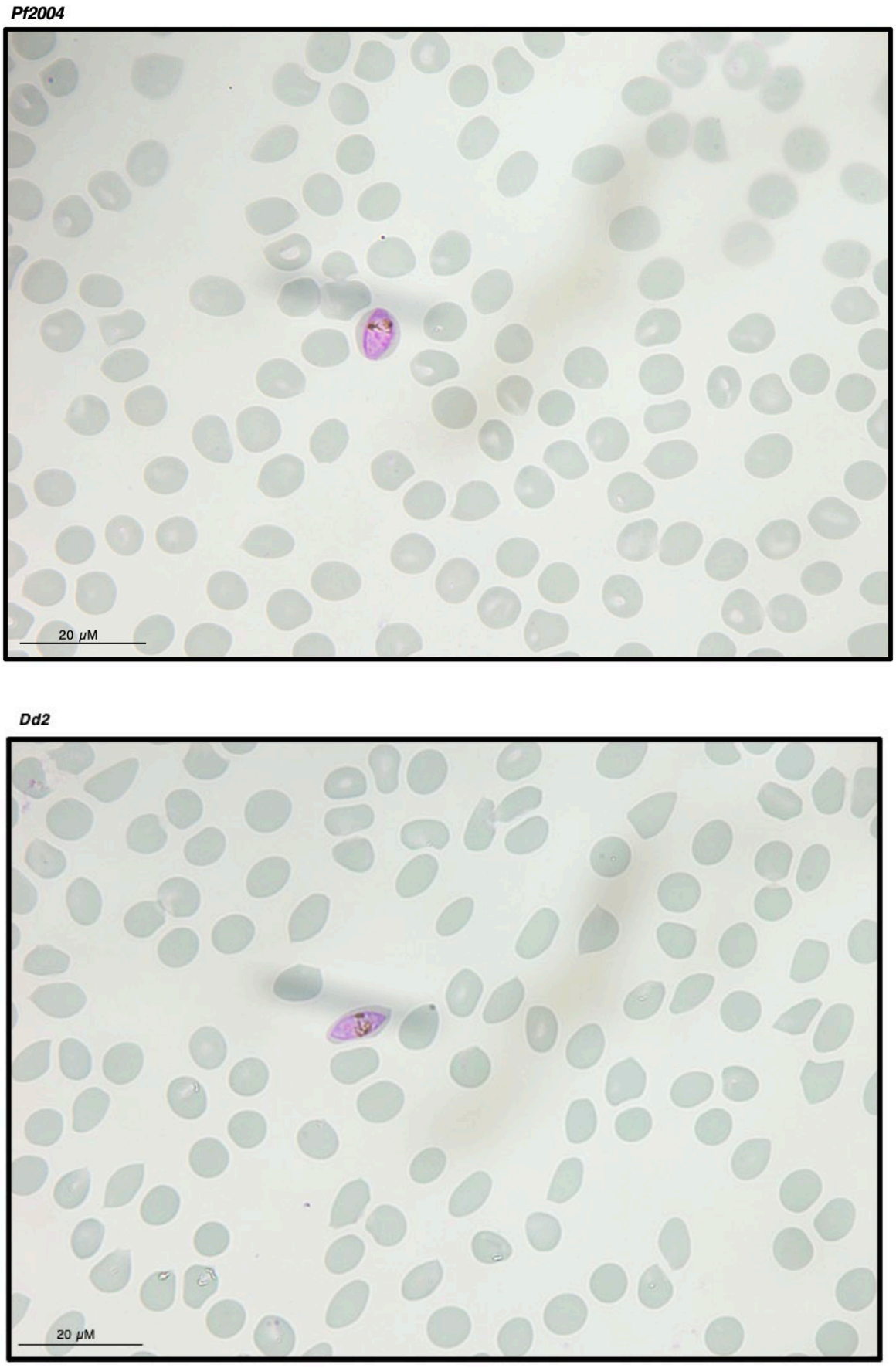

Figure 5-6. Blood smear of Pf2004 and Dd2 *in vitro* cultures confirms the presence of gametocytes following the sexual conversion assay.

5.4 Quality Control, Clustering and Annotation

5.4.1 Separating Pooled Strains

Pf2004 and Dd2 cells were pooled together prior to running on the 10X flow cell (**Figure 5-3B**). Pooling strains and using genetic-based separation reduces costs as fewer channels are used on the Chromium chip. To separate the two strains post hoc (i.e., computationally), strain-specific single nucleotide polymorphisms (SNPs) and competitive mapping were used. The genomes of Pf2004 and Dd2 were combined into a single genome and cells were mapped and assigned the strain with superior mapping for each replicate. Uniform manifold approximation and projection (UMAP) visualisation with low resolution clustering demonstrates the distinctive transcriptomes of these two *P. falciparum* strains (**Figure 5-7A**). After strain identities were assigned to each cell, the proportions of each strain per replicate was determined revealing approximately equal proportions of each strain in each replicate (**Figure 5-7B**).

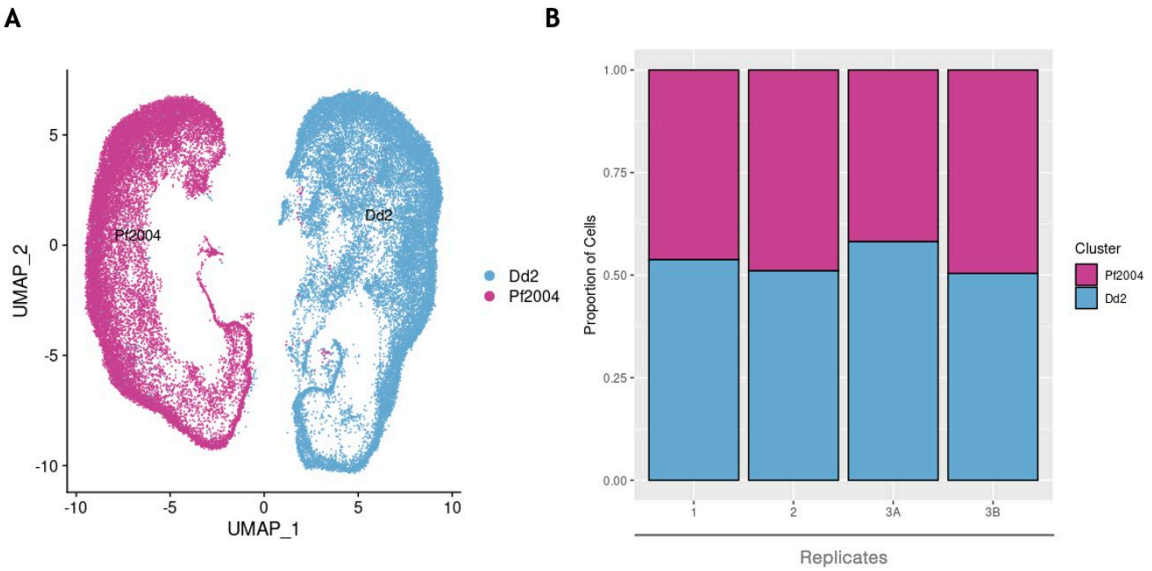

Figure 5-7. Separating pooled parasite strains computationally. Genomes of Pf2004 and Dd2 were combined into a single genome. (**A**) UMAP of combined Pf2004 and Dd2. (**B**) Proportion of cells assigned Pf2004 or Dd2 strain identities in each replicate. Replicate 3A and 3B are technical replicates of each other (the same sample was run twice due to a clogging failure in the 10X

Chromium machine). The aim was to pool strains in equal proportions for each replicate, as described in **Section 2.5.4**, which was successfully achieved.

Transcriptional differences between Pf2004 and Dd2 were explored using the combined Pf2004-Dd2 genome. Genes that have no sequence differences will be ignored in this analysis. Genes from the merozoite surface protein (MSP) multigene family were among top differentially expressed genes between the two strains. These genes included *msp1* (PF3D7_0930300), *msp2* (PF3D7_0206800), *msp4* (PF3D7_0207000) and *msp9* (PF3D7_1228600). This family of proteins is known to exhibit extensive polymorphisms with *msp1* and *msp2* commonly utilised for characterising genetic diversity in mixed infections or for identifying recrudescent infections (McBride et al., 1985, Soulama et al., 2009, Mwingira et al., 2011, Hamid et al., 2013, Sondo et al., 2019, Baina et al., 2023). The PfEMP1 variant, *var2csa*, was found to be a marker gene for Pf2004, likely attributed to prior cytoadherence selection for adhesion to immobilised CSA *in vitro* (**Figure 5-7**) (Hommel et al., 2010).

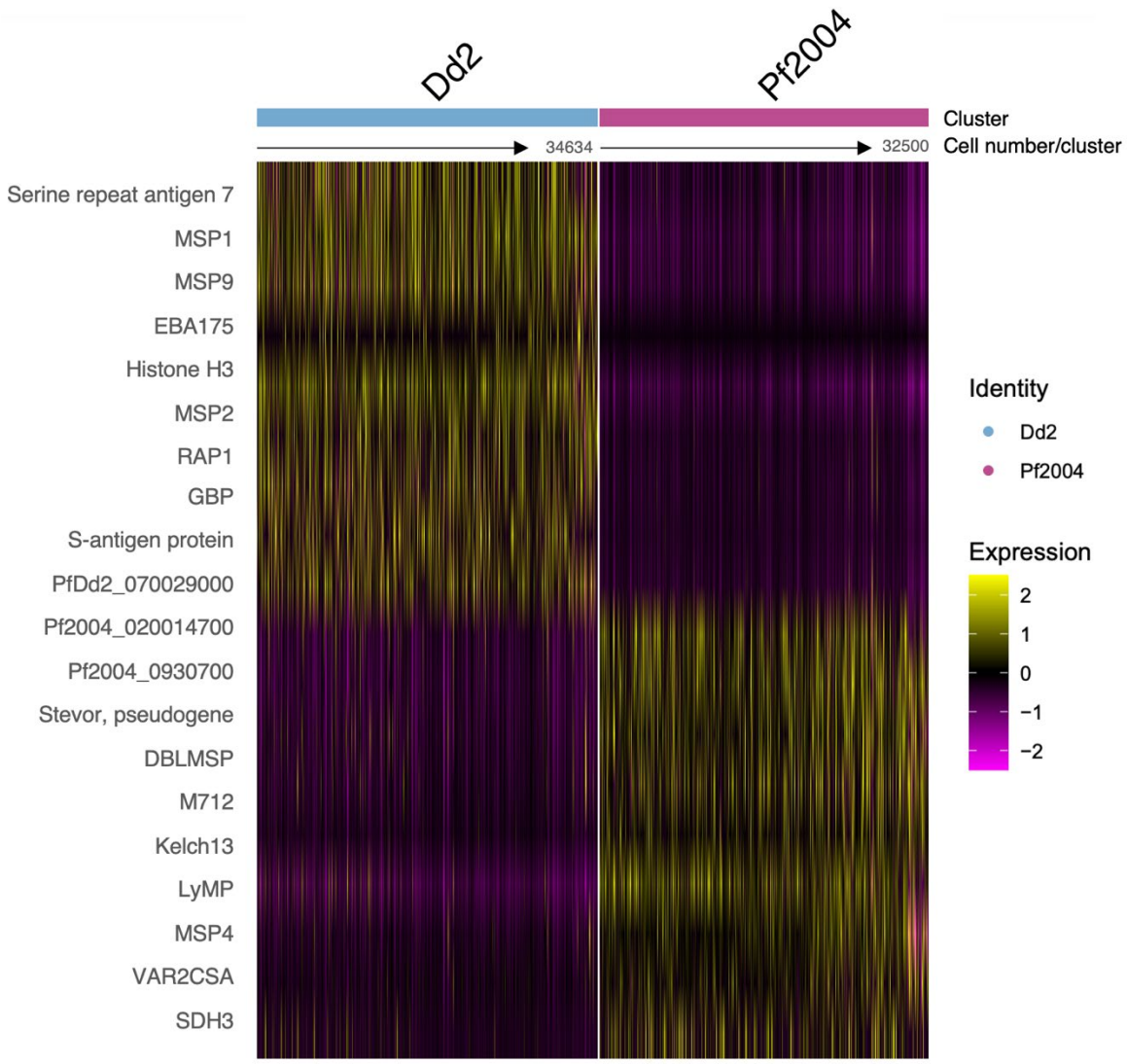

Figure 5-8. Heatmap of the top 10 differentially expressed marker genes between Pf2004 and Dd2. Genomes of Pf2004 and Dd2 were combined into a single genome and clustered at low resolution to identify a Pf2004 and a Dd2 cluster. Marker genes were determined for the Pf2004 and Dd2 clusters. The heatmap represents the expression level of the top 10 marker genes identified in each strain. Each column along the X axis of the heatmap represents a cell coloured by the expression level of the given gene on the Y axis.

5.4.2 Quality Control

Initial mapping of raw reads against the *P. falciparum* reference genome 3D7 with extended 3' untranslated regions was completed using Cell Ranger (v.7.0.0), performed by Thomas Otto. Despite employing the same experimental setup for each replicate, there was variation in the total number of cells returned for each run (**Table 5-1**). Although counting was performed by haemocytometer and flow cytometry before and after pooling, the Chromium chip was overloaded for

replicate 2 resulting in a higher number of doublets compared to other replicates. For replicate 3, a clogging failure on the 10X Chromium machine occurred due to an issue with a specific lot number of gel beads. Despite these technical setbacks, sequencing was performed on all samples allowing the recovery of 83,819 cells (46,938 cells for mFA and 36,881 for serum) across all replicates. Quality control was performed on individual samples before integration to remove noise and low quality cells (**Figure 5-9**) (Kolodziejczyk et al., 2015).

Across the three replicates, a median UMI/cell count ranging from 3684-5873 was achieved. This was higher than previous *Plasmodium* single cell datasets generated at the University of Glasgow, and up to 10 times higher than what was achieved in the first *P. falciparum* Malaria Cell Atlas which had a mean UMI/cell count of 587. The median genes/cell expressed across replicates was between 1151 to 1863 genes, representing an increase of up to 2-5 times higher compared to previous datasets (**Table 5-1**) (Howick et al., 2019, Hentzschel et al., 2022).

To deconvolute strain identity and eliminate multiplets, the computational tool Demuxlet was utilised. Demuxlet uses genetic variation (i.e., SNPs) to distinguish between sample identities within singlets (here between Pf2004 and Dd2) from multiple samples pooled together using barcoded single cell sequencing (Kang et al., 2018). After quality control, a total of 53,533 cells was retained (31,945 mFA and 21,588 serum) across the three replicates (**Figure 5-9, Table 5-1**). Therefore, 36% of cells were removed due to doublets or poor annotation.

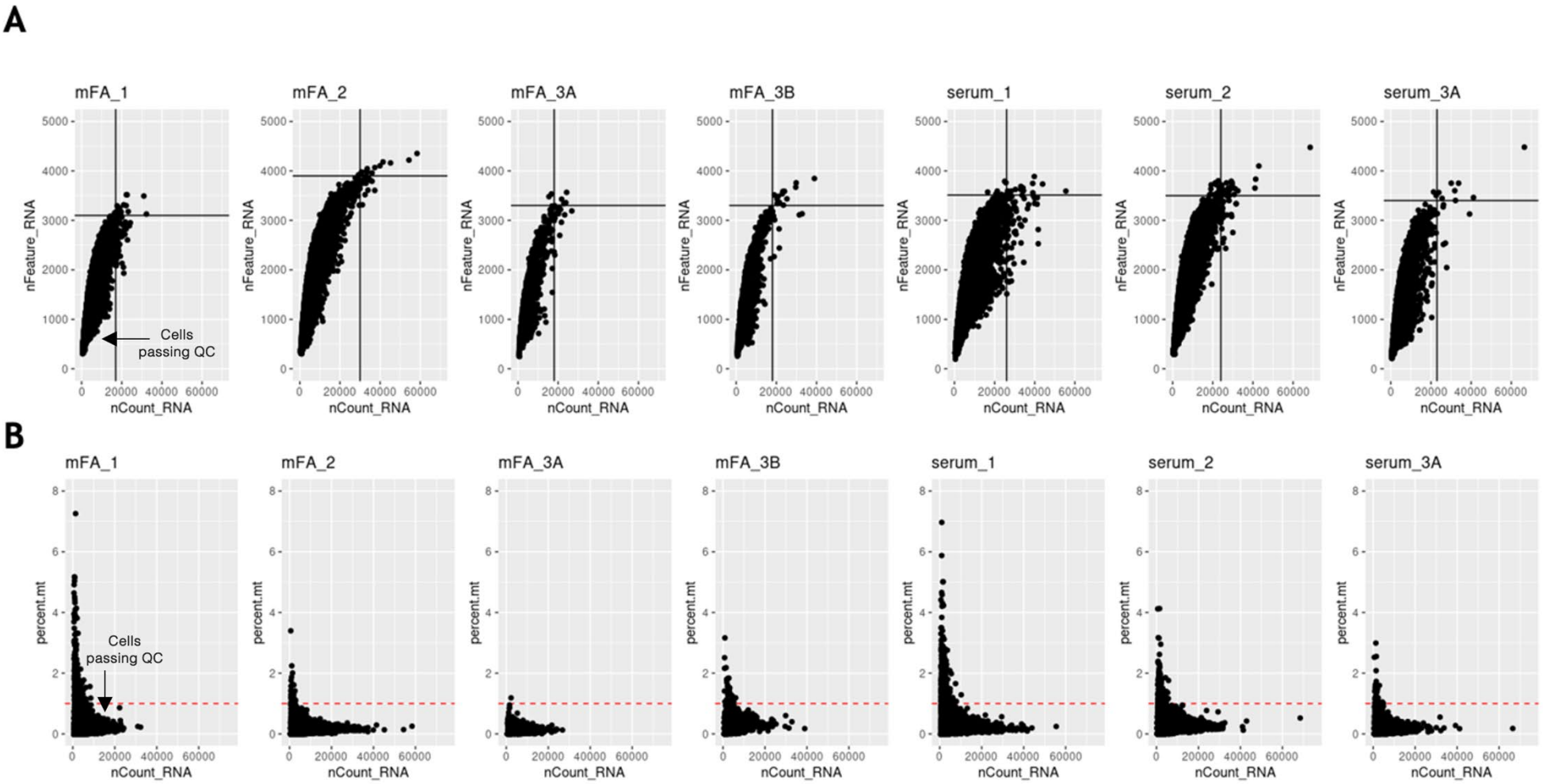

Figure 5-9. single cell RNA sequencing (scRNAseq) quality control (QC) thresholds for each sample. Scatterplots with quality control thresholds for filtering low quality cells where each point represents a cell. (**A**) nCount_RNA (i.e., UMI or unique transcript count) is plotted against nFeature_RNA (gene counts). A range of nCount_RNA and nFeature_RNA values are expected due to the varying expression levels and RNA content of different *Plasmodium* blood stages. Cells which

deviate from most cells in the dataset likely represent droplets containing multiple cells or droplets with ambient RNA contamination, and are therefore removed. Cells passing QC are located in the lower left quadrant highlighted in mFA_1. (**B**) nCount_RNA against the percentage of mitochondrial counts. Cells with a high percentage of mitochondrial counts often indicate cells which are stressed or dying and are therefore removed. Cells passing QC are below the red dashed line highlighted in mFA_1. Black or red dashed lines indicate threshold levels. Thresholds for each parameter can be found in **Section 2.6.1, Table 2-6**.

Table 5-1. Cell ranger outputs and cell counts.

	Cell Ranger Outputs							After QC Filtering		
	# Cells	**Median UMI / Cell**	**Median Genes / Cell**	**# Singlets**	**# Doublets**	**# Too Ambiguous**	**#Not Annotated**	**# Cells after QC**	**# Pf2004 Singlets**	**# Dd2 Singlets**
mFA_1	13533	3684	1151	8656	1637	2127	1113	8556	3911	4645
serum_1	11017	5557	1258	7314	1867	1256	580	7146	3112	4034
mFA_2	30659	5508	1863	21522	5664	2898	575	21432	12121	9311
serum_2	21566	4778	1499	13437	2563	3180	2386	13313	4893	8420
mFA_3A	1265	5423	1437	926	260	72	7	902	437	465
mFA_3B	1481	5267	1521	1110	266	92	13	1055	523	532
serum_3A	4298	5873	1239	3191	684	329	94	3129	1251	1878
Previously Published Datasets										
Hentzschel et al., 2022 (P. berghei)	5037	2338.4*	915*	-	-	-	-	-	-	-
Malaria Cell Atlas (P. berghei)	4884	1567.8*	799.8*	-	-	-	-	-	-	-
Malaria Cell Atlas (P. falciparum)	6737	587	373	-	-	-	-	-	-	-

*mean values instead of median.

5.4.3 Sample Integration & Unsupervised Clustering

After quality control, each strain was subset based on Demuxlet strain annotation and replicates were integrated together using Harmony (an algorithm for integrating single cell datasets) to generate two Seurat objects, one for each strain (Korsunsky et al., 2019) (**Figure 5-10**). Integrating both strains together and using different integration methods (Seurat integration) was tested. UMAP nonlinear dimensionality reduction was performed on the first 30 principal components. For both strains, cells were arranged in a circular fashion corresponding with the asexual life cycle. Objects were further refined by removing clusters with low UMI counts and gametocyte clusters (based on *pfs16* (PF3D7_0406200) expression). Gametocytes were removed since a gametocyte time point was not taken during this experiment, and therefore it was not possible to determine if gametocytes were the result of the sexual commitment assay or from previous cycles. Clusters were identified using a cluster resolution of 0.2 for Pf2004 and 0.25 for Dd2, respectively. This generated seven clusters for Pf2004 and six clusters for Dd2. The additional cluster identified in Pf2004 formed an inner ring of cells spanning the UMAP (**Figure 5-11**). The relevance of this inner ring of cells is discussed in **Section 5.6.2** (**Figure 5-24**). After quality control and the exclusion of specific clusters, 15,611 and 8340 cells were retained for Pf2004 in mFA and serum, respectively. Similarly, for Dd2, 8864 and 10,431 cells were retained in mFA and serum, respectively. Since Pf2004 and Dd2 were analysed separately, this difference in cell numbers after quality control will not be detrimental, particularly since a high number of cells was retained for both strains.

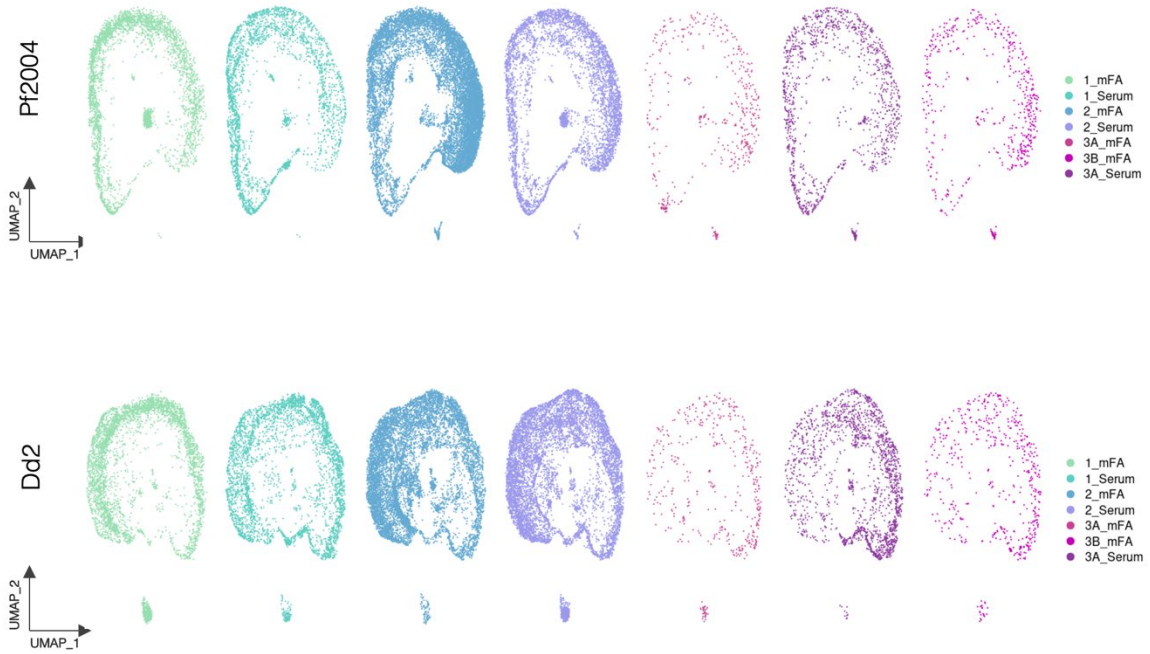

Figure 5-10. Minimal fatty acid (mFA) and Serum samples from each replicate were integrated into single Seurat objects depending on strain identity using Harmony. Replicates were integrated together using Harmony for each strain generating two Seurat objects: Pf2004 and Dd2 (Korsunsky et al., 2019). Each Seurat object (Pf2004 and Dd2) contains both cells grown in mFA and cells grown in Serum. Figure demonstrates the Pf2004 and Dd2 integrated objects separated according to the original sample (e.g., 1_mFA represents cells grown in mFA captured from the first replicate). This figure shows concordance in the uniform manifold approximation and projection (UMAP) for each replicate, and therefore successful integration. Each point represents an individual cell.

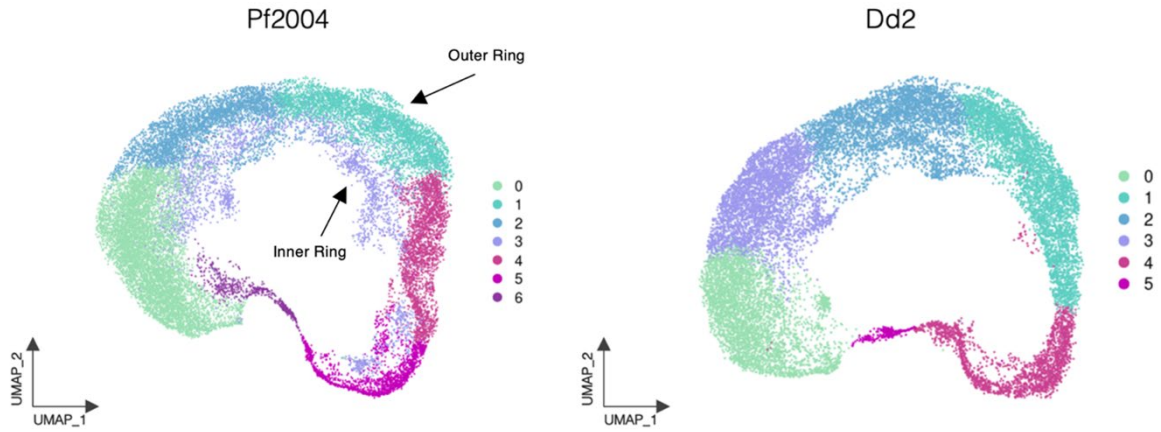

Figure 5-11. Pf2004 and Dd2 uniform manifold approximation and projections (UMAPs). Following the removal of cells with low unique molecular identifier (UMI) counts (i.e., low transcript counts) and gametocyte clusters, seven clusters were identified for Pf2004, and six clusters were identified for Dd2 at a cluster resolution of 0.2 and 0.25 respectively. Using these cluster resolutions, an additional cluster was identified in Pf2004 spanning the inner ring of the UMAP. Arrows on the Pf2004 UMAP indicate a separation into inner and outer clusters. The relevance of the inner and outer ring of cells is discussed in **Section 5.6.2, Figure 5-24**.

5.4.4 Correlating Clusters with Published Datasets

Clusters were annotated according to their correlation with the *P. falciparum* Smart-Seq2 Malaria Cell Atlas reference using scmap (Reid et al., 2018, Howick et al., 2019, Kiselev et al., 2018) (**Figure 5-12A**). scmap is a computational tool used to transfer cell type annotations from a reference scRNAseq dataset to a query scRNAseq dataset (Kiselev et al., 2018). Based on this reference mapping, 70% and 74% of cells for Pf2004 and Dd2 respectively were assigned a developmental stage. Cell identifications were confirmed using asexual marker genes ranging from rings to late schizonts (**Figure 5-13**). Marker genes corresponded with cell annotations based on the Malaria Cell Atlas reference mapping.

Despite harvesting only two time points, cells throughout the asexual intraerythrocytic cycle were identified. Most cells captured were early and late schizonts. In serum conditions, a small proportion of late rings were present. This was likely due to faster growth rates, reflected by a higher PMR in parasites grown in serum compared to parasites grown in mFA (**Figure 5-5, Figure 5-12B**).

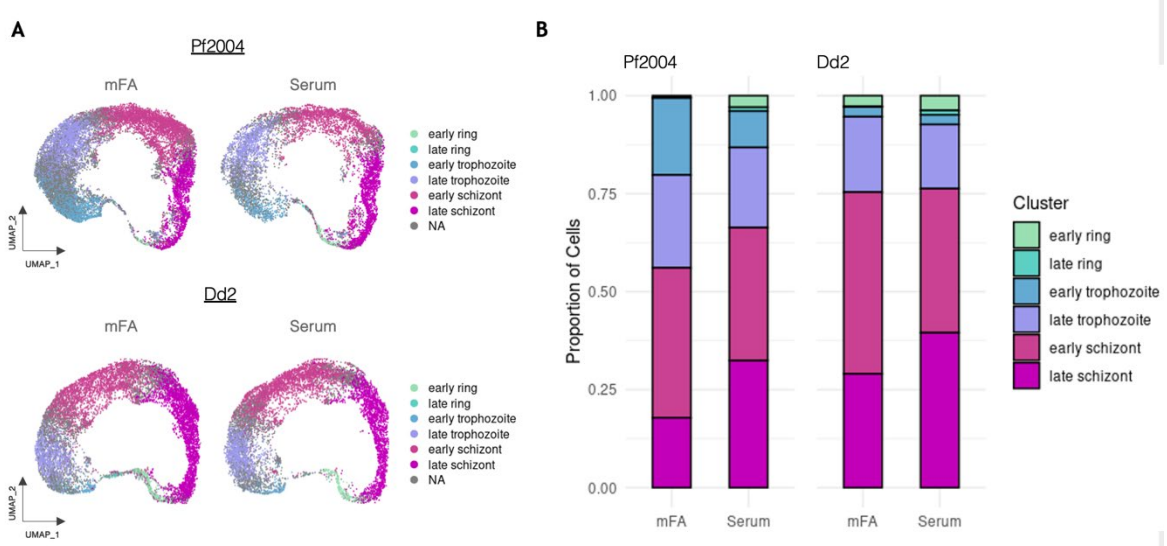

Figure 5-12. Assignment of asexual developmental stages to cells and their proportions after quality control. (**A**) Cell stage assignment was based on mapping of published *P. falciparum* Smart-Seq2 data from the Malaria Cell Atlas using scmap (Reid et al., 2018, Howick et al., 2019, Kiselev et al., 2018). Each point on the uniform manifold approximation and projection (UMAP) represent a cell. (**B**) Relative proportion of parasite clusters across conditions for each strain. Abbreviations: mFA, minimal fatty acid; NA, not assigned.

Pf2004

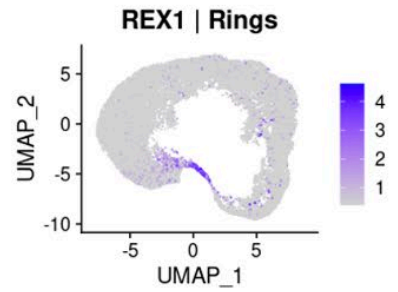
REX1 | Rings
UMAP_2
UMAP_1

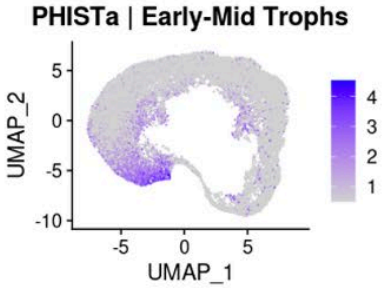
PHISTa | Early-Mid Trophs
UMAP_2
UMAP_1

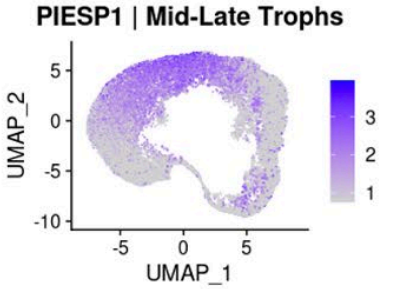
PIESP1 | Mid-Late Trophs
UMAP_2
UMAP_1

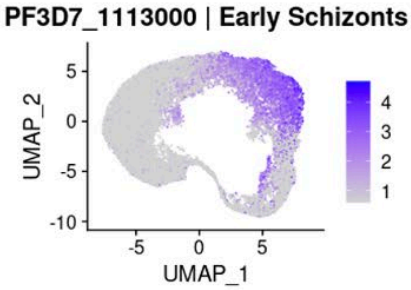
PF3D7_1113000 | Early Schizonts
UMAP_2
UMAP_1

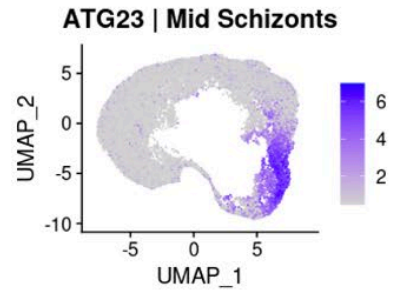
ATG23 | Mid Schizonts
UMAP_2
UMAP_1

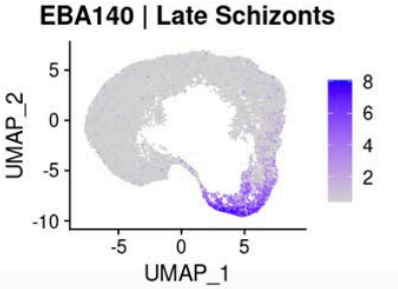
EBA140 | Late Schizonts
UMAP_2
UMAP_1

Dd2

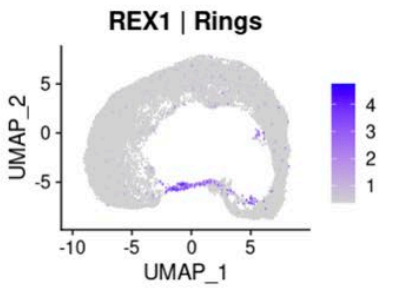
REX1 | Rings
UMAP_2
UMAP_1

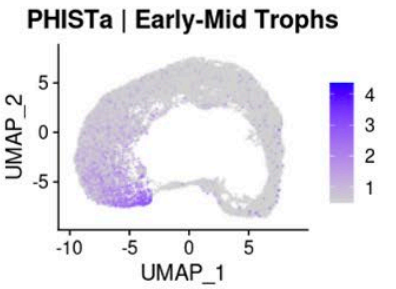
PHISTa | Early-Mid Trophs
UMAP_2
UMAP_1

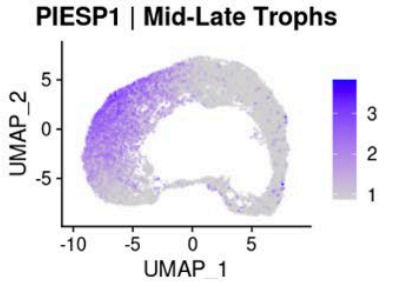
PIESP1 | Mid-Late Trophs
UMAP_2
UMAP_1

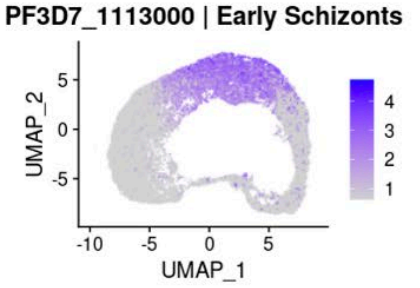
PF3D7_1113000 | Early Schizonts
UMAP_2
UMAP_1

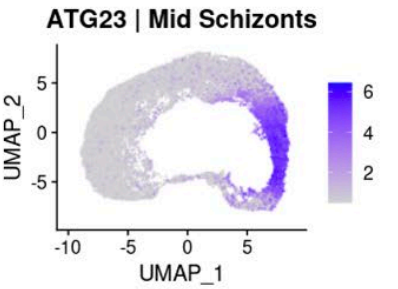
ATG23 | Mid Schizonts
UMAP_2
UMAP_1

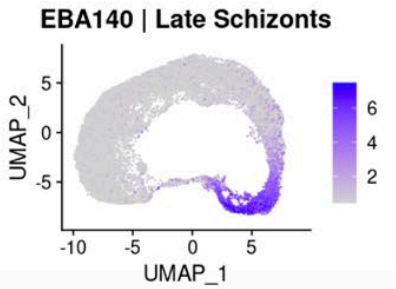
EBA140 | Late Schizonts
UMAP_2
UMAP_1

Figure 5-13. Uniform manifold approximation and projection (UMAP) of Pf2004 and Dd2 cells coloured by the expression level of cell stage marker genes. Expression patterns of marker genes from rings-late schizonts corresponded with clusters and scmap single cell reference annotation. Each strain is represented by a single UMAP which consists of both mFA and Serum grown cells integrated together (**Section 5.4.3**). Cell stage markers used: *rex1* (PF3D7_0935900), *piesp1* (parasite infected erythrocyte surface protein, PF3D7_0310400), *atg23* (PF3D7_1126700) and *eba140* (erythrocyte binding antigen 140, PF3D7_1301600).

5.5 Global Differences Between mFA vs Serum

Taking insights from bulk RNA sequencing and pseudo-single cell studies by Brancucci *et al.*, and given that parasites exhibited conversion rates of 20-35%, I hypothesised the existence of two distinct parasite populations within mFA: those committed to asexual development and those committed to sexual development (Brancucci et al., 2017, Brancucci et al., 2018). These two populations will likely share a metabolic response as a consequence of LysoPC depletion (Brancucci et al., 2018). Before exploring the transcriptomic profiles of sexually committed and asexual cells, the global differences between parasites grown in mFA compared to parasites grown in serum were first investigated. In doing so, results can be compared to existing bulk RNA sequencing datasets to validate the scRNAseq dataset generated here. In addition, this comparison may provide insight into the transcriptional signatures which define sexual and asexual populations.

5.5.1 DGE: mFA vs Serum

DGE of cells grown in mFA compared to cells grown in serum was initially investigated at the population level across all clusters. In Pf2004, 32 genes were found to be significantly upregulated (adjusted p-value <0.05, log2fold change > 0.5) while 606 genes were significantly downregulated. Amongst genes upregulated in mFA were *ap2-g* and *msrp1* representing the higher proportion of sexually committed cells present in mFA compared to serum (**Figure 5-5**). This overlaps with early transcriptional signatures of sexually committed cells in early scRNAseq studies (Poran et al., 2017, Brancucci et al., 2018). In addition, enzymes relating to metabolic responses to nutrient depletion were found to be upregulated in mFA. For example, *pmt* and s-adenosylhomocysteinase (*sahh,* PF3D7_0520900), which have previously been shown to be induced in LysoPC limiting conditions, were upregulated in mFA (**Figure 5-14A**). For the metabolic

pathway of PC biosynthesis and the alternative substrate arm of the Kennedy pathway, see **Section 1.4.4; Figure 1-8**). In connection with this metabolic pathway, ornithine aminotransferase (*oat,* PF3D7_0608800), which is involved in ornithine homeostasis and polyamine biosynthesis, was upregulated in mFA for Pf2004 (Gafan et al., 2001). Whereas, in serum conditions where LysoPC is available, an upregulation in choline kinase (*ck,* PF3D7_1401800) is observed (**Figure 5-14B**). *nt1* (PF3D7_1347200), an essential purine transporter, was among upregulated genes in mFA for Pf2004 alone likely in response to limiting nutrient availability in this media (El Bissati et al., 2006) (**Figure 5-14A, B**).

In Dd2, a similar DGE pattern in mFA compared to serum was observed but to a lesser extent. Here, only 9 genes were significantly upregulated in mFA while 156 genes were downregulated. Among those upregulated were *ap2-g, pmt* and *sahh* and those downregulated *clag3.1, clag3.2* and *clag2* (**Figure 5-14C, D**). The fewer genes differentially expressed between these two growth conditions for Dd2 reflects the hypersensitivity of Dd2 to LysoPC fluctuations resulting in higher commitment in serum conditions, and therefore more shared genes between the two media conditions (**Figure 5-5**).

In contrast, *rhoph2* (PF3D7_0929400), *rhoph3*, *clag3.1, clag3.2* (Pf3D7_0302200) and *clag2* were found to be upregulated in serum for both Pf2004 and Dd2 (**Figure 5-14**). These genes have been associated with the formation of a high molecular weight complex, the RhopH complex, which plays a critical role in merozoite invasion and solute transport (Goel et al., 2010, Nguitragool et al., 2011, Ito et al., 2017, Sherling et al., 2017, Schureck et al., 2021). The RhopH complex is comprised of three subunits, RhopH2, RhopH3 and CLAG. Once this complex is produced in its soluble form, it is packaged into the rhoptries to be released for invasion. Following invasion, this complex forms a nutrient channel, the PSAC, which is deposited onto the surface of the host RBC for solute uptake (Schureck et al., 2021). Contrary to the usual "just-in-time" model of transcription in *Plasmodium*, components of the RhopH complex are transcribed and translated in the cycle before they are required. Previous studies have demonstrated that the functionality of the PSAC is diminished in gametocytes and sexually committed schizonts, explaining the resistance of gametocytes to sorbitol lysis due to lower solute transport (Saul et al., 1990, Llorà-Batlle et al., 2020). Common to both

Pf2004 and Dd2, *surf4.1*, was upregulated in serum conditions compared to mFA. In contrast, *surf8.2* was upregulated in mFA for Pf2004 only (**Figure 5-14A, B**).

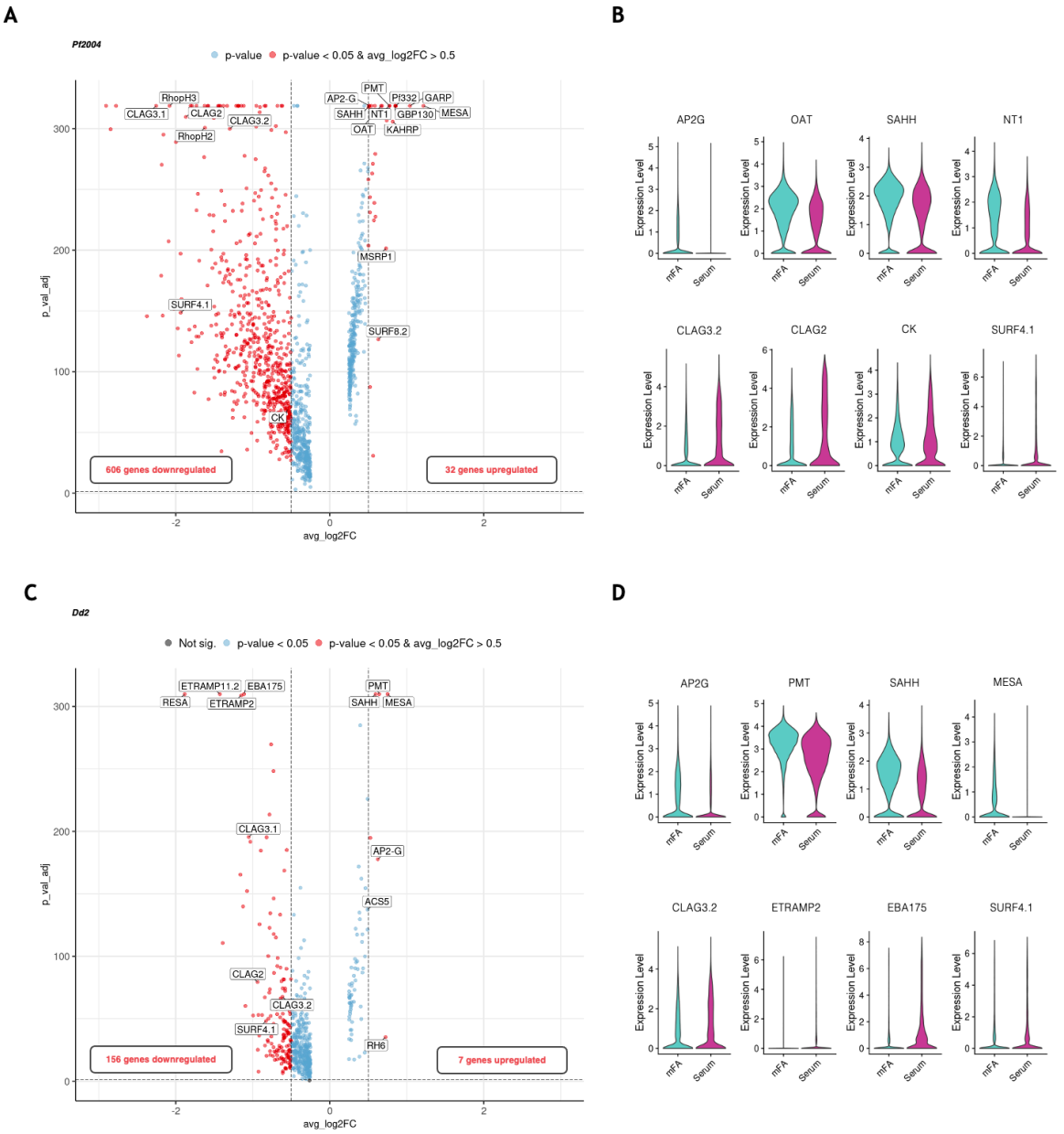

Figure 5-14. Global transcriptional changes between minimal fatty acid (mFA) and Serum for Pf2004 and Dd2. (**A**) Volcano plot of differential gene expression (DGE) between parasites (Pf2004) grown in mFA and Serum across all clusters or stages. (**B**) Expression levels of genes either upregulated (top panel) or downregulated (bottom panel) in Pf2004. (**C**) Volcano plot of DGE between parasites (Dd2) grown in mFA and Serum across all clusters or stages. (**D**) Expression levels of genes either upregulated (top panel) or downregulated (bottom panel) in Dd2.

To identify shared and unique genes upregulated and downregulated in mFA compared to serum between the two strains, Venn diagrams were utilised (**Figure**

5-15). For upregulated genes, 18.2% (6) of genes were shared between Pf2004 and Dd2 including *ap2-g, pmt,* and *sahh* (**Figure 5-15; Table5-2**). Alongside sexual commitment and metabolic markers, the reticulocyte binding homologue 6, (*rh6,* PF3D7_1335200), and the cytoadhesion associated gene, *mesa*, was upregulated in mFA for both Pf2004 and Dd2. The heat shock protein 70 (*hsp70,* PF3D7_0818900) was elevated in mFA for both Pf2004 and Dd2, whereas *hsp90* (PF3D7_0708400) was upregulated exclusively in Pf2004. The upregulation of heat shock proteins is likely part of a stress response (Banumathy et al., 2003, Przyborski et al., 2015).

For downregulated genes, 25.1% (153 genes) were shared between Pf2004 and Dd2, including *clag3.1, rhoph3,* and *clag2,* components of the RhopH complex/PSAC (**Figure 5-15; Table5-2**). The top downregulated gene shared between the two strains was ring-infected erythrocyte surface antigen (*resa*, PF3D7_0102200); this upregulation in serum might be explained by reinvasion events which were observed by smear when harvesting the late schizont time point, and as indicated in cell proportions of cells retained after quality control (**Figure 5-12B**). Other genes shared between the two strains were members of the ETRAMP multigene family, *etramp11.2* (PF3D7_1102800) and *etramp2* (PF3D7_0202500). These genes transcribe proteins which localise to the parasitophorous vacuole (PV) membrane and could mediate plasmodium-host cell interactions (Spielmann et al., 2003). Genes associated with merozoite RBC invasion belonging to the erythrocyte binding antigen family (EBA), such as *eba175* (PF3D7_0731500), *eba140* (PF3D7_1301600) and *eba181* (PF3D7_0102500), were amongst shared downregulated genes. Likewise, invasion related genes such as erythrocyte binding-like protein 1 (*ebl1,* PF3D7_1371600), *rh1* (PF3D7_0402300), *rh3* (PF3D7_1252400) and *msp2, msp3* (PF3D7_1035400) and *msp6* (PF3D7_1035500), were amongst shared downregulated genes in mFA for both strains (Tham et al., 2012, Molina-Franky et al., 2022).

Interestingly, several surface exported proteins and cytoadherence related genes were found to be exclusively upregulated in mFA in Pf2004 (**Figure 1-4**). These included, *garp* (PF3D7_0113000), *Pf332, kahrp, gbp130,* and *surf8.2*. The absence of *kahrp* is expected in Dd2 due to a chromosomal deletion from continuous culture (Ribacke et al., 2007, Jiang et al., 2008). Deletion of other surface

exported protein/cytoadherence related genes, such as *garp* and *pf332*, do not exist in Dd2 (PlasmoDB, release 66). Therefore, the upregulation of other surface antigen related genes in mFA for Pf2004 alone requires further investigation.

Together, these data validate previous bulk RNA sequencing findings which investigated the transcriptional differences between cells grown in mFA and serum at the population level (Brancucci et al., 2017). However, the advantage of performing scRNAseq is the ability to perform DGE analysis on specific cell types. Therefore, DGE between cells grown in mFA and serum was performed in early and late schizonts.

Table 5-2. Top 25 DGE genes between mFA vs Serum.

Upregulated (Pf2004)	Upregulated (Dd2)		Downregulated (Pf2004)	Downregulated (Dd2)
PF3D7_0500800 (MESA)	PF3D7_0500800 (MESA)		PF3D7_0102200 (RESA)	PF3D7_0102200 (RESA)
PF3D7_0113000 (GARP)	PF3D7_1335200 (RH6)		PF3D7_1102800 (ETRAMP11.2)	PF3D7_1102800 (ETRAMP11.2)
PF3D7_0112200 (MRP1)	PF3D7_0818900 (HSP70)		PF3D7_0731500 (EBA175)	PF3D7_0108500
PF3D7_1149000 (Pf332)	PF3D7_1343000 (PMT)		PF3D7_1149200 (RESA3)	PF3D7_1252400 (RH3)
PF3D7_1016300 (GBP130)	PF3D7_1222600 (AP2-G)		PF3D7_0202500 (ETRAMP2)	PF3D7_0202500 (ETRMP2)
PF3D7_0202000 (KAHRP)	PF3D7_0520900 (SAHH)		PF3D7_1252400 (RH3)	PF3D7_1301600 (EBA140)
PF3D7_1343000 (PMT)	PF3D7_1364100 (P92)		PF3D7_1301600 (EBA140)	PF3D7_0731500 (EBA175)
PF3D7_1347200 (NT1)			PF3D7_0102500 (EBA181)	PF3D7_1143100 (AP2-O)
PF3D7_0831700 (HSP70x)			PF3D7_0302500 (CLAG3.1)	PF3D7_0905400 (RhopH3)
PF3D7_0818900 (HSP70)			PF3D7_1411000	PF3D7_0302500 (CLAG3.1)
PF3D7_1335000 (MSRP1)			PF3D7_1035500 (MSP6)	PF3D7_1149200 (RESA3)
PF3D7_0731600 (ACS5)			PF3D7_0420300 (ApiAP2.1)	PF3D7_1327300 (SPM3)
PF3D7_0608800 (OAT)			PF3D7_1026600	PF3D7_0102500 (EBA181)
PF3D7_0830800 (SURF8.2)			PF3D7_0104300 (UBP1)	PF3D7_1401400 (ETRAMP14)
PF3D7_0708400 (HSP90)			PF3D7_0905400 (RhopH3)	PF3D7_0220800 (CLAG2)
PF3D7_1001600 (XL2)			PF3D7_0402300 (RH1)	PF3D7_1136900 (SUB2)
PF3D7_1307100 (UTP6)			PF3D7_1413700	PF3D7_0420300 (ApiAP2)
PF3D7_0532100 (ETRAMP5)			PF3D7_0108500	PF3D7_0220000 (LSA3)
PF3D7_1149100			PF3D7_1327300 (SPM3)	PF3D7_0903600
PF3D7_1335200 (RH6)			PF3D7_1143100 (AP2-O)	PF3D7_1023900 (CDH1)
PF3D7_1433900			PF3D7_0402200 (SURF4.1)	PF3D7_API03600 (ClpM)
PF3D7_0601900			PF3D7_1342600 (MyoA)	PF3D7_0613900 (MyoE)
PF3D7_0915400 (PFK9)			PF3D7_0220800 (CLAG2)	PF3D7_104300 (UBP1)
PF3D7_1132200 (TCP1)			PF3D7_1102700 (ETRAMP11.2)	PF3D7_0207100
PF3D7_1033900			PF3D7_1035400 (MSP3)	PF3D7_0402200 (SURF4.1)

Top 25 genes are ordered according to fold change, from highest to lowest. All top 25 genes have an adjusted p value < 0.05.

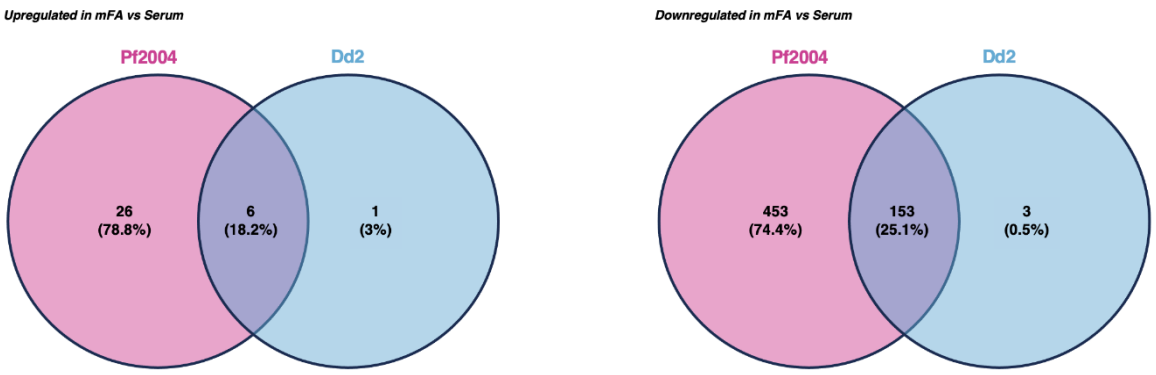

Figure 5-15. Venn diagram comparisons of differentially expressed genes in minimal fatty acid (mFA) vs Serum for Pf2004 and Dd2.

5.5.2 DGE: mFA vs Serum in Early and Late Schizonts

In Pf2004 early schizonts, 25 genes were significantly upregulated, and 126 genes were significantly downregulated in mFA compared to serum. Many upregulated genes mirrored that observed in global transcriptional changes (**Section 5.5.1**). For example, *ap2-g* and *msrp1* were significantly upregulated in addition to surface associated antigens such as *surf8.2, mesa, gbp130, pf332* and *garp,* with *mesa* and *gbp130* having the highest fold change. Genes related to the metabolic response of parasites to LysoPC limiting conditions, such as *pmt* and *ek* were amongst the top 25 genes significantly upregulated. In contrast, components of the RhopH complex/PSAC such as *clag3.1, rhoph3 and clag2* were downregulated and among the top 25 significant genes downregulated based on fold change. Similarly, members of the *etramp* family (e.g., *etramp11.2* and *etramp2*) were downregulated in mFA (**Figure 5-16A, B, Table 5-3**). These data reiterate the global transcriptional profile of cells grown in mFA compared to cells grown in serum matching existing bulk RNA sequencing and pseudo-single cell sequencing data (Brancucci et al., 2017, Brancucci et al., 2018). Similarly, in late schizonts in Pf2004, many of the same differentially expressed genes were identified with 48 genes significantly upregulated and 497 genes significantly downregulated in mFA compared to serum (**Figure 5-16C, D, Table 5-4**).

A similar expression pattern was observed in Dd2 however to a much lesser extent. In Dd2 early schizonts, only four genes were significantly upregulated, and 19 genes were significantly downregulated. In late schizonts, 29 genes were significantly upregulated whereas 93 genes were significantly downregulated. This

smaller difference between the two conditions may reflect the higher conversion rates in serum in Dd2 compared to Pf2004, suggesting that cells grown in mFA are more similar to cells grown in serum for Dd2, due to a greater sensitivity to LysoPC. Many of the same genes were significantly upregulated in schizonts such as *ap2-g, msrp1, ek, pmt, mesa, gbp130* and *rh6*. The highest fold change observed in upregulated genes for both Pf2004 and Dd2 in late schizonts was *rh6*. As observed in Pf2004, *clag3.1, clag2,* members of the *etramp* family and invasion related genes such as *eba175,* and *eba181,* were significantly downregulated in mFA. For both Pf2004 and Dd2, the highest fold change observed in downregulated genes in late schizonts grown in mFA was *resa* followed by *etramp11.2* (**Figure 5-17, Table 5-3, 5-4**). Overall, 11.5% (3) and 37.5% (21) of upregulated genes were shared between Pf2004 and Dd2 in early and late schizonts respectively. For downregulated genes, 14.2% (18) and 18.2% (91) of downregulated genes were shared between the two strains for early and late schizonts (**Figure 5-18**).

Interestingly, when investigating transcriptional changes between these two conditions at the cluster level, several ncRNAs were identified. These ncRNAs were found to be predominantly downregulated in mFA and amongst the top 25 significantly downregulated genes. In early schizonts, many of the differentially expressed ncRNAs were shared between Pf2004 and Dd2 including PF3D7_1370800, PF3D7_1244300, and PF3D7_1418800 (**Table 5-5**). While PF3D7_1148500 was only found in the top 25 for Pf2004, it was also significantly downregulated in Dd2 however it was below the FC threshold (log2FC: -0.45). Similarly, PF3D7_1478900 was found to be downregulated in Dd2 also, however, it was not part of the top25 downregulated genes in Pf2004 in early schizonts (**Table 5-4, 5-5**). To investigate these ncRNAs further, a BLASTn (basic local alignment search tool) search was performed. This search identified many regions of similarity between ncRNAs on chromosome 8, 11 and 13 (**Figure 5-19**). These regions of similarity might represent shared functions; however, this remains to be investigated.

In summary, DGE between media conditions for early and late schizonts exhibited many of the same DGE as identified in the population analysis in **Section 5.5.1**. However, by isolating clusters for analysis, stage specific transcriptional signatures are not masked. Interestingly, several ncRNAs were upregulated in serum in both Pf2004 and Dd2. Sequence similarity was determined between

ncRNAs revealing shared regions which may represent binding sites. The phenotypic relevance of these ncRNAs remains unknown.

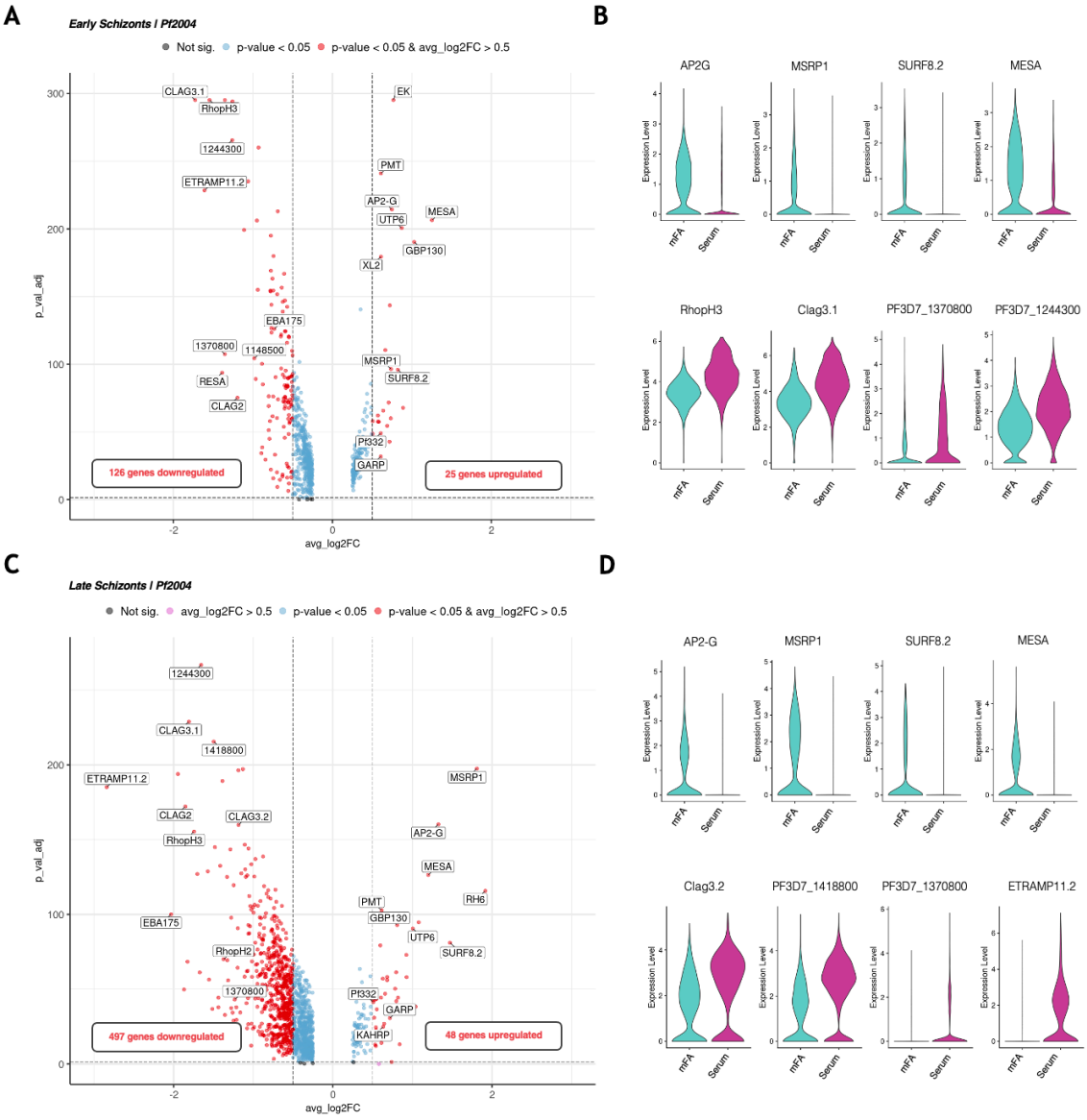

Figure 5-16. Transcriptional changes between schizonts in minimal fatty acid (mFA) and Serum in Pf2004. (**A**) Volcano plot of differential gene expression between parasites (Pf2004) grown in mFA for early schizonts. (**B**) Expression levels of genes either upregulated (top panel) or downregulated (bottom panel) in early schizonts (Pf2004). (**C**) Volcano plot of differential gene expression between Pf2004 parasites grown in mFA and Serum for late schizonts. (**D**) Expression levels of genes either upregulated (top panel) or downregulated (bottom panel) in late schizonts (Pf2004).

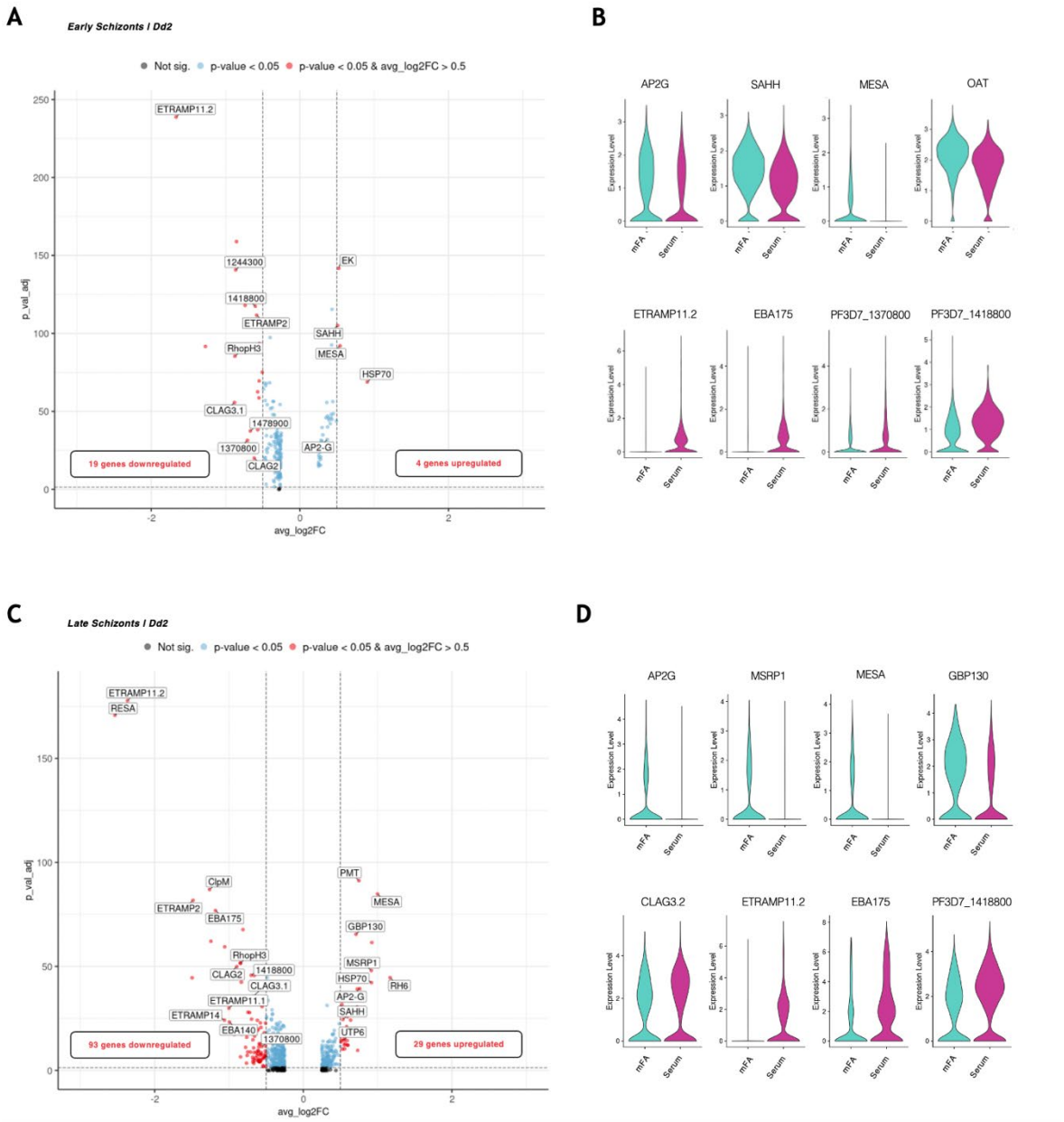

Figure 5-17. Transcriptional changes between schizonts in minimal fatty acid (mFA) and Serum in Dd2. (**A**) Volcano plot of differential gene expression between parasites (Dd2) grown in mFA for early schizonts. (**B**) Expression levels of genes either upregulated (top panel) or downregulated (bottom panel) in early schizonts (Dd2). (**C**) Volcano plot of differential gene expression between Dd2 parasites grown in mFA and Serum for late schizonts. (**D**) Expression levels of genes either upregulated (top panel) or downregulated (bottom panel) in late schizonts (Dd2).

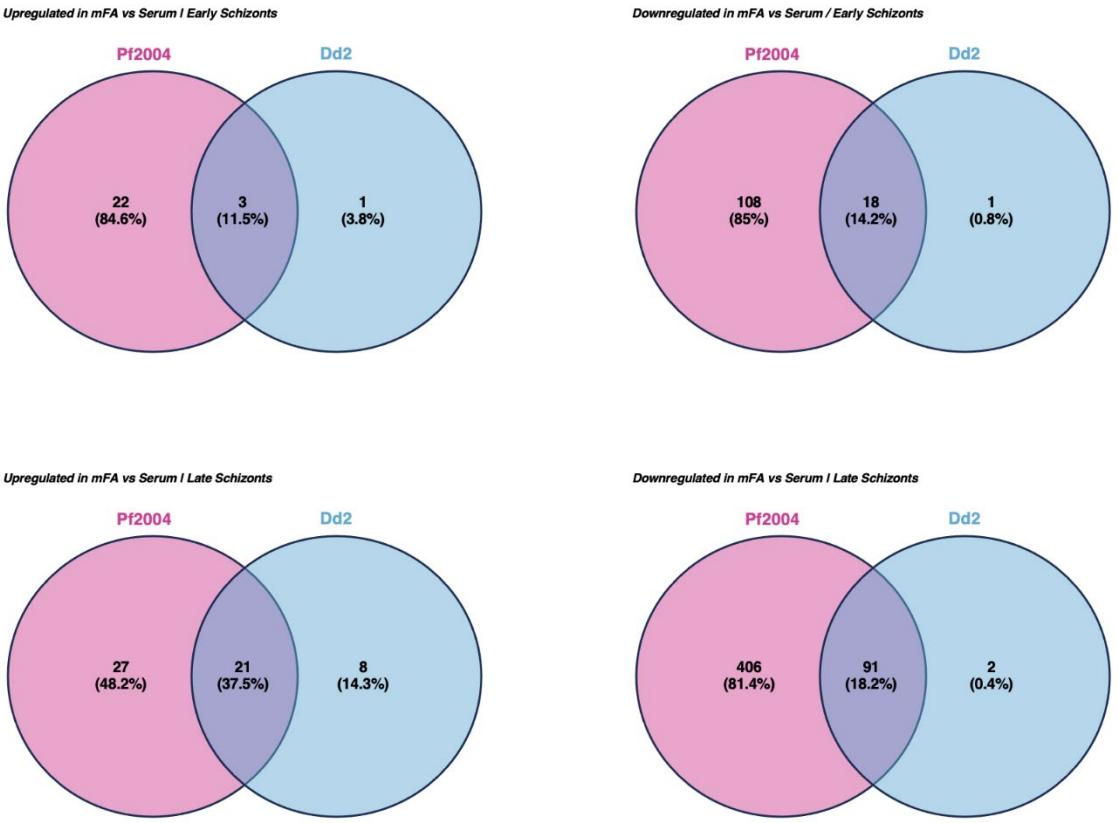

Figure 5-18. Venn diagram comparisons of differentially expressed genes between minimal fatty acid (mFA) vs Serum for Early and Late Schizonts (Pf2004 and Dd2).

Table 5-3. Top 25 DGE genes between mFA vs Serum in early schizonts.

Upregulated (Pf2004)	Upregulated (Dd2)		Downregulated (Pf2004)	Downregulated (Dd2)
PF3D7_0500800 (MESA)	PF3D7_0818900 (HSP70)		PF3D7_0302500 (CLAG3.1)	PF3D7_1102800 (ETRAMP11.2)
PF3D7_1016300 (GBP130)	PF3D7_0500800 (MESA)		PF3D7_1102800 (ETRAMP11.2)	PF3D7_0102200 (RESA)
PF3D7_0818900 (HSP70)	PF3D7_1124600 (EK)		PF3D7_0905400 (RhopH3)	PF3D7_0302500 (CLAG3.1)
PF3D7_1307100 (UTP6)	PF3D7_0520900 (SAHH)		PF3D7_0102200 (RESA)	PF3D7_0905400 (RhopH3)
PF3D7_0830800 (SURF8.2)			PF3D7_1370800	PF3D7_1244300
PF3D7_1124600 (EK)			PF3D7_0817900 (HMGB2)	PF3D7_0817900 (HMGB2)
PF3D7_1222600 (AP2-G)			PF3D7_1244300	PF3D7_0731500 (EBA175)
PF3D7_1335000 (MSRP1)			PF3D7_1418800	PF3D7_1370800
PF3D7_1140000 (CA)			PF3D7_0220800 (CLAG2)	PF3D7_1478900
PF3D7_1433900			PF3D7_0206800 (MSP2)	PF3D7_0108500
PF3D7_0532100 (ETRAMP5)			PF3D7_1434200 (CAM)	PF3D7_0220800 (CLAG2)
PF3D7_1033900			PF3D7_1148500	PF3D7_1418800
PF3D7_0708400 (HSP90)			PF3D7_1449200	PF3D7_0202500 (ETRAMP2)
PF3D7_0935200 (VPS33)			PF3D7_1335100 (MSP7)	PF3D7_0928000 (COX6B)
PF3D7_1444100			PF3D7_0928000 (COX6B)	PF3D7_0206800 (MSP2)
PF3D7_1001600 (XL2)			PF3D7_1038000	PF3D7_1449200
PF3D7_1343000 (PMT)			PF3D7_0722200 (RALP1)	PF3D7_1038000
PF3D7_0113000 (GARP)			PF3D7_0929400 (RhopH2)	PF3D7_1335100 (MSP7)
PF3D7_1149000 (Pf332)			PF3D7_1436200 (BCP1)	PF3D7_1010300 (SDH4)
PF3D7_0112200 (MRP1)			PF3D7_0831800 (HRP2)	
PF3D7_0819800			PF3D7_1012200 (RA)	
PF3D7_0731600 (ACS5)			PF3D7_0202500 (ETRAMP2)	
PF3D7_1149100			PF3D7_0105300 (CAP)	
PF3D7_0220200			PF3D7_1116000 (RON4)	
PF3D7_1431500 (MAPK1)			PF3D7_0511600 (ARNP)	

Top 25 genes are ordered according to fold change, from highest to lowest. All top 25 genes have an adjusted p value < 0.05. ncRNAs are highlighted in purple.

Table 5-4. Top 25 DGE genes between mFA vs Serum in late schizonts.

Upregulated (Pf2004)	Upregulated (Dd2)		Downregulated (Pf2004)	Downregulated (Dd2)
PF3D7_1335200 (RH6)	PF3D7_1335200 (RH6)		PF3D7_0102200 (RESA)	PF3D7_0102200 (RESA)
PF3D7_1335000 (MSRP1)	PF3D7_0500800 (MESA)		PF3D7_1102800 (ETRAMP11.2)	PF3D7_1102800 (ETRAMP11.2)
PF3D7_0830800 (SURF8.2)	PF3D7_0927500		PF3D7_0731500 (EBA175)	PF3D7_0108500
PF3D7_1222600 (AP2-G)	PF3D7_0818900 (HSP70)		PF3D7_1252400 (RH3)	PF3D7_0202500 (ETRAMP2)
PF3D7_0500800 (MESA)	PF3D7_1335000 (MSRP1)		PF3D7_1149200 (RESA3)	PF3D7_API03600 (ClpM)
PF3D7_1460000 (HCS2)	PF3D7_1222600 (AP2-G)		PF3D7_API03600 (ClpM)	PF3D7_1149200 (RESA3)
PF3D7_1307100 (UTP6)	PF3D7_1343000 (PMT)		PF3D7_1413700	PF3D7_0220000 (LSA3)
PF3D7_0819800	PF3D7_1117500 (TyrRSapi)		PF3D7_0202500 (ETRAMP2)	PF3D7_0731500 (EBA175)
PF3D7_0832100 (RIF)	PF3D7_1020100		PF3D7_0220800 (CLAG2)	PF3D7_1252400 (RH3)
PF3D7_1433900	PF3D7_1026100		PF3D7_0302500 (CLAG3.1)	PF3D7_1401400 (ETRAMP14)
PF3D7_1020100	PF3D7_1016300 (GBP130)		PF3D7_0319700 (ABC13)	PF3D7_API02900 (TUFA)
PF3D7_1016300 (GBP130)	PF3D7_1301900		PF3D7_1301600 (EBA140)	PF3D7_1102700 (ETRAMP11.1)
PF3D7_0927500	PF3D7_0819800		PF3D7_1244300	PF3D7_1301600 (EBA140)
PF3D7_1438800	PF3D7_0403600		PF3D7_0905400 (RhopH3)	PF3D7_0623800 (TKL4)
PF3D7_0403600	PF3D7_1433900		PF3D7_0108500	PF3D7_0220800 (CLAG2)
PF3D7_0704700 (PPAT)	PF3D7_1035700 (DBLMSP)		PF3D7_1418800	PF3D7_MIT02300 (CYTB)
PF3D7_1340500	PF3D7_1468200 (TLS1)		PF3D7_0102500 (EBA181)	PF3D7_1116800 (HSP101)
PF3D7_1301900	PF3D7_0802500		PF3D7_API02900 (TUFA)	PF3D7_0905400 (RhopH3)
PF3D7_0209500	PF3D7_0929600		PF3D7_0730300 (ApiAP2.1)	PF3D7_1010300 (SDH4)
PF3D7_1468200 (TLS1)	PF3D7_1340500		PF3D7_0622900 (AP2Tel)	PF3D7_0731400 (FIKK7.2)
PF3D7_0113000 (GARP)	PF3D7_1460000 (HCS2)		PF3D7_0220000 (LSA3)	PF3D7_MIT02100 (COX1)
PF3D7_1343000 (PMT)	PF3D7_1111900		PF3D7_0104300 (UBP1)	PF3D7_0102500 (EBA181)
PF3D7_0927900 (PSD)	PF3D7_1307100 (UTP6)		PF3D7_0611800	PF3D7_1023900 (CHD1)
PF3D7_0315300	PF3D7_0520900 (SAHH)		PF3D7_1321300	PF3D7_1321900
PF3D7_0202000 (KAHRP)	PF3D7_0406700		PF3D7_1035500 (MSP6)	PF3D7_1143100 (AP2-O)

Top 25 genes are ordered according to fold change, from highest to lowest. All top 25 genes have an adjusted p value < 0.05. ncRNAs are highlighted in purple.

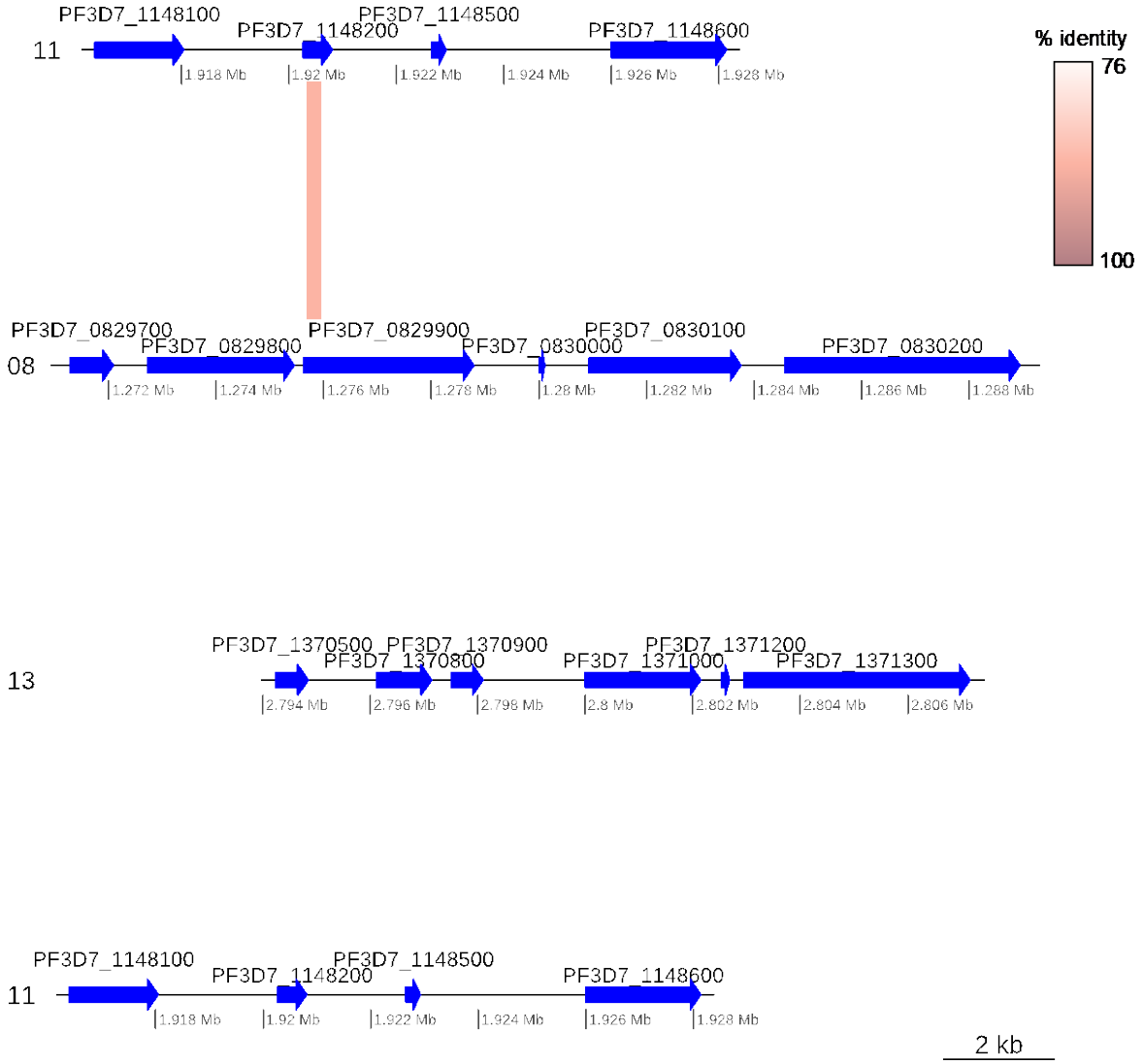

Figure 5-19. Regions of similarity between 3 non-coding RNAs (ncRNA) of chromosome, 8, 11. and 13. ncRNAs identified to be differentially expressed between mFA and Serum in schizonts (**Table 5-3, 5-4**) exhibited several regions of similarity, suggesting they may share functional roles. Blue arrows show the ncRNA positions in the *Plasmodium* reference genome (3D7). Pink to mauve links between chromosomes highlight the regions that BLAST against each other indicating regions of similarity between chromosomes. The ncRNA sequences in the regions PF3D7_08_v3:1270237-1290240, PF3D7_11_v3:1914041-1933278 and PF3D7_13_v3_2789345-2808200 were retrieved from PlasmoDB (release 66) and run against each other with blastn (v. 2.13.0).

5.6 Defining Asexual and Sexual Populations

5.6.1 Mapping Known Sexual Commitment Markers

As before described, Pf2004 and Dd2 represent two parasite strains with different sensitivities to LysoPC, with Dd2 being hypersensitive to fluctuations in LysoPC levels. The transcriptional pathway underlying different parasite responses to LysoPC remains unclear. To begin to explore this pathway, the gene expression

patterns of known sexual commitment markers (**Section 1.4.3**) were investigated along pseudotime. Pseudotime is a computational concept which infers a trajectory representing the temporal ordering of cells in a scRNAseq dataset (Reid and Wernisch, 2016). To map the expression of known sexual commitment markers over pseudotime, Pf2004 and Dd2 Seurat objects were split according to media (for example, Pf2004 mFA, **Figure 5-20A**). Since it was not possible to determine if rings originated from the previous cycle or the next cycle, ring clusters were removed. To easily draw a pseudotime trajectory, the cluster resolution was reduced allowing enough clusters for a start cluster and end cluster to be defined to build a slingshot trajectory (Street et al., 2018) (**Figure 5-20B**). Cluster resolution for Pf2004 mFA, Pf2004 serum, Dd2 mFA. Dd2 serum was reduced to 0.05, 0.08, 0.08 and 0.05 respectively. Using Slingshot, cells were ordered along pseudotime (Street et al., 2018) (**Figure 5-20C**). The average expression of the sexual commitment markers, *gdv1, gdv1as, ap2-g* and *msrp1,* were then visualised over pseudotime in each condition for Pf2004 and Dd2 (**Figure 5-21A, 5-22A**).

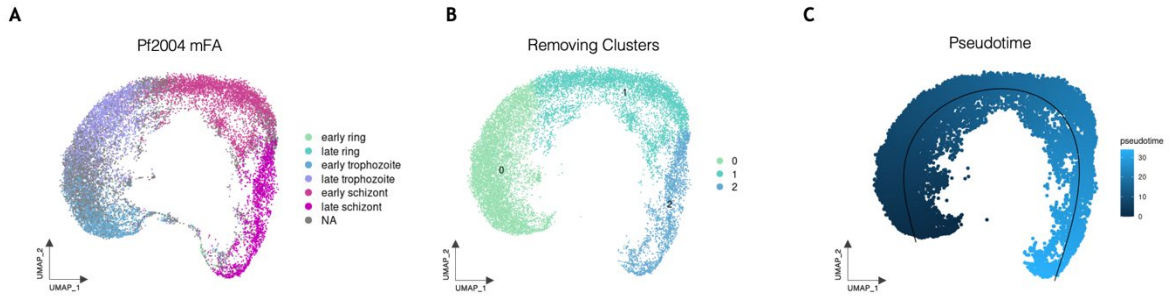

Figure 5-20. Representative figures demonstrating the ordering of cells along pseudotime. Representative images of how slingshot was used to draw a trajectory over pseudotime in Pf2004 (minimal fatty acid (mFA)). (**A**) Annotated uniform manifold approximation and projection (UMAP) of Pf2004 in mFA. To visualise the average expression of sexual commitment markers over pseudotime for each strain (Pf2004 and Dd2) and each condition (mFA and Serum), Seurat objects (e.g., Pf2004) were split according to condition (e.g., mFA). (**B**) Removal of ring clusters and reduction of cluster resolution. To allow a slingshot trajectory to be drawn over pseudotime, ring clusters were removed as it was not possible to determine if these rings were from the previous or subsequent cycle. After removal of ring clusters, the cluster resolution was reduced allowing enough clusters for a start and end cluster to be defined. For example, for Pf2004 mFA, cluster 0 was defined as the start cluster of the trajectory and cluster 2 was defined as the end cluster for slingshot (Street et al., 2018). (**C**) Slingshot trajectory along pseudotime in Pf2004 grown in mFA. Scale bar from dark to light blue indicates the progression of pseudotime from early to late stages in the trajectory. Referring to (**A**) this progression is from early trophozoites to late schizonts. Abbreviations: mFA, minimal fatty acid.

Overall, it was evident that the expression levels of, and the number of cells expressing, sexual commitment markers was lower in serum compared to mFA for Pf2004 (**Figure 5-21A, 5-22**). The transcriptional cascade of sexual commitment in Pf2004 can be deciphered over pseudotime where cells initially express *gdv1,* the expression of which is downregulated with the increase in expression levels of the ncRNA *gdv1as*. The expression of *gdv1* and *gdv1as* reduces with the increase in expression of *ap2-g*. Once the expression of *ap2-g* peaks in early schizonts, the expression of *msrp1* is increased and high throughout late schizonts. Following the decline in *msrp1* expression levels, the previously described positive feedback loop of *ap2-g* was observed (Kafsack et al., 2014, Poran et al., 2017). The expression patterns of sexual commitment markers were compared to parasites grown in serum (**Figure 5-21B**). This revealed a marked decrease in the average expression of sexual commitment markers over pseudotime (**Figure 5-21**).

The expression of sexual commitment markers in Pf2004 can be compared to that of Dd2 which is hypersensitive to LysoPC and therefore has a higher background conversion rate (**Figure 5-5**). While the overall expression was the same, there were a few notable differences. The peak in *ap2-g* expression in mFA appeared in the middle of early schizont growth in Dd2 whereas the peak in *ap2-g* expression in Pf2004 was towards the end of early schizonts. Like Pf2004, after the first peak of *ap2-g* expression, the expression of *msrp1* reached a peak (**Figure 5-21A**). With the decline in expression levels of *msrp1,* the second peak of *ap2-g* expression was evident in late schizonts in Dd2. When comparing the average expression of the same markers in serum, the average expression of *ap2-g* was higher in Dd2 than in Pf2004 (**Figure 5-21B**). This may reflect the higher background conversion in Dd2 compared to Pf2004. However, it is important to note that this is based on the average expression and therefore differences in cell numbers between strains may have an influence on the expression patterns visualised using this method (**Figure 5-21**).

Gene expression patterns can also be visualised on the UMAP for each strain in each condition (**Figure 5-22**). While this does not allow the identification of expression peaks as visualised in **Figure 5-21**, it allows for the visualisation of differences in the number of cells expressing each gene over time. From **Figure**

5-22, the number of cells expressing, and the level of expression, of sexual commitment associated markers was higher in mFA compared to serum for both strains. In contrast to Pf2004, the number of cells expressing *ap2-g* in serum was relatively higher in Dd2. Indeed, there were relatively more cells expressing all sexual commitment markers in serum for Dd2 compared to Pf2004 (**Figure 5-22**). This higher number of cells expressing sexual commitment markers in serum for Dd2 aligns with findings from DGE comparing mFA and serum conditions, where fewer transcriptional differences were observed between the two conditions in Dd2 (**Section 5.5**). As hypothesised in **Section 5.5**, this similarity between expression patterns of markers of sexual commitment, at least for *ap2-g*, in serum and mFA for Dd2 likely reflects the hypersensitivity of Dd2 to LysoPC fluctuations resulting in higher conversion rates in serum (**Figure 5-22**). While there were relatively similar cell numbers expressing *ap2-g* in Dd2 between mFA and serum, the second peak in *ap2-g* expression appeared to have fewer cells and lower expression levels in serum (**Figure 5-22**).

In both Pf2004 and Dd2, the sexual commitment pathway from the initial transcriptional response to LysoPC depletion until the positive feedback loop activating *ap2-g* was determined. Between the two strains, a similar transcriptional pattern was observed in sexual commitment markers. However, the relative number of cells expressing each sexual commitment marker differed between the two strains. It is unknown whether the transcriptional signature of sexually committed schizonts differs between these two strains and therefore requires further investigation.

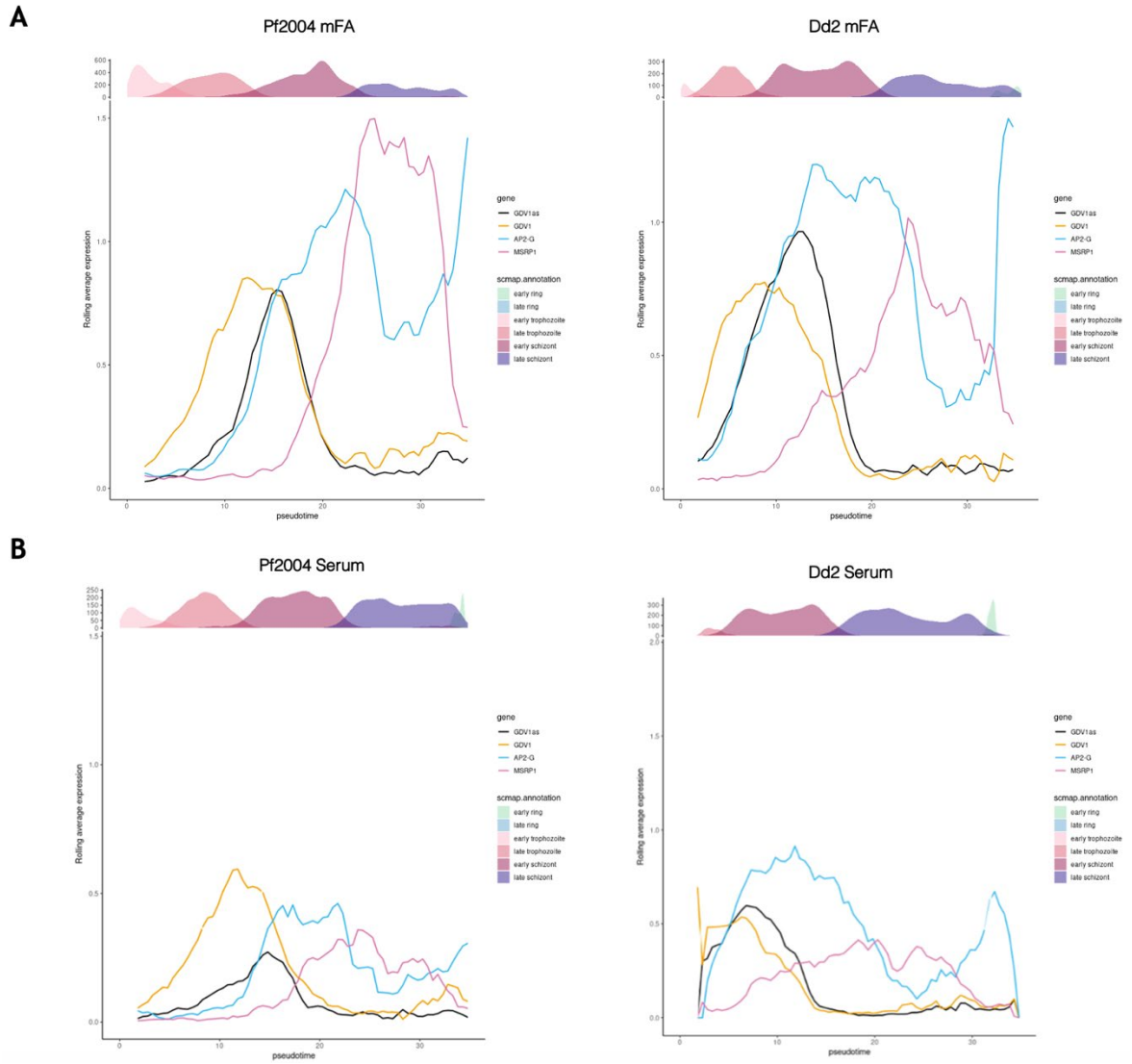

Figure 5-21. Temporal order of sexual commitment markers in mFA and Serum. (**A**) Average expression *of gdv1* (yellow), *gdv1as* (black), *ap2-g* (blue) and *msrp1* (pink) over pseudotime in mFA for Pf2004 and Dd2. Pseudotime, representing the temporal ordering of cells, is displayed on the x axis, with the corresponding cell type annotation from the Malaria Cell Atlas using scmap (scmap.annotation) shown above (Reid et al., 2018, Howick et al., 2019, Kiselev et al., 2018). (**B**) Average expression *of gdv1* (yellow), *gdv1as* (black), *ap2-g* (blue) and *msrp1* (pink) over pseudotime in Serum for Pf2004 and Dd2. Abbreviations: mFA, minimal fatty acid.

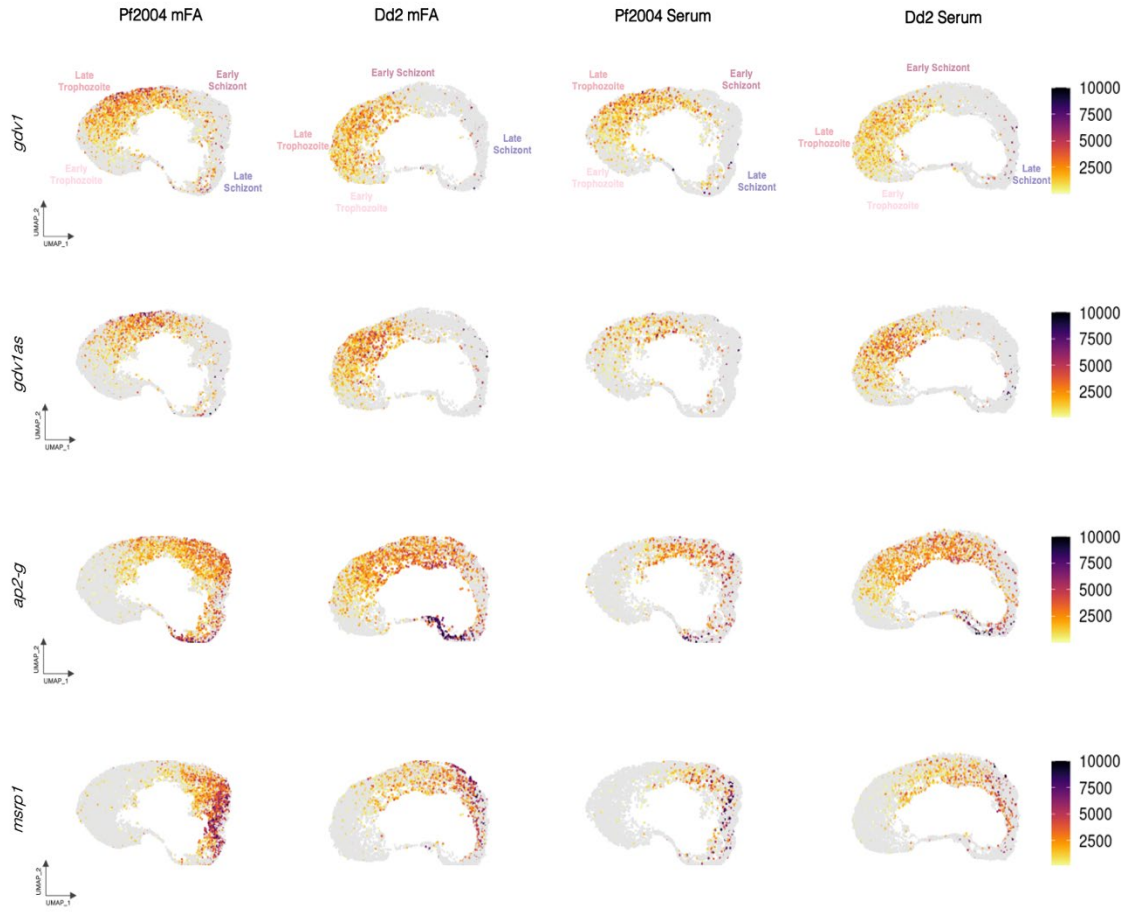

Figure 5-22. Expression of sexual commitment markers. Uniform manifold approximation and projection (UMAP) coloured by the expression levels of the sexual commitment associated marker, *gdv1, gdv1as, ap2-g* and *msrp1*. A UMAP is presented for each strain in each condition. Each point on the UMAP represents a cell which is coloured by the expression level of the given gene. Therefore, both expression level and the number if cells expressing the given gene can be assessed. Abbreviations: mFA, minimal fatty acid.

5.6.2 Mapping 'Sexual' and 'Asexual' Markers

To perform DGE analysis on sexual and asexual schizonts, it was necessary to identify sexual and asexual clusters. In **Section 5.4.3**, a cluster was identified in Pf2004 which formed an inner ring of cells spanning the UMAP (**Figure 5-23A)**. It was hypothesised that these cells clustered separately due to sexual commitment. To investigate this hypothesis, the expression of known sexual commitment markers in schizonts, and hypothesised asexual markers based on the data generated from mFA vs serum comparisons (**Section 5.6**) and previous publications, were plotted across all cells (Kafsack et al., 2014, Brancucci et al., 2014, Pelle et al., 2015, Brancucci et al., 2017, Poran et al., 2017, Brancucci et al., 2018, Llorà-Batlle et al., 2020, Dogga et al., 2024). Here, the expression of *ap2-g* was plotted in conjunction with either *clag3.1* or *rhoph3* which were both

consistently among the top 25 (based on fold change) downregulated genes in mFA conditions compared to serum (**Table A2-1 (Appendix 2), Figure 5-23**).

In Pf2004, *ap2-g* expression was predominantly localised to the outer ring of the UMAP. However, the expression of *clag3.1* and *rhoph3* did not result in a clear separation between sexual and asexual populations (**Figure 5-23**). Since *clag3.1* and *rhoph3* did not form a distinct cluster, it is likely that these are not good markers for non-committed populations. Indeed, there is conflicting evidence on whether *clag3.1* is enriched in sexual or asexual populations (Brancucci et al., 2017, Brancucci et al., 2018). In Dd2, cells expressing *ap2-g* did not form a distinct cluster which may make it more difficult to define sexual and asexual populations.

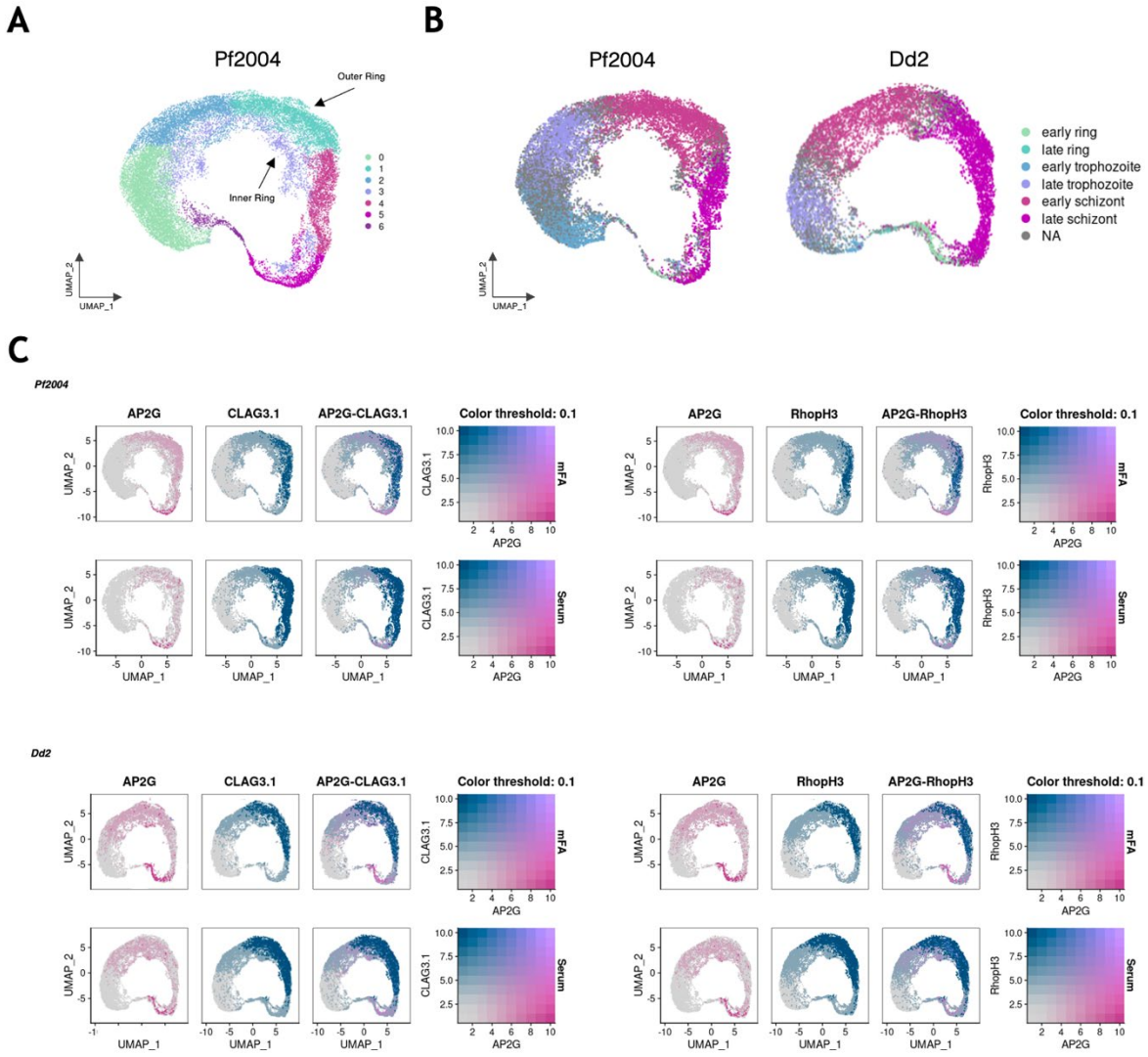

Figure 5-23. *clag3.1* and *rhoph3* were not markers of the cluster separation identified in Pf2004. (**A**) Uniform manifold approximation and projection (UMAP) of Pf2004 cells before cell

annotation revealing an inner ring cluster spanning the UMAP. (**B**) UMAP of Pf2004 and Dd2 (with mFA and Serum cells integrated together into a single object) annotated based on mapping of published *P. falciparum* Smart-Seq2 data from the Malaria Cell Atlas using scmap (Reid et al., 2018, Howick et al., 2019, Kiselev et al., 2018). (**C**) Pf2004 and Dd2 cells coloured by expression *ap2-g, clag3.1* and *rhoph3*. Pink coloured cells represent sexual commitment markers; blue coloured cell represents "asexual" markers. Each point on the UMAP represents an individual cell. Abbreviations: mFA, minimal fatty acids; NA, not assigned.

Given that there was conflicting evidence regarding the downregulation of *clag3.1* in induced (sexual) and uninduced (asexual) parasites (Brancucci et al., 2017, Brancucci et al., 2018), markers that were consistently downregulated in induced cells in at least two publications were investigated. This resulted in the identification of *pf332* and *garp* (Pelle et al., 2015, Brancucci et al., 2018, Llorà-Batlle et al., 2020). With these two markers, a clear separation of clusters was apparent in Pf2004. No distinct clusters were identified in Dd2 using these markers (**Figure 5-24**). Now that distinct "sexual" and "asexual" clusters were able to be identified, DGE analysis was performed using the clusters with the most marked separation in Pf2004. The presence of distinct clusters reflecting high (outer ring) and low *ap2-g* expression (inner ring) in mFA allows the exploration of DGE between sexual and asexual clusters in Pf2004.

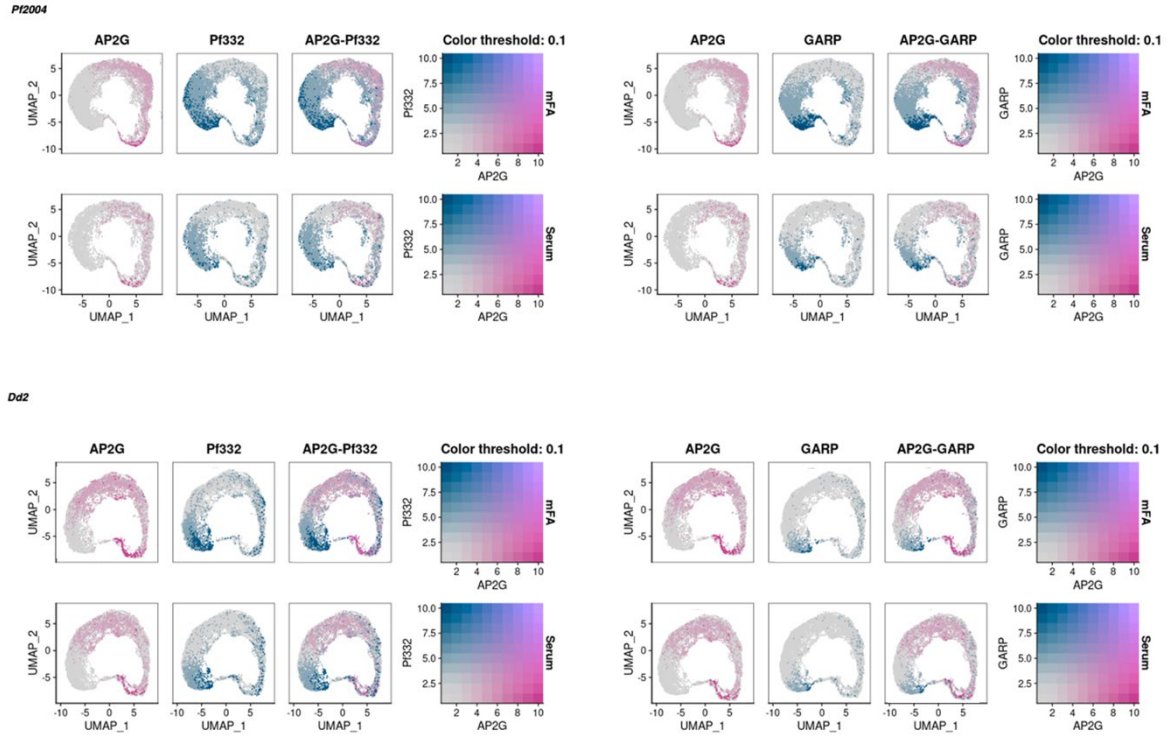

Figure 5-24. Uniform manifold approximation and projection (UMAP) of Pf2004 and Dd2 cells coloured by expression *ap2-g*, *garp*, and *pf332*. Cells expressing *pf332* and *garp* cluster in the inner ring of the UMAP while *ap2-g* expressing cells cluster in the outer ring (**Figure 23A**) for Pf2004. Using the same markers for Dd2, no distinct cluster separations were formed. Pink coloured cells represent *ap2-g* expression; blue coloured cell represents "asexual" markers. Each point on the UMAP represents an individual cell. Abbreviations: mFA, minimal fatty acids.

5.6.3 DGE: *ap2-g* High vs *ap2-g* Low Clusters in Pf2004

To investigate DGE between sexual and asexual populations, the cluster resolution was increased from 0.2 to 1.1 to increase the number of clusters. Three comparisons were made where a clear separation was identified in mFA for Pf2004. Since this separation of cell was most obvious in mFA, and to prevent serum signatures diluting sexual gene expression signatures, DGE was performed in cells in mFA conditions alone (**Figure 5-25**).

Across the three cluster comparisons, *ap2-g* was significantly upregulated with *msrp1* also upregulated in the last comparison (cluster 9 vs cluster 6). Amongst these, several transcription factors and genes involved in chromatin remodelling were upregulated. These included members of the ApiAP2 family of transcription factors (Pf3D7_0516800, PF3D7_0404100, PF3D7_0613800, PF3D7_0516800, PF3D7_0802100, PF3D7_1218300, PF3D7_1222400, and *sip2* (PF3D7_0604100)),

set9 (histone methyltransferase, PF3D7_0508100), *hda1* (histone deacetylase, PF3D7_1472200), and *hda2* (histone deacetylase, PF3D7_1008000). In addition, three ncRNAs were upregulated in sexual clusters (PF3D7_0419900, PF3D7_1478900, PF3D7_1244300). In the latest cluster comparison (cluster 9 vs cluster 6), *surf8.2*, which has previously been demonstrated to be associated with commitment, was ranked second highest based on gene expression fold change (**Table A2-1**, **Appendix 2**). Further the phospholipid scramblase, *plscr* (PF3D7_1022700) was amongst upregulated genes in this cluster comparison which has been hypothesised to play a role in sexual development (**Figure 5-25**) (Haase et al., 2021).

Among the most significantly downregulated genes in sexual clusters were genes relating to proteins which are exported. These genes were consistently downregulated throughout comparisons and included *garp, kahrp, gbp130, mesa*, exported protein 1 (*exp,* PF3D7_1121600) and *exp2* (PF3D7_1471100). In addition, the genes associated with the purine salvage pathway, such as hypoxanthine guanine phosphoribosyltransferase (*hgprt,* PF3D7_1012400) and nucleoside transporter 1 (*nt1*, PF3D7_1347200) and adenosine deaminase (*ada,* PF3D7_1029600), were downregulated in sexual clusters. In *P. berghei* infected mice, genes associated with purine metabolism were downregulated in sexual parasites within reticulocytes (Hentzschel et al., 2022). In addition, a ncRNA PF3D7_1370800, previously identified in mFA vs serum comparisons, was also found to be downregulated in sexual clusters (**Figure 5-25, Section 5.5.2, Table 5-3**). Both genes associated with cytoadherence and purine metabolism were consistently among the top 25 downregulated genes (based on fold change) across comparisons (**Table A2-1**, **Appendix 2**).

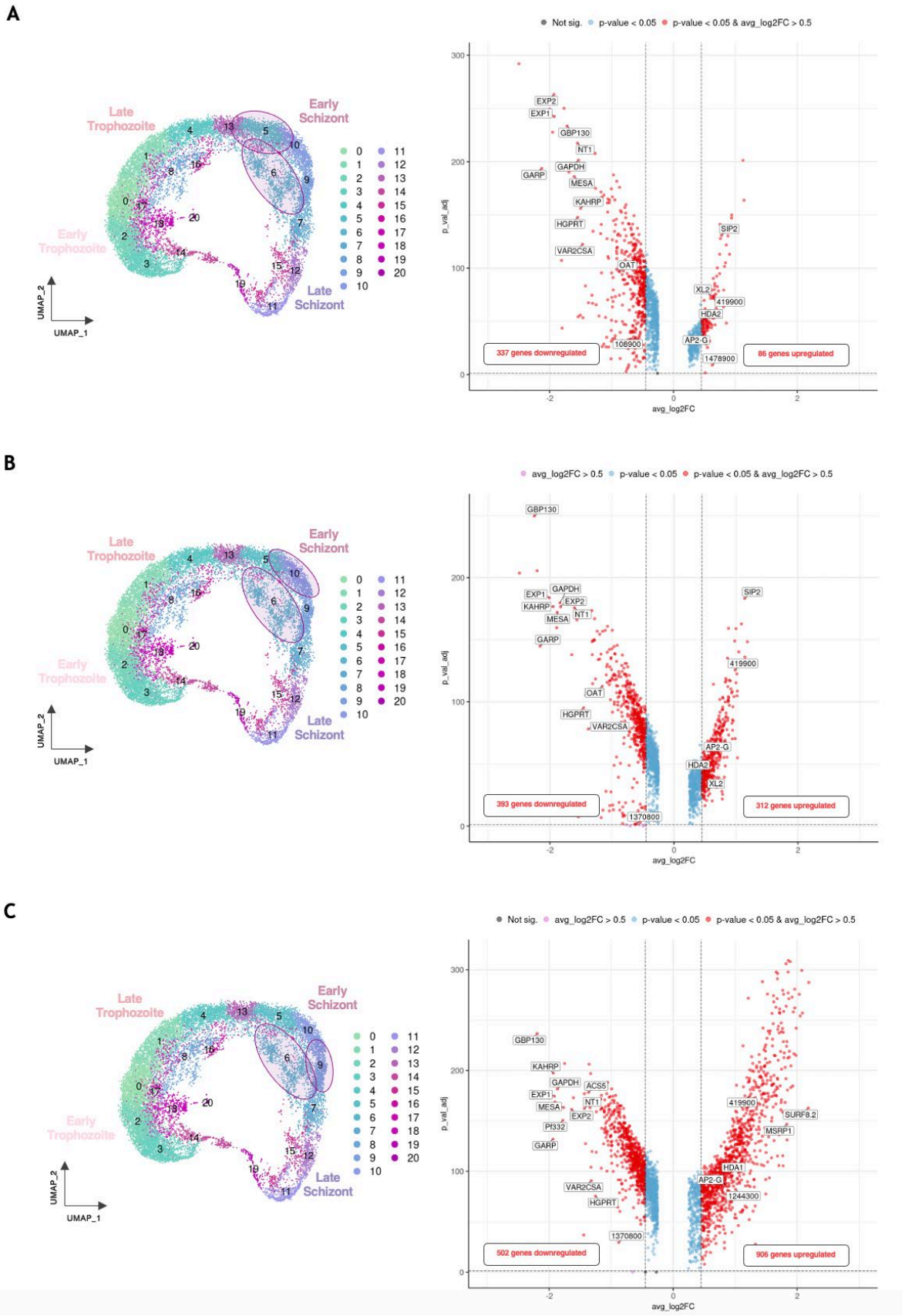

Figure 5-25. Differential gene expression (DGE) between *ap2-g* high and *ap2-g* low clusters. (**A**) Uniform manifold approximation and projection (UMAP) of Pf2004 cells at resolution 1.1. Cluster resolution was increased to allow DGE analysis to be performed between parallel clusters from the original asexual and sexual clusters. Clusters used for DGE analysis are highlighted with purple ovals (cluster 5 vs 6). Volcano plot of DGE of cluster 5 vs cluster 6. (**B**) Clusters used for DGE analysis are highlighted with purple ovals (cluster 10 vs 6). Volcano plot of DGE of cluster 10 vs cluster 6. (**C**) Clusters used for DGE analysis are highlighted with purple ovals (cluster 9 vs 6).

Volcano plot of DGE of cluster 9 vs cluster 6 The top 25 differentilly expressed genes (based on fold change) which were significantly upregulated or downregulated in each comparison can be found in **Table A2-1** (**Appendix 2**).

Now that several markers have been identified to be associated with either sexual or asexual clusters, their expression patterns were explored. As previously described (**Section 5.6.1**), the number of cells expressing sexual commitment markers (for example, *ap2*-g) was consistently lower in serum conditions compared to mFA. The expression of genes association with cytoadherence ((for example, *garp*) **Figure 1-4**), was highest early in the asexual cycle. However, in mFA conditions, there appeared to be a higher proportion of cells expressing these genes in a second peak of expression in early to late schizonts (**Figure 5-26**). It was clear from the average expression of genes associated with cytoadherence (for example, *garp, kahrp, mesa, gbp130* and *pf332*), that there were two separate expression patterns in mFA and serum. Across both conditions, the expression of these genes was consistently high in early trophozoites before declining in expression. In serum, this expression remained low for the remainder of the asexual life cycle. However, in mFA, the expression levels of these cytoadherence related genes began to increase again in early to late schizonts, although never to the expression level of the initial peak (**Figure 5-27A**). Interestingly, these genes were among the top 25 genes significantly upregulated genes in asexual clusters (**Table A2-1**, **Appendix 2**).

Genes encoding components of the RhopH complex/PSAC have previously been implicated as a marker of asexual stages (Llorà-Batlle et al., 2020). While these genes were downregulated in mFA compared to serum, the average expression level of these genes was higher in sexual clusters than in asexual clusters. These genes were therefore considered as not suitable asexual markers (**Figure 5-26**).

Several ncRNAs were identified from prior DGE analysis (**Section 5.5.2**), which were further investigated to determine if there were any candidates that may be involved in sexual commitment gene regulation. One ncRNA, PF3D7_1370800, had an interesting gene expression profile which may relate to commitment. In mFA, the average expression level of this ncRNA remained stable throughout the asexual life cycle. However, in serum conditions, the average expression level was 3 times

higher than sexual commitment markers. The expression of PF3D7_1370800 was similar in mFA and serum in trophozoites. However, as the expression of *ap2-g* increased in serum conditions, there was a subsequent peak in the expression of PF3D7_1370800 in early schizonts. Following this peak, the expression levels of both *ap2-g* and *msrp1* remained low throughout schizonts (**Figure 5-27B**).

surf8.2 was the second highest significantly expressed gene in sexually committed clusters (cluster 9 vs cluster 6) based on fold change. Members of the *surf* multigene family have been consistently upregulated in *ap2-g* high clusters from previous transcriptomic studies investigating sexual commitment (Brancucci et al., 2014, Pelle et al., 2015, Filarsky et al., 2018, Poran et al., 2017, Llorà-Batlle et al., 2020, Dogga et al., 2024). Therefore, the expression patterns of this *surf8.2* was investigated in relation to sexual commitment markers. The average expression of *ap2-g* and *msrp1* was plotted with *surf8.2*. The expression of *surf8.2* matched that of *msrp1* in mFA with both reaching a peak in expression levels at the same point in late schizonts. The expression of both genes follows a similar pattern in serum conditions suggesting that their gene expression is regulated similarly (**Figure 5-28A**). Based on the similar average expression pattern of *surf8.2* and *msrp1,* their co-expression was investigated. From co-expression plots of *msrp1* and *surf8.2,* it was evident that these two genes are co-expressed (**Figure 5-28B**). Through ChIP-Seq, SURF8.2 has been demonstrated to be bound to AP2-G suggesting that, like MSRP1, SURF8.2 is a direct target of AP2-G.

Based on these observations, two major transcriptional differences were identified between sexually committed and asexual schizonts under limiting conditions: i) induced expression of cytoadherence-linked genes, such as *kahrp, mesa, garp* and *pf332,* in asexual schizonts (in addition to their early-stage expression peak) and expression of genes associated with purine metabolism (such as *nt1* and *hgprt*), ii) induced expression of sexual commitment genes and gene expression/chromatin remodelling associated genes. In late schizonts in this second sexual population, the surface antigen *surf8.2* was co-expressed with *msrp1* suggesting a function for this surface antigen in sexually committed cells, or early gametocytes. Between these two populations in mFA, a metabolic response characterised by upregulation of genes of the alternative substrate arm of the Kennedy pathway, was shared. These two populations identified in mFA

differed from a third population of parasites in steady state conditions which were characterised by, iii) higher expression of nutrient channel components, invasion genes, and the ncRNA PF3D7_1370800 which may have a role in repressing sexual commitment akin to *gdv1as*.

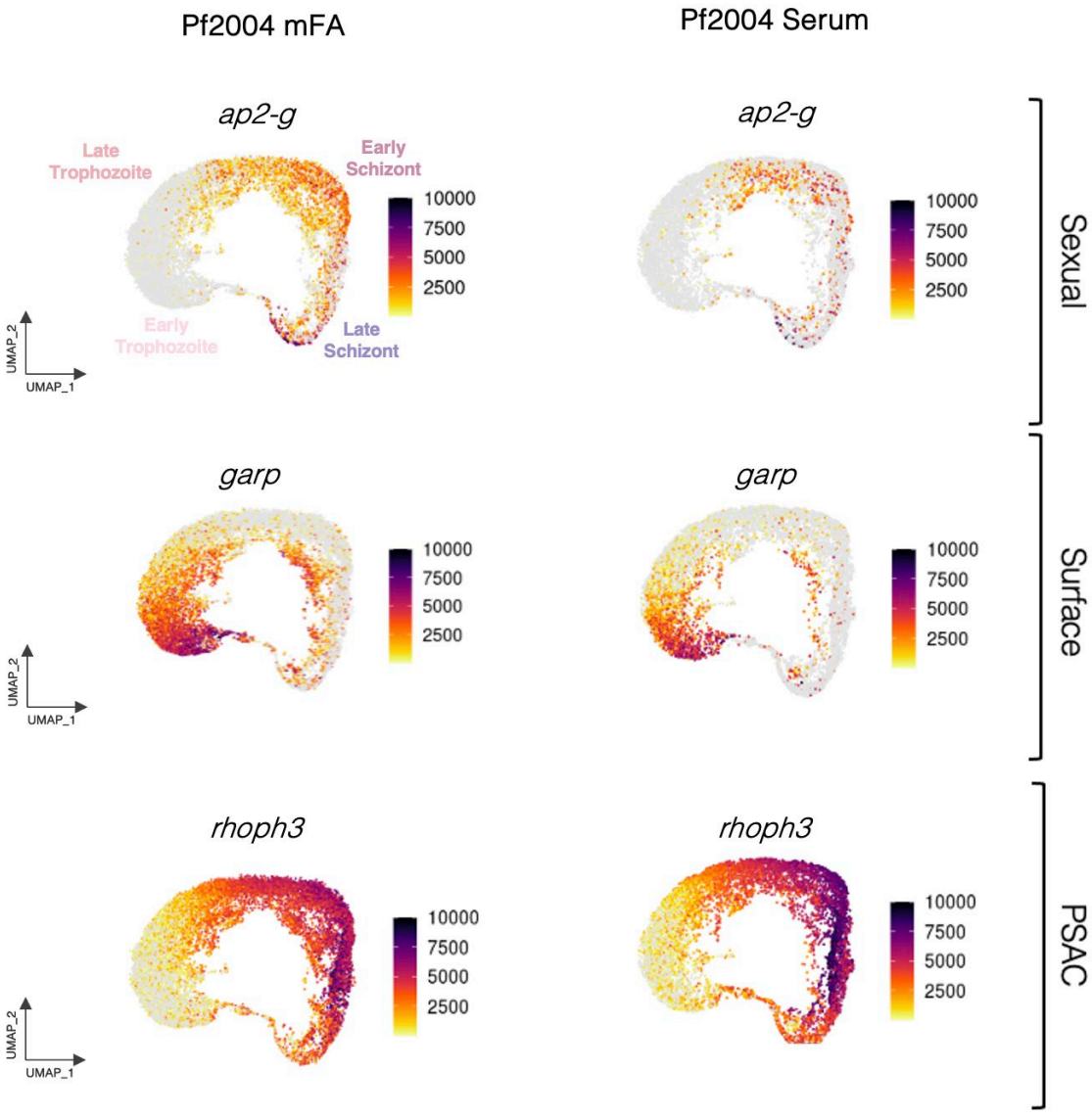

Figure 5-26. Uniform manifold approximation and projection (UMAPs) coloured by the expression of genes representing three identified schizont populations in Pf2004. Three populations with distinct transcriptional signatures were identified between minimal fatty acid (mFA) and Serum conditions. In mFA, two schizont populations were present: one upregulated in sexual commitment markers, such as *ap2*-g, and a second upregulated in cytoadherence related genes, such as garp. Genes involved in the RhopH/plasmodial surface anion channel (PSAC), such as *rhoph3*, exhibited higher expression in Serum than in mFA. Abbreviations: mFA, minimal fatty acid; PSAC, plasmodial surface anion channel.

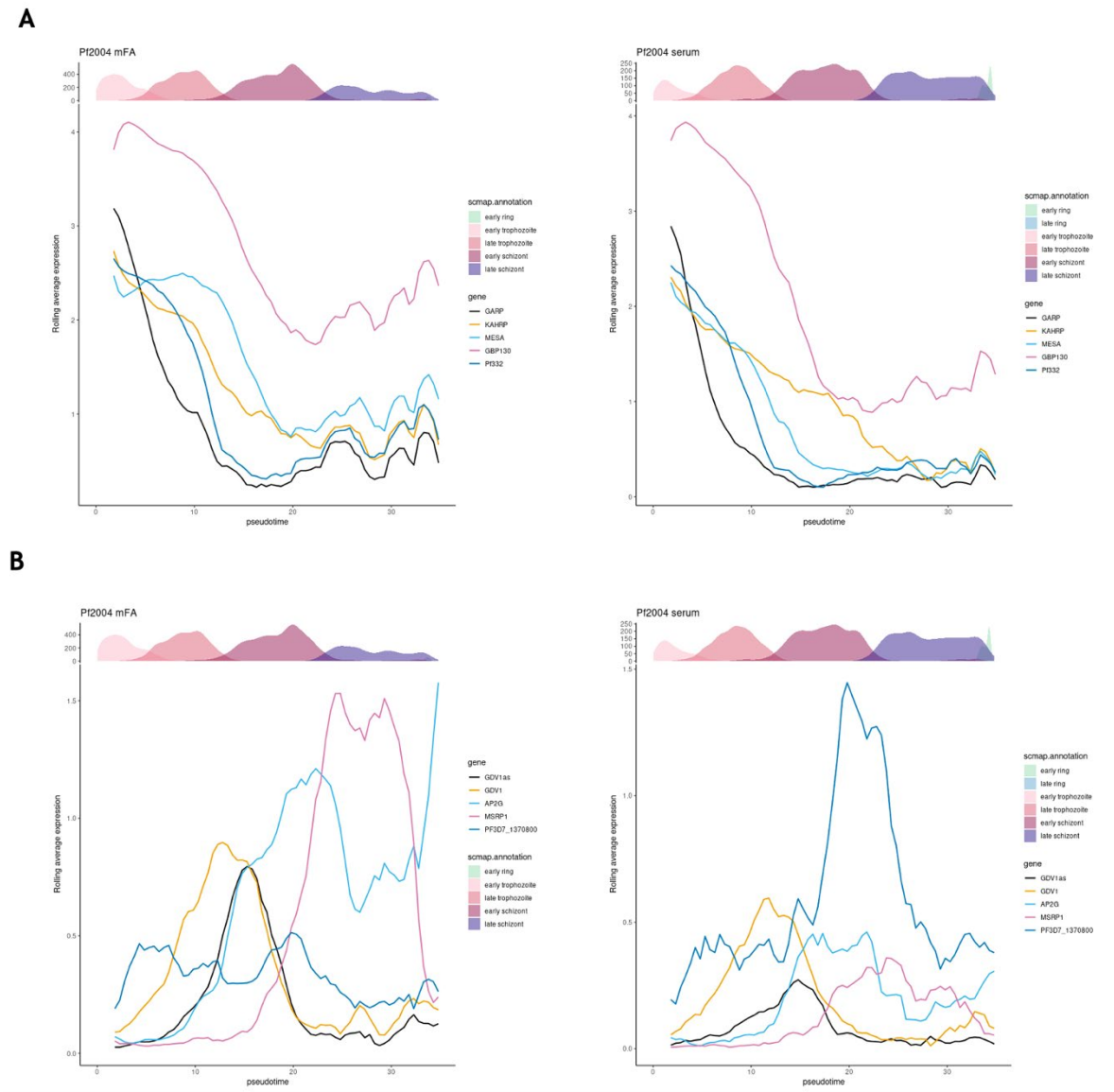

Figure 5-27. Average expression of differentially expressed genes identified in *ap2-g* high vs *ap2-g* low clusters over pseudotime in Pf2004. (**A**) Average expression of genes associated with cytoadherence (*garp* (black), *kahrp* (yellow), *mesa* (blue), *gbp130* (pink) and *pf332* (dark blue)) in minimal fatty acid (mFA) and Serum over pseudotime. Pseudotime, representing the temporal ordering of cells, is displayed on the X axis, with the corresponding cell type annotation from the Malaria Cell Atlas using scmap (scmap.annotation) shown above (Reid et al., 2018, Howick et al., 2019, Kiselev et al., 2018). In both mFA and Serum, expression of cytoadherence associated genes peaked in trophozoites. However, in mFA, the expression of these genes began to rise again in a similar manner in late schizonts. (**B**) Average expression of sexual commitment genes (*gdv1as* (black), *gdv1* (yellow), *ap2-g* (blue) and *msrp1* (pink)) and the ncRNA PF3D7_1370800 (dark blue) over pseudotime. Expression of the ncRNA was low throughout the cycle in mFA. However, expression peaked in early schizonts coinciding with the onset of *ap2-g* expression. Abbreviations: mFA, minimal fatty acid.

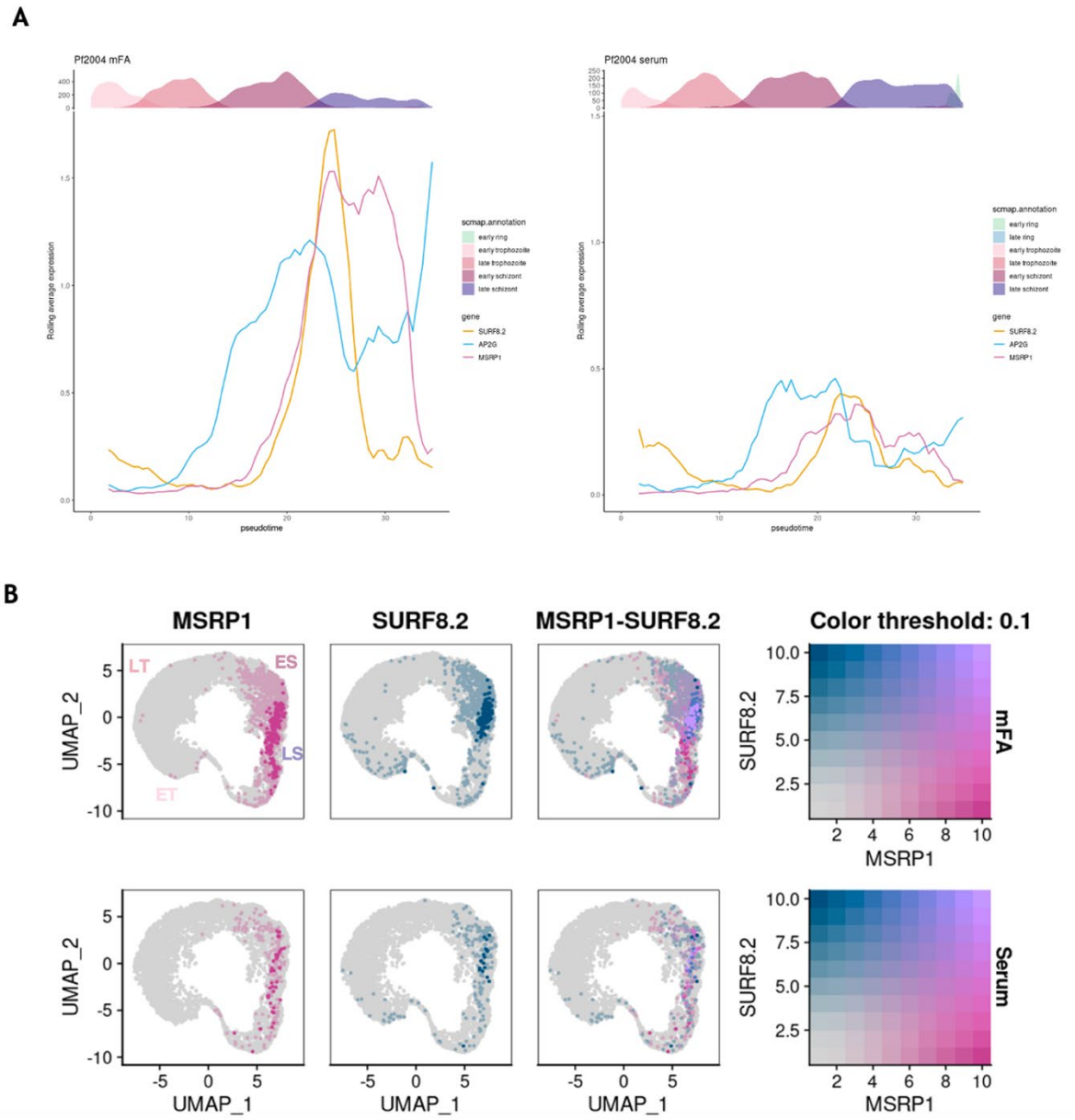

Figure 5-28. *surf8.2* is co-expressed with *msrp1* in Pf2004 late schizonts. (**A**) Average expression of *surf8.2, ap2-g* and *msrp1* over pseudotime. Pseudotime, representing the temporal ordering of cells, is displayed on the X axis, with the corresponding cell type annotation from the Malaria Cell Atlas using scmap (scmap.annotation) shown above (Reid et al., 2018, Howick et al., 2019, Kiselev et al., 2018). *surf8.1* (yellow) and *msrp1* (pink) exhibited similar expression profiles reaching peak expression at the same time in late schizonts. This shared expression pattern was observed in both minimal fatty acid (mFA) media and in Serum, although to a lesser extent in Serum. (**B**) Uniform manifold approximation and projection (UMAP) coloured by the expression, and co-expression, of *msrp1* (pink) and *surf8.2* (blue). Co-expression of *msrp1* and *surf8.2* was observed in late schizonts. Abbreviations: mFA, minimal fatty acid; ET, early trophozoites; LT, late trophozoites; ES, early schizonts; LS, late schizonts.

5.6.4 Investigating DGE Hits in Dd2

Now that three unique schizont populations, marked by genes associated with sexual commitment, cytoadherence and the RhopH complex, have been identified in Pf2004, the expression of markers of these populations were investigated in

Dd2. Based on UMAPs coloured by the expression of marker genes for these three schizont populations, the presence of these populations in Dd2 was not clear (**Figure 5-29**). In contrast to Pf2004, the expression of surface antigen or cytoadherence related genes did not differ greatly between media conditions (**Figure 5-29, 5-30A**). For Dd2, the expression of cytoadherence and surface antigen related genes did not exhibit a notable second peak in expression levels in late schizonts, as observed for Pf2004 (**Figure 5-27A, 5-30A**).

The average expression levels of the ncRNA, PF3D7_1370800, in relation to sexual commitment markers, was investigated in Dd2. While the expression of this ncRNA was higher in serum compared to mFA, the average peak expression of PF3D7_1370800 in serum conditions was notably lower than that observed in Pf2004 (**Figure 5-27B, 5-30B**). For Pf2004, the peak average expression of this ncRNA over pseudotime was 3 times higher than the expression of *ap2-g*. However, in Dd2, the expression of *ap2-g* in serum surpasses that of PF3D7_1370800 (**Figure 5-30B**). In relation to the hypothesis that this ncRNA could be involved in repressing sexual commitment, this finding in Dd2 would suggest that other mechanisms may regulate sexual commitment.

Overall, the transcriptional response of Dd2 to mFA largely differs to that of Pf2004. The relative number of cells expressing sexual commitment markers is comparable between mFA and serum. This may explain why fewer differentially expressed genes were identified between mFA and serum in Dd2 (**Section 5.5**). When investigating markers of asexual and sexually committed populations identified in Pf2004 (**Section 5.6.3**), Dd2 did not exhibit a population of asexual parasites characterised by a second peak in expression of cytoadherence related genes. Furthermore, the ncRNA, PF3D7_1370800, identified in asexual populations in Pf2004 was not as highly expressed in Dd2. The differences in expression patterns between these two strains might be due to their geographically distant origin. Pf2004 originated from a high transmission setting in West Africa whereas Dd2 originated from a low transmission setting in Southeast Asia (Elliot, 2007, Hommel et al., 2010, Wellems et al., 1990). In a low transmission setting, Dd2 likely must produce more gametocytes under the same environmental conditions, i.e., physiological range of LysoPC which may reflect the differences observed.

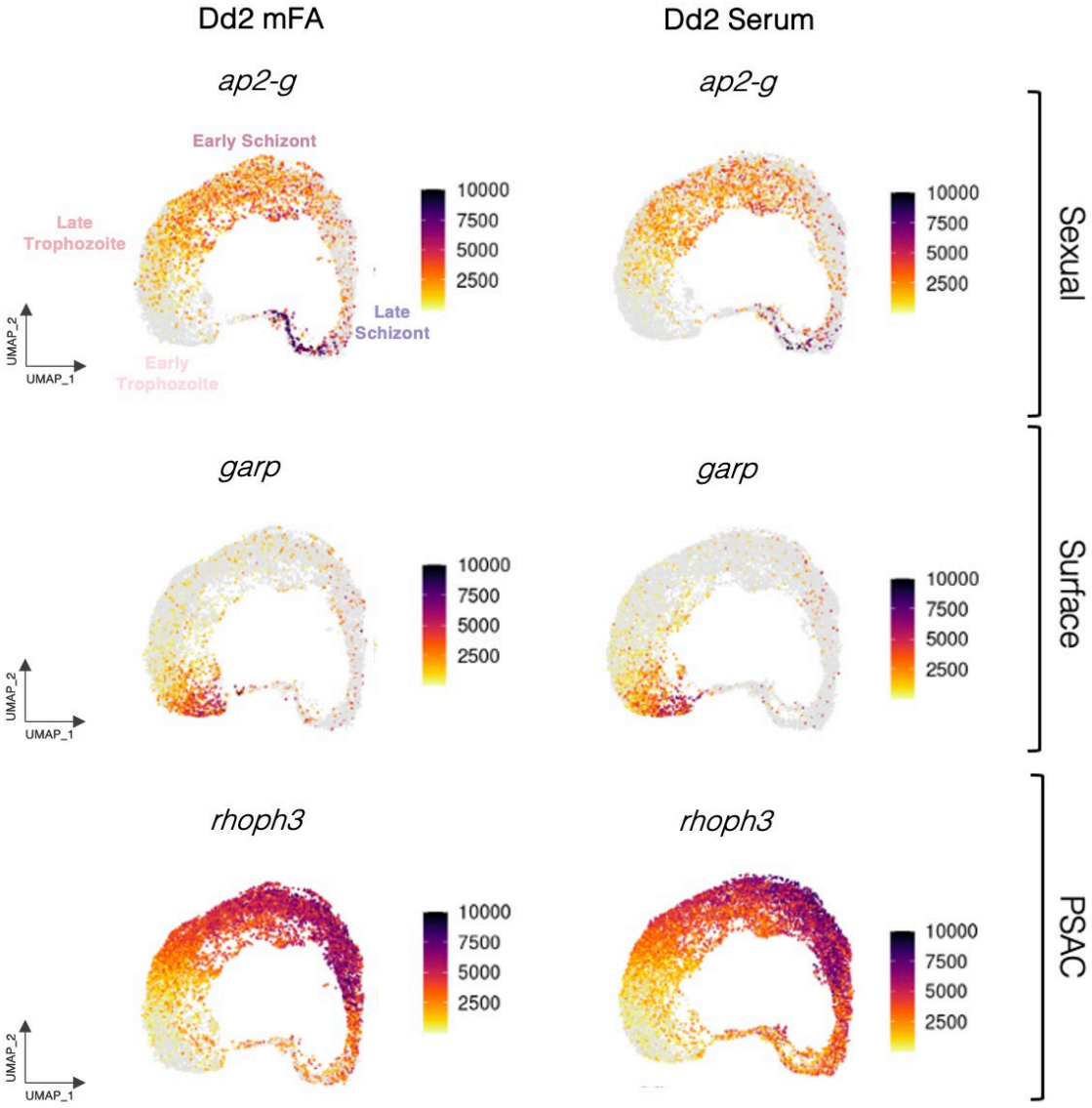

Figure 5-29. Uniform manifold approximation and projection (UMAPs) of Dd2 cells coloured by the expression of genes which represented three schizont populations identified in Pf2004. In Dd2, the three transcriptionally distinct populations identified in Pf2004 were not identified. A second population of *garp* expressing cells was not identified in early to late schizonts in minimal fatty acid (mFA) as observed in Pf2004 (Figure 5-26). The expression of sexual commitment associated genes, such as *ap2-g*, and components of the RhopH complex/plasmodial surface anion channel (PSAC) in Dd2 did not exhibit as much variation between the two media conditions as observed for Pf2004. Abbreviations: mFA, minimal fatty acid; PSAC, plasmodial surface anion channel.

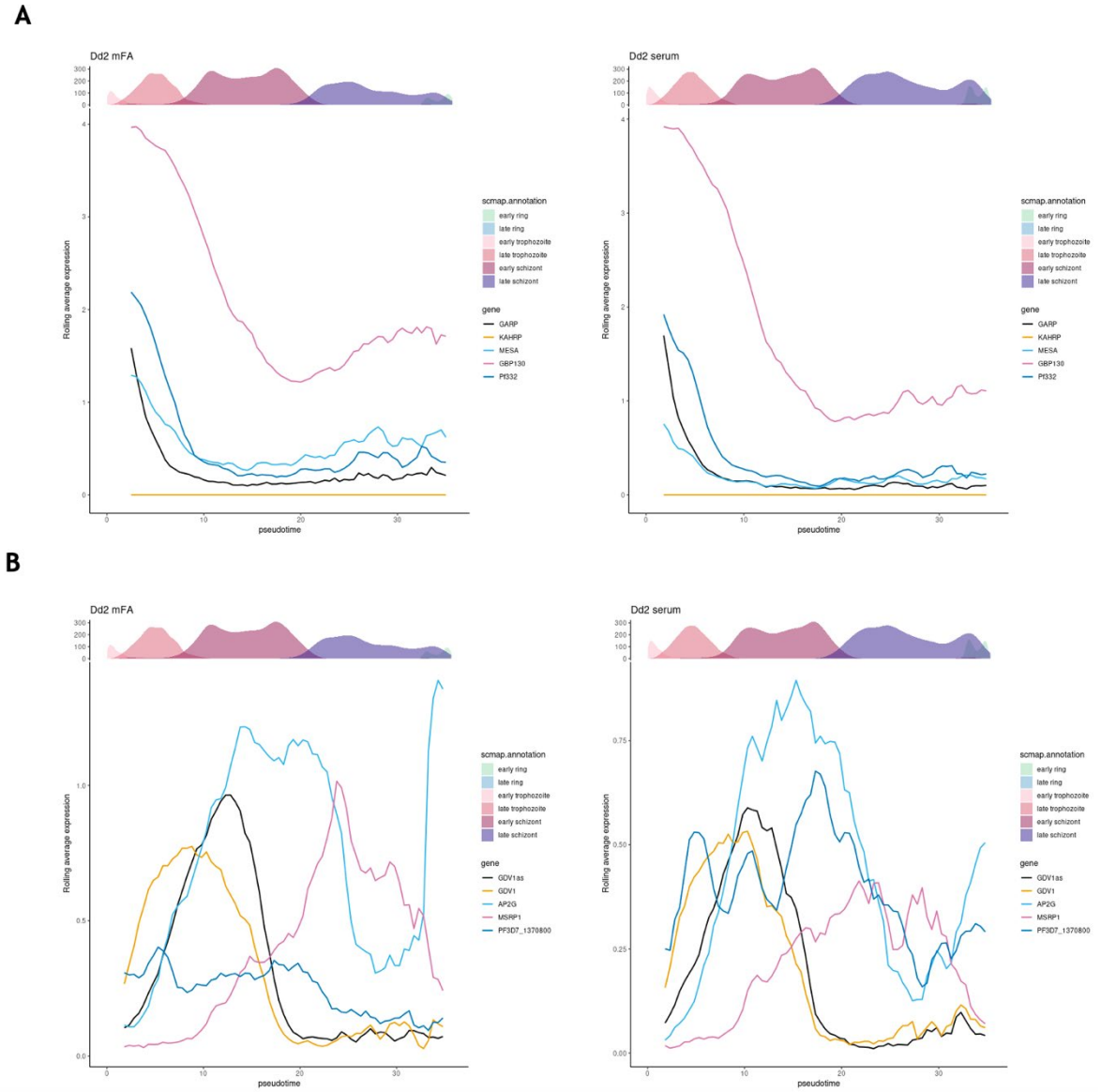

Figure 5-30. Average expression of markers over pseudotime in Dd2. (**A**) Average expression of genes associated with cytoadherence (*garp* (black), *kahrp* (yellow), *mesa* (blue), *gbp130* (pink) and *pf332* (dark blue)) over pseudotime in minimal fatty acid (mFA) and Serum. Pseudotime, representing the temporal ordering of cells, is displayed on the X axis, with the corresponding cell type annotation from the Malaria Cell Atlas using scmap (scmap.annotation) shown above (Reid et al., 2018, Howick et al., 2019, Kiselev et al., 2018). Expression of cytoadherence genes peaked in trophozoites for cells in minimal fatty acid (mFA) and Serum. In Dd2, there was a slight rise in the expression of these genes in late schizonts. However, this was to a lesser extent than observed in Pf2004 (**Figure 5-27A**). Note that the expression of *kahrp* is 0 in Dd2 due to a chromosomal deletion (Ribacke et al., 2007, Jiang et al., 2008). (**B**) Average expression of sexual commitment genes (*gdv1as* (black), *gdv1* (yellow), *ap2-g* (blue) and *msrp1* (pink)) and the ncRNA PF3D7_1370800 (dark blue) over pseudotime. In mFA, the expression of PF3D7_1370800 remained low throughout the cycle. In Serum, there was not a clear peak of this ncRNA above sexual commitment markers as observed in Pf2004 (**Figure 5-27B**). Abbreviations: mFA, minimal fatty acid.

5.7 Chapter Discussion

The conversion rate of parasites is known to vary between species in and transmission settings (Pollitt et al., 2011). In high transmission settings where there is ample opportunity to transmit and greater within-host competition, parasites exhibit a low conversion rate favouring asexual replication. The opposite is true of parasites in low transmission settings where there are fewer opportunities to transmit, favouring sexual commitment and gametocyte production (Greischar et al., 2016, Schneider and Reece, 2021). As such, different strains exhibit different levels of responsiveness to environmental factors known to induce sexual commitment. Conversion rate exhibits adaptive plasticity and is responsive to environmental factors such as LysoPC depletion (Brancucci et al., 2017). Different strains exhibit different levels of responsiveness to LysoPC; for example, Dd2 (Southeast Asian) is hypersensitive to LysoPC fluctuations (unpublished data from the Marti Lab). To investigate the transcriptional programme underlying the different parasite responses to this environmental trigger, scRNAseq was performed on Pf2004 (less sensitive to LysoPC fluctuations) and Dd2 (hypersensitive to LysoPC fluctuations) allowing the transcriptional signatures of asexual and sexually committed schizonts to be determined.

5.7.1 DGE: mFA vs Serum

DGE analysis was initially performed to compare the global and stage specific transcriptional differences between cells grown in mFA and serum (**Section 5.6**). While this comparison has previously been conducted using bulk RNA sequencing and pseudo single cell approaches, the repetition of this comparison serves to validate the experimental design here, corroborating findings against those obtained through previous analysis (Brancucci et al., 2017, Brancucci et al., 2018). Further, this initial analysis may provide insight into the distinct transcriptional signatures of sexually committed and asexual schizonts.

In mFA conditions, it was hypothesised that all cells grown in mFA would exhibit a shared metabolic response to the LysoPC depleted conditions. Indeed, in mFA, an alternative substrate arm of the Kennedy pathway was upregulated as evidenced by the increased expression of *pmt*, *sahh* and *ek*. In *P. falciparum*, choline is derived from the environment in the form of LysoPC. This is the preferred substrate that drives the biosynthesis of phosphatidylcholine, the most

abundant phospholipid in *Plasmodium* cell membranes. Under reduced LysoPC conditions (i.e., in mFA), an alternative substrate arm of the Kennedy pathway (**Section 1.4.4**) is upregulated, where ethanolamine is phosphorylated via ethanolamine kinase (EK) to produce phosphoethanolamine (P-Eth). P-Eth then enters the Kennedy pathway after transmethylation to phosphocholine (P-Cho) via PMT (Pessi et al., 2004, Pessi et al., 2005, Flammersfeld et al., 2018) using s-adenosylmethionine (SAM) as a methyl group donor. The S-adenosyl-l-homocysteine (SAH) produced is then recycled by SAH hydrolase (SAHH) (Tanaka et al., 2004). *oat* has been demonstrated to be responsive to fluctuations in SAM metabolism. Here, *oat* is upregulated in mFA in Pf2004 likely due to alterations in SAM metabolism due to the use of the alternative arm of the Kennedy pathway (van Brummelen et al., 2009, Schneider et al., 2023). In contrast, in LysoPC rich conditions (i.e., serum), LysoPC is obtained from the environment and converted to choline. Choline is subsequently phosphorylated to P-Cho through the action of CK. Cells grown in serum conditions displayed an upregulation of *ck* compared to mFA suggesting that PC is generated through the primary route of the Kennedy pathway. These findings validate previous bulk RNA sequencing studies using a similar experimental approach (Brancucci et al., 2017, Brancucci et al., 2018). For an outline of the Kennedy pathway, see **Section 1.4.4**.

In addition to genes involved in the alternative substrate arm of the Kennedy pathway, well described sexual commitment markers *ap2-g* and *msrp1* and the invasion ligand, *rh6* was upregulated in mFA for both strains. When performing DGE analysis on the population level, *rh6* was among the top 25 significantly upregulated genes (**Table 5-2**). At the cluster level, *rh6* was the top differentially expressed gene (based on fold change) between mFA and serum for late schizonts in both strains (**Table 5-4**). This upregulation is consistent with findings from earlier transcriptomic studies on sexual commitment which proposed that there could be localised activation, attributed to chromosomal topology, due to the proximity of *rh6* with *msrp1* (Poran et al., 2017, Llorà-Batlle et al., 2020, Szabo et al., 2019). It is unknown whether chromosomal topology is consistent between strains and species. Alternatively, this may represent a switch in invasion ligands in limiting conditions. While an upregulation of *rh6* is observed in mFA, other invasion related genes such as members of the *eba, ebl* and *msp* gene families are downregulated (**Table 5-4**). Merozoite invasion is mediated by specific merozoite

surface ligand interactions with the host RBC. The first step in merozoite invasion is initial contact which is mediated by low affinity interactions via MSPs, a highly polymorphic family (Beeson et al., 2016). The next step in invasion is apical reorientation. This apical reorientation involves high affinity interactions via EBL or RH proteins (Tham et al., 2012, Molina-Franky et al., 2022). The downregulation of invasion related genes may be explained, at least in part, by the reduced PMR observed in parasites grown in mFA (**Figure 5-5**). RH6 may play a role in the invasion of sexually committed merozoites; however, this is unknown.

Nutrient depletion (i.e., mFA) resulted in reduced expression of genes associated with the RhopH complex/PSAC such as *clag3.1, clag3.2, clag2, rhoph2* and *rhoph3*. This high molecular weight complex is composed of three subunits, RhopH2, RhopH3 and CLAG (sometimes referred to as RhopH1). RhopH2 and RhopH3 are encoded by *rhoph2* and *rhoph3* respectively while CLAG has five distinct isotypes encoded by members of the *clag* multigene family (*clag2, clag8, clag9* and the paralogues, *clag3.1* or *clag3.2*) (Kaneko et al., 2001, Kaneko et al., 2005). Once the complex is produced in a soluble form, it is packaged into the rhoptries for merozoite RBC invasion. The RhopH complex will subsequently cross the PV membrane to be deposited onto the host cell membrane to form a nutrient channel (PSAC) for solute uptake in trophozoites (**Figure 5-31**) (Schureck et al., 2021). Therefore, the transcription of components of the RhopH complex occurs in the cycle prior to their use. Components of the RhopH complex have previously been demonstrated to be downregulated in *ap2-g* induced vs uninduced cultures (Llorà-Batlle et al., 2020). The downregulation of expression of *clag3.1, clag2* and *rhoph3* has previously been demonstrated in a transgenic *P. falciparum* line where *ap2-g* was conditionally activated. Indeed, in this study, the same three genes were consistently among the top 25 genes significantly downregulated in mFA conditions for both strains. Llorà-Battle *et al.,* demonstrated that gametocytes had reduced PSAC activity explaining their resistance to sorbitol lysis (Saul et al., 1990, Llorà-Batlle et al., 2020, Bouyer et al., 2020). As such, the downregulation of genes that encode components of the RhopH complex may represent a preparatory step resulting in reduced permeability in gametocytes.

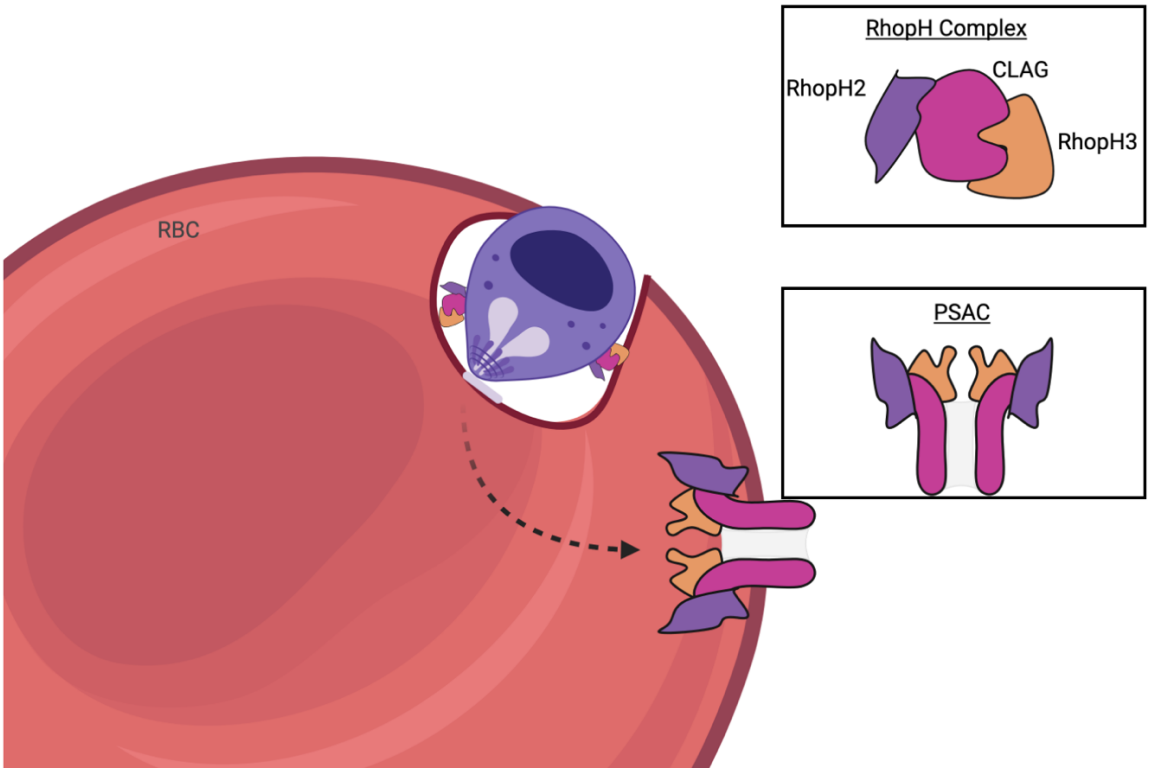

Figure 5-31.The RhopH complex and plasmodial surface anion channel (PSAC). The RhopH complex is comprised of three subunits: RhopH2, RhopH3 and CLAG. Once produced, the complex is packaged into the rhoptries for invasion of the merozoite. After invasion, the complex forms the PSAC which facilitates solute transport. Figure created with BioRender.com based on Schureck *et al.*, 2021 (Schureck et al., 2021).

Among the most differentially expressed genes between the two conditions were members of the ETRAMP family, which were predominantly downregulated in parasites grown in mFA conditions (except for *etramp5*). The ETRAMP family of proteins was first identified in *P. falciparum* in 2003 (Spielmann et al., 2003). Members of the ETRAMP family were demonstrated to have stage specific transcription and to associate with the PV membrane. Due to the location of these proteins, it was hypothesised that these proteins function largely in parasite-host cell interactions (Spielmann et al., 2006). However, the function of these proteins remains largely unknown. In previous studies, *etramp5* was demonstrated to be upregulated in sexually committed clusters (Dogga et al., 2024). Here, authors hypothesised that *etramp5,* alongside the upregulation of *mesa* and *gbp130* in sexual clusters (also observed in this dataset), may play a role in gametocyte sequestration. In contrast, *etramp11.2* and *etramp2* were consistently downregulated in mFA conditions in both strains. *etramp11.2,* in addition to

exp1/2, have previously been identified as some of the most highly transcribed genes in asexual stages (Le Roch et al., 2003). Few studies have been performed on *etramp11.2* in *P. falciparum;* however, in *P. vivax,* ETRAMP11.2 is recognised by *P. vivax* patient serum and has been demonstrated to elicit high antibody responses in mice (Chen et al., 2010, Cheng et al., 2015, Lee et al., 2019, Perrotti et al., 2023). Despite this protein being considered as a potential vaccine candidate for *P. vivax*, its function remains elusive. Similarly, few studies have investigated the function of *etramp2,* a ring stage specific ETRAMP in *P. falciparum*. It has been hypothesised that ETRAMP2, among other ETRAMPs, function in the early development of intraerythrocytic stages and comprise dominant protein components of the PV membrane (Spielmann et al., 2006).

In summary, DGE analysis of parasites grown in mFA compared to parasite grown in serum validated previous bulk RNA sequencing studies (Brancucci et al., 2017, Brancucci et al., 2018). From this comparison, parasites grown in serum are characterised by high expression of components of the RhopH complex and invasion ligands of the *rh, eba,* and *ebl* gene families. Nutrient depleted conditions induce the expression of the invasion ligand *rh6*, which has previously been identified to be upregulated in sexually committed parasites (Poran et al., 2017, Llorà-Batlle et al., 2020, Szabo et al., 2019). While there were several DGE genes shared between Pf2004 and Dd2, there were far fewer genes differentially expressed in Dd2. This is likely, at least in part, related to Dd2 exhibiting hypersensitivity to LysoPC fluctuations and consequently triggering the sexual commitment pathways in serum.

5.7.2 DGE: *ap2-g* High vs *ap2-g* Low Clusters

The sexual commitment pathway using known sexual markers was investigated in both Pf2004 and Dd2 over pseudotime. This revealed a transcriptional cascade from the initial transcriptional response to LysoPC depletion in which *gdv1as* was upregulated. This ultimately resulted in the positive feedback loop of *ap2-g* and its downstream targets (e.g., *msrp1*) (**Section 5.6.1**).

To investigate the transcriptional differences between hypothesised schizont populations in mFA, the expression of *ap2-g* was plotted alongside hypothesised asexual markers. Here, the aim was to determine distinct clusters which would

allow DGE analysis to be performed between sexual and asexual populations. From mFA vs serum comparisons, components of the RhopH complex were among top hits downregulated in mFA conditions (**Section 5.6**). Previous studies have demonstrated that the activity of the PSAC, which is comprised of components of the RhopH complex, is reduced in gametocytes (Llorà-Batlle et al., 2020). Since these genes are transcribed in the cycle prior to use, it was hypothesised that these genes were likely downregulated in sexually committed schizonts in preparation for gametocytogenesis and as such, could be markers of asexual schizonts. However, despite the downregulation of these genes observed in mFA, the expression of components of the RhopH complex remained high in mFA cells, although not as highly expressed as observed in serum. Since genes such as *clag3.1* and *rhoph3* were expressed in all cells in mFA and did not form distinct clusters from *ap2-g* or *msrp1* high clusters, they were deemed not suitable asexual markers.

To identify more suitable asexual markers, genes which had been consistently demonstrated to be downregulated in induced populations in at least two studies were investigated. These included genes with known functions in asexual stages such as *mesa, pf332, garp* and *kahrp* (Pelle et al., 2015, Brancucci et al., 2018, Llorà-Batlle et al., 2020). In doing so, two distinct cell populations were identified in early to late schizonts. Indeed, from initial unsupervised clustering, an inner ring of cells was clustered separately which is now known to be enriched for surface or cytoadherence related genes (indicated by arrows in **Figure 5-11**). Using these two distinct populations, DGE analysis was performed on *ap2-g* high and *ap2-g* low populations.

DGE analysis between *ap2-g* high and *ap2-g* low clusters revealed a downregulation of genes associated with the purine salvage pathway (*hgprt* and *nt1*) in sexually committed clusters. It is likely that these genes were downregulated due to a lower demand for purines in gametocytes, although this is unknown. An upregulation of several surface antigen or cytoadherence related genes such as *garp, mesa, pf332,* and *kahrp* was observed in asexual populations (**Figure 1-4, 5-25**, **Table A2-1** (**Appendix 2**)). In serum conditions, these genes were highly expressed in early trophozoites in preparation for knob formation before declining matching existing bulk RNA sequencing datasets (López-Barragán et al., 2011).

These genes remained lowly expressed for the remainder of the life cycle However, in mFA, the expression of surface antigen related genes began to rise again in early to late schizonts explaining their upregulation in mFA conditions observed in **Section 5.5**. As described in **Section 1.2.1, Figure 1-4**), these genes encode proteins which are involved in knob formation and cytoadherence (Taylor et al., 1987, Coppel, 1992, Mattei and Scherf, 1992, Crabb et al., 1997, Kun et al., 1999, Hodder et al., 2009, Maier et al., 2008, Maier et al., 2009, Almukadi et al., 2019). It is possible that in stress conditions, parasites upregulate these genes to increase cytoadherence capacity thereby protecting parasites from clearance. Therefore, in LysoPC depleted conditions, two parasite populations emerge. A population that invests in ensuring onward transmission through sexual commitment, and a population that increases binding capacity to avoid clearance.

From this analysis, a ncRNA located on chromosome 13, PF3D7_1370800, was identified which may function in repressing sexual commitment. This ncRNA has not been described previously except for in a PhD thesis where it was identified to be differentially expressed between ABO blood groups (Amanfo, 2018). Here, PF3D7_1370800 was upregulated in blood group A compared to blood group B and O. The role of this ncRNA was not investigated further in the scope of this thesis (Amanfo, 2018). Since all parasites were grown in O positive blood, this does not explain the differential expression observed between sexually committed and asexual clusters. When the average expression of PF3D7_1370800 was plotted over pseudotime for Pf2004 in mFA, the expression level was low and remained relatively stable throughout the intraerythrocytic developmental cycle. However, the average expression over pseudotime in serum grown parasites saw a dramatic peak in expression coinciding with the increase in expression of *ap2-g*. The expression of *ap2-g* reduces following the peak in expression of PF3D7_1370800 (**Figure 5-27B**). Interestingly, several ncRNAs identified in mFA and serum comparisons in schizonts were revealed. Between these ncRNAs regions of similarity were identified by BLAST. In some cases, for example PF3D7_137800 and PF3D7_1148200, shared 100% identity (**Figure 5-19**). These regions may represent shared functions; however, this remains unknown. Given that PF3D7_1370800 was strongly upregulated in asexual clusters, and the observed dramatic increase in expression following *ap2-g* expression in serum, it is possible that this ncRNA has a role in repressing sexual commitment. However, based on the data generated in

this study, it is not possible to draw any conclusions on the function of this ncRNA without further investigation.

Another gene of interest identified when investigating sexually committed schizonts was *surf8.2*. The SURFIN family of proteins was first identified in 2005 comprising of 10 genes which localise to close to or within sub-telomeres. These polymorphic proteins were identified on the surface of both merozoites and iRBCs; however, their function remains elusive (Winter et al., 2005). Members of this gene family (*surf1.2, surf4.1, surf4.2, surf8.1, surf8.2* and *surf13.1*) have previously been identified amongst upregulated genes in sexually committed parasites; however, their function in relation to commitment has not been investigated (Kafsack et al., 2014, Brancucci et al., 2014, Pelle et al., 2015, Poran et al., 2017, Brancucci et al., 2018, Brancucci et al., 2017). In this analysis, *surf8.2* was the second top upregulated gene in sexual clusters compared to asexual clusters (cluster 9 vs cluster 6). The expression of *surf8.2* coincided with the expression of *msrp1* in both mFA and serum, reaching a peak in expression levels in late schizonts (**Figure 5-28A**). Indeed, *surf8.2* was demonstrated to be co-expressed with *msrp1* (**Figure 5-28B**). To validate this co-expression, RNAscope could be performed with probes designed to detect *surf8.2* and *msrp1*. As such, a dual RNAscope experiment on blood clots containing sexually committed schizonts (as detailed in **Section 2.3.3**), could be performed. In earlier studies using ChIP-seq, SURF8.2 was found to be bound to AP2-G suggesting that it is a direct target of AP2-G, similar to MSRP1 (Llorà-Batlle et al., 2020). The function of SURF8.2 remains unknown, although it is possible that it plays a role in binding interactions in the BM of either the sexually committed schizont or gametocyte. To investigate this further, the BM blocks from the Malawi cohort could be utilised (**Section 2.1**). Here, antibodies could be designed to target SURF8.2. Through IHC, the spatial localisation of SURF8.2 positive cells may yield insights into potential interactions in the BM. Additionally, antibodies against AMA1 (schizonts) or Pfs16 (gametocytes) could indicate at what stages during which these interactions occur.

From this analysis in Pf2004, two transcriptionally distinct parasite populations were identified in mFA contrasting with a third population of parasites in serum. Within mFA, these two populations reflect: i) a sexually committed population,

marked by the upregulation of genes associated with sexual commitment, gene regulation, and *surf8.2*, and ii) a population committed to asexual replication, enriched in genes associated with cytoadherence and the ncRNA PF3D7-1370800. These two populations contrast, in part, with parasites grown in steady state conditions (serum), wherein parasites exhibit greater solute transport and invasion capacity (upregulation of genes encoding components of the RhopH complex and invasion related genes). The expression of the ncRNA PF3D7_1370800, which was identified in asexual parasite populations in mFA, was higher in serum.

While the experimental design utilised here allows the exploration of schizont populations that may exist in the BM through LysoPC depletion, there are many other factors which may influence the transcriptome of parasites within this niche. For example, the BM has an enrichment of erythroblasts and reticulocytes which are nutrient rich and more metabolically active than mature RBCs used here (Srivastava et al., 2015). Further, the experimental design could be improved by adding an additional time point after reinvasion collecting asexual or sexual rings. This additional time point would provide an endpoint for sexually committed or asexual schizonts that could be used to build commitment trajectories. Furthermore, this study could be expanded to investigate modification or gene regulation mechanisms beyond transcription, for example, post-transcriptional modifications.

5.7.3 Commitment in Dd2

Using markers identified in Pf2004, it was not possible to identify the same distinct populations relating to commitment in Dd2. In DGE analysis comparing mFA and serum in Dd2, far fewer genes were observed to be significantly differentially expressed between the two conditions compared to Pf2004. This suggested that Dd2 parasites grown in these two conditions were largely similar likely due to the sensitivity of Dd2 to LysoPC fluctuations (**Figure 5-5**). When comparing the average expression of sexual commitment markers over pseudotime between Pf2004 and Dd2, there were notable differences. The most notable differences were the higher expression levels of *gdv1-as*, and the lower average expression levels of *msrp1* in Dd2 compared to Pf2004 in mFA. In serum conditions, the average expression of *ap2-g* was higher in Dd2 than in Pf2004 partly explaining the slightly higher background conversion rates. However, the expression pattern of

the ncRNA PF3D7_1370800 in serum was markedly different in Dd2 compared to Pf2004. In Pf2004, this ncRNA was highly expressed in early schizonts with the expression of *ap2-g*. Following the peak in expression of this ncRNA, *msrp1* expression declined (**Figure 5-27B**). While the expression of this ncRNA was demonstrated to be upregulated in serum conditions in early schizonts, and to a lesser degree, late schizonts, PF3D7_1370800 exhibited lower average expression levels in serum than *ap2-g* for Dd2 compared to Pf2004. This suggests that, either this ncRNA does not play a role in repressing sexual commitment, or there are different or additional factors which regulate sexual commitment in Dd2 compared to Pf2004. For example, post-transcriptional regulation resulting in transcript or protein instability.

Both *mesa* and *gbp130* were among the top upregulated genes in mFA vs serum for Dd2 (**Figure 5-14**, **5-17, Table 5-3, 5-4**). Since these were among upregulated genes in Pf2004 also, it is possible that the two populations observed in Pf2004 (sexual commitment enriched and surface antigen/cytoadherence enriched) could also exist in Dd2. However, it was not possible to observe these distinct clusters with a global view of all cells. Instead, subsetting individual clusters, re-clustering and then plotting the expression of marker genes as before might reveal the distinct cell populations observed in Pf2004 through the reduction of noise from neighbouring clusters.

It is also possible that the difficulties observed in defining sexual and asexual populations in Dd2 relates to the geographical setting for which they originated from. In low transmission settings where Dd2 originated, *Plasmodium spp*. invest more in sexual conversion due to reduced within-host competition. As such, Dd2 responses to environmental stimuli may differ between that of the canonical Pf2004 strain analysed here. While no studies have investigated the relationship between inflammation, LysoPC and *ap2*-g expression in low transmission settings, this relationship was investigated in Kilifi, Kenya, where there are high and low transmission seasons. High inflammatory responses were associated with plasma LysoPC depletion and increased *ap2-g* expression in patients from Kilifi. This relationship was more pronounced with declining transmission (Abdi et al., 2023). As such, parasites from low transmission settings are more adaptive to environmental fluctuations to ensure onward transmission. Indeed, the higher

background conversion rate, and the higher number of cells expressing *ap2-g* in Dd2, suggests that there is greater investment in sexual conversion in this strain. By having a higher background conversion rate hardwired to ensure successful transmission, it is likely that there are differences between Dd2 and Pf2004 in sexual commitment. Therefore, different strategies to investigate sexual commitment in these two strains may need to be employed, such as the cluster by cluster approached which was previously suggested. It is also important to note that the two strains used here were culture-adapted, and so may have developed mutations through *in vitro* cultures. For example, the chromosomal deletion on chromosome 2 resulting in the absence of *kahrp* in Dd2 (Ribacke et al., 2007, Jiang et al., 2008). The precise nature of how sexual commitment is regulated in Dd2 remains elusive.

5.7.4 Limitations of scRNAseq

The use of scRNAseq platforms overcomes previous limitations in microarray and bulk RNA sequencing. By analysing transcriptional changes at the single cell level, rare cell populations, such as sexually committed schizonts, can be investigated. However, there are several limitations to these platforms. Droplet based approaches, such as Chromium 10X, allow for a high throughput of cells at a relatively low cost (Yang et al., 2020). This high throughput allows the detection of rare cell types. However, a technical limitation of single cell approaches, is the high dropout rate. A dropout event is where a transcript is not detected or captured resulting in an excess of cells where a given gene has an expression level of zero (Bacher and Kendziorski, 2016, Haque et al., 2017, Wang et al., 2021). In a comparative analysis of 10X and Smart-Seq2, 10X displayed a higher dropout ratio, particularly for low expressing genes (Wang et al., 2019). In such, there is a probability that genes will not be detected, even if they are expressed. Due to this dropout rate, it is not appropriate to perform DGE analysis comparing cells which are either positive or negative for the expression of a gene of interest. Instead, identification of clusters enriched with the expression of a gene(s) of interest, and comparing to clusters lacking such enrichment, is a more appropriate approach to DGE analysis in scRNAseq. The issue of dropout rate can be, in part, addressed by increasing sequencing depth (Haque et al., 2017). Further, specialised DGE tests such as MAST, which was used here, are designed for

datasets with a significant proportion of zero expression levels (Finak et al., 2015). Another technical limitation of scRNAseq is the high level of technical noise. It is therefore imperative to perform quality control steps which remove low quality cells to limit the noise in the transcriptional dataset (Kolodziejczyk et al., 2015, Chen et al., 2019). However, in this experiment, the number of UMIs was 10X higher than in previous studies, with >1000 genes per cell expressed (**Table 5-1**). The quality of this dataset lowers the effect of dropout as described by Haque *et al*. (Haque et al., 2017).

In addition to the strains analysed here, a non-gametocyte producing line could be informative. For example, if the non-gametocyte producing line had a deletion or mutation in *gdv1,* this may result in a different response to mFA compared to wild type. Importantly, the use of transcriptomics alone only provides one part of the story. Many processes in regulation of commitment may occur at the post-transcriptional level. Further, while genes may be transcribed, these genes may not be translated and therefore proteomics to confirm that these genes have a role either in the committed schizonts, or in the subsequent cycle, would be required.

5.7.5 Chapter Summary

In **Chapter 4**, sexually committed schizonts were identified in the BM of severe paediatric *P. falciparum* malaria cases suggesting that commitment can occur directly in the BM. This is likely triggered by the environmental factor, LysoPC, which has been demonstrated to be depleted in the BM compared to blood in *P. berghei* infected mice (Brancucci et al., 2017). Sexually committed schizonts and gametocytes collectively represented 22% of parasites in the BM (**Section 4.5, 4.6**); therefore, a population of asexual parasites exist in the BM. I hypothesised that sequestered parasites in the BM are transcriptionally distinct from those sequestered in other tissues.

Different parasite strains have differing conversion rates and sensitivities to environmental perturbations (Pollitt et al., 2011). Dd2, originating from a low transmission setting in Southeast Asia, is hypersensitive to fluctuations in LysoPC resulting in a greater background conversion rate in steady state conditions

compared to Pf2004 (originating from West Africa), which is less sensitive to LysoPC (Elliot, 2007, Hommel et al., 2010, Wellems et al., 1990). The transcriptional programme underlying different parasite responses to LysoPC remains unclear.

To deconvolute the transcriptional signature of sexual commitment in *P. falciparum* schizonts, scRNAseq was utilised comparing two culture-adapted strains with different LysoPC sensitivities (Pf2004 and Dd2).

Using this approach, two schizont populations in mFA were identified for Pf2004: i) a subset of parasites undergoing sexual commitment characterised by sexual commitment markers (e.g., *ap2-g* and *msrp1*), markers of gene regulation (e.g. *set9* and *hda1*) and the surface antigen *surf8.2*, ii) asexual schizonts marked by a second peak in expression of surface antigen and cytoadherence associated genes (e.g., *kahrp, mesa,* and *pf332*) in late schizonts, in addition to genes associated with purine metabolism (e.g., *nt1* and *hgprt*). These two populations exhibited a shared metabolic response to nutrient depletion upregulating genes associated with the alternative substrate arm of the Kennedy pathway. In steady state conditions, parasites exhibited higher expression of nutrient channel components (e.g., *rhoph2, rhoph,* and *clag3.1*) and invasion ligands (e.g., *eba140* and *eba175*) (**Figure 5-32**).

Several ncRNAs were identified when comparing the two media conditions. Identified ncRNAs on chromosomes 8, 11, and 13, shared regions of similarity suggesting shared function. The ncRNA PF3D7_1370800 on chromosome 13 was consistently found to be upregulated in asexual clusters, with the highest average expression in serum conditions. The onset of expression of this ncRNA coincided with that of *ap2-g*. Once this ncRNA reached peak expression levels, the expression levels of *ap2-g* reduced. The phenotypical relevance of this ncRNA remains to be investigated.

While the conversion rate in Pf2004 and Dd2 was not significantly different, the expression profile of sexual commitment markers was. There were hundreds of differentially expressed genes between media conditions for Pf2004, however, far fewer differentially expressed genes were found between these two conditions in

Dd2. This suggests that parasites within each condition are similar for Dd2. The relative number of cells expressing sexual commitment markers between mFA and serum appear to be similar in Dd2. As such, it was difficult to identify sexually committed and asexual clusters in this strain. The precise differences between these two strains in the transcriptional pathway of sexual commitment requires further investigation.

Overall, several markers associated with sexually committed and asexual schizonts in mFA and serum have been identified. These genes could play significant roles in the survival of these cell populations within the haematopoietic niches of the host. Further investigation is warranted to fully elucidate their functions in the haematopoietic niches of paediatric severe malaria cases using RNAscope or spatial transcriptomic approaches.

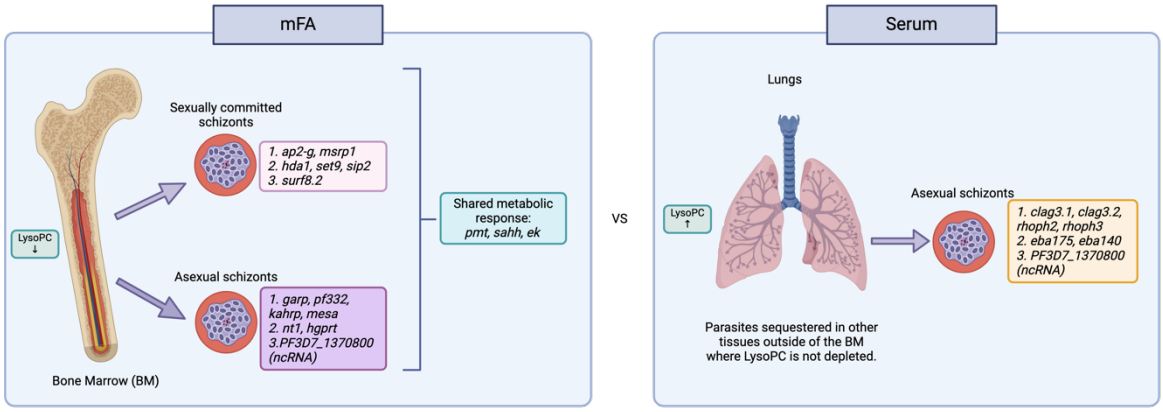

Figure 5-32. Summary of the transcriptional signatures of hypothesised schizont populations in the bone marrow (BM). The BM represents a unique environment which is depleted in lysophosphatidylcholine (LysoPC), an important substrate for phosphatidylcholine (PC) synthesis (Figure 1-8). Depletion of LysoPC has been demonstrated to induce sexual commitment in *P. falciparum*. Furthermore, the BM, which has been demonstrated to have a local LysoPC depletion and may represent a tissue compartment conducive of sexual commitment (Brancucci et al., 2017, Brancucci et al., 2018). To investigate the transcriptional signatures of schizonts which were hypothesised to exist in the BM, a single cell RNA sequencing (scRNAseq) experiment was designed using minimal fatty acid (mFA) media depleted of LysoPC to induce sexual commitment. Schizonts harvested from this media were compared with schizonts grown in steady state Serum conditions representing parasites sequestered elsewhere in the body, for example, in the lungs. Two schizont populations were identified in mFA conditions: i) a subset of parasites which were sexually committed characterised by upregulation of *ap2-g* and *msrp1*, in addition to genes associated with gene regulation, such as *hda1*. ii) a population of asexual parasites which were characterised by a second late peak of genes associated with cytoadherence such as *garp, kahrp, pf332* and *mesa*. These parasites also upregulated genes involved in purine metabolism (e.g., *nt1*). The two populations observed in mFA shared a metabolic response to nutrient depletion marked by upregulation of genes associated with the alternative substrate arm of the Kennedy pathway (e.g. *pmt*). In contrast, a third population was identified in Serum, which exhibited higher expression of genes of the RhopH complex/plasmodial surface anion channel (PSAC), such as *clag3.1* and

rhoph3, in addition to upregulation of genes associated with invasion, such as *eba175* and *eba140*. In both asexual populations, there was upregulation of an uncharacterised ncRNA, PF3D7_1370800, which may play a role in sexual commitment repression. While these three populations were identified in Pf2004, it was not possible to identify the same populations in Dd2. Abbreviations: mFA, minimal fatty acid; LysoPC, lysophosphatidylcholine; BM, bone marrow. Figure created with BioRender.com.

Chapter 6 | General Discussion

6.1 General Discussion

Malaria remains a disease of global importance, and a major target of malaria elimination efforts is to interrupt transmission (WHO, 2021). To achieve this goal, it is important to identify and characterise hidden reservoirs of *Plasmodium*. These reservoirs not only have the potential to contribute to transmission but could also contribute to recrudescent infections and the emergence of antimalarial resistance. The bone marrow (BM) represents an important reservoir of *Plasmodium* which is enriched in both replicative asexual stages and immature gametocytes. It is therefore essential for persistence and transmission (Joice et al., 2014, Aguilar et al., 2014, De Niz et al., 2018). The spleen has recently been identified to harbour a large hidden biomass of *Plasmodium,* including possibly gametocytes, with evidence to suggest the presence of an ongoing endosplenic asexual replication cycle. Characterising these two parasite reservoirs, both phenotypically and transcriptionally, in paediatric severe *P. falciparum* malaria patients is of crucial importance, as this group accounts for the highest malaria mortality rates.

This thesis presents a comparative analysis of post-mortem tissues collected from paediatric severe *P. falciparum* malaria patients from Blantyre, Malawi. Here, parasite distribution, density, and biomass were compared between the spleen, BM, lung, and peripheral circulation. It investigates the contribution of the spleen towards transmission and sexual commitment in the BM. In parallel, the transcriptional signatures of sexually and asexual schizonts within the BM reservoir were explored in two parasite strains with different sensitivities to an environmental trigger of sexual commitment.

6.2 Model of Splenic Accumulation in Malaria

In **Chapter 3**, basic histological techniques were utilised to investigate the histopathology of the BM and spleen and to generate preliminary results on the parasite distribution in the spleen. In both the spleen and the BM, histopathological changes were mild. In malaria cases, the BM had a greater presence of macrophages, eosinophils, infected red blood cells (iRBCs), pigment and a higher myeloid-to-erythroid (M:E) ratio, all parameters associated with malaria and a general response to infection. In the spleen, there were no major

differences between malaria cases and non-malarial controls. Overall, there was a minimal to mild disruption in the splenic microarchitecture across all cases which correlated with parasitaemia. Importantly, this histopathological examination of the spleen revealed that the spleen in this cohort was not haematopoietically active, did not exhibit a high percentage of immature red blood cells (RBCs), or marked congestion of blood. The lack of an enrichment of immature RBCs was confirmed by immunohistochemistry (IHC) using the reticulocyte marker CD71.

Using Giemsa-stained spleen sections and counting and staging criteria previously defined by Kho *et al.*, paediatric severe *P. falciparum* malaria spleens were evaluated for non-phagocytosed parasites (Kho et al., 2021a, Kho et al., 2021b). In the spleen, an enrichment of rings/early trophozoites was observed. Asexual parasites were predominantly distributed in the splenic cords with parasite densities significantly higher in the splenic cords and sinus lumens compared to the non-circulatory spaces of the spleen. This splenic distribution matches that observed in chronic asymptomatic malaria (Kho et al., 2021a, Kho et al., 2021b). Rings and trophozoite stage densities were significantly higher than schizonts and gametocytes across all splenic compartments analysed (sinus lumen, cords, perifollicular zone, and non-circulatory spaces). In this initial examination of the spleen, evidence of an endosplenic life cycle was investigated based on parasite stage distribution. For an endosplenic life cycle to exist in *P. falciparum,* parasite stages would be expected to be in proportions consistent with their duration across the entire asexual life cycle. For *P. falciparum*, rings and trophozoites combined (0 – 36 hours post invasion (hpi)) constitute ca. 75% of the intraerythrocytic life cycle, while schizonts constitute ca. 25%. Across all splenic compartments, the mean proportion of schizonts was 8.3%, less than what would be expected to be consistent with an endosplenic life cycle.

In **Chapter 4**, these findings were validated using IHC with antibodies targeting specific parasite and host markers. To investigate splenic tropism, the parasite distribution, density, and biomass, was compared between the spleen, BM, lung, and peripheral circulation. Between Giemsa and IHC, parasite distribution and densities were comparable. Parasite distribution in the lung was predominantly in small vessels likely due to classical sequestration. This contrasted with the BM and

spleen where the parasites were predominantly found in the extravascular spaces. When comparing parasite densities between organs and peripheral circulation, the spleen exhibited significantly higher parasite densities compared to the BM, lung, and peripheral circulation. These parasite densities could be explained by a retention of peripherally circulating parasites at a rate of 9.52%. This is consistent with previous observations of *P. falciparum* ring retention rates in *ex vivo* splenic perfusion experiments (Safeukui et al., 2008). Therefore, parasite densities in the spleen could be explained by retention of rings/early trophozoites in the slow circulation of the spleen. This contrasts with chronic asymptomatic malaria where the magnitude of splenic parasite densities could not be explained by retention of peripherally circulating parasites alone, even at parasite retention rates >90% (Kho et al., 2021a). Importantly, the total parasite biomass was compared between the BM, lung, and peripheral circulation to determine if there was a significant hidden biomass, and therefore tropism, in the spleen of paediatric severe *P. falciparum* malaria cases. While there were significantly higher parasite biomasses in the organs compared to peripheral circulation, there was no significant difference in parasite biomass between organs. Therefore, the spleen does not harbour a large hidden biomass of *P. falciparum* in paediatric severe malaria patients. Taken together, the low proportion of schizonts, parasite densities explainable by ring retention, and the absence of significant differences in organ biomass strongly suggest that there is no evidence to support the existence of an endosplenic life cycle in paediatric *P. falciparum* malaria cases.

In chronic asymptomatic *P. falciparum* malaria, gametocytes constituted 8.3% of the total parasites identified in the spleen (Kho et al., 2021a). Therefore, the contribution of the spleen towards gametocyte formation and development was investigated in relation to the BM which has previously been identified as a major site of gametocyte enrichment and development (Joice et al., 2014, Aguilar et al., 2014). Using antibodies against gametocytes (Pfs16) and sexually committed parasites (MSRP1), very few gametocytes and sexually committed parasites were identified in the spleen suggesting that the spleen, at least in paediatric severe *P. falciparum* malaria cases, does not contribute to gametocyte formation and development. In contrast, 26% of parasites identified in the BM were gametocytes, with 9% identified as sexually committed schizonts. This identification of sexually committed schizonts strongly suggests that sexual commitment can occur directly

in the BM. Two models have previously been proposed to explain the enrichment of gametocytes in the BM: i) sexually committed merozoites or early gametocytes preferentially home to the BM for gametocyte development, or ii) an exogenous asexual replication life cycle occurs in the BM, where the unique environment of the BM may be conducive of sexual commitment (Nilsson et al., 2015, De Niz et al., 2018). The presence of sexually committed schizonts in the BM supports the second model of gametocyte enrichment. However, this does not negate the existence of the first model as the two are mutually compatible and could exist in parallel.

Overall, in contrast to chronic asymptomatic malaria cases in adults, the spleen in paediatric severe *P. falciparum* malaria patients does not host a substantial hidden biomass of parasites. Furthermore, there is no evidence to support the presence of an endosplenic life cycle in this cohort. Instead, the density of parasites in the spleen could be explained by retention of rings in the slow circulation of the spleen. Based on these findings in paediatric severe *P. falciparum* malaria, and observations in chronic asymptomatic malaria (*P. vivax* and *P. falciparum*) in adults, these two cohorts likely represent two extremes. Here, I propose a model by which parasite accumulation in the spleen is related to disease severity (**Figure 4-26**). As such, parasite accumulation in the spleen is likely driven by parasite factors (e.g., slow growing phenotype) and host factors (e.g., tolerogenic environment) associated with disease severity.

6.3 Deconvoluting Transcriptional Signatures of Sexual Commitment

In **Chapter 5**, the transcriptional signatures associated with asexual and sexual commitment following environmental induction was investigated at the single cell level. In order to transmit, a subset of blood stage parasites must undergo sexual commitment, resulting in the production of gametocytes. The conversion rate, which indicates the proportion of gametocytes produced in a given cycle, demonstrates adaptive plasticity, responding to environmental factors such as the fluctuation in the serum phospholipid lysophosphatidylcholine (LysoPC) (Schneider et al., 2018, Brancucci et al., 2017). Different parasite strains exhibit varying levels of responsiveness to LysoPC concentration fluctuations; however, the

underlying transcriptional programme driving these diverse responses remains unclear. Importantly, the physiological levels of LysoPC fluctuates with inflammation and between tissue compartments (Abdi et al., 2023, Brancucci et al., 2017). Inflammation or inflammatory responses were negatively correlated with LysoPC concentrations in the blood, which in turn was associated with increased investment in gametocyte production (Abdi et al., 2023). Furthermore, LysoPC concentrations have been demonstrated to be reduced in the BM compared to the blood in mice, which suggests that parasites within the BM could respond to local LysoPC depletions by investing more in sexual commitment and gametocyte production (Brancucci et al., 2017).

From **Chapter 4**, the gametocyte and sexually committed schizont fraction in the BM was 22% combined. Therefore, the BM contains both sexually committed and asexual schizonts in LysoPC depleted conditions. To test the hypothesis that schizonts sequestered in the extravascular spaces of the BM are transcriptionally distinct from those sequestered in other tissues, a single cell RNA sequencing (scRNAseq) approach was used. Furthermore, to investigate the transcriptional programme underlying different responsiveness of parasite strains to limiting conditions (i.e., LysoPC depleted conditions), two *P. falciparum* strains with different sensitivities to LysoPC were used: Pf2004, originating from West Africa (high transmission, less sensitive to LysoPC fluctuations) and Dd2, originating from Southeast Asia (low transmission, hypersensitive to LysoPC fluctuations). These parasites were grown in either LysoPC depleted conditions (minimal fatty acid, mFA), or steady state conditions (serum).

Across replicates, the median unique molecular identifier (UMI)/cell (i.e., number of transcripts/cell) was up to 10 times higher than what was achieved in the first *P. falciparum* Malaria Cell Atlas. Similarly, the median number of genes expressed per cell were up to 5 times higher than this same dataset (Howick et al., 2019). After quality control, a total of 43,246 high quality cells were retrieved covering the different stages of the intraerythrocytic life cycle (rings through to schizonts). These parameters underscore the high quality of the dataset generated.

Using this dataset, published bulk RNA sequencing findings comparing parasites grown in mFA and serum were validated by taking a global view of all sequenced

cells (Brancucci et al., 2017, Brancucci et al., 2018). Differential gene expression (DGE) analysis between parasites grown in mFA and serum revealed an upregulation of sexual commitment markers, *ap2-g* and *msrp1*, alongside enzymes associated with the alternative arm of the Kennedy pathway, such as phophoethanolamine methyltransferase (*pmt*), S-adenosyl-l-homocysteine hydrolase (*sahh*), and ethanolamine kinase (*ek*) in mFA (**Figure 1-8**). In contrast, components of the RhopH complex and plasmodial anion surface channel (PSAC), such as *clag3.1, clag3.2, clag2, rhoph2,* and *rhoph3,* were downregulated in mFA conditions. These differentially expressed genes were shared between the two parasite strains, although there were far fewer differentially expressed genes in Dd2 compared to Pf2004.

This analysis was refined by performing DGE analysis on early schizonts and late schizonts grown in mFA compared to serum. Many of the same differentially expressed genes were identified as before such as *ap2-g, msrp1, ek, pmt* and *sahh*. Genes associated with surface antigens or cytoadherence were found to be significantly upregulated in mFA such as *mesa, gbp130, pf332, garp* and *kahrp* (**Figure 1-4**). In late schizonts, the highest upregulated gene in mFA shared between the two parasite stains was *rh6,* which has previously been demonstrated to be upregulated in sexually committed parasites (Poran et al., 2017, Llorà-Batlle et al., 2020). This upregulation in *rh6* has previously been attributed to chromosomal topology due to the close proximity of *rh6* to *msrp1* (Llorà-Batlle et al., 2020). However, it may suggest a switch in invasion ligands where members of the RH family have been associated with binding to receptors on the RBC surface for invasion (Beeson et al., 2016). Indeed, in serum conditions, there was an upregulation of invasion related genes such as *rh*, *eba, ebl,* and *msp* gene families. By refining this analysis to specific developmental stages, several ncRNAs were identified among the top 25 significantly downregulated genes in mFA for both Pf2004 and Dd2. The similarities of these ncRNA were investigated using basic local alignment search tool (BLAST) revealing regions of similarity between ncRNAs found on chromosome 8, 11 and 13. For example, region of the ncRNAs PF3D7_1370800 and PF3D7_1148500 had sequence identities of 100%. This suggests that these ncRNAs may have a shared function, although the phenotypic relevance of these ncRNAs remains unknown.

To begin to deconvolute the sexual commitment pathway in Pf2004 and Dd2, the expression patterns of known sexual commitment markers (*gdv1, gdv1as, ap2-g* and *msrp1*) was investigated. In Pf2004, *gdv1* is expressed in both mFA and serum in early to late trophozoites, although the average expression of *gdv1* was lower in serum compared to mFA. Limiting conditions triggers the expression of *gdv1as* in early schizonts which results in a decline in the average expression of both *gdv1* and *gdv1as*. With the rise in expression levels of *gdv1as, ap2-g* expression increases reaching a peak in expression in early to late schizonts. Following the peak in *ap2-g* expression, the expression of *msrp1* reaches a peak in late schizonts. After the peak in *msrp1* expression, the previously described positive feedback loop of *ap2-g* in late schizonts was observed (**Figure 5-21**) (Kafsack et al., 2014, Poran et al., 2017). This contrasts with serum conditions where, following the peak expression of *gdv1*, all sexual commitment markers exhibited low average expression throughout blood stages. In Dd2, the relative number of cells expressing sexual commitment markers appeared similar between mFA and serum. In serum, the average expression of *ap2-g* was higher in Dd2 compared to Pf2004. This higher expression of *ap2-g* likely reflects the higher background conversion rate of Dd2 in serum due to the hypersensitivity of Dd2 to fluctuations in LysoPC concentration.

The advantage of scRNAseq is that it allows the transcriptional signature of rare cell types to be defined, which would previously be masked by bulk RNA sequencing. In this experiment, parasites exhibited conversion rates between 20-35%. Consequently, sexually committed schizonts represent only a subset of parasites in mFA. In Pf2004, where sexually committed schizonts formed distinct clusters, DGE analysis could be performed between sexually committed and asexual clusters in schizonts. Two major transcriptional differences were identified between asexual and sexually committed schizonts in mFA. In asexual schizonts, there was induced expression of cytoadherence-linked genes, such as *kahrp, mesa, garp,* and *pf332,* in addition to their early-stage expression peak. Furthermore, the ncRNA PF3D7_1370800, was upregulated in asexual clusters. In sexually committed schizonts, genes associated with sexual commitment and gene regulation were upregulated. Since cytoadherence markers and sexual commitment markers were both upregulated in mFA compared to serum, this suggests that these two populations are in response to the nutrient limiting

conditions of mFA. In serum conditions, parasites exhibited higher expression levels of nutrient channel components (encoding the PSAC), invasion ligands, such as *eba175* and *eba140,* and the ncRNA PF3D7_1370800.

The ncRNA PF3D7_1370800 was consistently upregulated in serum conditions, and in asexual populations in mFA conditions. Investigation of the timing of this ncRNA in relation to sexual commitment markers revealed an interesting pattern. In serum, following the peak of *ap2-g,* PF3D7_1370800 was highly expressed and subsequently both *ap2-g* and *msrp1* expression remained low. The specific timing of this ncRNA, and its consistent upregulation in asexual populations suggests that this ncRNA may have a role in repressing sexual commitment, although this remains unknown.

In contrast to Pf2004, it was challenging to deconvolute distinct schizont populations in relation to sexual commitment in Dd2. Clusters defined by *ap2-g* expression were not identified in Dd2 meaning DGE between sexually committed and asexual clusters could not be performed. Based on the average expression of markers identified in Pf2004, the expression of genes associated with surface antigens and cytoadherence in mFA did not exhibit a notable second peak as observed in Pf2004. Furthermore, PF3D7_1370800 did not exhibit a strong expression peak in serum conditions for Dd2 as observed in Pf2004. Therefore, there is a difference in response to LysoPC depletion in Dd2 compared to Pf2004, the exact nature of which requires further investigation.

Overall, scRNAseq allowed for the first time the identification of three distinct schizont populations between mFA and serum: i) an asexual population which upregulates cytoadherence associated genes, and the ncRNA PF3D7_1370800, in response to LysoPC depletion, ii) a sexually committed population which upregulates genes associated with sexual commitment and gene regulation in response to LysoPC depletion, iii) and a final population in steady state conditions which exhibits higher expression of nutrient channel components, invasion related genes, and the ncRNA PF3D7_1370800 (**Figure 5-32**).

6.4 Future Directions

From this thesis, several findings require validation, and numerous questions remain unanswered. From **Chapter 3**, the lack of extramedullary haematopoiesis should be confirmed using antibodies against CD71 and CD163. The identification of schizonts in the spleen should be confirmed using schizont specific antibodies against the apical membrane antigen (AMA1) or KAHRP. Furthermore, since Giemsa staining failed in the BM, IHC with AMA1/KAHRP could be additionally performed in then BM. This would allow the proportion of schizonts that are sexually committed to be determined. In these circumstances, the use of both markers might be warranted in the event that schizonts in the spleen and/or the BM are knobless (i.e., KAHRP negative). This staining combination would also serve to verify that the enrichment of parasites on the periphery of the white pulp (WP), beyond the perifollicular zone, are mature stages (as identified by Giemsa). In the same location, parasitic "nests" (i.e., clusters of iRBCs and uninfected RBCs (uRBCs) enclosed within a membrane) were identified. By IHC, many of these parasitic "nests" were labelled by the macrophage marker CD68. However, there were cases where CD68 labelling was not evident. Alternatively, these "nests" may represent rosettes, where macrophages attempt to phagocytose the entire rosette explaining the membrane (Handunnetti et al., 1989). Antibodies against HSP70 and complement receptor 1, which has been implicated as an important factor in *P. falciparum* rosetting, including in field isolates, could determine if these clusters are examples of tissue rosettes (Rowe et al., 2000). Currently, there is no evidence of rosette formation in *in vivo* (Lee et al., 2022).

The identification of MSRP1 positive schizonts in the BM provides direct evidence of sexual commitment in the BM. This supports a previously proposed model of gametocyte enrichment whereby an endogenous asexual replication life cycle exists in the BM, with the unique microenvironment of the BM (e.g., local LysoPC depletion) being conducive of sexual commitment (Nilsson et al., 2015, De Niz et al., 2018, Brancucci et al., 2017). A second model of gametocyte enrichment in the BM was proposed in which sexually committed merozoites or early gametocyte stages preferentially home to the BM for invasion or gametocyte maturation. In *P. berghei* infected mice, the gametocyte dynamics were monitored using intravital microscopy revealing that early gametocytes preferentially home to the BM (De Niz et al., 2018). In this thesis, there were very few sexually committed schizonts

observed in the spleen. It was therefore concluded that the spleen does not contribute to gametocyte formation based on the tissue sections analysed. However, whether other tissues contribute to gametocyte formation is unknown. Brancucci *et al*. demonstrated that high parasite densities were associated with depletion in LysoPC, likely due to higher turnover of LysoPC by parasites (Brancucci et al., 2017). Therefore, a large comparative analysis of MSRP1 between different tissues with varying levels of vascular sequestration should be performed to determine if sexual commitment can occur outside of the BM (Seydel et al., 2006, Milner et al., 2015). For example, there may be a higher proportion of MSRP1 positive parasites in the brain or gastrointerinal tract which sequestration is high (Milner et al., 2015).

A limitation of the analysis of MSRP1 positive parasite density and distribution was the limited number of high powered fields (HPFs) analysed. Given that sexually committed parasites represent a rare parasite population, increasing the number of HPF analysed from 25 per compartment to 100 would increase confidence in the distribution observed. Furthermore, it would be interesting to investigate the host cell type (reticulocytes vs mature RBC) from which sexually committed schizonts and gametocytes reside. Therefore, MSRP1/CD71 and Pfs16/CD71 stains should be performed in this cohort. Based on the transcriptional signature of sexually committed schizonts observed by scRNAseq, it would also be interesting to determine if sexually committed schizonts were knobless and therefore perform IHC targeting MSRP1/KAHRP.

The major unanswered question from the scRNAseq analysis pertains to the transcriptional signatures of sexually and asexual parasites for Dd2. It is possible that noise from neighbouring clusters may have impacted the ability to isolate subpopulations of cells which are defined by sexual commitment markers. Therefore, utilising a cluster-by-cluster approach with markers identified in sexually and asexual schizonts in Pf2004 may aid the identification of these same populations in Dd2. Alternatively, since Dd2 has a different sensitivity to LysoPC depletion, it is possible that this altered sensitivity alters the sexual transcriptional programme of Dd2. Therefore, the transcriptional programme underlying the response of Dd2 to LysoPC depletion remains unclear and requires further investigation. It is also possible that factor influencing sexual commitment

regulation in Dd2 is at the post-transcriptional level. An interesting finding from the scRNAseq dataset was the identification of the ncRNA PF3D7_1370800 which may be involved in repressing sexual commitment. PF3D7_1370800 is located close to the chromosome end and therefore could be influenced by heterochromatin spread (Fraschka et al., 2018). To investigate the function of this ncRNA, it would be necessary to generate knock-out or knock-down parasite lines. Such parasite lines could be subjected to mFA to determine if sexual commitment could be induced.

To validate findings from scRNAseq, RNA *in situ* hybridisation methods such as RNAscope, could be used allowing detection of transcripts in tissues. RNAscope can be used to detect up to 12 RNA targets in formalin-fixed, paraffin embedded (FFPE) tissues (Wang et al., 2012). This can also be coupled with IHC allowing simultaneous detection of mRNA and proteins on the same tissue section. Three schizont populations were identified in Pf2004 (**Figure 5-32**). In mFA, two schizont populations were identified, one characterised by sexual commitment markers, and the other characterised be a second peak in expression of cytoadherence related genes. These two populations contrasted with schizonts grown in steady state serum conditions, where parasites exhibited higher expression of nutrient transport and invasion related genes. To validate these three populations, formalin-fixed, paraffin embedded (FFPE) blood clots consisting of either schizonts grown in mFA or serum could be made as detailed in **Section 2.3.3**. Probes could be designed against marker genes for each of these populations, for example, *ap2-g*, *kahrp,* and *clag3.1*. It was hypothesised that these first two populations represent populations present in the extravascular spaces of the BM, while the latter represents populations sequestered in other organs through vascular sequestration (**Figure 5-32**). To confirm this hypothesis, the same probes used on FFPE blood clots could be applied to tissues from the Malawi cohort. **Section 3.6.1** discussed the application of RNAscope in BM tissues highlighting the need to perform a quality control step using standard control probes in order to identify tissues which would be suitable for RNAscope.

RNA *in situ* hybridisation and IHC is limited in the number of genes or proteins that can be analysed simultaneously. However, the field of 'spatial transcriptomics' overcomes this limitation. Spatial transcriptomics allows the simultaneous

visualisation and quantitative analysis of transcriptomes with spatial resolution in tissues (Williams et al., 2022, Chen et al., 2023). This technique was first introduced and developed by Ståhl *et al*. and since commercialised by 10X Genomics (10X Genomics Visium) (Ståhl et al., 2016). Several other platforms are available including the widely used CosMx by NanoString (He et al., 2022). Utilising such approaches in the context of this project would allow the transcriptional characterisation of schizont populations directly in the tissues and would provide additional spatial context which could inform the interpretation of transcriptomic data.

6.5 Summary

In summary, the research presented in this thesis has expanded our understanding of the splenic reservoir revealing that the role of the spleen during *Plasmodium* infection is dynamic. As such, the accumulation of parasites in the spleen is likely to be driven by several host and parasite factors which are associated with disease severity. It has also provided the first *in vivo* evidence of sexual commitment in the human BM. This identification suggests that gametocyte enrichment in the BM is, at least in part, attributed to an endogenous asexual replication cycle within the BM which supports gametocyte formation. scRNAseq revealed transcriptionally distinct schizont populations characterised by the expression of genes associated with cytoadherence, sexual commitment, and nutrient transport/invasion. The phenotypic relevance of these different schizont populations remains to be determined. Finally, an uncharacterised ncRNA, PF3D7_1370800, was identified which may function in repressing sexual commitment.

Appendices

Appendix 1

Table A1-1. Histopathologic bone marrow (BM) scoring criteria.

PM =	
Histological Parameter	**H&E**
Sample Appearance	
Number of sections	
Integrity: 1 = Good / 2 = Suboptimal / 3 = Poor	
Bone remodeling/proliferation 1=Yes / 2=No	
Overall cellularity % compared to adipose	
Pigmentation (Needs Prussian blue to differantiate from iron)	
Megakaryocytes	
Average number under 40x objective	
Distribution: 1=Focal / 2=Diffuse	
Left shift: 1=Yes / 2=No	
Possible dysplastic changes: 1=Yes / 2=No	
Estimation of M:E ratio, better evaluated with Giemsa	
Granulocytic linage	
Linage complete ? Yes =1 / No=2	
Left shift ? Yes =1 / No=2	
Elevated eosinophils ? Yes =1 / No=2	
Erythroid linage	
Linage complete and ordely ? Yes =1 / No=2	
Left shift ? Yes =1 / No=2	
Can we define sinusoids/blood vessels? NEED thiner cuts in most of them	
Do we observe any suspected iRBCs ? Yes =1 / No=2	
Are susepcted parasites predominantly intravascular or extravascular? (intravascular=1 / extravascular =2)	
Increased Macrophages	
Haemorrhage/Congestion	
Evidence of inflammation	
Necrosis	
Fibrosis	
Other Features	

Table A1-2. Histopathologic spleen scoring criteria.

PM =	
Histological Parameter	**H&E**
Can we define sinusoids/blood vessels?	
Do we observe any suspected iRBCs? (Y/N)	
Are susepcted parasites predominantly intravascular or extravascular? (intravascular=1 / extravascular =2)	
Pigment Latent Cells	
Red Pullp	
White Pullp	
Free Pigment not sure we can really evalute this, what is free Vs ruptures cells	
Red Pullp	
White Pullp	
Whilte Pulp Hyperplasia	
Macrophages/Histiocytes	
Disorganised micro-architecture	
Limits between WP and RP blurred?	
Disruption of germnal centre archiecture	
Dissolution of Mantle zone	
Dissolution of Marginal zone	
Extramedullary Haematopoiesis	
Haemorrhage/Congestion	
Evidence of inflammation	
Necrosis	
Fibrosis	
Relative Lesion Burden	
Other Features	

Appendix 2

Table A2-1. Top 25 differentiallly expressed (DGE) genes between *ap2-g* high and *ap2-g* low clusters (Pf2004).

Upregulated (5vs6)	Upregulated (10vs6)	Upregulated (9vs6)	Downregulated (5vs6)	Downregulated (10vs6)	Downregulated (9vs6)
PF3D7_0704500	PF3D7_1113000	PF3D7_1401600	PF3D7_0532100 (ETRAMP5)	PF3D7_0532100 (ETRAMP5)	PF3D7_0532100 (ETRAMP5)
PF3D7_1029900	PF3D7_0704500	PF3D7_0830800 (SURF8.2)	PF3D7_0113000 (GARP)	PF3D7_1016300 (GBP130)	PF3D7_1016300 (GBP130)
PF3D7_0903300	PF3D7_1029900	PF3D7_1118700 (MLC-B)	PF3D7_0708400 (HSP90)	PF3D7_0708400 (HSP90)	PF3D7_0113000 (GARP)
PF3D7_0607700	PF3D7_0604100 (SIP2)	PF3D7_1009700	PF3D7_1149000 (Pf332)	PF3D7_0113000 (GARP)	PF3D7_0202000 (KAHRP)
PF3D7_1423500	PF3D7_0613800 (ApiAP2)	PF3D7_1436200 (BCP1)	PF3D7_1471100 (EXP2)	PF3D7_1121600 (EXP1)	PF3D7_1121600 (EXP1)
PF3D7_0829500	PF3D7_1138000	PF3D7_0105400	PF3D7_1121600 (EXP1)	PF3D7_0202000 (KAHRP)	PF3D7_0708400 (HSP90)
PF3D7_0207600 (SERA5)	PF3D7_1325400	PF3D7_0628100 (HECT1)	PF3D7_0908500	PF3D7_1149000 (Pf332)	PF3D7_1462800 (GAPDH)
PF3D7_0504800	PF3D7_1140000 (CA)	PF3D7_1206300	PF3D7_1356800 (ARK9)	PF3D7_0500800 (MESA)	PF3D7_1149000 (Pf332)
PF3D7_1033900	PF3D7_1313600	PF3D7_0405900 (ASP)	PF3D7_0220200	PF3D7_1462800 (GAPDH)	PF3D7_0500800 (MESA)
PF3D7_0516800 (ApiAP2.1)	PF3D7_0603800 (CEP76)	PF3D7_1437300	PF3D7_1126700 (ATG23)	PF3D7_1471100 (EXP2)	PF3D7_0112200 (MRP1)
PF3D7_0710000	PF3D7_1014900 (KIC8)	PF3D7_0810900	PF3D7_1016300 (GBP130)	PF3D7_0220200	PF3D7_1471100 (EXP2)
PF3D7_0419400	PF3D7_1252100 (RON3)	PF3D7_0522400	PF3D7_0818900 (HSP70)	PF3D7_0818900 (HSP70)	PF3D7_0220200
PF3D7_0606800 (VFT1)	PF3D7_0607700	PF3D7_0817600	PF3D7_0500800 (MESA)	PF3D7_1347200 (NT1)	PF3D7_0814200 (ALBA1)
PF3D7_0207700 (SERA4)	PF3D7_0404100 (ApiAP2.1)	PF3D7_1343800	PF3D7_1347200 (NT1)	PF3D7_0112200 (MRP1)	PF3D7_0113800
PF3D7_0404100 (ApiAP2.4)	PF3D7_0419900	PF3D7_1206000 (SHLP2)	PF3D7_1012400 (HGPRT)	PF3D7_1126700 (ATG23)	PF3D7_1420700 (P113)
PF3D7_0604100 (SIP2)	PF3D7_0919900 (RCC-PIP)	PF3D7_1107800 (ApiAP2)	PF3D7_1149100	PF3D7_1012400 (HGPRT)	PF3D7_1347200 (NT1)
PF3D7_0613900 (ApiAP2)	PF3D7_1019100	PF3D7_0614600	PF3D7_1035300 (GLURP)	PF3D7_1149100	PF3D7_0310400 (PIESP1)
PF3D7_0204100	PF3D7_1432200	PF3D7_0908500	PF3D7_1462800 (GAPDH)	PF3D7_1200600 (VAR2CSA)	PF3D7_0716300
PF3D7_0607600 (SAS6)	PF3D7_1455600 (FER2)	PF3D7_1145200	PF3D7_1021700	PF3D7_1308200 (cpsSII)	PF3D7_0731600 (ACS5)
PF3D7_0805700 (FIKK8)	PF3D7_1018200 (PPP8)	PF3D7_0722200 (RALP1)	PF3D7_0202000 (KAHRP)	PF3D7_1420700 (P113)	PF3D7_1308200 (cpsSII)
PF3D7_1113000	PF3D7_1224100	PF3D7_0214900 (RON6)	PF3D7_1200600 (VAR2CSA)	PF3D7_0220000 (LSA3)	PF3D7_0904900 (CuTP)
PF3D7_1221300 (TKL2)	PF3D7_1423500	PF3D7_1452000 (RON2)	PF3D7_1229800 (MyoJ)	PF3D7_0831700 (HSP70x)	PF3D7_1216900
PF3D7_1364100 (P92)	PF3D7_0308100	PF3D7_1014900 (KIC8)	PF3D7_0907500	PF3D7_0731600 (ACS5)	PF3D7_0220000 (LSA3)
PF3D7_0926500	PF3D7_0220800 (CLAG2)	PF3D7_1476300	PF3D7_1453700 (P23)	PF3D7_0814200 (ALBA1)	PF3D7_1149100
PF3D7_0314800	PF3D7_0531100	PF3D7_1321100	PF3D7_1107800 (ApiAP2.3)	PF3D7_0708800 (HSP110c)	PF3D7_1200600 (VAR2CSA)

Top 25 genes are ordered according to fold change, from highest to lowest. All top 25 genes have an adjusted p value < 0.05.

References

ABDI, A. I., ACHCAR, F., SOLLELIS, L., SILVA-FILHO, J. L., MWIKALI, K., MUTHUI, M., MWANGI, S., KIMINGI, H. W., ORINDI, B., ANDISI KIVISI, C., ALKEMA, M., CHANDRASEKAR, A., BULL, P. C., BEJON, P., MODRZYNSKA, K., BOUSEMA, T. & MARTI, M. 2023. Plasmodium falciparum adapts its investment into replication versus transmission according to the host environment. *eLife,* 12**,** e85140.

ACKLAND, J., OSMAN, K., SPALLUTO, C. M., CLEARY, D. W., CHRISTODOULIDES, M., WILKINSON, T. & STAPLES, K. J. 2019. Macrophage inflammatory responses to Non-typeable Haemophilus influenzae (NTHi) are strain-dependent. *European Respiratory Journal,* 54**,** PA5440.

ADIGWE, O. P., ONOJA, S. O. & ONAVBAVBA, G. 2023. A Critical Review of Sickle Cell Disease Burden and Challenges in Sub-Saharan Africa. *J Blood Med,* 14**,** 367-376.

ADJALLEY, S. H., CHABBERT, C. D., KLAUS, B., PELECHANO, V. & STEINMETZ, L. M. 2016. Landscape and Dynamics of Transcription Initiation in the Malaria Parasite Plasmodium falciparum. *Cell Rep,* 14**,** 2463-75.

AGUILAR, R., MAGALLON-TEJADA, A., ACHTMAN, A. H., MORALEDA, C., JOICE, R., CISTERÓ, P., LI WAI SUEN, C. S., NHABOMBA, A., MACETE, E., MUELLER, I., MARTI, M., ALONSO, P. L., MENÉNDEZ, C., SCHOFIELD, L. & MAYOR, A. 2014. Molecular evidence for the localization of Plasmodium falciparum immature gametocytes in bone marrow. *Blood,* 123**,** 959-66.

AHMAD, F., RANI, A., ALAM, A., ZARIN, S., PANDEY, S., SINGH, H., HASNAIN, S. E. & EHTESHAM, N. Z. 2022. Macrophage: A Cell With Many Faces and Functions in Tuberculosis. *Front Immunol,* 13**,** 747799.

AINGARAN, M., ZHANG, R., LAW, S. K., PENG, Z., UNDISZ, A., MEYER, E., DIEZ-SILVA, M., BURKE, T. A., SPIELMANN, T., LIM, C. T., SURESH, S., DAO, M. & MARTI, M. 2012. Host cell deformability is linked to transmission in the human malaria parasite Plasmodium falciparum. *Cell Microbiol,* 14**,** 983-93.

AL-MAAWI, S., VALENZUELA, P., DOHLE, E., HESELICH, A., SADER, R. & GHANAATI, S. 2022. Comparison of Different Fixation Methods for Combined Histological and Biomolecular Analysis of Fixed and Decalcified Bone Samples. *Methods and Protocols,* 5**,** 64.

ALMUKADI, H., SCHWAKE, C., KAISER, M. M., MAYER, D. C. G., SCHIEMER, J., BALDWIN, M. R., HEGDE, S., LU, Y., HANADA, T. & CHISHTI, A. H. 2019. Human erythrocyte band 3 is a host receptor for Plasmodium falciparum glutamic acid-rich protein. *Blood,* 133**,** 470-480.

ALTSCHUL, S. F., WOOTTON, J. C., ZASLAVSKY, E. & YU, Y.-K. 2010. The Construction and Use of Log-Odds Substitution Scores for Multiple Sequence Alignment. *PLOS Computational Biology,* 6**,** e1000852.

ALVES, F. A., PELAJO-MACHADO, M., TOTINO, P. R. R., SOUZA, M. T., GONÇALVES, E. C., SCHNEIDER, M. P. C., MUNIZ, J. A. P. C., KRIEGER, M. A., ANDRADE, M. C. R., DANIEL-RIBEIRO, C. T. & CARVALHO, L. J. M. 2015. Splenic architecture disruption and parasite-induced splenocyte activation and anergy in Plasmodium falciparum-infected Saimiri sciureus monkeys. *Malaria journal,* 14**,** 128-128.

AMANFO, S. A. 2018. *Parasite and Host Factors That Drive Heterogeneity in Human Malaria* PhD, University of Edinburgh.

AMINO, R., THIBERGE, S., MARTIN, B., CELLI, S., SHORTE, S., FRISCHKNECHT, F. & MÉNARD, R. 2006. Quantitative imaging of Plasmodium transmission from mosquito to mammal. *Nat Med,* 12**,** 220-4.

AMIT-AVRAHAM, I., POZNER, G., ESHAR, S., FASTMAN, Y., KOLEVZON, N., YAVIN, E. & DZIKOWSKI, R. 2015. Antisense long noncoding RNAs regulate var gene activation in the malaria parasite Plasmodium falciparum. *Proceedings of the National Academy of Sciences,* 112**,** E982-E991.

ANCELIN, M. L., CALAS, M., VIDAL-SAILHAN, V., HERBUTÉ, S., RINGWALD, P. & VIAL, H. J. 2003. Potent inhibitors of Plasmodium phospholipid metabolism with a broad spectrum of in vitro antimalarial activities. *Antimicrob Agents Chemother,* 47**,** 2590-7.

ANTWI-BAFFOUR, S., MENSAH, B. T., JOHNSON, G., ARMAH, D. N. O., ALI-MUSTAPHA, S. & ANNISON, L. 2023. Haematological parameters and their correlation with the degree of malaria parasitaemia among outpatients attending a polyclinic. *Malar J,* 22**,** 281.

ARESE, P. & SCHWARZER, E. 1997. Malarial pigment (haemozoin): a very active 'inert' substance. *Ann Trop Med Parasitol,* 91**,** 501-16.

ASAMI, M., OWHASHI, M., ABE, T. & NAWA, Y. 1992. A comparative study of the kinetic changes of hemopoietic stem cells in mice infected with lethal and non-lethal malaria. *Int J Parasitol,* 22**,** 43-7.

AURRECOECHEA, C., BRESTELLI, J., BRUNK, B. P., DOMMER, J., FISCHER, S., GAJRIA, B., GAO, X., GINGLE, A., GRANT, G., HARB, O. S., HEIGES, M., INNAMORATO, F., IODICE, J., KISSINGER, J. C., KRAEMER, E., LI, W., MILLER, J. A., NAYAK, V., PENNINGTON, C., PINNEY, D. F., ROOS, D. S., ROSS, C., STOECKERT, C. J., JR., TREATMAN, C. & WANG, H. 2009. PlasmoDB: a functional genomic database for malaria parasites. *Nucleic Acids Res,* 37**,** D539-43.

BACHER, R. & KENDZIORSKI, C. 2016. Design and computational analysis of single-cell RNA-sequencing experiments. *Genome Biology,* 17**,** 63.

BAIN, B. J., CLARK, D. M. & WILKINS, B. S. 2019. Infection and Reactive Changes. *Bone Marrow Pathology*. 5th ed. Hoboken, NJ: John Wiley & Sons, Inc.

BAINA, M. T., LISSOM, A., ASSIORO DOULAMO, N. V., DJONTU, J. C., UMUHOZA, D. M., MBAMA-NTABI, J. D., DIAFOUKA-KIETELA, S., MAYELA, J., MISSONTSA, G., WONDJI, C., ADEGNIKA, A. A., NGUIMBI, E., BORRMANN, S. & NTOUMI, F. 2023. Comparative study of Plasmodium falciparum msp-1 and msp-2 Genetic Diversity in Isolates from Rural and Urban Areas in the South of Brazzaville, Republic of Congo. *Pathogens,* 12.

BALAJI, S., BABU, M. M., IYER, L. M. & ARAVIND, L. 2005. Discovery of the principal specific transcription factors of Apicomplexa and their implication for the evolution of the AP2-integrase DNA binding domains. *Nucleic Acids Research,* 33**,** 3994-4006.

BANCELLS, C., LLORÀ-BATLLE, O., PORAN, A., NÖTZEL, C., ROVIRA-GRAELLS, N., ELEMENTO, O., KAFSACK, B. F. C. & CORTÉS, A. 2019. Revisiting the initial steps of sexual development in the malaria parasite Plasmodium falciparum. *Nature Microbiology,* 4**,** 144-154.

BANUMATHY, G., SINGH, V., PAVITHRA, S. R. & TATU, U. 2003. Heat Shock Protein 90 Function Is Essential for Plasmodium falciparum Growth in Human Erythrocytes*. *Journal of Biological Chemistry,* 278**,** 18336-18345.

BARBER, B. E., WILLIAM, T., GRIGG, M. J., PARAMESWARAN, U., PIERA, K. A., PRICE, R. N., YEO, T. W. & ANSTEY, N. M. 2015. Parasite Biomass-Related Inflammation, Endothelial Activation, Microvascular Dysfunction and Disease Severity in Vivax Malaria. *PLOS Pathogens,* 11**,** e1004558.

BARNWELL, J. W., ASCH, A. S., NACHMAN, R. L., YAMAYA, M., AIKAWA, M. & INGRAVALLO, P. 1989. A human 88-kD membrane glycoprotein (CD36) functions in vitro as a receptor for a cytoadherence ligand on Plasmodium falciparum-infected erythrocytes. *J Clin Invest,* 84**,** 765-72.

BARO, B., DEROOST, K., RAIOL, T., BRITO, M., ALMEIDA, A. C. G., DE MENEZES-NETO, A., FIGUEIREDO, E. F. G., ALENCAR, A., LEITÃO, R., VAL, F., MONTEIRO, W., OLIVEIRA, A., ARMENGOL, M. D. P., FERNÁNDEZ-BECERRA, C., LACERDA, M. V. & DEL PORTILLO, H. A. 2017. Plasmodium vivax gametocytes in the bone marrow of an acute malaria patient and changes in the erythroid miRNA profile. *PLOS Neglected Tropical Diseases,* 11**,** e0005365.

BÁRTFAI, R., HOEIJMAKERS, W. A. M., SALCEDO-AMAYA, A. M., SMITS, A. H., JANSSEN-MEGENS, E., KAAN, A., TREECK, M., GILBERGER, T.-W., FRANÇOIJS, K.-J. & STUNNENBERG, H. G. 2010. H2A.Z Demarcates Intergenic Regions of the Plasmodium falciparum Epigenome That Are

Dynamically Marked by H3K9ac and H3K4me3. *PLOS Pathogens,* 6**,** e1001223.

BARUCH, D. I., PASLOSKE, B. L., SINGH, H. B., BI, X., MA, X. C., FELDMAN, M., TARASCHI, T. F. & HOWARD, R. J. 1995. Cloning the P. falciparum gene encoding PfEMP1, a malarial variant antigen and adherence receptor on the surface of parasitized human erythrocytes. *Cell,* 82**,** 77-87.

BATUGEDARA, G., LU, X. M., HRISTOV, B., ABEL, S., CHAHINE, Z., HOLLIN, T., WILLIAMS, D., WANG, T., CORT, A., LENZ, T., THOMPSON, T. A., PRUDHOMME, J., TRIPATHI, A. K., XU, G., CUDINI, J., DOGGA, S., LAWNICZAK, M., NOBLE, W. S., SINNIS, P. & LE ROCH, K. G. 2023. Novel insights into the role of long non-coding RNA in the human malaria parasite, Plasmodium falciparum. *Nat Commun,* 14**,** 5086.

BAUOMY, A. A., DKHIL, M. A., DIAB, M. S. M., AMER, O. S. O., ZRIEQ, R. M. & AL-QURAISHY, S. 2014. Response of Spleen and Jejunum of Mice Infected with Schistosoma mansoni to Mulberry Treatment. *Pakistan journal of zoology,* 46**,** 753-761.

BEESON, J. G., DREW, D. R., BOYLE, M. J., FENG, G., FOWKES, F. J. & RICHARDS, J. S. 2016. Merozoite surface proteins in red blood cell invasion, immunity and vaccines against malaria. *FEMS Microbiol Rev,* 40**,** 343-72.

BELLUOCCIO, D., ROWLEY, L., LITTLE, C. B. & BATEMAN, J. F. 2013. Maintaining mRNA Integrity during Decalcification of Mineralized Tissues. *PLOS ONE,* 8**,** e58154.

BENNETT, L. F., LIAO, C. & PAULSON, R. F. 2018. Stress Erythropoiesis Model Systems. *Methods Mol Biol,* 1698**,** 91-102.

BENNETT, L. F., LIAO, C., QUICKEL, M. D., YEOH, B. S., VIJAY-KUMAR, M., HANKEY-GIBLIN, P., PRABHU, K. S. & PAULSON, R. F. 2019. Inflammation induces stress erythropoiesis through heme-dependent activation of SPI-C. *Sci Signal,* 12.

BERENDT, A. R., SIMMONS, D. L., TANSEY, J., NEWBOLD, C. I. & MARSH, K. 1989. Intercellular adhesion molecule-1 is an endothelial cell adhesion receptor for Plasmodium falciparum. *Nature,* 341**,** 57-9.

BERRY, A. E., GARDNER, M. J., CASPERS, G. J., ROOS, D. S. & BERRIMAN, M. 2004. Curation of the Plasmodium falciparum genome. *Trends Parasitol,* 20**,** 548-52.

BESSIS, M. 1958. Erythroblastic island, functional unity of bone marrow. *Rev Hematol,* 13**,** 8-11.

BETJES, M. G. H., HAKS, M. C., TUK, C. W. & BEELEN, R. H. J. 1991. Monoclonal Antibody EBM11 (Anti-CD68) Discriminates between Dendritic Cells and Macrophages after Short-Term Culture. *Immunobiology,* 183**,** 79-87.

BILAL, J. A., GASIM, G. I., KARSANI, A. H., ELBASHIR, L. M. & ADAM, I. 2016. Malaria Parasite Density Estimation using Actual and Assumed White Blood Cells Count in Children in Eastern Sudan. *J Trop Pediatr,* 62**,** 171-5.

BLAND, J. M. & ALTMAN, D. 1986. STATISTICAL METHODS FOR ASSESSING AGREEMENT BETWEEN TWO METHODS OF CLINICAL MEASUREMENT. *The Lancet,* 327**,** 307-310.

BÖHME, U., OTTO, T. D., SANDERS, M., NEWBOLD, C. I. & BERRIMAN, M. 2019. Progression of the canonical reference malaria parasite genome from 2002-2019. *Wellcome Open Res,* 4**,** 58.

BOUYER, G., BARBIERI, D., DUPUY, F., MARTEAU, A., SISSOKO, A., N'DRI, M.-E., NEVEU, G., BEDAULT, L., KHODABUX, N., ROMAN, D., HOUZÉ, S., SICILIANO, G., ALANO, P., MARTINS, R. M., LOPEZ-RUBIO, J.-J., CLAIN, J., DUVAL, R., EGÉE, S. & LAVAZEC, C. 2020. Plasmodium falciparum sexual parasites regulate infected erythrocyte permeability. *Communications Biology,* 3**,** 726.

BOZDECH, Z., LLINÁS, M., PULLIAM, B. L., WONG, E. D., ZHU, J. & DERISI, J. L. 2003. The Transcriptome of the Intraerythrocytic Developmental Cycle of Plasmodium falciparum. *PLOS Biology,* 1**,** e5.

BRADY, G., BARBARA, M. A. M. & ISCOVE, N. N. Representative in Vitro cDNA Amplification From Individual Hemopoietic Cells and Colonies. 1990.

BRANCUCCI, N. M., GOLDOWITZ, I., BUCHHOLZ, K., WERLING, K. & MARTI, M. 2015. An assay to probe Plasmodium falciparum growth, transmission stage formation and early gametocyte development. *Nat Protoc,* 10**,** 1131-42.

BRANCUCCI, N. M. B., BERTSCHI, N. L., ZHU, L., NIEDERWIESER, I., CHIN, W. H., WAMPFLER, R., FREYMOND, C., ROTTMANN, M., FELGER, I., BOZDECH, Z. & VOSS, T. S. 2014. Heterochromatin protein 1 secures survival and transmission of malaria parasites. *Cell Host Microbe,* 16**,** 165-176.

BRANCUCCI, N. M. B., DE NIZ, M., STRAUB, T. J., RAVEL, D., SOLLELIS, L., BIRREN, B. W., VOSS, T. S., NEAFSEY, D. E. & MARTI, M. 2018. Probing Plasmodium falciparum sexual commitment at the single-cell level. *Wellcome Open Res,* 3**,** 70.

BRANCUCCI, N. M. B., GERDT, J. P., WANG, C., DE NIZ, M., PHILIP, N., ADAPA, S. R., ZHANG, M., HITZ, E., NIEDERWIESER, I., BOLTRYK, S. D., LAFFITTE, M. C., CLARK, M. A., GRÜRING, C., RAVEL, D., BLANCKE SOARES, A., DEMAS, A., BOPP, S., RUBIO-RUIZ, B., CONEJO-GARCIA, A., WIRTH, D. F., GENDASZEWSKA-DARMACH, E., DURAISINGH, M. T., ADAMS, J. H., VOSS, T. S., WATERS, A. P., JIANG, R. H. Y., CLARDY, J. & MARTI, M. 2017.

Lysophosphatidylcholine Regulates Sexual Stage Differentiation in the Human Malaria Parasite Plasmodium falciparum. *Cell,* 171, 1532-1544.e15.

BRIGGS, E. M., WARREN, F. S. L., MATTHEWS, K. R., MCCULLOCH, R. & OTTO, T. D. 2021. Application of single-cell transcriptomics to kinetoplastid research. *Parasitology,* 148, 1223-1236.

BROADBENT, K. M., BROADBENT, J. C., RIBACKE, U., WIRTH, D., RINN, J. L. & SABETI, P. C. 2015. Strand-specific RNA sequencing in Plasmodium falciparum malaria identifies developmentally regulated long non-coding RNA and circular RNA. *BMC Genomics,* 16, 454.

BROADBENT, K. M., PARK, D., WOLF, A. R., VAN TYNE, D., SIMS, J. S., RIBACKE, U., VOLKMAN, S., DURAISINGH, M., WIRTH, D., SABETI, P. C. & RINN, J. L. 2011. A global transcriptional analysis of Plasmodium falciparum malaria reveals a novel family of telomere-associated lncRNAs. *Genome Biology,* 12, R56.

BROWN, W. M., YOWELL, C. A., HOARD, A., VANDER JAGT, T. A., HUNSAKER, L. A., DECK, L. M., ROYER, R. E., PIPER, R. C., DAME, J. B., MAKLER, M. T. & VANDER JAGT, D. L. 2004. Comparative structural analysis and kinetic properties of lactate dehydrogenases from the four species of human malarial parasites. *Biochemistry,* 43, 6219-29.

BUCHHOLZ, K., BURKE, T. A., WILLIAMSON, K. C., WIEGAND, R. C., WIRTH, D. F. & MARTI, M. 2011. A high-throughput screen targeting malaria transmission stages opens new avenues for drug development. *The Journal of infectious diseases,* 203, 1445-1453.

BUCKLING, A., RANFORD-CARTWRIGHT, L. C., MILES, A. & READ, A. F. 1999. Chloroquine increases Plasmodium falciparum gametocytogenesis in vitro. *Parasitology,* 118 (Pt 4), 339-46.

BUFFET, P. A., MILON, G., BROUSSE, V., CORREAS, J.-M., DOUSSET, B., COUVELARD, A., KIANMANESH, R., FARGES, O., SAUVANET, A., PAYE, F., UNGEHEUER, M.-N., OTTONE, C., KHUN, H., FIETTE, L., GUIGON, G., HUERRE, M., MERCEREAU-PUIJALON, O. & DAVID, P. H. 2006. Ex vivo perfusion of human spleens maintains clearing and processing functions. *Blood,* 107, 3745-3752.

BUFFET, P. A., SAFEUKUI, I., DEPLAINE, G., BROUSSE, V., PRENDKI, V., THELLIER, M., TURNER, G. D. & MERCEREAU-PUIJALON, O. 2011. The pathogenesis of Plasmodium falciparum malaria in humans: insights from splenic physiology. *Blood,* 117, 381-392.

BUNNIK, E. M., COOK, K. B., VAROQUAUX, N., BATUGEDARA, G., PRUDHOMME, J., CORT, A., SHI, L., ANDOLINA, C., ROSS, L. S., BRADY, D., FIDOCK, D. A., NOSTEN, F., TEWARI, R., SINNIS, P., AY, F., VERT, J.-P., NOBLE, W. S. & LE ROCH, K. G. 2018. Changes in genome organization of parasite-specific

gene families during the Plasmodium transmission stages. *Nature Communications,* 9**,** 1910.

BUNNIK, E. M., POLISHKO, A., PRUDHOMME, J., PONTS, N., GILL, S. S., LONARDI, S. & LE ROCH, K. G. 2014. DNA-encoded nucleosome occupancy is associated with transcription levels in the human malaria parasite Plasmodium falciparum. *BMC Genomics,* 15**,** 347.

CALIS, J. C. J., PHIRI, K. S., FARAGHER, E. B., BRABIN, B. J., BATES, I., CUEVAS, L. E., DE HAAN, R. J., PHIRI, A. I., MALANGE, P., KHOKA, M., HULSHOF, P. J. M., VAN LIESHOUT, L., BELD, M. G. H. M., TEO, Y. Y., ROCKETT, K. A., RICHARDSON, A., KWIATKOWSKI, D. P., MOLYNEUX, M. E. & VAN HENSBROEK, M. B. 2008. Severe Anemia in Malawian Children. *New England Journal of Medicine,* 358**,** 888-899.

CHAAL, B. K., GUPTA, A. P., WASTUWIDYANINGTYAS, B. D., LUAH, Y.-H. & BOZDECH, Z. 2010. Histone Deacetylases Play a Major Role in the Transcriptional Regulation of the Plasmodium falciparum Life Cycle. *PLOS Pathogens,* 6**,** e1000737.

CHAPPELL, L., ROSS, P., ORCHARD, L., RUSSELL, T. J., OTTO, T. D., BERRIMAN, M., RAYNER, J. C. & LLINÁS, M. 2020. Refining the transcriptome of the human malaria parasite Plasmodium falciparum using amplification-free RNA-seq. *BMC Genomics,* 21**,** 395.

CHASIS, J. A. & MOHANDAS, N. 2008. Erythroblastic islands: niches for erythropoiesis. *Blood,* 112**,** 470-478.

CHATZOPOULOS, K., TREECK, B. V., VENABLE, E., SERLA, V., WIRTH, T., AMIRAHMADI, F., PETERSON, A. & LIN, P. T. 2020. Formalin pigment artifact deposition in autopsy tissue: predisposing factors, patterns of distribution and methods for removal. *Forensic Science, Medicine and Pathology,* 16**,** 435-441.

CHAU, J. Y., TIFFANY, C. M., NIMISHAKAVI, S., LAWRENCE, J. A., PAKPOUR, N., MOONEY, J. P., LOKKEN, K. L., CAUGHEY, G. H., TSOLIS, R. M. & LUCKHART, S. 2013. Malaria-associated L-arginine deficiency induces mast cell-associated disruption to intestinal barrier defenses against nontyphoidal Salmonella bacteremia. *Infect Immun,* 81**,** 3515-26.

CHAUBEY, S., GROVER, M. & TATU, U. 2014. Endoplasmic reticulum stress triggers gametocytogenesis in the malaria parasite. *J Biol Chem,* 289**,** 16662-74.

CHEN, G., NING, B. & SHI, T. 2019. Single-Cell RNA-Seq Technologies and Related Computational Data Analysis. *Frontiers in Genetics,* 10.

CHEN, I., CLARKE, S. E., GOSLING, R., HAMAINZA, B., KILLEEN, G., MAGILL, A., O'MEARA, W., PRICE, R. N. & RILEY, E. M. 2016. "Asymptomatic" Malaria: A Chronic and Debilitating Infection That Should Be Treated. *PLOS Medicine,* 13**,** e1001942.

CHEN, J. H., JUNG, J. W., WANG, Y., HA, K. S., LU, F., LIM, C. S., TAKEO, S., TSUBOI, T. & HAN, E. T. 2010. Immunoproteomics profiling of blood stage Plasmodium vivax infection by high-throughput screening assays. *J Proteome Res,* 9**,** 6479-89.

CHEN, L., WANG, J., LIU, J., WANG, H., HILLYER, C. D., BLANC, L., AN, X. & MOHANDAS, N. 2021. Dynamic changes in murine erythropoiesis from birth to adulthood: implications for the study of murine models of anemia. *Blood Adv,* 5**,** 16-25.

CHEN, T. Y., YOU, L., HARDILLO, J. A. U. & CHIEN, M. P. 2023. Spatial Transcriptomic Technologies. *Cells,* 12.

CHENG, Y., LU, F., LEE, S.-K., KONG, D.-H., HA, K.-S., WANG, B., SATTABONGKOT, J., TSUBOI, T. & HAN, E.-T. 2015. Characterization of Plasmodium vivax Early Transcribed Membrane Protein 11.2 and Exported Protein 1. *PLOS ONE,* 10**,** e0127500.

CHISTIAKOV, D. A., KILLINGSWORTH, M. C., MYASOEDOVA, V. A., OREKHOV, A. N. & BOBRYSHEV, Y. V. 2017. CD68/macrosialin: not just a histochemical marker. *Laboratory Investigation,* 97**,** 4-13.

CHOTIVANICH, K., UDOMSANGPETCH, R., DONDORP, A., WILLIAMS, T., ANGUS, B., SIMPSON, J. A., PUKRITTAYAKAMEE, S., LOOAREESUWAN, S., NEWBOLD, C. I. & WHITE, N. J. 2000. The Mechanisms of Parasite Clearance after Antimalarial Treatment of Plasmodium falciparum Malaria. *The Journal of Infectious Diseases,* 182**,** 629-633.

CHUA, C. L. L., BROWN, G., HAMILTON, J. A., ROGERSON, S. & BOEUF, P. 2013. Monocytes and macrophages in malaria: protection or pathology? *Trends in Parasitology,* 29**,** 26-34.

CHUA, C. L. L., NG, I. M. J., YAP, B. J. M. & TEO, A. 2021. Factors influencing phagocytosis of malaria parasites: the story so far. *Malar J,* 20**,** 319.

COETZEE, N., SIDOLI, S., VAN BILJON, R., PAINTER, H., LLINÁS, M., GARCIA, B. A. & BIRKHOLTZ, L.-M. 2017. Quantitative chromatin proteomics reveals a dynamic histone post-translational modification landscape that defines asexual and sexual Plasmodium falciparum parasites. *Scientific Reports,* 7**,** 607.

COLEMAN, B. I., SKILLMAN, K. M., JIANG, R. H. Y., CHILDS, L. M., ALTENHOFEN, L. M., GANTER, M., LEUNG, Y., GOLDOWITZ, I., KAFSACK, B. F. C., MARTI, M., LLINÁS, M., BUCKEE, C. O. & DURAISINGH, M. T. 2014. A Plasmodium falciparum histone deacetylase regulates antigenic variation and gametocyte conversion. *Cell Host Microbe,* 16**,** 177-186.

COPPEL, R. L. 1992. Repeat structures in a Plasmodium falciparum protein (MESA) that binds human erythrocyte protein 4.1. *Mol Biochem Parasitol,* 50**,** 335-47.

CORTÉS, A. & DEITSCH, K. W. 2017. Malaria Epigenetics. *Cold Spring Harb Perspect Med,* 7.

COX, F. E. G. 2010. History of the discovery of the malaria parasites and their vectors. *Parasites & Vectors,* 3**,** 5.

COX-SINGH, J. & SINGH, B. 2008. Knowlesi malaria: newly emergent and of public health importance? *Trends Parasitol,* 24**,** 406-10.

CRABB, B. S., COOKE, B. M., REEDER, J. C., WALLER, R. F., CARUANA, S. R., DAVERN, K. M., WICKHAM, M. E., BROWN, G. V., COPPEL, R. L. & COWMAN, A. F. 1997. Targeted gene disruption shows that knobs enable malaria-infected red cells to cytoadhere under physiological shear stress. *Cell,* 89**,** 287-96.

CRANSTON, H. A., BOYLAN, C. W., CARROLL, G. L., SUTERA, S. P., WILLIAMSON, J. R., GLUZMAN, I. Y. & KROGSTAD, D. J. 1984. Plasmodium falciparum maturation abolishes physiologic red cell deformability. *Science,* 223**,** 400-3.

CUI, L., FAN, Q., CUI, L. & MIAO, J. 2008. Histone lysine methyltransferases and demethylases in Plasmodium falciparum. *International Journal for Parasitology,* 38**,** 1083-1097.

CUI, L., MIAO, J., FURUYA, T., LI, X., SU, X. Z. & CUI, L. 2007. PfGCN5-mediated histone H3 acetylation plays a key role in gene expression in Plasmodium falciparum. *Eukaryot Cell,* 6**,** 1219-27.

CULVENOR, J. G., DAY, K. P. & ANDERS, R. F. 1991. Plasmodium falciparum ring-infected erythrocyte surface antigen is released from merozoite dense granules after erythrocyte invasion. *Infect Immun,* 59**,** 1183-7.

DA SILVA, A. M., CORRÊA, C. L., NEVES, R. H. & MACHADO-SILVA, J. R. 2012. A high-fat diet associated with acute schistosomiasis mansoni causes disorganization in splenic architecture in mice. *Exp Parasitol,* 132**,** 193-9.

DE NIZ, M., MEIBALAN, E., MEJIA, P., MA, S., BRANCUCCI, N. M. B., AGOP-NERSESIAN, C., MANDT, R., NGOTHO, P., HUGHES, K. R., WATERS, A. P., HUTTENHOWER, C., MITCHELL, J. R., MARTINELLI, R., FRISCHKNECHT, F., SEYDEL, K. B., TAYLOR, T., MILNER, D., HEUSSLER, V. T. & MARTI, M. 2018. Plasmodium gametocytes display homing and vascular transmigration in the host bone marrow. *Science Advances,* 4**,** eaat3775.

DÉCHAMPS, S., SHASTRI, S., WENGELNIK, K. & VIAL, H. J. 2010a. Glycerophospholipid acquisition in Plasmodium - a puzzling assembly of biosynthetic pathways. *Int J Parasitol,* 40**,** 1347-65.

DÉCHAMPS, S., WENGELNIK, K., BERRY-STERKERS, L., CERDAN, R., VIAL, H. J. & GANNOUN-ZAKI, L. 2010b. The Kennedy phospholipid biosynthesis pathways

are refractory to genetic disruption in Plasmodium berghei and therefore appear essential in blood stages. *Mol Biochem Parasitol,* 173**,** 69-80.

DECHERING, K. J., CUELENAERE, K., KONINGS, R. N. & LEUNISSEN, J. A. 1998. Distinct frequency-distributions of homopolymeric DNA tracts in different genomes. *Nucleic Acids Res,* 26**,** 4056-62.

DELACRÉTAZ, F., PEREY, L., SCHMIDT, P. M., CHAVE, J. P. & COSTA, J. 1987. Histopathology of bone marrow in human immunodeficiency virus infection. *Virchows Arch A Pathol Anat Histopathol,* 411**,** 543-51.

DELAHUNT, C., HORNING, M. P., WILSON, B. K., PROCTOR, J. L. & HEGG, M. C. 2014. Limitations of haemozoin-based diagnosis of Plasmodium falciparum using dark-field microscopy. *Malar J,* 13**,** 147.

DEPLAINE, G., SAFEUKUI, I., JEDDI, F., LACOSTE, F., BROUSSE, V., PERROT, S., BILIGUI, S., GUILLOTTE, M., GUITTON, C., DOKMAK, S., AUSSILHOU, B., SAUVANET, A., CAZALS HATEM, D., PAYE, F., THELLIER, M., MAZIER, D., MILON, G., MOHANDAS, N., MERCEREAU-PUIJALON, O., DAVID, P. H. & BUFFET, P. A. 2011. The sensing of poorly deformable red blood cells by the human spleen can be mimicked in vitro. *Blood,* 117**,** e88-e95.

DI IORGI, N., ROSOL, M., MITTELMAN, S. D. & GILSANZ, V. 2008. Reciprocal Relation between Marrow Adiposity and the Amount of Bone in the Axial and Appendicular Skeleton of Young Adults. *The Journal of Clinical Endocrinology & Metabolism,* 93**,** 2281-2286.

DOGGA, S. K., ROP, J. C., CUDINI, J., FARR, E., DARA, A., OUOLOGUEM, D., DJIMDÉ, A. A., TALMAN, A. M. & LAWNICZAK, M. K. N. 2024. A single cell atlas of sexual development in Plasmodium falciparum. *Science,* 384**,** eadj4088.

DONDORP, A. M., DESAKORN, V., PONGTAVORNPINYO, W., SAHASSANANDA, D., SILAMUT, K., CHOTIVANICH, K., NEWTON, P. N., PITISUTTITHUM, P., SMITHYMAN, A. M., WHITE, N. J. & DAY, N. P. J. 2005. Estimation of the Total Parasite Biomass in Acute Falciparum Malaria from Plasma PfHRP2. *PLOS Medicine,* 2**,** e204.

DONDORP, A. M., FANELLO, C. I., HENDRIKSEN, I. C., GOMES, E., SENI, A., CHHAGANLAL, K. D., BOJANG, K., OLAOSEBIKAN, R., ANUNOBI, N., MAITLAND, K., KIVAYA, E., AGBENYEGA, T., NGUAH, S. B., EVANS, J., GESASE, S., KAHABUKA, C., MTOVE, G., NADJM, B., DEEN, J., MWANGA-AMUMPAIRE, J., NANSUMBA, M., KAREMA, C., UMULISA, N., UWIMANA, A., MOKUOLU, O. A., ADEDOYIN, O. T., JOHNSON, W. B., TSHEFU, A. K., ONYAMBOKO, M. A., SAKULTHAEW, T., NGUM, W. P., SILAMUT, K., STEPNIEWSKA, K., WOODROW, C. J., BETHELL, D., WILLS, B., ONEKO, M., PETO, T. E., VON SEIDLEIN, L., DAY, N. P. & WHITE, N. J. 2010. Artesunate versus quinine in the treatment of severe falciparum malaria in African children (AQUAMAT): an open-label, randomised trial. *Lancet,* 376**,** 1647-57.

DONDORP, A. M., NOSTEN, F., YI, P., DAS, D., PHYO, A. P., TARNING, J., LWIN, K. M., ARIEY, F., HANPITHAKPONG, W., LEE, S. J., RINGWALD, P., SILAMUT, K., IMWONG, M., CHOTIVANICH, K., LIM, P., HERDMAN, T., AN, S. S., YEUNG, S., SINGHASIVANON, P., DAY, N. P. J., LINDEGARDH, N., SOCHEAT, D. & WHITE, N. J. 2009. Artemisinin Resistance in Plasmodium falciparum Malaria. *New England Journal of Medicine,* 361, 455-467.

DUFFIER, Y., LORTHIOIS, A., CISTERÓ, P., DUPUY, F., JOUVION, G., FIETTE, L., MAZIER, D., MAYOR, A., LAVAZEC, C. & MORENO SABATER, A. 2016. A humanized mouse model for sequestration of Plasmodium falciparum sexual stages and in vivo evaluation of gametocytidal drugs. *Scientific Reports,* 6, 35025.

DUMARCHEY, A., LAVAZEC, C. & VERDIER, F. 2022. Erythropoiesis and Malaria, a Multifaceted Interplay. *International Journal of Molecular Sciences,* 23, 12762.

EKSI, S., MORAHAN, B. J., HAILE, Y., FURUYA, T., JIANG, H., ALI, O., XU, H., KIATTIBUTR, K., SURI, A., CZESNY, B., ADEYEMO, A., MYERS, T. G., SATTABONGKOT, J., SU, X. Z. & WILLIAMSON, K. C. 2012. Plasmodium falciparum gametocyte development 1 (Pfgdv1) and gametocytogenesis early gene identification and commitment to sexual development. *PLoS Pathog,* 8, e1002964.

EL BISSATI, K., ZUFFEREY, R., WITOLA, W. H., CARTER, N. S., ULLMAN, B. & BEN MAMOUN, C. 2006. The plasma membrane permease PfNT1 is essential for purine salvage in the human malaria parasite Plasmodium falciparum. *Proceedings of the National Academy of Sciences,* 103, 9286-9291.

ELLIOT, S. R. P., PAUL D. DUFFY, MICHAEL F. BYRNE, TIMOTHY J. THAM, WAI-HONG ROGERSON, STEPHEN J. BROWN, GRAHAM V. EISEN, DAMON P. 2007. Antibody Recognition of Heterologous Variant Surface Antigens after a Single Plasmodium falciparum Infection in Previously Naïve Adults. *The American Journal of Tropical Medicine and Hygiene Am J Trop Med Hyg,* 76, 860-864.

ELMORE, S. A. 2006. Enhanced histopathology of the bone marrow. *Toxicologic pathology,* 34, 666-686.

EMMANUEL, B. N., CHESSED, G., ERUKAINURE, F. E., EKEUHIE, J. C. & PHILIPS, V. 2023. Prevalence of malaria parasite and its effects on some hematological parameters amongst pregnant women in Yola, Nigeria. *Journal of Umm Al-Qura University for Applied Sciences.*

EPP, C., LI, F., HOWITT, C. A., CHOOKAJORN, T. & DEITSCH, K. W. 2009. Chromatin associated sense and antisense noncoding RNAs are transcribed from the var gene family of virulence genes of the malaria parasite Plasmodium falciparum. *Rna,* 15, 116-27.

EVERS, D. L., FOWLER, C. B., CUNNINGHAM, B. R., MASON, J. T. & O'LEARY, T. J. 2011. The effect of formaldehyde fixation on RNA: optimization of formaldehyde adduct removal. *J Mol Diagn,* 13, 282-8.

FARFOUR, E., CHARLOTTE, F., SETTEGRANA, C., MIYARA, M. & BUFFET, P. 2012. The extravascular compartment of the bone marrow: a niche for Plasmodium falciparum gametocyte maturation? *Malaria Journal,* 11, 285.

FARRINGTON, L., VANCE, H., REK, J., PRAHL, M., JAGANNATHAN, P., KATUREEBE, A., ARINAITWE, E., KAMYA, M. R., DORSEY, G. & FEENEY, M. E. 2017. Both inflammatory and regulatory cytokine responses to malaria are blunted with increasing age in highly exposed children. *Malar J,* 16, 499.

FILARSKY, M., FRASCHKA, S. A., NIEDERWIESER, I., BRANCUCCI, N. M. B., CARRINGTON, E., CARRIÓ, E., MOES, S., JENOE, P., BÁRTFAI, R. & VOSS, T. S. 2018. GDV1 induces sexual commitment of malaria parasites by antagonizing HP1-dependent gene silencing. *Science,* 359, 1259.

FINAK, G., MCDAVID, A., YAJIMA, M., DENG, J., GERSUK, V., SHALEK, A. K., SLICHTER, C. K., MILLER, H. W., MCELRATH, M. J., PRLIC, M., LINSLEY, P. S. & GOTTARDO, R. 2015. MAST: a flexible statistical framework for assessing transcriptional changes and characterizing heterogeneity in single-cell RNA sequencing data. *Genome Biology,* 16, 278.

FIORI, P. L., RAPPELLI, P., MIRKARIMI, S. N., GINSBURG, H., CAPPUCCINELLI, P. & TURRINI, F. 1993. Reduced microbicidal and anti-tumour activities of human monocytes after ingestion of Plasmodium falciparum-infected red blood cells. *Parasite Immunol,* 15, 647-55.

FLAMMERSFELD, A., LANG, C., FLIEGER, A. & PRADEL, G. 2018. Phospholipases during membrane dynamics in malaria parasites. *International Journal of Medical Microbiology,* 308, 129-141.

FLATEAU, C., LE LOUP, G. & PIALOUX, G. 2011. Consequences of HIV infection on malaria and therapeutic implications: a systematic review. *The Lancet. Infectious diseases,* 11, 541-556.

FLUECK, C., BARTFAI, R., VOLZ, J., NIEDERWIESER, I., SALCEDO-AMAYA, A. M., ALAKO, B. T. F., EHLGEN, F., RALPH, S. A., COWMAN, A. F., BOZDECH, Z., STUNNENBERG, H. G. & VOSS, T. S. 2009. Plasmodium falciparum Heterochromatin Protein 1 Marks Genomic Loci Linked to Phenotypic Variation of Exported Virulence Factors. *PLOS Pathogens,* 5, e1000569.

FOLEY, M., TILLEY, L., SAWYER, W. H. & ANDERS, R. F. 1991. The ring-infected erythrocyte surface antigen of Plasmodium falciparum associates with spectrin in the erythrocyte membrane. *Mol Biochem Parasitol,* 46, 137-47.

FRASCHKA, S. A., FILARSKY, M., HOO, R., NIEDERWIESER, I., YAM, X. Y., BRANCUCCI, N. M. B., MOHRING, F., MUSHUNJE, A. T., HUANG, X., CHRISTENSEN, P. R., NOSTEN, F., BOZDECH, Z., RUSSELL, B., MOON, R. W.,

MARTI, M., PREISER, P. R., BÁRTFAI, R. & VOSS, T. S. 2018. Comparative Heterochromatin Profiling Reveals Conserved and Unique Epigenome Signatures Linked to Adaptation and Development of Malaria Parasites. *Cell Host Microbe,* 23**,** 407-420.e8.

FRÖBEL, J., LANDSPERSKY, T., PERCIN, G., SCHRECK, C., RAHMIG, S., ORI, A., NOWAK, D., ESSERS, M., WASKOW, C. & OOSTENDORP, R. A. J. 2021. The Hematopoietic Bone Marrow Niche Ecosystem. *Frontiers in Cell and Developmental Biology,* 9.

FUJIMOTO, A., HAMAGUCHI, S. & SUZUKI, R. 2022. Case of Pulmonary Extramedullary Hematopoiesis Responding to Ruxolitinib. *Leukemia Research Reports,* 17**,** 100290.

GAFAN, C., WILSON, J., BERGER, L. C. & BERGER, B. J. 2001. Characterization of the ornithine aminotransferase from Plasmodium falciparum. *Molecular and Biochemical Parasitology,* 118**,** 1-10.

GALLOWAY, J. L. & ZON, L. I. 2003. 3 Ontogeny of hematopoiesis: Examining the emergence of hematopoietic cells in the vertebrate embryo. *Current Topics in Developmental Biology*. Academic Press.

GAMAIN, B., CHÊNE, A., VIEBIG, N. K., TUIKUE NDAM, N. & NIELSEN, M. A. 2021. Progress and Insights Toward an Effective Placental Malaria Vaccine. *Front Immunol,* 12**,** 634508.

GARDNER, M. J., HALL, N., FUNG, E., WHITE, O., BERRIMAN, M., HYMAN, R. W., CARLTON, J. M., PAIN, A., NELSON, K. E., BOWMAN, S., PAULSEN, I. T., JAMES, K., EISEN, J. A., RUTHERFORD, K., SALZBERG, S. L., CRAIG, A., KYES, S., CHAN, M.-S., NENE, V., SHALLOM, S. J., SUH, B., PETERSON, J., ANGIUOLI, S., PERTEA, M., ALLEN, J., SELENGUT, J., HAFT, D., MATHER, M. W., VAIDYA, A. B., MARTIN, D. M. A., FAIRLAMB, A. H., FRAUNHOLZ, M. J., ROOS, D. S., RALPH, S. A., MCFADDEN, G. I., CUMMINGS, L. M., SUBRAMANIAN, G. M., MUNGALL, C., VENTER, J. C., CARUCCI, D. J., HOFFMAN, S. L., NEWBOLD, C., DAVIS, R. W., FRASER, C. M. & BARRELL, B. 2002. Genome sequence of the human malaria parasite Plasmodium falciparum. *Nature,* 419**,** 498-511.

GHOSH, D. & STUMHOFER, J. S. 2021. The spleen: “epicenter” in malaria infection and immunity. *Journal of Leukocyte Biology,* 110**,** 753-769.

GIFRE-RENOM, L., DAEMS, M., LUTTUN, A. & JONES, E. A. V. 2022. Organ-Specific Endothelial Cell Differentiation and Impact of Microenvironmental Cues on Endothelial Heterogeneity. *Int J Mol Sci,* 23.

GLENISTER, F. K., COPPEL, R. L., COWMAN, A. F., MOHANDAS, N. & COOKE, B. M. 2002. Contribution of parasite proteins to altered mechanical properties of malaria-infected red blood cells. *Blood,* 99**,** 1060-3.

GOEL, S., VALIYAVEETTIL, M., ACHUR, R. N., GOYAL, A., MATTEI, D., SALANTI, A., TRENHOLME, K. R., GARDINER, D. L. & GOWDA, D. C. 2010. Dual stage synthesis and crucial role of cytoadherence-linked asexual gene 9 in the surface expression of malaria parasite var proteins. *Proc Natl Acad Sci U S A,* 107, 16643-8.

GOMEZ-PEREZ, G., VAN BRUGGEN, R., GROBUSCH, M. & DOBAÑO LÁZARO, C. 2014. Plasmodium falciparum malaria and invasive bacterial co-infection in young African children: The dysfunctional spleen hypothesis. *Malaria journal,* 13, 335.

GÓMEZ-PÉREZ, G. P., VAN BRUGGEN, R., GROBUSCH, M. P. & DOBAÑO, C. 2014. Plasmodium falciparum malaria and invasive bacterial co-infection in young African children: the dysfunctional spleen hypothesis. *Malaria Journal,* 13, 335.

GONZALES, S. J., REYES, R. A., BRADDOM, A. E., BATUGEDARA, G., BOL, S. & BUNNIK, E. M. 2020. Naturally Acquired Humoral Immunity Against Plasmodium falciparum Malaria. *Frontiers in Immunology,* 11.

GREISCHAR, M. A., MIDEO, N., READ, A. F. & BJØRNSTAD, O. N. 2016. Predicting optimal transmission investment in malaria parasites. *Evolution,* 70, 1542-58.

GRIFFITH, J. F. 2017. Age-Related Changes in the Bone Marrow. *Current Radiology Reports,* 5, 24.

GRIFFITHS, R. E., KUPZIG, S., COGAN, N., MANKELOW, T. J., BETIN, V. M., TRAKARNSANGA, K., MASSEY, E. J., PARSONS, S. F., ANSTEE, D. J. & LANE, J. D. 2012. The ins and outs of human reticulocyte maturation: autophagy and the endosome/exosome pathway. *Autophagy,* 8, 1150-1.

GROOM, A. C., SCHMIDT, E. E. & MACDONALD, I. C. 1991. Microcirculatory pathways and blood flow in spleen: new insights from washout kinetics, corrosion casts, and quantitative intravital videomicroscopy. *Scanning Microsc,* 5, 159-73; discussion 173-4.

GROOMES, P. V., KANJEE, U. & DURAISINGH, M. T. 2022. RBC membrane biomechanics and Plasmodium falciparum invasion: probing beyond ligand-receptor interactions. *Trends Parasitol,* 38, 302-315.

GRUENBERG, J., ALLRED, D. R. & SHERMAN, I. W. 1983. Scanning electron microscope-analysis of the protrusions (knobs) present on the surface of Plasmodium falciparum-infected erythrocytes. *J Cell Biol,* 97, 795-802.

GUO, L., WANG, Z., ANDERSON, C. M., DOOLITTLE, E., KERNAG, S., COTTA, C. V., ONDREJKA, S. L., MA, X. J. & COOK, J. R. 2018. Ultrasensitive automated RNA in situ hybridization for kappa and lambda light chain mRNA detects B-cell clonality in tissue biopsies with performance comparable or superior to flow cytometry. *Mod Pathol,* 31, 385-394.

GUPTA, A. P., CHIN, W. H., ZHU, L., MOK, S., LUAH, Y.-H., LIM, E.-H. & BOZDECH, Z. 2013. Dynamic Epigenetic Regulation of Gene Expression during the Life Cycle of Malaria Parasite Plasmodium falciparum. *PLOS Pathogens,* 9**,** e1003170.

GUPTA, S., KRISHNAN, A. S., SINGH, J., GUPTA, A. & GUPTA, M. 2022. Clinicopathological characteristics and management of extramedullary hematopoiesis: A review. *Pediatric Hematology Oncology Journal,* 7**,** 182-186.

GUPTA, S., SNOW, R. W., DONNELLY, C. A., MARSH, K. & NEWBOLD, C. 1999. Immunity to non-cerebral severe malaria is acquired after one or two infections. *Nat Med,* 5**,** 340-3.

HAASE, S., CONDRON, M., MILLER, D., CHERKAOUI, D., JORDAN, S., GULBIS, J. M. & BAUM, J. 2021. Identification and characterisation of a phospholipid scramblase in the malaria parasite Plasmodium falciparum. *Mol Biochem Parasitol,* 243**,** 111374.

HALDAR, K., MURPHY, S. C., DAN A. MILNER, J. & TAYLOR, T. E. 2007. Malaria: Mechanisms of Erythrocytic Infection and Pathological Correlates of Severe Disease. *Annual Review of Pathology: Mechanisms of Disease,* 2**,** 217-249.

HAMID, M. M., MOHAMMED, S. B. & EL HASSAN, I. M. 2013. Genetic Diversity of Plasmodium falciparum Field Isolates in Central Sudan Inferred by PCR Genotyping of Merozoite Surface Protein 1 and 2. *N Am J Med Sci,* 5**,** 95-101.

HANDUNNETTI, S. M., DAVID, P. H., PERERA, K. L. & MENDIS, K. N. 1989. Uninfected erythrocytes form "rosettes" around Plasmodium falciparum infected erythrocytes. *Am J Trop Med Hyg,* 40**,** 115-8.

HAO, Y., HAO, S., ANDERSEN-NISSEN, E., MAUCK, W. M., ZHENG, S., BUTLER, A., LEE, M. J., WILK, A. J., DARBY, C., ZAGER, M., HOFFMAN, P., STOECKIUS, M., PAPALEXI, E., MIMITOU, E. P., JAIN, J., SRIVASTAVA, A., STUART, T., FLEMING, L. M., YEUNG, B., ROGERS, A. J., MCELRATH, J. M., BLISH, C. A., GOTTARDO, R., SMIBERT, P. & SATIJA, R. 2021. Integrated analysis of multimodal single-cell data. *Cell,* 184**,** 3573-3587.e29.

HAQUE, A., ENGEL, J., TEICHMANN, S. A. & LÖNNBERG, T. 2017. A practical guide to single-cell RNA-sequencing for biomedical research and clinical applications. *Genome Medicine,* 9**,** 75.

HE, S., BHATT, R., BROWN, C., BROWN, E. A., BUHR, D. L., CHANTRANUVATANA, K., DANAHER, P., DUNAWAY, D., GARRISON, R. G., GEISS, G., GREGORY, M. T., HOANG, M. L., KHAFIZOV, R., KILLINGBECK, E. E., KIM, D., KIM, T. K., KIM, Y., KLOCK, A., KORUKONDA, M., KUTCHMA, A., LEWIS, Z. R., LIANG, Y., NELSON, J. S., ONG, G. T., PERILLO, E. P., PHAN, J. C., PHAN-EVERSON, T., PIAZZA, E., RANE, T., REITZ, Z., RHODES, M., ROSENBLOOM, A., ROSS, D., SATO, H., WARDHANI, A. W., WILLIAMS-WIETZIKOSKI, C. A., WU, L. &

BEECHEM, J. M. 2022. High-plex imaging of RNA and proteins at subcellular resolution in fixed tissue by spatial molecular imaging. *Nat Biotechnol,* 40**,** 1794-1806.

HEDLUND, E. & DENG, Q. 2018. Single-cell RNA sequencing: Technical advancements and biological applications. *Molecular Aspects of Medicine,* 59**,** 36-46.

HELLER, T., TACCARI, F., RAMBIKI, K., KUMWENDA, T., BRUNETTI, E. & WALLRAUCH, C. 2023. “Sponge pattern” of the spleen: a rarely described high-frequency ultrasound pattern in HIV-positive patients. *The Ultrasound Journal,* 15**,** 6.

HENDRIKSEN, I. C. E., MWANGA-AMUMPAIRE, J., VON SEIDLEIN, L., MTOVE, G., WHITE, L. J., OLAOSEBIKAN, R., LEE, S. J., TSHEFU, A. K., WOODROW, C., AMOS, B., KAREMA, C., SAIWAEW, S., MAITLAND, K., GOMES, E., PAN-NGUM, W., GESASE, S., SILAMUT, K., REYBURN, H., JOSEPH, S., CHOTIVANICH, K., FANELLO, C. I., DAY, N. P. J., WHITE, N. J. & DONDORP, A. M. 2012. Diagnosing Severe Falciparum Malaria in Parasitaemic African Children: A Prospective Evaluation of Plasma PfHRP2 Measurement. *PLOS Medicine,* 9**,** e1001297.

HENTZSCHEL, F., GIBBINS, M. P., ATTIPA, C., BERALDI, D., MOXON, C. A., OTTO, T. D. & MARTI, M. 2022. Host cell maturation modulates parasite invasion and sexual differentiation in Plasmodium berghei. *Sci Adv,* 8**,** eabm7348.

HERMIDA, M. D. E.-R., DE MELO, C. V. B., LIMA, I. D. S., OLIVEIRA, G. G. D. S. & DOS-SANTOS, W. L. C. 2018. Histological Disorganization of Spleen Compartments and Severe Visceral Leishmaniasis. *Frontiers in cellular and infection microbiology,* 8**,** 394-394.

HO, M., WHITE, N. J., LOOAREESUWAN, S., WATTANAGOON, Y., LEE, S. H., WALPORT, M. J., BUNNAG, D. & HARINASUTA, T. 1990. Splenic Fc receptor function in host defense and anemia in acute Plasmodium falciparum malaria. *J Infect Dis,* 161**,** 555-61.

HODDER, A. N., MAIER, A. G., RUG, M., BROWN, M., HOMMEL, M., PANTIC, I., PUIG-DE-MORALES-MARINKOVIC, M., SMITH, B., TRIGLIA, T., BEESON, J. & COWMAN, A. F. 2009. Analysis of structure and function of the giant protein Pf332 in Plasmodium falciparum. *Mol Microbiol,* 71**,** 48-65.

HOFFMAN, S., BANCROFT, W., GOTTLIEB, M., JAMES, S., BURROUGHS, E., STEPHENSON, J. & MORGAN, M. 1997. Funding for malaria genome sequencing. *Nature,* 387**,** 647.

HOLLIN, T., CHAHINE, Z. & LE ROCH, K. G. 2023. Epigenetic Regulation and Chromatin Remodeling in Malaria Parasites. *Annu Rev Microbiol,* 77**,** 255-276.

HOLLIN, T. & LE ROCH, K. G. 2020. From Genes to Transcripts, a Tightly Regulated Journey in Plasmodium. *Frontiers in Cellular and Infection Microbiology,* 10.

HOMMEL, M., ELLIOTT, S. R., SOMA, V., KELLY, G., FOWKES, F. J., CHESSON, J. M., DUFFY, M. F., BOCKHORST, J., AVRIL, M., MUELLER, I., RAIKO, A., STANISIC, D. I., ROGERSON, S. J., SMITH, J. D. & BEESON, J. G. 2010. Evaluation of the antigenic diversity of placenta-binding Plasmodium falciparum variants and the antibody repertoire among pregnant women. *Infect Immun,* 78**,** 1963-78.

HOUZÉ, S., BOLY, M. D., LE BRAS, J., DELORON, P. & FAUCHER, J. F. 2009. PfHRP2 and PfLDH antigen detection for monitoring the efficacy of artemisinin-based combination therapy (ACT) in the treatment of uncomplicated falciparum malaria. *Malar J,* 8**,** 211.

HOWICK, V. M., RUSSELL, A. J. C., ANDREWS, T., HEATON, H., REID, A. J., NATARAJAN, K., BUTUNGI, H., METCALF, T., VERZIER, L. H., RAYNER, J. C., BERRIMAN, M., HERREN, J. K., BILLKER, O., HEMBERG, M., TALMAN, A. M. & LAWNICZAK, M. K. N. 2019. The Malaria Cell Atlas: Single parasite transcriptomes across the complete Plasmodium life cycle. *Science,* 365.

HOWIE, S. R. 2011. Blood sample volumes in child health research: review of safe limits. *Bull World Health Organ,* 89**,** 46-53.

HSIEH, F. L., TURNER, L., BOLLA, J. R., ROBINSON, C. V., LAVSTSEN, T. & HIGGINS, M. K. 2016. The structural basis for CD36 binding by the malaria parasite. *Nat Commun,* 7**,** 12837.

HUANG, L. & APPLETON, J. A. 2016. Eosinophils in Helminth Infection: Defenders and Dupes. *Trends in parasitology,* 32**,** 798-807.

HUANG, Y. H., SCHÄFER-ELINDER, L., WU, R., CLAESSON, H. E. & FROSTEGÅRD, J. 1999. Lysophosphatidylcholine (LPC) induces proinflammatory cytokines by a platelet-activating factor (PAF) receptor-dependent mechanism. *Clin Exp Immunol,* 116**,** 326-31.

HUNT, M., SILVA, N. D., OTTO, T. D., PARKHILL, J., KEANE, J. A. & HARRIS, S. R. 2015. Circlator: automated circularization of genome assemblies using long sequencing reads. *Genome Biol,* 16**,** 294.

ICRP 2020. Paediatric Computational Reference Phantoms. ICRP Publication 143. Ann. ICRP 49(1) ed.

IHC-WORLD. 2022. *Methods and Protocols for Decalcification of Bone Material* [Online]. Available: https://ihcworld.com/2024/01/25/methods-and-protocols-for-decalcification-of-bone-material/ [Accessed 14th Nov 2022].

IQBAL, J., SIDDIQUE, A., JAMEEL, M. & HIRA, P. R. 2004. Persistent histidine-rich protein 2, parasite lactate dehydrogenase, and panmalarial antigen reactivity after clearance of Plasmodium falciparum monoinfection. *J Clin Microbiol,* 42**,** 4237-41.

ITO, D., SCHURECK, M. A. & DESAI, S. A. 2017. An essential dual-function complex mediates erythrocyte invasion and channel-mediated nutrient uptake in malaria parasites. *eLife,* 6**,** e23485.

IWANAGA, S., KANEKO, I., KATO, T. & YUDA, M. 2012. Identification of an AP2-family Protein That Is Critical for Malaria Liver Stage Development. *PLOS ONE,* 7**,** e47557.

JACKSON, A., NANTON, M. R., O'DONNELL, H., AKUE, A. D. & MCSORLEY, S. J. 2010. Innate immune activation during Salmonella infection initiates extramedullary erythropoiesis and splenomegaly. *J Immunol,* 185**,** 6198-204.

JAURÉGUIBERRY, S., NDOUR, P. A., ROUSSEL, C., ADER, F., SAFEUKUI, I., NGUYEN, M., BILIGUI, S., CICERON, L., MOURI, O., KENDJO, E., BRICAIRE, F., VRAY, M., ANGOULVANT, A., MAYAUX, J., HALDAR, K., MAZIER, D., DANIS, M., CAUMES, E., THELLIER, M., BUFFET, P. & GROUP, T. F. A. W. 2014. Postartesunate delayed hemolysis is a predictable event related to the lifesaving effect of artemisinins. *Blood,* 124**,** 167-175.

JIANG, H., YI, M., MU, J., ZHANG, L., IVENS, A., KLIMCZAK, L. J., HUYEN, Y., STEPHENS, R. M. & SU, X. Z. 2008. Detection of genome-wide polymorphisms in the AT-rich Plasmodium falciparum genome using a high-density microarray. *BMC Genomics,* 9**,** 398.

JING, Q., CAO, L., ZHANG, L., CHENG, X., GILBERT, N., DAI, X., SUN, M., LIANG, S. & JIANG, L. 2018. Plasmodium falciparum var Gene Is Activated by Its Antisense Long Noncoding RNA. *Front Microbiol,* 9**,** 3117.

JOICE, R., FRANTZREB, C., PRADHAM, A., SEYDEL, K. B., KAMIZA, S., WIRTH, D. F., DURAISINGH, M. T., MOLYNEUX, M. E., TAYLOR, T. E., MARTI, M. & MILNER JR, D. A. 2016. Evidence for spleen dysfunction in malaria-HIV co-infection in a subset of pediatric patients. *Modern Pathology,* 29**,** 381-390.

JOICE, R., NILSSON, S. K., MONTGOMERY, J., DANKWA, S., EGAN, E., MORAHAN, B., SEYDEL, K. B., BERTUCCINI, L., ALANO, P., WILLIAMSON, K. C., DURAISINGH, M. T., TAYLOR, T. E., MILNER, D. A. & MARTI, M. 2014. Plasmodium falciparum transmission stages accumulate in the human bone marrow. *Sci Transl Med,* 6**,** 244re5.

KADEKOPPALA, M., OGUN, S. A., HOWELL, S., GUNARATNE, R. S. & HOLDER, A. A. 2010. Systematic genetic analysis of the Plasmodium falciparum MSP7-like family reveals differences in protein expression, location, and importance in asexual growth of the blood-stage parasite. *Eukaryot Cell,* 9**,** 1064-74.

KAFSACK, B. F. C., ROVIRA-GRAELLS, N., CLARK, T. G., BANCELLS, C., CROWLEY, V. M., CAMPINO, S. G., WILLIAMS, A. E., DROUGHT, L. G., KWIATKOWSKI, D. P., BAKER, D. A., CORTÉS, A. & LLINÁS, M. 2014. A transcriptional switch underlies commitment to sexual development in malaria parasites. *Nature,* 507**,** 248-252.

KANEKO, O., LIM, B. Y. S. Y., IRIKO, H., LING, I. T., OTSUKI, H., GRAINGER, M., TSUBOI, T., ADAMS, J. H., MATTEI, D., HOLDER, A. A. & TORII, M. 2005. Apical expression of three RhopH1/Clag proteins as components of the Plasmodium falciparum RhopH complex. *Molecular and Biochemical Parasitology,* 143**,** 20-28.

KANEKO, O., TSUBOI, T., LING, I. T., HOWELL, S., SHIRANO, M., TACHIBANA, M., CAO, Y.-M., HOLDER, A. A. & TORII, M. 2001. The high molecular mass rhoptry protein, RhopH1, is encoded by members of the clag multigene family in Plasmodium falciparum and Plasmodium yoelii. *Molecular and Biochemical Parasitology,* 118**,** 223-231.

KANG, H. M., SUBRAMANIAM, M., TARG, S., NGUYEN, M., MALISKOVA, L., MCCARTHY, E., WAN, E., WONG, S., BYRNES, L., LANATA, C. M., GATE, R. E., MOSTAFAVI, S., MARSON, A., ZAITLEN, N., CRISWELL, L. A. & YE, C. J. 2018. Multiplexed droplet single-cell RNA-sequencing using natural genetic variation. *Nature Biotechnology,* 36**,** 89-94.

KAPILA, V., WEHRLE, C. J. & TUMA, F. 2023. Physiology, Spleen. *StatPearls*. Treasure Island (FL) ineligible companies. Disclosure: Chase Wehrle declares no relevant financial relationships with ineligible companies. Disclosure: Faiz Tuma declares no relevant financial relationships with ineligible companies.: StatPearls Publishing
Copyright © 2023, StatPearls Publishing LLC.

KHALIL, S. H., NOUNOU, R. M., FRAYHA, H., HALIM, M. A., ELLIS, M. & BLACK, F. T. 1996. Bone Marrow Morphologic Findings in Patients with Human Immunodeficiency Virus (HIV) Infection. *Annals of Saudi Medicine,* 16**,** 16-19.

KHO, S., QOTRUNNADA, L., LEONARDO, L., ANDRIES, B., WARDANI, P. A. I., FRICOT, A., HENRY, B., HARDY, D., MARGYANINGSIH, N. I., APRIYANTI, D., PUSPITASARI, A. M., PRAYOGA, P., TRIANTY, L., KENANGALEM, E., CHRETIEN, F., BROUSSE, V., SAFEUKUI, I., DEL PORTILLO, H. A., FERNANDEZ-BECERRA, C., MEIBALAN, E., MARTI, M., PRICE, R. N., WOODBERRY, T., NDOUR, P. A., RUSSELL, B. M., YEO, T. W., MINIGO, G., NOVIYANTI, R., POESPOPRODJO, J. R., SIREGAR, N. C., BUFFET, P. A. & ANSTEY, N. M. 2021a. Evaluation of splenic accumulation and colocalization of immature reticulocytes and Plasmodium vivax in asymptomatic malaria: A prospective human splenectomy study. *PLOS Medicine,* 18**,** e1003632.

KHO, S., QOTRUNNADA, L., LEONARDO, L., ANDRIES, B., WARDANI, P. A. I., FRICOT, A., HENRY, B., HARDY, D., MARGYANINGSIH, N. I., APRIYANTI, D., PUSPITASARI, A. M., PRAYOGA, P., TRIANTY, L., KENANGALEM, E., CHRETIEN, F., SAFEUKUI, I., DEL PORTILLO, H. A., FERNANDEZ-BECERRA,

C., MEIBALAN, E., MARTI, M., PRICE, R. N., WOODBERRY, T., NDOUR, P. A., RUSSELL, B. M., YEO, T. W., MINIGO, G., NOVIYANTI, R., POESPOPRODJO, J. R., SIREGAR, N. C., BUFFET, P. A. & ANSTEY, N. M. 2021b. Hidden Biomass of Intact Malaria Parasites in the Human Spleen. *New England Journal of Medicine,* 384**,** 2067-2069.

KHOURY, D. S., CROMER, D., BEST, S. E., JAMES, K. R., KIM, P. S., ENGWERDA, C. R., HAQUE, A. & DAVENPORT, M. P. 2014. Effect of mature blood-stage Plasmodium parasite sequestration on pathogen biomass in mathematical and in vivo models of malaria. *Infect Immun,* 82**,** 212-20.

KIM, Y. L., IM, Y. J., HA, N. C. & IM, D. S. 2007. Albumin inhibits cytotoxic activity of lysophosphatidylcholine by direct binding. *Prostaglandins Other Lipid Mediat,* 83**,** 130-8.

KISELEV, V. Y., YIU, A. & HEMBERG, M. 2018. scmap: projection of single-cell RNA-seq data across data sets. *Nature Methods,* 15**,** 359-362.

KLEI, T. R. L., MEINDERTS, S. M., VAN DEN BERG, T. K. & VAN BRUGGEN, R. 2017. From the Cradle to the Grave: The Role of Macrophages in Erythropoiesis and Erythrophagocytosis. *Frontiers in Immunology,* 8.

KOLODZIEJCZYK, ALEKSANDRA A., KIM, J. K., SVENSSON, V., MARIONI, JOHN C. & TEICHMANN, SARAH A. 2015. The Technology and Biology of Single-Cell RNA Sequencing. *Molecular Cell,* 58**,** 610-620.

KOPERSKA, M. 2023. *Pediatric Blood Volume Calculator* [Online]. Available: https://www.omnicalculator.com/health/pediatric-blood-volume [Accessed 2nd January 2024].

KORSUNSKY, I., MILLARD, N., FAN, J., SLOWIKOWSKI, K., ZHANG, F., WEI, K., BAGLAENKO, Y., BRENNER, M., LOH, P.-R. & RAYCHAUDHURI, S. 2019. Fast, sensitive and accurate integration of single-cell data with Harmony. *Nature Methods,* 16**,** 1289-1296.

KRIEK, N., TILLEY, L., HORROCKS, P., PINCHES, R., ELFORD, B. C., FERGUSON, D. J. P., LINGELBACH, K. & NEWBOLD, C. I. 2003. Characterization of the pathway for transport of the cytoadherence-mediating protein, PfEMP1, to the host cell surface in malaria parasite-infected erythrocytes. *Molecular Microbiology,* 50**,** 1215-1227.

KROTOSKI, W. A. 1985. Discovery of the hypnozoite and a new theory of malarial relapse. *Trans R Soc Trop Med Hyg,* 79**,** 1-11.

KUN, J. F., WALLER, K. L. & COPPEL, R. L. 1999. Plasmodium falciparum: structural and functional domains of the mature-parasite-infected erythrocyte surface antigen. *Exp Parasitol,* 91**,** 258-67.

LAISHRAM, D. D., SUTTON, P. L., NANDA, N., SHARMA, V. L., SOBTI, R. C., CARLTON, J. M. & JOSHI, H. 2012. The complexities of malaria disease manifestations with a focus on asymptomatic malaria. *Malaria Journal,* 11**,** 29.

LAMBROS, C. & VANDERBERG, J. P. 1979. Synchronization of Plasmodium falciparum erythrocytic stages in culture. *J Parasitol,* 65**,** 418-20.

LAMIKANRA, A. A., BROWN, D., POTOCNIK, A., CASALS-PASCUAL, C., LANGHORNE, J. & ROBERTS, D. J. 2007. Malarial anemia: of mice and men. *Blood,* 110**,** 18-28.

LANGHORNE, J., NDUNGU, F. M., SPONAAS, A.-M. & MARSH, K. 2008. Immunity to malaria: more questions than answers. *Nature Immunology,* 9**,** 725-732.

LANGRETH, S. G., JENSEN, J. B., REESE, R. T. & TRAGER, W. 1978. Fine structure of human malaria in vitro. *J Protozool,* 25**,** 443-52.

LAW, S. H., CHAN, M. L., MARATHE, G. K., PARVEEN, F., CHEN, C. H. & KE, L. Y. 2019. An Updated Review of Lysophosphatidylcholine Metabolism in Human Diseases. *Int J Mol Sci,* 20.

LE ROCH, K. G., ZHOU, Y., BLAIR, P. L., GRAINGER, M., MOCH, J. K., HAYNES, J. D., DE LA VEGA, P., HOLDER, A. A., BATALOV, S., CARUCCI, D. J. & WINZELER, E. A. 2003. Discovery of Gene Function by Expression Profiling of the Malaria Parasite Life Cycle. *Science,* 301**,** 1503-1508.

LEE, R. S., WATERS, A. P. & BREWER, J. M. 2018. A cryptic cycle in haematopoietic niches promotes initiation of malaria transmission and evasion of chemotherapy. *Nature Communications,* 9**,** 1689.

LEE, S.-K., HAN, J.-H., PARK, J.-H., HA, K.-S., PARK, W. S., HONG, S.-H., NA, S., CHENG, Y. & HAN, E.-T. 2019. Evaluation of antibody responses to the early transcribed membrane protein family in Plasmodium vivax. *Parasites & Vectors,* 12**,** 594.

LEE, W.-C., RUSSELL, B. & RÉNIA, L. 2022. Evolving perspectives on rosetting in malaria. *Trends in Parasitology,* 38**,** 882-889.

LEE, W.-C., RUSSELL, B., SOBOTA, R. M., GHAFFAR, K., HOWLAND, S. W., WONG, Z. X., MAIER, A. G., DORIN-SEMBLAT, D., BISWAS, S., GAMAIN, B., LAU, Y.-L., MALLERET, B., CHU, C., NOSTEN, F. & RENIA, L. 2020. Plasmodium-infected erythrocytes induce secretion of IGFBP7 to form type II rosettes and escape phagocytosis. *eLife,* 9**,** e51546.

LEECH, J. H., BARNWELL, J. W., MILLER, L. H. & HOWARD, R. J. 1984. Identification of a strain-specific malarial antigen exposed on the surface of Plasmodium falciparum-infected erythrocytes. *J Exp Med,* 159**,** 1567-75.

LEONG, Y. W., RUSSELL, B., MALLERET, B. & RÉNIA, L. 2022. Erythrocyte tropism of malarial parasites: The reticulocyte appeal. *Frontiers in Microbiology,* 13.

LEOWATTANA, W., KRUDSOOD, S., TANGPUKDEE, N., BRITTENHAM, G. & LOOAREESUWAN, S. 2008. Defective erythropoietin production and reticulocyte response in acute Plasmodium falciparum malaria-associated anemia. *Southeast Asian J Trop Med Public Health,* 39**,** 581-8.

LEWIS, S. M., WILLIAMS, A. & EISENBARTH, S. C. 2019. Structure and function of the immune system in the spleen. *Science immunology,* 4**,** eaau6085.

LI, H., LIU, Z. L., LU, L., BUFFET, P. & KARNIADAKIS, G. E. 2021a. How the spleen reshapes and retains young and old red blood cells: A computational investigation. *PLOS Computational Biology,* 17**,** e1009516.

LI, J., SHAMI, G. J., CHO, E., LIU, B., HANSSEN, E., DIXON, M. W. A. & TILLEY, L. 2022. Repurposing the mitotic machinery to drive cellular elongation and chromatin reorganisation in Plasmodium falciparum gametocytes. *Nat Commun,* 13**,** 5054.

LI, Y., BAPTISTA, R. P., SATERIALE, A., STRIEPEN, B. & KISSINGER, J. C. 2021b. Analysis of Long Non-Coding RNA in Cryptosporidium parvum Reveals Significant Stage-Specific Antisense Transcription. *Frontiers in Cellular and Infection Microbiology,* 10.

LINDBLADE, K. A., STEINHARDT, L., SAMUELS, A., KACHUR, S. P. & SLUTSKER, L. 2013. The silent threat: asymptomatic parasitemia and malaria transmission. *Expert Rev Anti Infect Ther,* 11**,** 623-39.

LIU, J., FIKE, K. R., DAPPER, C. & KLEMBA, M. 2024. Metabolism of host lysophosphatidylcholine in Plasmodium falciparum-infected erythrocytes. *Proceedings of the National Academy of Sciences,* 121**,** e2320262121.

LIU, J., ZHANG, J., GINZBURG, Y., LI, H., XUE, F., DE FRANCESCHI, L., CHASIS, J. A., MOHANDAS, N. & AN, X. 2013. Quantitative analysis of murine terminal erythroid differentiation in vivo: novel method to study normal and disordered erythropoiesis. *Blood,* 121**,** e43-e49.

LLINÁS, M., BOZDECH, Z., WONG, E. D., ADAI, A. T. & DERISI, J. L. 2006. Comparative whole genome transcriptome analysis of three Plasmodium falciparum strains. *Nucleic Acids Research,* 34**,** 1166-1173.

LLORÀ-BATLLE, O., MICHEL-TODÓ, L., WITMER, K., TODA, H., FERNÁNDEZ-BECERRA, C., BAUM, J. & CORTÉS, A. 2020. Conditional expression of PfAP2-G for controlled massive sexual conversion in <em>Plasmodium falciparum</em&gt. *Science Advances,* 6**,** eaaz5057.

LOKKEN, K. L., STULL-LANE, A. R., POELS, K. & TSOLIS, R. M. 2018. Malaria Parasite-Mediated Alteration of Macrophage Function and Increased Iron Availability Predispose to Disseminated Nontyphoidal Salmonella Infection. *Infect Immun,* 86.

LOMBERK, G., WALLRATH, L. & URRUTIA, R. 2006. The Heterochromatin Protein 1 family. *Genome Biology,* 7**,** 228.

LOOKER, O., BLANCH, A. J., LIU, B., NUNEZ-IGLESIAS, J., MCMILLAN, P. J., TILLEY, L. & DIXON, M. W. A. 2019. The knob protein KAHRP assembles into a ring-shaped structure that underpins virulence complex assembly. *PLOS Pathogens,* 15**,** e1007761.

LÓPEZ-BARRAGÁN, M. J., LEMIEUX, J., QUIÑONES, M., WILLIAMSON, K. C., MOLINA-CRUZ, A., CUI, K., BARILLAS-MURY, C., ZHAO, K. & SU, X. Z. 2011. Directional gene expression and antisense transcripts in sexual and asexual stages of Plasmodium falciparum. *BMC Genomics,* 12**,** 587.

LOPEZ-RUBIO, J.-J., MANCIO-SILVA, L. & SCHERF, A. 2009. Genome-wide Analysis of Heterochromatin Associates Clonally Variant Gene Regulation with Perinuclear Repressive Centers in Malaria Parasites. *Cell Host & Microbe,* 5**,** 179-190.

LOUBENS, M., VINCENSINI, L., FERNANDES, P., BRIQUET, S., MARINACH, C. & SILVIE, O. 2021. Plasmodium sporozoites on the move: Switching from cell traversal to productive invasion of hepatocytes. *Mol Microbiol,* 115**,** 870-881.

LUCAS, D. 2017. The Bone Marrow Microenvironment for Hematopoietic Stem Cells. *In:* BIRBRAIR, A. (ed.) *Stem Cell Microenvironments and Beyond.* Cham: Springer International Publishing.

LUCAS, D. 2021. Structural organization of the bone marrow and its role in hematopoiesis. *Curr Opin Hematol,* 28**,** 36-42.

LUGER, K., MÄDER, A. W., RICHMOND, R. K., SARGENT, D. F. & RICHMOND, T. J. 1997. Crystal structure of the nucleosome core particle at 2.8 Å resolution. *Nature,* 389**,** 251-260.

LUN, A., MCCARTHY, D. & MARIONI, J. 2016. A step-by-step workflow for low-level analysis of single-cell RNA-seq data with Bioconductor [version 2; peer review: 3 approved, 2 approved with reservations]. *F1000Research,* 5.

MACHADO SIQUEIRA, A., LOPES MAGALHÃES, B. M., CARDOSO MELO, G., FERRER, M., CASTILLO, P., MARTIN-JAULAR, L., FERNANDEZ-BECERRA, C., ORDI, J., MARTINEZ, A., LACERDA, M. V. G. & DEL PORTILLO, H. A. 2012. Spleen Rupture in a Case of Untreated Plasmodium vivax Infection. *PLOS Neglected Tropical Diseases,* 6**,** e1934.

MAIER, A. G., COOKE, B. M., COWMAN, A. F. & TILLEY, L. 2009. Malaria parasite proteins that remodel the host erythrocyte. *Nature Reviews Microbiology,* 7, 341-354.

MAIER, A. G., RUG, M., O'NEILL, M. T., BROWN, M., CHAKRAVORTY, S., SZESTAK, T., CHESSON, J., WU, Y., HUGHES, K., COPPEL, R. L., NEWBOLD, C., BEESON, J. G., CRAIG, A., CRABB, B. S. & COWMAN, A. F. 2008. Exported proteins required for virulence and rigidity of Plasmodium falciparum-infected human erythrocytes. *Cell,* 134, 48-61.

MAIR, Y., ZHENG, Y. & CAI, D. 2013. Dysmegakaryocytopoiesis and maintaining platelet count in patients with plasma cell neoplasm. *N Am J Med Sci,* 5, 316-9.

MALLERET, B., XU, F., MOHANDAS, N., SUWANARUSK, R., CHU, C., LEITE, J. A., LOW, K., TURNER, C., SRIPRAWAT, K., ZHANG, R., BERTRAND, O., COLIN, Y., COSTA, F. T. M., ONG, C. N., NG, M. L., LIM, C. T., NOSTEN, F., RÉNIA, L. & RUSSELL, B. 2013. Significant Biochemical, Biophysical and Metabolic Diversity in Circulating Human Cord Blood Reticulocytes. *PLOS ONE,* 8, e76062.

MANDALA, W. L., GONDWE, E. N., MACLENNAN, J. M., MOLYNEUX, M. E. & MACLENNAN, C. A. 2017. Age- and sex-related changes in hematological parameters in healthy Malawians. *J Blood Med,* 8, 123-130.

MANSON, P. 1900. Experimental Proof of the Mosquitomalaria Theory. *Br Med J,* 2, 949-51.

MANSON, P. T. 1901. Experimental Malaria: Recurrence after Nine Months. *Br Med J,* 2, 77.

MANTEL, P. Y., HOANG, A. N., GOLDOWITZ, I., POTASHNIKOVA, D., HAMZA, B., VOROBJEV, I., GHIRAN, I., TONER, M., IRIMIA, D., IVANOV, A. R., BARTENEVA, N. & MARTI, M. 2013. Malaria-infected erythrocyte-derived microvesicles mediate cellular communication within the parasite population and with the host immune system. *Cell Host Microbe,* 13, 521-534.

MARCHIAFAVA, E. B., A. 1894. A. Sulle febbri estivo annali. *E. Loescher*.

MARCIAL-JUÁREZ, E., PÉREZ-TOLEDO, M., NAYAR, S., PIPI, E., ALSHAYEA, A., PERSAUD, R., JOSSI, S. E., LAMERTON, R., BARONE, F., HENDERSON, I. R. & CUNNINGHAM, A. F. 2023. Salmonella infection induces the reorganization of follicular dendritic cell networks concomitant with the failure to generate germinal centers. *iScience,* 26, 106310.

MARKUS, M. B. 2017. Malaria Eradication and the Hidden Parasite Reservoir. *Trends in Parasitology,* 33, 492-495.

MARTINS, R. M., MACPHERSON, C. R., CLAES, A., SCHEIDIG-BENATAR, C., SAKAMOTO, H., YAM, X. Y., PREISER, P., GOEL, S., WAHLGREN, M., SISMEIRO, O., COPPÉE, J.-Y. & SCHERF, A. 2017. An ApiAP2 member regulates expression of clonally variant genes of the human malaria parasite Plasmodium falciparum. *Scientific Reports,* 7**,** 14042.

MASUDA, N., OHNISHI, T., KAWAMOTO, S., MONDEN, M. & OKUBO, K. 1999. Analysis of chemical modification of RNA from formalin-fixed samples and optimization of molecular biology applications for such samples. *Nucleic Acids Res,* 27**,** 4436-43.

MATANGILA, J. R., MITASHI, P., INOCÊNCIO DA LUZ, R. A., LUTUMBA, P. T. & VAN GEERTRUYDEN, J.-P. 2015. Efficacy and safety of intermittent preventive treatment for malaria in schoolchildren: a systematic review. *Malaria Journal,* 14**,** 450.

MATTEI, D. & SCHERF, A. 1992. The Pf332 gene of Plasmodium falciparum codes for a giant protein that is translocated from the parasite to the membrane of infected erythrocytes. *Gene,* 110**,** 71-9.

MAYER, J. & DONNELLY, T. M. 2013. Reticulocyte Count. *Clinical Veterinary Advisor*. Saint Louis: W.B. Saunders.

MAYXAY, M., PUKRITTAYAKAMEE, S., CHOTIVANICH, K., LOOAREESUWAN, S. & WHITE, N. J. 2001. Persistence of Plasmodium falciparum HRP-2 in successfully treated acute falciparum malaria. *Trans R Soc Trop Med Hyg,* 95**,** 179-82.

MCBRIDE, J. S., NEWBOLD, C. I. & ANAND, R. 1985. Polymorphism of a high molecular weight schizont antigen of the human malaria parasite Plasmodium falciparum. *Journal of Experimental Medicine,* 161**,** 160-180.

MCCUTCHAN, T. F., PIPER, R. C. & MAKLER, M. T. 2008. Use of malaria rapid diagnostic test to identify Plasmodium knowlesi infection. *Emerg Infect Dis,* 14**,** 1750-2.

MCGREGOR, A., DOHERTY, T., LOWE, P., CHIODINI, P. & NEWSHOLME, W. 2015. Hyperreactive Malarial Splenomegaly Syndrome--Can the Diagnostic Criteria Be Improved? *Am J Trop Med Hyg,* 93**,** 573-6.

MCMURRAY, H. F., PARTHASARATHY, S. & STEINBERG, D. 1993. Oxidatively modified low density lipoprotein is a chemoattractant for human T lymphocytes. *J Clin Invest,* 92**,** 1004-8.

MEBIUS, R. E. & KRAAL, G. 2005. Structure and function of the spleen. *Nature Reviews Immunology,* 5**,** 606-616.

MEREMIKWU, M. M., DONEGAN, S., SINCLAIR, D., ESU, E. & ORINGANJE, C. 2012. Intermittent preventive treatment for malaria in children living in areas with seasonal transmission. *Cochrane Database Syst Rev,* 2012**,** Cd003756.

MESCHER, A. L. 2018. Hemopoiesis. *Junqueira's Basic Histology: Text and Atlas, 15e*. New York, NY: McGraw-Hill Education.

MESIN, L., ERSCHING, J. & VICTORA, GABRIEL D. 2016. Germinal Center B Cell Dynamics. *Immunity,* 45**,** 471-482.

MIAO, J., FAN, Q., CUI, L., LI, J., LI, J. & CUI, L. 2006. The malaria parasite Plasmodium falciparum histones: Organization, expression, and acetylation. *Gene,* 369**,** 53-65.

MIKKOLA, H. K. A. & ORKIN, S. H. 2006. The journey of developing hematopoietic stem cells. *Development,* 133**,** 3733-3744.

MILNER, D., JR., FACTOR, R., WHITTEN, R., CARR, R. A., KAMIZA, S., PINKUS, G., MOLYNEUX, M. & TAYLOR, T. 2013a. Pulmonary pathology in pediatric cerebral malaria. *Hum Pathol,* 44**,** 2719-26.

MILNER, D. A., JR., LEE, J. J., FRANTZREB, C., WHITTEN, R. O., KAMIZA, S., CARR, R. A., PRADHAM, A., FACTOR, R. E., PLAYFORTH, K., LIOMBA, G., DZAMALALA, C., SEYDEL, K. B., MOLYNEUX, M. E. & TAYLOR, T. E. 2015. Quantitative Assessment of Multiorgan Sequestration of Parasites in Fatal Pediatric Cerebral Malaria. *J Infect Dis,* 212**,** 1317-21.

MILNER, D. A., JR., WHITTEN, R. O., KAMIZA, S., CARR, R., LIOMBA, G., DZAMALALA, C., SEYDEL, K. B., MOLYNEUX, M. E. & TAYLOR, T. E. 2014. The systemic pathology of cerebral malaria in African children. *Frontiers in cellular and infection microbiology,* 4**,** 104-104.

MILNER, D. A., VALIM, C., CARR, R. A., CHANDAK, P. B., FOSIKO, N. G., WHITTEN, R., PLAYFORTH, K. B., SEYDEL, K. B., KAMIZA, S., MOLYNEUX, M. E. & TAYLOR, T. E. 2013b. A histological method for quantifying Plasmodium falciparum in the brain in fatal paediatric cerebral malaria. *Malaria Journal,* 12**,** 191.

MIQUELESTORENA-STANDLEY, E., JOURDAN, M.-L., COLLIN, C., BOUVIER, C., LAROUSSERIE, F., AUBERT, S., GOMEZ-BROUCHET, A., GUINEBRETIÈRE, J.-M., TALLEGAS, M., BRULIN, B., LE NAIL, L.-R., TALLET, A., LE LOARER, F., MASSIERE, J., GALANT, C. & DE PINIEUX, G. 2020. Effect of decalcification protocols on immunohistochemistry and molecular analyses of bone samples. *Modern Pathology,* 33**,** 1505-1517.

MOHANTY, S., SAHU, P. K., PATTNAIK, R., MAJHI, M., MAHARANA, S., BAGE, J., MOHANTY, A., MOHANTY, A., BENDSZUS, M., PATTERSON, C., GUPTA, H., DONDORP, A. M., PIRPAMER, L., HOFFMANN, A. & WASSMER, S. C. 2022. Evidence of Brain Alterations in Noncerebral Falciparum Malaria. *Clin Infect Dis,* 75**,** 11-18.

MOLINA, D. K., PINNERI, K., STASH, J. A., LI, L., VANCE, K. & CROSS, C. 2019. Organ Weight Reference Ranges for Ages 0 to 12 Years. *Am J Forensic Med Pathol,* 40**,** 318-328.

MOLINA-FRANKY, J., PATARROYO, M. E., KALKUM, M. & PATARROYO, M. A. 2022. The Cellular and Molecular Interaction Between Erythrocytes and Plasmodium falciparum Merozoites. *Frontiers in Cellular and Infection Microbiology,* 12.

MONS, B. 1986. Intra erythrocytic differentiation of Plasmodium berghei. *Acta Leiden,* 54**,** 1-124.

MOONEY, J. P., LOKKEN, K. L., BYNDLOSS, M. X., GEORGE, M. D., VELAZQUEZ, E. M., FABER, F., BUTLER, B. P., WALKER, G. T., ALI, M. M., POTTS, R., TIFFANY, C., AHMER, B. M., LUCKHART, S. & TSOLIS, R. M. 2015. Inflammation-associated alterations to the intestinal microbiota reduce colonization resistance against non-typhoidal Salmonella during concurrent malaria parasite infection. *Sci Rep,* 5**,** 14603.

MOTA, M. M., PRADEL, G., VANDERBERG, J. P., HAFALLA, J. C., FREVERT, U., NUSSENZWEIG, R. S., NUSSENZWEIG, V. & RODRÍGUEZ, A. 2001. Migration of Plasmodium sporozoites through cells before infection. *Science,* 291**,** 141-4.

MOURA, P. L., LIZARRALDE IRAGORRI, M. A., FRANÇAIS, O., LE PIOUFLE, B., DOBBE, J. G. G., STREEKSTRA, G. J., EL NEMER, W., TOYE, A. M. & SATCHWELL, T. J. 2019. Reticulocyte and red blood cell deformation triggers specific phosphorylation events. *Blood Adv,* 3**,** 2653-2663.

MOXON, C. A., GIBBINS, M. P., MCGUINNESS, D., MILNER, D. A., JR. & MARTI, M. 2020. New Insights into Malaria Pathogenesis. *Annu Rev Pathol,* 15**,** 315-343.

MWINGIRA, F., NKWENGULILA, G., SCHOEPFLIN, S., SUMARI, D., BECK, H. P., SNOUNOU, G., FELGER, I., OLLIARO, P. & MUGITTU, K. 2011. Plasmodium falciparum msp1, msp2 and glurp allele frequency and diversity in sub-Saharan Africa. *Malar J,* 10**,** 79.

MYLES, P. S. & CUI, J. 2007. I. Using the Bland–Altman method to measure agreement with repeated measures. *BJA: British Journal of Anaesthesia,* 99**,** 309-311.

NASH, G. B., O'BRIEN, E., GORDON-SMITH, E. C. & DORMANDY, J. A. 1989. Abnormalities in the mechanical properties of red blood cells caused by Plasmodium falciparum. *Blood,* 74**,** 855-61.

NDOUR, P. A., LOPERA-MESA, T. M., DIAKITÉ, S. A., CHIANG, S., MOURI, O., ROUSSEL, C., JAURÉGUIBERRY, S., BILIGUI, S., KENDJO, E., CLAESSENS, A., CICERON, L., MAZIER, D., THELLIER, M., DIAKITÉ, M., FAIRHURST, R. M. & BUFFET, P. A. 2015. Plasmodium falciparum clearance is rapid and pitting

independent in immune Malian children treated with artesunate for malaria. *J Infect Dis,* 211**,** 290-7.

NDOUR, P. A., SAFEUKUI, I., DIAKITÉ, S., DUEZ, J., JAURÉGUIBERRY, S. & BUFFET, P. 2014. Role of the Spleen in Human Malaria. *In:* HOMMEL, M. & KREMSNER, P. G. (eds.) *Encyclopedia of Malaria*. New York, NY: Springer New York.

NEVEU, G., RICHARD, C., DUPUY, F., BEHERA, P., VOLPE, F., SUBRAMANI, P. A., MARCEL-ZERROUGUI, B., VALLIN, P., ANDRIEU, M., MINZ, A. M., AZAR, N., MARTINS, R. M., LORTHIOIS, A., GAZEAU, F., LOPEZ-RUBIO, J.-J., MAZIER, D., SILVA, A. K. A., SATPATHI, S., WASSMER, S. C., VERDIER, F. & LAVAZEC, C. 2020. Plasmodium falciparum sexual parasites develop in human erythroblasts and affect erythropoiesis. *Blood,* 136**,** 1381-1393.

NEWTON, P. N., CHOTIVANICH, K., CHIERAKUL, W., RUANGVEERAYUTH, R., TEERAPONG, P., SILAMUT, K., LOOAREESUWAN, S. & WHITE, N. J. 2001. A comparison of the in vivo kinetics of Plasmodium falciparum ring–infected erythrocyte surface antigen–positive and –negative erythrocytes. *Blood,* 98**,** 450-457.

NGUITRAGOOL, W., BOKHARI, A. A. B., PILLAI, A. D., RAYAVARA, K., SHARMA, P., TURPIN, B., ARAVIND, L. & DESAI, S. A. 2011. Malaria parasite clag3 genes determine channel-mediated nutrient uptake by infected red blood cells. *Cell,* 145**,** 665-677.

NILSSON, S., ANGELETTI, D., WAHLGREN, M., CHEN, Q. & MOLL, K. 2012. Plasmodium falciparum Antigen 332 Is a Resident Peripheral Membrane Protein of Maurer's Clefts. *PLOS ONE,* 7**,** e46980.

NILSSON, S. K., CHILDS, L. M., BUCKEE, C. & MARTI, M. 2015. Targeting Human Transmission Biology for Malaria Elimination. *PLOS Pathogens,* 11**,** e1004871.

NOEDL, H., SE, Y., SCHAECHER, K., SMITH, B. L., SOCHEAT, D. & FUKUDA, M. M. 2008. Evidence of artemisinin-resistant malaria in western Cambodia. *N Engl J Med,* 359**,** 2619-20.

NÖTZEL, C. & KAFSACK, B. F. C. 2021. There and back again: malaria parasite single-cell transcriptomics comes full circle. *Trends Parasitol,* 37**,** 850-852.

OBALDIA, N., 3RD, MEIBALAN, E., SA, J. M., MA, S., CLARK, M. A., MEJIA, P., MORAES BARROS, R. R., OTERO, W., FERREIRA, M. U., MITCHELL, J. R., MILNER, D. A., HUTTENHOWER, C., WIRTH, D. F., DURAISINGH, M. T., WELLEMS, T. E. & MARTI, M. 2018. Bone Marrow Is a Major Parasite Reservoir in Plasmodium vivax Infection. *mBio,* 9**,** e00625-18.

ORISH, V. N., OFORI-AMOAH, J., AMEGAN-AHO, K. H., OSISIOGU, E. U., OSEI-YEBOAH, J., LOKPO, S. Y., ALLOTEY, E. A., ADU-AMANKWAAH, J., AZUMA, D. E. & AGORDOH, P. D. 2021. Eosinophilia in school-going children with

Plasmodium falciparum and helminth infections in the Volta Region of Ghana. *Pan Afr Med J,* 38**,** 277.

ORKIN, S. H. & ZON, L. I. 2008. Hematopoiesis: an evolving paradigm for stem cell biology. *Cell,* 132**,** 631-44.

ORPHANIDOU-VLACHOU, E., TZIAKOURI-SHIAKALLI, C. & GEORGIADES, C. S. 2014. Extramedullary Hemopoiesis. *Seminars in Ultrasound, CT and MRI,* 35**,** 255-262.

OTTO, T. D., BÖHME, U., JACKSON, A. P., HUNT, M., FRANKE-FAYARD, B., HOEIJMAKERS, W. A. M., RELIGA, A. A., ROBERTSON, L., SANDERS, M., OGUN, S. A., CUNNINGHAM, D., ERHART, A., BILLKER, O., KHAN, S. M., STUNNENBERG, H. G., LANGHORNE, J., HOLDER, A. A., WATERS, A. P., NEWBOLD, C. I., PAIN, A., BERRIMAN, M. & JANSE, C. J. 2014. A comprehensive evaluation of rodent malaria parasite genomes and gene expression. *BMC Biology,* 12**,** 86.

OTTO, T. D., BÖHME, U., SANDERS, M., REID, A., BRUSKE, E. I., DUFFY, C. W., BULL, P. C., PEARSON, R. D., ABDI, A., DIMONTE, S., STEWART, L. B., CAMPINO, S., KEKRE, M., HAMILTON, W. L., CLAESSENS, A., VOLKMAN, S. K., NDIAYE, D., AMAMBUA-NGWA, A., DIAKITE, M., FAIRHURST, R. M., CONWAY, D. J., FRANCK, M., NEWBOLD, C. I. & BERRIMAN, M. 2018. Long read assemblies of geographically dispersed Plasmodium falciparum isolates reveal highly structured subtelomeres. *Wellcome Open Res,* 3**,** 52.

OTTO, T. D., SANDERS, M., BERRIMAN, M. & NEWBOLD, C. 2010a. Iterative Correction of Reference Nucleotides (iCORN) using second generation sequencing technology. *Bioinformatics,* 26**,** 1704-7.

OTTO, T. D., WILINSKI, D., ASSEFA, S., KEANE, T. M., SARRY, L. R., BÖHME, U., LEMIEUX, J., BARRELL, B., PAIN, A., BERRIMAN, M., NEWBOLD, C. & LLINÁS, M. 2010b. New insights into the blood-stage transcriptome of Plasmodium falciparum using RNA-Seq. *Molecular Microbiology,* 76**,** 12-24.

OVCHYNNIKOVA, E., AGLIALORO, F., VON LINDERN, M. & VAN DEN AKKER, E. 2018. The Shape Shifting Story of Reticulocyte Maturation. *Front Physiol,* 9**,** 829.

PAINTER, H. J., CAMPBELL, T. L. & LLINÁS, M. 2011. The Apicomplexan AP2 family: integral factors regulating Plasmodium development. *Mol Biochem Parasitol,* 176**,** 1-7.

PAINTER, H. J., CHUNG, N. C., SEBASTIAN, A., ALBERT, I., STOREY, J. D. & LLINÁS, M. 2018. Genome-wide real-time in vivo transcriptional dynamics during Plasmodium falciparum blood-stage development. *Nature Communications,* 9**,** 2656.

PATIL, V., LESCAULT, P. J., LIRUSSI, D., THOMPSON, A. B. & MATRAJT, M. 2012. Disruption of the expression of a non-coding RNA significantly impairs cellular differentiation in Toxoplasma gondii. *Int J Mol Sci,* 14**,** 611-24.

PAULSON, R. F., RUAN, B., HAO, S. & CHEN, Y. 2020. Stress Erythropoiesis is a Key Inflammatory Response. *Cells,* 9**,** 634.

PAULSON, R. F., SHI, L. & WU, D.-C. 2011. Stress erythropoiesis: new signals and new stress progenitor cells. *Current Opinion in Hematology,* 18.

PEATEY, C. L., LEROY, D., GARDINER, D. L. & TRENHOLME, K. R. 2012. Anti-malarial drugs: how effective are they against Plasmodium falciparum gametocytes? *Malaria Journal,* 11**,** 34.

PEATEY, C. L., WATSON, J. A., TRENHOLME, K. R., BROWN, C. L., NIELSON, L., GUENTHER, M., TIMMINS, N., WATSON, G. S. & GARDINER, D. L. 2013. Enhanced gametocyte formation in erythrocyte progenitor cells: a site-specific adaptation by Plasmodium falciparum. *J Infect Dis,* 208**,** 1170-4.

PEI, X., GUO, X., COPPEL, R., BHATTACHARJEE, S., HALDAR, K., GRATZER, W., MOHANDAS, N. & AN, X. 2007. The ring-infected erythrocyte surface antigen (RESA) of Plasmodium falciparum stabilizes spectrin tetramers and suppresses further invasion. *Blood,* 110**,** 1036-42.

PELLE, K. G., OH, K., BUCHHOLZ, K., NARASIMHAN, V., JOICE, R., MILNER, D. A., BRANCUCCI, N. M. B., MA, S., VOSS, T. S., KETMAN, K., SEYDEL, K. B., TAYLOR, T. E., BARTENEVA, N. S., HUTTENHOWER, C. & MARTI, M. 2015. Transcriptional profiling defines dynamics of parasite tissue sequestration during malaria infection. *Genome Medicine,* 7**,** 19.

PÉREZ-TOLEDO, K., ROJAS-MEZA, A. P., MANCIO-SILVA, L., HERNÁNDEZ-CUEVAS, N. A., DELGADILLO, D. M., VARGAS, M., MARTÍNEZ-CALVILLO, S., SCHERF, A. & HERNANDEZ-RIVAS, R. 2009. Plasmodium falciparum heterochromatin protein 1 binds to tri-methylated histone 3 lysine 9 and is linked to mutually exclusive expression of var genes. *Nucleic Acids Research,* 37**,** 2596-2606.

PERRIN, A. J., BARTHOLDSON, S. J. & WRIGHT, G. J. 2015. P-selectin is a host receptor for Plasmodium MSP7 ligands. *Malaria Journal,* 14**,** 238.

PERROTTI, E., L'EPISCOPIA, M., MENEGON, M., SOARES, I. S., ROSAS-AGUIRRE, A., SPEYBROECK, N., LLANOS-CUENTAS, A., MENARD, D., FERREIRA, M. U. & SEVERINI, C. 2023. Reduced polymorphism of Plasmodium vivax early transcribed membrane protein (PvETRAMP) 11.2. *Parasites & Vectors,* 16**,** 238.

PESSI, G., CHOI, J.-Y., REYNOLDS, J. M., VOELKER, D. R. & MAMOUN, C. B. 2005. In Vivo Evidence for the Specificity of Plasmodium falciparum Phosphoethanolamine Methyltransferase and Its Coupling to the Kennedy Pathway*. *Journal of Biological Chemistry,* 280**,** 12461-12466.

PESSI, G., KOCIUBINSKI, G. & MAMOUN, C. B. 2004. A pathway for phosphatidylcholine biosynthesis in Plasmodium falciparum involving phosphoethanolamine methylation. *Proc Natl Acad Sci U S A,* 101**,** 6206-11.

PHYO, A. P., DAHAL, P., MAYXAY, M. & ASHLEY, E. A. 2022. Clinical impact of vivax malaria: A collection review. *PLOS Medicine,* 19**,** e1003890.

POLLITT, L. C., MIDEO, N., DREW, D. R., SCHNEIDER, P., COLEGRAVE, N. & REECE, S. E. 2011. Competition and the evolution of reproductive restraint in malaria parasites. *The American naturalist,* 177**,** 358-367.

PONGPONRATN, E., RIGANTI, M., BUNNAG, D. & HARINASUTA, T. 1987. Spleen in falciparum malaria: ultrastructural study. *Southeast Asian J Trop Med Public Health,* 18**,** 491-501.

PONGPONRATN, E., RIGANTI, M., HARINASUTA, T. & BUNNAG, D. 1989. Electron microscopic study of phagocytosis in human spleen in falciparum malaria. *Southeast Asian J Trop Med Public Health,* 20**,** 31-9.

PONTS, N., HARRIS, E. Y., LONARDI, S. & LE ROCH, K. G. 2011. Nucleosome occupancy at transcription start sites in the human malaria parasite: a hard-wired evolution of virulence? *Infect Genet Evol,* 11**,** 716-24.

PORAN, A., NÖTZEL, C., ALY, O., MENCIA-TRINCHANT, N., HARRIS, C. T., GUZMAN, M. L., HASSANE, D. C., ELEMENTO, O. & KAFSACK, B. F. C. 2017. Single-cell RNA sequencing reveals a signature of sexual commitment in malaria parasites. *Nature,* 551**,** 95-99.

PORTUGAL, S., MOEBIUS, J., SKINNER, J., DOUMBO, S., DOUMTABE, D., KONE, Y., DIA, S., KANAKABANDI, K., STURDEVANT, D. E., VIRTANEVA, K., PORCELLA, S. F., LI, S., DOUMBO, O. K., KAYENTAO, K., ONGOIBA, A., TRAORE, B. & CROMPTON, P. D. 2014. Exposure-Dependent Control of Malaria-Induced Inflammation in Children. *PLOS Pathogens,* 10**,** e1004079.

PROYTCHEVA, M. 2013. Bone marrow evaluation for pediatric patients. *International Journal of Laboratory Hematology,* 35**,** 283-289.

PRZYBORSKI, J. M., DIEHL, M. & BLATCH, G. L. 2015. Plasmodial HSP70s are functionally adapted to the malaria parasite life cycle. *Front Mol Biosci,* 2**,** 34.

QIN, X., QIU, C. & ZHAO, L. 2014. Lysophosphatidylcholine perpetuates macrophage polarization toward classically activated phenotype in inflammation. *Cell Immunol,* 289**,** 185-90.

QUINN, M. T., PARTHASARATHY, S. & STEINBERG, D. 1988. Lysophosphatidylcholine: a chemotactic factor for human monocytes and its potential role in atherogenesis. *Proc Natl Acad Sci U S A,* 85**,** 2805-9.

RAABE, C. A., SANCHEZ, C. P., RANDAU, G., ROBECK, T., SKRYABIN, B. V., CHINNI, S. V., KUBE, M., REINHARDT, R., NG, G. H., MANICKAM, R., KURYSHEV, V. Y., LANZER, M., BROSIUS, J., TANG, T. H. & ROZHDESTVENSKY, T. S. 2010.

A global view of the nonprotein-coding transcriptome in Plasmodium falciparum. *Nucleic Acids Res,* 38**,** 608-17.

REAL, E., HOWICK, V. M., DAHALAN, F. A., WITMER, K., CUDINI, J., ANDRADI-BROWN, C., BLIGHT, J., DAVIDSON, M. S., DOGGA, S. K., REID, A. J., BAUM, J. & LAWNICZAK, M. K. N. 2021. A single-cell atlas of Plasmodium falciparum transmission through the mosquito. *Nature Communications,* 12**,** 3196.

REBELATTO, M. C. 2018. Chapter 24 - Spleen, Lymph Nodes, and Thymus. *In:* SUTTIE, A. W. (ed.) *Boorman's Pathology of the Rat (Second Edition)*. Boston: Academic Press.

REBELO, M., SHAPIRO, H. M., AMARAL, T., MELO-CRISTINO, J. & HÄNSCHEID, T. 2012. Haemozoin detection in infected erythrocytes for Plasmodium falciparum malaria diagnosis-prospects and limitations. *Acta Trop,* 123**,** 58-61.

REGEV-RUDZKI, N., WILSON, D. W., CARVALHO, T. G., SISQUELLA, X., COLEMAN, B. M., RUG, M., BURSAC, D., ANGRISANO, F., GEE, M., HILL, A. F., BAUM, J. & COWMAN, A. F. 2013. Cell-cell communication between malaria-infected red blood cells via exosome-like vesicles. *Cell,* 153**,** 1120-33.

REICHARD, A., WANNER, N., FARHA, S. & ASOSINGH, K. 2023. Hematopoietic stem cells and extramedullary hematopoiesis in the lungs. *Cytometry Part A,* 103**,** 967-977.

REID, A. J., TALMAN, A. M., BENNETT, H. M., GOMES, A. R., SANDERS, M. J., ILLINGWORTH, C. J. R., BILLKER, O., BERRIMAN, M. & LAWNICZAK, M. K. 2018. Single-cell RNA-seq reveals hidden transcriptional variation in malaria parasites. *Elife,* 7.

REID, J. E. & WERNISCH, L. 2016. Pseudotime estimation: deconfounding single cell time series. *Bioinformatics,* 32**,** 2973-80.

RIBACKE, U., MOK, B. W., WIRTA, V., NORMARK, J., LUNDEBERG, J., KIRONDE, F., EGWANG, T. G., NILSSON, P. & WAHLGREN, M. 2007. Genome wide gene amplifications and deletions in Plasmodium falciparum. *Molecular and Biochemical Parasitology,* 155**,** 33-44.

RIECHMANN, J. L. & MEYEROWITZ, E. M. 1998. The AP2/EREBP family of plant transcription factors. *Biol Chem,* 379**,** 633-46.

ROBERT, C., POUVELLE, B., MEYER, P., MUANZA, K., FUJIOKA, H., AIKAWA, M., SCHERF, A. & GYSIN, J. 1995. Chondroitin-4-sulphate (proteoglycan), a receptor for Plasmodium falciparum-infected erythrocyte adherence on brain microvascular endothelial cells. *Res Immunol,* 146**,** 383-93.

RODRIGUES, P. T., VALDIVIA, H. O., DE OLIVEIRA, T. C., ALVES, J. M. P., DUARTE, A., CERUTTI-JUNIOR, C., BUERY, J. C., BRITO, C. F. A., DE SOUZA, J. C., JR., HIRANO, Z. M. B., BUENO, M. G., CATÃO-DIAS, J. L., MALAFRONTE, R. S., LADEIA-ANDRADE, S., MITA, T., SANTAMARIA, A. M., CALZADA, J. E., TANTULAR, I. S., KAWAMOTO, F., RAIJMAKERS, L. R. J., MUELLER, I., PACHECO, M. A., ESCALANTE, A. A., FELGER, I. & FERREIRA, M. U. 2018. Human migration and the spread of malaria parasites to the New World. *Sci Rep,* 8**,** 1993.

ROGERSON, S. J., CHAIYAROJ, S. C., NG, K., REEDER, J. C. & BROWN, G. V. 1995. Chondroitin sulfate A is a cell surface receptor for Plasmodium falciparum-infected erythrocytes. *J Exp Med,* 182**,** 15-20.

ROGERSON, S. J. & ORDI, J. 2014. Pathology and Pathophysiology of Placental Malaria. *In:* HOMMEL, M. & KREMSNER, P. G. (eds.) *Encyclopedia of Malaria*. New York, NY: Springer New York.

ROSCHE, K. L., ALJASHAM, A. T., KIPFER, J. N., PIATKOWSKI, B. T. & KONJUFCA, V. 2015. Infection with Salmonella enterica Serovar Typhimurium Leads to Increased Proportions of F4/80+ Red Pulp Macrophages and Decreased Proportions of B and T Lymphocytes in the Spleen. *PLoS One,* 10**,** e0130092.

ROSENTHAL, P. J., ASUA, V. & CONRAD, M. D. 2024. Emergence, transmission dynamics and mechanisms of artemisinin partial resistance in malaria parasites in Africa. *Nature Reviews Microbiology*.

ROWE, J. A., ROGERSON, S. J., RAZA, A., MOULDS, J. M., KAZATCHKINE, M. D., MARSH, K., NEWBOLD, C. I., ATKINSON, J. P. & MILLER, L. H. 2000. Mapping of the region of complement receptor (CR) 1 required for Plasmodium falciparum rosetting and demonstration of the importance of CR1 in rosetting in field isolates. *J Immunol,* 165**,** 6341-6.

RUG, M., PRESCOTT, S. W., FERNANDEZ, K. M., COOKE, B. M. & COWMAN, A. F. 2006. The role of KAHRP domains in knob formation and cytoadherence of P falciparum-infected human erythrocytes. *Blood,* 108**,** 370-378.

RUIZ, J. L., TENA, JUAN J., BANCELLS, C., CORTÉS, A., GÓMEZ-SKARMETA, JOSÉ L. & GÓMEZ-DÍAZ, E. 2018. Characterization of the accessible genome in the human malaria parasite Plasmodium falciparum. *Nucleic Acids Research,* 46**,** 9414-9431.

RUSSELL, A. J. C., SANDERSON, T., BUSHELL, E., TALMAN, A. M., ANAR, B., GIRLING, G., HUNZIKER, M., KENT, R. S., MARTIN, J. S., METCALF, T., MONTANDON, R., PANDEY, V., PARDO, M., ROBERTS, A. B., SAYERS, C., SCHWACH, F., CHOUDHARY, J. S., RAYNER, J. C., VOET, T., MODRZYNSKA, K. K., WATERS, A. P., LAWNICZAK, M. K. N. & BILLKER, O. 2023. Regulators of male and female sexual development are critical for the transmission of a malaria parasite. *Cell Host Microbe,* 31**,** 305-319.e10.

SAFEUKUI, I., CORREAS, J.-M., BROUSSE, V., HIRT, D., DEPLAINE, G., MULÉ, S., LESURTEL, M., GOASGUEN, N., SAUVANET, A., COUVELARD, A., KERNEIS, S., KHUN, H., VIGAN-WOMAS, I., OTTONE, C., MOLINA, T. J., TRÉLUYER, J.-M., MERCEREAU-PUIJALON, O., MILON, G., DAVID, P. H. & BUFFET, P. A. 2008. Retention of Plasmodium falciparum ring-infected erythrocytes in the slow, open microcirculation of the human spleen. *Blood,* 112**,** 2520-2528.

SAIDI, A. M., GUENTHER, G., IZEM, R., CHEN, X., SEYDEL, K. & POSTELS, D. 2021. Plasmodium falciparum clearance time in Malawian children with cerebral malaria: a retrospective cohort study. *Malaria Journal,* 20**,** 408.

SAIDI, A. M., ZHANG, B., JIANG, M., KAWAZA, K., MUSAYA, J., TAYLOR, T. & SEYDEL, K. 2023. Differential Effects of Antimalarial Drugs on Parasite Clearance Rates Are Reflected by Plasmodium falciparum Ring Ratio. *Open Forum Infectious Diseases,* 10.

SALANTI, A., STAALSOE, T., LAVSTSEN, T., JENSEN, A. T., SOWA, M. P., ARNOT, D. E., HVIID, L. & THEANDER, T. G. 2003. Selective upregulation of a single distinctly structured var gene in chondroitin sulphate A-adhering Plasmodium falciparum involved in pregnancy-associated malaria. *Mol Microbiol,* 49**,** 179-91.

SALCEDO-AMAYA, A. M., VAN DRIEL, M. A., ALAKO, B. T., TRELLE, M. B., VAN DEN ELZEN, A. M. G., COHEN, A. M., JANSSEN-MEGENS, E. M., VAN DE VEGTE-BOLMER, M., SELZER, R. R., INIGUEZ, A. L., GREEN, R. D., SAUERWEIN, R. W., JENSEN, O. N. & STUNNENBERG, H. G. 2009. Dynamic histone H3 epigenome marking during the intraerythrocytic cycle of Plasmodium falciparum. *Proceedings of the National Academy of Sciences,* 106**,** 9655-9660.

SALMON, C. R., SILVÉRIO, K. G., GIORGETTI, A. P. D. O., SALLUM, E. A., CASATI, M. Z. & NOCITI, F. H. J. 2012. Gene Expression Analysis in Microdissected Samples from Decalcified Tissues. *Diagnostic Molecular Pathology,* 21**,** 120-126.

SANGER, F. & COULSON, A. R. 1975. A rapid method for determining sequences in DNA by primed synthesis with DNA polymerase. *J Mol Biol,* 94**,** 441-8.

SANGER, F., NICKLEN, S. & COULSON, A. R. 1977. DNA sequencing with chain-terminating inhibitors. *Proc Natl Acad Sci U S A,* 74**,** 5463-7.

SANTOS, J. M., JOSLING, G., ROSS, P., JOSHI, P., ORCHARD, L., CAMPBELL, T., SCHIELER, A., CRISTEA, I. M. & LLINÁS, M. 2017. Red Blood Cell Invasion by the Malaria Parasite Is Coordinated by the PfAP2-I Transcription Factor. *Cell Host & Microbe,* 21**,** 731-741.e10.

SARAF, A., CERVANTES, S., BUNNIK, E. M., PONTS, N., SARDIU, M. E., CHUNG, D.-W. D., PRUDHOMME, J., VARBERG, J. M., WEN, Z., WASHBURN, M. P., FLORENS, L. & LE ROCH, K. G. 2016. Dynamic and Combinatorial Landscape

of Histone Modifications during the Intraerythrocytic Developmental Cycle of the Malaria Parasite. *Journal of Proteome Research,* 15, 2787-2801.

SASOU, S. 2021. The perifollicular zone of the spleen as a distributor and filter of blood components. *J Clin Exp Hematop,* 61, 58-60.

SAUL, A., GRAVES, P. & EDSER, L. 1990. Refractoriness of erythrocytes infected with Plasmodium falciparum gametocytes to lysis by sorbitol. *Int J Parasitol,* 20, 1095-7.

SCHENA, M., SHALON, D., DAVIS, R. W. & BROWN, P. O. 1995. Quantitative monitoring of gene expression patterns with a complementary DNA microarray. *Science,* 270, 467-70.

SCHMIDT, E. E., MACDONALD, I. C. & GROOM, A. C. 1993. Comparative aspects of splenic microcirculatory pathways in mammals: the region bordering the white pulp. *Scanning Microsc,* 7, 613-28.

SCHNEIDER, P., GREISCHAR, M. A., BIRGET, P. L. G., REPTON, C., MIDEO, N. & REECE, S. E. 2018. Adaptive plasticity in the gametocyte conversion rate of malaria parasites. *PLOS Pathogens,* 14, e1007371.

SCHNEIDER, P. & REECE, S. E. 2021. The private life of malaria parasites: Strategies for sexual reproduction. *Mol Biochem Parasitol,* 244, 111375.

SCHNEIDER, VICTORIA M., VISONE, JOSEPH E., HARRIS, CHANTAL T., FLORINI, F., HADJIMICHAEL, E., ZHANG, X., GROSS, MACKENSIE R., RHEE, KYU Y., BEN MAMOUN, C., KAFSACK, BJÖRN F. C. & DEITSCH, KIRK W. 2023. The human malaria parasite Plasmodium falciparum can sense environmental changes and respond by antigenic switching. *Proceedings of the National Academy of Sciences,* 120, e2302152120.

SCHNITZER, B., SODEMAN, T., MEAD, M. L. & CONTACOS, P. G. 1972. Pitting Function of the Spleen in Malaria: Ultrastructural Observations. *Science,* 177, 175-177.

SCHURECK, M. A., DARLING, J. E., MERK, A., SHAO, J., DAGGUPATI, G., SRINIVASAN, P., OLINARES, P. D. B., ROUT, M. P., CHAIT, B. T., WOLLENBERG, K., SUBRAMANIAM, S. & DESAI, S. A. 2021. Malaria parasites use a soluble RhopH complex for erythrocyte invasion and an integral form for nutrient uptake. *eLife,* 10, e65282.

SCHWARZER, E., TURRINI, F., ULLIERS, D., GIRIBALDI, G., GINSBURG, H. & ARESE, P. 1992. Impairment of macrophage functions after ingestion of Plasmodium falciparum-infected erythrocytes or isolated malarial pigment. *J Exp Med,* 176, 1033-41.

SCORZA, T., MAGEZ, S., BRYS, L. & DE BAETSELIER, P. 1999. Hemozoin is a key factor in the induction of malaria-associated immunosuppression. *Parasite Immunology,* 21**,** 545-554.

SCOVINO, A. M., TOTINO, P. R. R. & MORROT, A. 2022. Eryptosis as a New Insight in Malaria Pathogenesis. *Front Immunol,* 13**,** 855795.

SEE, P., LUM, J., CHEN, J. & GINHOUX, F. 2018. A Single-Cell Sequencing Guide for Immunologists. *Frontiers in Immunology,* 9.

SEY, I. C. M., EHIMIYEIN, A. M., BOTTOMLEY, C., RILEY, E. M. & MOONEY, J. P. 2020. Does Malaria Cause Diarrhoea? A Systematic Review. *Frontiers in Medicine,* 7.

SEYDEL, K. B., KAMPONDENI, S. D., VALIM, C., POTCHEN, M. J., MILNER, D. A., MUWALO, F. W., BIRBECK, G. L., BRADLEY, W. G., FOX, L. L., GLOVER, S. J., HAMMOND, C. A., HEYDERMAN, R. S., CHILINGULO, C. A., MOLYNEUX, M. E. & TAYLOR, T. E. 2015. Brain Swelling and Death in Children with Cerebral Malaria. *New England Journal of Medicine,* 372**,** 1126-1137.

SEYDEL, K. B., MILNER, D. A., JR, KAMIZA, S. B., MOLYNEUX, M. E. & TAYLOR, T. E. 2006. The Distribution and Intensity of Parasite Sequestration in Comatose Malawian Children. *The Journal of Infectious Diseases,* 194**,** 208-215.

SHAO, Y. Y., WANG, L., HICKS, D. G. & BALLOCK, R. T. 2006. Analysis of gene expression in mineralized skeletal tissues by laser capture microdissection and RT-PCR. *Laboratory Investigation,* 86**,** 1089-1095.

SHAPIRO, H. M., APTE, S. H., CHOJNOWSKI, G. M., HÄNSCHEID, T., REBELO, M. & GRIMBERG, B. T. 2013. Cytometry in Malaria—A Practical Replacement for Microscopy? *Current Protocols in Cytometry,* 65**,** 11.20.1-11.20.23.

SHERLING, E. S., KNUEPFER, E., BRZOSTOWSKI, J. A., MILLER, L. H., BLACKMAN, M. J. & OOIJ, C. V. 2017. The Plasmodium falciparum rhoptry protein RhopH3 plays essential roles in host cell invasion and nutrient uptake. *eLife,* 6**,** e23239.

SHONHAI, A., BOSHOFF, A. & BLATCH, G. L. 2007. The structural and functional diversity of Hsp70 proteins from Plasmodium falciparum. *Protein Sci,* 16**,** 1803-18.

SHRESTHA, S., LUCKY, A. B., BRASHEAR, A. M., LI, X., CUI, L. & MIAO, J. 2022. Distinct Histone Post-translational Modifications during Plasmodium falciparum Gametocyte Development. *Journal of Proteome Research,* 21**,** 1857-1867.

SIEGEL, T. N., HON, C.-C., ZHANG, Q., LOPEZ-RUBIO, J.-J., SCHEIDIG-BENATAR, C., MARTINS, R. M., SISMEIRO, O., COPPÉE, J.-Y. & SCHERF, A. 2014. Strand-

specific RNA-Seq reveals widespread and developmentally regulated transcription of natural antisense transcripts in Plasmodium falciparum. *BMC Genomics,* 15**,** 150.

SIMANTOV, K., GOYAL, M. & DZIKOWSKI, R. 2022. Emerging biology of noncoding RNAs in malaria parasites. *PLOS Pathogens,* 18**,** e1010600.

SINGH, B. & DANESHVAR, C. 2013. Human Infections and Detection of Plasmodium knowlesi. *Clinical Microbiology Reviews,* 26**,** 165-184.

SINGH, B., KIM SUNG, L., MATUSOP, A., RADHAKRISHNAN, A., SHAMSUL, S. S., COX-SINGH, J., THOMAS, A. & CONWAY, D. J. 2004. A large focus of naturally acquired Plasmodium knowlesi infections in human beings. *Lancet,* 363**,** 1017-24.

SINGH, I., MIKITA, G., GREEN, D., RISQUEZ, C. & SANDERS, A. 2017. Pulmonary extra-medullary hematopoiesis and pulmonary hypertension from underlying polycythemia vera: a case series. *Pulm Circ,* 7**,** 261-267.

SINHA, A., HUGHES, K. R., MODRZYNSKA, K. K., OTTO, T. D., PFANDER, C., DICKENS, N. J., RELIGA, A. A., BUSHELL, E., GRAHAM, A. L., CAMERON, R., KAFSACK, B. F. C., WILLIAMS, A. E., LLINÁS, M., BERRIMAN, M., BILLKER, O. & WATERS, A. P. 2014. A cascade of DNA-binding proteins for sexual commitment and development in Plasmodium. *Nature,* 507**,** 253-257.

SMALLEY, M. E., ABDALLA, S. & BROWN, J. 1981. The distribution of Plasmodium falciparum in the peripheral blood and bone marrow of Gambian children. *Trans R Soc Trop Med Hyg,* 75**,** 103-5.

SMITH, J. D., CHITNIS, C. E., CRAIG, A. G., ROBERTS, D. J., HUDSON-TAYLOR, D. E., PETERSON, D. S., PINCHES, R., NEWBOLD, C. I. & MILLER, L. H. 1995. Switches in expression of Plasmodium falciparum var genes correlate with changes in antigenic and cytoadherent phenotypes of infected erythrocytes. *Cell,* 82**,** 101-10.

SMITH, J. D., CRAIG, A. G., KRIEK, N., HUDSON-TAYLOR, D., KYES, S., FAGEN, T., PINCHES, R., BARUCH, D. I., NEWBOLD, C. I. & MILLER, L. H. 2000. Identification of a Plasmodium falciparum intercellular adhesion molecule-1 binding domain: A parasite adhesion trait implicated in cerebral malaria. *Proceedings of the National Academy of Sciences,* 97**,** 1766-1771.

SOLOGUB, L., KUEHN, A., KERN, S., PRZYBORSKI, J., SCHILLIG, R. & PRADEL, G. 2011. Malaria proteases mediate inside-out egress of gametocytes from red blood cells following parasite transmission to the mosquito. *Cell Microbiol,* 13**,** 897-912.

SONDO, P., DERRA, K., LEFEVRE, T., DIALLO-NAKANABO, S., TARNAGDA, Z., ZAMPA, O., KAZIENGA, A., VALEA, I., SORGHO, H., OUEDRAOGO, J. B., GUIGUEMDE, T. R. & TINTO, H. 2019. Genetically diverse Plasmodium

falciparum infections, within-host competition and symptomatic malaria in humans. *Sci Rep,* 9**,** 127.

SORBER, K., CHIU, C., WEBSTER, D., DIMON, M., RUBY, J. G., HEKELE, A. & DERISI, J. L. 2008. The Long March: A Sample Preparation Technique that Enhances Contig Length and Coverage by High-Throughput Short-Read Sequencing. *PLOS ONE,* 3**,** e3495.

SOULAMA, I., NÉBIÉ, I., OUÉDRAOGO, A., GANSANE, A., DIARRA, A., TIONO, A. B., BOUGOUMA, E. C., KONATÉ, A. T., KABRÉ, G. B., TAYLOR, W. R. J. & SIRIMA, S. B. 2009. Plasmodium falciparum genotypes diversity in symptomatic malaria of children living in an urban and a rural setting in Burkina Faso. *Malaria Journal,* 8**,** 135.

SPIELMANN, T., FERGUSEN, D. J. & BECK, H. P. 2003. etramps, a new Plasmodium falciparum gene family coding for developmentally regulated and highly charged membrane proteins located at the parasite-host cell interface. *Mol Biol Cell,* 14**,** 1529-44.

SPIELMANN, T., GARDINER, D. L., BECK, H.-P., TRENHOLME, K. R. & KEMP, D. J. 2006. Organization of ETRAMPs and EXP-1 at the parasite–host cell interface of malaria parasites. *Molecular Microbiology,* 59**,** 779-794.

SRIVASTAVA, A., CREEK, D. J., EVANS, K. J., DE SOUZA, D., SCHOFIELD, L., MÜLLER, S., BARRETT, M. P., MCCONVILLE, M. J. & WATERS, A. P. 2015. Host Reticulocytes Provide Metabolic Reservoirs That Can Be Exploited by Malaria Parasites. *PLOS Pathogens,* 11**,** e1004882.

ST JOHN, A. L. & ABRAHAM, S. N. 2009. Salmonella disrupts lymph node architecture by TLR4-mediated suppression of homeostatic chemokines. *Nat Med,* 15**,** 1259-65.

STÅHL, P. L., SALMÉN, F., VICKOVIC, S., LUNDMARK, A., NAVARRO, J. F., MAGNUSSON, J., GIACOMELLO, S., ASP, M., WESTHOLM, J. O., HUSS, M., MOLLBRINK, A., LINNARSSON, S., CODELUPPI, S., BORG, Å., PONTÉN, F., COSTEA, P. I., SAHLÉN, P., MULDER, J., BERGMANN, O., LUNDEBERG, J. & FRISÉN, J. 2016. Visualization and analysis of gene expression in tissue sections by spatial transcriptomics. *Science,* 353**,** 78-82.

STEBEGG, M., KUMAR, S. D., SILVA-CAYETANO, A., FONSECA, V. R., LINTERMAN, M. A. & GRACA, L. 2018. Regulation of the Germinal Center Response. *Frontiers in Immunology,* 9.

STEINIGER, B., BARTH, P. & HELLINGER, A. 2001. The perifollicular and marginal zones of the human splenic white pulp : do fibroblasts guide lymphocyte immigration? *Am J Pathol,* 159**,** 501-12.

STEINIGER, B. S. 2015. Human spleen microanatomy: why mice do not suffice. *Immunology,* 145**,** 334-46.

STONE, A. P., NASCIMENTO, T. F. & BARRACHINA, M. N. 2022. The bone marrow niche from the inside out: how megakaryocytes are shaped by and shape hematopoiesis. *Blood,* 139, 483-491.

STREET, K., RISSO, D., FLETCHER, R. B., DAS, D., NGAI, J., YOSEF, N., PURDOM, E. & DUDOIT, S. 2018. Slingshot: cell lineage and pseudotime inference for single-cell transcriptomics. *BMC Genomics,* 19, 477.

STURGEON, P. 1951. Volumetric and microscopic pattern of bone marrow in normal infants and children. III. Histologic pattern. *Pediatrics,* 7 6, 774-81.

STURM, A., AMINO, R., VAN DE SAND, C., REGEN, T., RETZLAFF, S., RENNENBERG, A., KRUEGER, A., POLLOK, J. M., MENARD, R. & HEUSSLER, V. T. 2006. Manipulation of host hepatocytes by the malaria parasite for delivery into liver sinusoids. *Science,* 313, 1287-90.

SU, X. Z., HEATWOLE, V. M., WERTHEIMER, S. P., GUINET, F., HERRFELDT, J. A., PETERSON, D. S., RAVETCH, J. A. & WELLEMS, T. E. 1995. The large diverse gene family var encodes proteins involved in cytoadherence and antigenic variation of Plasmodium falciparum-infected erythrocytes. *Cell,* 82, 89-100.

SZABO, Q., BANTIGNIES, F. & CAVALLI, G. 2019. Principles of genome folding into topologically associating domains. *Science Advances,* 5, eaaw1668.

TANAKA, N., NAKANISHI, M., KUSAKABE, Y., SHIRAIWA, K., YABE, S., ITO, Y., KITADE, Y. & NAKAMURA, K. T. 2004. Crystal Structure of S-Adenosyl-l-Homocysteine Hydrolase from the Human Malaria Parasite Plasmodium falciparum. *Journal of Molecular Biology,* 343, 1007-1017.

TANG, F., BARBACIORU, C., WANG, Y., NORDMAN, E., LEE, C., XU, N., WANG, X., BODEAU, J., TUCH, B. B., SIDDIQUI, A., LAO, K. & SURANI, M. A. 2009. mRNA-Seq whole-transcriptome analysis of a single cell. *Nature Methods,* 6, 377-382.

TAVARES, J., FORMAGLIO, P., THIBERGE, S., MORDELET, E., VAN ROOIJEN, N., MEDVINSKY, A., MÉNARD, R. & AMINO, R. 2013. Role of host cell traversal by the malaria sporozoite during liver infection. *J Exp Med,* 210, 905-15.

TAYLOR, D. W., PARRA, M., CHAPMAN, G. B., STEARNS, M. E., RENER, J., AIKAWA, M., UNI, S., ALEY, S. B., PANTON, L. J. & HOWARD, R. J. 1987. Localization of Plasmodium falciparum histidine-rich protein 1 in the erythrocyte skeleton under knobs. *Mol Biochem Parasitol,* 25, 165-74.

TAYLOR, S. M., PAROBEK, C. M. & FAIRHURST, R. M. 2012. Haemoglobinopathies and the clinical epidemiology of malaria: a systematic review and meta-analysis. *The Lancet Infectious Diseases,* 12, 457-468.

TAYLOR, T. E., FU, W. J., CARR, R. A., WHITTEN, R. O., MUELLER, J. G., FOSIKO, N. G., LEWALLEN, S., LIOMBA, N. G. & MOLYNEUX, M. E. 2004. Differentiating the pathologies of cerebral malaria by postmortem parasite counts. *Nature Medicine,* 10**,** 143-145.

TEMPLETON, T. J., IYER, L. M., ANANTHARAMAN, V., ENOMOTO, S., ABRAHANTE, J. E., SUBRAMANIAN, G. M., HOFFMAN, S. L., ABRAHAMSEN, M. S. & ARAVIND, L. 2004. Comparative analysis of apicomplexa and genomic diversity in eukaryotes. *Genome Res,* 14**,** 1686-95.

TER KUILE, F., WHITE, N. J., HOLLOWAY, P., PASVOL, G. & KRISHNA, S. 1993. Plasmodium falciparum: in vitro studies of the pharmacodynamic properties of drugs used for the treatment of severe malaria. *Exp Parasitol,* 76**,** 85-95.

TESEMA, G. A., WORKU, M. G., TESSEMA, Z. T., TESHALE, A. B., ALEM, A. Z., YESHAW, Y., ALAMNEH, T. S. & LIYEW, A. M. 2021. Prevalence and determinants of severity levels of anemia among children aged 6-59 months in sub-Saharan Africa: A multilevel ordinal logistic regression analysis. *PLoS One,* 16**,** e0249978.

THAM, W.-H., HEALER, J. & COWMAN, A. F. 2012. Erythrocyte and reticulocyte binding-like proteins of Plasmodium falciparum. *Trends in Parasitology,* 28**,** 23-30.

THOMSON, J. G. & ROBERTSON, A. 1935. The structure and development of plasmodium falciparum gametocytes in the internal organs and peripheral circulation. *Transactions of the Royal Society of Tropical Medicine and Hygiene,* 29**,** 31-40.

TOENHAKE, C. G. & BÁRTFAI, R. 2019. What functional genomics has taught us about transcriptional regulation in malaria parasites. *Briefings in Functional Genomics,* 18**,** 290-301.

TRAGER, W. & JENSEN, J. B. 1976. Human malaria parasites in continuous culture. *Science,* 193**,** 673-5.

TRAN, P. N., BROWN, S. H. J., RUG, M., RIDGWAY, M. C., MITCHELL, T. W. & MAIER, A. G. 2016. Changes in lipid composition during sexual development of the malaria parasite Plasmodium falciparum. *Malaria Journal,* 15**,** 73.

TRAVLOS, G. S. 2006. Normal Structure, Function, and Histology of the Bone Marrow. *Toxicologic Pathology,* 34**,** 548-565.

TRELLE, M. B., SALCEDO-AMAYA, A. M., COHEN, A. M., STUNNENBERG, H. G. & JENSEN, O. N. 2009. Global Histone Analysis by Mass Spectrometry Reveals a High Content of Acetylated Lysine Residues in the Malaria Parasite Plasmodium falciparum. *Journal of Proteome Research,* 8**,** 3439-3450.

TREUTIGER, C. J., HEDDINI, A., FERNANDEZ, V., MULLER, W. A. & WAHLGREN, M. 1997. PECAM-1/CD31, an endothelial receptor for binding Plasmodium falciparum-infected erythrocytes. *Nat Med,* 3**,** 1405-8.

TURNER, L., LAVSTSEN, T., BERGER, S. S., WANG, C. W., PETERSEN, J. E., AVRIL, M., BRAZIER, A. J., FREETH, J., JESPERSEN, J. S., NIELSEN, M. A., MAGISTRADO, P., LUSINGU, J., SMITH, J. D., HIGGINS, M. K. & THEANDER, T. G. 2013. Severe malaria is associated with parasite binding to endothelial protein C receptor. *Nature,* 498**,** 502-5.

TYBERGHEIN, A., DEROOST, K., SCHWARZER, E., ARESE, P. & VAN DEN STEEN, P. E. 2014. Immunopathological effects of malaria pigment or hemozoin and other crystals. *BioFactors,* 40**,** 59-78.

UNAIDS 2023a. 2022 Malawi HIV estimates.

UNAIDS 2023b. The path that ends AIDS: UNAIDS Global AIDS Update 2023. Geneva: Joint United Nations Programme on HIV/AIDS.

URBAN, B. C., HIEN, T. T., DAY, N. P., PHU, N. H., ROBERTS, R., PONGPONRATN, E., JONES, M., MAI, N. T., BETHELL, D., TURNER, G. D., FERGUSON, D., WHITE, N. J. & ROBERTS, D. J. 2005a. Fatal Plasmodium falciparum malaria causes specific patterns of splenic architectural disorganization. *Infect Immun,* 73**,** 1986-94.

URBAN, B. C., HIEN, T. T., DAY, N. P., PHU, N. H., ROBERTS, R., PONGPONRATN, E., JONES, M., MAI, N. T. H., BETHELL, D., TURNER, G. D. H., FERGUSON, D., WHITE, N. J. & ROBERTS, D. J. 2005b. Fatal Plasmodium falciparum Malaria Causes Specific Patterns of Splenic Architectural Disorganization. *Infection and Immunity,* 73**,** 1986-1994.

USUI, M., PRAJAPATI, S. K., AYANFUL-TORGBY, R., ACQUAH, F. K., CUDJOE, E., KAKANEY, C., AMPONSAH, J. A., OBBOH, E. K., REDDY, D. K., BARBEAU, M. C., SIMONS, L. M., CZESNY, B., RAICIULESCU, S., OLSEN, C., ABUAKU, B. K., AMOAH, L. E. & WILLIAMSON, K. C. 2019. Plasmodium falciparum sexual differentiation in malaria patients is associated with host factors and GDV1-dependent genes. *Nature communications,* 10**,** 2140-2140.

VALIHRACH, L., ANDROVIC, P. & KUBISTA, M. 2018. Platforms for Single-Cell Collection and Analysis. *International Journal of Molecular Sciences,* 19**,** 807.

VAN BRUMMELEN, A. C., OLSZEWSKI, K. L., WILINSKI, D., LLINÁS, M., LOUW, A. I. & BIRKHOLTZ, L.-M. 2009. Co-inhibition of Plasmodium falciparum S-Adenosylmethionine Decarboxylase/Ornithine Decarboxylase Reveals Perturbation-specific Compensatory Mechanisms by Transcriptome, Proteome, and Metabolome Analyses*. *Journal of Biological Chemistry,* 284**,** 4635-4646.

VAUGHAN, A. M., MIKOLAJCZAK, S. A., WILSON, E. M., GROMPE, M., KAUSHANSKY, A., CAMARGO, N., BIAL, J., PLOSS, A. & KAPPE, S. H. 2012. Complete Plasmodium falciparum liver-stage development in liver-chimeric mice. *J Clin Invest,* 122**,** 3618-28.

VEMBAR, S. S., DROLL, D. & SCHERF, A. 2016. Translational regulation in blood stages of the malaria parasite Plasmodium spp.: systems-wide studies pave the way. *WIREs RNA,* 7**,** 772-792.

VENUGOPAL, K., HENTZSCHEL, F., VALKIŪNAS, G. & MARTI, M. 2020. Plasmodium asexual growth and sexual development in the haematopoietic niche of the host. *Nature Reviews Microbiology,* 18**,** 177-189.

VIAL, H. J., ELDIN, P., TIELENS, A. G. & VAN HELLEMOND, J. J. 2003. Phospholipids in parasitic protozoa. *Mol Biochem Parasitol,* 126**,** 143-54.

VILLEVAL, J. L., LEW, A. & METCALF, D. 1990. Changes in hemopoietic and regulator levels in mice during fatal or nonfatal malarial infections. I. Erythropoietic populations. *Exp Parasitol*, 71**,** 364-74.

VOSS, T. S. & BRANCUCCI, N. M. B. 2024. Regulation of sexual commitment in malaria parasites — a complex affair. *Current Opinion in Microbiology,* 79**,** 102469.

WALLER, K. L., NUNOMURA, W., AN, X., COOKE, B. M., MOHANDAS, N. & COPPEL, R. L. 2003. Mature parasite-infected erythrocyte surface antigen (MESA) of Plasmodium falciparum binds to the 30-kDa domain of protein 4.1 in malaria-infected red blood cells. *Blood,* 102**,** 1911-4.

WANG, F., FLANAGAN, J., SU, N., WANG, L.-C., BUI, S., NIELSON, A., WU, X., VO, H.-T., MA, X.-J. & LUO, Y. 2012. RNAscope: A Novel in Situ RNA Analysis Platform for Formalin-Fixed, Paraffin-Embedded Tissues. *The Journal of Molecular Diagnostics,* 14**,** 22-29.

WANG, X., HE, Y., ZHANG, Q., REN, X. & ZHANG, Z. 2021. Direct Comparative Analyses of 10X Genomics Chromium and Smart-seq2. *Genomics Proteomics Bioinformatics,* 19**,** 253-266.

WANG, Y. J., SCHUG, J., LIN, J., WANG, Z., KOSSENKOV, A., CONSORTIUM, T. H. & KAESTNER, K. H. 2019. Comparative analysis of commercially available single-cell RNA sequencing platforms for their performance in complex human tissues. *bioRxiv***,** 541433.

WARNCKE, J. D., VAKONAKIS, I. & BECK, H.-P. 2016. Plasmodium Helical Interspersed Subtelomeric (PHIST) Proteins, at the Center of Host Cell Remodeling. *Microbiology and molecular biology reviews : MMBR,* 80**,** 905-927.

WATSON, J. A., UYOGA, S., WANJIKU, P., MAKALE, J., NYUTU, G. M., MTURI, N., GEORGE, E. C., WOODROW, C. J., DAY, N. P. J., BEJON, P., OPOKA, R. O., DONDORP, A. M., JOHN, C. C., MAITLAND, K., WILLIAMS, T. N. & WHITE, N. J. 2022. Improving the diagnosis of severe malaria in African children using platelet counts and plasma PfHRP2 concentrations. *Sci Transl Med,* 14, eabn5040.

WEATHERALL, D. J. 2008. Genetic variation and susceptibility to infection: the red cell and malaria. *British Journal of Haematology,* 141, 276-286.

WEIN, S., MAYNADIER, M., BORDAT, Y., PEREZ, J., MAHESHWARI, S., BETTE-BOBILLO, P., TRAN VAN BA, C., PENARETE-VARGAS, D., FRAISSE, L., CERDAN, R. & VIAL, H. 2012. Transport and pharmacodynamics of albitiazolium, an antimalarial drug candidate. *British Journal of Pharmacology,* 166, 2263-2276.

WEISS, G. E., TRAORE, B., KAYENTAO, K., ONGOIBA, A., DOUMBO, S., DOUMTABE, D., KONE, Y., DIA, S., GUINDO, A., TRAORE, A., HUANG, C.-Y., MIURA, K., MIRCETIC, M., LI, S., BAUGHMAN, A., NARUM, D. L., MILLER, L. H., DOUMBO, O. K., PIERCE, S. K. & CROMPTON, P. D. 2010. The Plasmodium falciparum-Specific Human Memory B Cell Compartment Expands Gradually with Repeated Malaria Infections. *PLOS Pathogens,* 6, e1000912.

WEISS, L., JOHNSON, J. & WEIDANZ, W. 1989. Mechanisms of splenic control of murine malaria: tissue culture studies of the erythropoietic interplay of spleen, bone marrow, and blood in lethal (strain 17XL) Plasmodium yoelii malaria in BALB/c mice. *Am J Trop Med Hyg,* 41, 135-43.

WELLEMS, T. E., PANTON, L. J., GLUZMAN, I. Y., DO ROSARIO, V. E., GWADZ, R. W., WALKER-JONAH, A. & KROGSTAD, D. J. 1990. Chloroquine resistance not linked to mdr-like genes in a Plasmodium falciparum cross. *Nature,* 345, 253-255.

WHITE, N. J. 2011. Determinants of relapse periodicity in Plasmodium vivax malaria. *Malar J,* 10, 297.

WHITE, N. J. 2018. Anaemia and malaria. *Malaria Journal,* 17, 371.

WHO 2021. Global technical strategy for malaria 2016–2030. Geneva.

WHO 2023a. WHO guidelines for malaria.

WHO 2023b. World malaria report 2023. Geneva.

WHO. 2024. *Malaria* [Online]. Available: https://www.who.int/health-topics/malaria#tab=tab_1 [Accessed 1st March 2024].

WICKRAMASINGHE, S. N., PHILLIPS, R. E., LOOAREESUWAN, S., WARRELL, D. A. & HUGHES, M. 1987. The bone marrow in human cerebral malaria: parasite sequestration within sinusoids. *Br J Haematol,* 66, 295-306.

WILLIAMS, C. G., LEE, H. J., ASATSUMA, T., VENTO-TORMO, R. & HAQUE, A. 2022. An introduction to spatial transcriptomics for biomedical research. *Genome Medicine,* 14, 68.

WILLIAMS, D. W., ENGLE, E. L., SHIRK, E. N., QUEEN, S. E., GAMA, L., MANKOWSKI, J. L., ZINK, M. C. & CLEMENTS, J. E. 2016. Splenic Damage during SIV Infection: Role of T-Cell Depletion and Macrophage Polarization and Infection. *Am J Pathol,* 186, 2068-2087.

WILSON, R. J. M., GARDNER, M. J., FEAGIN, J. E. & WILLIAMSON, D. H. 1991. Have malaria parasites three genomes? *Parasitology Today,* 7, 134-136.

WINTER, G., KAWAI, S., HAEGGSTRÖM, M., KANEKO, O., VON EULER, A., KAWAZU, S.-I., PALM, D., FERNANDEZ, V. & WAHLGREN, M. 2005. SURFIN is a polymorphic antigen expressed on Plasmodium falciparum merozoites and infected erythrocytes. *The Journal of experimental medicine,* 201, 1853-1863.

WITMER, K., DAHALAN, F. A., METCALF, T., TALMAN, A. M., HOWICK, V. M. & LAWNICZAK, M. K. N. 2021. Using scRNA-seq to Identify Transcriptional Variation in the Malaria Parasite Ookinete Stage. *Front Cell Infect Microbiol,* 11, 604129.

YANG, M., ROARKE, M. & NGUYEN, B. 2017. Diagnosis of Diffuse Pulmonary Extramedullary Hematopoiesis in Myelofibrosis with Technetium-99m Sulfur Colloid Bone Marrow Scintigraphy. *Journal of Nuclear Medicine,* 58, 596-596.

YANG, S., CORBETT, S. E., KOGA, Y., WANG, Z., JOHNSON, W. E., YAJIMA, M. & CAMPBELL, J. D. 2020. Decontamination of ambient RNA in single-cell RNA-seq with DecontX. *Genome Biology,* 21, 57.

YAP, G. S. & STEVENSON, M. M. 1992. Plasmodium chabaudi AS: erythropoietic responses during infection in resistant and susceptible mice. *Exp Parasitol,* 75, 340-52.

YOUNG, J. A., FIVELMAN, Q. L., BLAIR, P. L., DE LA VEGA, P., LE ROCH, K. G., ZHOU, Y., CARUCCI, D. J., BAKER, D. A. & WINZELER, E. A. 2005. The Plasmodium falciparum sexual development transcriptome: a microarray analysis using ontology-based pattern identification. *Mol Biochem Parasitol,* 143, 67-79.

YUDA, M., IWANAGA, S., SHIGENOBU, S., KATO, T. & KANEKO, I. 2010. Transcription factor AP2-Sp and its target genes in malarial sporozoites. *Molecular Microbiology,* 75, 854-863.

ZHANG, H. 2019. The review of transcriptome sequencing: principles, history and advances. *IOP Conference Series: Earth and Environmental Science,* 332**,** 042003.

ZHANG, L. & WANG, C.-C. 2014. Inflammatory response of macrophages in infection. *Hepatobiliary & Pancreatic Diseases International,* 13**,** 138-152.

ZHENG, G. X. Y., TERRY, J. M., BELGRADER, P., RYVKIN, P., BENT, Z. W., WILSON, R., ZIRALDO, S. B., WHEELER, T. D., MCDERMOTT, G. P., ZHU, J., GREGORY, M. T., SHUGA, J., MONTESCLAROS, L., UNDERWOOD, J. G., MASQUELIER, D. A., NISHIMURA, S. Y., SCHNALL-LEVIN, M., WYATT, P. W., HINDSON, C. M., BHARADWAJ, R., WONG, A., NESS, K. D., BEPPU, L. W., DEEG, H. J., MCFARLAND, C., LOEB, K. R., VALENTE, W. J., ERICSON, N. G., STEVENS, E. A., RADICH, J. P., MIKKELSEN, T. S., HINDSON, B. J. & BIELAS, J. H. 2017. Massively parallel digital transcriptional profiling of single cells. *Nature Communications,* 8**,** 14049.

ZHU, L., MOK, S., IMWONG, M., JAIDEE, A., RUSSELL, B., NOSTEN, F., DAY, N. P., WHITE, N. J., PREISER, P. R. & BOZDECH, Z. 2016. New insights into the Plasmodium vivax transcriptome using RNA-Seq. *Scientific Reports,* 6**,** 20498.

ZIEGENHAIN, C., VIETH, B., PAREKH, S., REINIUS, B., GUILLAUMET-ADKINS, A., SMETS, M., LEONHARDT, H., HEYN, H., HELLMANN, I. & ENARD, W. 2017. Comparative Analysis of Single-Cell RNA Sequencing Methods. *Molecular Cell,* 65**,** 631-643.e4.